

PROCEEDINGS OF THE 41ST JOINT  
MEETING OF U.S.-JAPAN PANEL ON  
WIND AND SEISMIC EFFECTS  
UJNR

Edited by

Keiichi Tamura, Secretary-General  
Japan-side Panel on Wind and Seismic Effects

**Synopsis**

This publication contains the proceedings of the 41st Joint Meeting of the U.S.-Japan Panel on Wind and Seismic Effects, UJNR. The meeting was held at the National Institute for Land and Infrastructure Management, Tsukuba, Japan during May 18-20, 2009. Twenty-two technical papers were authored for the meeting, which were organized into seven themes; Next-Generation Building and Infrastructure Systems, Dams, Wind Engineering, Transportation Systems, Storm Surge and Tsunami, Sustainable Design for Buildings and Infrastructure - Focus on Natural Disaster Prevention, and Disaster Resilient Buildings and Infrastructure.

**Keywords:** *wind engineering, earthquake engineering, sustainable design, natural disaster prevention, UJNR*

## **PREFACE**

This publication contains the proceedings of the 41st Joint Meeting of the U.S.-Japan Panel on Wind and Seismic Effects, UJNR. The meeting was held at the National Institute for Land and Infrastructure Management, Tsukuba, Japan during May 18-20, 2009. The proceedings include the program, list of members, task committee reports, and technical papers submitted to the Joint Panel Meeting, and a summary of the technical site visits.

## **BACKGROUND**

Responding to the need for improving engineering and scientific practices through exchange of technical data and information, research personnel and research equipments, the United States and Japan created the U.S.-Japan Cooperative Science Program in 1961. The U.S.-Japan Cooperative Program in Natural Resources (UJNR) was created in January 1964. The objective of UJNR is to exchange information on research results and scientists and engineers in natural resources of benefit of both countries. UJNR is of 18 Panels each responsible for specific technical subjects.

The Panel on Wind and Seismic Effects was established in 1969. Twenty-one U.S. and seven Japanese agencies currently participate to develop and exchange technologies aimed at reducing damage from high winds, earthquakes, storm surge, and tsunamis. This work is produced through collaboration between U.S. and Japanese member researchers working in five Task Committees. Each Task Committee focuses on specific technical issues, e.g., next-generation building and infrastructure systems. The Panel provides the vehicle to exchange technical data and information on design and construction of civil engineering infrastructures, buildings, and to exchange high wind and seismic measurement records. Annual Joint Panel Meetings alternate in the U.S. and Japan. These one-week technical meetings including technical site visits provide the forum to discuss on-going research and research results.

The National Institute of Standards and Technology (NIST) provides the U.S.-side chairman and secretary-general. The Public Works Research Institute (PWRI) provides the Japan-side chairman and secretary-general.

These annual Joint Panel Meetings provide the mechanism for interaction with U.S. and Japanese researchers in wind and earthquake engineering which provides opportunities to gain valuable information and to engage in cooperative research. Through these opportunities the Panel member organizations have realized important advances in building and structure technology.

The Panel provides the vehicle to exchange technical data and information on design and construction of civil engineering lifelines, buildings, waterfront, and coastal structures. The data produced by the Panel influence on-going structural engineering research and contribute to the revision and creation of U.S.

building codes and standards. Examples of Panel benefits include:

- Created and exchanged digitized earthquake records used as the basis of design and research for Japan and the U.S.
- Produced full-scale test data that advanced seismic design standards for buildings.
- Translated into English a Port and Harbour Research Institute handbook on *Liquefied Remediation of Reclaimed Land*, A. A. Balkema, The Netherlands, publisher that provided general guidance for the US design profession on remediation of liquefiable soils.
- In collaboration with Japan's Geotechnical Society translated into English a report from the Port and Harbour Research Institute, *Remedial Measures Against Soil Liquefaction: From Investigation and Design to Implementation*, A. A. Balkema, The Netherlands, 1998, publisher that served as background and guidance for the Corps of Engineers in performing dam remediation at Clemson University.
- Developed a protocol for testing bridge columns subjected to earthquake loads that facilitated the exchange of experimental data between both countries. The protocol serves as a basis for FHWA's development of new seismic design criteria for bridge columns.
- Facilitated an USACE Team to Kobe within days after the Kobe Earthquake that allowed access to data and information through performing post disaster investigations. This investigation would not have been possible without the Panel's endorsement.
- Performed joint post disaster investigations whose findings influenced revisions to and development of new seismic design and rehabilitation criteria in the US.
- Accessed a large US and Japan database that helped develop an USACE Guidance Criteria in Geotechnical Engineering.
- Provided access to data to help characterize gravely soils in determining the seismic instability of gravely soils for dams and were used to improve USACE construction criteria.
- Through a Japan Guest Researcher from the Port and Harbour Research Institute working at ERDC/WES, Vicksburg geotechnical research findings were transferred into USACE documents.
- Created a database comparing Japanese and US standard penetration tests to improve prediction of soil liquefaction.
- Influenced the creation of a NIST base isolation research program using data from translated Japan reports into English on base isolation systems.
- Increased awareness of wind engineering practice, problems, and breakthroughs in Japan and the U.S.
- Improved cross-discipline research among wind engineers/meteorologists/sociologists in each country.
- Increased the dissemination of latest research findings in wind engineering, especially post-storm events (typhoons/hurricanes) to each country.
- Stimulated interest to create Joint quick-response storm survey teams with interdisciplinary research thrusts to examine storm damage in both countries.
- Developed field test data for use in aerodynamic retrofit of bridge structures.
- Produced data that advanced retrofit techniques for bridge structures.
- Advanced technology for repairing and strengthening reinforced concrete, steel, and masonry structures, improved in-situ measurement methods for soil liquefaction and stability under seismic loads.
- Created database on storm surge and tsunamis and verified mathematical models of tsunami and storm

surge warning systems.

- Established a library resource of current research on wind and earthquake engineering and on storm surge and tsunamis.
- Exchanged more than 250 guest researchers between Japan and the US that has resulted in advancing their respective organizations mission research, advanced the state-of-technology, and provided career growth opportunities for these guest researchers.
- Performed joint research in more than 10 collaborative research projects that resulted in new US seismic design criteria for buildings and bridges.
- Published proceedings of Panel meetings, Task Committee Workshops, and special publications such as List of Panel Publications, translated two-volume series on earthquake resistant construction using base isolation systems, newsletter, website of Panel activities, and more.
- Gained better knowledge of both countries research, design and construction capabilities from in-depth visits to host country's laboratories and building and public works projects. Results of such visits contribute to creation of new Task Committees, agendas for Joint Panel meetings and task committee workshops, special visits of US-Japan researchers, and joint collaborative research.

The Panel's efforts are exemplary of effective joint research and of technology delivery between researchers in the U.S. and Japan. Since its creation, about 2000 papers were presented in 40 Joint Panel Meetings and Task Committee Workshops and over 250 guest researchers were exchanged. The Panel provides important information about the U.S. and Japan's civil engineering thrusts which influence both countries' research and provide the basis for improvements in building and structure codes and standards.

# TABLE OF CONTENTS

<b>PREFACE</b> .....	i
<b>AGENDA OF JOINT MEETING AND TECHNICAL SITE VISITS</b> .....	1
<b>LIST OF PANEL MEMBERS</b> .....	9
<b>RESOLUTIONS</b> .....	27
<b>STRATEGIC PLAN</b> .....	31
<b>PAPERS</b> .....	43
<b>THEME 1. Next-Generation Building and Infrastructure Systems</b> .....	45
Continuity and/or Resiliency of Building Function after Disasters	
Hiroshi Fukuyama*, Koichi Morita, Tomohisa Mukai, Taiki Saito, Hitomitsu Kikitsu, Yoshihiro Iwata, Yoshio Wakiyama and Seitaro Tajiri .....	47
<b>THEME 2. Dams</b> .....	61
Improvement of Distance Attenuation Formula of Acceleration and Lower Limit Acceleration Response Spectrum to Evaluate Seismic Performance of Dams	
Shinya Mitsuishi, Tomoki Otani*, Yoshikazu Yamaguchi and Tomoya Iwashita .....	63
Developing Regional Exercises Involving Multiple Dams	
Enrique Matheu, Yazmin Seda-Sanabria and Robert Hughes* .....	76
Damage to Dams due to the Iwate-Miyagi Nairiku Earthquake in 2008	
Yoshikazu Yamaguchi*, Tomoya Iwashita and Shinya Mitsuishi .....	86
<b>THEME 3. Wind Engineering</b> .....	95
Experimental Studies on Internal Pressure and Debris Strike for Improved Tornado Induced Loads of Low-Rise Buildings	
Partha Sarkar* and Hitomitsu Kikitsu .....	97
Damage to Buildings by EF5 Tornado in Iowa, U.S. on May 25, 2008	
Hitomitsu Kikitsu* and Partha Sarkar .....	110
New Scales for the Destructive Potential of Tropical Cyclones	
Mark Powell and Timothy Reinhold (Presented by John Gaynor*) .....	124
<b>THEME 4. Transportation Systems</b> .....	133
Damage Investigation of Maturube Bridge during the 2008 Iwate-Miyagi Nairiku Earthquake	
Shigeki Unjoh*, Takashi Tamakoshi, Koichi Ikuta and Junichi Sakai .....	135
The Lessons Learned from Wenchuan Earthquake on Highway Bridges	
Phillip Yen*, Genda Chen and Mark Yashinski .....	148
Quick Earthquake Damage Detection System for Bridges	

Junichi Sakai* and Shigeki Unjoh .....	165
Shake Table Testing of Bridge Reinforced Concrete Columns under Combined Actions	
Juan Arias-Acosta and David Sanders* .....	180
Shake Table Experiment on RC Bridge Columns Using E-Defense	
Kazuhiko Kawashima*, Tomohiro Sasaki, Koichi Kajiwara, Hiromichi Ukon, Shigeki Unjoh, Junichi Sakai, Kenji Kosa, Yoshikazu Takahashi, Masaaki Yabe and Hiroshi Matsuzaki .....	188
Outline of the Damage of Transportation Facilities and Geotechnical Structures by the 2009 L'Aquila, Italy Earthquake	
Kazuhiko Kawashima*, Omer Aydan, Kazuo Konagai, Atsushi Yamashita and Sven-Peter Teodori .....	202
<b>THEME 5. Storm Surge and Tsunami</b> .....	215
Decision Making on Evacuation from the Tsunami Following the Earthquake off Kuril Islands in 2006	
Yoshio Suwa and Fuminori Kato* .....	217
Practical Model to Estimate Behavior of Tsunami-Drifted Bodies	
Takashi Tomita* and Kazuhiko Honda .....	227
Manual for Forecasting Earthquake and Tsunami Damage to Public Civil Engineering Facilities (Proposal)	
Osamu Okamoto, Kentaro Kumagai and Katsuya Oda .....	235
<b>THEME 6. Sustainable Design for Buildings and Infrastructure - Focus on Natural Disaster Prevention</b> .....	243
Earthquake Disaster Management in Japan	
Koji Ikeuchi* and Masamitsu Waga .....	245
Study on Landslide Orientation Bias Triggered by 1994 Northridge Earthquake	
Hiroshi P. Sato* .....	260
<b>THEME 7. Disaster Resilient Buildings and Infrastructure</b> .....	269
On the Variation of Fundamental Frequency (Period) of an Undamaged Building - A Continuing Discussion	
Mehmet Celebi* .....	271
System Dynamics Modeling and Simulation of Disaster Recovery Process of Interdependent Infrastructure Systems	
Shojiro Kataoka* .....	282
Modal-Pushover-based Ground Motion Scaling Procedure for Nonlinear Analysis of Structures	
Erol Kalkan* and Anil Chopra .....	289
Climate Change Adaptive Strategies for Buildings and Public Health	
Fuyuen Yip, Josephine Malilay, George Luber and Paul Garbe .....	310
<b>APPENDIX</b> .....	317
<b>TASK COMMITTEE REPORTS</b> .....	319

TECHNICAL SITE VISITS.....333

**AGENDA OF JOINT MEETING AND  
TECHNICAL SITE VISITS**

## JOINT MEETING

### May 17 (Sunday)

Arrival of U.S.-side Delegation

Hotel: Okura Frontier Hotel Tsukuba Epochal

Phone/Fax: +81-(0)29-860-7700/+81-(0)29-860-7701

### May 18 (Monday)

10:00

#### **Opening Ceremonies**

[8F Conference Room]

Call to order by Keiichi Tamura, Secretary-General, Japan-side Panel

Opening remarks by Hiroaki Taniguchi, Vice-Minister for Engineering Affairs,  
Ministry of Land, Infrastructure, Transport and Tourism

Remarks by Bart D. Cobbs, Unit Chief, Environment, Science and Technology Unit,  
Economic Affairs, Embassy of the United States of America

Remarks by Masanobu Morita, Director, International Science and Technology Affairs  
Division, Science and Technology Policy Bureau, Ministry of Education, Culture,  
Sports, Science and Technology

Remarks by Tadahiko Sakamoto, Chairman, Japan-side Panel on Wind and Seismic  
Effects, Chief Executive, Public Works Research Institute

Remarks by H. S. Lew, Acting Chairman, U.S.-side Panel on Wind and Seismic Effects,  
Building and Fire Research Laboratory, National Institute of Standards and Technology,  
Department of Commerce

Introduction of Japan-side Members by Japan-side Panel Chairman

Introduction of U.S.-side Members by U.S.-side Panel Chairman

Elect Joint Panel Meeting Chairman

Adopt Agenda

Adjourn

11:10

Group Photograph

11:30	<b>Technical Session 1 - Transportation Systems</b> Chairman - Dr. H. S. Lew	
11:30	<i>Damage Investigation of Maturube Bridge during the 2008 Iwate-Miyagi Nairiku Earthquake</i> , Shigeki Unjoh*, Takashi Tamakoshi, Koichi Ikuta, NILIM; and Junichi Sakai, PWRI	
11:50	<i>The Lessons Learned from Wenchuan Earthquake on Highway Bridges</i> , Phillip Yen*, FHWA; Genda Chen, MUST; and Mark Yashinski, CALTRANS	
12:10	Discussion	
12:20	Lunch	[1F Conference Room]
13:20	<b>Technical Session 2 - Transportation Systems</b> Chairman - Dr. H. S. Lew	
13:20	<i>Quick Earthquake Damage Detection System for Bridges</i> , Junichi Sakai*, PWRI; and Shigeki Unjoh, NILIM	
13:40	<i>Shake Table Testing of Bridge Reinforced Concrete Columns under Combined Actions</i> , Juan Arias-Acosta and David Sanders*, UNR	
14:00	<i>Shake Table Experiment on RC Bridge Columns Using E-Defense</i> , Kazuhiko Kawashima*, Tomohiro Sasaki, Tokyo Institute of Technology; Koichi Kajiwara, Hiromichi Ukon, NIED; Shigeki Unjoh, NILIM; Junichi Sakai, PWRI; Kenji Kosa, Kyushu Institute of Technology; Yoshikazu Takahashi, Kyoto University; Masaaki Yabe, Chodai; and Hiroshi Matsuzaki, Tokyo Institute of Technology	
14:20	<i>Outline of the Damage of Transportation Facilities and Geotechnical Structures by the 2009 L'Aquila, Italy Earthquake</i> , Kazuhiko Kawashima*, Tokyo Institute of Technology; Omer Aydan, Tokai University; Kazuo Konagai, University of Tokyo; Atsushi Yamashita, Gifu University; and Sven-Peter Teodori, Nippon Koei Co., Ltd. / <i>Highlights of the L'Aquila, Italy Earthquake of April 6, 2009</i> , Mehmet Celebi*	
14:45	Discussion	
15:05	Break	
15:20	<b>Task Committee Meetings</b>	
	B: Next-Generation Building and Infrastructure Systems	[Room #524]
	C: Dams	[Room #532]
	D: Wind Engineering	[Room #616]
	G: Transportation Systems	[Room #617]
	H: Storm Surge and Tsunami	[Room #601]
17:00	Conclusion of Day 1	

18:30 Japan-side Panel Hosted Reception  
(Okura Frontier Hotel Tsukuba)

**May 19 (Tuesday)**

9:00 **Technical Session 3 - Sustainable Design for Buildings and Infrastructure - Focus on Natural Disaster Prevention, and Disaster Resilient Buildings and Infrastructure**

Chairman - Dr. Tadahiko Sakamoto

9:00 *Earthquake Disaster Management in Japan*, Koji Ikeuchi\* and Masamitsu Waga, Cabinet Office

9:20 *On the Variation of Fundamental Frequency (Period) of an Undamaged Building - A Continuing Discussion*, Mehmet Celebi\*, USGS

9:40 *System Dynamics Modeling and Simulation of Disaster Recovery Process of Interdependent Infrastructure Systems*, Shojiro Kataoka\*, NILIM

10:00 *Modal-Pushover-based Ground Motion Scaling Procedure for Nonlinear Analysis of Structures*, Erol Kalkan\*, USGS; and Anil Chopra, UCB

10:20 Discussion

10:40 Break

10:55 **Technical Session 4 - Wind Engineering**

Chairman - Dr. Tadahiko Sakamoto

10:55 *Experimental Studies on Internal Pressure and Debris Strike for Improved Tornado Induced Loads of Low-Rise Buildings*, Partha Sarkar\*, ISU; and Hitomitsu Kikitsu, NILIM

11:15 *Damage to Buildings by EF5 Tornado in Iowa, U.S. on May 25, 2008*, Hitomitsu Kikitsu\*, NILIM; and Partha Sarkar, ISU

11:35 *New Scales for the Destructive Potential of Tropical Cyclones*, Mark Powell, NOAA; and Timothy Reinhold, IBHS (Presented by John Gaynor\*)

11:55 Discussion

12:10 Lunch [1F Conference Room]

13:10 **Technical Session 5 - Next-Generation Building and Infrastructure Systems, and Sustainable Design for Buildings and Infrastructure - Focus on Natural Disaster Prevention**

Chairman - Dr. Tadahiko Sakamoto

13:10 *Continuity and/or Resiliency of Building Function after Disasters*, Hiroshi Fukuyama\*,

- Koichi Morita, Tomohisa Mukai, Taiki Saito, BRI; Hitomitsu Kikitsu, NILIM;  
Yoshihiro Iwata, Yoshio Wakiyama and Seitaro Tajiri, BRI
- 13:30 *Study on Landslide Orientation Bias Triggered by 1994 Northridge Earthquake*,  
Hiroshi P. Sato\*, GSI
- 13:50 Discussion
- 14:00 Break
- 14:15 **Strategic Planning Session**
- 17:00 Conclusion of Day 2
- 18:30 Individual Japan-side Members Hosted Dinners

### May 20 (Wednesday)

- 9:00 **Technical Session 6 - Dams**  
Chairman - Dr. H. S. Lew
- 9:00 *Analysis of Remediation Alternatives for Success Dams*, Michael Sharp\*, USACE
- 9:20 *Improvement of Distance Attenuation Formula of Acceleration and Lower Limit  
Acceleration Response Spectrum to Evaluate Seismic Performance of Dams*, Shinya  
Mitsuishi, NILIM; Tomoki Otani\*, Japan Water Agency; Yoshikazu Yamaguchi and  
Tomoya Iwashita, PWRI
- 9:40 *Developing Regional Exercises Involving Multiple Dams*, Enrique Matheu, DHS;  
Yazmin Seda-Sanabria, USACE; and Robert Hughes\*, DHS
- 10:00 *Damage to Dams due to the Iwate-Miyagi Nairiku Earthquake in 2008*, Yoshikazu  
Yamaguchi\*, Tomoya Iwashita, PWRI; and Shinya Mitsuishi, NILIM
- 10:20 *Developing Structural Performance Criteria for Concrete Hydraulic Structures*, Robert  
Hall, USACE (Presented by Michael Sharp\*)
- 10:40 Discussion
- 11:05 Break
- 11:20 **Technical Session 7 - Storm Surge and Tsunami**  
Chairman - Dr. H. S. Lew
- 11:20 *Decision Making on Evacuation from the Tsunami Following the Earthquake off Kuril  
Islands in 2006*, Yoshio Suwa and Fuminori Kato\*, NILIM
- 11:40 *Practical Model to Estimate Behavior of Tsunami-Drifted Bodies*, Takashi Tomita\* and  
Kazuhiko Honda, PARI
- 12:00 Discussion

12:10 Lunch [1F Conference Room]

13:10 **Workshop and Task Committee Reports**  
Chairman - Dr. Tadahiko Sakamoto

14:30 Break

14:50 **Adoption of Final Resolutions**  
Chairman - Dr. Tadahiko Sakamoto

15:50 Break

16:00 **Closing Ceremonies**  
Call to order by Keiichi Tamura, Secretary-General, Japan-side Panel  
  
Remarks by H. S. Lew, Acting Chairman, U.S.-side Panel on Wind and Seismic Effects  
  
Remarks by Tadahiko Sakamoto, Chairman, Japan-side Panel on Wind and Seismic Effects

16:30 Conclusion of 41st Joint Panel Technical Sessions

18:30 U.S.-side Panel Hosted Reception  
(Restaurant ESPOIR, Epochal Tsukuba International Congress Center)

## TECHNICAL SITE VISITS

### May 21 (Thursday)

- 8:12-9:05 Move to Akihabara from Tsukuba by TX
- 9:20-10:00 Move to Ariake by bus
- 10:00-10:30 Visit Ariake Yard for fabrication of main truss span of Tokyo Rinkai Oh-hashii Bridge
- 10:30-12:00 Visit construction site of Tokyo Rinkai Oh-hashii Bridge, Tokyo Bay by ferry
- 12:00-12:30 Move to Tokyo International Airport (Haneda)
- 12:30-13:30 Lunch at meeting room of Tokyo International Airport Development Office
- 13:30-15:30 Visit construction site for new runway at Tokyo International Airport (Haneda) by ferry
- 15:30-16:00 Move to Ariake by bus
- 16:00-17:30 Visit Disaster Management Center (DMC) at Ariake
- 17:30-18:00 Move to hotel by bus  
Stay at Mitsui Garden Hotel Ginza Premier (Shimbashi, Tokyo)

### May 22 (Friday)

- 9:20-10:00 Move to Tokyo Main Office, Takenaka Corporation at Toyo-cho by bus
- 10:00-12:00 Introduction of sustainable works and Tokyo Main Office (sustainable building) at Tokyo Main Office, Takenaka Corporation
- 12:00-12:30 Move to Shimizu Institute of Technology at Etchujima by bus
- 12:30-13:30 Lunch at meeting room of Shimizu Institute of Technology
- 13:30-16:30 Introduction of sustainable building concept, floating isolation, wind tunnel facility, etc at Shimizu Institute of Technology
- 16:30-17:00 Move to hotel by bus  
Stay at Mitsui Garden Hotel Ginza Premier (Shimbashi, Tokyo)

### May 23 (Saturday)

- 9:10-9:30 Move to Japan Meteorological Agency (JMA) Headquarters at Ohtemachi by bus
- 9:30-10:30 Introduction of earthquake early warning system of JMA
- 10:30-10:45 Move to Japan Life Insurance Corporation Building at Tokyo by bus
- 10:45-12:00 Introduction of sustainable building and advanced seismic response controls system
- 12:00-13:00 Lunch around Tokyo Station

### May 24 (Sunday)

- Departure of U.S.-side Delegation

# **LIST OF PANEL MEMBERS**

## U.S.-SIDE DELEGATION

Dr. H. S. Lew  
Acting-Chairman, U.S.-side Panel  
Senior Research Structural Engineer  
Materials and Construction Research Division  
Building and Fire Research Laboratory  
National Institute of Standards and Technology  
100 Bureau Drive Stop 8611  
Gaithersburg, MD 20899-8611  
(T) 301-975-6060 (F) 301-869-6275  
hls@nist.gov

Dr. Mehmet K. Celebi  
Research Civil Engineer  
U.S. Geological Survey  
U.S. Department of the Interior  
345 Middlefield Road, MS 977  
Menlo Park, CA 94025  
(T) 650-329-5623 (F) 650-329-5163  
celebi@usgs.gov

Mr. John Gaynor  
Director, Office of Weather and Air Quality  
Office of Oceanic and Atmospheric Research  
National Oceanic and Atmospheric Administration  
Silver Spring, MD 20910  
(T) 301-734-1178 (F) 301-713-3515  
john.gaynor@noaa.gov

Mr. Robert Cris Hughes  
Dams Sector Branch  
Sector Specific Agency Executive Management Office  
Office of Infrastructure Protection  
US Department of Homeland Security  
Washington, DC 20528  
(T) 703-235-2838  
C.Hughes@dhs.gov

Dr. Erol Kalkan  
Senior Research Engineer  
Earthquake Hazards Team  
U.S. Geological Survey  
U.S. Department of the Interior  
345 Middlefield Road, MS 977  
Menlo Park, CA 94025  
(T) 650-329-5146 (F) 650-329-5163 U.S.  
ekalkan@usgs.gov

Mr. Noël Raufaste  
NIST Guest Researcher/Engineer Emeritus  
Building and Fire Research Laboratory  
National Institute of Standards and Technology  
100 Bureau Drive, Stop 8611  
Gaithersburg, MD 20899-8611  
(T) 301-975-6062  
noel.raufaste@nist.gov

Dr. David H. Sanders  
Professor  
Department of Civil and Environmental Engineering  
University of Nevada  
Reno, NV 89557  
(T) 775-784-4288 (F) 775-784-1390  
sanders@unr.edu

Dr. Partha P. Sarkar  
Professor and Wilson Chair  
Director of Wind Simulation and Testing Laboratory  
2271 Howe Hall, Rm. 1200  
Department of Aerospace Engineering  
Iowa State University  
Ames, IA 50011-2271  
(T) 515-294-0719  
ppsarkar@iastate.edu

Dr. Michael K. Sharp  
Technical Director, Civil Works Infrastructure  
Geotechnical and Structures Laboratory  
US Army Engineer Research and Development Center  
3909 Halls Ferry Road  
Vicksburg, MS 39180-6199  
(T) 601-634-4127 (F) 601-634-4894  
michael.k.sharp@erdc.usace.army.mil

Dr. W. Phillip Yen  
Program Manager  
Seismic Hazard Mitigation Program  
Office of Infrastructure, R&D  
Federal Highway Administration  
6300 Georgetown Pike  
McLean, VA 22101  
(T) 202-493-3056 (F) 202-493-3442  
Wen-huei.Yen@fhwa.dot.gov

## U.S.-SIDE PANEL ON WIND AND SEISMIC EFFECTS MEMBERSHIP LIST

Mr. Stephen A. Cauffman  
Secretary-General, U.S.-side Panel  
Deputy Chief, Materials and Construction Research  
Division  
Building and Fire Research Laboratory  
National Institute of Standards and Technology  
100 Bureau Drive, Stop 8611  
Gaithersburg, MD 20899-8611  
301-975-6051 (F) 301-869-6275  
stephen.cauffman@nist.gov

Mr. John Baals  
Seismic Safety Coordinator  
P.O. Box 25007 (D-8110)  
Bureau of Reclamation  
U.S. Department of the Interior  
Denver, CO 80225  
303-236-9129 x304 (F) 303-236-9099  
jbaals@do.usbr.gov

Dr. Eddie N. Bernard  
Director, Pacific Marine Environmental Laboratory  
National Oceanic and Atmospheric Administration  
U.S. Department of Commerce  
7600 Sand Point Way, NE  
BIN C15700/Building 3  
Seattle, WA 98115-0070  
206-526-6800 (F) 206-526-4576  
Eddie.N.Bernard@noaa.gov

Dr. David M. Boore  
U.S. Geological Survey  
345 Middlefield Road MS 977  
Menlo Park, CA 94025  
650-329-5616 (F) 650-329-5163  
boore@usgs.gov

Dr. Roger D. Borchardt  
U.S. Geological Survey  
U.S. Department of the Interior  
345 Middlefield Road, MS 977  
Menlo Park, CA 94025  
650-329-5619 (F) 650-329-5163  
borcherdt@usgs.gov

Dr. Mehmet K. Celebi  
Research Civil Engineer  
U.S. Geological Survey  
U.S. Department of the Interior  
345 Middlefield Road, MS 977  
Menlo Park, CA 94025  
650-329-5623 (F) 650-329-5163  
celebi@usgs.gov

Dr. C. Y. Chen  
Senior Civil/Geotechnical Engineer  
Office of Foreign Buildings  
Department of State  
Code SA-6, Rm. 347

Washington, DC 20520  
703-875-6207 (F) 703-875-6204  
chency@state.gov

Dr. Anjana Chudgar  
Structural Engineer  
U.S. Army Corps of Engineers  
550 Main Street, RM 10-031  
Cincinnati, OH 45202  
513-684-6210 (F) 513-684-2460 (C) 5020345-0743  
anjana.k.chudgar@hq02.usace.army.mil

Dr. Amr Elnashai  
Director, Mid-America Earthquake Center  
Professor of Civil Engineering  
University of Illinois  
1245 Newmark Laboratory  
205 North Mathews Avenue  
Urbana, IL 61801  
217-265-5497 (F) 217-333-3821  
aelnash@uiuc.edu

Mr. John Gaynor  
Director, Office of Weather and Air Quality  
Office of Oceanic and Atmospheric Research  
National Oceanic and Atmospheric Administration  
Silver Spring, MD 20910  
301-734-1178 (F) 301-713-3515  
john.gaynor@noaa.gov

Dr. Hamid Ghasemi  
Bridge Safety, Reliability and Security  
Office of Infrastructure and Security  
Office of Infrastructure R&D  
Federal Highway Administration  
6300 Georgetown Pike  
McLean VA 22101  
202-493-3042 (F) 202-493-3443  
hamid.ghasemi@fhwa.dot.gov

Dr. John Gross  
Research Structural Engineer  
Materials and Construction Research Division  
Building and Fire Research Laboratory  
National Institute of Standards and Technology  
100 Bureau Drive, Stop 8611  
Gaithersburg, MD 20899-8611  
301-975-6068 (F) 301-869-6275  
john.gross@nist.gov

Dr. Robert L. Hall  
Chief, Geosciences and Structures Division  
Geotechnical and Structures Laboratory  
US Army Engineer Research and Development Center  
CEERD-GS  
3909 Halls Ferry Road  
Vicksburg, MS 39180-6199  
601-634-2567 (F) 601-634-3412  
(C) 601-618-0644

Robert.L.Hall@erdc.usace.army.mil

Dr. Mary Ellen Hynes  
Director of Research, Infrastructure, and Geophysical  
Division  
Science and Technology Directorate  
Department of Homeland Security  
Washington, DC 20528  
1499 Massachusetts Avenue, NW Apt 113A, Washington,  
DC 20005  
202-254-5807  
Maryellen.hynes@dhs.gov

Dr. Nicholas P. Jones  
Dean, Whiting School of Engineering  
Johns Hopkins University  
Baltimore, MD 21218  
410-516-4050 (Jeannie Pugh) 443-834-3740  
npjones@jhu.edu

Mr. Michael Keever  
Chief, Earthquake Engineering Office  
California Department of Transportation Division of  
Engineering Services, MS9-2/7J  
P.O. Box 168041  
Sacramento, CA 95816  
916-227-8806 (F) 916-227-8242  
mike\_keever@dot.ca.gov

Dr. George C. Lee  
Task Director, Multidisciplinary Center for Earthquake  
Engineering Research (MCEER)  
University at Buffalo  
122 Red Jacket Quad  
Buffalo, NY 14261  
716-645-3391 x111 (F) 716-645-3399  
716-645-2039 716-310-1078 (C)  
gcllee@mceermail.buffalo.edu

Dr. H. S. Lew  
Senior Research Structural Engineer  
Materials and Construction Research Division  
Building and Fire Research Laboratory  
National Institute of Standards and Technology  
100 Bureau Drive Stop 8611  
Gaithersburg, MD 20899-861  
301-975-6060 (F) 301-869-6275  
hai.lew@nist.gov

Mr. Michael Mahoney  
Physical Scientist  
Federal Emergency Management Agency  
500 C Street, SW  
Washington, DC 20472  
202-646-2794 (F) 202-646-4387  
mike.mahoney@dhs.gov

Dr. Josephine Malilay  
Associate Director for Science (Acting)  
Division of Environmental Hazards and Health Effects  
National Center for Environmental Health  
Centers for Disease Control and Prevention  
4770 Buford Hwy., NE (Mail stop F-52)  
Atlanta, GA 30341  
770-488-3465 (F) 770-488-3460  
JMalilay@cdc.gov

Dr. Enrique E. Matheu  
Chief, Dams Sector Branch  
Sector Specific Agency Executive Management Office  
Office of Infrastructure Protection  
US Department of Homeland Security  
Washington, DC 20528  
703-235-2863 (F) 703-235-3053  
enrique.matheu@dhs.gov

Mr. Noël Raufaste  
NIST Emeritus/Guest Researcher  
Building and Fire Research Laboratory  
National Institute of Standards and Technology  
Gaithersburg, MD 20899-8611  
301-975-6062  
noel.raufaste@nist.gov

Dr. Andrei M. Reinhorn  
Clifford C. Furnas Professor of Structural Engineering and  
Director, Structural Engineering and Earthquake  
Simulation Laboratory (SEESL)  
University at Buffalo, State University of New York  
231 Ketter Hall, Buffalo, NY 14260  
716-645-2114 X2419  
(F) 716-645-3733  
Reinhorn@buffalo.edu

Dr. William E. Roper  
School of Computational Sciences  
Center for Earth Observing and Space Research  
George Mason University  
4400 University Drive, MS 5C3  
Fairfax, VA 22030  
703-993-1648 (F) 703-993-1521  
wroper@gmu.edu

Dr. Michael K. Sharp  
Technical Director, Civil Works Infrastructure  
Geotechnical and Structures Laboratory  
US Army Engineer Research and Development Center  
3909 Halls Ferry Road  
Vicksburg, MS 39180-6199  
601-634-4127 (F) 601-634-4894  
michael.k.sharp@erdc.usace.army.mil

Dr. M. P. Singh  
Program Director  
Structural Systems and Hazard Mitigation of Structures  
(SSHM)  
Room 550 S  
National Science Foundation  
4201 Wilson Boulevard  
Arlington, VA 22230  
703-292-7081  
mpsingh@nsf.gov

Dr. Charles E. Smith  
Senior Technical Advisor  
Accident Investigation Board  
U. S. Minerals Management Service  
381 Elden Street, MS 4021  
Herndon, VA 20170-4817  
703-787-1561 (F) 703-787-1549  
smithc@mms.gov or Charles.E.Smith@mms.gov

Dr. W. Phillip Yen  
Program Manager  
Seismic Hazard Mitigation Program  
Federal Highway Administration  
Office of Infrastructure, R&D  
6300 Georgetown Pike  
McLean, VA 22101  
202-493-3056 (F) 202-493-3442 (C) 202-468-6113  
Wen-huei.Yen@fhwa.dot.gov

Dr. Solomon C. Yim  
Professor  
Structural and Ocean Engineering  
Oregon State University  
202 Apperson Hall  
Corvallis, OR 97331-2302  
541-737-6894 (F) 541-737-3052  
solomon.yim@oregonstate.edu

# JAPAN-SIDE PANEL ON WIND AND SEISMIC EFFECTS

## MEMBERSHIP LIST

### STEERING COMMITTEE MEMBERS

Dr. Tadahiko Sakamoto  
Chairman, Japan-side Panel on Wind and Seismic Effects  
Chief Executive, Public Works Research Institute  
1-6 Minamihara, Tsukuba-shi, Ibaraki-ken 305-8516  
Tel: 029-879-6700  
Fax: 029-879-6741  
E-mail: sakamoto@pwri.go.jp

Dr. Keiichi Tamura  
Secretary-General, Japan-side Panel on Wind and Seismic Effects  
Research Coordinator for Earthquake Engineering  
Center for Advanced Engineering Structural Assessment and Research (CAESAR)  
Public Works Research Institute  
1-6 Minamihara, Tsukuba-shi, Ibaraki-ken 305-8516  
Tel: 029-879-6721  
Fax: 029-879-6739  
E-mail: ke-tamura@pwri.go.jp

Mr. Tomonori Abe  
Director, Hydraulic Engineering Research Group  
Public Works Research Institute  
1-6 Minamihara, Tsukuba-shi, Ibaraki-ken 305-8516  
Tel: 029-879-6723  
Fax: 029-879-6737  
E-mail: to-abe@pwri.go.jp

Mr. Yoshikazu Fukushima  
Director, Geographic Department  
Geographical Survey Institute  
Ministry of Land, Infrastructure, Transport and Tourism  
1 Kitasato, Tsukuba-shi, Ibaraki-ken 305-0811  
Tel: 029-864-1111  
Fax: 029-864-1804  
E-mail: fukushima@gsi.go.jp

Dr. Hiroshi Fukuyama  
Chief Research Engineer and Research Coordinator  
Department of Structural Engineering  
Building Research Institute  
1 Tachihara, Tsukuba-shi, Ibaraki-ken 305-0802  
Tel: 029-864-6647  
Fax: 029-864-6773  
E-mail: fukuyama@kenken.go.jp

Dr. Hiromichi Higashihara  
Director, Earthquake Disaster Mitigation Research Center  
National Research Institute for Earth Science and Disaster Prevention  
1-5-2 Wakinohama Kaigandori, Chuo-ku, Kobe-shi, Hyogo-ken 651-0073  
Tel: 078-262-5520  
Fax: 078-262-5526  
E-mail: higashi@edm.bosai.go.jp

Dr. Jun-ichi Hoshikuma  
Chief Researcher, Bridge and Structural Technology Research Group  
Center for Advanced Engineering Structural Assessment and Research (CAESAR)  
Public Works Research Institute  
1-6 Minamihara, Tsukuba-shi, Ibaraki-ken 305-8516  
Tel: 029-879-6793  
Fax: 029-879-6739  
E-mail: hoshikuma@pwri.go.jp

Dr. Masanori Iiba  
Director, Department of Structural Engineering  
Building Research Institute  
1 Tachihara, Tsukuba-shi, Ibaraki-ken 305-0802  
Tel: 029-864-6633  
Fax: 029-864-6773  
E-mail: iiba-m@kenken.go.jp

Dr. Takashi Iijima  
President, Civil Engineering Research Laboratory  
1-18 Kanda Suda-cho Chiyoda-ku, Tokyo 101-0041  
Tel: 03-3254-9481  
Fax: 03-3254-9448  
E-mail: iijima@crl.or.jp

Mr. Munehiro Igarashi  
Director, Disaster Risk Management Office  
River Bureau  
Ministry of Land, Infrastructure, Transport and Tourism  
2-1-3 Kasumigaseki, Chiyoda-ku, Tokyo 100-8918  
Tel: 03-5253-8111  
Fax: 03-5253-1608  
E-mail: igarashi-m2ag@milt.go.jp

Mr. Koji Ikeuchi  
Director for Earthquake, Volcanic and Large-scale Flood Disaster Management  
Disaster Management Bureau  
Cabinet Office  
1-2-2 Kasumigaseki, Chiyoda-ku, Tokyo 100-8969  
Tel: 03-3501-5693  
Fax: 03-3501-5199  
E-mail: koji.ikeuchi@cao.go.jp

Mr. Yasuo Katsumi  
Director for International Building Code Coordination  
Housing Bureau  
Ministry of Land, Infrastructure, Transport and Tourism  
2-1-3 Kasumigaseki, Chiyoda-ku, Tokyo 100-8918  
Tel: 03-5253-8513  
Fax: 03-5253-1630  
E-mail: katsumi-y2ym@milt.go.jp

Dr. Naohito Kawai  
Chief Research Engineer, Department of Structural

Engineering  
Building Research Institute  
1 Tachihara, Tsukuba-shi, Ibaraki-ken 305-0802  
Tel: 029-864-6753  
Fax: 029-864-6773  
E-mail: kawai@kenken.go.jp

Dr. Kazuhiko Kawashima  
Professor, Department of Civil Engineering  
Tokyo Institute of Technology  
2-12-1 O-okayama, Meguro-ku, Tokyo 152-8552  
Tel: 03-5734-2922  
Fax: 03-5734-3810  
E-mail: kawasima.k.ae@m.titech.ac.jp

Mr. Naoki Kawashima  
Director, Disaster Risk Management Office  
Coast Administration and Disaster Reduction Division  
Ports and Harbors Bureau  
Ministry of Land, Infrastructure, Transport and Tourism  
2-1-3 Kasumigaseki, Chiyoda-ku, Tokyo 100-8918  
Tel: 03-5253-8111  
Fax: 03-5253-1654  
E-mail: kawashima-n2jv@mlit.go.jp

Dr. Shuzo Murakami  
Chief Executive, Building Research Institute  
1 Tachihara, Tsukuba-shi, Ibaraki-ken 305-0802  
Tel: 029-864-2151  
Fax: 029-864-2989  
E-mail: murakami@kenken.go.jp

Mr. Jun Murakoshi  
Chief Researcher, Bridge and Structural Technology  
Research Group  
Center for Advanced Engineering Structural Assessment  
and Research (CAESAR)  
Public Works Research Institute  
1-6 Minamihara, Tsukuba-shi, Ibaraki-ken 305-8516  
Tel: 029-879-6792  
Fax: 029-879-6739  
E-mail: murakosi@pwri.go.jp

Dr. Masayoshi Nakashima  
Director, Hyogo Earthquake Engineering Center  
National Research Institute for Earth Science and Disaster  
Prevention  
1501-21, Mituta, Nishikameya, Shijimi-cho, Miki-shi,  
Hyogo-ken 673-0515  
Tel: 0794-85-8211  
Fax: 0794-85-7994  
E-mail: naka@bosai.go.jp

Dr. Shinsuke Nakata  
Professor, Infrastructure System Engineering Course  
Kochi University of Technology  
185 Miyanokuchi, Tosa-Yamada-cho, Kochi-ken 782-8502  
Tel: 0887-53-1040  
Fax: 0887-57-2420  
E-mail: nakata.shinsuke@kochi-tech.ac.jp

Mr. Masaaki Nakayasu  
Director, Planning and Research Administration  
Department  
National Institute for Land and Infrastructure Management  
Ministry of Land, Infrastructure, Transport and Tourism

1 Asahi, Tsukuba-shi, Ibaraki-ken 305-0804  
Tel: 029-864-2868  
Fax: 029-864-1527  
E-mail: nakayasu-m92ta@nilim.go.jp

Mr. Yoshiaki Nanami  
Director, International Policy Unit for Infrastructure  
Policy Bureau  
Ministry of Land, Infrastructure, Transport and Tourism  
2-1-3 Kasumigaseki, Chiyoda-ku, Tokyo 100-8918  
Tel: 03-5253-8111  
Fax: 03-5253-1562  
E-mail: nanami-y2qp@mlit.go.jp

Dr. Isao Nishiyama  
Director, Building Department  
National Institute for Land and Infrastructure Management  
Ministry of Land, Infrastructure, Transport and Tourism  
1 Tachihara, Tsukuba-shi, Ibaraki-ken 305-0802  
Tel: 029-864-4277  
Fax: 029-864-6774  
E-mail: nishiyama-i92ta@nilim.go.jp

Mr. Akihiko Nunomura  
Director-General  
National Institute for Land and Infrastructure Management  
Ministry of Land, Infrastructure, Transport and Tourism  
1 Asahi, Tsukuba-shi, Ibaraki-ken 305-0804  
Tel: 029-864-2210  
Fax: 029-864-2148  
E-mail: nunomura-a2ij@nilim.go.jp

Dr. Hisashi Okada  
Director, Testing and Research Laboratory  
Japan Housing and Wood Technology Center  
3-4-2 Shinsuna, Koto-ku, Tokyo 136-0075  
Tel: 03-3589-1788  
Fax: 03-3589-1766  
E-mail: h-okada@howtec.or.jp

Dr. Izuru Okawa  
Senior Research Fellow, Department of Structural  
Engineering  
Building Research Institute  
1 Tachihara, Tsukuba-shi, Ibaraki-ken 305-0802  
Tel: 029-864-6627  
Fax: 029-864-6773  
E-mail: okawa@kenken.go.jp

Dr. Yasuo Okuda  
Chief Research Engineer, Department of Structural  
Engineering  
Building Research Institute  
1 Tachihara, Tsukuba-shi, Ibaraki-ken 305-0802  
Tel: 029-864-6618  
Fax: 029-864-6773  
E-mail: y\_okuda@kenken.go.jp

Dr. Hiroshi Sato  
Professor, Graduate School of Systems and Information  
Engineering  
University of Tsukuba  
1-1-1 Tennodai, Tsukuba-shi, Ibaraki-ken 305-8573  
Tel: 029-853-5549  
Fax: 029-853-5549  
E-mail: hsato@sk.tsukuba.ac.jp

Dr. Koji Sekiguchi  
Head, Outreach Division  
Strategic Planning Department  
National Research Institute for Earth Science and Disaster  
Prevention  
3-1 Tennodai, Tsukuba-shi, Ibaraki-ken 305-0006  
Tel: 029-863-7768  
Fax: 029-851-1622  
E-mail: ksekigut@bosai.go.jp

Dr. Hideki Sugita  
Team Leader, Soil Mechanics and Dynamics Research  
Team  
Material and Geotechnical Engineering Research Group  
Public Works Research Institute  
1-6 Minamihara, Tsukuba-shi, Ibaraki-ken 305-8516  
Tel: 029-879-6770  
Fax: 029-879-6735  
E-mail: sugita@pwri.go.jp

Mr. Morito Takahashi  
Director, Cold-Region Construction Engineering Research  
Group  
Civil Engineering Research Institute for Cold Region  
Public Works Research Institute  
1-3-1-34 Hiragishi, Toyohira-ku, Sapporo-shi, Hokkaido  
062-8602  
Tel: 011-841-1698  
Fax: 011-841-3502  
E-mail: morito@ceri.go.jp

Dr. Susumu Takamiya  
Head, Earthquake Prevention Division  
Research Center for Disaster Risk Management  
National Institute for Land and Infrastructure Management  
Ministry of Land, Infrastructure, Transport and Tourism  
1 Asahi, Tsukuba-shi, Ibaraki-ken 305-0804  
Tel: 029-864-3244  
Fax: 029-864-0598  
E-mail: takamiya-s92tc@nilim.go.jp

Dr. Takashi Tomita  
Tsunami Research Director, Tsunami Research Center  
Port and Airport Research Institute  
3-1-1 Nagase, Yokosuka-shi, Kanagawa-ken 239-0826  
Tel: 046-844-5052  
Fax: 046-844-1274  
E-mail: tomita@pari.go.jp

Mr. Mitsuru Ueno  
Director, Typhoon Research Department  
Meteorological Research Institute  
Japan Meteorological Agency  
Ministry of Land, Infrastructure, Transport and Tourism  
1-1 Nagamine, Tsukuba-shi, Ibaraki-ken 305-0052  
Tel: 029-853-8663  
Fax: 029-853-8735  
E-mail: mueno@mri-jma.go.jp

Dr. Shigeki Unjoh  
Research Coordinator for Earthquake Disaster Prevention,  
Research Center for Disaster Risk Management  
National Institute for Land and Infrastructure Management  
Ministry of Land, Infrastructure, Transport and Tourism  
1 Asahi, Tsukuba-shi, Ibaraki-ken 305-0804

Tel: 029-864-2926  
Fax: 029-864-0598  
E-mail: unjoh-s92ta@nilim.go.jp

Mr. Atsushi Watanabe  
Director, Office of Reduction Research  
Research and Development Bureau  
Ministry of Education, Culture, Sports, Science and  
Technology  
3-2-2 Kasumigaseki, Chiyoda-ku, Tokyo 100-8959  
Tel: 03-6734-4134  
Fax: 03-6734-4139  
E-mail: watanabe@mext.go.jp

Mr. Kazushige Watanabe  
Director, Division of Road Risk Management  
Road Bureau  
Ministry of Land, Infrastructure, Transport and Tourism  
2-1-3 Kasumigaseki, Chiyoda-ku, Tokyo 100-8918  
Tel: 03-5253-8111  
Fax: 03-5253-1620  
E-mail: watanabe-k22av@milt.go.jp

Dr. Yoshikazu Yamaguchi  
Team Leader, Dam Structure Research Team  
Hydraulic Engineering Research Group  
Public Works Research Institute  
1-6 Minamihara, Tsukuba-shi, Ibaraki-ken 305-8516  
Tel: 029-879-6780  
Fax: 029-879-6737  
E-mail: yamaguti@pwri.go.jp

Mr. Yoshiji Yokote  
Senior Coordinator for Research and Development,  
Planning Division, Administration Department  
Japan Meteorological Agency  
1-3-4 Ote-machi, Chiyoda-ku, Tokyo 100-8122  
Tel: 03-3212-8341  
Fax: 03-3211-2032  
E-mail: yokote@met.kishou.go.jp

Dr. Koichi Yokoyama  
Professor, Department of Urban and Civil Engineering  
Ibaraki University  
4-12-1 Nakanarusawa, Hitachi-shi, Ibaraki-ken 316-8511  
Tel: 0294-38-5161  
Fax: 0294-38-5268  
E-mail: yokoyama@mx.ibaraki.ac.jp

Dr. Sumio Yoshikawa  
Director, Seismology and Volcanology Research  
Department  
Meteorological Research Institute  
Japan Meteorological Agency  
1-1 Nagamine, Tsukuba-shi, Ibaraki-ken 305-0052  
Tel: 029-853-8675  
Fax: 029-851-3730  
E-mail: syosikaw@mri-jma.go.jp

Mr. Atsushi Yoshioka  
Director, Bridge and Structural Technology Research  
Group  
Center for Advanced Engineering Structural Assessment  
and Research (CAESAR)  
Public Works Research Institute  
1-6 Minamihara, Tsukuba-shi, Ibaraki-ken 305-8516

Tel: 029-879-6726  
Fax: 029-879-6739

E-mail: [yoshioka@pwri.go.jp](mailto:yoshioka@pwri.go.jp)

## SECRETARIES COMMITTEE MEMBERS

Dr. Keiichi Tamura  
Secretary-General, Japan-side Panel on Wind and Seismic Effects  
Research Coordinator for Earthquake Engineering  
Center for Advanced Engineering Structural Assessment and Research (CAESAR)  
Public Works Research Institute  
1-6 Minamihara, Tsukuba-shi, Ibaraki-ken 305-8516  
Tel: 029-879-6721  
Fax: 029-879-6739  
E-mail: ke-tamura@pwri.go.jp

Mr. Tatsuya Azuhata  
Head, Structural Standard Division  
Building Department  
National Institute for Land and Infrastructure Management  
Ministry of Land, Infrastructure, Transport and Tourism  
1 Tachihara, Tsukuba-shi, Ibaraki-ken 305-0802  
Tel: 029-864-4299  
Fax: 029-864-6774  
E-mail: azuhata-t92ta@nilim.go.jp

Dr. Hiroshi Fukuyama  
Chief Research Engineer and Research Coordinator  
Department of Structural Engineering  
Building Research Institute  
1 Tachihara, Tsukuba-shi, Ibaraki-ken 305-0802  
Tel: 029-864-6647  
Fax: 029-864-6773  
E-mail: fukuyama@kenken.go.jp

Dr. Jun-ichi Hoshikuma  
Chief Researcher, Bridge and Structural Technology Research Group  
Center for Advanced Engineering Structural Assessment and Research (CAESAR)  
Public Works Research Institute  
1-6 Minamihara, Tsukuba-shi, Ibaraki-ken 305-8516  
Tel: 029-879-6793  
Fax: 029-879-6739  
E-mail: hoshikuma@pwri.go.jp

Mr. Hiroyuki Ishikawa  
Team Leader, Structures Research Team  
Cold-Region Construction Engineering Research Group  
Civil Engineering Research Institute for Cold Region  
Public Works Research Institute  
1-3-1-34 Hiragishi, Toyohira-ku, Sapporo-shi, Hokkaido 062-8602  
Tel: 011-841-1698  
Fax: 011-841-3502  
E-mail: hi-iskw@ceri.go.jp

Mr. Toshio Kitahara  
Head, Planning Division, Geographic Department  
Geographical Survey Institute  
Ministry of Land, Infrastructure, Transport and Tourism  
1 Kitasato, Tsukuba-shi, Ibaraki-ken 305-0811  
Tel: 029-864-5917  
Fax: 029-864-1804  
E-mail: kitahara@gsi.go.jp

Dr. Shin Koyama  
Chief Research Engineer, International Institute of Seismology and Earthquake Engineering  
Building Research Institute  
1 Tachihara, Tsukuba-shi, Ibaraki-ken 305-0802  
Tel: 029-864-6677  
Fax: 029-864-6777  
E-mail: skoyama@kenken.go.jp

Mr. Jun Murakoshi  
Chief Researcher, Bridge and Structural Technology Research Group  
Center for Advanced Engineering Structural Assessment and Research (CAESAR)  
Public Works Research Institute  
1-6 Minamihara, Tsukuba-shi, Ibaraki-ken 305-8516  
Tel: 029-879-6792  
Fax: 029-879-6739  
E-mail: murakosi@pwri.go.jp

Mr. Shoichi Nakatani  
Chief Researcher, Bridge and Structural Technology Research Group  
Center for Advanced Engineering Structural Assessment and Research (CAESAR)  
Public Works Research Institute  
1-6 Minamihara, Tsukuba-shi, Ibaraki-ken 305-8516  
Tel: 029-879-6794  
Fax: 029-879-6739  
E-mail: nakatani@pwri.go.jp

Dr. Tetsuo Nakazawa  
Head, The Second Research Laboratory  
Typhoon Research Department  
Meteorological Research Institute  
Japan Meteorological Agency  
Ministry of Land, Infrastructure, Transport and Tourism  
1-1 Nagamine, Tsukuba-shi, Ibaraki-ken 305-0052  
Tel: 029-853-8671  
Fax: 029-853-8735  
E-mail: nakazawa@mri-jma.go.jp

Dr. Yasuo Okuda  
Chief Research Engineer, Department of Structural Engineering  
Building Research Institute  
1 Tachihara, Tsukuba-shi, Ibaraki-ken 305-0802  
Tel: 029-864-6618  
Fax: 029-864-6773  
E-mail: y\_okuda@kenken.go.jp

Dr. Koji Sekiguchi  
Head, Outreach Division  
Strategic Planning Department  
National Research Institute for Earth Science and Disaster Prevention  
3-1 Tennodai, Tsukuba-shi, Ibaraki-ken 305-0006  
Tel: 029-863-7768  
Fax: 029-851-1622  
E-mail: ksekigut@bosai.go.jp

Dr. Hideki Sugita

Team Leader, Soil Mechanics and Dynamics Research Team  
Material and Geotechnical Engineering Research Group  
Public Works Research Institute  
1-6 Minamihara, Tsukuba-shi, Ibaraki-ken 305-8516  
Tel: 029-879-6770  
Fax: 029-879-6735  
E-mail: sugita@pwri.go.jp

Dr. Susumu Takamiya  
Head, Earthquake Prevention Division  
Research Center for Disaster Risk Management  
National Institute for Land and Infrastructure Management  
Ministry of Land, Infrastructure, Transport and Tourism  
1 Asahi, Tsukuba-shi, Ibaraki-ken 305-0804  
Tel: 029-864-3244  
Fax: 029-864-0598  
E-mail: takamiya-s92tc@nilim.go.jp

Dr. Takashi Tomita  
Tsunami Research Director  
Tsunami Research Center  
Port and Airport Research Institute  
3-1-1 Nagase, Yokosuka-shi, Kanagawa-ken 239-0826  
Tel: 046-844-5052  
Fax: 046-844-1274  
E-mail: tomita@pari.go.jp

Dr. Shigeki Unjoh

Research Coordinator for Earthquake Disaster Prevention,  
Research Center for Disaster Risk Management  
National Institute for Land and Infrastructure Management  
Ministry of Land, Infrastructure, Transport and Tourism  
1 Asahi, Tsukuba-shi, Ibaraki-ken 305-0804  
Tel: 029-864-2926  
Fax: 029-864-0598  
E-mail: unjoh-s92ta@nilim.go.jp

Dr. Yoshikazu Yamaguchi  
Team Leader, Dam Structure Research Team  
Hydraulic Engineering Research Group  
Public Works Research Institute  
1-6 Minamihara, Tsukuba-shi, Ibaraki-ken 305-8516  
Tel: 029-879-6780  
Fax: 029-879-6737  
E-mail: yamaguti@pwri.go.jp

Mr. Atsushi Yoshioka  
Director, Bridge and Structural Technology Research Group  
Center for Advanced Engineering Structural Assessment and Research (CAESAR)  
Public Works Research Institute  
1-6 Minamihara, Tsukuba-shi, Ibaraki-ken 305-8516  
Tel: 029-879-6726  
Fax: 029-879-6739  
E-mail: yoshioka@pwri.go.jp

## **TEMPORARY MEMBERS**

Dr. Shojiro Kataoka	National Institute for Land and Infrastructure Management
Mr. Fuminori Kato	National Institute for Land and Infrastructure Management
Dr. Hitomitsu Kikitsu	National Institute for Land and Infrastructure Management
Mr. Tomoki Ootani	Japan Water Agency
Dr. Junichi Sakai	Public Works Research Institute
Dr. Hiroshi P. Sato	Geographical Survey Institute

## ASSOCIATE MEMBERS

Mr. Tomomitsu Fujii	Foundation of River Basin Integrated Communications
Dr. Minoru Fujiwara	Formerly, Nippon Slag Association
Dr. Masami Fukuoka	Management System Assessment Center
Dr. Masaya Hirosawa	Professor Emeritus, Kogakuin University
Dr. Shiro Ibukiyama	Professor Emeritus, Kogyokusha College of Technology
Dr. Kaoru Ichihara	Public Works Research Center
Dr. Takashi Iijima	Civil Engineering Research Laboratory
Mr. Yasutake Inoue	Fukuda Corporation
Dr. Toshio Iwasaki	Public Works Research Center
Mr. Shunichiro Kamijo	KICTEC Inc.
Mr. Takashi Kaminosono	Center for Better Living
Mr. Kenji Kawakami	Kubota Corporation
Dr. Kazuhiko Kawashima	Professor, Tokyo Institute of Technology
Dr. Eiichi Kuribayashi	Professor Emeritus, Toyohashi University of Technology
Dr. Kiyoshi Nakano	Professor Emeritus, Tokyo Denki University
Dr. Shinsuke Nakata	Professor, Kochi University of Technology
Dr. Kazuto Nakazawa	Formerly, Public Works Research Institute
Dr. Nobuyuki Narita	Public Works Research Center, Japanese Technical Association for Steel Pipe Piles
Dr. Setsuo Noda	Coastal Development Institute of Technology
Dr. Hisashi Okada	Japan Housing and Wood Technology Center
Dr. Michio Okahara	Advanced Construction Technology Center
Dr. Shin Okamoto	Japan Association for Building Research Promotion
Mr. Kei-ichi Ohtani	Formerly, National Research Institute for Earth Science and Disaster Prevention
Mr. Yoshiji Sakagami	Formerly, Japan Development Construction Corporation
Dr. Yasushi Sasaki	Japan Institute of Construction Engineering
Dr. Yukihiro Sumiyoshi	Central Consultant Inc.
Mr. Jiro Taguchi	Sakurada Co., Ltd.
Dr. Masateru Tominaga	Public Works Research Center, Central Consultant Inc.
Dr. Hajime Tsuchida	Echo Corporation
Mr. Seizo Tsuji	Japan Utility Subway Company Inc.
Dr. Hiroyuki Yamanouchi	The Building Center of Japan, Inc.
Dr. Koichi Yokoyama	Professor, Ibaraki University

## TASK COMMITTEE MEMBERS

\* denotes Task Committee Chair.

### B. Next-Generation Building and Infrastructure Systems

George C. Lee*	MCEER
Douglas Foutch*	NSF
Fu-Kuo Chang	Stanford University
Mete A. Sozen	Purdue University
B. F. Spencer	University of Illinois
K. Thirumalai	DOT
Ming Wang	University of Illinois
Hiroshi Fukuyama*	Building Research Institute
Masayoshi Nakashima*	National Research Institute for Earth Science and Disaster Prevention
Tatsuya Azuhata	National Institute for Land and Infrastructure Management
Namihiko Inoue	National Institute for Land and Infrastructure Management
Yoshihiro Iwata	Building Research Institute
Takashi Kaminosono	Center for Better Living
Hitomitsu Kikitsu	National Institute for Land and Infrastructure Management
Koichi Kusunoki	Yokohama National University
Chikahiro Minowa	National Research Institute for Earth Science and Disaster Prevention
Koichi Morita	Building Research Institute
Akiyoshi Mukai	National Institute for Land and Infrastructure Management
Isao Nishiyama	National Institute for Land and Infrastructure Management
Taiki Saito	Building Research Institute
Hitoshi Shiohara	University of Tokyo
Masaomi Teshigawara	Nagoya University
Shigeki Unjoh	National Institute for Land and Infrastructure Management
Akira Wada	Tokyo Institute of Technology

### C. Dams

Robert L. Hall*	USACE-ERDC
Enrique E. Matheu*	DHS
Anjuna Chudgar	USACE
Richard C. Dove	USACE-ERDC
Ziyad H. Duron	Harvey Mudd College
Larry K. Nuss	U.S. Bureau of Reclamation
Richard S. Olsen	USACE-ERDC
Rick Poepelman	USACE
Donald E. Yule	USACE-ERDC
Yoshikazu Yamaguchi*	Public Works Research Institute
Tomonori Abe	Public Works Research Institute
Noriaki Hakoishi	Public Works Research Institute
Takashi Ikeda	Japan Dam Engineering Center
Tomoya Iwashita	Public Works Research Institute
Tatsuo Ohmachi	Tokyo Institute of Technology
Yoshio Ohne	Aichi Institute of Technology
Tsutomu Sakurai	Japan Water Agency
Hiroyuki Satoh	Public Works Research Institute
Choshiro Tamura	University of Tokyo
Yasuya Watanabe	Japan Institute of Construction Engineering

### D. Wind Engineering

John Gaynor*	NOAA
Nicholas P. Jones*	Johns Hopkins University
Earl J. Baker	Florida State University
Bogusz Bienkiewicz	Colorado State University
Harold Bosch	FHWA
Donald Burgess	NOAA

Ahsan Kareem	University of Notre Dame
Joseph Main	NIST
Mark D. Powell	NOAA
Liz Ritchie	University of New Mexico
Partha Sarkar	Iowa State University
Emil Simiu	NIST
Jun Murakoshi*	Public Works Research Institute
Yasuo Okuda*	Building Research Institute
Hiroshi Katsuchi	Yokohama National University
Hiromasa Kawai	Kyoto University
Hitomitsu Kikitsu	National Institute for Land and Infrastructure Management
Kichiro Kimura	Kyushu Institute of Technology
Masao Mikami	Meteorological Research Institute
Hisashi Okada	Japan Housing and Wood Technology Center
Hiromichi Shirato	Kyoto University
Tetsuro Tamura	Tokyo Institute of Technology
Yukio Tamura	Tokyo Institute of Polytechnics
Yasushi Uematsu	Tohoku University
Mitsuru Ueno	Meteorological Research Institute
Hitoshi Yamada	Yokohama National University
Ikuo Yamada	Honshu-Shikoku Bridge Expressway Company Limited

### **G. Transportation Systems**

W. Phillip Yen*	FHWA
Harold Bosch	FHWA
Michel Bruneau	MCEER
Peter Chang	University of Maryland
Hamid Ghasemi	FHWA
Nicholas P. Jones	Johns Hopkins University
David H. Sanders	University of Nevada
Atsushi Yoshioka*	Public Works Research Institute
Yozo Fujino	University of Tokyo
Susumu Fukunaga	Honshu-Shikoku Bridge Expressway Company Limited
Yoshihei Horie	Hanshin Expressway Company Limited
Jun-ichi Hoshikuma	Public Works Research Institute
Yasuo Inokuma	Central Nippon Expressway Company Limited
Hiroyuki Ishikawa	Public Works Research Institute
Yasushi Josen	Public Works Research Institute
Kazuhiko Kawashima	Tokyo Institute of Technology
Motoki Kazama	Tohoku University
Jun Murakoshi	Public Works Research Institute
Shoichi Nakatani	Public Works Research Institute
Atsushi Nozu	Port and Airport Research Institute
Takeshi Suzuki	National Institute for Land and Infrastructure Management
Katsuya Ogihara	Honshu-Shikoku Bridge Expressway Company Limited
Masasumi Okada	Metropolitan Expressway Company Limited
Masahiro Shirato	Public Works Research Institute
Takahiro Sugano	Port and Airport Research Institute
Junichi Sakai	Public Works Research Institute
Hideki Sugita	Public Works Research Institute
Shunsuke Tanimoto	Public Works Research Institute
Takashi Tamakoshi	National Institute for Land and Infrastructure Management
Keiichi Tamura	Public Works Research Institute
Shigeaki Unjoh	National Institute for Land and Infrastructure Management
Koichi Yokoyama	Ibaraki University

### **H. Storm Surge and Tsunami**

Solomon C. Yim*	OSU
Eddie Bernard*	NOAA
Michael Briggs	USACE
Frank Gonzalez	NOAA
Laura Kong	ITIC

Harry Yeh  
Philip Liu

OSU  
Cornell University

Takashi Tomita\*  
Koji Fujima  
Fumihiko Imamura  
Hiroyasu Kawai  
Nadao Kohno  
Takeshi Suzuki  
Yoshio Suwa

Port and Airport Research Institute  
National Defense Academy of Japan  
Tohoku University  
Port and Airport Research Institute  
Japan Meteorological Agency  
National Institute for Land and Infrastructure Management  
National Institute for Land and Infrastructure Management

# **RESOLUTIONS**

**RESOLUTIONS OF THE FORTY-FIRST JOINT MEETING  
U.S.-JAPAN PANEL ON WIND AND SEISMIC EFFECTS (UJNR)**

National Institute for Land and Infrastructure Management, Tsukuba, Japan  
18-20 May, 2009

The following resolutions are hereby adopted:

1. The Forty-first Joint Panel Meeting provided the forum to exchange valuable technical information that is beneficial to both countries. In view of the importance of cooperative programs on the subject of wind and seismic effects, the continuation of Joint Panel Meetings is considered essential. Both sides agreed to follow the recommendations of the Panel's 2nd Five-Year Strategic Plan and will give emphasis to identifying opportunities, primarily through its Task Committees, and to share and develop technologies that lead to new design and construction practices, and provide users with improved procedures.
2. The following activities have been conducted since the Fortieth Joint Meeting:
  - a. Technology Exchanges. Technical experts and technical documents have been exchanged. These exchanges have contributed to the development of new research and enhanced ongoing research programs in both countries.
  - b. Task Committee Workshops. The Panel held two workshops:
    1. Task Committee (H), 5th International Workshop on Coastal Disaster Prevention, 22 July 2008, Yogyakarta, Indonesia.
    2. Task Committee (G), 24th U.S.-Japan Bridge Engineering Workshop, 22-24 September 2008, Minneapolis, MN, U.S.
  - c. Major Products. The Panel members produced or made significant contributions to advancing the Panel's mission through its Task Committees:
    1. Task Committee (C) continued to conduct collaborative research on non-linear response analysis of concrete dams.
    2. Task Committee (H) members contributed to conducting experimental research and developing various numerical models to simulate tsunamis in coast areas in the U.S. and Japan.
3. The Panel accepted the Task Committee reports presented during the Forty-first Joint Panel Meeting. Each report included objectives, scope of work, accomplishments and future plans.
4. The Panel continues to work toward streamlining its structure, encouraging and expanding the collaboration of researchers in both countries.
5. The Panel conducted its annual Strategic Planning Session. Based on its 2nd Five-Year Strategic Plan, the Panel evaluated its accomplishments and Task Committees activities and recommended the following actions:

- a. The Panel recognizes the importance of disaster resilient buildings and infrastructure, and encourages conducting the related research.
  - b. The results of the Panel's work should be widely disseminated to improve the quality of life globally. The Panel encourages greater use of e-mail, the Panel's eNewsletter, and the Panel's Web Site to share and disseminate data and information to Panel members and other researchers.
  - c. The Panel encourages partnering opportunities identified by respective Task Committees.
  - d. The Panel encourages each Task Committee to develop methods to evaluate progress of their respective Task Committee.
6. The Panel endorses the following two proposed Task Committee Workshops during the coming year:
- a. Task Committee (G), 25th U.S.-Japan Bridge Engineering Workshop, 19-21 October 2009, Tsukuba, Japan
  - b. Task Committee (H), 6th International Workshop on Coastal Disaster Prevention, late 2009, Japan

In the event that T/C co-chairs recommend conducting a joint meeting or workshop prior to the next annual meeting, that is not included in the above list, the T/C co-chairs will make a request to conduct the meeting through their respective Secretary-General for approval by the Joint Panel Chairmen.

7. The U.S. and Japan sides will plan, conduct, and share as appropriate, joint investigations following earthquake and wind disasters in the U.S., Japan and other countries.
8. The Forty-second Joint Panel Meeting of the UJNR Panel on Wind and Seismic Effects will be organized by the U.S.-side Panel, to be held in the U.S. in May 2010. The U.S.-side secretariat will propose dates, program, location, and itinerary with the concurrence of the Japan-side Panel.

# **STRATEGIC PLAN**

ADDENDUM 1  
Panel Expectations During 2006-2010

STRATEGIC PLAN  
U.S.-JAPAN JOINT PANEL ON WIND AND SEISMIC EFFECTS

**1. Introduction**

This document is Addendum 1 of the Strategic Plan for the US-Japan Panel on Wind and Seismic Effects 2001-2005 (attachment). The Panel's 2001 Strategic Plan serves as the base of the Panel's operations and structure. This Addendum 1 provides a roadmap of outlined technical approaches for the Panel's operations during the next five-year period 2006-2010. As background, the Panel's Charter, developed in 1987 at the 19th Joint Panel Meeting, is to:

- a. Encourage, develop, and implement the exchange of wind and seismic technology between appropriate US and Japanese organizations to share scientific and technological knowledge.
- b. Develop strong technical links of scientific and engineering researchers between the two countries and encourage exchanges of guest researchers.
- c. Conduct joint research in areas of winds and seismic technology including exchange of available research equipment and facilities in both countries. Publish findings from joint research efforts.
- d. Conduct cooperative programs to improve engineering design and construction practices and other wind and earthquake hazard mitigation practices. Publish results from cooperative programs.

**2. Panel Approaches During 2006-2010**

The Panel's operational procedure is defined in the attached Strategic Plan (2001-2005). Annually the Panel performs a self-evaluation during a Strategic Planning session held during its May Joint Panel Meeting. Based on the Panel's evaluation, incremental modifications are carried out to enhance the Panel's operations and to bring 'value-added' to its users.

**2.1. Panel Mission and Vision for 2006-2010**

1. Continue performing post disaster investigations and reconnaissance and sharing findings with Panel members and others as was carried out for:
  - a) Earthquakes: (2004 Niigata, 2004 Indonesia, 2005 Pakistan, and others)
  - b) Typhoons and Hurricanes: (2005 Katrina and Rita, 2004 Typhoon)
2. Share US and Japan National Disaster Mitigation Plan among the Panel members such as:
  - a) USA. NSTC/SDR: *Grand Challenge for Disaster Prevention- a 10-year strategy for disaster reduction through science and technology; Windstorm Impact Reduction Implementation Plan*; the NEHRP Annual Plan.
  - b) Japan. *Central Disaster Prevention Council: Reduction by half of human damage and economic damage in coming 10 years*, Technology Development Plan at "Council for Science and Technology"
3. Identify methods that support each countries efforts in disaster mitigation through cooperation between the US and Japan and explore opportunities for joint research projects.

4. During 2006-2010 the Panel will focus on topics such as:
  - a) Continue to understand causes and effects of wind and seismic hazards and pursue the accumulation and interpretation of data
  - b) Evaluate and estimate risk of natural hazards
  - c) Improve/develop disaster mitigation technology and methodology, and dissemination of disaster response technology into practical applications
  - d) Promote attention to increase research that considers societal implications of natural disasters
  - e) Integrate technology development and the viewpoint of social/civil engineering by increasing the importance of the cooperative works between related UJNR Panels, the Panel's Task Committees, and the private sector and academia
  - f) Create methods to better integrate comprehensive technology information as a base for transmitting information throughout the Panel member's organizations
  - g) Contribute to dissemination of cooperative products that will facilitate global standardization of related civil engineering technologies

2.2. Evaluate Task Committees. The Panel operates under seven Task Committees; an optimum number for Panel management and productivity. The Task Committees serve as the heart of the Panel's operations:

- |                   |   |
|-------------------|---|
| Task Committee A. | Geotechnical Engineering and Ground Motion          |
| Task Committee B. | Next Generation Building and Infrastructure Systems |
| Task Committee C. | Dams  |
| Task Committee D. | Wind Engineering                                    |
| Task Committee G. | Transportation Systems                              |
| Task Committee H. | Storm Surge and Tsunami                             |
| Task Committee I. | Fire Performance of Structures                      |

Findings from Task Committees' evaluations will help the Task Committees 1) measure achievements, productivity, and impact on contributions to improving design and construction practices, 2) identify opportunities for making contributions and addressing emerging technical challenges, and 3) assess when they completed their mission and are ready for retirement. Task Committee Evaluation Criteria includes: 1) one or more workshop conducted at least every three-years, 2) implementing recommendations from workshops, 3) publications and other outreach, and 4) collaborations beyond their Task Committee.

The Panel will encourage its respective Task Committees to identify thematic focuses requiring technology sharing and joint collaborations. These Themes will be discussed at annual Panel Meetings. The Panel will consider the merits of creating new Task Committees that meet special needs and eliminating Task Committees that have completed their mission or can be strengthened through consolidation with other Task Committee(s).

2.3. Partnering Opportunities. Identify partnering opportunities through clustering appropriate Panel's Task Committees, collaborating with other UJNR Panels, and working together with the private sector and academia. Clustering provides Task Committee optimization of resources (human and financial). Partnering and clustering will be discussed at annual Panel Meetings including increasing participation from the private sector and academia.

2.4. Joint Research. Perform joint research initiated by the Panel and its Task Committees. The Task Committees are encouraged to identify key joint-research opportunities to improve the state-of-knowledge or to consider engaging in a significant long-term research funded from one or more sponsoring organizations. For the latter, below are the Panel Cooperative Research Projects performed during the past 27-years that improved design and construction practices for both countries.

1. Reinforced Concrete Structures (1979-1987); accomplishments include testing six-story full scale buildings which led to improve seismic design methods of reinforced concrete buildings.
2. Seismic Performance of Lifeline Facilities (1982-1989); accomplishments included development of improved seismic design methods of bridge columns.
3. *In-situ* Testing Methods for Soil Liquefaction (1983-1986); accomplishments include development of rationale for Standard Penetration Test (SPT) data based on energy ratio.
4. Masonry Structures (1984-1988); accomplishments include development of strength-based design guidelines for reinforced masonry buildings.
5. Steel-Frame Structures (1985-1987); accomplishments include testing of a full-scale five-story building to confirm prediction of performance based on components and subassemblages.
6. Bridge Hybrid Control Systems (1990-1994); accomplishments include development of hybrid control algorithms that require less energy for controlling bridge response.
7. Precast Seismic Structural Systems (1991-1992); accomplishments include development of strength-based design guidelines.
8. Seismic Performance of Composite and Hybrid Structures (1993-1998); accomplishments include development of design guidelines for composite and hybrid system, and development of new materials.
9. Countermeasures for Soil Liquefaction (1994-2004); accomplishments include contributions on the revision of design guidelines for building foundations and formulation of soil experiment plans using E-Defense.
10. Development of Smart Structural Systems (1998-2003); accomplishments include development of structural performance detection technology and structural members using intelligent materials.
11. Develop Comparative Analysis of Seismic Performance Testing Guidelines for Bridge Piers (1999-2006); accomplishments included a joint publication on the comparative analysis of US and Japan bridge piers.

The respective Task Committees will identify candidate joint research for discussion at annual Panel meetings.

2.5. Panel Communications. More broadly disseminate Panel's activities, accomplishments, and impacts including findings from post-disaster investigations using the Panel's eNewsletter, a more active Web Site, Task Committee publications, and identify Panel accomplishments and impacts. The Panel will increase information sharing among its member organizations and include links to related organizations in both countries. Task Committees will serve as a knowledge base of information on their respective themes and share their information to users following methods described above.

### **3. Conclusion**

This Addendum represents the Panel's focus to address panel's activities of the next five-years. The strategic plan is annually evaluated during its annual May Meetings.

# U.S.-Japan Joint Panel on Wind and Seismic Effects Strategic Plan

## **1. Introduction**

### 1.1 Context

The U.S. and Japan must maintain an awareness of international developments in earthquake and wind mitigation technology. The international exchange of information is achieved through a combination of formal and informal mechanisms, including: attendance at conferences and workshops; cooperative research projects and programs; and exchange of scientists and engineers. There is a long-established tradition of joint research activities between Japan and the United States. The U.S.-Japan Cooperative Program in Natural Resources (UJNR) Panel on Wind and Seismic Effects (WSE Panel) provides a formal government-to-government mechanism for cooperation between the two countries in the area of earthquake and wind mitigation technology.

At the 32nd Joint Panel Meeting, a resolution was passed to establish a joint Ad-Hoc Committee for the purpose of developing a strategic plan for the WSE Panel. The catalyst for this effort was the need to address immediate issues related to cost and participation. While the Panel recognized the importance of addressing these immediate issues, it also realized that an opportunity existed to strengthen the WSE Panel's focus on its core mission and foster greater collaboration between researchers in the U.S. and Japan while streamlining the overall operation of the Panel. It was with this goal in mind that the ad-hoc committee developed the strategic plan contained in this document.

### 1.2 Approach

Before meeting to develop the strategic plan, each side held domestic panel meetings and conducted one-on-one meetings with participating agencies to identify issues that needed to be addressed by the strategic plan and to understand which features of the Panel and its operation should be retained and which needed to be changed or adapted to meet current and future needs. Each side developed a concept paper to capture these ideas. The concept papers, however, tended to focus on addressing the immediate issues rather than positioning the Panel to address the needs and challenges of the future. Through the exchange of the concept papers and subsequent discussion, the two sides moved close to agreement on near-term changes to the Panel's operation. Thus, the strategic plan emphasizes longer-term goals for the operation and growth of the Panel and a time-phased approach to implementation of steps to achieve these goals.

The strategic plan is intended to establish a course for the WSE Panel over the next 5-10 years. It recognizes that there are many ways in which the Panel may work to achieve the goals identified, and so while some steps in the implementation process are clear, others are left open to be determined through experimentation. However, the Panel believes working toward the goals identified will strengthen its role in engineering and scientific communities of the U.S. and Japan and will allow our countries to make more efficient use of resources to conduct research and disseminate results to the benefit of both countries.

## **2. Role of the Panel**

## 2.1 Guide Research Agendas

As a government-to-government mechanism for collaboration, the WSE Panel is in a unique position to guide the development and execution of each country's research agenda. Currently, each country defines its own research priorities, projects are formulated in a fragmented manner, and results are reported through vehicles such as the Annual Joint Panel Meeting. By strengthening its ties to industry and academia, the Panel will be able to identify specific research needs and align those with government priorities. The Panel shall work toward a coordinated research agenda that permits the efficient use of human resources, funding, and research facilities to achieve mutual research objectives.

The new Task Committees formed through implementation of this strategic plan shall work to identify areas where joint research projects can be established and conducted as a part of a coordinated research agenda. Joint research projects may include participation by university or industry researchers in addition to member agency researchers.

## 2.2 Leverage Resources

The U.S. and Japan each possess significant expertise in the fields of earthquake and wind engineering and have a substantial investment in equipment and facilities to perform testing and measurements in support of research in these fields. Historically, the WSE Panel has facilitated the exchange of researchers between the U.S. and Japan but has not made a concerted effort to leverage the resources of the two countries. There is an opportunity for the Panel to coordinate research activities to efficiently utilize testing and measurement facilities in both countries to address mutual research needs and avoid duplication. This is an area in which the Panel can significantly strengthen its efforts and provide a tangible benefit to each country by working to establish strong partnerships for coordinated research.

## 2.3 Foster Cooperation

From its founding, the WSE Panel has promoted cooperation between the U.S. and Japan through annual Joint Panel Meetings, Task Committee activities, and exchange of researchers. One of the hallmarks of success for the WSE Panel through the years has been the high level of cooperation. The model these cooperative efforts have been built around, however, is one of information exchange. While the exchange of information and research results is an important facet of the WSE Panel's work, there is the opportunity to greatly expand the scope and importance of cooperative efforts to leverage resources (people, funding, facilities) through joint research projects of bilateral importance. Additionally, the Panel should look beyond the government agencies that participate to be more inclusive of universities and the private sector. At a minimum, this will include broadening participation in the Joint Panel Meetings to include industry and university participants. As industry and universities become more engaged, exchanges of researchers among government, university, and industry participants may be possible. Joint programs that include participation by government, industry, and university partners shall also be considered. These activities would broaden the reach of the Panel and provide a means for more rapid diffusion of research results into practice.

## 2.4 Technical Exchange

The WSE Panel has, throughout its history, been an effective mechanism for the exchange of

technical information between Japan and the United States. Further, the WSE Panel has provided a means for disseminating measurements and research results to other nations affected by earthquake, wind, tsunami, and storm surge hazards. Annual Joint Panel Meetings, Task Committee Meetings and Workshops, researcher exchange programs, and personal relationships among researchers have fostered this exchange. The Panel recognizes this as one of its strengths and should seek to broaden its reach to include participation by researchers in other nations. The Panel should explore means of increasing collaboration with other countries through inclusion of representatives from other nations in Joint Panel Meetings, encouraging joint projects through the Task Committees that include partners outside the U.S. and Japan, and through the exchange of researchers with other countries.

### 2.5 Engage Private Sector

The WSE Panel has engaged the private sector to a limited extent in its activities during its history, although the work of the Panel and the participating agencies can have a direct benefit to industry and ultimately the public in our respective countries. Further, some larger companies have research capabilities and programs that could enrich the Panel. More actively engaging the private sector will provide a means for obtaining input in setting priorities and for more rapidly diffusing the results of research activities into practice within Japan and the United States. The involvement of the private sector may include participation in the development of coordinated research agendas and dissemination of information perhaps through special sessions at the annual Joint Panel Meetings. The Panel should also consider involving the private sector in research projects coordinated at the Task Committee level that will have broad-based benefits to industry in both countries. Longer-term, the involvement of the private sector will facilitate dialogue between practicing engineers and builders in Japan with their counterparts in the U.S. The Joint Panel will examine ways to increase industry participation, initially by inviting key industry representatives to participate in Joint Panel Meetings and to speak about the work of their company or organization and explore possibilities for greater collaboration.

### 2.6 Web Page Development

The Joint Panel will explore ways to increase utilization of the Internet as a means of communication both among Panel members and with outside organizations. The Japan-side has offered to take the lead in developing an Internet presence for the Joint Panel and has begun work on an initial concept for the site. Once the site is established, the Task Committees will be relied on to provide, maintain, and update content related to their activities. The Joint Panel will also explore ways of using Internet resources as a means of facilitating communication among researchers as well as the exchange and dissemination of information and research results.

## **3. Implementation**

### 3.1 Strategic Plan Development and Approval

This strategic plan was prepared through the efforts of the Joint Ad-Hoc Committee appointed by the Chairmen following the 32nd Joint Panel Meeting. The Joint Panel shall work toward approval of the Strategic Plan during the 33rd Joint Panel Meeting May 28-30, 2001. The approved document will reflect comments received from Panel members on the draft. Implementation of the strategic plan will begin with approval and require 12-24 months for full implementation.

### 3.2 Task Committee Charters and Recommended Committees

The US- and Japan-side Panels have agreed on the following seven themes around which Task Committees may be formed:

- Theme A: Geotechnical Engineering and Ground Motion
- Theme B: Buildings
- Theme C: Dams
- Theme D: Wind
- Theme E: Lifelines
- Theme F: Seismic Information and IT
- Theme G: Transportation
- Theme H: Storm Surge and Tsunami
- Theme I: Public Health

Task Committee formed to address one of these themes will be approved by the Joint Panel on annual basis, provided that the Task Committee remains active. The criteria for active Task Committees are following:

- a) Conducts joint workshops or technical meetings on a regular basis for the purpose of exchanging technical information, research results, or data for the mutual benefit of both countries.
- b) Engages in frequent exchange of researchers for the purpose of technical interchange and collaboration on research.
- c) Conducts one or more joint research projects having clearly defined technical objectives, finite duration, and shared responsibility for producing technical results.

Task Committees will report results through papers presented during the joint panel meeting and through task committee reports. The Joint Panel will review task committee results and future plans on an annual basis and will approve task committees for the next year based on this information.

For this year, new task committees may be established by requesting approval through the Secretary-Generals at any time before the 34th Joint Panel Meeting.

### 3.3 Transition to New Annual Panel Meeting Format

A number of alternative formats for the annual Joint Panel Meeting were considered. Based upon the input received from Panel members, the basic format of the Joint Panel Meeting be retained. Session topics will be principally driven by the Task Committees. Each Task Committee would be given one session during which it would be able to present research results. This Task Committee-driven format should strengthen the role of the Task Committees and is intended to stimulate greater cooperation among researchers in each country. This format will foster the exchange of information that many have expressed is a desirable feature of the Joint Panel Meeting.

The Joint Panel meeting will be shortened by one day (from 4 days to 3 days). The shorter meeting, coupled with a shorter Technical Site Tour will reduce the time commitment for

participants to one week. This is intended to encourage greater participation in the Panel Meetings and Site Tours, particularly by members of the visiting Panel.

Finally, the Joint Panel will explore streamlining the Joint Panel Meeting to maximize the opportunity for technical exchange.

The shortened Panel Meeting/Technical Site Tour format is implemented for the first time at the 33rd Joint Panel Meeting. The Task Committee-driven technical meeting format will be implemented at a later date when the revised Task Committee organization is in place.

#### **4. Conclusion**

The plan outlined above represents a strategic plan for positioning the Joint Panel to meet the challenges of the future, while retaining those aspects that have contributed to its success through its 32 year history. This plan is intended to address the current realities of the Panel, as well as increase the value and contribution of the Panel to the U.S. and Japan. Full implementation of the strategic plan will take approximately two years.

# PAPERS

# **THEME 1**

## **Next-Generation Building and Infrastructure Systems**

# Continuity and/or Resiliency of Building Function after Disasters

by

Hiroshi Fukuyama<sup>1</sup>, Koichi Morita<sup>2</sup>, Tomohisa Mukai<sup>2</sup>, Taiki Saito<sup>1</sup>, Hitomitsu Kikitsu<sup>4</sup>,  
Yoshihiro Iwata<sup>3</sup>, Yoshio Wakiyama<sup>3</sup>, and Seitaro Tajiri<sup>3</sup>

## ABSTRACT

Building Research Institute (BRI) has started research project on “Development of Performance-Based Structural Design System for Evaluating Continuity and/or Resiliency of Building Function after Disasters” in 2007 as a 3-year research project. The expected final results of the project are research and development of (1) Structural design framework and (2) Structural design data base for evaluation of “Continuity and/or Resiliency of Building Function, and (3) Guidebook for dissemination of the concept on “continuity and/or resiliency of building function after disasters”.

**KEYWORDS:** Functional Continuity, Disaster Resiliency, Structural Performance Evaluation, Structural Design Framework, Database, Accountability

## 1. INTRODUCTION

Securing human life in disasters is one of the most important objectives of the design of buildings, and the Building Standard Law of Japan which specifies the minimal requirements contains the provisions to be observed for securing the human life in disasters. In earthquake disasters in recent years, however, there occurred serious damages of losing the functions of buildings as the dwelling and as the field of human activities. Thus, adding to the safety viewpoint, the design has recognized the necessity of the viewpoint of “how to maintain the building functions” or “how rapidly recover the deteriorated functions”. The recognition also relates to the request of the Central Disaster Prevention Council of the Cabinet Office for the business enterprises to establish their Business Continuity Plan (BCP), along with the increase

of achievement rate of earthquake-resistant structures, in order to decrease the amount of damages by about half at the expected Tokai Earthquake, Tonankai Earthquake, Nankai Earthquake, strong local earthquake in the Tokyo metropolitan area, etc.

Building Research Institute (BRI) began the 3-year research and development project “Development of Performance-based Structural Design System for Evaluating Continuity and/or Resiliency of Building Function after Disasters” in 2007, aiming at not only the safety evaluation in disasters but also the difficulty evaluation in social, economic, and human activities after disasters. A Framework and a database system for structural design, and guidebooks for dissemination information for general users, etc. will be developed as useful outputs of building design allowing functional continuity and disaster resilience. This paper describes the overview of the research project and the individual research subjects.

## 2. BACKGROUND OF PROJECT RESEARCH

The Southern Hyogo Earthquake (Kobe Earthquake) occurred in 1995 resulted in collapse of large number of buildings, killed many people, and also paralyzed variety of city functions to force citizens to live at emergency evacuation areas outside their home for a long period. This is because many residential buildings lost their functions as the “dwelling”. In addition, there appeared not a small number of cases that, although the buildings designed

---

1 Chief Research Engineer, Building Research Institute, Tsukuba, Ibaraki 305-0802, JAPAN

2 Senior Research Engineer, ditto

3 Research Engineer, ditto

4 Senior Research Engineer, National Institute for Land and Infrastructure Management, MLIT, Tsukuba, Ibaraki 305-0804, JAPAN

according to the current seismic code did not collapse as requested by the codes and protected the human life, the damages of structural frame were serious, which needed very large restoration cost, thus the damaged buildings were finally tore down and reconstructed, (refer to Photo 1 as an example.) The cases show the importance of design to have a viewpoint of damage control and of functional resilience. The Geiyo Earthquake in 2001, the Tokachi-Oki Earthquake in 2003, and the Southern Miyagi Earthquake in 2005 generated damages caused by dropping large scale space ceiling. The West-Off Fukuoka Earthquake in 2005 generated damages of window glass of office buildings and of walls and fittings of condominiums (Photo 2). Thus, there appeared the cases that also the damages of those nonstructural members induce danger of human life similar to the cases of damages of structural framework, and that the loss of building function and of dwelling ability results in the difficulty of continuous use of the buildings after disasters.

Review of the cases of building damages in the earthquakes occurred in recent years clearly showed the actual state that owners and residents of buildings do not expect the conditions of disasters, and they do not prepare action plan after the disasters. On that matter, the suppliers of buildings might also lack the efforts to convey information and special field knowledge to the owners and the residents. The Kobe Earthquake drew attention about the damages of nonstructural members and equipment and fixtures, whose damages were relatively not recognized in the past hidden by the serious damage or collapse of structural framework. Furthermore, the Kobe Earthquake showed a feature that the residents of damaged buildings emphasized not only the direct loss of the building structure but also the indirect economic loss resulted from the disaster.

Through the experiences of above earthquake damages, business enterprises strongly recognized the importance of preventive measures to enable the business to continue in disaster and to enable the core business operation to rapidly recover to the level before the disaster. In this regard, the “Business

Continuity Plan (BCP)” has drawn attention inside and outside Japan. The BCP is a strategy of protection of business enterprise from critical profit loss and from deterioration of enterprise rating by avoiding stop operation of important business in disaster and by, even when the business operation is stopped, resuming the important function within a target restoration period. In Japan, “Special Field Survey Committee relating to the Disaster Preventive Power Improvement utilizing Private Sector Power and Market Power”, organized under the Central Disaster Prevention Council of the Cabinet Office, published the 1st edition of the Business Continuity Guidelines and the Check List in August 2005, and the Committee requested all the business enterprises to prepare their own BCP. Not limited to the activities of the government, the general constructors have recently begun practical application of earthquake risk evaluation system which supports BCP of, for example, semiconductor production facilities. In this manner, the development of structural design technology proceeds targeting not only the damage evaluation but also the evaluation of restoration period and of cost-effectiveness. Many of the above activities, however, use the statistical data of past earthquake damages, and do not reach the level of evaluation in depth to the response of individual buildings and to the relation between the damages and the deterioration of functions.

### 3. PERFORMANCE DESIGN SYSTEM BASED ON THE “FUNCTIONAL RESILIENCY”

#### 3.1 Definition of “Functional Resiliency”

On the background of Chapter 2, this section newly defines the “Functional Resiliency” as the performance indicating the easiness of disaster resilience of building function after disasters, especially earthquakes.

BRI selected three basic structural performances of buildings in the performance design, “Serviceability”, “Safety”, and “Reparability”, in the “Development of New Building Structural System (hereinafter referred to as the “New Structural System Project”) as

one of the Comprehensive Technological Development Project of the Ministry of Construction, and promoted the practical application of the design process based on these three basic structural performances. The concept of the “Functional Resiliency” defined in the research, however, is the one with an extension of the concept of “Reparability” defined in the New Structural System Project. Therefore, those two concepts differ from each other on the following points.

- The concept of “Reparability” in the New Structural System Project: The main object is the “property preservation” for buildings after earthquake; the easiness of restoration of buildings after the earthquake is secured by suppressing the building damages within a physical restoration limit of the building specified in each performance evaluation article.

- The concept of “Functional Resiliency” in this research: Easiness of functional resilience of buildings after earthquake is secured by, adding to the concept of “Reparability” of the New Structural System Project, keeping the restoration cost and the restoration period of the building after the earthquake within the target restoration cost and the target restoration period, respectively, determined by the owner (with an agreement with the designer) in view of functions of the building. Although the Business Continuity Plan (BCP) expects the damages of surrounding area of the building and the damages of lifeline, the concept of “Functional Resiliency” of the research deals with the controllable range in the design of individual buildings, and the influence caused by the variables other than those of the building is considered afterward as an additional condition

### 3.2 Design Verification Flow Scheme Based on the “Functional Resiliency”

The design verification flow scheme based on the “Functional Resiliency” is illustrated in Fig. 1. Main articles of the flow are outlined below.

i) *Uses of buildings (“Occupancy category” in Fig.1)*

Since the functions of buildings have close relation mainly with their uses, and since the

applied structural methods and specifications of every position of the building depend on the uses, the design verification based on the “Functional Resiliency” positively counts the building uses.

ii) *Process up to the 1st level verification*

The cross sectional dimensions of structural members are firstly determined. Then, the model of structural members is prepared, and the earthquake motion is determined. Next, the response evaluation is given to thus prepared model to calculate the response values of engineering indexes (such as maximum story drift and response acceleration) necessary to the damage evaluation. Also to the nonstructural members and the building equipment and contents, detail specifications are prepared, and their response values of engineering indexes required in the damage evaluation are calculated based on the values of maximum story drift and of response acceleration derived from the response evaluation of the structural members. Finally, using the database relating to the damage conditions, the physical restoration limit state of individual positions of the building, determined at the target performance level, is converted into the limit value of corresponding engineering index, thus comparing the limit value with the response value to complete the 1st level verification of the Reparability. The 1st level verification is a verification based on the performance evaluation article of the conventional Reparability.

iii) *Process up to the 2nd level verification*

On the basis of the damage condition of each position of the building, revealed up to the 1st level verification, firstly the restoration target of entire building is determined, and the method for restoration is determined. Then, the restoration cost and the restoration period, corresponding to the determined restoration method, are calculated using the database relating to the restoration method. Finally, these values are compared with the target restoration cost and the target restoration period expected by the owner and the resident in their Business Continuity Plan, etc. to complete the 2nd level verification. If the result of the 2nd level

verification gives NG, the preparation of restoration plan is executed again, and the same procedure is applied again. (If the second time of the 2nd level verification gives NG, and if the sole change of the restoration plan is judged as non-effective, the design itself has to be changed from the beginning.)

#### iv) *Indication of performance*

The evaluation result of the “Functional Resiliency” of the building, confirmed through the 1st and the 2nd level verifications, is explained to the owner and the resident in an understandable format. The “database relating to the damage condition corresponding to the occupancy category of building” given in the flow was prepared gathering experimental data and other findings to give a total image of the relation between [the damage conditions of each position of structural members, nonstructural members, and equipment and fixtures] and [the engineering indexes describing the damages, based on the experimental data, etc.] The “database relating to the restoration method” is the collected data relating to the restoration cost and the restoration period for each restoration method, based on the existing findings and knowledge.

## 4. APPLICATION EXAMPLE OF EVALUATION SYSTEM BASED ON “FUNCTIONAL RESILIENCY”

### 4.1 Buildings for Evaluation

The target building is an existed hospital in Niigata Prefecture. Table 1 shows the outline of the building. The room arrangement of each floor is: 1st and 2nd basement for machinery of core equipment; 1st and 2nd floor for diagnostic and treatment departments; 3rd floor for operation of each medical section; 4th and upper floors for wards; and roof top for elevated water tank and cooling tower. The building suffered damage due to the Niigata-Chuetsu Earthquake in 2004, and the restoration was conducted, thus the building is still in operation as hospital. After the earthquake, a survey of building damages was given, and detail records exist including the analysis of restoration work. The hospital was selected as the target building because these

records are effective reference materials in the research.

### 4.2 Time history response analysis

The applied vibration analysis model was an equivalent shear model with seven mass points, giving the 1st floor as the fixed end. The viscosity damping was assumed as an instantaneous stiffness proportional type of 3% to the primary natural period. The earthquake motion for the study was selected to the simulated earthquake motion 3 wave which was prepared using the phases of EL CENTRO NS (1940), TAFTEW (1952), and HACHINOHE NS (1968), in accordance with the “extremely rarely occurring earthquake motion” specified in the Notification No. 1461.

The maximum response acceleration and the maximum drift at each floor are given in the following, (Figs. 3 and 4). The response acceleration distributes in a range from 300 to 700 gal. The maximum story drift angle is almost 1/200 or less, though it gives about 1/140 at the maximum in the Y direction at lower floors.

### 4.3 Evaluation of Functional Resiliency

#### (1) Evaluation of damage conditions

Degree of damages is evaluated for structural frame, exterior/interior, building equipment, lift facility, and medical equipment and devices. As of these, the medical equipment and devices were subjected to on-site sampling survey focusing on the fixing conditions, and confirmed 6 units of fixed-to-floor type, 21 units of direct-positioned (nonfixed) type, and 19 units of mobile type. If only the fixed type equipment and devices were designed according to the Design and Construction Guidelines of Building Equipments (2005) published by the Building Center of Japan, etc., they are judged not to induce sliding or falling at the response acceleration of this research. For the equipment and devices of direct-positioned type, the possibility of falling is calculated based on the equipment dimensions and the maximum response acceleration, (adding 0.30 of vertical seismic intensity), to give the possibility of falling of 17 units among 21 units. Therefore, the direct-positioned type equipment and

devices and the mobile type equipment and devices presumably suffer damages. To estimate the amount of damages, there are needed materials relating to the characteristics and the purchased price of the equipment and devices, which materials are however difficult to obtain at present. Accordingly, the medical equipment and devices are limited to obtain the above damage estimation, and the expected amount of damages is left as an issue. Thus, the targets of the research are limited to the building and the building equipment. The damages of targets other than that of medical equipment and devices were evaluated based on the vibration analysis result, the report of damage survey, and the above literature. Responding to the degree of damage, the necessary restoration period was speculated. The result is given in Table 2.

## (2) Estimated amount of damages

The fractional damages of building caused by earthquake, (the ratio of the restoration work cost for the damage to the initial investment), is calculated by the following equation.

$$L_T = \sum_i p_i \cdot L_i \quad (1)$$

where  $L_i$  : the fractional damage at each position based on the vibration analysis result  
 $p_i$  : the fraction of work cost at each position to the total work cost

Table 3 shows the breakdown of cost ratio for each work article at the initial construction. The table does not contain temporary work expenses and miscellaneous expenses.

The fractional damage ( $L_i$ ) corresponding to the degree of various damages for each article is defined corresponding to the five damage stages: large damage; medium damage; small damage; slight damage; and non-damage.

The values used in the damage evaluation are assumed as given in Table 4. From the above assumptions, the fractional damage is expected to:

$$L_T = 0.185 \times 0.200 + 0.078 \times 0.125 + 0.187 \times 0.010 + 0.366 \times 0.010 = 0.052 \quad (2)$$

That is, the damage is determined to that of 5.2% of the initial investment. Based on the current building price level, if the total construction work (including miscellaneous expenses and temporary work expenses) is assumed to 2,114,000,000 yen, the restoration work cost is estimated to 109,900,000 yen.

## (3) Period of restoration

As shown in Table 2, the restoration period can be determined mainly by the period for restoring the structural frame. The period of complete restoration of the hospital from the Niigata-Chuetsu Earthquake was slightly more than 5 months. The level of the earthquake under research is presumably lower than the level of the Niigata-Chuetsu Earthquake, thus the expected restoration period of 3.5 months is considered reasonable.

## 5. DATABASE FOR EVALUATING THE “FUNCTIONAL RESILIENCY”

The database developed in the project has a structure largely classifying the building elements, relating to “Functional Resiliency”, into four: (structural members, nonstructural members, equipment (including piping), and furniture). To obtain necessary data, individual positions are further grouped in detail, and the data relating to the following articles are collected for each of thus grouped in detail.

- i) Engineering (response) quantity contributing to the damages
- ii) Quantity of damages generated from a certain response, (specifically the damage relating to Reparability)
- iii) Restoration method corresponding to the quantity of damage
- iv) Cost and period for the restoration method
- v) Period and cost of functional resilience taking into account the restoration cost and restoration period

Next, for structuring the database, the data of damage evaluation relating to the Reparability are collected from a vast amount of data, and thus collected data are reviewed to pick up the

articles necessary for the “Functional Resiliency”. To this point, among the three stages of data, “Collection”, “Review”, and “Pick up”, the research conducts the “Review” by a work sheet, and the data reflecting the result of the “Pick up” are positioned to the “Database”, (refer to Fig. 5). The following is the description about the investigation method and the progress of the investigation relating to the database structuring for evaluating damages at each position.

#### 5.1. Structural Members

In principle, the target data are those for damage evaluation, which satisfy the following two requirements.

- i) The damage article which allows estimating the restoration period and cost shall be clearly given: for example, an RC member has the description of damage information about the quantity of cracks and the yield of reinforcing bars.
- ii) The article which allows calculating stiffness (including stiffness reduction ratio) and proof stress shall be given: for example, there shall be described cross section, reinforcement arrangement, strength of applied material, and loading conditions (degree of end-fixation and loading history).

To prepare the work sheet, there is specifically necessary the information of damages required for the restoration. Furthermore, the degree of influence of the damages of structural members on the other positions and on the building functions will be considered.

#### 5.2 Nonstructural Members

A questionnaire survey was conducted on manufacturers and suppliers of nonstructural members to collect data for the damage evaluation. The collected data are then arranged in the work sheet. In addition, investigation on papers, academic or related guidelines and standards is also conducted.

#### 5.3 Equipment and Devices

Similar to the nonstructural members, a questionnaire survey is given to the related manufacturers to collect data relating to the damage evaluation, which collected data are then arranged in the work sheet. In addition, investigation on papers, academic guidelines and standards collected data are also conducted.

#### 5.4 Furniture (Contents)

On the existing papers, guidelines and standards are reviewed to collect the data having clear indication of the input magnitude and the response value, which are then arranged in the work sheet.

### 6. OCCURRENCE OF EARTHQUAKE DAMAGE AND MEANS OF FUNCTIONAL RESILIENCE

According to the research articles, the object is to review the information relating to the building damages of earthquake and to the functional resilience after earthquake, and to investigate the preparation of explanation and expression tool to convey the information to general users in an understandable format.

In the first fiscal year of the research project, there was reviewed the expectedly occurring damages of earthquake and means of functional resilience on the examples of houses, hospitals, and offices. Since the functions required to buildings differ with the uses of buildings, the research assumed the three uses of buildings: houses, hospitals, and offices. Then the possible damages on earthquake and the means of functional resilience were reviewed. As the method of review, the damage phenomena were divided along the time axis into I (immediately after the earthquake), II (within several days after the earthquake), and III (afterward), and there were reviewed the influence of each phenomenon on the functions, the hardware measures, and the software measures including human actions. In addition, the software measures were further divided into the pre-measures applying before appearing the earthquake damages and the post-measures applying immediately after the earthquake.

### 6.1 Earthquake Damage of Houses and Means of Functional Resilience

The function requested for houses was determined as the maintaining of living, thus the recovery from the condition of difficulty in living after earthquake was determined as the functional resilience. Table 5 shows the generation of earthquake damages and outline of the means of functional resilience. The characteristics of houses include that the citizens suffered from earthquake are forced to live in an emergency evacuation area or temporary houses owing to the lack of substitute facilities, and that restoration cost becomes a heavy economical load. In the initial period of living in an emergency evacuation area, washroom is not available, and other damages of lifeline seriously affect the maintaining living

### 6.2 Earthquake damages in hospitals and means of functional resilience

The function requested to hospitals was determined as the continuity of medical activities, thus the recovery of medical activities was determined as the functional resilience. Table 6 shows the generation of earthquake damages and outline of the means of functional resilience. Since the assurance of life of patients and medical treatment take the priority, the characteristics of hospital include that transfer of patients to an emergency evacuation area or to other hospital is requested after the earthquake, and that, if dialysis patients exist, water stoppage becomes a critical problem. Furthermore, many of medical equipment and devices have casters, which need special care for the transfer under earthquake.

### 6.3 Earthquake Damage of Offices and Means of Functional Resilience

The function requested to offices was determined as the continuity of business, thus the recovery of the business was determined as the functional resilience. Table 7 shows the generation of earthquake damages and outline of the means of functional resilience. The features of office buildings include that substitute facilities for the head office building and the branch building are relatively easily available. Consequently, it is important that, as

the preliminary measures, the Business Continuity Plan (BCP) in disaster is prepared assuming the use of substitute facilities. Since many kinds of business rely on computers, it is necessary to secure the earthquake resistance of computer facilities and to attain early restoration.

## 7. CONCLUSION

As a new requirement of society aiming at safety and security, the rapid functional resilience of buildings after earthquake disasters is discussed. As described in Chapter 2, considering the problems recognized in the earthquake damages of recent years, and the disaster-preventive strategy at national level, it is expected that the necessity of technology development relating to the functional continuity and disaster resilience should be emphasized more than ever. Continuing the technology development is expected under sustainable cooperation of organizations relating to the subject.

The research project promotes the activity organically and effectively under the same sense of purpose among Japan Structural Consultants Association (JSCA), NPO Japan Aseismic Safety Organization (JASO), university members, and many relating organizations. Toward the structuring a performance-based design system which has a true significance requested by the society, we strongly hope to have cooperation of relating sectors in wide fields.

## 8. ACKNOWLEDGEMENT

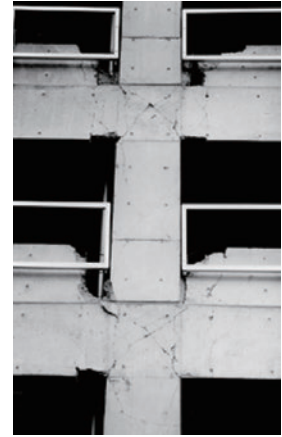
This research was conducted as a part of “Development of Performance-Based Structural Design System for Evaluating Continuity and/or Resiliency of Building Function after Disasters” of a research subject of BRI, (Chairman: Dr. Hitoshi Shiobara, Associate Professor of the University of Tokyo). We would like to express our appreciation to the related persons and organizations.



(a) Full view of the building (RC rigid joint structure)



(b) Shearing fracture and damage of pillar



(c) Damage of beams and joints of pillar with beam

Photo 1 Building designed in accordance with the New Earthquake Resistance Standards: Seriously damaged by the Southern Hyogo Earthquake in 2005, though not collapsed



Photo 2 Crack damage of nonstructural wall of corridor of a condominium by the West-Off Fukuoka Earthquake in 2005

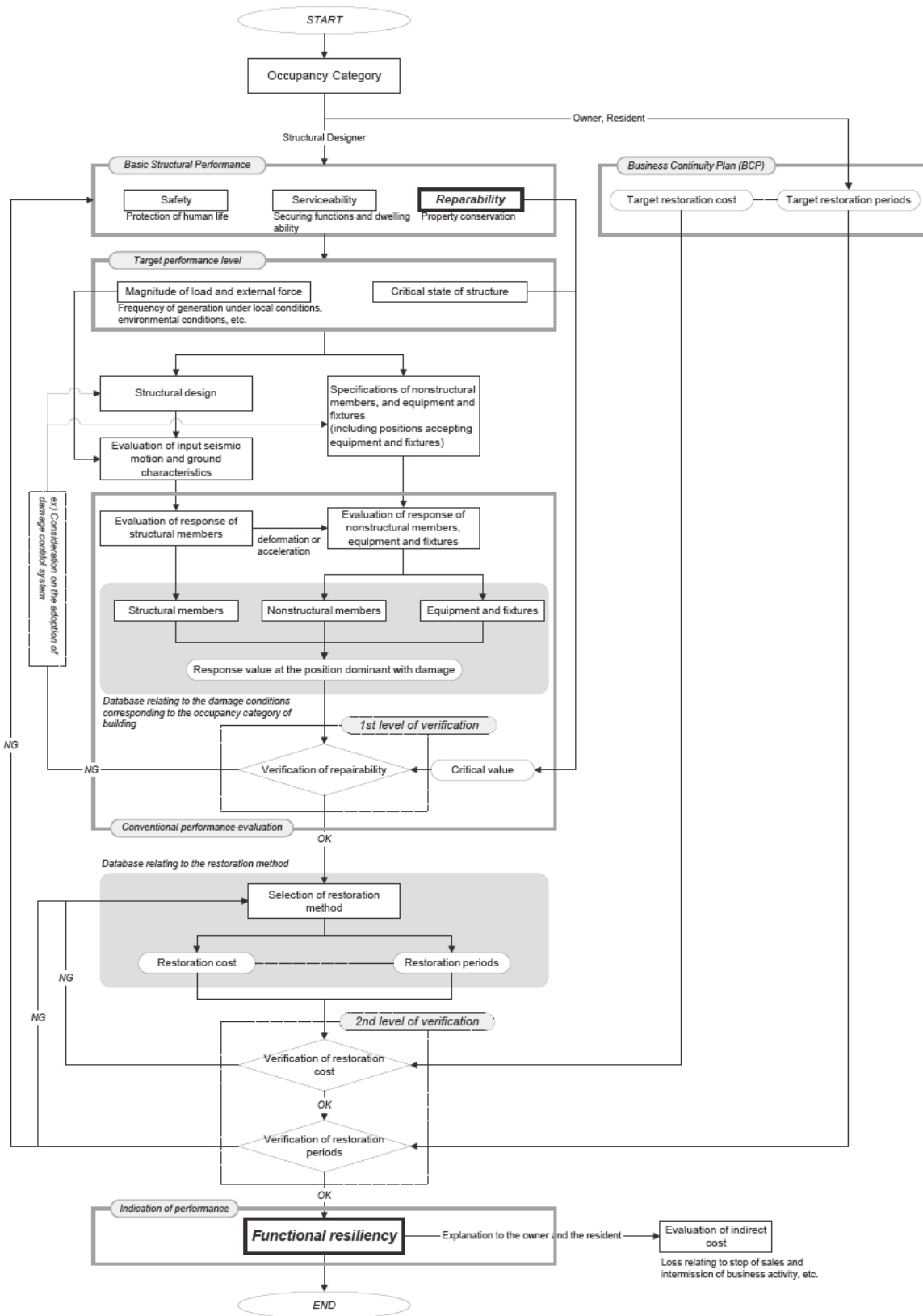


Figure 1 Design verification flow scheme based on the “Functional Resiliency”

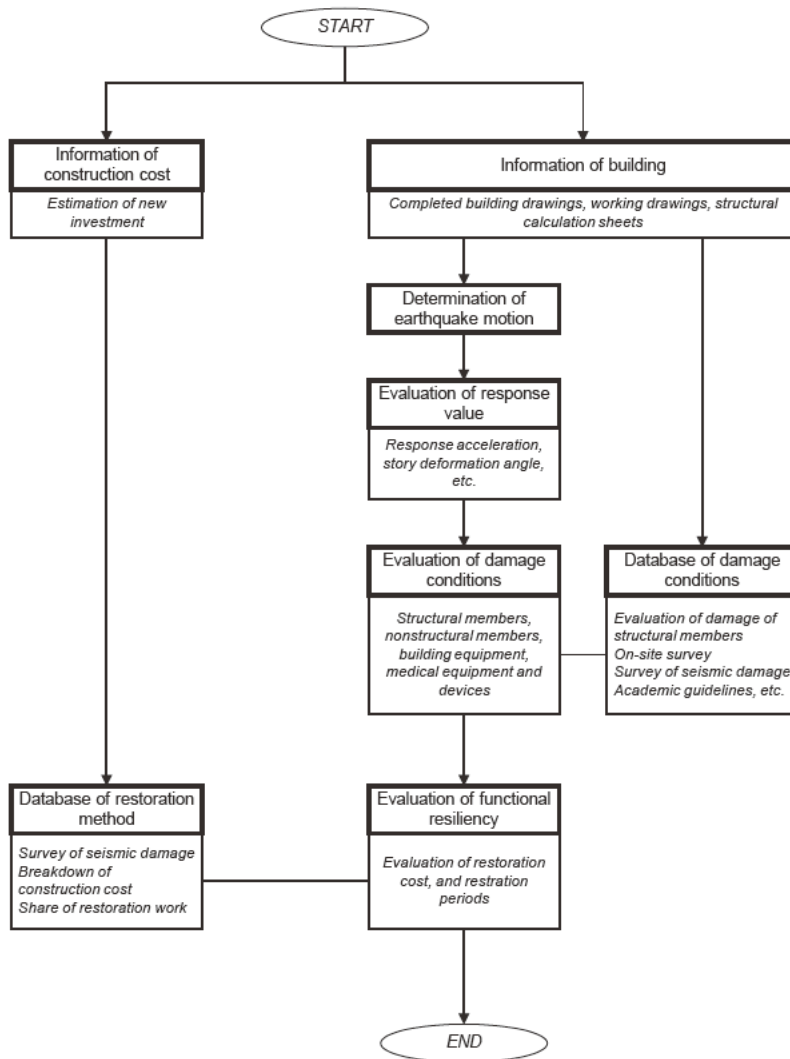


Figure 2 Evaluation flow diagram

Table 1 Outline of building

Time of construction	September, 1980
Scale	1st and 2nd basements and 1st to 8th floors, with a penthouse
Total floor area	7,974m <sup>2</sup>
Structure	SRC (from 2nd basement to 3rd floor), RC (from 4th floor to penthouse)
Foundation structure	Direct foundation

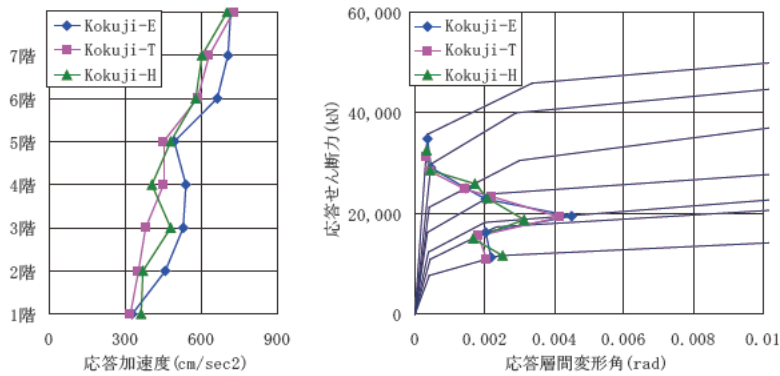


Figure 3 Result of time history response analysis (X direction)

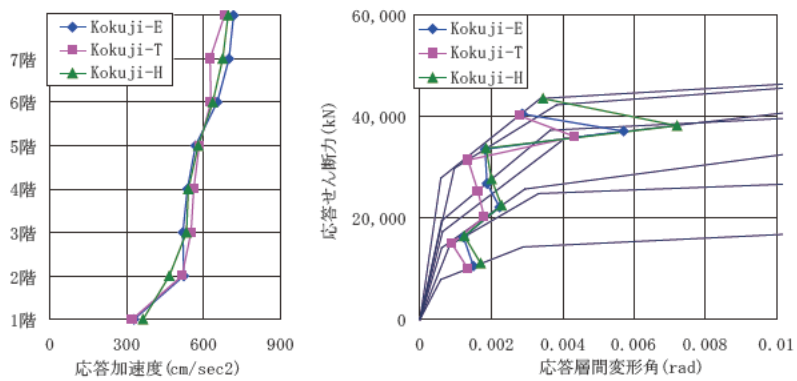


Figure 4 Result of time history response analysis (Y direction)

Table 2 Evaluation of damage condition

Position	Damage evaluation	Restoration work period
Structural frame	Medium damage	within 3 months
Exterior non-structural member	Small damage – Medium damage	within 3 weeks
Interior non-structural member	Slight damage	within 3 days
Air conditioning and hygiene equipment	Slight damage	within 3 days
Electric equipment	Non-damage	
Lift equipment	Non-damage	

Table 3 Breakdown of construction work

Work article	Share of work cost, $p_i$
Structural member	0.185
Exterior non-structural member	0.078
Interior non-structural member	0.187
Air conditioning and hygiene equipment	0.366
Electric equipment	0.160
Lift equipment	0.023
Total	1.000

Table 4 Fractional damage of each position responding to the degree of damage

Position	Degree of damage				
	Large damage	Medium damage	Small damage	Slight damage	Non-damage
Structural member	0.50	0.20	0.05	0.02	0.00
Exterior non-structural member	0.50	0.20	0.05	0.01	0.00
Interior non-structural member	0.50	0.20	0.05	0.01	0.00
Air conditioning and hygiene equipment	0.50	0.20	0.05	0.01	0.00
Electric equipment	0.50	0.20	0.05	0.01	0.00
Lift equipment	0.50	0.20	0.05	0.01	0.0

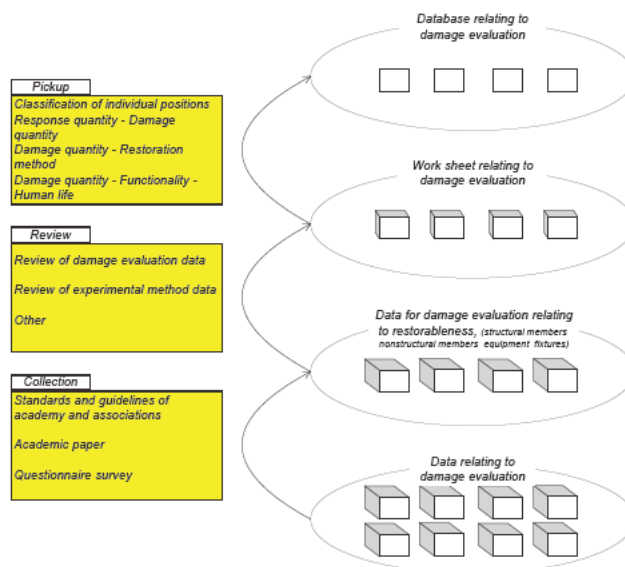


Figure 5 Method for developing structuring database

Table 5 Earthquake-induced damage and means of functional resilience (Houses)

Phase	Damage phenomena	Influence on functions	Hardware measures	Software measures (preliminary action)	Software measures (after earthquake)
I	Collapse, half collapse, part damage of building	Occurrence of killed and injured citizens	Increase in the earthquake resistance of building	Diagnosis of earthquake resistance of building	Confirmation of safety of family Rescue operation
	Difficult for opening/closing door	Interference with evacuation	Making door earthquake resistant		
	Falling and dropping of furniture and fixtures	Injury by direct earthquake attack Interference with evacuation	Fixation and support of furniture and fixtures	Room safety check	
	Electric power failure	Interference with collecting information Inconvenience in living (especially at night)		Preparation of portable radio Preparation of flashlight and candle	
	Stop of lift	Interference with evacuation			Request for restoration of lift
I - II	Water stoppage, gas stoppage	Inconvenience in living (drinking water, toilet, face wash, bath)		Storing drinking water Storing water for toilet	
II	Unserviceable building	Poor living condition			Moving to an emergency evacuation area
	Fire	Occurrence of killed and injured citizens	Increase in the fire proof of building		Fire fighting
III	Worsened living environment	Psychological stress			Psychological care
	Elongation of period of living in an emergency evacuation area	Psychological stress			Moving to temporary houses
	Poor economical condition	Delay of building restoration		Joining earthquake insurance	Contribution, emergency aid

Table 6 Earthquake-induced damage and means of functional resilience (Hospitals)

Phase	Damage phenomena	Influence on functions	Hardware measures	Software measures (preliminary action)	Software measures (after earthquake)
I	Collapse, half collapse, part damage of building	Occurrence of killed and injured citizens	Increase in the earthquake resistance of building	Diagnosis of earthquake resistance of building	Confirmation of safety of patients and staffs Rescue operation
	Falling medical equipment and devices, etc Break of glass	Injury by direct earthquake attack Interference with evacuation	Fixation and support of medical equipment and devices	Room safety check	Guiding evacuation of inpatients
	Stop of lift	Interference with evacuation		Acceptance of seriously ill patients at lower floors	Guiding evacuation through emergency staircases
	Electric power failure	Stopping functioning of medical equipment and devices Deletion of computer data Inconvenience in living (especially at night)	Securing emergency power source	Backup of data	
I - II	Water stoppage	Inconvenience in living (drinking water, toilet, face wash, bath) Interference with medical treatment (dialysis patients)	Securing emergency water source (groundwater, etc )	Storing daily life water	Use of water tank trucks Moving patients to other hospitals
II	Unserviceable building	Stopping medical treatment activities	Preparation of temporary tents		Emergency medical treatment at temporary tents
	Increase in the number of sufferers	Stagnant medical treatment activities Shortage of acceptance area		Structuring network with other hospitals	Gathering staffs Request for other hospitals to accept patients
	Shortage of drugs and medicines		Cool storage of drugs and medicines	Securing drugs and medicines which can be stored in cool space	
III	Worsening hospital environment	Stress of patients			Psychological care for patients
	Lump of waste	Hygienic problems		Establishing cooperation scheme with local government	

Table 7 Earthquake-induced damage and means of functional resilience (Offices)

Phase	Damage phenomena	Influence on functions	Hardware measures	Software measures (preliminary action)	Software measures (after earthquake)
I	Collapse, half collapse, part damage of building	Occurrence of killed and injured citizens	Increase in the earthquake resistance of building	Preparation of BCP, Diagnosis of earthquake resistance of building	Confirmation of safety of staffs Rescue operation
	Drop of ceiling Break and scattering of window glass Difficult for opening/closing door Damage of sprinkler	Injury by direct earthquake attack Injury of passers-by Interference with evacuation Fire extinguishing unavailable	Preventive measure against falling of ceiling Protective film against scattering of glass Making door earthquake resistant Making equipment earthquake resistant		
	Moving and falling of heavy equipment such as copying machine	Injury by direct earthquake attack	Fixation and support of equipment	Room safety check	
	Failure of computer network	Stopping communication, deletion of data	Making computers seismic isolation	Backup of data	Request for restoration of network
	Stop of lift	Interference with evacuation			Evacuation through emergency staircases Request for restoration of lift
	Electric power failure	Deletion of computer data	Securing emergency power source		
I - II	Water stoppage	Inconvenience in living (drinking water, toilet, face wash, bath) Interference with medical treatment (dialysis patients)	Securing emergency water source (groundwater, etc )	Storing daily life water	Use of water tank trucks Moving patients to other hospitals
II	Unserviceable building	Stopping sales activity	Securing substitute facilities	Preparation of BCP	Continuation of sales activity at substitute facilities

I: immediately after the earthquake  
 II: within several days after the earthquake  
 III: afterward

## **THEME 2**

### **Dams**

# Improvement of Distance Attenuation Formula of Acceleration and Lower Limit Acceleration Response Spectrum to Evaluate Seismic Performance of Dams

by

Shinya Mitsuishi<sup>1</sup>, Tomoki Otani<sup>2</sup>, Yoshikazu Yamaguchi<sup>3</sup> & Tomoya Iwashita<sup>4</sup>

## ABSTRACT

In 2005, River Bureau of Ministry of Land, Infrastructure, Transport and Tourism (MLIT) issued "Guidelines for Seismic Performance Evaluation of Dams during Large Earthquakes (Draft) [1] (hereinafter referred to as the "Draft Guidelines") as new technical guidelines systematically explaining the evaluation methods for seismic performance of dams during large earthquakes.

The Draft Guidelines show a standard regulation to evaluate of the seismic performance of dams for *Level 2 earthquake motions*. The definition of "Level 2 earthquake motions" is "Motions having the maximum-scale level of intensity conceivable at the dam site, at the present and in the future", which is equivalent to the Maximum Credible Earthquake.

The Draft Guidelines show three important matters to evaluate the seismic performance of dams against large earthquakes.

- i) The definition of earthquake motions that should be taken into consideration in evaluations
- ii) The concepts of the required seismic performance of dams.
- iii) The methods of seismic performance evaluation of dam bodies and appurtenant structures

The Draft Guidelines were applied as a "trial implementation" to verify the applicability in the technical viewpoint. Verification was conducted at several existing dams to find out various problems in working-level and solve them.

The Draft Guidelines provide the lower limit acceleration response spectrum for evaluation as

the minimum level of the earthquake motions to be considered for seismic performance evaluation. This spectrum is set on the basis of the distance attenuation formula for dams.

In the trial implementation, the distance attenuation formula for dams has been used to determine Level 2 earthquake motions. The evaluation using models dams conducted as a trial application of the Draft Guidelines found several problems originating from the distance attenuation formula for dams to determine earthquake motions. To deal with these problems, the distance attenuation formula for dams was revised. This was followed by the review of the lower limit acceleration response spectrum for dam evaluation using the revised distance attenuation formula for dams.

*KEYWORDS: Distance Attenuation Formula, Lower Limit Acceleration Response Spectrum, Seismic performance evaluation*

## 1. IMPROVEMENT OF THE DISTANCE ATTENUATION FORMULA FOR DAMS

### 1.1 Setting of Level 2 Earthquake Motions

Based on the Draft Guidelines, Level 2 earthquake motions should be determined by thoroughly investigating and collecting information about past earthquakes, near the dam site. Level 2 earthquake motions for each dam are determined as the estimated earthquake

---

1 Head, Water Management and Dam Division, River Department, National Institute for Land and Infrastructure Management, Ministry of Land, Infrastructure, Transport and Tourism (MLIT), Tsukuba 305-0804 Japan

2 Former Researcher, ditto (Kansai Regional Bureau, Japan Water Agency)

3 Team Leader, Dam Structure Research Team, Hydraulic Engineering Research Group, Public Works Research Institute, Tsukuba 305-8516 Japan

4 Deputy Team Leader, ditto

motions at each dam site and caused by selected earthquakes that could have the largest impact on the dam (*Scenario Earthquakes*). For determination of the Scenario Earthquakes for each dam, information such as location and magnitude of past earthquakes, active faults and plate boundaries that might suggest to the occurrence of future earthquakes, should be gathered from reports provided by various earthquake research organs. For determination of the Scenario Earthquakes for each dam, information such as location and magnitude of past earthquakes, active faults and plate boundaries that might suggest to the occurrence of future earthquakes, should be gathered from reports provided by various earthquake research organs.

The Scenario Earthquakes for each dam should be selected by comparing the estimated earthquake motions at the site caused by potential earthquakes that might occur near the dam site. The effects of individual potential earthquakes is basically estimated by comparison of acceleration response spectra evaluated using the *Distance attenuation formula for dams* on acceleration response spectrum [2], which is a set of empirical equations derived from earthquake motions observed at rock foundation or dam basement of numerous dams in Japan.

The largest acceleration response spectrum calculated by the formula is applied for the target spectrum. The acceleration time history of Level 2 earthquake motion for a dam is produced by fitting the acceleration response spectrum of the original earthquake motion to the target spectrum.

In addition to the empirical method of using the distance attenuation formula for dams, earthquake motions could be determined by the semi-empirical methods such as the empirical Green's function method and the statistical Green's function method or the theoretical method. However, these methods still have problems in regard to their application, including the need for appropriate modeling of the rupture process at the source fault surfaces

and of the characteristics of the propagation from the source fault to the dam site. For these reasons, the empirical method of the distance attenuation formula for dams is used to determine Level 2 earthquake motions for dams, in the present trial implementation of the Draft Guidelines.

## 1.2 Concerns of the Distance Attention Formula for Dams

In the trial implementation of the Draft Guidelines, the distance attenuation formula for dams prepared in 2001 (hereinafter referred to as the "2001 Formula") was used to determine Level 2 earthquake motions. Two types of equation were produced as the distance attenuation formula for dams as shown below.

- Shortest distance equation

$$\log S_A(T) = C_m(T)M + C_h(T)H_c - C_d(T) \log \{R + 0.334 \exp(0.653M)\} + C_o(T) \dots\dots\dots(1)$$

- Equivalent hypocentral distance equation

$$\log S_A(T) = C_m(T)M + C_h(T)H_c - C_d(T)X_{eq} - \log X_{eq} + C_o(T) \dots\dots\dots(2)$$

Where, T is period (seconds),  $S_A(T)$  is the acceleration response spectrum, M is the Japan Meteorological Agency Magnitude,  $H_c$  is the depth at the center of the source fault plane (km), R is the shortest distance to the source fault plane (km),  $X_{eq}$  is the equivalent hypocentral distance (km) and  $C_m$ ,  $C_h$ ,  $C_d$ ,  $C_{dh}$  and  $C_o$  are the constants.

These equations were established by the regression analysis of the relationship between the scale of the earthquake, distance to the fault plane and depth at the center of the fault plane and acceleration response spectrum for each period based on seismic data recorded by the seismographs installed at the inspection gallery at the bottom of a dam in Japan in the period from 1974 to 2000.

The earthquake motions prepared by the application of the 2001 Formula to the dams for evaluation in the trial implementation showed

Table 1 Number of Regression Analysis Data for Distance Attenuation Formula for Dams

	Data Period	Subject Earthquakes	Number of Dams	Number of Observation Data (Horizontal Motions)	Number of Observation Data (Vertical Motions)
2001 Formula	1974 to 2000	63	91	293	—
2008 Formula	1974 to 2008	88	213	642	318

that there was a major discrepancy in the estimation results of the earthquake motions between the shortest distance equation and the equivalent hypocentral distance equation in the case where the source fault plane of the Scenario Earthquake was located near the dam site and also in some other cases.

The reason for such discrepancy was thought to be the application of the distance attenuation formula for dams to different ranges of the distance to the source fault and the earthquake magnitude of earthquake observation data used as regression analysis data for the distance attenuation formula for dams. The number of earthquake observation data close to the source fault is quite few. While the maximum magnitude observed of an inland fault earthquake was 7.3, a larger earthquake was estimated in the evaluation.

In view of these issues, the equation structure of the distance attenuation formula for dams was modified. In addition, observation data on earthquakes which have occurred since 2001 was added as regression analysis data. The modification of the equation structure also incorporated the latest research developments on earthquake motion estimating equations.

The 2001 formula is applied to estimate the acceleration response spectrum only for horizontal earthquake motions. There was no formula to estimate the vertical motions. In the past of the trial implementation, the latter was determined by multiplying the acceleration response spectrum of horizontal earthquake motions determined by the distance attenuation formula for dams by the ratio between the horizontal acceleration response spectrum and the vertical acceleration response spectrum for each frequency. As consideration of the vertical motions is needed to be more appropriate for evaluation of the seismic performance of dams,

Table 2 Main Earthquakes for Which Data Was Added Newly for Regression Analysis to Produce Distance Attenuation Formula

Name of Earthquake/Epicenter	Date of Occurrence	JMA Magnitude
Miyagiken-oki	26/05/2003	7.1
Tokachi-oki	26/09/2003	8.0
Niigataken-Chuetsu	23/10/2004	6.8
Fukuoka-ken Seiho-oki	20/04/2005	7.0
Noto Hanto	25/03/2007	6.9
Niigata-ken Chuetsu-oki	16/07/2007	6.8
Iwate-Miyagi Nairiku	14/06/2008	7.2

it was decided to prepare new distance attenuation equations for vertical motions as part of the review of the distance attenuation formula.

### 1.3 Improvement of Distance Attenuation Formula for Dams

#### 1.3.1 Acceleration Record Data Used for Analysis

The earthquake observation data used to decide the values of the constants for the distance attenuation formula for dams was that observed at the dam foundation with an epicentral distance of not more than 200 km in the case of earthquakes of which the magnitude and the hypocenter depth are at least 5.0 and not deeper than 100 km respectively. The number of observation data used for the 2001 Formula and the latest formula suggested in this paper (hereinafter referred to as "the 2008 Formula") is shown in Table 1. The main earthquake of the observation data newly added as regression analysis data is listed in Table 2.

#### 1.3.2 Modification of Formula Structure

Because of the issues of the distance attenuation formula described in Section 1.2, the structure of the equations was modified and the resulting equations are given below.

▪ Shortest distance equation

$$\log S_A(T) = C_{m1}(T)M + C_h(T)H_c - \log(R + C_1(T) \cdot 10^{0.5M}) - (C_d(T) + C_{dh}(T)H_c)R + C_0(T) \quad (M \leq M_0) \dots\dots\dots(3)$$

$$\log S_A(T) = C_{m1}(T)M + C_{m2}(T)(M_0 - M)^2 + C_h(T)H_c - \log(R + C_1(T) \cdot 10^{0.5M}) - (C_d(T) + C_{dh}(T)H_c)R + C_0(T) \quad (M > M_0) \dots\dots\dots(4)$$

▪ Equivalent hypocentral distance equation

$$\log S_A(T) = C_{m1}(T)M + C_h(T)H_c - \log(X_{eq} + C(T)) - (C_d(T) + C_{dh}(T)H_c)X_{eq} + C_0(T) \quad (M \leq M_0) \dots\dots\dots(5)$$

$$\log S_A(T) = C_{m1}(T)M + C_{m2}(T)(M_0 - M)^2 + C_h(T)H_c - \log(X_{eq} + C(T)) - (C_d(T) + C_{dh}(T)H_c)X_{eq} + C_0(T) \quad (M > M_0) \dots\dots\dots(6)$$

Where, T is period (sec),  $S_A$  is the acceleration response spectrum, M is the Japan Meteorological Agency magnitude,  $H_c$  is the depth at the center of the fault plane (km), R is the shortest distance to the fault plane (km),  $X_{eq}$  is the equivalent hypocentral distance (km) and  $C_{m1}$ ,  $C_h$ ,  $C_1$ ,  $C_d$ ,  $C_{dh}$ ,  $C_0$  and C are the constants.

The 2001 Formula was modified in the following manners.

- Adding of restricting term for considering against overestimate for large magnitude

Although the number of the observation data is quite few, in the case of an earthquake with an extremely large magnitude the earthquake motions estimated by the 2001 Formula tend to be quite larger than the observation data. In the 2001 Formula, a linear relationship is assumed between the logarithm for the amplitude of the earthquake motions and the earthquake magnitude. Therefore, it has been pointed out that the estimation of earthquake motions appropriately reflecting the characteristics of earthquake motions near the source fault based on the scaling rules of the hypocenter is quite difficult in the 2001 Formula. In consideration of these points, it was decided to innovate a

square root term for the magnitude into the equation. The impact of this square root term is considered when the earthquake magnitude exceeds a certain level. It was, therefore, determine the value which best conforms to the observation data for the minimum magnitude of which the impact must be taken into consideration. The adequate magnitude determined is  $M_0=5.0$  for the shortest distance equation and  $M_0=6.0$  for the equivalent hypocentral distance equation.

- Modification of the distance attenuation term in the shortest distance equation

The characteristic of the distance attenuation of earthquake motions is expressed as the sum of the effect of geometric attenuation and the effect of internal attenuation in the equivalent hypocentral distance equation of the 2001 Formula. In the shortest distance equation, however, it is collectively expressed in the form corresponding to the internal attenuation, making the effect of geometric attenuation unclear. Therefore, the modified shortest distance equation has both a geometric attenuation term and an internal attenuation term to express the characteristic of the distance attenuation of earthquake motions as the sum of the effects of these two types of attenuation.

- Modification of the restricting term for the shortest distance in the shortest distance equation.

The correction term in order to consider the restriction dependent on the earthquake magnitude for distance attenuation was added in the term expressing the geometric attenuation. The constant value for the restriction of earthquake motions relating to the distance attenuation was newly calculated by the latest regression analysis. The constant value for the magnitude was set to 0.5 based on the past research findings.

- Adding of a restricting term for the equivalent hypocentral distance to the equivalent hypocentral distance equation

The correction term for the distance was added in the term expressing the distance attenuation as in the case of the shortest distance equation so that the restriction on earthquake motions near the source fault could be considered appropriately. Where, as the equivalent hypocentral distance was defined as an indicator for the distance where the effects of the two-dimensional spread of the fault rupture surface could be considered, a relevant constant value for the correction for the distance was installed instead of relying on the earthquake magnitude corresponding to the area of the fault rupture surface.

- Consideration of the dependence of the distance attenuation on the depth of the hypocenter

According to the past research findings [3], the gradient of the distance attenuation equation also depends on the depth of the hypocenter. The geometric attenuation term in both the shortest distance equation and the equivalent hypocentral distance equation were modified to enable consideration of such dependence on the depth of the hypocenter.

### 1.3.3 Types of Earthquakes

For application of the 2001 formula, earthquakes were classified into three types: earthquake occurring on faults (inland earthquakes), subduction-zone earthquake within a hypocenter depth of 60 km or less (interplate earthquakes) and deep earthquakes inside the subducted plate. In this classification, subduction-zone earthquakes were considered to be shallow earthquakes with a hypocenter depth of 60 km

or less other than inland earthquakes and included shallow earthquakes within the subducting plates. However, as earthquake within subducting plate and interplate earthquake have different characteristics, it was thought that they should be clearly distinguished for the proposal of a distance attenuation formula.

As a result, it was decided to divide the subduction-zone earthquakes into two types based on the hypocenter depth, producing the four types of earthquakes listed below. Figure 1 shows the conceptual location of the earthquake hypocenter of each earthquake type.

- Type A: earthquake occurring on faults
- Type B: inter plate earthquake
- Type C: shallow earthquake within the subducting plate
- Type D: intermediate depth earthquake within the subducted plate

### 1.3.4 Regression Analysis Results for Each Constant

Regression analysis regarding the 2008 Formula was conducted using the earthquake data shown in Table 1 and the regression constants for horizontal motions and vertical motions were determined for both the shortest distance equation and the equivalent hypocentral distance equation.

The maximum likelihood estimation method was used for the regression of each constant of the distance attenuation formula for dams. Figures 2 and 3 show the resulting regression constants (parameters) calculated for the distance attenuation formula for dams.

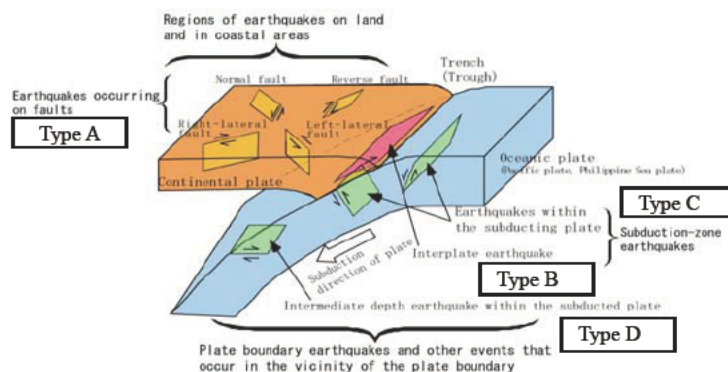


Fig. 1 Illustration of Rupture Zones for Each Type of Earthquakes in the 2008 Formula

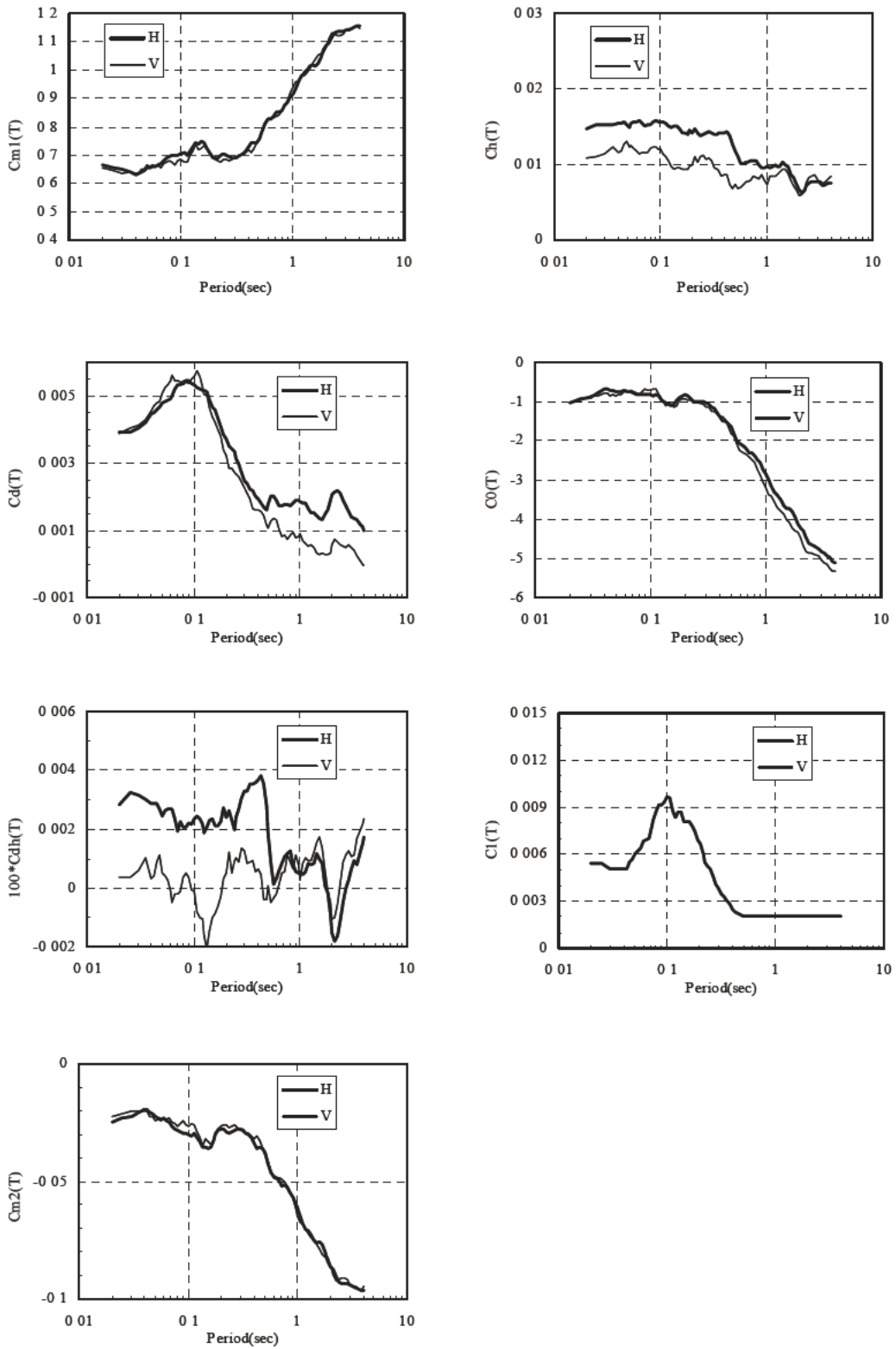


Fig. 2 Parameters on Shortest Distance Equation

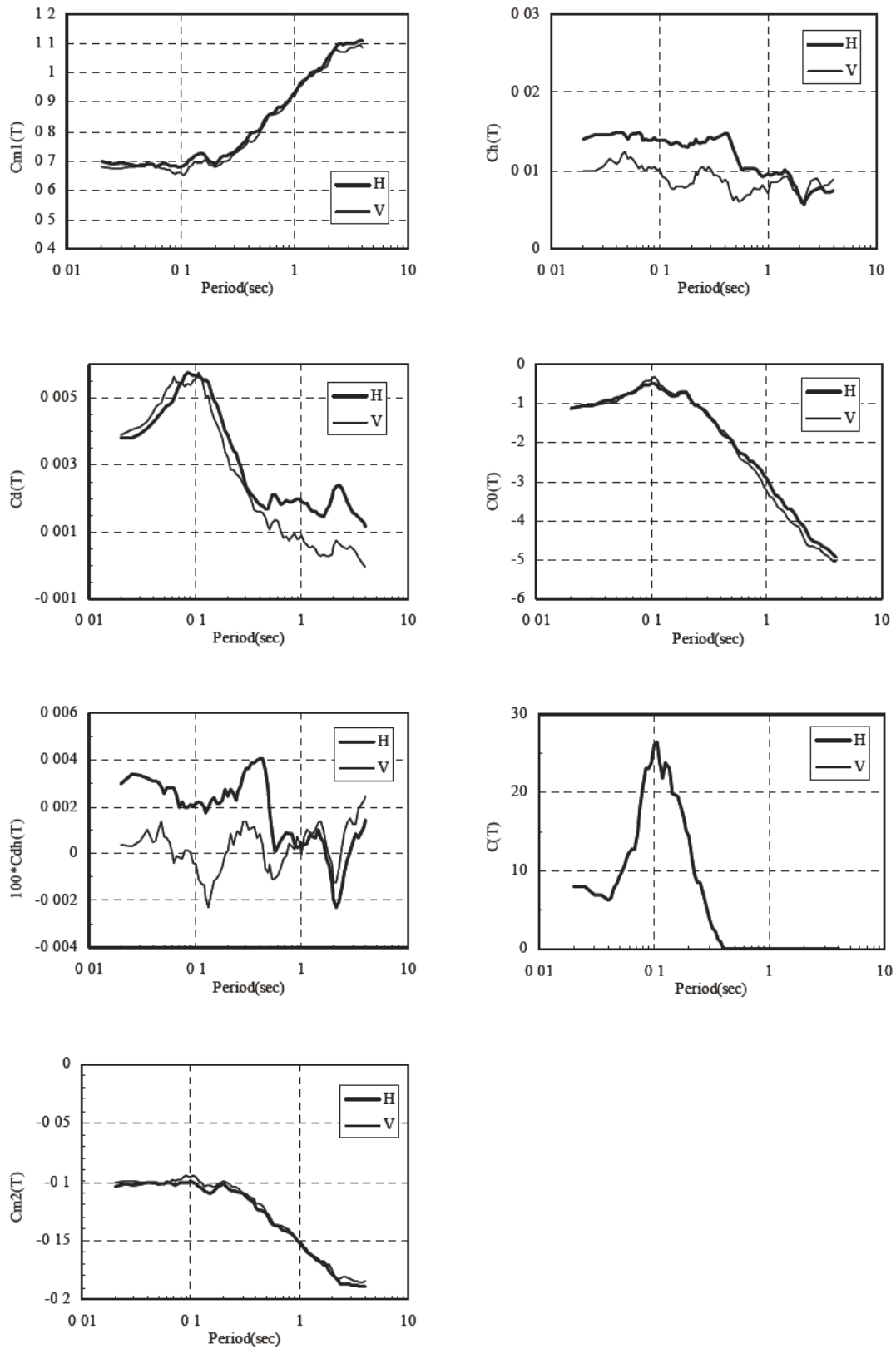
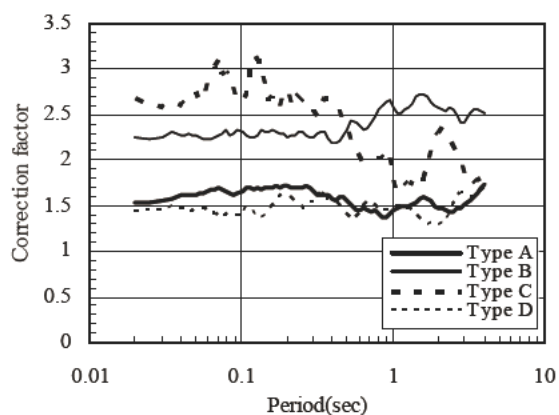
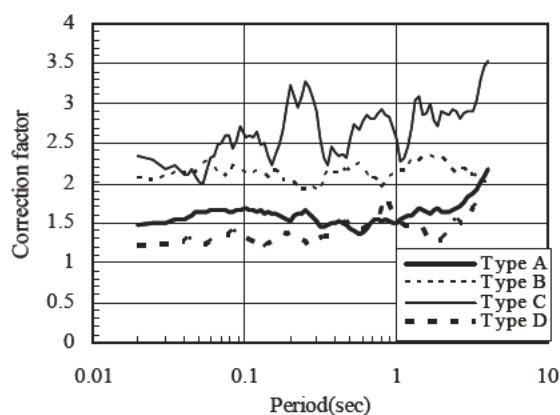


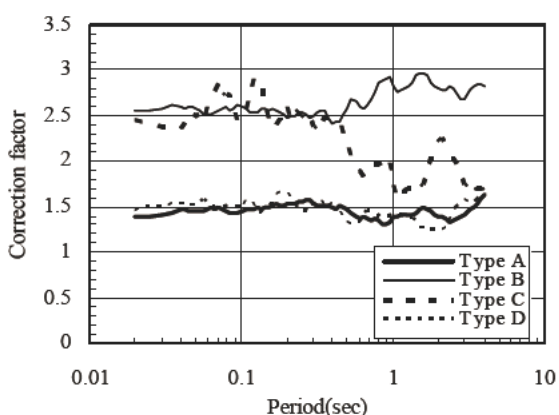
Fig. 3 Parameters on Equivalent Hypocentral Distance Equation



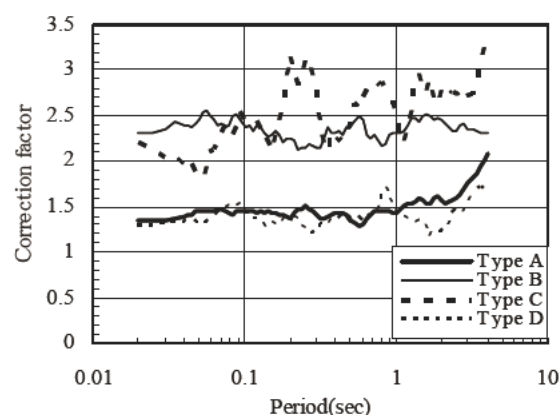
(a) Shortest distance equation(horizontal component)



(b) Shortest distance equation(vertical component)



(c) Equivalent hypocentral distance equation(horizontal component)



(d) Equivalent hypocentral distance equation(vertical component)

Fig. 4 Correction Factors for Each Type of Earthquakes

Figure 4 shows the correction factor for each type of earthquake. In this figure, the proportion of each type of earthquake in the mean earthquake motions is calculated. This figure indicates the value of the mean plus the standard deviation for the multiplying power for correction in consideration of the dispersion of earthquake motions.

For the determination of Level 2 earthquake motions, the acceleration response spectrum is firstly established by inserting the parameter values for the fault surface, etc. of the Scenario Earthquake, the distance to the fault surface and the regression constant values shown in Fig. 2 and Fig. 3 to Equations (3) to (6). The acceleration response spectrum of the Scenario Earthquake is then determined by multiplying the calculated acceleration response spectrum by the correction factor for each type of earthquake shown in Fig. 4.

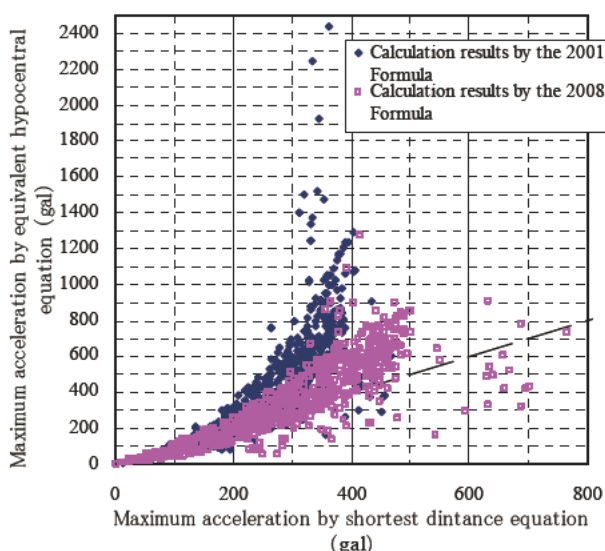


Fig. 5 Comparison of Maximum Acceleration Calculated by Shortest Distance Equation and Equivalent Hypocentral Distance Equation

#### 1.4 Verification of Improved Distance Attenuation Formula for Dams

- Decrease of deviation of both the calculation results by the shortest distance equation and equivalent hypocentral distance equation

Figure 5 shows the relationship between the maximum acceleration calculated by the shortest distance equation and equivalent hypocentral distance equation. Compared to the results between the 2001 Formula and the 2008 Formula, the overall deviation is much more compact.

- Improved compatibility for deep earthquakes

Figure 6 shows the observation data and calculation results of the distance attenuation formula for dams at the dam foundation for the Miyagiken-oki Earthquake (M7.1,  $H_c=77$  km) occurred on May, 2003. Modification of the term expressing the distance attenuation to the term dependent on the depth of the hypocenter has improved the compatibility of the calculation results with the observation data at a dam foundation.

- Verification by comparison with dam observation data for actual earthquakes

Figure 7 shows the horizontal maximum acceleration observed at the dam foundation during two major earthquakes and the attenuation curve of the horizontal acceleration response spectrum at the period of 0.02sec using the distance attenuation formula for dams (the 2001 and 2008 Formulas). The attenuation curves of maximum acceleration (acceleration response spectrum at the period of 0.02sec) calculated by the 2008 Formula agree well the maximum acceleration data observed at the dam foundations.

## 2. EVALUATION OF LOWER LIMIT ACCELERATION RESPONSE SPECTRUM FOR DAM EVALUATION

### 2.1 Theory for Determination of Lower Limit Acceleration Response Spectrum for Dam Evaluation

The Draft Guidelines provide “*Lower-limit acceleration response spectrum for Dam evaluation*” that should be considered as the mandatory minimum Level 2 earthquake motions. The reason for stipulating this minimum spectrum is that the earthquake motion used for seismic performance evaluation should be determined taking into consideration the possibility of an earthquake occurring directly at an active fault under the dam site even when no active fault is identified by the investigations.

The Draft Guidelines determine the earthquake magnitude based on the following theories to prepare the lower limit acceleration response spectrum for evaluation and the same method was used for the present review.

- Few earthquakes of M6.5 or smaller produce surface earthquake faults.
- Many earthquakes of M6.8 or greater produce surface earthquake faults.
- The number of earthquakes of M6.6 or M6.7 is much smaller compared to M6.5 or smaller, or, M6.8 or greater. This is not coincidental as a discontinuous scale of magnitude occurs due to the effect of the causative fault plane piercing through the ground surface.
- In exceptional cases, earthquakes exceeding M6.5 may not produce surface earthquake faults. The damage caused by these earthquakes little differs from the maximum damage caused by earthquakes of M6.5 or smaller.
- A surface earthquake fault may not be produced by earthquakes up to approximately M7.3. In the case of the Tottori-ken Seibu Earthquake (M7.3) on October, 2000, the causative fault was not identified prior to the earthquake.

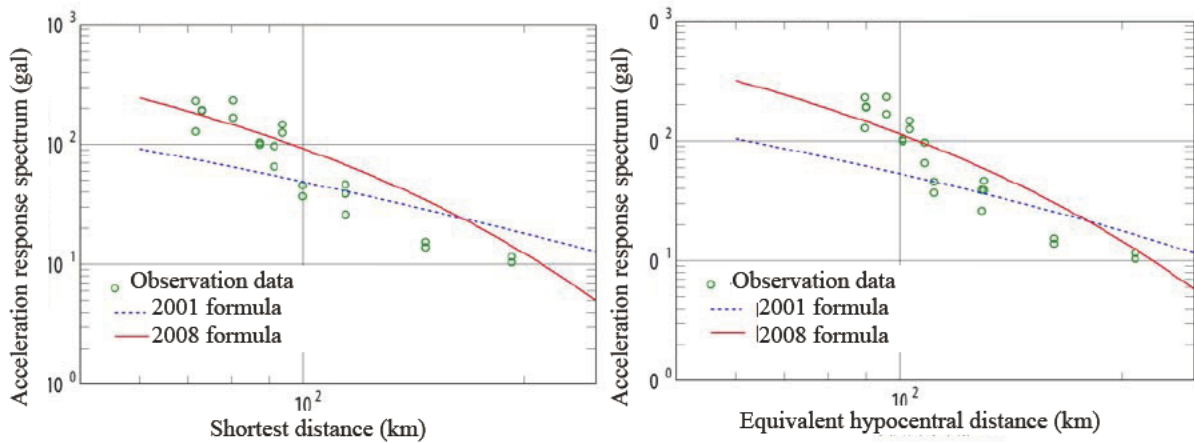
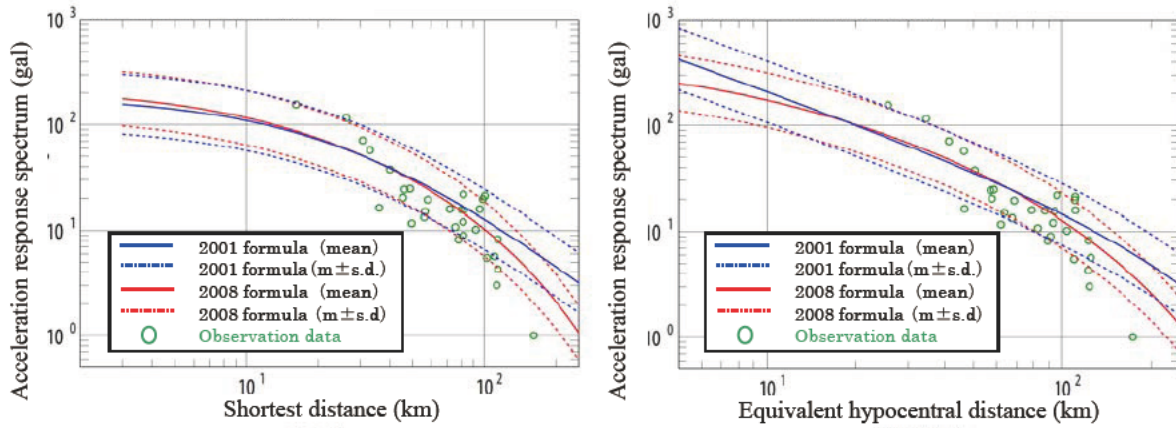
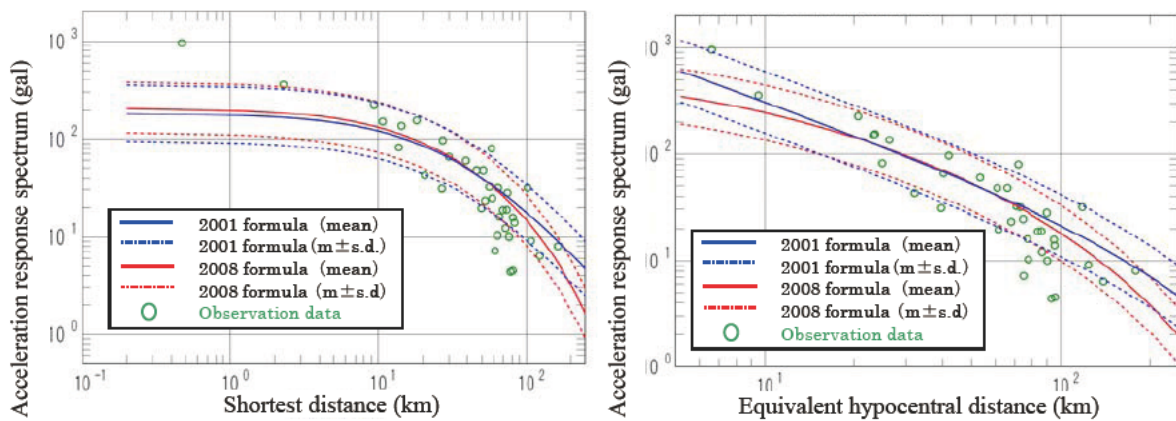


Fig. 6 Comparison of Acceleration Response Spectrum ( $t=0.02\text{sec}$ ) Between Observation Data and Calculation Results by Distance Attenuation Formulas for Dams in the Case of Miyagiken-oki Earthquake on May, 2003



(1) Niigata-ken Chuetsu-oki Earthquake in 2007 (M6.8)



(2) Iwate-Miyagi Nairiku Earthquake in 2008 (M7.2)

Fig. 7 Comparison of Maximum Acceleration (Acceleration Response Spectrum at  $t=0.02\text{sec}$ ) Between Observation Data and Calculation Results by Distance Attenuation Formulas for Dams

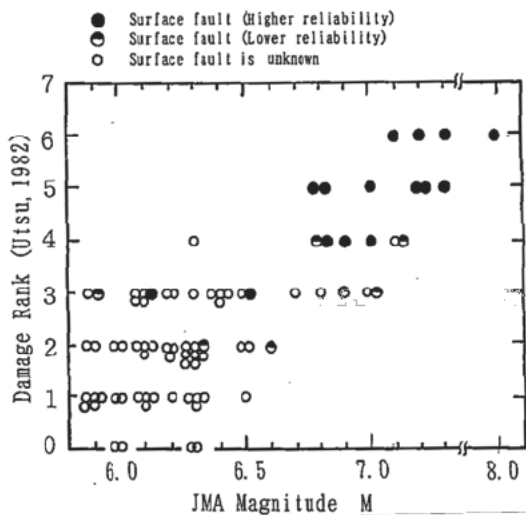


Fig. 8 Relations of damage rank, JMA Magnitude and the occurrence of surface earthquake faults.

The above theories descriptions are based on the JSCE Guideline of Seismic Design for Infrastructures [4] which refers to the relationships of the magnitude, damage rank and the occurrence of surface earthquake faults of past earthquakes in Japan as shown in Fig. 8.

Based on the above, M6.5 and M7.3 were used to establish the lower limit acceleration response spectrum for evaluation. In the case of M6.5, it was decided to use the spectrum corresponding

to the "mean + standard deviation" in the distance attenuation formula for dams. In the case of M7.3, the "mean" of the 2008 formula was used based on the idea that the fault plane could have been identified in advance in many cases of M7.3 or greater earthquakes.

Assuming the occurrence of an earthquake with the magnitude referred to above, the 2008 Formula was used to establish the acceleration response spectrum at each dam site using the locational relationship between the dam and the fault plain and the different gradients of the fault plane.

## 2.2 Setting of Lower Limit Acceleration Response Spectrum for Dam Evaluation

Using the method described in Section 2.1, the 84% fractile value for the earthquake with M6.5 above its epicenter was calculated using the 2008 formula (mean + standard deviation). Similarly, the 84% fractile value for the earthquake with M7.3 above its epicenter was calculated using the same equation (mean). Figure 9 shows the current lower limit acceleration response spectrum and its draft modification. The lower limit acceleration response spectrum for dam evaluation in the present Draft Guidelines found that the calculated spectra using the 2008 Formula exceed the

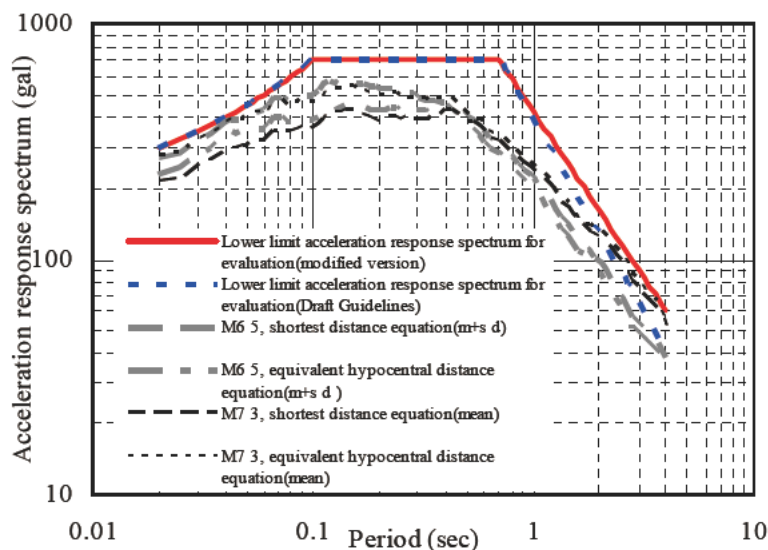


Fig. 9 Modification of Lower Limit Acceleration Response Spectrum for Dam Evaluation (Horizontal Motions)

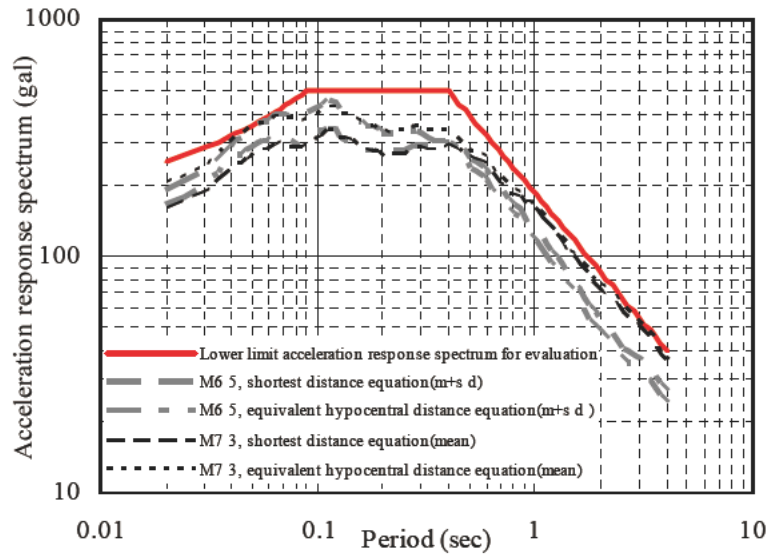


Fig. 10 Determination of Lower Limit Acceleration Response Spectrum for Dam Evaluation (Vertical Motions)

current spectrum in the range of period longer than 2sec. To correct this, the long period side of the lower limit acceleration response spectrum for dam evaluation was modified to envelop the 84% fractile values of M6.5 (mean + standard deviation) and M7.3 (mean) for horizontal motions.

For vertical motions, the 84% fractile values for M6.5 (mean + standard deviation) and M7.3 (mean) were calculated using the distance attenuation formula (the 2008 Formula) for vertical motion. The lower limit acceleration response spectrum for evaluation for vertical motions was set to envelop these fractile values as shown in Fig. 10.

### 3. CONCLUDING REMARKS

Various examinations have been conducted up to the present to solve the problems discovered through the trial implementation of “Guidelines for Seismic Performance Evaluation of Dams During Large Earthquakes (Draft)”. This paper described the review of the problems associated with the distance attenuation formula of acceleration and the determination of the lower limit acceleration response spectrum for seismic evaluation of dams.

Level 2 earthquake motions for the seismic

evaluation of dams were determined mainly using the distance attenuation formula for dams. In the trial implementation of the Draft Guidelines, the formula proposed in 2001 had been used but this formula caused several problems as described in this paper. Efforts were made to solve these problems by modifying the structure of the formula. At the same time, data observed during recent large earthquakes was added as regression analysis data. As a result, distance attenuation equation for horizontal motions was improved and that for vertical motions was established. Following the review of the distance attenuation formula for dams, the lower limit acceleration response spectrum for dam evaluation was also examined. The spectrum for horizontal motions was modified while the spectrum for vertical motions was newly developed.

Evaluation of the seismic performance of dams in Japan will be conducted using the distance attenuation formula for dams and the lower limit acceleration response spectrum for dam evaluation described in this paper.

### REFERENCES

1. River Bureau, MLIT: *Guidelines for Seismic Performance Evaluation of Dams during*

- Large Earthquakes(Draft) , 2005*
2. Matsumoto, N., Ohmachi, T., Yasuda, N., Sasaki, T. and Annaka, T.: Acceleration Response Spectra at Dam Foundations, *Proceedings of the 22nd Congress of ICOLD*, 2006
  3. Annaka, T., Morita, M., Aikyo, Y. and Harada, M.: An Attenuation Model for 5 % damped Acceleration Response Spectra Considering the Effect of Earthquake Type, *JSCE Earthquake Engineering Symposium*, 2005
  4. Japan Society for Civil Engineers: *Guideline of Seismic Design for Infrastructures*, 2001
  5. Matsumoto, N., Yoshida, H., Sasaki, T. and Annaka, T.: Response Spectra of Earthquake Motion at Dam Foundations, *Proceedings of the 21st Congress of ICOLD*, 2003

# DEVELOPING REGIONAL EXERCISES INVOLVING MULTIPLE DAMS

by

Enrique E. Matheu, PhD <sup>1</sup>, Yazmin Seda-Sanabria <sup>2</sup>, and Robert C. Hughes, PE <sup>3</sup>

## ABSTRACT

Owners and operators of dams across the United States are focused on enhancing protection efforts against natural or manmade disasters and improving preparedness, response, and rapid recovery in the event of dam failures or other emergencies. In a collaborative effort led by the U.S. Department of Homeland Security (DHS), multiple dam owners are actively participating in several exercise efforts aligned with the Homeland Security Exercise and Evaluation Program (HSEEP). This performance-based exercise program provides a standardized methodology for exercise design, development, execution, evaluation, and improvement planning, and can be adapted to a variety of scenarios and events.

The HSEEP framework is particularly useful for exercise efforts involving multiple dams, which have dominant regional and multi-jurisdictional characteristics when the corresponding scenarios trigger significant cascading impacts affecting extended areas. These types of exercises provide an effective mechanism to identify any required improvements to the Emergency Action Plans (EAPs) of the facilities involved. An example of these types of regional initiatives is a recently conducted effort that tested communications protocols between government and non-government entities facing a catastrophic event involving two dams located along the same river basin in the Midwest. Another example is a current series of exercises involving significant flooding in the Pacific Northwest, affecting several dams along the Columbia River Basin. This paper describes these efforts and their relevance as an important vehicle to increase preparedness and resilience at the regional level.

**KEYWORDS:** HSEEP methodology; emergency preparedness; resilience; exercise series; regional perspective; emergency action plan.

## 1.0 INTRODUCTION

Comprehensive emergency management planning is the most effective approach to prepare for, prevent, respond to, and recover from catastrophic emergency situations. This is especially important for dam owners in the event of a dam failure. Although emergency management efforts for dams in the U.S. officially began over thirty years ago, efforts have intensified in recent years due to terrorist attacks against the U.S. in 1993, 1995, and 2001. Since 2001, officials in all areas of emergency management, at all levels of government, and in all types of communities have been focused on enhancing protection efforts against both natural and manmade disasters. These efforts include the creation of the U.S. Department of Homeland Security (DHS) in 2002, and dedicated efforts by the dam safety and security communities toward improving preparedness, response, and rapid recovery in the event of dam failures or other emergencies.

Developing and maintaining a comprehensive emergency exercise program plays a crucial role in these efforts. Conducting emergency exercises provides opportunities for emergency responders and officials to practice notification and response actions and assess their collective capabilities. Conducting emergency exercises is one of the primary activities that help safeguard against the loss of life and property damage that can result from the failure of a high-hazard potential dam.

---

<sup>1</sup> Chief, Dams Sector Branch, Sector-Specific Agency Executive Management Office, Office of Infrastructure Protection, U.S. Department of Homeland Security, Washington DC, 20528, [enrique.matheu@dhs.gov](mailto:enrique.matheu@dhs.gov)

<sup>2</sup> Program Manager, Critical Infrastructure Security Program, Office of Homeland Security, Directorate of Civil Works, U.S. Army Corps of Engineers, Headquarters, Washington DC, 20314, [yazmin.seda-sanabria@usace.army.mil](mailto:yazmin.seda-sanabria@usace.army.mil)

<sup>3</sup> Civil Engineer, Dams Sector Branch, Sector-Specific Agency Executive Management Office, Office of Infrastructure Protection, U.S. Department of Homeland Security, Washington DC, 20528, [c.hughes@dhs.gov](mailto:c.hughes@dhs.gov)

The Homeland Security Exercise and Evaluation Program (HSEEP) was developed by DHS to provide exercise policy and program guidance that constitutes a national standard for exercises. During the past two years, the DHS Dams Sector Branch has utilized the HSEEP framework as part of joint exercise efforts developed in collaboration with the U.S. Army Corps of Engineers (USACE), other federal agencies, State and local agencies, and private dam owners/operators.

## 2.0 THE HSEEP METHODOLOGY

The HSEEP methodology was developed by DHS in response to the need for a comprehensive and consistent emergency exercise program. It is a capabilities- and performance-based exercise program that provides standardized methodology and terminology for exercise design, development, conduct, evaluation, and improvement planning. It can be adapted to a variety of scenarios and events from natural disasters to manmade incidents. HSEEP promotes the use of consistent terminology that can be used by all exercise planners, regardless of the nature and composition of their sponsoring agency or organization. It provides tools to help exercise managers plan, conduct, and evaluate exercises to improve their overall emergency preparedness. HSEEP also provides guidance and resources to facilitate the management of self-sustaining exercise programs.

Development of the HSEEP methodology incorporated lessons learned and best practices from existing exercise programs. HSEEP integrates language and concepts from the National Response Plan, National Incident Management System, National Preparedness Goal, Universal Task List (UTL), Target Capabilities List (TCL), existing exercise programs, and prevention and response protocols from all levels of government. It has been accepted as the standardized policy and methodology for the execution of the National Exercise Program (NEP). The NEP is the Nation's overarching exercise program formulated by the National Security Council / Homeland Security Council. All interagency partners in the U.S. have adopted HSEEP as the methodology for all exercises that will be

conducted as part of the NEP. It is also being used at the State, regional, county, and city levels, in addition to usage by private company and other organizations.

### 2.1 Exercise Program Management

The HSEEP methodology provides the user with information and guidance to promote effective exercise program management. The functions required for a user to sustain a variety of exercises targeted toward preparedness priorities on an ongoing basis are provided within the HSEEP framework. These include project management, multi-year planning, budget development, grant management, staff hiring, funding allocation, and expenditure tracking.

Effective exercise program management should function as a cyclic process. To support this, the development of a Multi-Year Training and Exercise Plan is recommended by considering the user's preparedness priorities. As a first step, a Training and Exercise Plan Workshop should be conducted. During the workshop, participants typically review priority preparedness capabilities and coordinate exercise and training activities that can improve and validate those capabilities. Next, specific training and exercise activities are planned and conducted according to the multi-year plan's schedule. Finally, exercise planners consider post-exercise After Action Reports / Improvement Plans (AARs/IPs) when developing priorities for the next multi-year plan, as well as updating plans and procedures, acquiring new equipment, and conducting additional training.

### 2.2 Exercise Project Management

Exercise project management is an important component of exercise program management. It is used to carry out the activities needed to execute an individual exercise. Exercise project management involves five phases, which are collectively known as the *exercise cycle*. Exercises conducted in accordance with the phases of the exercise cycle lead to tangible preparedness improvements.

The five phases of the exercise cycle, as provided by HSEEP, are as follows:

1. **Foundation:** The following activities must be accomplished to provide the foundation for an effective exercise: create a base of support (i.e., establish buy-in from the appropriate entities and/or senior officials); develop a project management timeline and establish milestones; identify an exercise planning team; and schedule planning conferences.

2. **Design and Development:** Building on the exercise foundation, the design and development process focuses on identifying objectives, designing the scenario, creating documentation, coordinating logistics, planning exercise conduct, and selecting an evaluation and improvement methodology.

3. **Conduct:** After the design and development steps are complete, the exercise takes place. Exercise conduct steps include setup, briefings, facilitation/control/evaluation, and wrap-up activities.

4. **Evaluation:** The evaluation phase for all exercises includes a formal exercise evaluation, an integrated analysis, and an AAR/IP that identifies strengths and areas for improvement in an entity's preparedness, as observed during the exercise. Recommendations related to areas for improvement are identified to help develop corrective actions to be tracked throughout the improvement planning phase.

5. **Improvement Planning:** During improvement planning, the corrective actions identified in the evaluation phase are assigned, with due dates, to responsible parties; tracked to implementation; and then validated during subsequent exercises.

### 2.3 Exercise Options

HSEEP is a very versatile tool that allows the user to tailor an exercise to address specific objectives and meet the particular user needs. Integral to this versatility are the multiple exercise options, documentation capabilities, and planning and after action report options that are defined within the HSEEP methodology.

Seven types of exercises are defined within the HSEEP methodology along with guidance for their application. The exercises range from

small scale seminar style events to full scale events (see Figure 1). Each of the exercises is considered to be either discussion-based or operation-based activities.

Discussion-based exercises are used to familiarize participants with current plans, policies, agreements and procedures, or may be used to develop new plans, policies, agreements, and procedures.

Types of discussion-based exercises include:

*Seminar.* An informal discussion, designed to orient participants to new or updated plans, policies, or procedures (e.g., a seminar to review a new Evacuation Standard Operating Procedure).

*Workshop.* Resembles a seminar, but is employed to build specific products, such as a draft plan or policy (e.g., a Training and Exercise Plan Workshop is used to develop a Multi-year Training and Exercise Plan).

*Tabletop Exercise (TTX).* Involves key personnel discussing simulated scenarios in an informal setting. TTXs can be used to assess plans, policies, and procedures, and is probably the most utilized of all exercise types.

*Games.* A simulation of operations that often involves two or more teams, usually in a competitive environment, using rules, data, and procedure designed to depict an actual or assumed real-life situation.

Operation-based exercises are used to validate plans, policies, agreements and procedures, clarify roles and responsibilities, and identify resource gaps in an operational environment.

The types of operation-based exercises include:

*Drill.* A coordinated, supervised activity usually employed to test a single, specific operation or function within a single entity (e.g., a fire department conducts a decontamination drill).

*Functional Exercise (FE).* Examines and/or validates the coordination, command, and control between various multi-agency

coordination centers (e.g., emergency operation center, joint field office, etc.). A functional exercise does not involve any "boots on the ground" (i.e., first responders or emergency officials responding to an incident in real time).

*Full-Scale Exercises (FSE).* A multi-agency, multi-jurisdictional, multi-discipline exercise involving functional (e.g., joint field office, emergency operation centers, etc.) and "boots on the ground" responses (e.g., firefighters decontaminating mock victims).

## 2.4 Exercise Documentation

Documentation is a very important part of any exercise. HSEEP provides information and guidance for seven important document types that can be used for most exercises. The list below briefly describes each of these documents.

*Situation Manual (SitMan).* A participant handbook for discussion-based exercises, particularly TTXs. It provides background information on exercise scope, schedule, and objectives. It also presents the scenario narrative that will drive participant discussions during the exercise.

*Exercise Plan (ExPlan).* Typically used for operation-based exercises. Provides a synopsis of the exercise and is published and distributed to players and observers prior to the start of the exercise. The ExPlan includes the exercise objectives and scope, safety procedures, and logistical considerations such as an exercise schedule. The ExPlan does not contain detailed scenario information.

*Controller and Evaluator (C/E) Handbook.* Supplements the ExPlan for operation-based exercises. Contains more detailed information about the exercise scenario, and describes exercise controllers' and evaluators' roles and responsibilities. Because the C/E Handbook contains information on the scenario and exercise administration, it is distributed only to those individuals specifically designated as controllers or evaluators.

*Master Scenario Events List (MSEL).* A chronological timeline of expected actions and scripted events (i.e., injects) to be inserted into operation-based exercise play by controllers in order to generate or prompt player activity. It ensures necessary events happen so that all exercise objectives are met.

*Player Handout.* A 1-2 page document, usually handed out the morning of an exercise, which provides a quick reference for exercise players on safety procedures, logistical considerations, exercise schedule, and other key factors and information.

*Exercise Evaluation Guides (EEGs).* Help evaluators collect and interpret relevant exercise observations. EEGs provide evaluators with information on the tasks they should expect to see accomplished during an exercise, space to record observations, and questions to address after the exercise as a first step in the analysis process. In order to assist entities in exercise evaluation, standardized EEGs have been created that reflect capabilities-based planning tools, such as the TCL and UTL. The EEGs are not meant to be interpreted as report cards. Rather, they are intended to guide an evaluator's observations so that the evaluator focuses on capabilities and tasks relevant to exercise objectives to support development of the AAR/IP.

*After Action Report/Improvement Plan (AAR/IP).* The final product of an exercise. The AAR/IP has two components: an AAR, which captures observations and recommendations based on the exercise objectives as associated with the capabilities and tasks; and an IP, which identifies specific corrective actions, assigns them to responsible parties, and establishes target dates for completion. The lead evaluator and exercise planning team draft the AAR and submit it to conference participants prior to an After Action Conference (see below). The draft AAR is distributed to conference participants for review no more than 30 days after exercise conduct. The final AAR/IP is an outcome of the After Action Conference

and should be disseminated to participants no more than 60 days after exercise conduct.

## 2.5 Planning and After Action Conferences

The HSEEP methodology defines a variety of planning and after action conferences. The need for each of these conferences varies depending on the type and scope of the exercise. They include:

- Concepts and Objectives Meeting
- Initial Planning Conference
- Mid-Term Planning Conference
- Master Scenario Events List Conference
- Final Planning Conference
- After Action Conference

## 3.0 EMERGENCY ACTION PLANS

The EAP constitutes an essential component of a comprehensive emergency management framework for dam owners and operators, as it plays a crucial role in preventing the loss of life and property damage that can result from the failure of a high-hazard potential dam. The document identifies potential emergency conditions at a dam and specifies pre-planned actions to be followed in order to minimize property damage and loss of life. It is essential because it identifies the area below a dam that would be flooded as a result of a failure; establishes communication between the dam owner and State/local emergency responders; provides for notifications and evacuations conducted by police, fire, and rescue teams; and predicts the timing of the impending flood wave.

It is essential that dam owners develop this critical information and provide it to appropriate responders to effect safe and successful evacuations, save lives, and help keep responders out of danger. An EAP contains procedures and information to assist the dam owner in issuing early warning and notification messages to responsible downstream emergency management authorities of the emergency situation. It also contains inundation maps to show emergency management authorities the critical areas for action in case of an emergency.

The effectiveness of an EAP can be enhanced by using uniform guidelines during its

development. This helps to ensure that all aspects of emergency planning are covered in each plan. Uniform EAPs and advance coordination with local and State emergency management officials and organizations should facilitate a timely response to a developing or actual emergency situation.

### 3.1 EAP Structure

The following guidelines are provided for preparing or revising EAPs for all high and significant hazard potential dams. Ownership and development of the floodplain downstream from each dam varies; therefore, the potential for loss of life as a result of failure or operation of a dam will also vary. It is very important that the EAP for a given dam be tailored to the particular needs and site-specific conditions that exist at that dam.

An EAP generally contains six basic informational elements:

1. Notification Flowchart
2. Emergency Detection, Evaluation, and Classification
3. Responsibilities
4. Preparedness
5. Inundation Maps
6. Appendices

While the dam owner is responsible for the development or revision of the EAP, it must be done in coordination with those having emergency management responsibilities for the affected areas at the State and local levels. Emergency management agencies need and will use the information in a dam owner's EAP to facilitate the implementation of their responsibilities. Brief descriptions of the six basic elements of an EAP are listed below.

1. *Notification Flowchart*. Shows the priority chain of notification. The information on the notification flowchart is necessary for the timely notification of persons responsible for taking emergency actions.
2. *Emergency Detection, Evaluation, and Classification*. Early detection and evaluation of the situation(s) or triggering event(s) that initiate or require an emergency

action are crucial. The establishment of procedures for reliable and timely classification of an emergency situation is imperative to ensure that the appropriate course of action is taken based on the urgency of the situation. It is better to activate the EAP while confirming the extent of an emergency than to wait for the extent of the emergency to be confirmed.

3. *Responsibilities.* A determination of responsibility for EAP-related tasks must be made during the development of the plan. Dam owners are responsible for developing, maintaining, and implementing the EAP. State and local emergency management officials having statutory obligation are responsible for warning and evacuation within affected areas. The EAP must clearly specify the dam owner's responsibilities to ensure that effective, timely action is taken should an emergency occur at the dam. The EAP must be site-specific because conditions at the dam and downstream of all dams are different.
4. *Preparedness.* Actions taken to moderate or alleviate the effects of a dam failure or operational spillway release and to facilitate response to emergencies. This section identifies actions that should be taken before an emergency.
5. *Inundation Maps.* Delineate the areas that would be flooded as a result of a dam failure. Inundation maps are used both by the dam owner and emergency management officials to facilitate timely notification and evacuation of areas affected by a dam failure or flood condition. These maps greatly facilitate notification by graphically displaying flooded areas and showing travel times for flood peaks at critical locations.
6. *Appendices.* Contain information that supports and supplements the material used in the development and maintenance of the EAP.

It is vital that development of the EAP be coordinated with all stakeholders, jurisdictions, and agencies that would be affected by a dam failure and/or flooding as a result of large operational releases, or that have statutory

responsibilities for warning, evacuation, and post-flood actions. The finished product should be user friendly as it realistically takes into account each organization's capabilities and responsibilities.

Coordination with State and local emergency management officials at appropriate levels of management responsible for warning and evacuation of the public is essential to ensure that there is agreement on their individual and group responsibilities. Participation in the preparation of the EAP and in exercises where the EAP is tested will enhance confidence in the EAP and in the accuracy of its components. Coordination will provide opportunities for discussion and determination of the order in which public officials would be notified, backup personnel, alternate means of communication, and special procedures for nighttime, holidays, and weekends.

The tasks and responsibilities of the dam owner and emergency management officials during dam emergencies need to be as compatible as possible. To facilitate compatibility, the dam owner should coordinate emergency response actions with local emergency management officials who have the responsibility to provide a timely warning and evacuation notice to the population at risk. This should help prevent over, or under, reaction to the incident by various organizations.

#### 4.0 APPLICATION TO REGIONALLY-BASED, MULTIPLE DAMS EXERCISES

The HSEEP framework is particularly useful for exercise efforts involving multiple dams, which have dominant regional and multi-jurisdictional characteristics when the corresponding scenarios trigger significant cascading impacts affecting extended areas. These types of exercises provide an effective mechanism to identify any required improvements to the EAPs of the individual facilities and the local, State, and Federal agencies involved. They are an important vehicle to increase preparedness and resilience at the regional level.

DHS has utilized HSEEP for conducting two separate exercise efforts involving multiple dams and cascading impacts with regional and

multi-jurisdictional effects. The first effort was conducted in 2008 in collaboration with USACE and other partners across the Dams Sector. It consisted of as a series of exercises focused on enhancing protection efforts against manmade attacks and improving preparedness, response, and rapid recovery in the event of an attack, natural disaster, or other emergency. The second effort is currently underway and involves significant flooding of several dams and communities along the Columbia River Basin in the Pacific Northwest. It also consists of a series of exercises and is a collaborative effort with USACE and other partners across the Dams Sector.

#### 4.1 2008 Dam Security Exercise Series–Bagnell/Truman (DSES-08)

The 2008 Dam Security Exercise Series–Bagnell/Truman (DSES-08) was a series of exercises designed to test existing interoperability and communications protocols between government and non-government entities facing a catastrophic security-related event involving two dams located along the same river basin. DSES-08 was comprised of multiple events, including a series of workshops, a tabletop exercise, and a functional exercise.

The events associated with DSES-08 involved Bagnell Dam, owned by AmerenUE, and Harry S. Truman Dam and Reservoir, owned by the USACE Kansas City District. Additional participants included DHS, the Missouri State Emergency Management Agency, and other Federal, State, local agencies, and private entities. DSES-08 was developed by an Exercise Planning Team comprised of representatives from all participating entities. The exercise series consisted of four main activities: an EAP Workshop, an Inundation Modeling and Mapping Workshop, a Security TTX, and a Functional Exercise (FE). The first three activities were conducted on August 7, 2008 in Lake of the Ozarks, Missouri. The fourth activity was conducted on September 17, 2008 in Jefferson City, MO. A total of 311 personnel from 64 organizations attended all DSES-08 events.

DSES-08 sought to exercise interagency interoperability and communications in response

to all-hazard, dam emergencies to improve Truman Dam and Bagnell Dam EAPs, and readiness of associated critical infrastructure and key resources (CIKR). Exercise participants successfully exercised the EAPs in workshop and FE forums that validated the plans and will guide refinements to established procedures. The FE scenario involved a response to terrorist attacks. The FE scenario facilitated participants' review of roles and responsibilities, coordinate and integrate capabilities, examine planning processes, identify issues and seek solutions. The FE included agency participation from Missouri and Washington DC, as well as representatives from the Dams Government Coordinating Council and the Sector Coordinating Council, who participated from their respective locations across the US (see Figure 2).

DSES-08 provided many valuable lessons learned in five functional areas: Exercise Organization Planning and Execution; Communications, Information Sharing and Interoperability; EAP Scope; Inundation Modeling and Mapping; and Interaction with Local and State Agencies. In particular, challenges in communication protocols faced during the exercise underscored the critical need to ensure that plans incorporate redundant means of communications, and that users receive adequate training on the use of incident management communications systems.

DSES-08 successfully utilized the HSEEP program in achieving exercise objectives, including exercising interagency interoperability and communications in response to almost-simultaneous security-related incidents at multiple dams. These efforts clearly assisted in improving the readiness conditions at the participating projects, as well as the information dissemination framework established across the sector.

#### 4.2 2009 Dams Sector Exercise Series–Columbia River Basin (DSES-09)

The 2009 Dams Sector Exercise Series–Columbia River Basin (DSES-09) consists of a series of exercises involving significant flooding in the Pacific Northwest, affecting several dams along the Columbia River Basin. Participants in this effort include the Pacific Northwest Economic Region, DHS, USACE, and various

stakeholders in the Pacific Northwest region. The primary objective of DSES-09 is to facilitate the development of an Integrated Regional Strategy to improve disaster resilience and preparedness initially for the Tri-Cities area of Washington State (Kennewick, Pasco, and Richland) and ultimately for the broader Columbia River basin.

The DSES-09 effort consists of pre-exercise training seminars, a series of TTXs, and follow-up after action/strategy workshops. DSES-09 is currently underway and is utilizing the HSEEP methodology as the framework for all exercise components. The versatility of HSEEP is proving integral to achieving the primary objective of the exercise series, which is the development of an Integrated Regional Strategy to improve disaster resilience and preparedness across multiple sectors and jurisdictions.

DSES-09 is being conducted with a somewhat unique approach. The effort has been divided into five tracks. Each track is being conducted separately with completion scheduled to complement the other tracks as the overall effort progresses. Each track is briefly described below.

*Track 1 - Modeling and Mapping.* Use existing models to estimate hydrological and hydraulic conditions based on weather and dam operations, update inundation maps, and identify additional modeling requirements.

*Track 2 - Pre-Disaster Operational Response.* Examine the effectiveness of plans and procedures for dams with regards to communication, coordination, roles and responsibilities, information-sharing, and response and mitigation procedures associated with cascading events that could create a potentially catastrophic inundation scenario in the Tri-Cities area.

*Track 3 - State and Local Preparedness/Emergency Response.* Identify disaster management challenges during a major regional flood within multiple highly populated communities that consist of CIKR, some of which pose unique environmental concerns.

*Track 4 - Long-term Restoration/Economic Resilience.* Address issues related to assessing consequences of a major flood event on CIKR and associated regional infrastructure interdependencies, duration of disruptions, impacts on recovery and longer-term restoration, and potential prevention and mitigation measures.

*Track 5 - Integrated Regional Strategy.* Develop an Integrated Regional Strategy that leverages lessons learned from the series of exercises in order to improve regional disaster resilience.

Track 1 entailed the creation of a Modeling and Mapping Workgroup to address modeling approaches and capabilities that can be leveraged from other efforts. The initial focus was on updating inundation maps and refining the scenario, which is being used during Tracks 2, 3 and 4. The workgroup conducted a Modeling and Mapping Workshop to assist with exercise development.

Tracks 2, 3, and 4 consist of a concepts and objectives meeting, training seminar, TTX, and post-exercise workshop for each track. These tracks are designed to help build the Integrated Regional Strategy. The workgroups for Tracks 2-4 are being tailored to include additional stakeholder organizations beyond those in Track 1, as appropriate.

Finally, Track 5 will include development of an AAR/IP to identify lessons learned and assign responsibilities for areas that require improvement. The results of the first 4 tracks as well as the AAR/IP will be integrated into a regional strategy for the Columbia River basin in the Pacific Northwest region.

## 5.0 CONCLUDING REMARKS

EAPs and exercises are essential components of comprehensive emergency management planning for dam owners and operators. An EAP is essential for major dams in order to save lives and reduce property damage in areas that would be affected by dam failure. Exercises are the primary tool for dam owners to test EAPs and other emergency procedures, assess emergency response capabilities, and identify

areas for improvement. The HSEEP methodology is a capabilities and performance-based tool that provides guidance for exercise design, development, conduct, evaluation, and improvement planning. The HSEEP framework is scalable and easily applied to regionally-based, multi-dam scenarios that involve multi-jurisdictional and multi-agency components. It is an invaluable tool for dam owners and operators for improving their preparedness, response, and recovery capabilities. Large scale exercises such as DSES-08 and DSES-09 provide an excellent opportunity for building coordination and compatibility.

## 6.0 REFERENCES

1. "Homeland Security Exercise and Evaluation Program, (HSEEP), Volume 1: Overview and Exercise Program Management," Federal Emergency Management Agency, National Preparedness Directorate, U.S. Department of Homeland Security.
2. Seda-Sanabria, Yazmin, Norton, Douglas J., Matheu, Enrique E., Empson, William B., and Hunter, John W., "Application of the Homeland Security Exercise and Evaluation Program (HSEEP) Framework to the 2008 Dam Security Exercise Series (DSES-08)," *29<sup>th</sup> USSD Annual Meeting and Conference*, Nashville, TN.
3. "Emergency Action Planning for State Regulated High-Hazard Potential Dams, FEMA 608," Federal Emergency Management Agency, August 2006.
4. "Federal Guidelines for Dam Safety: Emergency Action Planning for Dam Owners, FEMA 64," Interagency Committee of Dam Safety, U. S. Department of Homeland Security, Federal Emergency Management Agency, 1998.

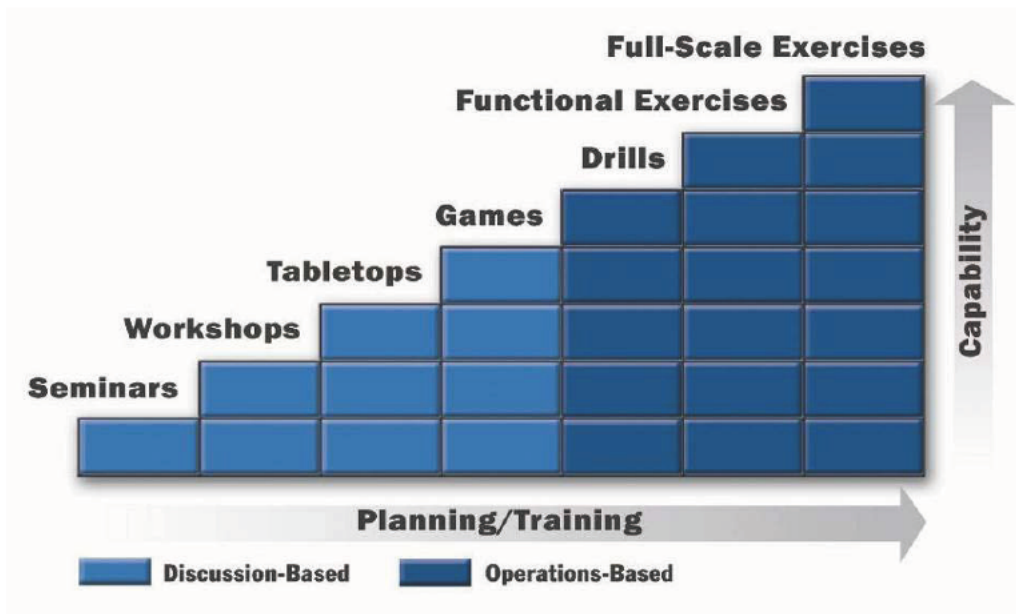


Figure 1. Exercise Types

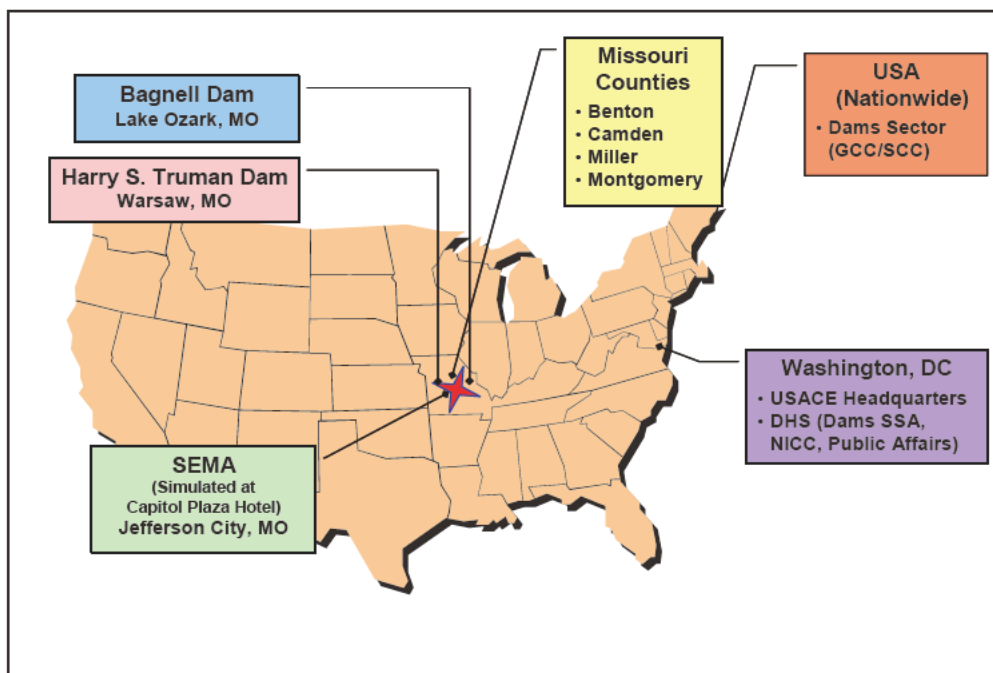


Figure 2. DSES-08 Functional Exercise Locations

## Damage to Dams due to the Iwate-Miyagi Nairiku Earthquake in 2008

by

Yoshikazu Yamaguchi<sup>1</sup>, Tomoya Iwashita<sup>2</sup> and Shinya Mitsuishi<sup>3</sup>

### ABSTRACT

The large earthquake, the Iwate-Miyagi Nairiku Earthquake in 2008 mainly struck the mid Tohoku Region in northeastern Honshu Island, Japan on June 14, 2008. The magnitude of the event was estimated as 7.2 in the JMA scale. Based on the results of the emergency inspections of 134 dams by the site officers immediately after the earthquake, on June 15 and 16, dam engineering experts carried out site investigation at the five dams where damage had been found. This paper described the outlines of the results of the preliminary investigations of the five dams. According to the investigation, no problems severe enough to threaten the structural safety of any of the five dams were found. This verified the high level of seismic resistance of the dams in Japan.

**KEYWORDS:** Dam, Damage, Deformation, Earthquake, Investigation, Leakage

### 1. INTRODUCTION

The large earthquake, the Iwate-Miyagi Nairiku Earthquake in 2008 mainly struck the mid Tohoku Region in northeastern Honshu Island, Japan at 8:43 am on Saturday morning, June 14, 2008. The strongest shaking was measured in Oshu City, Iwate Prefecture and Kurihara City, Miyagi Prefecture, both at 6 Upper of the Japan Meteorological Agency (JMA) seismic intensity.

Landslides triggered by this earthquake crushed structures, buried people, cut off road traffic, and isolated local communities. Mud from landslides dammed up rivers to form lakes, so called "quake lakes", which could threaten the safety of their downstream areas. By 13:30, July 30, 13 people were confirmed dead, 450 injured, and 10 still missing. A total of 28 homes were destroyed, 99 partly destroyed, and 1,382 partly damaged. (Fire and Disaster Management

Agency, 2008) [1]

No nuclear power plant was shut down following this earthquake, unlike the case of Kashiwazaki-Kariwa nuclear power plant after the Niigataken Chuetsu-oki Earthquake in 2007. Several sections of express highways in the Tohoku Region were closed, then all were reopened by nightfall, except for one section where a traffic restriction was maintained because of repair works. Some JR East train services were suspended on Shinkansen, Japanese superexpress, and local lines, then resumed from the first trains on the following day. (Cabinet Office, 2008) [2]

The Technical Emergency Control Force (TEC-FORCE) organized by Ministry of Land, Infrastructure, Transport and Tourism (MLIT) dispatched many experts to the event area to investigate damage to infrastructures and houses and provide technical support for emergency countermeasures on the day of the earthquake. To conduct emergency investigations of dams, the authors, all dam engineering experts, were dispatched to five dams damaged by this earthquake from June 14 through 16, 2008. This paper reports the results of the on-site survey of damage to and safety evaluation of the dams which were surveyed.

### 2. PROFILE OF THE EARTHQUAKE

The earthquake occurred at 8:43 am on June 14, 2008. The Japan Meteorological Agency (JMA) named the event the Iwate-Miyagi Nairiku

---

<sup>1</sup> Team Leader, Dam Structure Research Team, Hydraulic Engineering Research Group, Public Works Research Institute (PWRI), Tsukuba City, 305-8516 Japan

<sup>2</sup> Deputy Team Leader, ditto

<sup>3</sup> Head, Water Management and Dam Division, River Department, National Institute for Land and Infrastructure Management (NILIM), Ministry of Land, Infrastructure, Transport and Tourism (MLIT), Tsukuba City, 305-0804 Japan

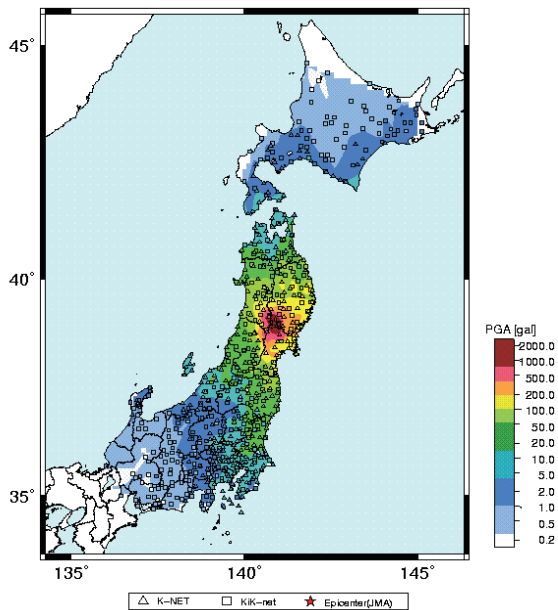


Fig.1 Peak ground acceleration contour map based on KiK-net and K-NET operated by NIED (NIED, 2008) [3]

Earthquake in 2008. Here, the term of “Nairiku” means inland. The magnitude of the event was estimated as 7.2 in the JMA scale and its epicenter was located at 39°01.7’N, 140°52.8’E, about 85 kilometres north of Sendai City and about 385 kilometres north-northeast of Tokyo. The depth of the epicenter is estimated at about 8km. The fault is a thrust fault in the compression in the WNW to ESE direction.

National Research Institute for Earth Science and Disaster Prevention (NIED) operates the strong motion instrumentation networks, K-NET and KiK-net. Strong motions were recorded at 330 and 325 stations respectively. Based on their data, a peak ground acceleration contour map was drawn as shown in Figure 1. The KIK-net station, IWTH25 almost on the earthquake fault recorded over 1g of peak acceleration at the location of underground level -260m where S-wave velocity is 1.8km.

### 3. SPECIAL SAFETY INSPECTION OF DAMS BY SITE OFFICERS

Immediately after the earthquake, special safety inspections of dams were made by the site officers within the river reaches administered

under the River Act. The special safety inspections consisted of primary and secondary inspections; the former were visual inspections immediately after the earthquake, and the latter were detailed visual inspections and safety checks using data measured by installed instruments.

The primary emergency inspections were conducted at 134 dams, with secondary inspections performed at 77 of these dams. The results of the emergency inspection confirmed damage to the dam bodies and the slopes around dam reservoirs at 12 dams.

### 4. EMERGENCY INVESTIGATION OF DAMS BY TEC-FORCE EXPERTS

As a result of emergency inspections by dam site officers, of those dams reported to be damaged, the authors who were expert members of TEC-FORCE, performed site surveys of dams managed and operated directly by the national or prefectural government which were reported damaged, in response to requests by site officers to perform surveys. The on-site surveys were performed on June 15 and 16 at five dams operated by MLIT, Miyagi Prefecture, and Akita Prefecture. The locations of five dams surveyed are shown in Figure 2. The following are outlines of the results of the surveys of the five dams. Note that because this paper reports the results of the preliminary investigation, the information and the observed data could be corrected afterwards.

#### 4.1 Ishibuchi Dam

Ishibuchi Dam is a concrete faced rockfill dam (CFRD) with a dam height of 53m completed in 1953, and managed by Tohoku Regional Bureau, MLIT. Figure 3 is the cross section and longitudinal section of the dam. The upstream concrete face maintains the watertightness of dam body of this type of dam. No severe damage was found in the concrete face and its joints shown in Photo. 1.

At the crest of the dam, the pavement was wavy and cracked shown in Photos. 2 and 3. And gaps appeared on the boundary between the

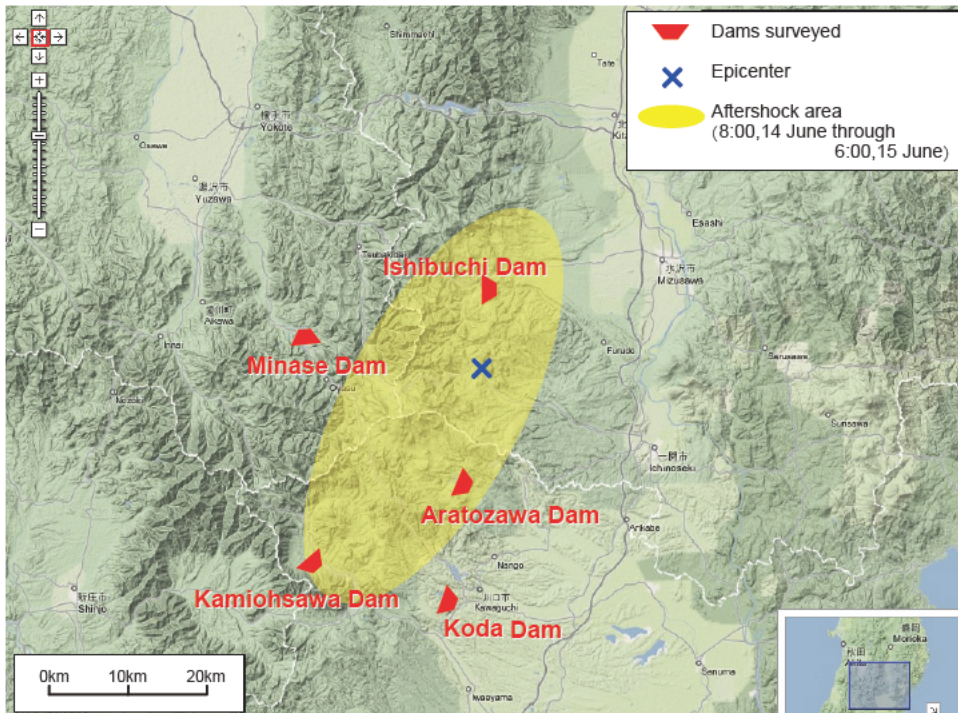


Fig. 2 Location map of the five dams surveyed immediately after the earthquake by TEC-FORCE experts

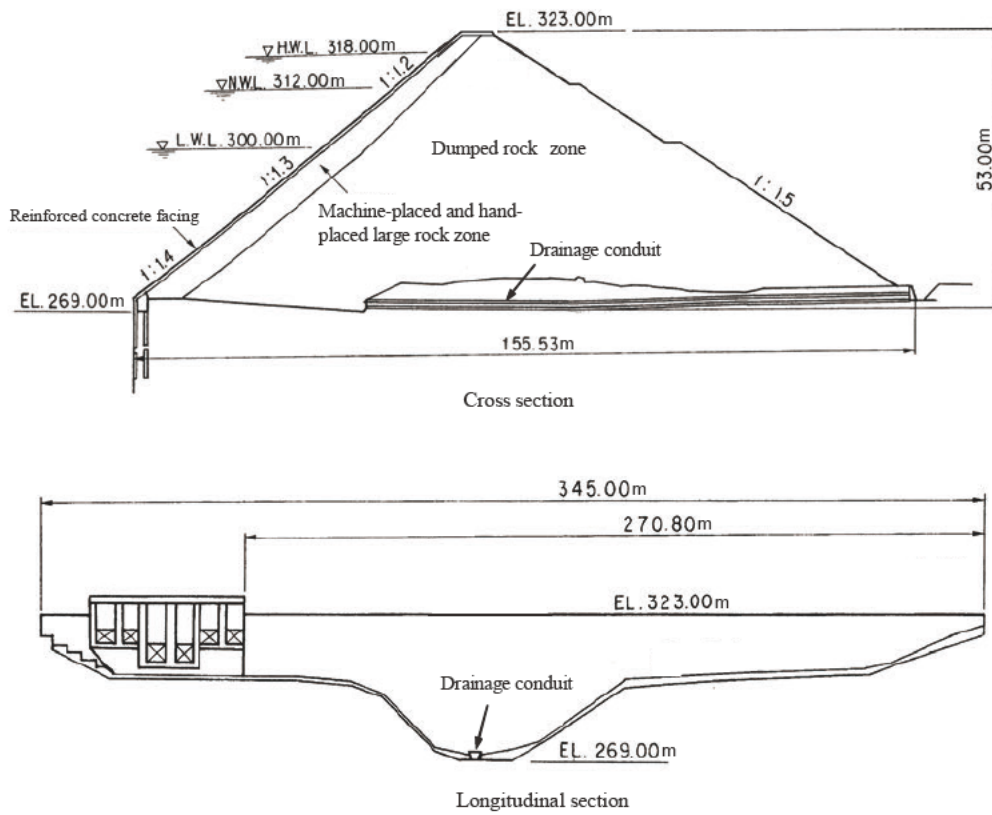


Fig. 3 Cross section and longitudinal section of Ishibuchi Dam

railing and pavement on the shoulder of the slope at the crest. On the downstream slope surface of the dam, projections were observed on the rock materials at the protruding parts of the wave on the crest pavement shown in Photos. 4 and 5, but damage of this kind was limited to high elevations. This dam was constructed by the dumped rock construction method as shown in Photo. 6 taken during construction. The piers for the railroad from where trucks dropped rock materials were left buried in the dam body. It is hypothesized that the whole dam body settled due to the earthquake, while the areas near the buried piers only settled a little. The maximum differential settlement is supposed to be about 50cm.

Leakage through the upstream concrete face and the shallow foundation, which is measured at the downstream slope toe, has increased since the occurrence of the earthquake. However, its amount was below the maximum amount which had ever been observed at the dam and has performed a stable behavior with a dependence on the reservoir level. Turbid leakage water was also observed after the earthquake, but it returned to normal after a few days.

A seismometer installed on the top of the downstream slope (elevation of the crest) recorded the maximum acceleration of 1,461 gal in the stream direction and 2,070 gal in the vertical direction, but this record might include



Photo.1 Concrete faced upstream slope on which no damage was found (Ishibuchi Dam) (Photographed by Public Works Research Institute (PWRI) on June 15, 2008)



Photo.2 Overview of the crest and downstream slope (Ishibuchi Dam) (Photographed by PWRI on June 15, 2008)



Photo.3 Cracks and waving of the crest pavement (Ishibuchi Dam) (Photographed by PWRI on June 15, 2008)



Photo.4 Gaps between the railing and pavement on the crest (Ishibuchi Dam) (Photographed by PWRI on June 15, 2008)



Photo.5 Projection of the riprap rocks around the top of the downstream slope (Ishibuchi Dam) (Photographed by PWRI on June 15, 2008)



Photo.6 Ishibuchi Dam under construction by the dumped rock method in 1950's (The piers of tramway were buried.) (Courtesy by Kitakami River Integrated Dam Management Office, MLIT)

local shaking of the large size rock on which the seismometer was installed, so further analysis is necessary.

Based on the results of emergency investigation, it was decided that no serious problems threatened the safety of the dam, but careful monitoring has been continued and the technical committee has been established to make a detailed survey to prepare for restoration of the dam.

#### 4.2 Aratozawa Dam

Aratozawa Dam is an earth core rockfill dam (ECRD) with a dam height of 74.4m completed in 1998. It was constructed by Tohoku Regional Agricultural Administration Office, Ministry of Agriculture, Forestry and Fisheries (MAFF) and is managed by Miyagi Prefecture.

Huge landslides occurred around the reservoir on the left bank upstream from the dam. The largest landslide was 1.3km long, 0.8km wide, and approximately 67 million m<sup>3</sup> in volume as shown in Photo. 7 of an aerial photograph. Approximately 1.5 million m<sup>3</sup> of this landslide soil flowed into the reservoir. This corresponds to about 10% of the reservoir capacity of 14.13 million m<sup>3</sup>.

Maximum settlement of about 20cm was



Photo.7 Huge landslides around the reservoir of Aratozawa Dam (Photographed by PWRI on June 15, 2008)

measured at the upstream slope shoulder of the dam crest. The surveying target was installed on the rock zone surface. Because the pipe of a crossarm gauge protruded about 40cm shown in Photo. 8, it is hypothesized that the large settlement occurred at the core zone in the center of the crest rather than at the rock zone. Regardless of the large settlement, no conspicuous cracks were found on the crest pavement surface shown in Photo. 9. In addition, no deformation of the riprap on the upstream



Photo.8 The pipe of a crossarm gauge protruded, as a result of the settlement of the dam body (Aratozawa Dam) (Photographed by PWRI on June 16, 2008)



Photo.9 Few cracks in the crest pavement in spite of the dam body settlement (Aratozawa Dam) (Photographed by PWRI on June 16, 2008)

and downstream surfaces was found.

In the inspection gallery beneath the impervious core zone, a small amount of leakage was discovered through fine cracks in its ceiling and from the boundary between the upstream side wall and invert. And small openings caused by the earthquake were observed at the joints of blocks of the gallery.

The measured leakage through the dam body and shallow foundation increased immediately after the earthquake, but it was steadily declining by the time of our survey on June 16, 2008.

A seismometer installed in the dam foundation recorded earthquake motion dominant in the high frequency domain and maximum acceleration of about 1g in the stream direction. At the crest, a maximum acceleration of 525gal was recorded in the stream direction.

Based on the results of emergency investigation, it was judged that no serious problems threatened the safety of the dam at the time of our investigation. MAFF has established a technical committee and started a detailed survey to prepare for restoration of the dam.

#### 4.3 Minase Dam

Minase Dam is a CFRD with a dam height of

66.5m completed in 1963. The surface concrete facing had already been repaired with asphalt paving for the appropriate watertightness. It was constructed by MILT (then Ministry of Construction (MOC)) and is managed by Akita Prefecture.

No cracks were confirmed on the pavement at the crest. Crest settlement of about maximum 14cm was observed, and at the connection of the spillway and the rockfill dam body, a level difference of about 15cm formed shown in Photo. 10. No deformation was confirmed on the upstream facing and the downstream rock slope surface.

The amount of leakage through the upstream concrete face and shallow foundation increased until 210L/min on the day after the earthquake, but after then it decreased with falling the reservoir level.

At the time of the investigation, it was decided that its condition was not in a state that would immediately threaten the safety of the dam.

#### 4.4 Kamiohsawa Dam

Kamiohsawa Dam is an earthfill dam with a dam height of 19m completed in 2003. It was constructed and is managed by Miyagi Prefecture.

A few cracks with maximum width of 10mm

stream direction was a maximum of 5 to 6cm,

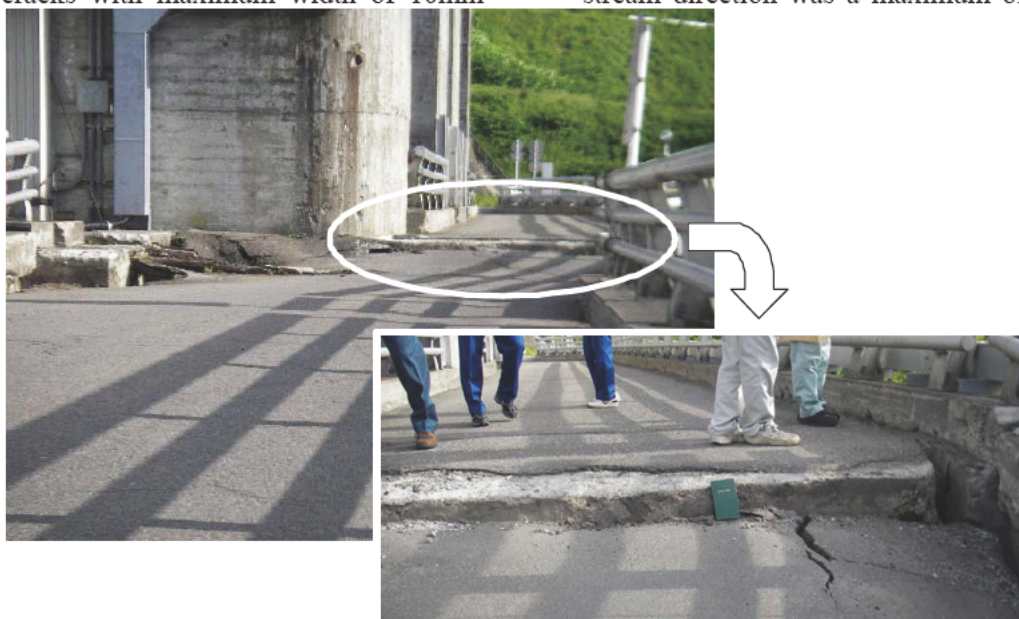


Photo.10 Level difference occurred at the connection of the spillway concrete and the rockfill dam body as a result of the settlement of the dam body (Minase Dam) (Photographed by PWRI on June 15, 2008)

occurred on the crest pavement. The L-shaped curbstones on the crest were pushed up at one place. Maximum settlement of 14.4cm was observed at the dam crest, but this is hypothesized to be largely an impact of foundation settlement whose maximum value is 14.8cm.

Leakage increased by about 10L/min from 27.27L/min before the earthquake to a maximum of 39.34L/min after the earthquake, but it had stabilized by the time of our survey on June 15, 2008.

It was judged that the no conditions which could threaten the safety of the dam existed.

#### 4.5 Koda Dam

Koda Dam is an ECRD with a dam height of 43.5m completed in 2005. It was constructed by Tohoku Regional Agricultural Administration Office, MAFF and is managed by Miyagi Prefecture.

The settlement at the crest was a maximum of 3.8cm and the horizontal displacement in the



Photo.11 The damaged curbstone on the crest shoulder (Koda Dam) (Photographed by PWRI on June 16, 2008)

but the horizontal displacement in the dam axis direction was a little large at a maximum of about 13cm. And the curbstones on the crest were partially damaged by compression as shown in Photo. 11. No conspicuous cracks were, however, found on the crest pavement. And the riprap on the upstream and downstream sides was free of any deformation.

Leakage doubled from 90.8L/min before the

earthquake to a maximum of 194.4L/min. after the earthquake, but at the time of our survey on June 16, 2008, it was gradually decreasing. The turbidity of the leakage rose after the earthquake, but was tending to decline by the time of our survey.

It was judged that there were no conditions which could threaten the safety of the dam.

## 5. CONCLUSIONS

The Iwate-Miyagi Nairiku Earthquake of 2008 did not cause any damage to dams which were severe enough to possibly threaten their safety. This verifies the high level of seismic resistance of the dams.

Based on the results of the emergency inspections of the dams by the site officers immediately after the earthquake, dam engineering experts carried out site investigation at the five dams where damage had been found. According to the preliminary investigation, no problems severe enough to threaten the structural safety of any of the five dams were found. At present, repair works for damaged dams have already been started or finished based on the results of detailed inspections and surveys.

In Japan, dam sites are selected after a detailed geological survey. The dams are designed by performing careful structural analyses based on the design criteria, and are constructed under strict management with high quality materials. These careful survey, design and construction efforts help to ensure the safety of the dams. However, dams are large, important structures

which must not fail. This earthquake caused the most severe damage to dams of any earthquake which has occurred in Japan in recent years. In the seismic acceleration observed at the dams, although the high frequency range was dominant, the maximum acceleration level was the highest ever recorded. Based on these facts, in the future, we plan to perform detailed surveys of the effect of this earthquake to dams and reflect the findings in development of future seismic research and technology for dams.

## 6. ACKNOWLEDGEMENTS

This survey was conducted with the generous cooperation of River Bureau and Tohoku Regional Bureau of MLIT, and Miyagi Prefecture and Akita Prefecture. The authors are deeply grateful to members of these organizations for their kind assistance.

## 7. REFERENCES

1. Fire and Disaster Management Agency, Government of Japan (2008): *The Iwate-Miyagi Nairiku Earthquake in 2008, 72nd edition*, <http://www.fdma.go.jp/detail/811.html> (in Japanese)
2. Cabinet Office, Government of Japan (2008): *About the Iwate-Miyagi Nairiku Earthquake in 2008*, <http://www.bousai.go.jp/kinkyu/iwate/2008-iwate-cao-027.pdf> (in Japanese)
3. National Research Institute for Earth Science and Disaster Prevention (NIED) (2008): *Strong Motions due to the Iwate-Miyagi Nairiku Earthquake in 2008*, <http://www.hinet.bosai.go.jp/topics/iwate-miyagi080614/> (in Japanese)

## **THEME 3**

# **Wind Engineering**

# Experimental Studies on Internal Pressure and Debris Strike for Improved Tornado Induced Loads of Low-Rise Buildings

by

Partha P Sarkar<sup>1</sup> and Hitomitsu Kikitsu<sup>2</sup>

## ABSTRACT

This paper presents the results of experimental studies on transient wind loads on a low-rise building induced by a tornado. The ISU Tornado Simulator at Iowa State University was used for these experiments. The internal pressure and risk of wind-borne debris strike was considered for improved prediction of these dynamic wind loads. It is shown that the magnitude of internal pressure determines the total wind uplift force on the roof and that its characteristics depend on the extent of natural leakage in the building walls as well as location of dominant openings on any of these walls. Further, the laboratory experiments show that the risk of wind-borne debris strike in a tornado increases with decreasing distance between potential wind-borne debris and target building and the characteristic of this risk depends on whether the potential debris is located within or outside the region defined by a distance of one tornado-core radius from the target building.

**KEYWORDS:** Tornado, Tornado simulator, Wind loads, Internal-pressure, Wind-borne debris

## 1.0 INTRODUCTION

Tornadoes produce rotating winds with updraft and downdraft and radial flows that intensify significantly near the ground. In most commonly occurring tornadoes that are EF-2 or of less intensity on the newly implemented Enhanced Fujita Scale, winds could reach 60 m/s (135 mph, 3-sec gust) near the ground. As a result of passage of a tornado directly over a building, transient loads are produced that peaks when the center of the tornado is within one core radius, where maximum tangential wind speed occurs, from the center of the building (Sengupta et al., 2008). In this study, only external surface

pressures were measured to evaluate the loads on a low-rise cubic building. The importance of internal pressure inside a building in modifying the resultant uplift force on the roof of the building was recognized in this study but not explored because of some limitations in the model. It is known that the internal pressure inside a building is a function of air leakages through the building envelope because of intrinsic porosity that is present in the envelope and any dominant opening that could be triggered by a puncture in the envelope by wind-borne debris. This paper studies the role of internal pressure in producing the resultant wind loads in a tornado-like vortex as a function of porosity and dominant opening in a building envelope and attempts to find the strike probabilities of wind-borne debris that could create these dominant openings as a function of their relative location to the building. This work will improve the predictions of wind loads on low-rise buildings in a tornado and contribute to a probability-based design framework.

## 2.0 ISU TORNADO SIMULATOR PARAMETERS USED

Laboratory experiments in this study were carried out using the ISU tornado simulator at Iowa State University (ISU). Figure 1 illustrates the concept of the simulator with a schematic diagram. The details of this facility are given in Haan, et al. (2008). In these experiments, the translation speed of the tornado was fixed at 0.15m/s. The other tornado simulator parameters such as fan speed, vane angle and floor height were the same as those of “Vane 5” test case in the study by Haan, et al. (2008). A tornado-like vortex with a swirl ratio of 1.14 and radius of the tornado core of 0.53 m, where the maximum tangential velocity (= 9.7 m/s in this case) occurs, was obtained by fixing these parameters.

### 3.0 EVALUATION OF WIND FORCE CHARACTERISTICS

#### 3.1 Pressure Model Details

Tornado-induced surface pressures were measured on a low-rise building model with 152.4mm by 97.5mm (6.0in. by 3.8in.) in plan dimensions and an eave height of 48.8mm (1.92in.). The shallow roof angle of the model was 1/12 (4.76°) with the roof ridge parallel to the longer dimension. The configuration of this model is the same as that used in the study by Oh et al. (2007). The model was made out of plexiglass and contained 20 pressure taps on the roof surface and 16 pressure taps on the four walls to measure the external pressure distribution and a single pressure tap to measure the internal pressure.

The geometric and velocity scale ratios were 1/250 ( $\lambda_L$ ) and 1/10 ( $\lambda_{vel}$ ), respectively. The internal volume of the model was scaled also to maintain similarity of the dynamic response of the volume at model scale to that in full scale. The internal volume scale ( $\lambda_{vol}$ ), as defined below, was calculated as follows:

$$\lambda_{vol} = \frac{\lambda_L^3}{\lambda_{vel}^2} = \frac{1}{156,250} \quad (1)$$

In order to achieve this scale, a sealed volume chamber was installed at the bottom of the model so that its internal volume was increased proportionately based on the scaling law above.

Dominant openings and leakage through the building envelope were taken into consideration to evaluate the characteristics of internal pressure during the passage of a tornado with the building placed along the centerline of the tornado path. The building was oriented with its shorter wall normal to the translation direction of the tornado. Table 1 shows the geometry and opening ratio of dominant openings and leakage, where the opening ratio ( $r$ ) is defined as the area of the opening to the total surface area of the building walls. Leakage in a real building will be distributed uniformly on the building envelope, comprising of walls and roof, and is a result of

the porosity that naturally occurs in the building material.

#### 3.2 Wind Pressure Measurement

High speed electronic pressure scanner (Scanivalve ZOC33/64Px) was used to measure the pressure distribution on the building model. Data were sampled for 24 seconds at the rate of 500Hz (12,000 data points). The initiation of data acquisition and the crane movement were synchronized using a common external trigger. The overall forces acting on the model were estimated by integrating the surface pressures. Wind pressure coefficients, as shown in the next section, were normalized using the respective maximum tangential velocity,  $V_{\theta max}$ , and then ensemble averaged over 10 identical data runs.

#### 3.3 Results of Wind Pressure Experiments

##### 3.3.1 Characteristics of wind force on the roof (z-direction)

Figures 3 and 4 show the results of wind force coefficients in  $z$  direction as obtained from the pressure coefficients. Horizontal axis is the distance between the center of the tornado vortex and the center of the building model,  $x$ , normalized by the diameter of the tornado core,  $D$ .

(1) *Experimental cases where there are only leakages on walls (see Figure 3)*

Absolute value of external wind pressure coefficient,  $C_{pe}$ , increased as the simulator approached the model. It became maximum when  $x/D$  was  $\approx \pm 0.5$  and minimum when  $x/D$  was zero. In contrast, absolute value of internal wind pressure (suction) coefficient,  $C_{pi}$ , became maximum when  $x/D$  was zero where the maximum value increased with the opening ratio ( $r$ ) of leakage which resulted in the maximum value of wind force coefficient,  $C_{Fz}$ , at  $x/D$  of  $\approx \pm 0.5$ ; these values were around 2.6 in the case of  $r=0.04\%$  and around 1.8 in the case of  $r = 0.13\%$ .

(2) *Experimental cases where there are leakages ( $r=0.13\%$ ) on walls and a dominant opening on*

one wall (see Figure 4)

In the experimental cases where there were not only distributed leakages but also a dominant opening on one wall, it was found that characteristics of the wind force on the roof depend on the location of the dominant opening. First, for the cases of dominant opening on wall #1 or #4, the value of  $C_{Fz}$  became maximum when  $x/D$  was  $\approx 0.5$ , since the absolute value of  $C_{pi}$  was bigger when  $x/D$  was negative. In contrast, for the cases of dominant opening on wall #2 or #3 the characteristics of  $C_{Fz}$  showed different tendency from those above and it became maximum when  $x/D$  was  $\approx -0.5$ . The internal pressure helped to reduce the peak uplift force on the roof significantly with a dominant opening present on wall # 1 or # 3 but not so much when the opening was on wall # 2 or # 4. The rotating wind enters the building through the opening on walls # 2 or # 4 and induces a positive internal pressure that reduces the magnitude of the internal pressure (suction) inside the building as induced by the static pressure drop inside the tornado core.

The value of  $C_{Fz}$  in each case discussed above was zero, when the center of vortex reached the center of model. The value of  $C_{pi}$  in each case had high correlation with the value of  $C_{pe}$  of the tap that was nearest to the dominant opening.

### 3.3.2 Characteristics of wind force on the wall ( $x$ - and $y$ -direction)

Figure 5 shows the results of wind force coefficients in both  $x$  and  $y$  directions for the case where there are only distributed leakages ( $r=0.13\%$ ). As the tornado moves from the negative to the positive  $x$  direction, the value of  $C_{Fx}$  shows that the model was pulled first in the negative direction and then in the positive direction. The value of  $C_{Fy}$  follows the pattern of the tangential velocity component of the vortex. The tangential velocity exerted a positive  $C_{Fy}$  as the vortex first encountered the model, and then the value changed sign as the opposite side of the core passed over the model. The maximum of both  $C_{Fx}$  and  $C_{Fy}$  occurred very close to  $x/D = \pm 0.5$  (i.e. at the radius of the vortex). This result is similar to those reported in Sengupta et al.

(2008), where internal pressures were not considered, proving that internal pressure does not influence the overall loads on the walls that occur because of leakage.

## 4.0 PROBABILITY OF WIND-BORNE DEBRIS STRIKE

### 4.1 Experimental Setup

The low-rise building model and its orientation with respect to the tornado's translation axis, as used for the experiments discussed in this section of the paper, are the same as those of experiments discussed earlier in Section 3.1. Models of most commonly occurring wind-borne debris, i.e. 2 x 4 timber components, were made out of thick paper. Mass and reference area of the debris model were chosen to match those of the full scale based on Tachikawa number,  $K$ , as defined here:

$$K = \frac{\rho_a V^2 A}{2Mg} \quad (2)$$

where  $\rho_a$  is air density,  $V$  is tornado wind velocity,  $A$  is reference area,  $M$  is mass, and  $g$  is acceleration due to gravity, respectively, where velocity scale was calculated as 1/7. Table 2 shows the values of  $V$ ,  $A$ , and  $M$  used here.

### 4.2 Method for Evaluation of the Strike Risk

For the case where the tornado approaches the building along its centerline, the probability of wind-borne debris striking the building walls was estimated in the following way. Figure 6 shows the number of each wall and location of potential wind-borne debris in normalized coordinates ( $x^*$ ,  $y^*$ ) as normalized by the radius of the vortex core,  $R$ .

Two hundred debris models were put at each location of potential wind-borne debris and then forced to scatter through the passage of the tornado simulator. By counting the number of the debris models which entered the model through the opening on the target wall ( $\#k$ ), the probability ( $p_k$ ) of wind-borne debris striking the target wall  $\#k$  were generated for each

location  $(x^*, y^*) = (i, j)$ , as follows:

$$p_k(i, j) = \frac{n_k}{n_0} \quad (k=1, \dots, 4) \quad (3)$$

$$= \frac{1}{n_0} \cdot \left[ \bar{N}_k(i, j) + \frac{t_\alpha}{\sqrt{3}} \cdot S_k(i, j) \right]$$

where  $n_0=200$ ,  $\bar{N}_k$  and  $S_k$  are mean and standard deviation of the sample number of debris models entering through the target opening in three trials, and  $t_\alpha$  is 4.3 as listed in the Table of T distribution. Based on Equation (3) and the assumption that the strike of wind-borne debris on each wall are mutually independent, probability of wind-borne debris striking the building as a function of its location  $(x^*, y^*) = (i, j)$ ,  $P$ , can be obtained by the following equation:

$$P(i, j) = \sum_{k=1}^4 p_k(i, j) \quad (4)$$

### 4.3 Results of Experiment and Risk Evaluation

Figure 7 shows a snap shot of debris models flying around the building model and Figure 8 shows the probability of strike by wind-borne debris on each wall,  $p_k$ . The dark-gray filled circles in Figure 8 indicate the locations where the highest five probabilities were obtained.

Compared with the probability of strike on wall #2 or #4, probability corresponding to wall #1 was very small. This is because the direction of tangential wind velocity at  $y^*=0$  is not perpendicular but parallel to that of wall #1. Strike probability corresponding to wall #3 was the same as that of wall #1. Strike probability corresponding to wall #2 or #4 increased with decrease in distance between potential location of debris generation and target building model. Moreover, while distribution of probabilities of strike on wall #4 was symmetric with respect to  $x^*$  axis, strike probabilities corresponding to wall #2 was not symmetric in the region of  $-1 < x^*$ . It is noted that probability was quite small in the region, defined by the dotted line  $-1 < x^*$  and  $0 < y^*$ , because as the tornado simulator passes over the building model the debris models within the dotted region are picked up and thrown away from the model instead of striking wall # 2

which is located on the other side of this region.

Probabilities of debris strike based on Equation (4) are summarized in Figure 9. With respect to the potential debris locations in the region of  $x^* < -1$ , all the probabilities shows a trend of inverse proportionality to the value of  $x^*$  raised to some power ( $1/x^{*n}$ ). The power exponent (n) of  $x^*$  was calculated as 0.51 for  $y^* = 0$ , and 0.30 for  $y^* = \pm 1$ . In contrast, in the region of  $-1 \leq x^* \leq 0$ , probabilities for different  $y^*$  follows different trend from one another. While the value for  $y^* = -1$  is constant, approximately 0.45, the value for  $y^* = 1$  had a gap at  $x^* = -1$ , which is seen in Figure 8(b). Further, the probability for  $y^* = 0$ , the value for  $-1 < x^* < 0$  can be estimated by interpolating values between  $x^* = -1$  and 0.

According to the results as discussed above, it is concluded that the characteristics of the risk of wind-borne debris strike on a building depends on whether or not the potential debris are located within a distance equivalent to the radius of tornado core from the center of the target building.

### 5.0 CONCLUSION

This paper summarizes the results of experimental studies related to wind hazards to low-rise buildings posed by tornadoes. The ISU tornado simulator at Iowa State University was used for these experiments. With respect to the results of wind pressure experiments, it was observed that the magnitude of internal pressure determines the total wind uplift force affecting the roof and that its characteristics depend on the magnitude of the distributed leakage and location of a dominant opening on the wall. Further, with respect to assessing risk of wind-borne debris strike, the experimental results show that the probability generally increases with decreasing distance between potential wind-borne debris and target building and the characteristics of the probability depends on whether the location of the potential debris is within or outside the region defined by one core radial distance of the tornado from the building center.

## 6.0 REFERENCES

Haan, F.L., Sarkar, P.P. and Gallus, W.A. (2008). "Design, Construction and Performance of a Large Tornado Simulator for Wind Engineering Applications." *Engineering Structures*, Vol. 30 (4), 1146-1159.

Oh, J.H., Kopp, G.A. and Inculet, D.R. (2007). "The UWO Contribution to the NIST Aerodynamic Database for Wind Load on Low Buildings: Part 3. Internal pressures." *Journal of Wind Engineering and Industrial Aerodynamics*, Vol. 95, 755-779.

Sengupta, A., Haan, F.L., Sarkar, P.P. and Balaramudu, V. (2008). "Transient Loads on Buildings in Microburst and Tornado Winds." *Journal of Wind Engineering and Industrial Aerodynamics*, Vol. 96 (10-11), 2173-2187.

Tachikawa, M. (1983). "Trajectories of Flat Plates in Uniform Flow with Application to Wind-Generated Missiles." *Journal of Wind Engineering and Industrial Aerodynamics*, Vol.14, 443-453.

Table 1: Geometry and ratio of dominant openings and leakage

Description of opening		Dimension (model scale)	Opening ratio, $r$
Distributed leakage	Two holes on each wall #1, 3	d=1.0mm	~0.04%
	Four holes on each wall #2, 4	d=1.8mm	~0.13%
Dominant opening		20.8mm x 7.6mm (wall #1, 3) 32.5mm x 7.6mm (wall #2, 4)	3.3%

Table 2: Parameters related to  $V$ ,  $A$ , and  $M$

	Full scale ( $f$ )	Model scale ( $m$ )
V	68m/s	9.7m/s
A	53cm x 10cm	3cm x 1.7cm
Mg	910g	0.2g

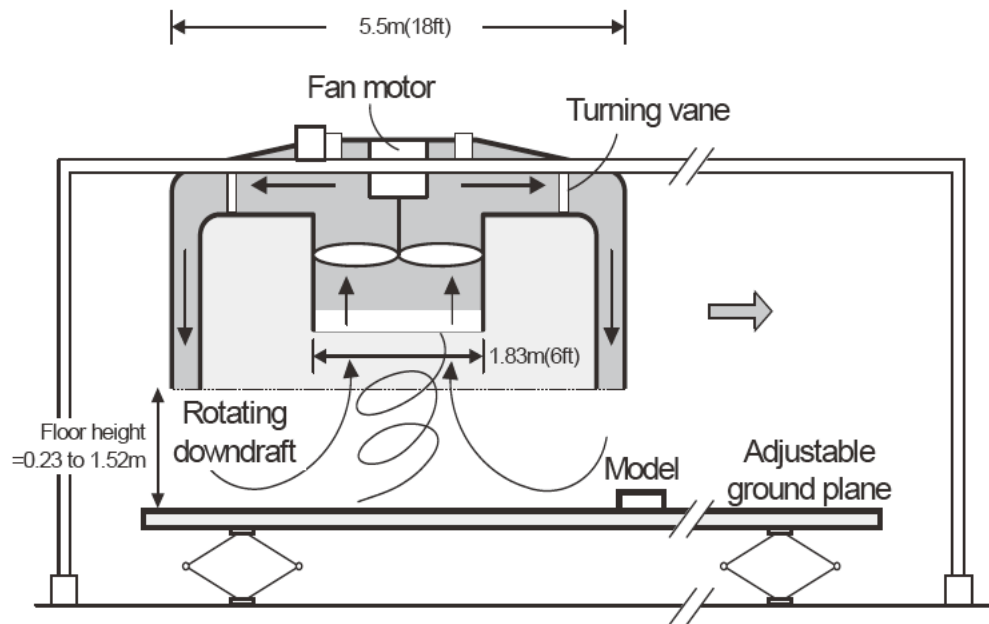


Figure 1: Schematic illustration of ISU Tornado Simulator

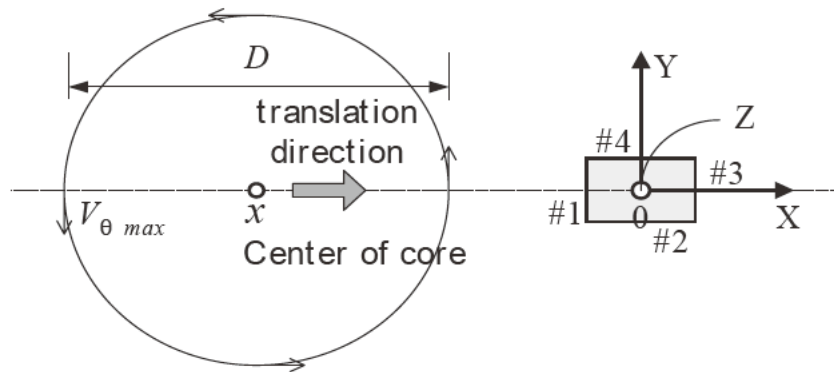
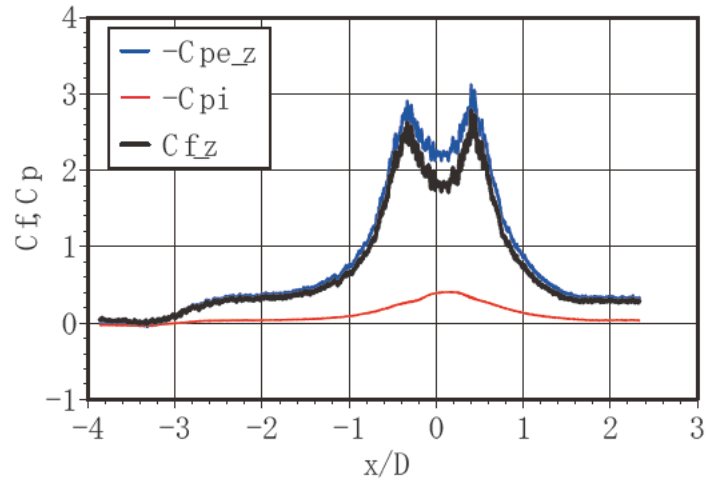
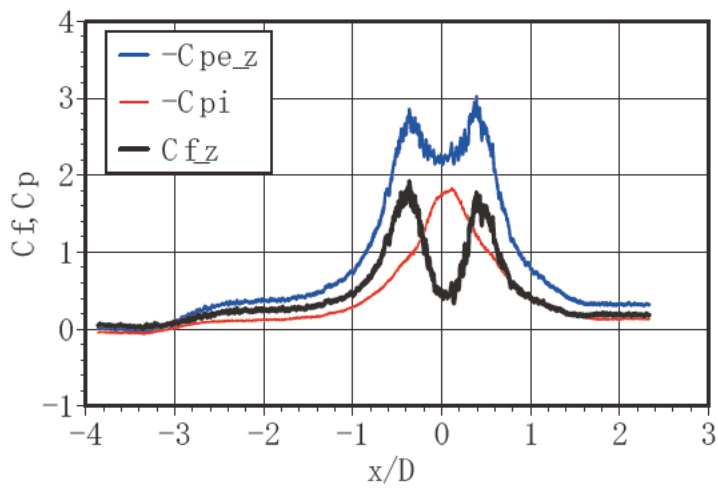


Figure 2: Definition of wall number and coordinates

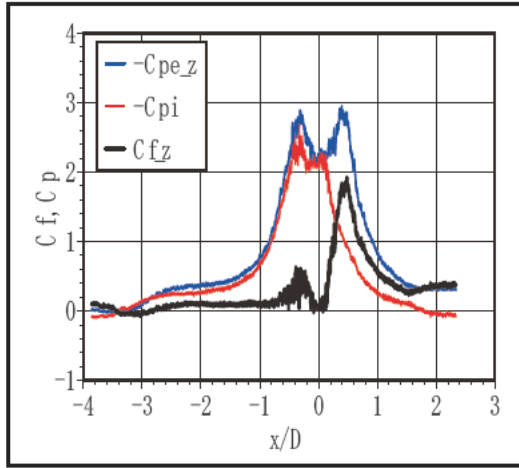


(a)  $r = \sim 0.04\%$

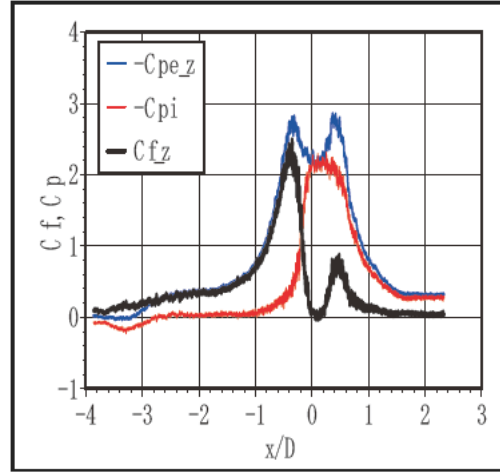


(b)  $r = \sim 0.13\%$

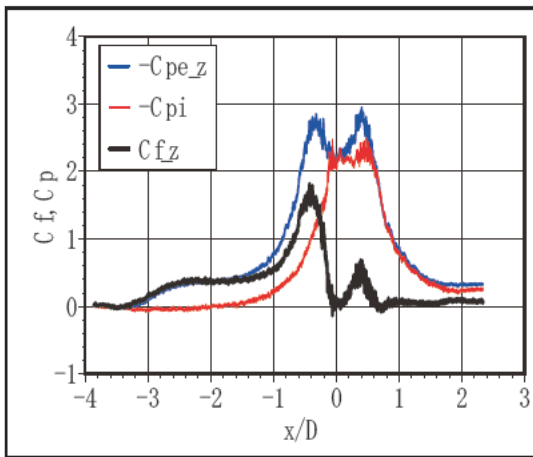
Figure 3: Wind Force Coefficients,  $C_{Fz}$  (Leakages Only)



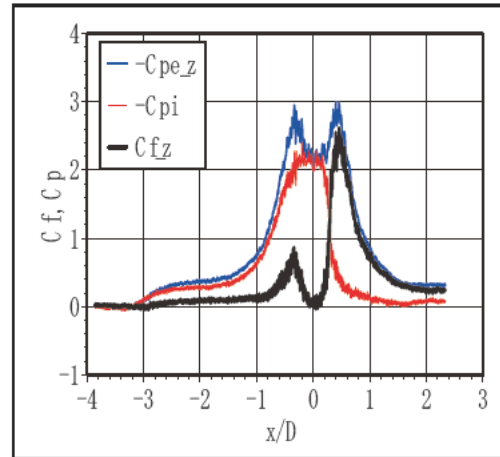
(a) Opening on Wall #1



(b) Opening on Wall #2



(c) Opening on Wall #3



(d) Opening on Wall #4

Figure 4: Wind Force Coefficients,  $C_{Fz}$ , (Dominant Opening plus Leakage)

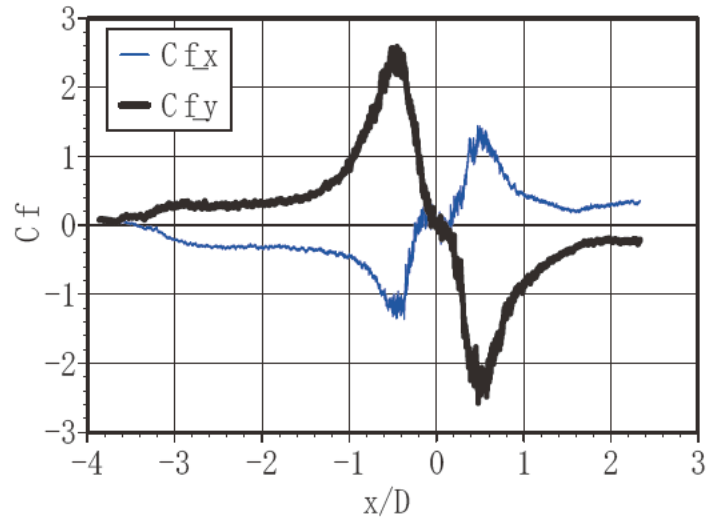


Figure 5: Wind Force Coefficients,  $C_{Fx}$ ,  $C_{Fy}$

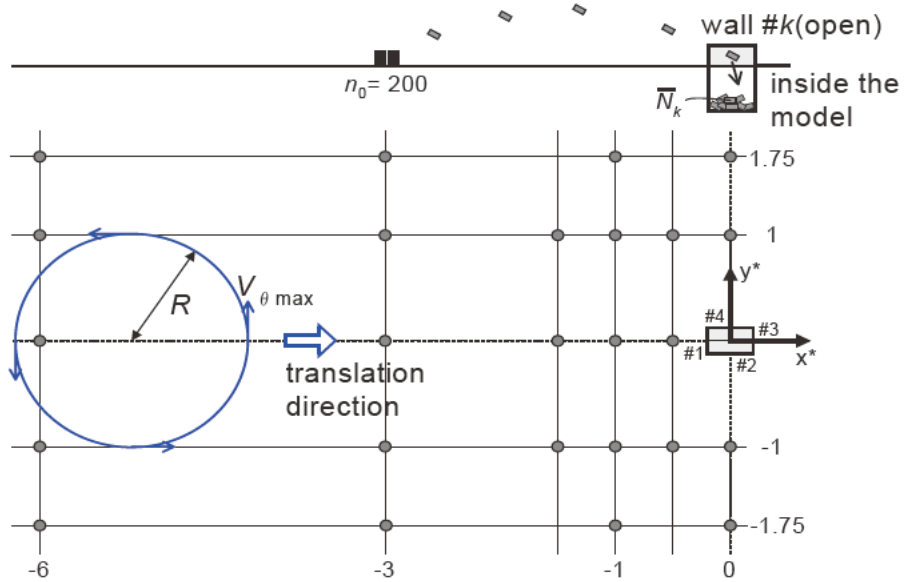
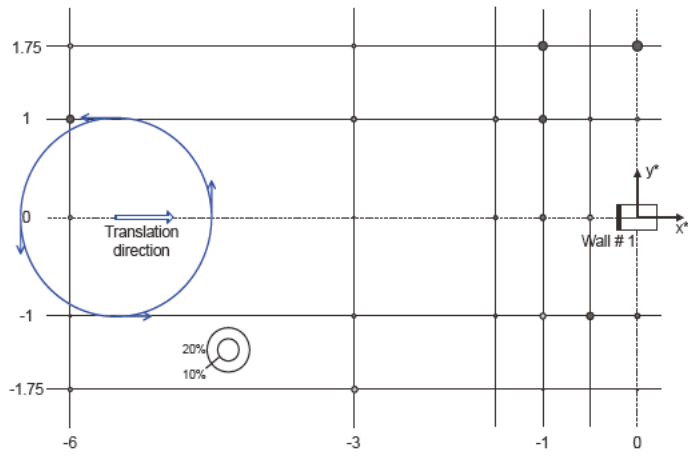


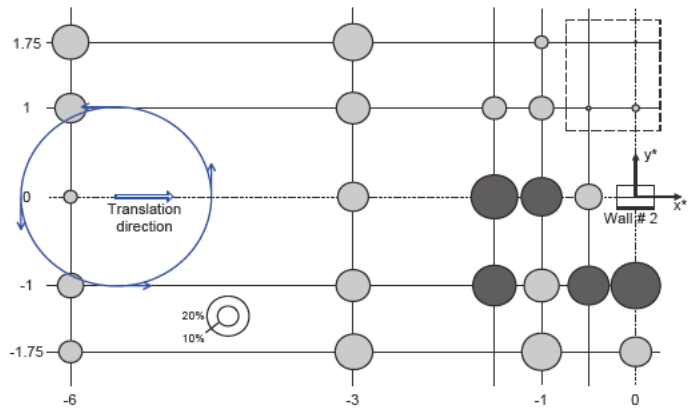
Figure 6: Definition of Wall Number, Coordinates, and Location of potential wind-borne debris in normalized coordinates ( $x^* = x/R$ ,  $y^* = y/R$ ) shown as dark dots.



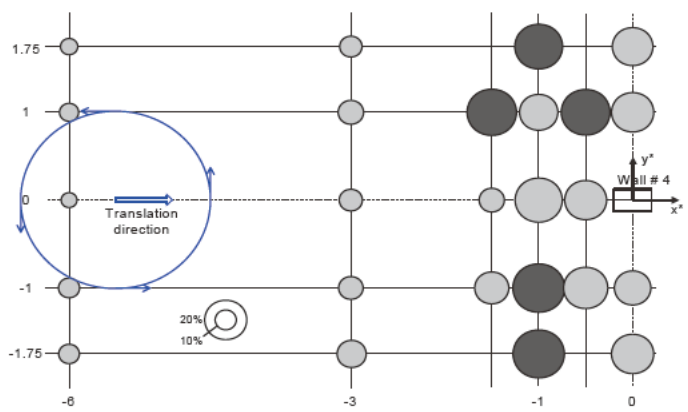
Figure 7: Debris models flying around building model



(a) Probability of Debris Strike on Wall #1,  $p_1(i, j)$



(b) Probability of Debris Strike on Wall #2,  $p_2(i, j)$



(c) Probability of Debris Strike on Wall #4,  $p_4(i, j)$

Figure 8: Probability of debris strike on each wall

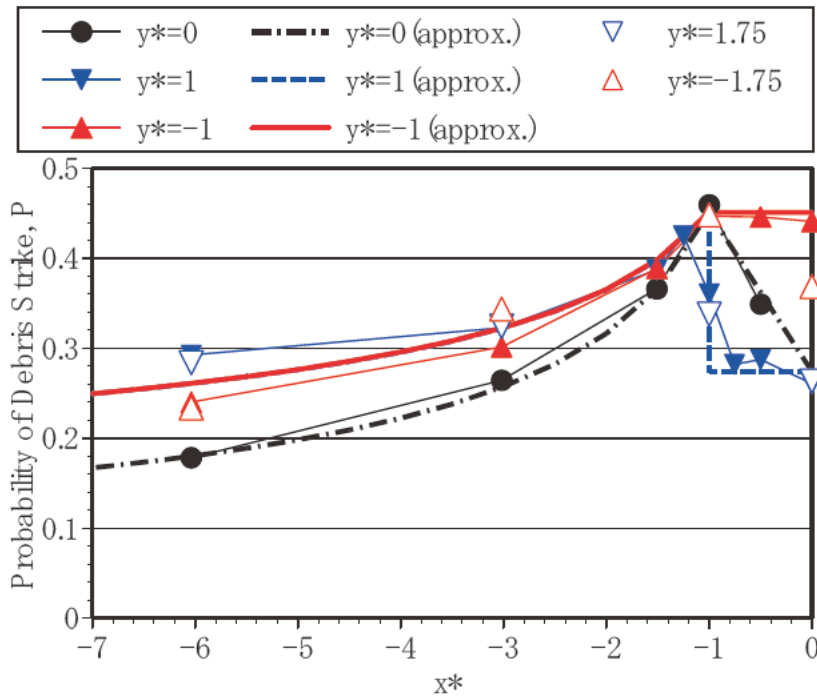


Figure 9: Probability of debris strike vs. Location of potential wind-borne debris

# Damage to Buildings by EF5 Tornado in Iowa, U.S. on May 25, 2008

by

Hitomitsu Kikitsu<sup>1</sup> and Partha P Sarkar<sup>2</sup>

## ABSTRACT

A major tornado struck the towns of Parkersburg and New Hartford, located in the north-central region of Iowa in United States, on May 25, 2008. This is the only EF5 tornado to occur in 2008. This paper summarizes the extent of the structural damage to buildings induced by this tornado. Results of field survey show the region where there were lots of seriously damaged buildings and typical modes of damage of these residential, public and commercial buildings. Further, based on the post disaster survey, rates of progress in recovery and replacement of damaged houses are shown.

**KEYWORDS:** Tornado, Damage Survey, Enhanced Fujita Scale

## 1. INTRODUCTION

A major tornado struck the towns of Parkersburg and New Hartford, located in the north-central region of Iowa in United States, on May 25, 2008 (Sunday) around 5 pm (CST). These towns are located slightly north of highway US-20 and east of Interstate I-35. Parkersburg, a town of 1,900, is about 80 miles northeast of Des Moines, the capital of Iowa. The counties that were affected by this natural disaster were Black Hawk, Buchanan, Butler and Delaware. The tornado touched down at 4:48 pm (CST) two miles south of Aplington near the Butler-Grundy county line, and moved 43 miles to the east until it lifted off at 5:58 pm (CST). The 43-mile damage path was 0.5 mile (800 m) wide near Parkersburg, 1/4-mile wide east of New Hartford and 1.2 miles wide north of Dunkerton before the tornado dissipated.

As per the clarification on damage assessment by Iowa Homeland Security and FEMA released on May 30, 621 houses were estimated to be damaged of which 394 were destroyed, 65 had

major damage and 162 had minor damage. There were eight casualties, six at Parkersburg and two at New Hartford. These casualties contributed to the rising national death toll from tornadoes in 2008 (111 to date) which has already proven to be the worst year in a decade in terms of number of tornado occurrences (605 total to date).

Of the 1,691 tornado occurrences in 2008<sup>1)</sup>, 207 or ~12% of the total were rated EF2 or higher - 148 EF2, 49 EF3, 9 EF4 and 1 EF5. The Parkersburg-New Hartford tornado is the only EF5 tornado to occur in the US this year and the only EF5 tornado to occur in Iowa in last 32 years; the last F5 tornado occurred in the Boone and Story counties of Iowa in 1976 in which 88 houses were destroyed but there were no serious injuries.

The co-authors of this paper carried out a field survey of the damaged area and buildings on May 26-27 and May 30 at Parkersburg and New Hartford. Assistance during the field survey from the office of National Weather Service at Johnston, Iowa is acknowledged.

## 2. TORNADO INTENSITY AND RELATED DAMAGE

Information on the tornado intensity and related damage as it appeared in the press releases of State of Iowa<sup>2)</sup>, the local newspapers (e.g. the Des Moines Register<sup>3)</sup>), and US National Weather Service is summarized below.

The US National Weather Service has rated this tornado as EF5 on the newly adopted Enhanced Fujita Damage Scale or EF-Scale with an estimated wind speed of 205 mph (92 m/s). Although EF5 is the highest rating on the

---

<sup>1</sup> Senior Researcher, National Institute for Land and Infrastructure Management, MLIT, Tsukuba-shi, Ibaraki-ken 305-0804 JAPAN

<sup>2</sup> Professor, Iowa State University, IA, USA

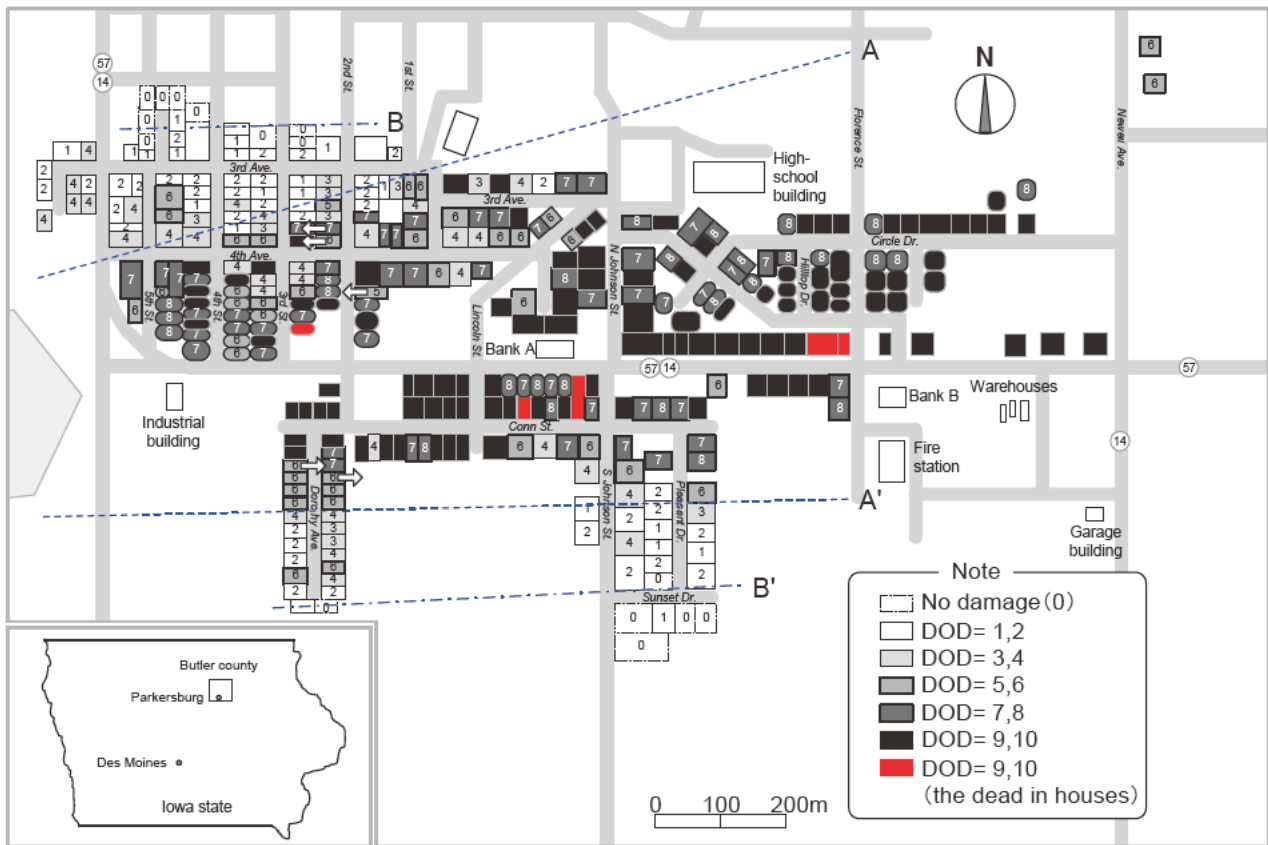


Figure 1 Distribution of damage to buildings in Parkersburg, IA

tornado intensity scale, the estimated wind speeds barely exceeded the range of wind speeds assigned to the EF4 scale (166-200 mph). In this regard, the tornado was at the low end of the EF5 scale.

Statistics of structural and other types of damages and fatalities are as follows:

- As of May 30, in Butler, Buchanan, Black Hawk, and Delaware counties, 621 houses were estimated to be damaged in the storm of which 394 were destroyed, 65 had major damage and 162 had minor damage. In addition, 21 businesses including 4 major ones and a high school were damaged. The City Hall in Parkersburg was also destroyed.
- As of May 28, 7 persons were dead because of the storm. The ages of the 5 persons who died in Parkersburg range from 71 to 80 years and the 2 persons who died in New Hartford were 48 and 71 years old. At least 50 persons were injured of which one was in critical condition.
- There were 1,002 electrical outages in Parkersburg. Of these, 320 were in homes or businesses that were destroyed.

### 3. TORNADO-INDUCED STRUCTURAL DAMAGE

#### 3.1 Damage Distribution of Buildings in Parkersburg

A rough map of Parkersburg showing the locations of the damaged buildings is given in Figure 1. Damage state of each house correspond to the degree of damage or DOD regulated for one- or two-family residences as shown in Table 1<sup>4)</sup>. The damage state is defined as DOD of 1 to 10 in EF scale. DOD of 1 to 4 indicate damage states in which non-structural components are mainly damaged, while DOD of 5 and more indicate damage states related to structural components including destruction of entire structure.

The most severe damage area, where almost all the houses were collapsed, is along highway 57th, Conn street, N Johnson street, and Circle street. Therefore, it can be estimated that the center of tornado vortex passed through highway 57th. According to the local newspaper, the casualties occurred in several

houses that were located along the estimated path.

Generally, it can be noted that the boundary between severely damaged area and quite less damaged one is more distinguishable in tornado-induced damage than in the case of typhoon-induced damage<sup>5)</sup>. Based on that, line A – A' (Fig. 1) can be approximate boundary between structural components' related damage and non-structural components' related damage. Also line B – B' can be approximate threshold of visible damage to buildings. This result shows that houses suffering structural damage range in width of approximately 400 – 600m, and that houses suffering mostly non structural damage range in width of approximately 200m in both sides.

Table 1 Degree of damage for one- or two-family residences in EF scale<sup>4)</sup>

DOD	Damage description
1	Threshold of visible damage
2	Loss of roof covering material (<20%); gutters and/or awning; loss of vinyl or metal siding
3	Broken glass in doors and windows
4	Uplift of roof deck and loss of significant roof covering material (>20%); collapse of chimney; garage doors collapse inward; failure of porch or carport
5	Entire house shifts off foundation
6	Large sections of roof structure removed; most walls remain standing
7	Exterior walls collapsed
8	Most walls collapsed, except small interior rooms
9	All walls
10	Destruction of engineered and/or well constructed residence; slab swept clean

### 3.2 Damage to Public and Commercial Buildings

Under this category of buildings is High-School, Bank, Car-Wash, Garage, Warehouse, Fire-Station and Industrial Buildings and Grain Bins or Tanks. Most of these were engineered buildings. Damage to each of these categories is described next.

#### (1) High-school Building

Damage to the high school building is shown below. The walls were made out of one external layer of brick and mortar and one internal layer of unreinforced concrete masonry unit (or CMU) and mortar, placed side by side while spanning between reinforced concrete columns. The roof was flat and it was supported by light steel truss spanning between the walls. It is observed that walls of the classrooms along the west side (Photos 1, 2) and those along the east side (Photos 3 – 4) were completely destroyed. Photo 5 shows the exposed steel reinforcement of the collapsed column that was part of a wall along the east side. Extensive roof damage of the school gymnasium can be seen in Photos 2, 3 and lots of broken glass were found scattered all around. The clock in Photo 1 shows the time of destruction when it stopped at 4:55 pm (CST).

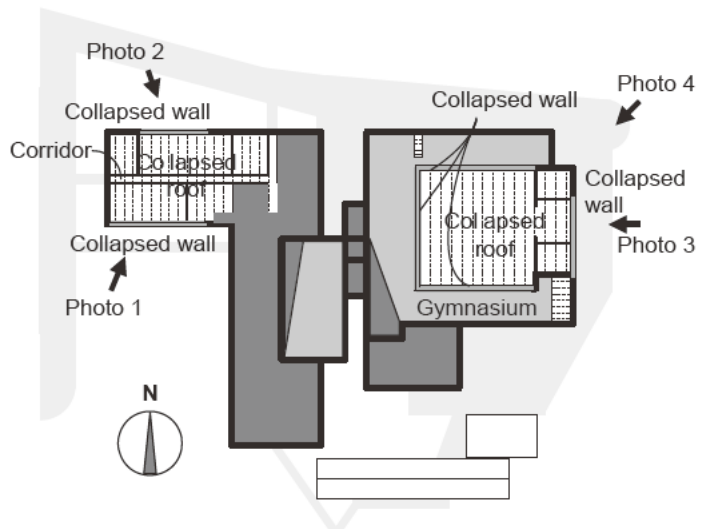


Figure 2 Damage to high-school building



Photo 1 Collapse of wall of classroom



Photo 2 Collapse of wall and roof of classroom



Photo 3 Collapse of wall and roof



Photo 4 View of collapsed wall



Photo 5 Failure of structural elements reinforced with bars

### (2) *Bank Buildings*

Damage to Bank A and Bank B buildings is shown in Photos 6, 7, and Photo 8, respectively. These were regular timber constructions with a brick veneer. The structural damage to Bank A building such as collapse of a wall resulted in much more devastation than that of Bank B building. It is surprising to note that although Bank A building, in spite of its location right along the tornado path, was the only building that stood and was not completely demolished. It should be noted that this was a newer construction.



Photo 6 View of damage from the south (Bank A)



Photo 7 View of south west corner showing collapse of a portion of south wall (Bank A)



Photo 8 Damage to roof canopy (Bank B)

### (3) Fire Station

Damage to a fire station is shown in Photos 9 – 10 below. The fire station sustained minor damage but all seven out of its eight overhead shutters on the western side were completely lost (Photo 9). This is a typical metal building

structure with metal cladding and steel frame. This building was not in the direct tornado path and is located close to the water tank on the southern side of the tornado path.



Photo 9 West side of fire-station



Photo 10 North side of fire-station

### (4) Industrial Building

An industrial steel framed building with gable roof and a large roof span took the first hit from the tornado as it was located at the south-western corner of the town where the tornado first approached Parkersburg. The entire building was destroyed and only the concrete slab remained. The twisted steel frame and corrugated sheet metal are seen in Photo 11 and failed steel components and sheared welded joints are seen in Photo 12. All the columns of the building were sheared from their base.



Photo 11 Destroyed structural elements



Photo 12 Failed steel component

*(5) Warehouses and Garage Building*

There were three warehouses (A, B and C) on Figure 1. Each of three warehouses has individual compartment rooms attached with shutters, which are arranged in line in both east and west sides. Damage to Warehouse A is shown in Photos 13 – 15. This one is located on the eastern-most end of the three warehouses that were built side by side and is the largest amongst the three warehouses. The end-most roof truss of this warehouse on the north side (Photo 15) and most of the roof on the east side are lost (Photo 13).

This warehouse sustained much more damage to its roof and shutters compared to the garage. This could be because it was closer to the path of the tornado than the garage. It is evident that a few of the shutters in the warehouse were pulled outward that is consistent with the loading produced by suction in the tornado vortex (Photo 14).

Figure 3 shows distribution of damage to roof

cover, shutter and wall of all the three warehouses in plan view. This shows marked contrast of damage states between east and west sides in each warehouse: there are severe damage to roofing systems and not so much damage to shutters in east side of each warehouse, while there are severe damage to shutters in west side of each one. Moreover, with respect to damage to shutters, almost all the damaged shutters in east sides were pulled outward as shown in Photo 14, while all the damaged ones in west side were pushed inward.

Damage to a vehicle garage is shown in Photos 16 – 17. The roof cover on the west side of the vehicle garage is lost. This building has a gable roof with its ridge oriented along the east-west direction. It is observed in Photo 16 that the damage to the roof and its gable end occurred at the west end which was the leading edge of the rotating flow. The overhead shutters that were on the north side performed very well, as seen in the photo. Photo 17 shows flying debris impact on the west wall.



Photo 13 Damaged shutters and roof frames



Photo 14 Pulled-out shutters



Photo 15 Loss of roof truss and wall



Photo 16 Damage in west and north side



Figure 3 Plan view of damage to warehouses



Photo 17 Flying debris impact on the west wall

(6) *Grain Bins and Tanks*

Damage to grain bins and tanks is shown below. This grain bin complex is located approximately two miles east of the most damaged area of Parkersburg along the tornado path. All the grain bin structures lost its dome-shaped roof (Photo 18). Severe buckling of the cylindrical shell (Photo 19) and overturning of the smaller tanks (Photo 20) could be observed. The buckling of the shell usually occurred in the top third or in the upper half portion of the structure. It was unclear whether these grain bins or tanks were empty or full or partially full.



Photo 19 Severe buckling of the cylindrical shells



Photo 20 Overturning of smaller tanks



Photo 18 Loss of dome-shaped roof

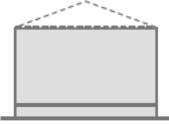
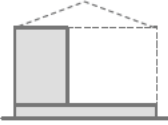
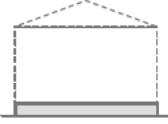
3.3 Damage to Residential Buildings

Severe damage was observed in residential buildings not only to non-structural elements such as roofing material and cladding but also to the structural elements. These buildings are typically timber houses. Damage to structural elements can be categorized under several modes as follows:

- Partial or complete loss of roofing system
- Partial loss or collapse of walls
- Lateral shifting of entire house from foundation
- Partial loss or collapse of the entire house with basement exposed

Examples of these damage modes, as observed in this tornado damage survey, are given below.

Table 2 Modes of structural damage to houses

(1)	(2)
 <p>Partial or complete loss of roofing system</p>	 <p>Partial loss or collapse of walls</p>
(3)	(4)
 <p>Lateral shifting of entire house from foundation</p>	 <p>Partial loss or collapse of the entire house with basement exposed</p>

(1) *Partial or complete loss of roofing system*

While most walls of buildings, as shown in Photos 21 – 23, are still intact, the roof is partially or completely lost. In addition, Photo 23 shows partial or complete collapse of one wall.



Photo 21 Complete loss of the roof



Photo 22 Complete loss of roof



Photo 23 Loss of roof and overturn of the wall

(2) *Partial loss or collapse of walls*

There were many damaged houses in which most walls (external or internal) had collapsed and the roof is completely destroyed. Photo 25 shows collapse of walls on three sides of the house resulting in the vertical collapse of the entire roof structure. In some cases, for example as seen in Photo 26, one room with interior walls remained intact.



Photo 24 Partial loss of walls



Photo 25 Collapse of walls



Photo 27 Lateral shifting of entire house



Photo 26 Intact small room



Photo 28 Collapse of continuous footing

*(3) Lateral shifting of entire house from foundation*

The entire house in Photo 27 is seen shifted off to the west direction. Another view of this house is shown in Photo 28. Entire house in Photo 29 is observed to be shifted in the east direction. This is consistent with the counterclockwise rotational direction of the wind where winds to the south of the path are in the east direction causing damage to buildings in Photo 29 and winds to the north of the path are in the west direction causing damage to building in Photo 27.



Photo 29 Lateral shifting of entire house

*(4) Partial loss or collapse of the entire house with basement exposed*

Loss of entire house can be categorized into two damage modes — one where the floor slab remains on the foundation (Photo 30) and the other where the floor slab is swept clean (Photo 31).



Photo 30 Loss of entire house



Photo 33 Scattered timber components



Photo 31 Loss of entire house and swept-clean floor slab

Moreover, in partially damaged houses, impact of flying debris on walls or glasses could be seen in Photo 32. Most of the debris is timber structural component from failed homes (Photo 33).



Photo 32 Damage of wall by wind-borne debris impact

#### 4. COMMENTS RELATED TO THE DISASTER

Based on the press releases by State of Iowa and the news in the local newspaper (e.g. the Des Moines Register), comments related to the disaster are summarized as follows. CNN news related to this disaster is also shown in Photo 34.

- Gov. Chet Culver declared Butler, Buchanan, and Black Hawk counties on May 25 and Delaware County on May 26 to be state disaster areas, respectively. President Bush declared Butler County a federal disaster area on May 27, which will help bring federal assistance to residents of the Parkersburg area. He also declared Buchanan, Black Hawk, and Delaware counties federal disaster area on May 30.
- Casualties in this disaster contribute to the rising national death toll by tornadoes this year and this year is the worst in a decade.
- The weather service issued a tornado warning that specifically mentioned Parkersburg at 4:46pm. The Butler County sheriff's office said sirens wailed in the town for at least five minutes before the tornado struck at about 4:53 pm. In Parkersburg, an additional siren was installed a few days before the storm. This action reduced the number of fatalities.
- In New Hartford, the siren began 15 minutes before the tornado, but lasted only a few minutes before power was knocked out. Firefighters drove through the streets, using their truck sirens to alert residents.
- Wisconsin residents have been finding

debris from a tornado more than 100 miles away in Iowa. Most of them are lightweight materials such as photographs, personal papers and check stubs.



Photo 34 CNN News (Evening, May 25)

These figures show that the recovery of damaged houses did not occur in the first month since the disaster struck, and that new construction has not started since two months after the disaster struck. At the elapsed time of four months, new construction of approximately half of the seriously damaged houses has been in progress, but construction of just only 10% of those has been completed.

This post disaster survey also revealed that new construction method in all the seriously damaged houses chose continuous footing made from reinforced concrete as shown in Photo 35, because continuous footing that were damage and exposed, as shown in Photo 28, showed inadequate reinforcement.

## 5. POST DISASTER SURVEY

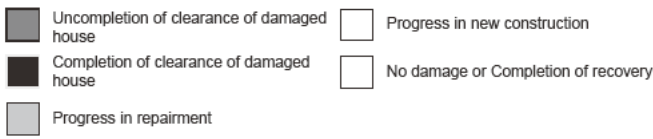
The author carried out post disaster survey to obtain the status of residents' activities related to the recovery from the disaster. This survey was carried out on June 17, July 18, August 24, and September 19, approximately every one month after May 25.

Progress in recovery of houses damaged by the tornado is shown in Figure 4. Figure 5 shows the recovery progress of houses which suffered serious damage. Vertical axis in this figure indicates the ratio of recovery or completion, calculated as follows:

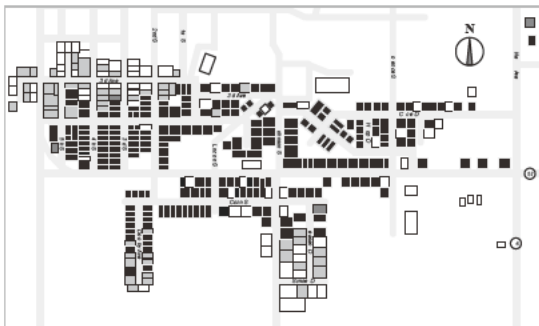
$$R_{rec}(t) = \frac{N_{rec}(DOD \geq 5, t)}{N(DOD \geq 5)} \quad (1)$$

$$R_{com}(t) = \frac{N_{com}(DOD \geq 5, t)}{N(DOD \geq 5)} \quad (2)$$

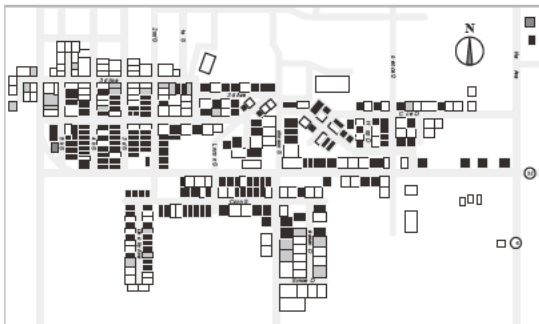
where  $R_{rec}(t)$ : ratio of recovery,  $R_{com}(t)$ : ratio of completion,  $t$ : elapsed time from the date of disaster,  $N(DOD \geq 5)$ : number of damaged houses with DOD of five or more,  $N_{rec}(DOD \geq 5, t)$ : number of damaged houses with DOD of five or more whose recovery has been already in progress at  $t$ ,  $N_{com}(DOD \geq 5, t)$ : number of damaged houses with DOD of five or more which has been replaced by new construction at  $t$ , respectively.



(a) June 17, 2008



(b) July 18, 2008



(c) August 24, 2008



(d) September 19, 2008

Figure 4 Progress in recovery of houses damaged by the tornado

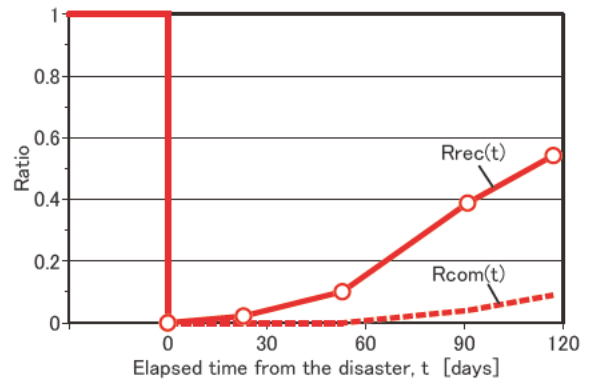


Figure 5 Ratio of recovery or completion of seriously damaged house vs. elapsed time



Photo 35 New construction of continuous footing and basement

## 6. CONCLUSION

This paper presents the outline of structural damage induced by EF-5 tornado in Iowa, U.S. on May 2008. This is the only EF5 tornado to occur in 2008. Results of field survey shows width of region where there were lots of seriously damaged houses and typical damage modes of residential, public and commercial buildings. Further, based on the post disaster survey, rates of progress in recovery of damaged houses and completion of newly constructed houses to replace the damaged houses are shown.

## 7. REFERENCES

- 1) [http://en.wikipedia.org/wiki/Tornadoes\\_of\\_2008](http://en.wikipedia.org/wiki/Tornadoes_of_2008)
- 2) Press Release of State of Iowa
- 3) The Des Moines Register

- 4) <http://www.wind.ttu.edu/EFScale.pdf>
- 5) Damage Survey Report on Saroma, Japan,  
Tornado of 2006 (in Japanese),  
[http://www.kenken.go.jp/japanese/contents/  
activities/other/disaster/kaze/2006saroma/2  
006saroma.pdf](http://www.kenken.go.jp/japanese/contents/activities/other/disaster/kaze/2006saroma/2006saroma.pdf)

# New Scales for the Destructive Potential of Tropical Cyclones<sup>1</sup>

by  
Mark D. Powell<sup>2</sup> and Timothy A. Reinhold<sup>3</sup>

## ABSTRACT

Tropical cyclone intensity defined by maximum wind speed in the storm fails to consider the area impact of damaging winds. A more appropriate intensity measure scales with the physical processes of ocean surface stress and structural wind loading and takes into account the spatial coverage of the wind field, thereby including the potential for a storm to create damage through wind, waves, or storm surge.

**KEYWORDS:** Hurricanes, IKE, Tropical Cyclones, Saffir-Simpson Scale

## 1. TROPICAL CYCLONE INTENSITY AND DAMAGE SCALES

Tropical cyclone intensity in the Atlantic Basin is defined by the maximum sustained wind (1): the maximum 1 min mean wind that might be measured anywhere in the storm at a particular instant in time, and then classified by a 1-5 rating according to the Saffir-Simpson (SS) scale (2,3). Determination of tropical cyclone intensity is subjective, and often depends on indirect estimates from visible satellite imagery (4), pressure-wind relationships (5), or empirical surface-reduction of flight-level reconnaissance wind measurements<sup>6</sup>. Coastal communities are warned for tropical cyclone wind, wave, and storm surge impacts based on intensity information with uncertainties of 10-20% (depending on the method and measurement platform (6,7)), and forecasts (24 h) with ~5 m/s mean absolute intensity errors (8), or approximately one half an SS category. Here we propose an alternative measure of intensity that may be produced from an integrated system of aircraft- space-, land- and marine-based observing platforms. The integrated kinetic energy (IKE) is more physically linked to the damage process than the maximum wind speed or Saffir-Simpson Scale, and provides a measure of intensity forecast accuracy that is less sensitive to uncertainty in the maximum wind speed. Furthermore the IKE provides an intensity measure that is equivalent to earthquake energy release.

Tropical cyclone intensity in the Atlantic Basin is defined by the maximum sustained wind (1):

the maximum 1 min mean wind that might be measured anywhere in the storm at a particular instant in time, and then classified by a 1-5 rating according to the Saffir-Simpson (SS) scale (2,3). Determination of tropical cyclone intensity is subjective, and often depends on indirect estimates from visible satellite imagery (4), pressure-wind relationships (5), or empirical surface-reduction of flight-level reconnaissance wind measurements<sup>6</sup>. Coastal communities are warned for tropical cyclone wind, wave, and storm surge impacts based on intensity information with uncertainties of 10-20% (depending on the method and measurement platform (6,7)), and forecasts (24 h) with ~5 m/s mean absolute intensity errors (8), or approximately one half an SS category. Here we propose an alternative measure of intensity that may be produced from an integrated system of aircraft- space-, land- and marine-based observing platforms. The integrated kinetic energy (IKE) is more physically linked to the damage process than the maximum wind speed or Saffir-Simpson Scale, and provides a measure of intensity forecast accuracy that is less sensitive to uncertainty in the maximum wind speed. Furthermore the IKE provides an intensity measure that is equivalent to earthquake energy release.

The potential of a tropical cyclone to inflict damage is currently described by the SS scale, originally defined according to peak 3 s wind gusts (2). Subsequently, SS has been interpreted to be associated with the maximum sustained wind (9). While the SS scale has been used extensively to convey storm intensity to the public, it is subjective and can be misleading especially applied to storms of different sizes. Alternative measures to assess hurricane intensity or damage potential include Hurricane Destructive Potential and Accumulated Cyclone Energy (ACE) (10), Hurricane Outer and Inner core Strengths (11,12), and kinetic energy dissipation or Power (13). Each of these measures has limitations related to the lack of consideration for the spatial extent of damaging winds. For example ACE and Power are computed from the square or cube of the maximum sustained wind speed alone. Since experts often disagree on measured or estimated maximum sustained wind speeds, we seek an alternative intensity metric less sensitive to a single wind value.

<sup>1</sup> Portions of this paper were published in Powell and Reinhold, 2007: Tropical cyclone destructive potential by integrated kinetic energy. *Bulletin of the American Meteorological Society*, 88, 513-526. Portions will be also presented at the 11th ACWE Conference and proceedings.

<sup>2</sup> Atmospheric Scientist, NOAA-AOML-HRD COAPS-FSU Tallahassee, FL 32301, USA

<sup>3</sup> VP Engineering, Institute for Business and Home Safety, Tampa, FL, 33617 USA

## 2. IKE

As numerical modeling of tropical cyclones progresses, it is important to validate model forecasts objectively based on observations. It is also important that critical natural hazard information be based on an objective assessment of the available observations. The recent development of air-, space-, land-, and sea-based measurement systems now provide sufficient observations to depict the horizontal distribution of tropical cyclone wind fields in the Western Atlantic and Caribbean basin. The Integrated Kinetic Energy (IKE) takes into account the destructive potential of the wind field. IKE is computed from the surface wind field by integrating the kinetic energy per unit volume ( $V$ ) over the storm domain (or the contribution over specific wind speed ( $w_s$ ) thresholds) for a 1 m thick air layer of unit density centered at the 10 m level.

$$IKE = \int \frac{1}{2} \rho w_s^2 dV \quad (1)$$

Kinetic energy scales with wind loads on structures (14) since it correlates with the wind pressure acting on a vertical structure. However, weighting of IKE is generally necessary for assessing wind damage potential because damage to most of the built environment at risk increases almost exponentially with increased wind speed once damage is initiated. Waves and storm surge are generated by shear stress of the wind on the ocean surface, which also scales with IKE. While the initial dependence of sea surface drag coefficient is linear with wind speed, supporting a cubic dependence for stress, recent analysis of wind profiles in hurricanes (15) find that the drag coefficient levels off or slightly decreases at winds above 33 m/s, suggesting a continued dependence on the square of the wind speed. It is clear from recent storms such as Opal, Ivan, Katrina and Rita that the potential for storm surge is correlated with the size and intensity of the storm in the hours and days before landfall as well as the actual wind field characteristics during landfall. Consequently, the history of IKE components in the hours and days before landfall are likely to

provide a robust estimate of surge damage potential.

## 3. H\*Wind GRIDS and IKE

Measurement of IKE in a hurricane requires sufficient observations for an analysis of the wind field. The NOAA Hurricane Research Division Hurricane Wind Analysis System (16,17) (H\*Wind) provides an objective analysis of all available observations and since 1999, these have been available in a gridded format to facilitate research and experimental use in storm surge and wave models, as well as for validation of remotely sensed winds and numerical weather prediction models. Analyses are conducted on an experimental basis when a tropical cyclone is monitored by reconnaissance aircraft. Uncertainty of the analysis maximum sustained wind speed depends on data coverage and the quality of the individual platforms contributing to the peak wind measurement, but is estimated at 10% when the peak wind is sampled at the surface (8), or 20% if the peak wind is estimated by a simple flight level reduction factor (6). Outside the eyewall where radial gradients are weaker, more plentiful in-situ observations are available and wind uncertainty is probably closer to 10%. While estimates of the maximum sustained wind in a landfalling hurricane can vary by agency, the IKE depends on the spatial characteristics of the tropical cyclone and is not very sensitive to changes in the maximum wind.

In order to better differentiate between intense but small tropical cyclones such as Camille and Andrew and broader but less intense storms such as Hugo and Katrina it is necessary to further refine the IKE analysis. Analysis options were explored by evaluating several threshold wind speed values for a selection of 22 hurricanes comprising large and small wind fields in the H\*Wind archive<sup>4</sup> over an 8 degree latitude domain. A wind speed of 10 m/s was selected for the low end ( $IKE_{>10}$ ), with additional thresholds chosen to relate to storm surge and wave damage ( $V_{MS} > 18 \text{ m s}^{-1}$ , the highest one-minute average wind at an elevation of 10m: tropical storm

---

<sup>4</sup> [www.aoml.noaa.gov/hrd/data2.html](http://www.aoml.noaa.gov/hrd/data2.html)

force  $IKE_{TS} > 33$  m/s:  $IKE_H$ ), light (25-40 m/s,  $IKE_{25-40}$ ) and moderate (41-55 m/s,  $IKE_{41-55}$ ) wind damage and severe building envelope wind damage ( $IKE_{>55}$ ) for winds  $> 55$  m/s. After experimenting during the 2006 and 2007 hurricane seasons, the  $IKE_{TS}$  was the most relevant quantity for assessing Surge and Wave Damage Potential (SDP) and continuous multiplier approach was formulated for Wind Damage Potential (WDP).

#### 4. SURGE DESTRUCTIVE POTENTIAL

Based on the largest and most intense hurricanes observed since 2000, a continuous spline fit relationship was assigned between  $IKE_{TS}$  and SDP (Fig. 1) based on the familiar 0-5 range of the SS scale.

Ultimately the damage scale should be based on an objective measure of damage realized but such depends on the infrastructure and population of an affected area and the difficulty of attributing damage to wind, wave or surge. The SDP is an objective measure of the forcing available from the wind field. Based on simple scaled storm surge modeling results (private communication, Jennifer Irish, Texas A&M) the SDP has a strong relationship to the extent of coastal inundation greater than 1 m, but a poor relationship to peak surge. Given that bathymetric and coastline orientation details are missing from SDP, the relationship to inundation is useful for emergency management and storm preparedness applications. The strength of the SDP scale is that it provides an objective means to compare a current storm to historical storms in the same area based on a level playing field. When decisions need to be made regarding evacuation and warnings 1-2 days before expected landfall, forecast uncertainty is such that the precise landfall location (and associated local bottom slope and coastline shape factors that ultimately affect surge) is unknown. Although peak surge is important, it usually covers a very small area so the extent of inundation levels known to threaten safety or encumber evacuation take on an increased importance. Its practical to base the damage potential rating on an integrated wind

forcing rather than some peak value that can misrepresent the severity of the event.

#### 5. WIND DESTRUCTIVE POTENTIAL

From a direct wind damage perspective, it is important to develop a meaningful way to relate the IKE values to damage experience. The response of residential structures to wind is a highly non-linear process, as evidenced by residential insurance losses (17) (by zip code) compared to H\*Wind analyses of open terrain wind speeds in Hurricanes Andrew, Hugo, and Opal (Fig. 2). The kinetic energy per unit volume ( $KE_V$  in Joules) for a wind field analysis grid cell was related to the co-located damage data (Fig. 3). A multiplier was fit based on a reference value corresponding to the kinetic energy per unit volume associated with the initiation of light structural damage in winds of  $\sim 25$  m s<sup>-1</sup> (Fig. 4).

$$M_G = 3.45 ( 49.785 * [ 1 + \text{TanH} (0.002469 * ( KE_V - 1602.94 ) ) ] )$$

The weighted IKE for a tropical cyclone ( $IKE_{WT}$ ) is found by summing each grid cell's product of  $M_G * KE_V$ , for all grid cells with winds in excess of 25 m s<sup>-1</sup>.

Since the concept of a damage scale with a 1-5 range is familiar to the public, we evaluated IKE threshold contributions and assigned a 1-5 rating scale. For wind damage, categories 4-5 are based on a prerequisite of winds  $> 55$  m s<sup>-1</sup>.

The Wind Damage Potential (WDP) is defined as:

$$WDP > 4: V_{MS} \geq 55.0 \text{ m s}^{-1}$$

$$WDP > 4 = 3.974 - 0.0002 \text{ } IKE_{WT} + 0.0373 (IKE_{WT})^5 + 0.085 \text{ Log}_{10} (IKE_{WT})$$

where  $IKE_{WT}$  is in TJ.

$$WDP < 4: V_{MS} > 55.0 \text{ m s}^{-1}$$

$$WDP < 4 = .8828 + 0.0183 (IKE_{WT})^5 + 0.802 \text{ Log}_{10} (IKE_{WT})$$

## 6. HURRICANES KATRINA AND IKE

As an example, consider two stages of Hurricane Katrina's wind field as depicted in post-storm analysis of all available observations during two ~ 6 h periods on 28 and 29 August, 2005. When considered to be a SS Category (Cat) Five (Fig. 5a) the day before landfall, Katrina's wind field contained maximum winds estimated at 71 m/s with an IKE of 117 TJ over an 8 degree domain. At landfall in Southern Louisiana and Mississippi, Katrina had weakened to Cat 3 status (52 m/s) but the wind field had expanded (Fig. 5b) with an IKE of 112 TJ. Therefore, based on the IKE, Katrina at landfall was of similar destructive capacity to when it was an SS Cat 5 in the central Gulf of Mexico, and about twice as destructive as the prior standard of destruction for the Gulf of Mexico coast (SS Cat 5 Hurricane Camille of 1969 with max winds near 67 m s<sup>-1</sup> and IKE of ~ 63 TJ). The tremendous wave and storm surge related destruction of Katrina at landfall was not well represented by the SS scale<sup>5</sup>.

In 2008 Hurricane Ike passed over western Cuba and emerged into the Gulf of Mexico as a marginal hurricane. Ike gradually developed a huge wind field despite maximum winds < 50 m s<sup>-1</sup>. The day before landfall Ike's IKE<sub>TS</sub> values (Fig 5c) were comparable to those for Katrina (Fig. 5a,b) despite being rated as an SS Category 2 storm. There is some evidence that the relatively low SS rating of Hurricane Ike, during this critical period for undertaking evacuation and preparation activities, may have influenced some coastal residents to stay rather than evacuate, with catastrophic results in the vicinity of the Bolivar Peninsula.

## 7. DISCUSSION

An advantage of using an IKE-based approach is that it makes no distinction on whether a tropical cyclone is classified as a hurricane or tropical storm ( a large, strong tropical storm could have more damage potential than a small, weak

---

<sup>5</sup> Many people on the Mississippi based their evacuation plans on comparing Katrina to 1969 Cat 5 Hurricane Camille, a destructive but much smaller storm.

hurricane), the scale could also be applied to non tropical storms. IKE<sub>TS</sub> may be compared to objective measures of earthquake Seismic Moment Magnitude (SMM) (18,19), which conveys earthquake size in terms of radiated energy. A SSM 7.0 earthquake corresponds to an energy release of 2000 TJ. However, unlike SMM, with 10<sup>3</sup> increases in energy between two integer gradations, the entire range in IKE<sub>TS</sub> between a selection of the smallest and largest hurricanes in the H\*Wind archive is on the order of 200 TJ. Considering that we are focusing here on a 1 m thick layer of air near the surface, the IKE<sub>TS</sub> values would increase by a factor of ~ 10<sup>3</sup>-10<sup>4</sup> if we integrated to the top of the tropical cyclone, which would approach the energy release of severe earthquakes<sup>6</sup>. The influence of bathymetry, coastline shape, surface topography, and roughness could be used as modifiers for the surge estimation, much the same as soil modification factors are used to estimate site specific ground motions. A limitation of IKE as a damage potential indicator include the inability to account for localized areas susceptible to storm surge and waves due to coastline shape and bathymetry. During the 2009 Hurricane Season we will continue to issue wind field analysis research products containing IKE<sub>TS</sub>, IKE<sub>H</sub>, SDP, and WDP as shown in Fig. 5c. With future advances in satellite and airborne monitoring of ocean surface wind vectors, we envision that all tropical cyclone basins will eventually contain sufficient observations for global assessments of tropical cyclone intensity by IKE, and more meaningful measures of basin wide tropical cyclone destructiveness from one season to the next.

## ACKNOWLEDGEMENTS

This research was supported by NOAA 2005 hurricane supplemental and the U.S. Army Corps of Engineers IPET Project.

---

<sup>6</sup> The energy release associated with the Magnitude 9.2 Alaska earthquake of 1964 has been estimated as 3.9 x 10<sup>6</sup> TJ.

## REFERENCES

1. National Hurricane Operations Plan, FCM-P12-2005, OFCM, Silver Spring, MD.  
<http://www.ofcm.gov/nhop/05/nhop05.htm>, (2005).
2. Saffir, H. Low Cost construction resistant to earthquakes and hurricanes. ST/ESA/23, United Nations, 149-162, (1975).
3. Weatherwise, The hurricane disaster potential scale. *Weatherwise*, **27**, 169-186, (1974).
4. Dvorak, V. F., Tropical cyclone intensity analysis using satellite data. NOAA Tech. Memo. NESDIS-11, 47 pp. (1984).
5. Kraft, R. H., The hurricane's central pressure and highest wind. *Mar. Wea. Log.*, **5**, 157, (1961).
6. Franklin, J.L., M.L. Black, and K. Valde. GPS dropwindsonde wind profiles in hurricanes and their operational implications. *Wea. Forecasting*, **18**, 32-44 (2003).
7. Uhlhorn, E. and P. G. Black, Verification of remotely sensed sea surface winds in hurricanes. *J. Atmos and Ocean Tech.*, **20**, 99-116, (2003).
8. National Hurricane Center, National Hurricane Center Forecast Verification, <http://www.nhc.noaa.gov/verification/index.shtml>? (2006).
9. National Hurricane Center, The Saffir-Simpson Hurricane Scale. <http://www.nhc.noaa.gov/aboutsshs.shtml> (2006).
10. Bell, G. D. & coauthors, a. Climate assessment for 1999. *Bull. Amer. Meteor. Soc.*, **81**, 1328 (2000).
11. Weatherford, C. L., and Gray, W. M., Typhoon structure as revealed by aircraft reconnaissance. Part I Data analysis and climatology. *Mon. Wea. Rev.*, **116**, 1032-1043, (1988).
12. Croxford, M. and G. M. Barnes, Inner core strength of Atlantic tropical cyclones. *Mon. Wea. Rev.*, **130**, 127-139, (2002).
13. Emanuel, K., Increasing destructiveness of tropical cyclones over the past 30 years. *Nature*, **436**, 686-688, (2005).
14. ASCE 7-02: Minimum design loads for buildings and other structures. American Society of Civil Engineers, 1801 Alexander Bell Dr., Reston, VA 20191, (2006).
15. Powell, M.D., P.J. Vickery, and T.A. Reinhold, Reduced drag coefficient for high wind speeds in tropical cyclones, *Nature*, **422**, 279-283, (2003).
16. Powell, M. D., S. H. Houston, and T. Reinhold, Hurricane Andrew's landfall in south Florida. Part I: Standardizing measurements for documentation of surface wind fields. *Wea. Forecasting.*, **11**, 304-328, (1996).
17. Powell, M. D., S. H. Houston, L. R. Amat, and N. Morisseau-Leroy, The HRD real-time hurricane wind analysis system. *J. Wind Engineer. and Indust. Aerodyn.* **77&78**, 53-64, (1998).
18. Kanamori, H., The energy release in great earthquakes, *J. Geophys. Res.*, **82**, p.2981-2987, (1977).
19. Hanks, T. C., and H. Kanamori, A moment magnitude scale, *J. Geophys. Res.*, **84**, 2348-2350, (1979).

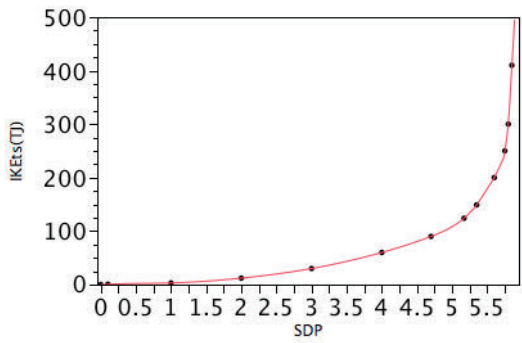


Fig. 1 Spline fit of  $IKE_{TS}$  (in TJ) vs. SDP.

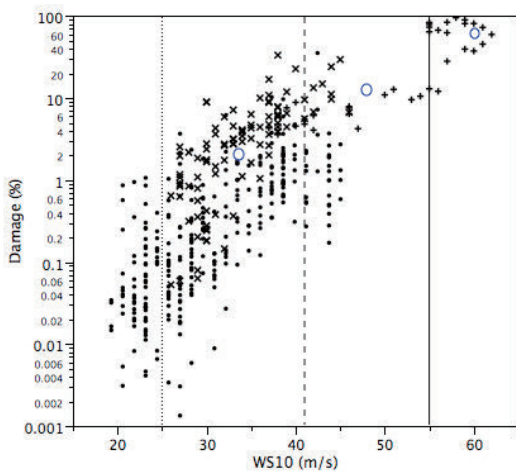


Fig. 2 Residential damage (claim to insured value ratio) as a function of 10 m open-terrain maximum sustained wind speed in Hurricanes Andrew, Hugo, and Opal. The 25-41, 42-55, and  $>55$  m/s thresholds are shown by vertical lines and mean damage by blue circles.

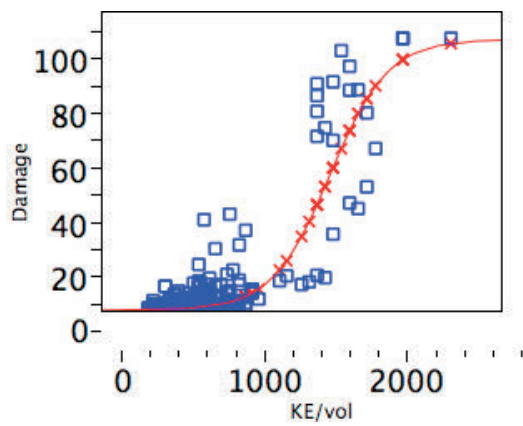


Fig. 3 Fit of damage ratio to grid cell kinetic energy per unit volume.

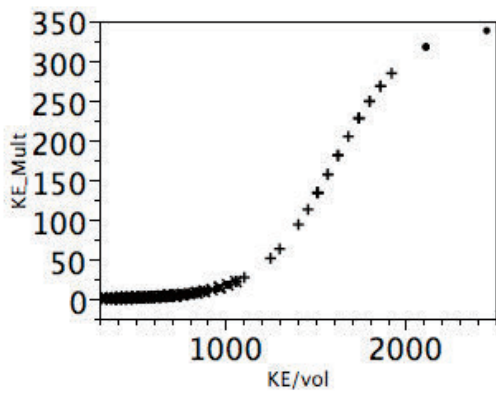
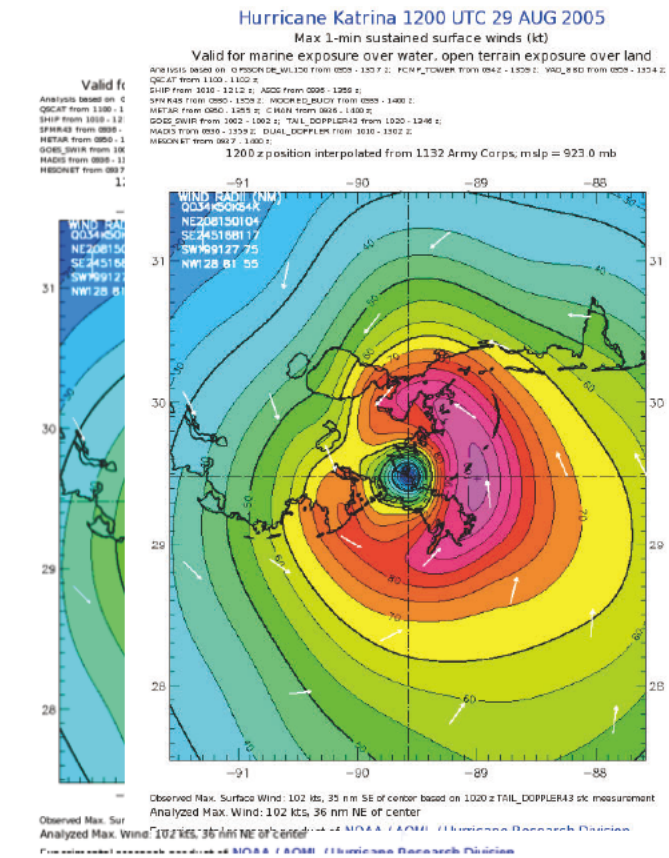
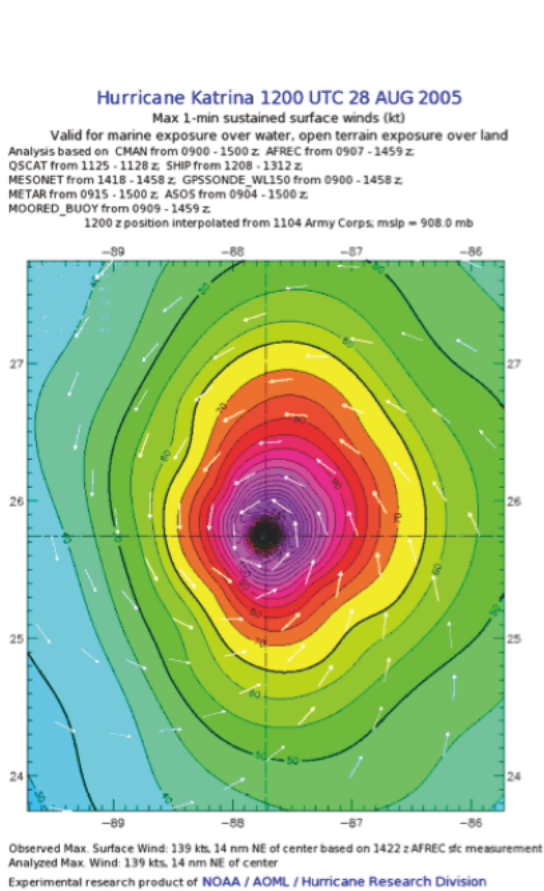
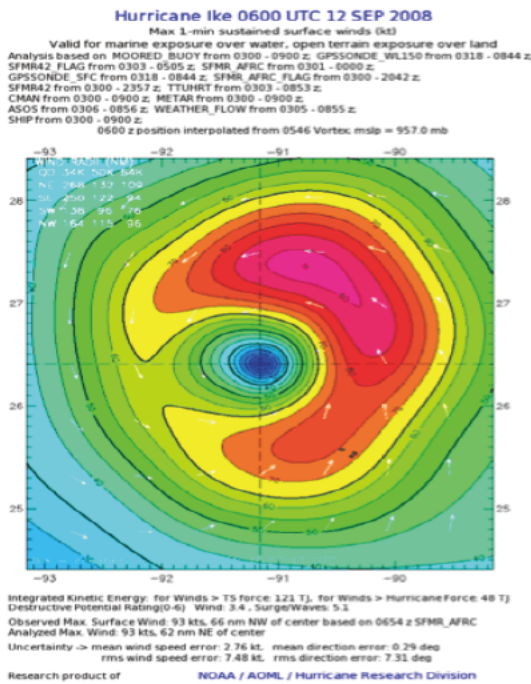


Fig. 4 Grid cell multiplier factor for computing weighted IKE in the WDP calculation.



a

b



c

Fig. 5 H\*Wind analysis of Hurricane Katrina's surface wind field at a) peak maximum wind speed, b) landfall, c) Hurricane Ike 24 h before landfall.

## **THEME 4**

# **Transportation Systems**

# Damage Investigation of Maturube Bridge during the 2008 Iwate-Miyagi-Nairiku Earthquake

by

Shigeki Unjoh<sup>1</sup>, Takashi Tamakoshi<sup>2</sup>, Koichi Ikuta<sup>3</sup>, and Junichi Sakai<sup>4</sup>

## ABSTRACT

The Maturube Bridge on National Highway Route #342 was collapsed during the 2008 Iwate-Miyagi-Nairiku Earthquake. The slope, which supported the abutment and pier foundations, displaced about 10m to the bridge center because of the landslide caused by the strong ground motion. The bridge was moved with the landslide, and one pier completely failed and overturned, and finally the bridge superstructure fell down to the ground. This paper presents the results of damage investigation of the Maturube Bridge, and the damage mechanism and the lessons learned from this particular type of damage is discussed.

**KEYWORDS:** Collapse, Iwate-Miyagi-Nariku Earthquake, Landslide, Maturube Bridge

## 1. INTRODUCTION

The Iwate-Miyagi-Nairiku Earthquake with magnitude of 7.2 occurred on June 14, 2008 at the border between Iwate and Miyagi prefectures, Tohoku region. There were serious damage including about 500 casualties and damage to about 2,500 houses. During the earthquake, large-scale landslides occurred in mountain areas and caused river closures which resulted in the development of natural dams, and road closures. Although bridge structures in the area were not affected so much by the strong ground motion, the Maturube Bridge on national highway route #342 was collapsed during the earthquake. The bridge was managed by the Iwate prefectural government. MLIT dispatched the emergency investigation team including the experts of bridge structures to the site of the Maturube Bridge just after the earthquake in

order to technically support the Iwate prefectural government. The team reported their investigation result to the Iwate prefectural government and the media for the early recovery of the national highway route #342.

The superstructure of the Maturube Bridge was a 3-span continuous steel girder with total length of 94.9m. The superstructure was supported by two piers in the middle spans and two abutments at both ends. The strong earthquake shaking caused landslide at the slope where the abutment and pier were located, and the abutment and pier moved by about 10m to the opposite side. One pier was completely failed and overturned and finally the superstructure fell down to the ground as a jackknife. This particular type of damage has not been found in the past earthquakes.

This paper presents the results of damage investigation of the collapsed Maturube Bridge, and the damage mechanism and the lessons learned from this particular type of damage is discussed.

- 
- <sup>1</sup> Research Coordinator for Earthquake Disaster Prevention, National Institute for Land and Infrastructure Management (NILIM), Ministry of Land, Infrastructure, Transport and Tourism (MLIT), Asahi-1, Tsukuba-shi, Ibaraki-ken 305-0804 Japan
  - <sup>2</sup> Head, Bridge and Structures Division Engineering, Road Department, NILIM, MLIT
  - <sup>3</sup> Researcher, Bridge and Structures Division Engineering, Road Department, NILIM, MLIT
  - <sup>4</sup> Senior Researcher, Bridge and Structural Technology Group, Center for Advanced Engineering Structural Assessment and Research (CAESAR), Public Works Research Institute (PWRI), Minamihara 1-6, Tsukuba-shi, Ibaraki-ken 305-8516 Japan

## 2. DAMAEG INVESTIGATION OF MATSURUBE BRIDGE

### 2.1 Iwate-Miyagi-Nairiku Earthquake [1]

The Iwate-Miyagi Nairiku Earthquake occurred at around 8:43AM on June 16, 2008. The magnitude of the earthquake was 7.2 and the depth of epicenter was 8km. Japan Meteorological Intensity (JMA Intensity) was the 6 Upper in the epicentral area. The high intensities were observed in the wide area in Iwate and Miyagi prefectures.

Damage extended to the 5 prefectures in the Tohoku region, in particular heavy damage was reported in the Iwate and Miyagi prefectures. Casualties of 23 (dead: 13, missing: 10), injured: 451, damage to houses: 2557, were reported. The total damage was evaluated as 152 billion Yen. Since the earthquake occurred in the mountain area, large landslides and slope failures occurred and caused river closures and road closures.

The National Research Institute for Earth Science and Disaster Prevention (NIED) reported the strong motion observation data. The strongest ground motion was observed at the IWTH25 station which was located by just a distance of 1.3 km from the collapsed bridge site. The maximum PGA was 1,143gal in NS, 1,433gal in EW, 3,866gal in UD, and 4,022gal as a combined value of these 3 components. It should be noted here that very strong UD acceleration with a very short period, which has not yet observed in the past earthquakes, was recorded.

**Fig.1** shows the response acceleration spectrum of the IWTH25 record. It is found that the ground motion was very strong in the short natural period range less than 0.3s, but the shaking intensity decreases in longer natural period range than 0.3s. That means that the earthquake seriously affected on the short natural period structures but not so much on the longer natural period structures. For example, typical bridge structures with general spans and general height of substructures have the natural period of 0.5 to 1.0s, therefore, it was estimated that the shaking was not so strong effect on such bridge structures.

### 2.2 MLIT TEC-FORCE

MLIT has established TEC-FORCE (Technical Emergency Control Force) in April 2008 [2]. Objectives of the TEC-FORCE are to provide technical emergency supports to the local governments where the large scale disasters occur or where the risk of disasters is high. The TEC-FORCE operates in order to make the local governments' countermeasures quicker and more effective. The TEC-FORCE teams are established at MLIT Headquarters Office, NILIM, Geographical Survey Institute (GSI), MLIT Regional Bureau and JMA, and consist of several units including advance unit, field support unit, information communication unit, high tech leading unit, damage investigation unit, emergency operation unit, transport support unit, geographic information unit, meteorological and terrestrial information unit. When a large scale natural disaster occurs, MLIT dispatches the TEC-FORCE and they work to support the local governments through the damage investigation, prevention of damage expansion, and early recovery works.

During the Iwate-Miyagi-Nairiku Earthquake, total number of days and engineers are about 1,400 in the first month after the earthquake. As for this bridge collapse, 5 engineers including bridge experts were dispatched as TEC-FORCE team just after the earthquake to investigate what happened at this bridge [3].

### 2.3 Bridge Design Condition

The Maturube Bridge was constructed in 1978 and managed by the Iwate prefectural government. It was 3-span continuous steel girder bridge with length of 94.9m (27m+40m+27m) as shown in **Fig.2**. The width of deck is about 10m. Two piers in the middle spans were RC wall type piers with height of 25m, and both abutments were an inverted T-shaped RC wall type. Ground condition is Type I (Stiff) according to the JRA highway bridge design specifications and therefore all foundations of piers and abutments were a spread type. Seismic coefficient

employed in the original design was 0.15 with allowable stress design method. The superstructure consisted of 4 steel plate girders with concrete slab deck. The fixed steel bearing was provided at the A1 abutment and others on two piers and A2 abutment were movable steel bearings in the longitudinal direction. In the transverse direction, all bearings had side stoppers to constraint the transverse movement.

## 2.4 Damage to Maturube Bridge

**Photo 1** shows an aerial photo of the collapsed bridge. The photo was taken and provided by the Pasco Corporation and the Kokusai Kogyo Co., Ltd. It is understood that P2 pier was collapsed and a part of superstructure between A2 and P1 fell down to the ground. Deck end at A1 abutment also fell down from the seat of the A1 abutment. Looking at the mountain area at the back of A1 abutment, some large cracks and slope deformation were recognized. It was estimated that the landslide in the part of mountain slope occurred and that the slope moved to the bridge and affected on the collapse.

The detailed damage situation of the bridge members is shown in the followings.

### 1) Superstructure (**Photo 2, 3**)

As wrote in the above, the superstructure between A2 abutment and P1 pier fell down to the ground as a jackknife. Deck end also fell down from the seat of the A1 abutment. At P1 pier, the steel girders were broken and overturned laterally because of the falling down of the superstructure between A2 abutment and P1 pier.

### 2) A1 Abutment (**Photo 4, 5**)

Road surface at the backward of A1 abutment failed heavily and large cracks and slips of the soils were developed. Significant cracks from parapet wall to the abutment wall were also found at the side of abutment.

### 3) P1 Pier (**Photo 3, 6**)

Small cracks were observed at the mid-height section of the column, they were possibly at the section of the concrete placement joint. But the columns itself was not damaged remarkably. The pier was inclined so that the pier top is close to A1 abutment and the

bottom to the direction of A2 abutment.

### 4) P2 Pier (**Photo 7**)

P2 pier failed in the particular failure mode. The column was broken and separated into 3 parts. Two parts fell down just around the bottom of original column. Top part of the column just fell down in the A2 abutment side and stood just along the bottom part column. The middle part of column fell down and overturned in the opposite A1 abutment side. The bottom part still remained at the original position.

### 5) A2 Abutment (**Photo 8, 9**)

The particular failure mode was also found at the A2 abutment. Parapet wall was failed and pushed into the backfill soil. The push-into distance was about 4m. The evidence to show the impact between the deck end and the parapet wall was recognized at the surface of the parapet wall and the end section of the steel girders.

### 6) Measurement of Geometry of the Bridge

The distance between the locations of substructures was measured by using simple method at the site. Although it is necessary to measure more accurate manner, **Fig.3** shows the measured values. The distance between A1 abutment and A2 abutment shortened to about 85m. Since the original distance was about 95m, so the distance shortened by about 10m. The distance between A1 abutment and adjacent P1 pier was about 26m. Original distance was 27m, so some shortening was found. On the other hand, the distance between P1 pier and A2 abutment was 59m. Since original distance was about 68m, therefore, about 9m shortened. The distance between A1 abutment and P1 pier was not so much change but the distance change between P1 pier and A2 abutment was about 10m. That means that the A1 abutment and P1 Pier moved toward P2 pier and A2 abutment.

## 2.5 Estimation of Damage Mechanism

Based on the detailed damage investigation and the measurement of the distance between substructures, the damage mechanism was estimated. The more detailed measurement and investigation including the boring of soils was needed but the failure was estimated to be developed in the following

mechanism. **Fig.4** shows the estimated sequences of the collapse of the bridge.

- 1) The failure and slide of the mountain slope was developed by the earthquake shaking and the abutment and pier which were supported by the slope moved with the landslide.
- 2) In particular, considering the evidence of the heavy damage and cracks at the backside soil of A1 abutment, A1 abutment and P1 pier moved to the direction of A2 abutment. At the same time, the superstructure was pushed to the direction of A2 abutment and P2 pier. That resulted in the collapse of P2 pier and damage to the parapet wall of A2 abutment, then the superstructure fell down like a jackknife.
- 3) P1 pier was separated into 3 parts. The column had two termination sections of longitudinal re-bars at mid-height. It was estimated that the terminated section became relative weak sections when the column was subjected to the extreme large displacement. The upper section with termination of longitudinal re-bars of P2 pier firstly failed because of the large displacement of superstructure, the top part fell down to the A2 abutment side. Then the superstructure was broken and settled down because of dead weight with losing the support from P1 pier and the continuous displacement from the slope, finally the superstructure fell down as a jackknife. When the falling down of the superstructure to the ground, the middle part of column of P2 pier was overturned to the P1 side with the falling superstructure.

### 3. ANALYTICAL SIMULATION

#### 3.1 Bridge Model

To simulate this particular bridge collapse mode, the preliminary analytical study was conducted. There were discussions that the damage was caused by the ground shaking, ground displacement or both. But the critical damage was developed only at P2 pier but almost no damage to P1 pier which had completely the same dimensions and re-bar arrangement with P2

pier. Therefore it was estimated the damage was caused by the displacement rather than the ground shaking. This estimation corresponded to the response spectrum of observed data. Therefore, the pushover analysis method applying the displacement to the foundations of A1 abutment and P1 pier was employed in this study. Dynamic analysis was also made using the observed strong motion data but in this preliminary study the pushover analysis is shown here.

**Fig.5** shows the mathematical model of the bridge. The superstructure was modeled as concrete slab and 4 steel girders considering the nonlinear behavior of materials. Movable bearing was modeled as nonlinear spring element considering the strength and fail of side stoppers. RC columns were modeled using fiber element model. The termination sections of the longitudinal re-bars were also considered. Abutments were modeled as linear element but the parapet walls were modeled as nonlinear fiber element model. Also to simulate the push-out failure of the parapet wall, the nonlinear shear spring element was provided at the bottom of the parapet wall. Backfill soil was model as spring element and the general soil stiffness was assumed because of the lack of the accurate soil data. Since foundations were spread type on the stiff ground, they are model as fixed to the ground.

In the pushover analysis, the displacements were given in the 3 dimensional directions. The displacement at A1 abutment and P1 pier used in this analysis was by the detailed measurement of the bridge by the Iwate prefectural government [4].

#### 3.2 Preliminary Analytical Results

**Fig.6** shows the preliminary results obtained from the pushover analyses. Upper section of the termination of longitudinal re-bars was found to be failed firstly and the top part of P2 pier pushed to the direction of A2 abutment. It is estimated from the analyses that the failure and falling down of the top part of the P2 pier was caused by the large displacement of the superstructure. The failure of the parapet wall of A2

abutment also found because of the push-into of the end of the superstructure. Therefore, the failure mode in the first stage was almost reproduced by the simulation analysis.

#### 4. LESSONS LEARNED AND DISCUSSIONS

The damage mode of the Maturube Bridge was particular. The landslide of the backward slope of the bridge caused the large displacement of about 10m and the abutment and pier were displaced with the landslide. Then the pier failed and the superstructure broken as a jackknife. The collapsed pier was separated into 3 parts and the parapet wall pushed into backfill soils by the superstructure. These damage modes had not found in the past earthquakes.

The preliminary lessons and discussions are summarized as follows.

- 1) The damage was basically caused by the landslide. Therefore, it is important to investigate the possibility of the occurrence of landslides around the bridge construction sites.
- 2) At this moment, it is very difficult to evaluate the earthquake shaking intensity accurately when the landslides occur at each slope. It is important to study and to accumulate the data in order to improve the slope investigation method and the stability evaluation method.
- 3) It is impossible to stop the movement of large slope by a bridge structure. In the structural design point of view, it is essential to select the route carefully and to study the design consideration on the placement of foundations. Also, it is important to study the methods to improve the redundancy of road networks.

It should be noted here that Iwate prefectural government established the investigation committee to study the damage mechanism of the Maturube Bridge (Chairman: Prof. Motoyuki Suzuki, Tohoku University) more in detail. The final report will be published soon. The interim report already can be downloaded from the Iwate prefecture web site as [4].

#### 5. REFERENCES

1. MLIT: Press Release on the establishment of TEC-FORCE (In Japanese)  
([http://www.mlit.go.jp/kisha/kisha08/05/050425\\_4\\_.html](http://www.mlit.go.jp/kisha/kisha08/05/050425_4_.html))
2. NILIM: Report of Damage Investigation of 2008 Iwate-Miyagi Nairiku Earthquake, August 26, 2008 (In Japanese)  
(<http://www.nilim.go.jp/engineer/index.html>)
3. MLIT TEC-FORCE Team: Report of Investigation of Maturube Bridge on National Highway Route #342, Reported to the Iwate Prefectural Government and Media, June 18, 2008 (In Japanese)
4. Iwate Prefectural Government : Committee Report on Damage Investigation of Maturube Bridge on natibal Higway Roure #342 (In Japanese)  
(<http://www.pref.iwate.jp/view.rbz?of=1&ik=0&pnp=14&cd=17790>)

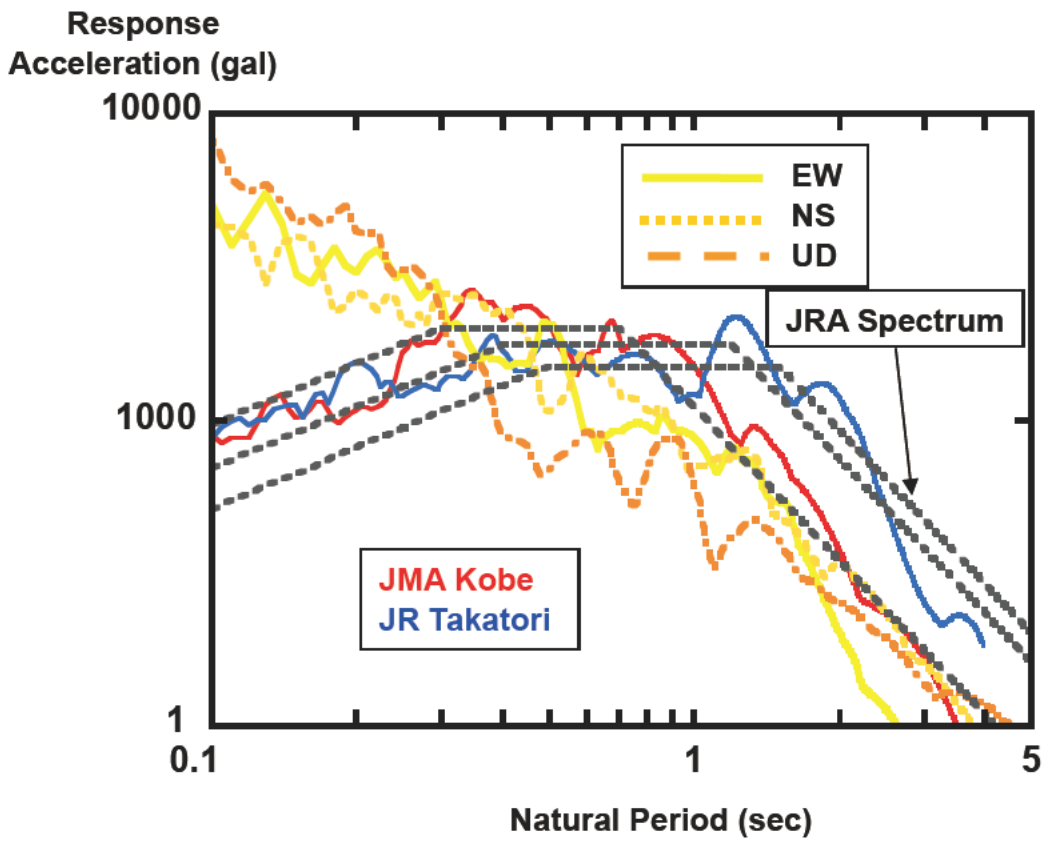


Fig. 1 Response Acceleration Spectrum of IWTH25 Station (NIED, KiK-Net)

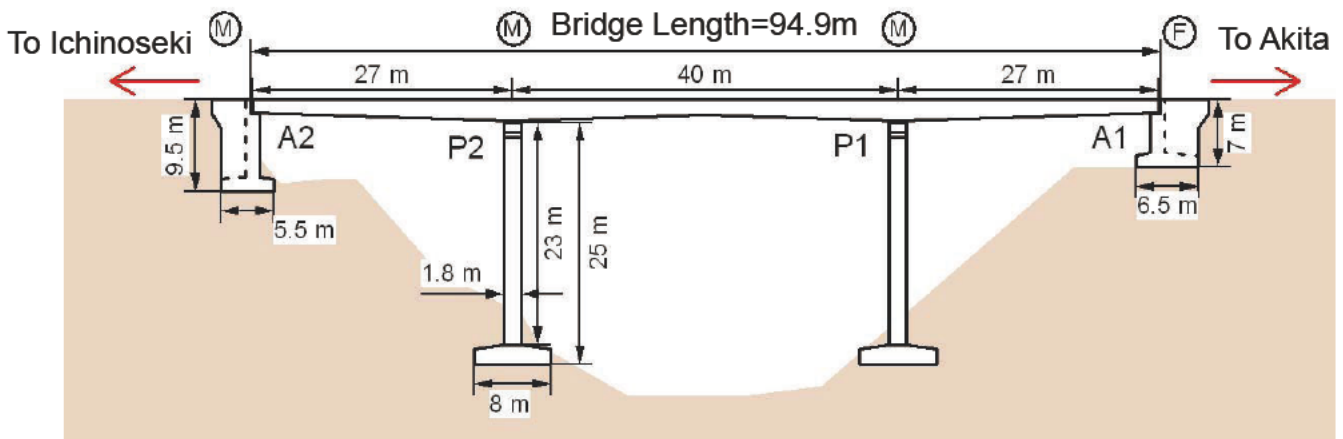
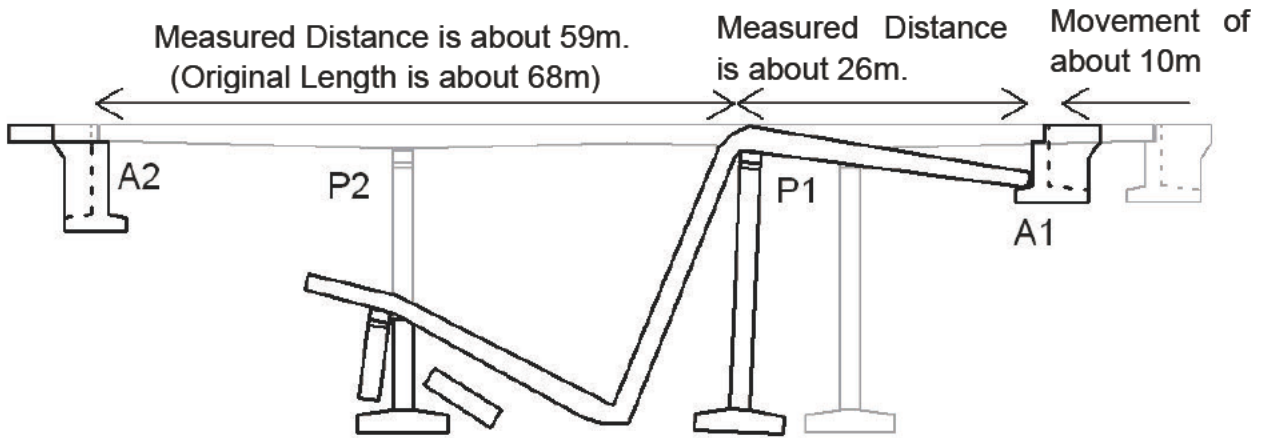
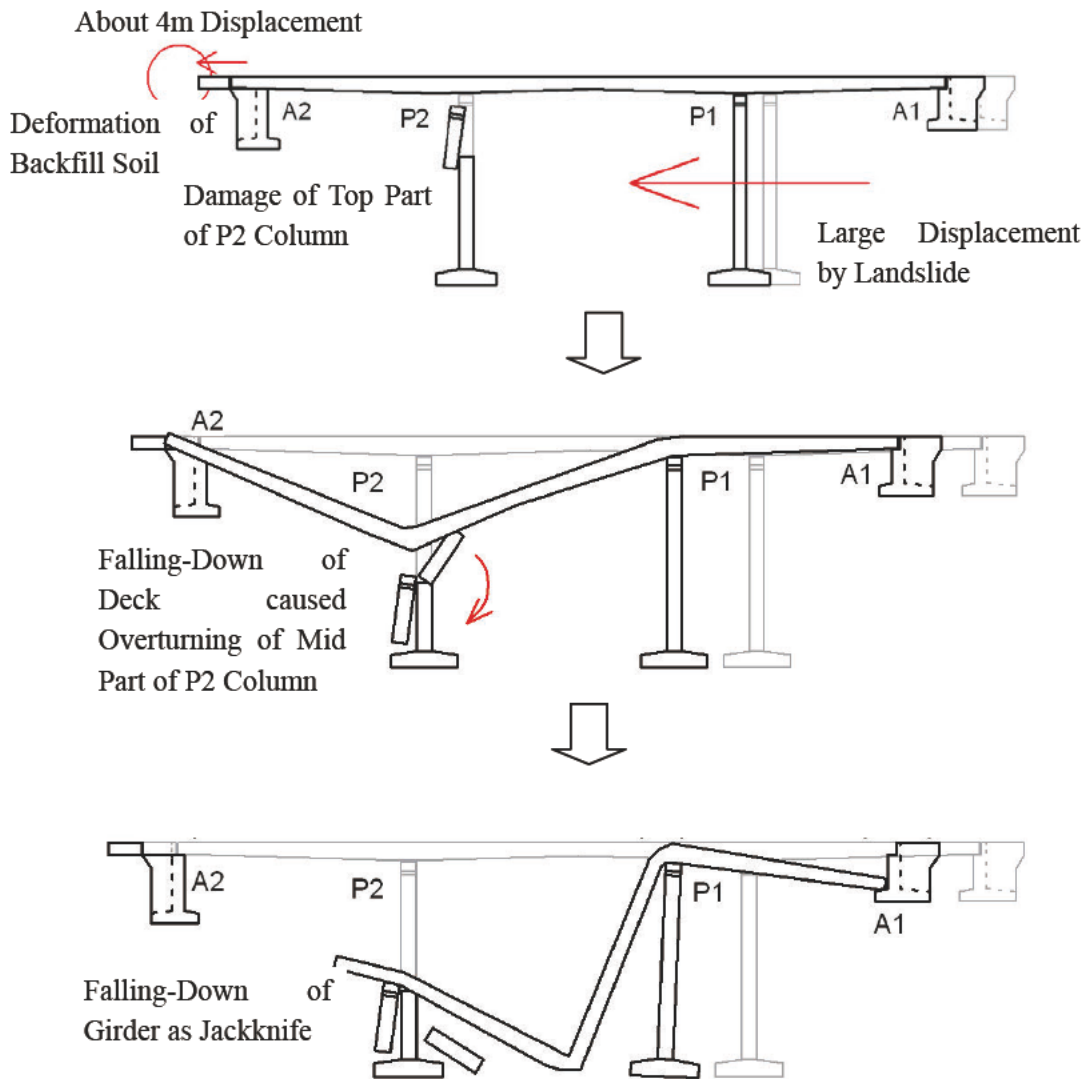


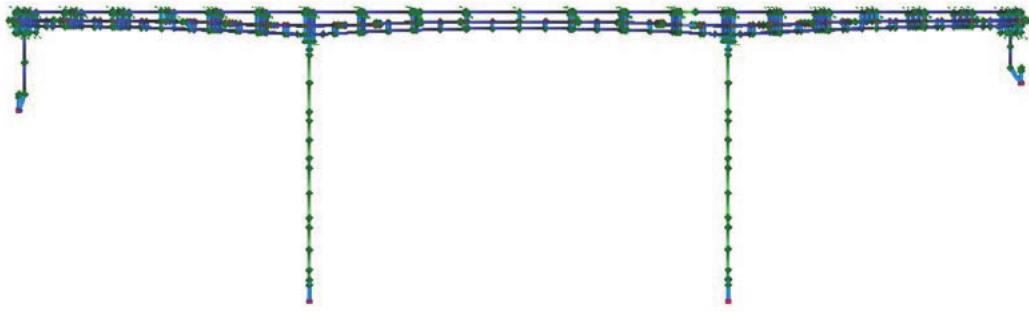
Fig. 2 Side View of the Maturube Bridge



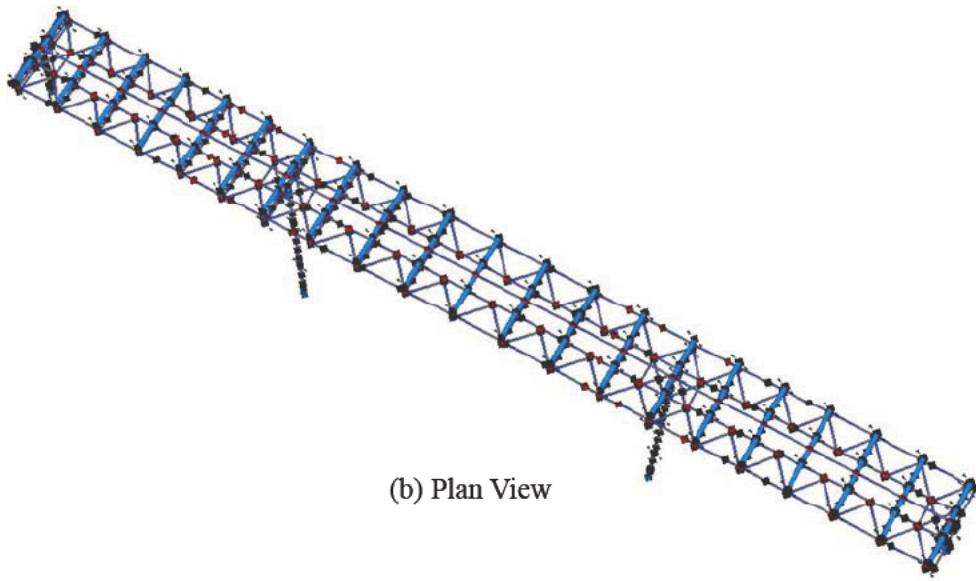
**Fig. 3** Measured Distance Changes between Substructures



**Fig. 4** Estimated Sequences of the Bridge Collapse



(a) Side View

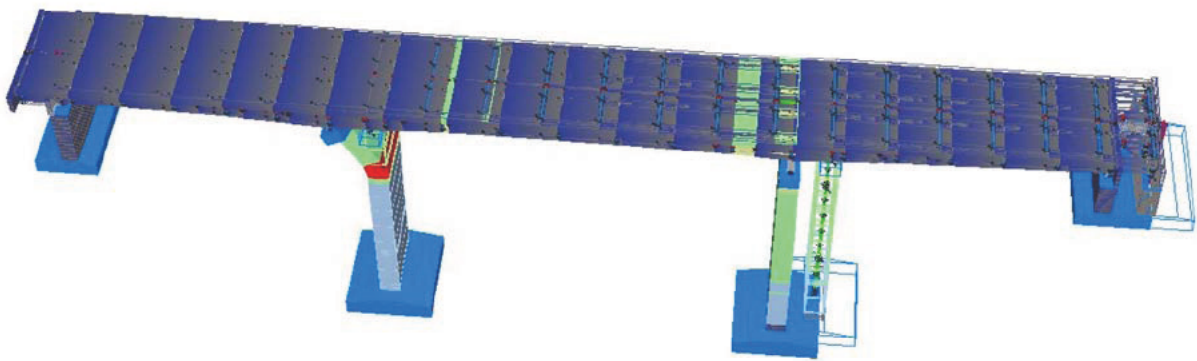
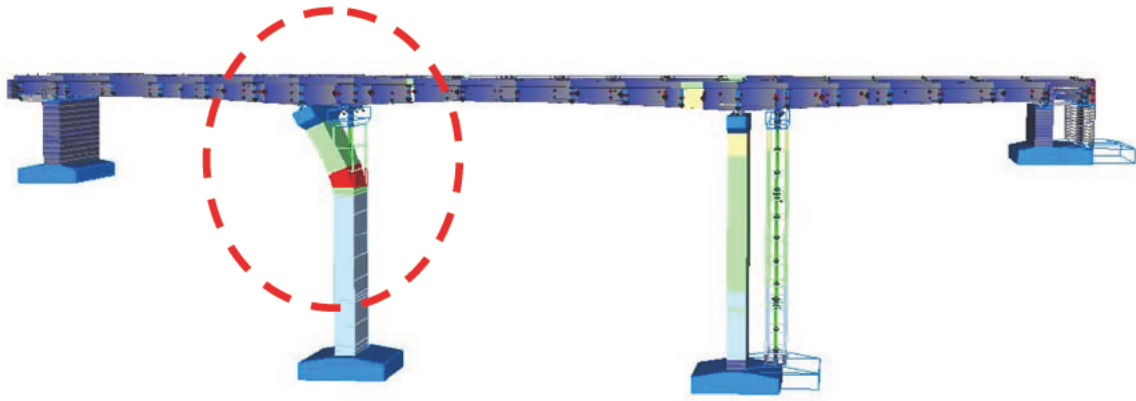


(b) Plan View

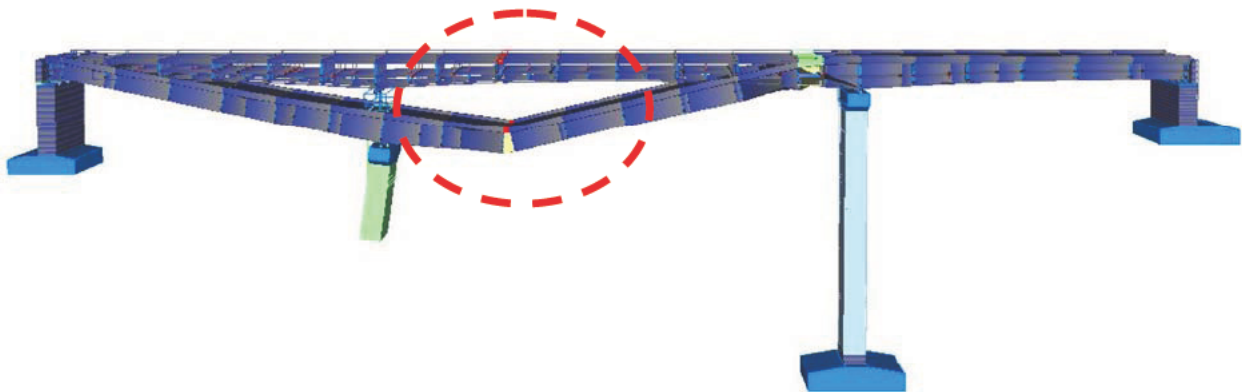


(c) Solid Illustration

**Fig. 5** Mathematical Model to Simulate Bridge Collapse



(a) Failure of Top Part of P2 Pier caused by the Displacement



(b) Possibility of Jackknife Failure of Girder with Losing Vertical Support by P2 Pier

**Fig. 6** Preliminary Results of Push-over Analyses to Simulate the Bridge Collapse

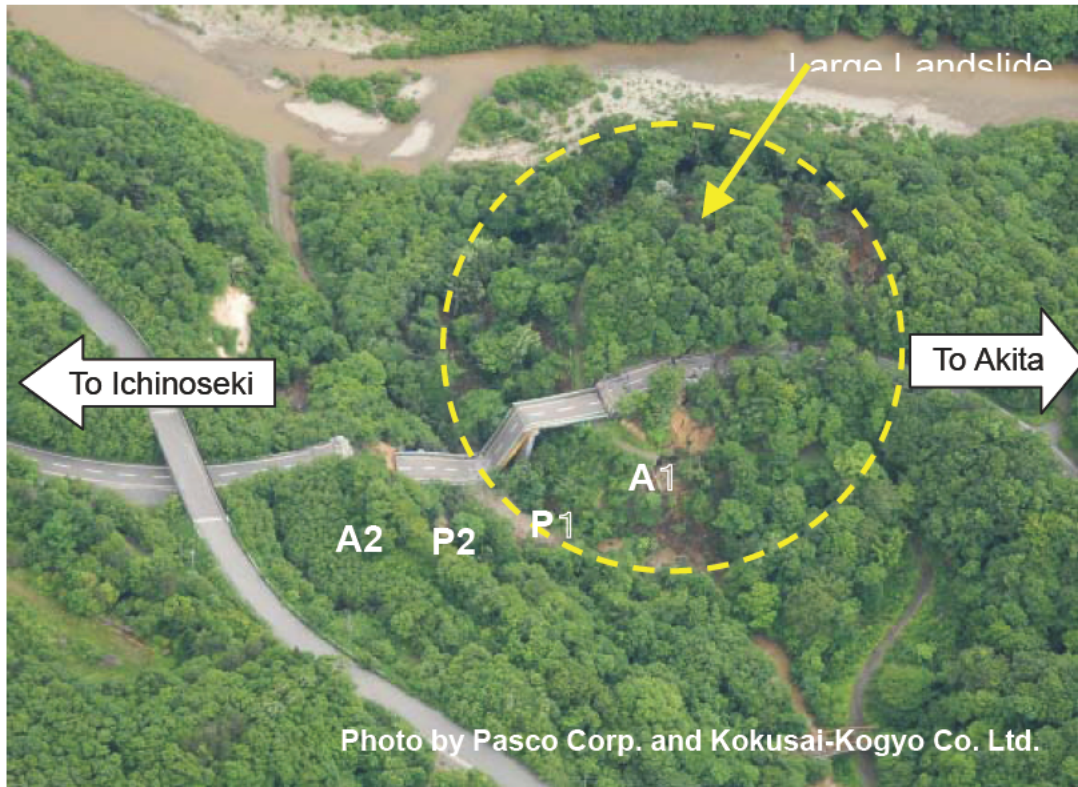


**Photo 1** Aerial Photo of Maturube Bridge



**Photo 2** Collapse of Superstructure



**Photo 3** Damage of Girder on P1 Pier



**Photo 4** Large Cracks and Slips of Backfill Soils at A1 Abutment



**Photo 5** Crack at Slopes in the Back of A1 Abutment

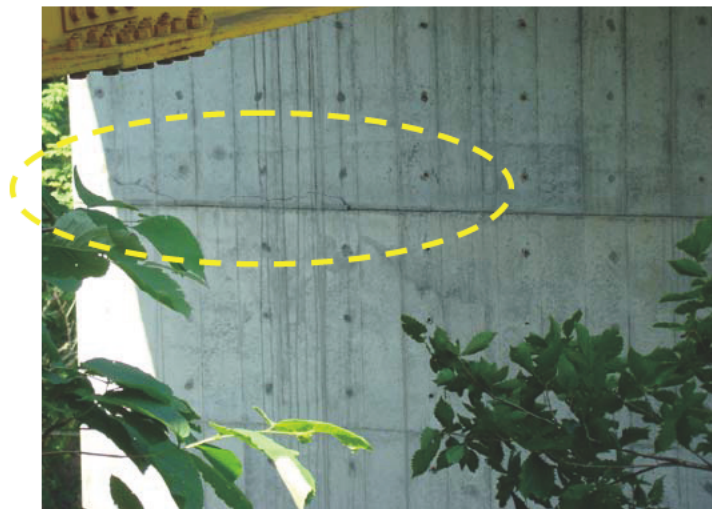


**Photo 6** Crack at the Pier P1 (Around Joint of Concrete Placement)

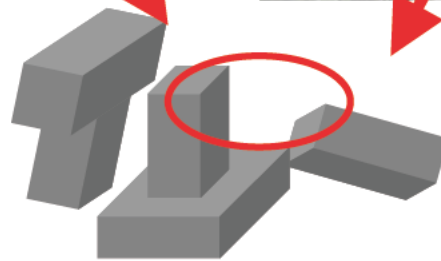


**Photo 7** Damage of P2 Pier

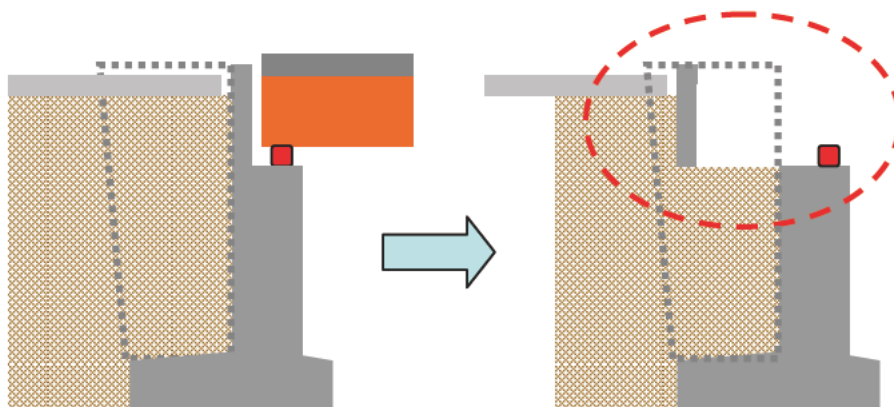
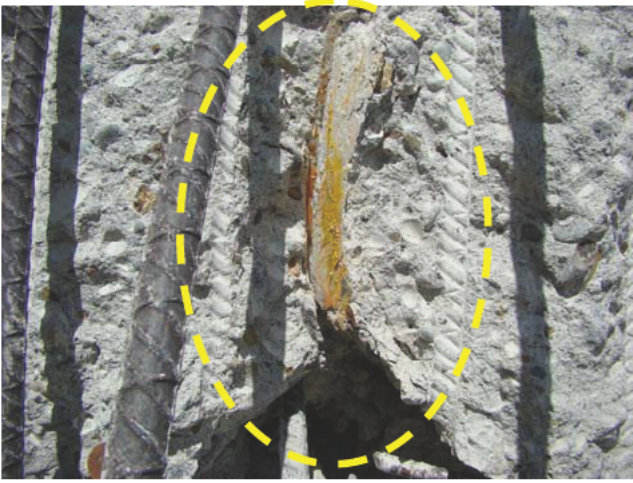


**Photo 8** Damaged of A2 Abutment (Failure of Parapet Wall)



(a) Surface of Parapet Wall



(b) Girder End

**Photo 9** Evidence of Impact between Parapet Wall and Girder End

# The Lessons Learned from Wenchuan Earthquake on Highway Bridges

by

W. Phillip Yen<sup>1</sup>, Genda Chen<sup>2</sup>, Mark Yashinski<sup>3</sup>,

## ABSTRACT

A strong earthquake of M7.9 occurred in the Wenchuan County in Sichuan Province, China, on May 12, 2008. Shortly after the earthquake, the Turner-Fairbank Highway Research Center of Federal Highway Administration led a reconnaissance team, partnering with Chinese counterpart, the Research Institute of Highway from the Ministry of Communication of China, to conduct a post-earthquake bridge performance investigation in the earthquake affected areas of transportation system. The U.S. transportation system reconnaissance team visited the earthquake affected areas on July 20 – 24, 2008. This report is a briefing of the findings and lessons that the team learnt from the earthquake event.

**KEYWORDS:** bridge engineering, earthquake engineering, post earthquake investigations.

## 1.0 INTRODUCTION

A team of five U.S. engineers was invited by the Ministry of Communication of China to study bridge damage from the M7.9 (M8.0 according to China Earthquake Administration or CEA) Wenchuan earthquake of May 12, 2008. The team included Dr. Phillip W. Yen (Team Leader) from the Turner-Fairbank Highway Research Center of Federal Highway Administration (FHWA), Mr. Mark Yashinsky from the California Department of Transportation representing the Earthquake Engineering Research Institute (EERI), Dr. Genda Chen from the Center for Transportation Infrastructure and Safety (CTIS), a national University Transportation Center at Missouri

University of Science and Technology, Dr. Youssef Hashash from Geo-Engineering Earthquake Reconnaissance (GEER), and Mr. Curtis Holub from the Mid-America Earthquake Center (MAE). The reconnaissance team was hosted by Dr. Kehai Wang of the Research Institute of Highway from the Ministry of Communication of China and Mr. Xiaodong Guo of the Sichuan Province Highway Planning, Survey, Design, and Research Institute.

## 2.0 EARTHQUAKE AND SURFACE RUPTURE

The May 12, 2008, Wenchuan Earthquake:

The M7.9 Wenchuan earthquake occurred at 06:28:01 (UTC) on May 12, 2008 in the Longmen-Shan thrust zone. Its epicenter is located at 30.989° N /103.329° E near a town called Yingxiu in Wenchuan County, Sichuan Province. The focal depth of the earthquake is approximately 10 km. The highest recorded peak ground acceleration is 0.65g (Xie et al., 2008). At least 35 aftershocks with magnitudes equal to or greater than M5.0 were recorded within the first three months after the main shock with the strongest aftershock of M6.4 (M6.5 according to CEA). This region has continually experienced large earthquakes as indicated in Table 1 & Figure 2. The largest earthquake over M7.0 prior to the Wenchuan earthquake occurred in 1973.

The Longmen-Shan thrust zone was formed by the Eastern Tibetan Plateau pushing against the Sichuan Basin (Burchfiel et al., 2008). The thrust zone has three faults: the front fault (Guanxian-Jiangyu-Guangyuan), the center fault (Yingxiu-Beichuan-Chaba-Linjueshi), and the back fault

---

1 Seismic Research program Manager, Turner-Fairbank Highway Research Center of Federal Highway Administration (FHWA)

2 Professor, the Center for Transportation Infrastructure and Safety (CTIS), a national University Transportation Center at Missouri University of Science and Technology

3 Senior Bridge Engineer, California Department of Transportation representing the Earthquake Engineering Research Institute (EERI)

(Wenchuan-Maoxian-Qingchuan). Based on the distribution of aftershocks, approximately 300 km of the faults was estimated to have ruptured, breaking the ground surface along the Yingxiu-Beichuan segment of the center fault (210 km) and the Guanxia-Jiangyu segment of the front fault (70 km). According to Xie et al. (2008), the vertical fault displacements measured were over 5 m.

The M7.9 Wenchuan earthquake and several strong aftershocks resulted in massive landslides and rockfalls. These events caused approximately 70,000 fatalities and economic loss of over \$110B. They damaged more than 1,000 bridges, approximately 20 of which had to be replaced. The severity of bridge damage greatly increased with proximity to the fault, with the worst damage occurring in mountainous terrains. This made the recovery more difficult. Most mountain roads are switchbacks with steep grades over narrow passes with little room for detour. Massive landslides covered or undermined the roads, making it difficult to bring in equipment and supplies.

### 2.1 Surface Feature of Fault Rupture at the Earthquake Epicenter

The epicenter of the May 12 Wenchuan earthquake is located near Yingxiu in Wenchuan County, Sichuan Province. The surface rupture of the center fault in the Longmen-Shan fault zone was observed in Yingxiu as illustrated in Figure 5. The thrust fault appeared to cross the Ming River in right angle. As shown in Figure 5, the earthquake left behind a distinct dislocation on the river bed at the northeast (NE) end of the surface rupture. The northwest (NW) side of the fault on the upstream of the River moves upward against the southeast (SE) side of the fault. The fact that one deck panel along the expressway elevated bridge was still supported by one pier in Figure 3 indicated the sudden push by a near-field pulsing effect.

On the other side of the Ming River was a five-story building with a construction joint between two similar parts. The right side of the building as shown in Figure 5 was completely collapsed while the left side of the building only lost the second story and suffered structural damage in walls. A

sudden change was also evidenced as shown in Figure 5 on the slope of the mountain behind the building. A closer look at the old Dujiangyan-Wenchuan highway in front of the building indicated that the vertical dislocation is approximately 1.5 m as illustrated in Figure 4.

## 3.0 OBSERVED BRIDGE DAMAGES

Although many bridges performance were inspected, only the three most severely damaged and collapsed bridges are discussed due to the limitation of the paper size. More discussions on other bridges will be published soon.

### 3.1 Bridges in Nanba Town

Three bridges crossed a river (river's name was not known) near Nanba Town as shown in Figure 5. The west structure was a concrete and masonry three-span arch bridge built in the 1970s. The old arch bridge completely collapsed during the earthquake as shown in Figure 6. Immediately downstream of the arch bridge was a 10-span river crossing (on a 10° skew) that was under construction during the earthquake, as shown in Figure 7. Each 6 m long span was simply supported on two-column bents and seat-type abutments with 560 mm seats. As shown in Figure 8, each span consisted of eight precast box girders with a cross section of 1067 mm by 1520 mm. Each girder was supported on two 200 mm round elastomeric bearings at each end. The girders were in place but the concrete deck had not yet been poured at the time of the earthquake as seen from Figure 5.

As shown in Figures 7 and 8, most of the box girders of the new bridge dropped into the river and the two-column bents were distorted. The end box girders were transversely displaced by approximately 760 mm. The deck hadn't been poured, there wasn't any real transverse bracing or shear keys, and girders were on a slight skew, all of which contributed to the damage. Also, many of the bents were leaning or distorted, but with no damage visible above the waterline.

There was no indication that the ten-span bridge suffered any damage due to a fault crossing. As

such, the three-span arch bridge must have been damaged by ground shaking, perhaps exacerbated by soil movement. Liquefaction, lateral spreading, or other soil movement may have been also responsible for the distortion of the two column bents. The reconnaissance team was not able to discern what type of foundation system the bents were supported on, but apparently they were not sufficiently embedded into good material.

On the east side of the old and new bridges is a temporary structure that was being constructed by launching Bailey Bridges onto new RC pier walls at the time of field reconnaissance. As shown in Figure 9, vehicles were driving across the river on fill material laid over culverts in the meantime.

### 3.2 Miaozhiping Bridge

Miaozhiping Highway from Dujiangyan to Wenchuan was under construction during the earthquake. It consists of a tunnel at Zhipingpu and a bridge over the Ming River as schematically shown in Figure 10. The Tunnel is shown in Figure 11 and experienced little damage during the earthquake. The highway was scheduled to open in October, 2008. Near the highway is the well-known Dujiangyan Dam. The bridge of approximately 1.4 km long consists of three parts: a main span and two approach spans as shown in Figure 12.

As shown in Figure 13, the approach span near the tunnel is a two-span, RC girder structure with 50 m span length each. The bridge deck is supported on five RC girders and two-column bents with several cross struts. As indicated in Figure 13, the bridge deck is continuous but the girders are simply supported on the bents. The main bridge is a continuous, non-prismatic, three-span structure supported on two intermediate wall piers with 125 m, 220m, and 125m length, respectively. The superstructure is a single-cell box girder structure. The depth of girders varies to a maximum depth of 4.0 ~ 4.5 m.

The approach bridge on the other side of the main span has three parts of 250 m, 250 m, and 100 m, respectively. Any of the first three parts has five

spans of 50 m long, supporting ten RC girders. All girders are simply supported on the bents for dead load but the bridge deck is continuous for live load. The bents are as tall as 105 m. In some locations, they are 40 m deep into water in the Zidingdu reservoir of the Dujiangyan Dam in the main span of the bridge. Expansion joints are used between the parts and between the approach and main bridge.

The construction of the bridge was near completion except for the installation of expansion joints at the time of the earthquake. The most severe damage was to the end span of a five-span T-girder segment that became unseated at the expansion joint end, fractured in the continuous deck at the other end due to gravity load, and fell off the supporting bent caps during the earthquake. The bent seats were approximately 300 mm in length but the bridge experienced at least 500 mm of longitudinal movement due to earthquake shaking. Since the columns of each bent are approximately 105 m tall, the accumulated displacement at the bent cap was likely significant during the earthquake. There were other indications of large longitudinal movement. The barrier rails were overlapped by about 300 mm at the southeast expansion joint. The barrier also displaced transversely for approximately 250 mm. Divers found cracks at the bottom of the main span columns due to earthquake shaking. Shear key failure was also observed as shown in Figure 50. After the earthquake, the bridge deck was jacked back into place with hydraulic jacks.

The end of the Miaozhiping Bridge near the tunnel is divided into two parallel elevated structures in order to guide two ways of traffic in alignment with the twin tunnels as indicated in Figure 16. Over the southeast approach is a four-span RC girder bridge built in 2004. The bridge supports the old highway from Dujiangyan to Wenchuan and Juzhaigou. The old highway was built along the mountain terrain, perpendicular to the Zhipingpu Highway at Zhipingpu Town. The bridge showed shear key failures and embankment cracking as shown in Figure 17.

In the vicinity of Miaozhiping Bridge there are several RC girder bridges as shown in Figure 18.

These bridges appeared to suffer little damage. No weight limits were posted on these bridges.

### 3.2 Baihua Bridge

Baihua Bridge is part of a Class 2 Highway from Dujiangyan to Wenchuan. It was built in 2004 by the owner of a nearby hydroelectric plant to bring in workers. As schematically shown in Figure 19, the bridge is an 18-span, RC structure with a total length of 450 m. The bridge superstructure was supported on two-column bents of varying heights as it climbs over the hilly terrain. The tallest bents have one or two struts to provide transverse restraint between the columns. The bridge has both straight and curve spans. For convenience, the bridge structure can be divided into six sections as summarized in Table 2. The superstructure was a prestressed box girder with a drop-in T-girder span between Bent 9 and Bent 10. There were expansion joints at Bents 2, 6, 9, 10, 14, and at the two seat-type abutments. For the drop-in span, the bridge deck just rested on the bent cap at its both ends.

During the earthquake, the more highly curved section of the bridge completely collapsed as illustrated in Figure 20. The rest of the bridge suffered varying degrees of damage, including shear cracks and failure at columns and struts, shear key failure, and bearing failure as shown in Figures 21-24 for Bents 3, 9, 15, and 18, respectively. At Bent 3, typical damage occurred between the strut and columns in the form of spalling and cracks. At Bent 9 with expansion joints, the superstructure had significant transverse displacement, knocking off the shear key. At Bent 15, the bridge section was completely collapsed due likely to the shear and flexural failure of columns. At Bent 18, in addition to cracks between column and strut, significant spalling occurred underneath the bridge deck.

At the curve part of the bridge, the bridge is likely subjected to higher deformation and stress under the earthquake, resulting in collapse. Even for the straight part of the bridge, due to tall columns, the damage in various sections under the earthquake results in tilting of the columns that would push the superstructure almost off their support at

several locations. A detour had been graded along the side of the damaged bridge. Considering the high risk of a further collapse during an aftershock, endangering people using the detour, the rest of the bridge was demolished with dynamite as illustrated in Figure 25.

Similar to the previously described Xiaoyudong Bridge, this bridge could have been damaged by surface faulting though there is no clear surface fault feature that the reconnaissance team has ever found near the bridge site. Considering the complex vibration system of the irregular structure with varying column heights and lack of continuity between the substructure and superstructure, severe shaking alone could result in collapse. Still, the bridge is very close to the fault and several photos (taken immediately after the earthquake) show what looks to be a surface fault under the bridge. During the field reconnaissance after nearly three months later, all signs of the fault were gone and the bridge was lying on the ground.

### 4.0 LESSONS LEARNED FROM EARTHQUAKE RECONNAISSANCE

The bridge damage observed during the May 12, 2008, Wenchuan Earthquake reminded us of what California suffered during the February 9, 1971 San Fernando Earthquake. The U.S. in the 1960's and 1970's was expanding their highway network similar to China's efforts today. Before the San Fernando earthquake, Caltrans' maximum seismic coefficient was 0.10g, similar to China's current maximum seismic coefficient of 0.10g. After the San Fernando earthquake, Caltrans greatly increased the seismic hazard used to design California's bridges, similar to how Japan increased the hazard for its bridges following the 1995 Kobe earthquake. It is hoped that this earthquake will have the same significance for China's bridge engineers and the seismic hazard for areas near known faults will be greatly increased. Also, the bridges we studied had few seismic details such as long seats, large shear keys, or tightly-spaced transverse reinforcement. These details would greatly reduce bridge damage during future earthquakes. The various fault traces through the region need to be carefully identified and bridges should be designed for the seismic hazards at the

bridge site, based on a low probability of the hazard being exceeded during the life of the bridge.. This would ensure that China could rely on its highway infrastructure during the frequent earthquakes that strike this and other regions.

4.1 Based on the field reconnaissance, the following are the observations:

- The collapse of most arch and girder bridges is associated with surface rupturing of the faults in the Longmen-Shan Thrust Zone. A significant portion of roadways and bridges were pushed away or buried by overwhelming landslides in the mountainous terrain of steep slopes.
- The representative damage types in bridge superstructure include unseating of girders, longitudinal and transverse offset of decks, pounding at expansion joints, and shear key failure.
- The bearings of several girder bridges were either crushed or displaced significantly.
- The substructure and foundation of bridges were subjected to shear and flexural cracks, concrete spalling, stirrup rupture, excessive displacement, and loss of stability.
- More damage occurred in simply-supported bridges in comparison with continuous spans. The curve bridges either collapsed or suffered more severe damage.
- The directivity effects on the bridges near the earthquake epicenter were evidenced during the earthquake.

## 5.0 REFERENCES

Burchfiel, B.C., L.H. Royden, R.D. van der Hilst, B.H. Hager, Z. Chen, R.W. King, C. Li, J. Lü, H. Yao, and E. Kirby, 2008, A geological and geophysical context for the Wenchuan earthquake of 12 May 2008, Sichuan, People's Republic of China, *GSA Today*, 18, p. 4-11.

Stone, R., 2008, Landslides, flooding poses threats as experts survey quake's impact, *Science*, 320, p. 996-997.

Wang, Z. M., 2008, "May 12, 2008, Sichuan China Earthquake Reconnaissance." Presentation posted at [http://www.uky.edu/KGS/geologic hazards/Sichuan\\_Earthquake.pdf](http://www.uky.edu/KGS/geologic hazards/Sichuan_Earthquake.pdf), Kentucky Geological Survey, 228 MMRB, University of Kentucky, Lexington, KY 40506, [zmwang@uky.edu](mailto:zmwang@uky.edu).

Xie, F.R., Z. M. Wang, Y. Du, and X.L. Zhang, 2008, Preliminary observations of the faulting and damage pattern of M8.0 Wenchuan, China, earthquake, submitted to a journal for possible publication.

Table 1: Longmen-Shan Significant Earthquake  $M \geq 7.0$

Year	Month	Day	Time	Latitude	Longitude	Depth	Magnitude
1917	07	30	2354	29.000	104.000	0	7.3
1923	03	24	1240	30.553	101.258	25	7.2
1933	08	25	0750	31.810	103.541	25	7.3
1947	03	17	0819	33.000	99.500	0	7.5
1948	05	25	0711	29.500	100.500	0	7.2
1950	08	15	1409	28.500	96.500	0	8.6
1955	04	14	0129	29.981	101.613	10	7.5
1967	08	30	0422	31.631	100.232	8.1	7.0
1973	02	06	1037	31.361	100.504	6.6	7.4

Table 2: Parameters of the Baihua Bridge

Section	No. of Span	Span Length (m)	Section Length (m)
1	5	25	125
2	4	25	100
3	1	50	50
4	3	25	75
5	5	20	100
6	2	25	50

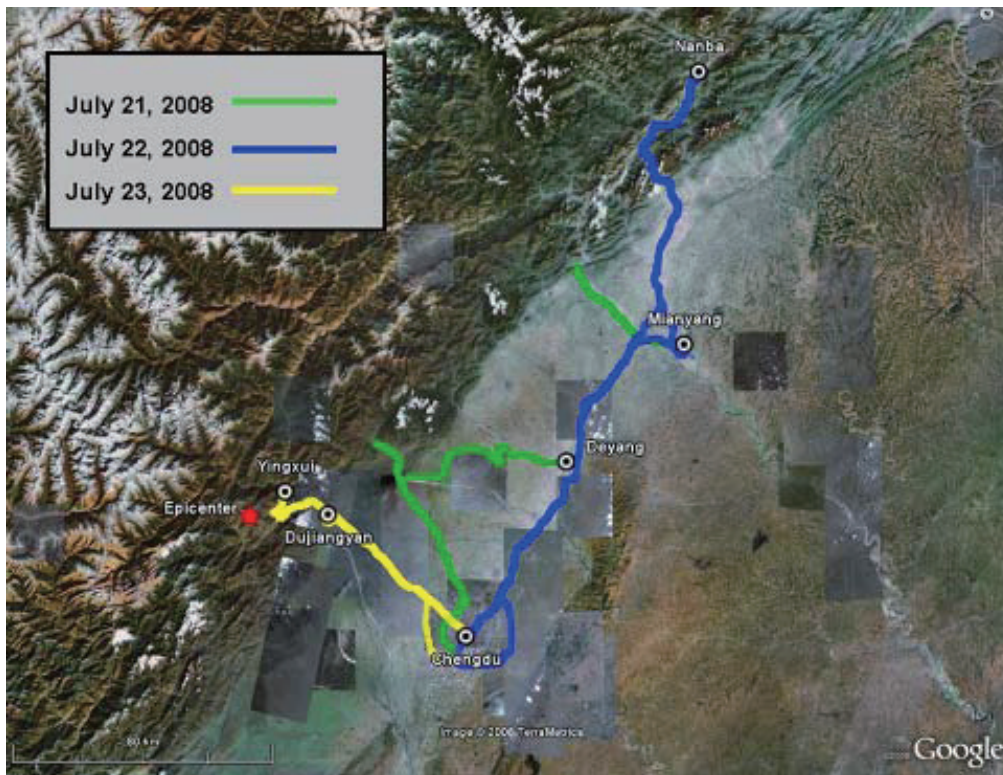


Figure 1: Bridge Sites Investigated by Reconnaissance Team



Figure 2: Historical Earthquake Activity

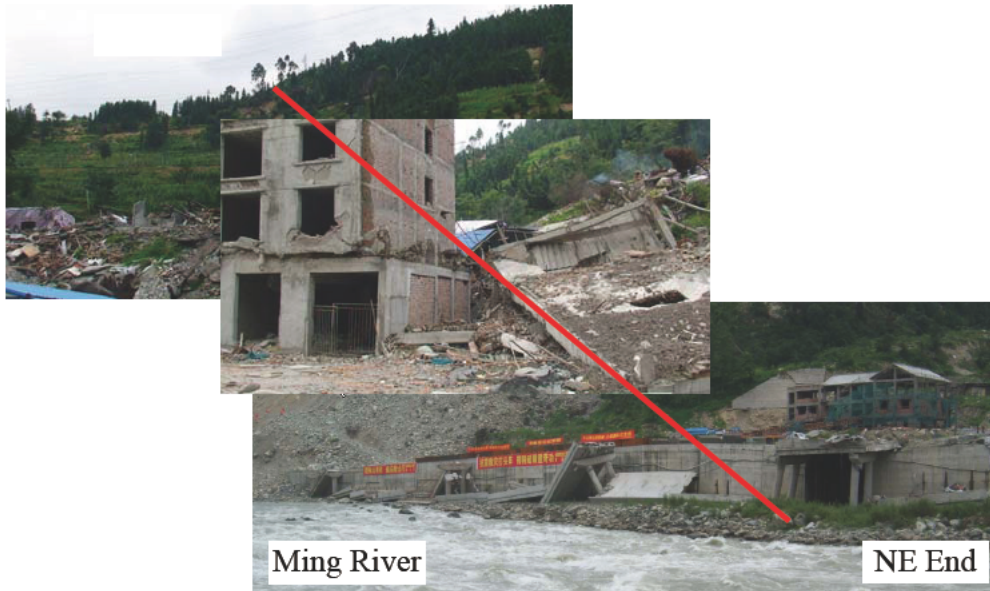


Figure 3: Surface Rupture of the Earthquake Fault



Figure 4: Surface Rupture along the Old Highway near the Collapsed Building

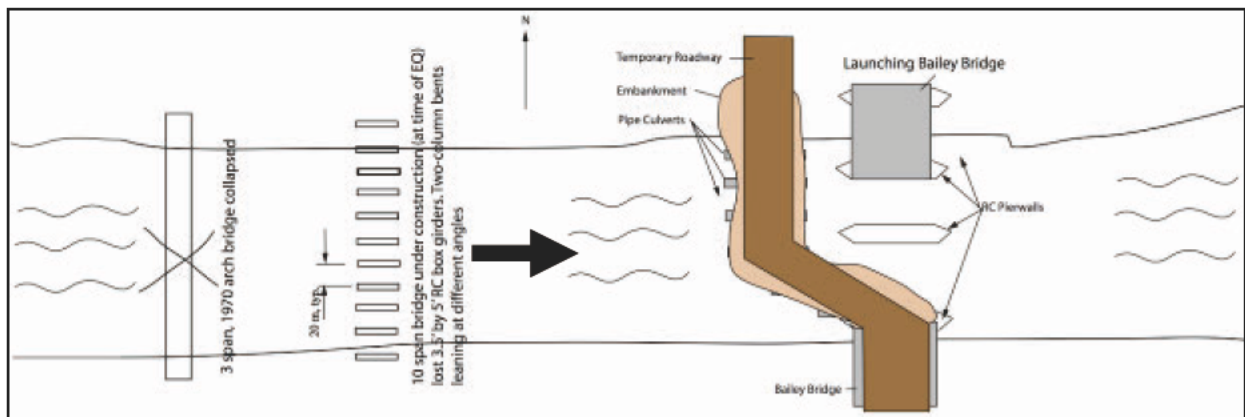


Figure 5: Three Bridges at Nanba Town



Figure 6: Collapse of the Old Three-Arch Bridge



Figure 7: Damage Scenario of the 10-span Bridge under Construction during the Earthquake



Figure 8: Damage to the 10-Span Bridge under Construction

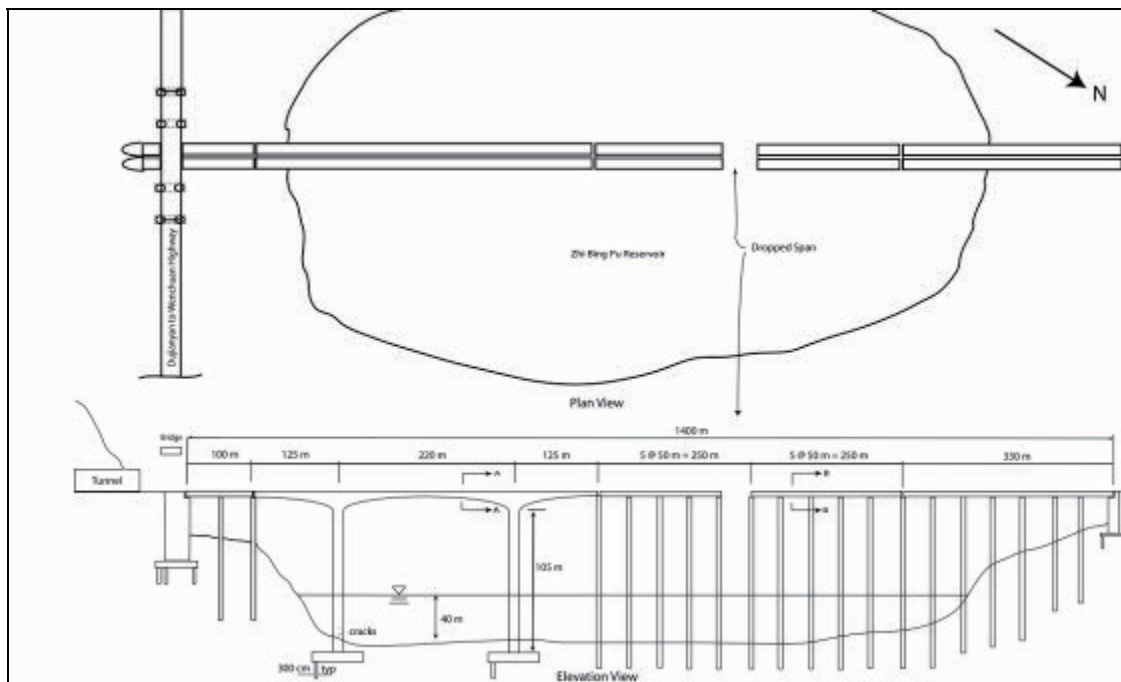


(a) Overview of a Temporary Bridge Construction

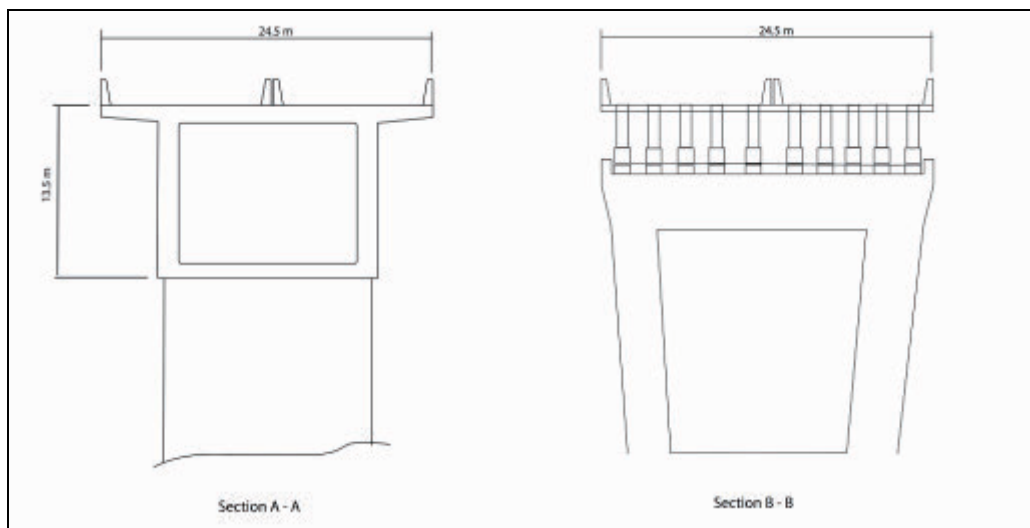


(b) Bailey Bridge Pushed in Place

Figure 9: Construction of a Temporary Bridge



(a) Plan and Elevation



(b) Cross Section of Main Span and Approach Bridge

Figure 10: Schematic View of the Miaozhiping Bridge



Figure 11: Miaozihiping Tunnel



Figure 12: Overview of the Miaozihiping Bridge



Figure 13: Drop-off Span and Construction Details between Two Spans



Figure 14: Longitudinal and Transverse Offset of Bridge Deck



Figure 15: Shear Key Failure



Figure 16: End of the Miaozhiping Bridge and its Overpass for the Old Highway



Figure 17: Damage to Shear Key and Embankment of the Overpass



Figure 18: Bridges in the Vicinity of Miaozhiping Bridge

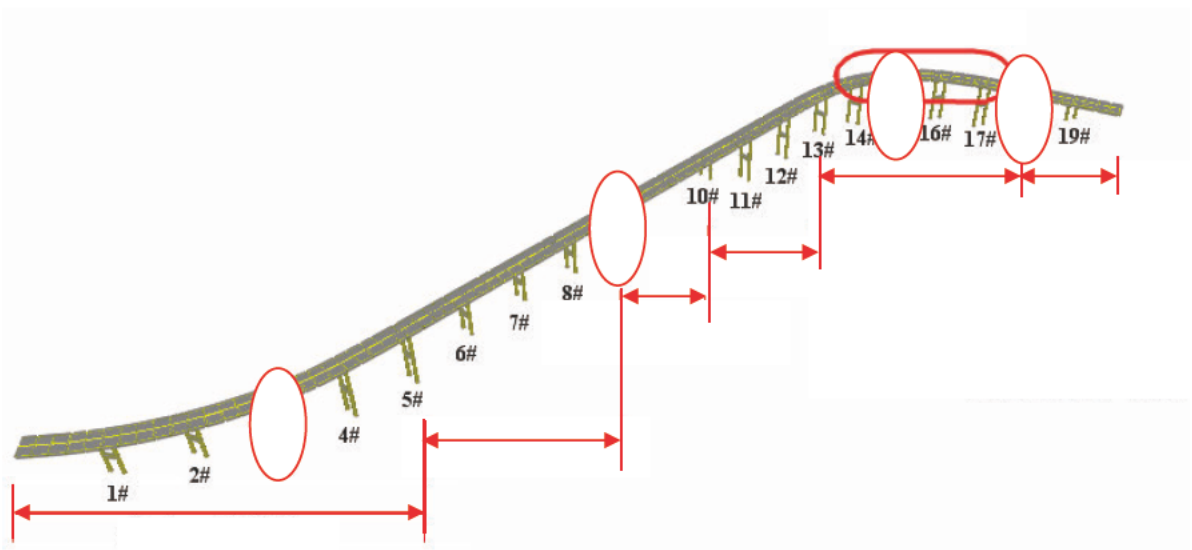


Figure 19: Schematic View of the Baihua Bridge before the Earthquake



Figure 20: Post-Earthquake Damage



Figure 21: Damage at Bent 3



Figure 22: Damage at Bent 9



(a) Column Shear and Flexural Failure



(b) Column Shear Failure and Section 5 Collapse

Figure 23: Earthquake Damage at Bent 15

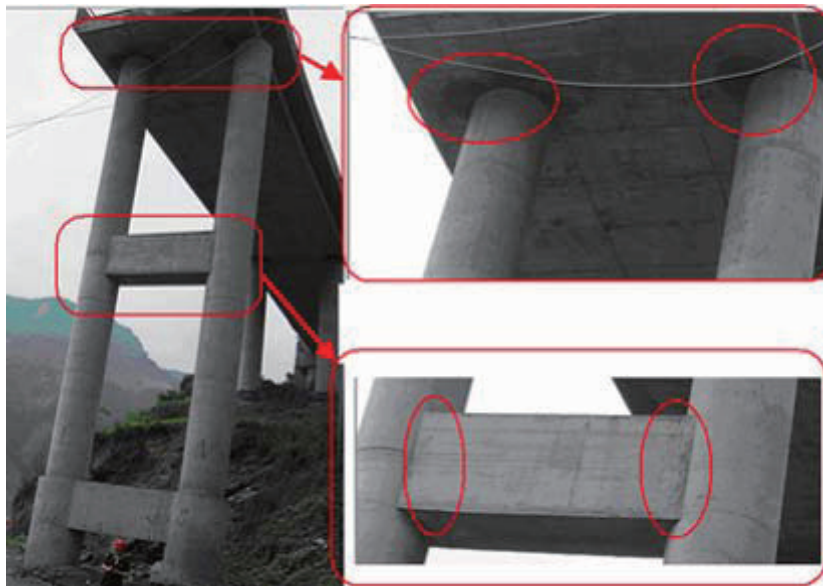


Figure24: Damage at Bent 18



(a) Blast Demolition



(b) After Demolition

Figure 25: Post-Earthquake Demolition of Baihua Bridge

# Quick Earthquake Damage Detection System for Bridges

by

Junichi Sakai<sup>1</sup> and Shigeki Unjoh<sup>2</sup>

## ABSTRACT

When an extreme earthquake occurs, roads and bridges are fundamental infrastructures to evacuate the affected people and to transport the emergency equipment and materials. For these emergency activities, it is essential to detect immediately after the earthquake the severe structural damage that affects the performance of structures. This paper proposes a method for quick earthquake damage detection/evaluation of reinforced concrete bridge columns, which has been developed through investigations of dynamic response properties of reinforced concrete bridge columns obtained from shake table tests. An intelligent sensor unit was developed that captures changes of response period of a bridge column. Field measurements of traffic induced vibrations of bridges were also conducted to evaluate the efficiency and to improve the applicability of the proposed method.

**KEYWORDS:** Earthquake Damage, Damage Detection, Intelligent Sensor Unit, Reinforced Concrete Bridge Column

## 1. INTRODUCTION

When an extreme earthquake occurs, it is significant to ensure the emergency road network to evacuate the affected people and to transport the emergency equipment and materials. In particular, bridges are fundamental structures in the network because the damaged bridges are likely to result in long-term closer of the road.

For these emergency activities, it is essential to obtain the information of the structural safety and serviceability of bridge structures immediately after the event and to conduct repair works as soon as possible if needed. Therefore, there is a strong need to develop a

method for quick detection and evaluation of severe damage that affects the structural safety and serviceability, and also a method for subsequent rapid repair works. The authors have been conducting research projects for developing these methods for bridge structures, and have proposed rapid repair methods [1] for the latter part of the project.

In terms of the earthquake damage detection, detection/evaluation of the degree of damage and structural safety of bridge structures are currently done by visual inspection of experts; however, there are various problems on this procedure, such as: the lack of uniform standards for quantitative evaluation of the degree of damage, the difficulty of visual inspection for underground/underwater structures, and the time-consuming process for gathering and analyzing the information with a limited number of personnel. Therefore, it is necessary to develop a method for accurate and speedy determination of the degree of damage without experts' inspection.

For detecting and evaluating the seismic damage without visual inspections, research projects have been conducted to develop sensing technologies in two approaches. One is a method to evaluate the change of the global dynamic response, and the other is a method to detect a local damage. Kiremidjian et al. have proposed statistical pattern recognition based damage detection algorithms, and verified its efficiency by analyzing the data from a real three span prestressed concrete frame type bridge [2]. Some researchers proposed detection

---

<sup>1</sup> Senior Researcher, Bridge and Structural Technology Research Group, Center for Advanced Engineering Structural Assessment and Research, Public Works Research Institute, Tsukuba, Ibaraki, 305-8516, Japan

<sup>2</sup> Research Coordinator for Earthquake Disaster Prevention, Research Center for Disaster Risk Management, National Institute of Land and Infrastructure Management, Tsukuba, Ibaraki, 305-0804, Japan

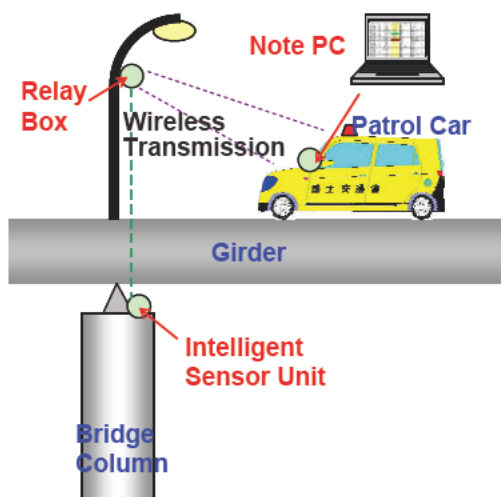


Figure 1 Seismic Damage Detection System

methods by measuring vibration characteristics [3] [4] [5]. Nihei et al. have proposed a method by measuring a maximum response rotation at column-beam connection for frame type bridge columns [6]. On the other hand, some researchers proposed methods to detect local damage of structures, such as concrete cracking, strain distribution, etc. by utilizing optical fiber sensors, or sensors made of new materials [7] [8] [9]. The authors have also been conducting a research project to develop a method to detect seismic damage by capturing the changes of vibration characteristics of global response [10] [11] because the global behavior generally has stronger correlation with the serviceability and safety of the structures.

In this paper, an algorithm estimating seismic damage of reinforced concrete bridge columns by measuring the change of response natural period is proposed. The method estimating the response ductility was developed through the analyses of shake table test results of reinforced concrete bridge column models. The field measurements were also conducted to evaluate the efficacy and the applicability of the proposed method.

## 2. DAMAGE DETECTION SYSTEM

Figure 1 shows the damage detection system proposed in this research project [11]. This is a system intended to be used by road administrators for an emergency patrol after the

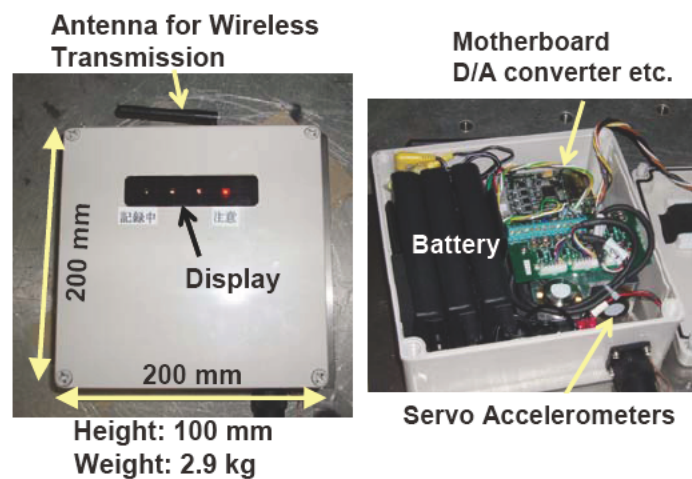


Figure 2 Prototype Intelligent Sensor Unit

big event. The system contains an intelligent sensor unit that includes an accelerometer and a microcomputer, a relay box (if necessary), and a personal computer that indicates results. The key features of the system are:

- Ability for quick damage detection,
- Easy handling of sensor units,
- Low cost for manufacture and installation,
- Ability for obtaining the information of bridge damage in a running patrol car, and
- Emergency battery in case of electrical power failure due to earthquake.

The intelligent sensor unit is placed on a column top to detect the change of response natural period of the column, and the microcomputer calculates the estimated response ductility using the proposed algorithm and judge whether the column suffers considerable damage by the proposed method. The results are wirelessly transmitted from the intelligent sensor unit to the personal computer. If the signal condition is not good enough to transmit the results, a relay box is needed to help the transmission. This system enables road administrators to gather information on the damage and safety of structures in a running patrol car during an emergency patrol.

Figure 2 shows the prototype of the intelligent sensor unit. The unit includes servo accelerometers for two horizontal directions (additional sensor for vertical response is

Table 1 Shake Table Tests Analyzed

No.	Spec.	ID., Shape	Input GM	Case	Amplitude	Time SF	Reference	
1	1	00S, Saure	JR Takatori, 2 Horizontal	00S-020x, y	20%	50%	[12] (2004) Nishida & Unjoh	
2				00S-100x, y	100%			
3	2	01C, Circular	JR Takatori, 2 Horizontal	01C-015x, y	15%	50%		
4				01C-080x, y	80%			
5	3	02R, Rectangular	JR Takatori, 2 Horizontal	02R-015x, y	15%	50%		
6				02R-090x, y	90%			
7	4	03R, Rectangular	JR Takatori, 1 Horizontal	03R-015	15%	50%		[10] (2005) Kobayashi & Unjoh 2005
8				03R-050	50%			
9				03R-060	60%			
10				03R-080a	80%			
11				03R-080b	80%			
12				03R-080c	80%			
13	5	04R, Rectangular	JR Takatori, 3 Dimensional	04R-015x, y	15%	50%	[13] (2006) Nishida & Unjoh	
14				04R-090x, y	90%			
15				04R-050x, y	50%			
16	6	05R, Rectangular	JR Takatori, 1 Horizontal	05R-015-1x	15%	50%	[14] (2006) Nishida & Unjoh	
17			K-NET	05R-015-2x, y	15%			
18			Chokubetsu, 3 Dimensional	05R-040x, y	40%			
19			05R-170x, y	170%				
20	7	05C, Circular	Tsugaru Oh- hashi,	05C-020x, y	20%	50%	[15] (2006) Sakai & Unjoh	
21				05C-400x, y	400%			
22	8	06F, Circular	JR Takatori, 3 Dimensional	06F-010x, y	10%	50%	[16] (2008) Sakai & Unjoh	
23				06F-020Mx, y	20%			
24				06F-020Ax, y				
25				06F-030Mx, y	30%			
26				06F-030Ax, y				
27				06F-050Mx, y	50%			
28				06F-050Ax, y				
29				06F-060Mx, y	60%			
30	06F-060Ax, y							
31	9	06ED, Circular	JR Takatori, 3 Dimensional	06ED-F010x, y	10%	60%	[17] (2008) Sakai, Unjoh & Ukon	
32				06ED-F080x, y	80%			

optional), a microcomputer, a D/A converter, a memory, a wireless transmitter and a battery. The dimension of the sensor is 200 mm square, the height is 100 mm and the weight is 2.9 kg. The prototype sensor unit is small and light enough for easy installation. The cost to manufacture the unit is about 1.5 million yen. The cost is yet high because servo accelerometers are used to ensure the accuracy of measurements. If large amounts of the sensor units are produced, the cost can be reduced. Although the use of less expensive accelerometers such as MEMS sensor can also reduce the cost, further research is needed to ensure the accuracy of measurements.

### 3. QUICK EARTHQUAKE DAMAGE DETECTION METHOD FOR COLUMN THAT FAILS IN FLEXURE AT BOTTOM

#### 3.1 Test Specimens and Conditions

To develop the damage detection method, results from shaking table tests for reinforced concrete bridge column specimens [10] [12] [13] [14] [15] [16] [17] were investigated. Table 1 summarizes the tests analyzed in this study. Figure 3 shows cross sections of the specimens. The size of the cross section was about 0.6 m. The height from the bottom of the column to the center of gravity of the top mass was about 3 m. The aspect ratio of the specimens was larger than 4, and no cutoff of longitudinal

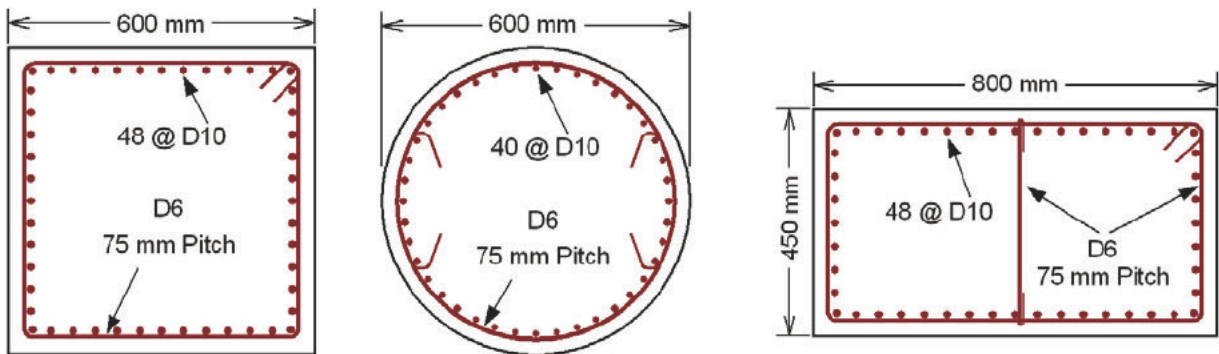


Figure 3 Typical Cross Sections of Specimens

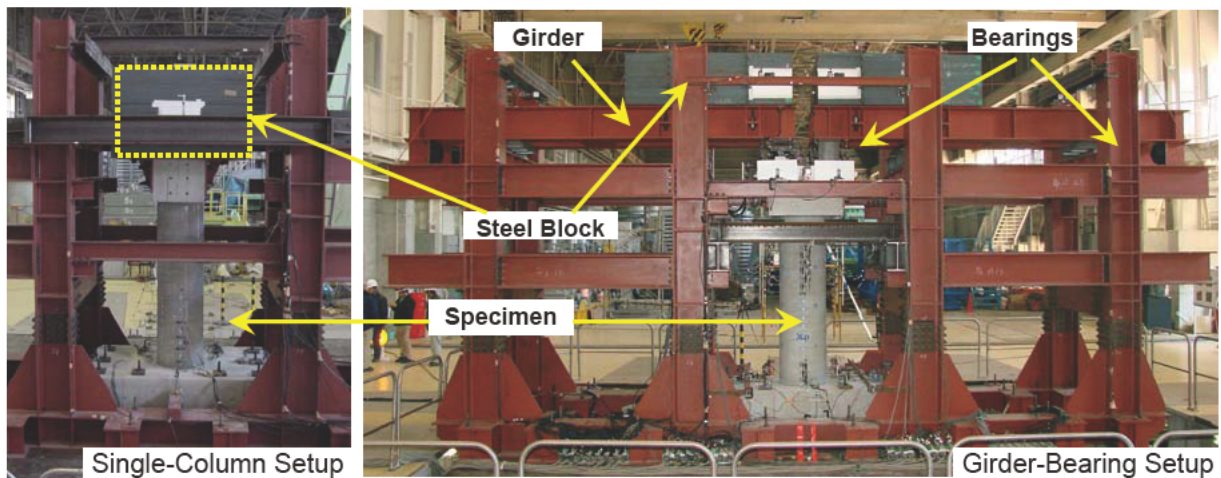


Figure 4 Test Setup

reinforcement was provided to have all the specimens fail in flexure at the bottom of the column. The scale factor of the models was assumed to be 3 or 4. The time of ground motions was scaled using a scale factor considering the similitude requirements of each specimen.

Figure 4 shows the test setup. Two types of setup were used; a single-column style setup and a setup with girders and bearings. For the single-column setup, the mass block modeling the inertia mass and axial force of a superstructure was directly fixed to the top of the columns. For the girder-bearing setup, the girders that the mass blocks were fixed onto were supported by fixed bearings on the top of the column and a longitudinal-movable/transverse-fixed bearing at each end. In this study, the response at the center of gravity of the inertia mass was analyzed for the tests with single-column setup while the response at the

top of the column was analyzed for the tests with the girder-bearing setup.

Each shake table test had two phases; one was for dynamic response in elastic range, and the other was for that in nonlinear range. Because the method was developed to estimate the damage, only tests for nonlinear response, which are 19 test cases from 32 cases shown in Table 1, were used in the analysis. As shown in Table 1, 8 specimens were tested under two horizontal (+vertical) ground motions. Thus, total cases analyzed are 33 cases because each horizontal response was analyzed individually without consideration of interaction of two horizontal responses. For the rectangular columns, the stronger axis was defined as x axis while the weaker axis was defined as y axis.

The ground motions recorded at the JR Takatori Station during the 1995 Hyogo-ken Nanbu, Japan, earthquake (Kobe earthquake), which is

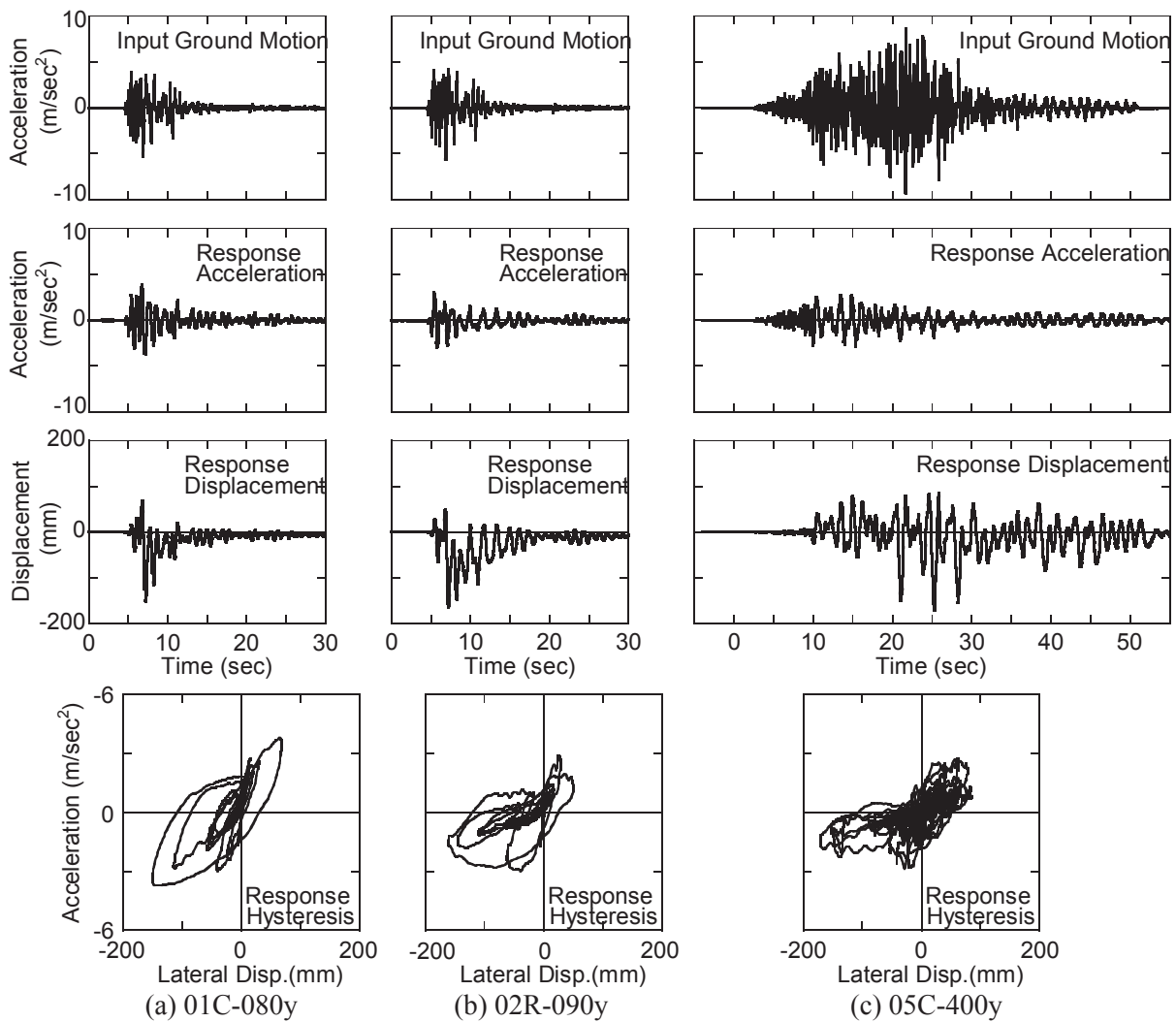


Figure 5 Dynamic Response of Specimen

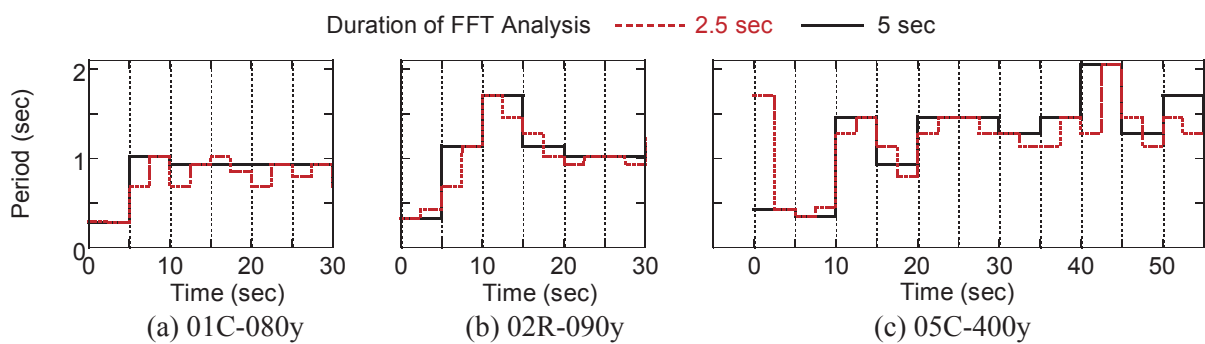


Figure 6 Changes of Response Period Due to Flexural Damage

commonly used as a near-field ground motion, was used in the most cases of the tests. Far field ground motions that have longer duration were used in some tests.

### 3.2 Dynamic Response and Change of Response Period

Figure 5 shows the time histories of the input ground motion, response acceleration and displacement at the center of gravity of the inertia mass, and acceleration versus lateral

displacement hystereses. Flexural damage, such as spalling of the cover concrete and buckling and fracture of the longitudinal reinforcement were observed at the bottom after the test. The time histories of the response indicate that the response natural period elongates after the flexural damage occurred due to the large lateral response displacement.

To evaluate such changes of vibration characteristics due to the seismic damage, response period of the column in certain duration was calculated by the Fast Fourier Transform (FFT) analysis of the response acceleration. Figure 6 shows the time histories of the changes of response period for the specimens. Here the duration of the FFT analysis of 2.5 seconds and 5 seconds were used. Considering the time scale factor ( $= 2$ ), the durations used are equivalent to 5 and 10 seconds, respectively, for real size columns. The band path filter with the cutoff frequencies of 0.333 and 10 Hz was used in the FFT analyses to eliminate the effects of the vibration characteristics of the shake table and test setup. As shown in Figures 5 and 6, when the response displacement increases during the main pulses of the ground motion, the response period increases from the initial value, which indicates the seismic damage. Change of response period is minor after the main pulses. Some case shows large response period during the main pulses of input ground motions such as the response of Case 02R-090y. This is because the response acceleration included the effects of the dominant natural period of the input ground motions.

### 3.3 Algorithm Estimating Earthquake Damage

To predict the degree of earthquake damage based on the changes of response period, a bridge column is idealized as a single-degree-of-freedom (SDOF) system shown in Figure 7.

The natural period  $T$  of the SDOF system is given as

$$T = 2\pi \sqrt{\frac{M}{K}} \quad (1)$$

where  $M$  and  $K$  are the inertia mass and

stiffness of the system, respectively. The change of natural period before and after the damage is captured by the following equation:

$$\frac{T_d}{T_0} = \sqrt{\frac{K_0}{K_d}} \quad (2)$$

where  $T_0$  and  $K_0$  are the natural period and stiffness of the system before damage, and  $T_d$  and  $K_d$  are the natural period and stiffness of the damaged structure.

Assuming an elastoplastic skeleton curve of the restoring force versus deformation relation, as shown in Figure 8, the virgin stiffness  $K_0$  is given as

$$K_0 = \frac{P_y}{d_y} \quad (3)$$

The damaged stiffness  $K_d$  is given as a secant stiffness of the point at the maximum response displacement  $d_{r\cdot\max}$  for simplicity sake although  $K_d$  is dependent on the hysteretic characteristics of the structure.

$$K_d = \frac{P_y}{d_{r\cdot\max}} \quad (4)$$

By substituting Equations (3) and (4) for Equation (2), the maximum response ductility  $\mu_{QEDDM}$  can be given as

$$\mu_{QEDDM} = \frac{d_{r\cdot\max}}{d_y} = \left( \frac{T_d}{T_0} \right)^2 \quad (5)$$

The response ductility is estimated from the following equation using the empirical coefficient for structural properties  $\alpha$ , which is determined based on hysteretic characteristics.

$$\mu = \alpha \cdot \mu_{QEDDM} \quad (6)$$

Because the maximum response ductility  $\mu$

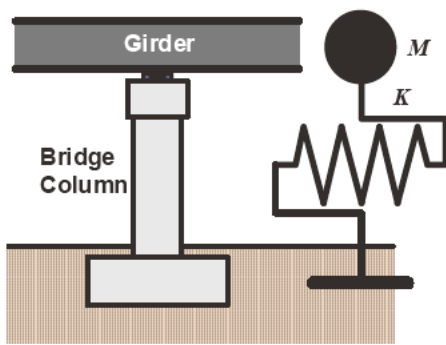


Figure 7 SDOF System Idealization

Table 2 Flexural Damage of Reinforced Concrete Column

Damage	Minor	Moderate	Severe
Schematic Image of Damage			
	Flexural Cracks	Flaking, Minor Spalling of Cover Concrete	Spalling of Concrete Buckling/Fracture of Longitudinal Rebar Fracture of Hoops

has strong correlation with the structural damage, the degree of damage can be estimated by the proposed method.

The empirical coefficient for structural properties  $\alpha$  is determined from the analyses of the test results for the reinforced concrete bridge columns, which will be described in 3.5. The empirical coefficient  $\alpha$  is the coefficient determined depending on materials and failure mechanism of structures, and thus, this algorithm can be applied to any columns by determining the structural coefficient for each structures.

### 3.4 Quick Earthquake Damage Detection Method

Using the proposed algorithm introduced in 3.3, a method detecting/evaluating earthquake damage is developed. Firstly, the relation between estimated response ductility and earthquake damage was clarified, and subsequently, the data processing method is developed.

Table 2 shows the degree of damage of reinforced concrete bridge columns that fail in flexure at the bottom of the column. It is commonly known that for the columns designed according to the Japanese specifications for highway bridges that were published after 1996, flexural cracks are observed when the response ductility is about 2 or 3, and then flaking and minor spalling are observed. Spalling of cover concrete, buckling/fracture of longitudinal

reinforcement and fracture of transverse reinforcement occurs when the response ductility exceeds about 8. On the other hand, for the columns designed according to the older specifications, the earthquake damage observed in much smaller response ductility due to insufficient reinforcement details.

Based on these facts, the relation between the degree of earthquake damage and response ductility is determined as shown in Figure 9 depending on the applied specifications. The applied specification was categorized in three categories; pre-1980 specifications, 1980 and 1990 specifications and post-1996 specifications. This categorization is based on the fact that seismic damage of bridge columns designed according to pre-1980 specification was severe during the 1995 Kobe earthquake. In fact, the allowable shear stress of concrete and the design details for cutoff points of longitudinal reinforcement were improved in the 1980 specifications. Figure 9 also considers that the design ground motions were increased and the ductility design method was included as a design method in the specifications after the 1995 Kobe earthquake. Figure 9 would be improved based on the calibration through results of field testing because the test cases used in this study are still limited.

To install the proposed method in the intelligent sensor unit, sequence of data processing was developed. Figure 10 shows the sequence as a flowchart and Figure 11 shows the definitions of

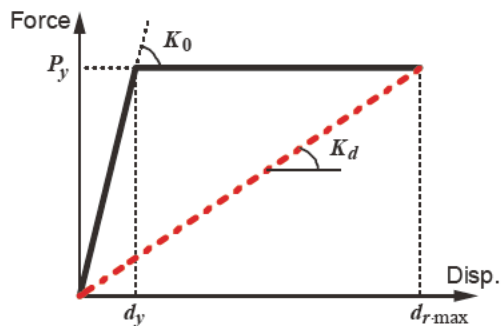


Figure 8 Assumption of Skeleton Curve

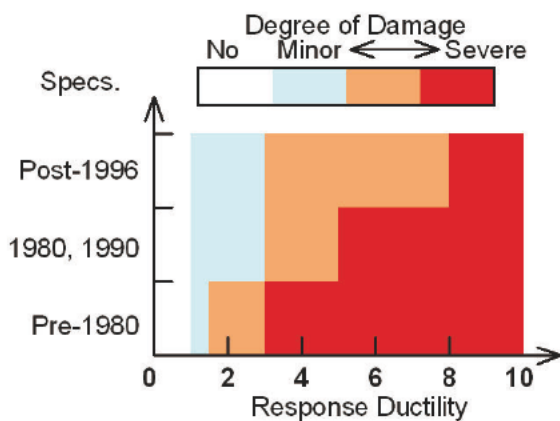


Figure 9 Relation between Earthquake Damage and Response Ductility

the delay time, the start trigger, and the end trigger.

The sensor always monitors response acceleration at the top of the column, and buffers it on the memory. If the acceleration exceeds the start trigger, which the road administrator presets, the sensor initiates recording the acceleration. The data is recorded from 10 seconds, which is a delay time, before the start trigger to 170 seconds after the trigger. Consequently, the total recording duration is 180 seconds. To record the response from the beginning of the response and to estimate the undamaged period, the delay time was introduced in this procedure.

The change of response period was calculated by the FFT analysis of the response acceleration for certain duration as examples have been shown in Figure 6. The recommended duration of the FFT analysis is determined based on the

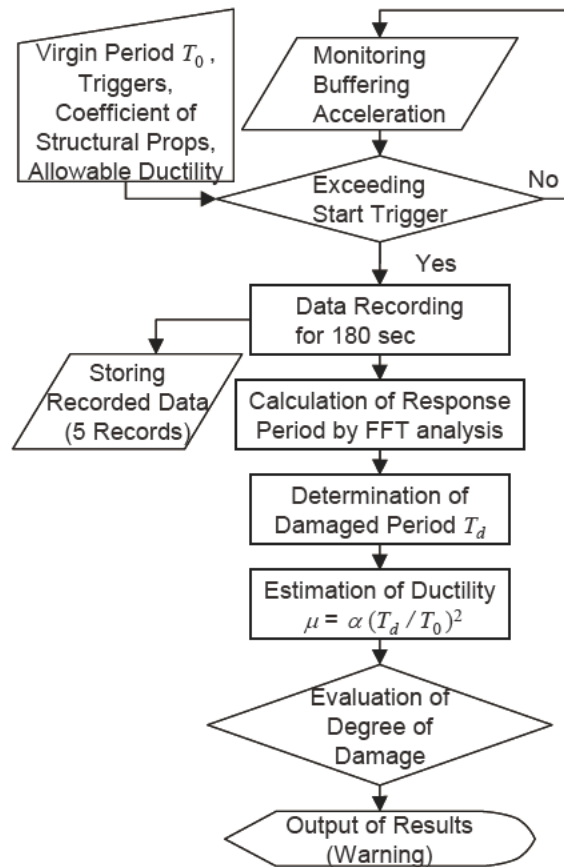


Figure 10 Sequence of Data Processing

analysis of test results as described later.

The sampling frequency and number of data for FFT analysis are 100 Hz and 2048, respectively. These values might be changed based on the performance of the microcomputer installed in the sensor unit. An appropriate band-path filter may be used to eliminate noise.

The degree of damage is estimated from the estimated response ductility obtained from Equation (6) and the relation shown in Figure 9. Therefore, it is significant to appropriately determine the virgin (undamaged) and damaged response period,  $T_0$  and  $T_d$ , respectively. Figure 11 schematically shows these periods. The virgin response period is defined as the period when the data recording initiated. Because the period at this point may be affected by the traffic vibrations as described in Chapter 4, however, the virgin response period shall be predetermined based on the preliminary

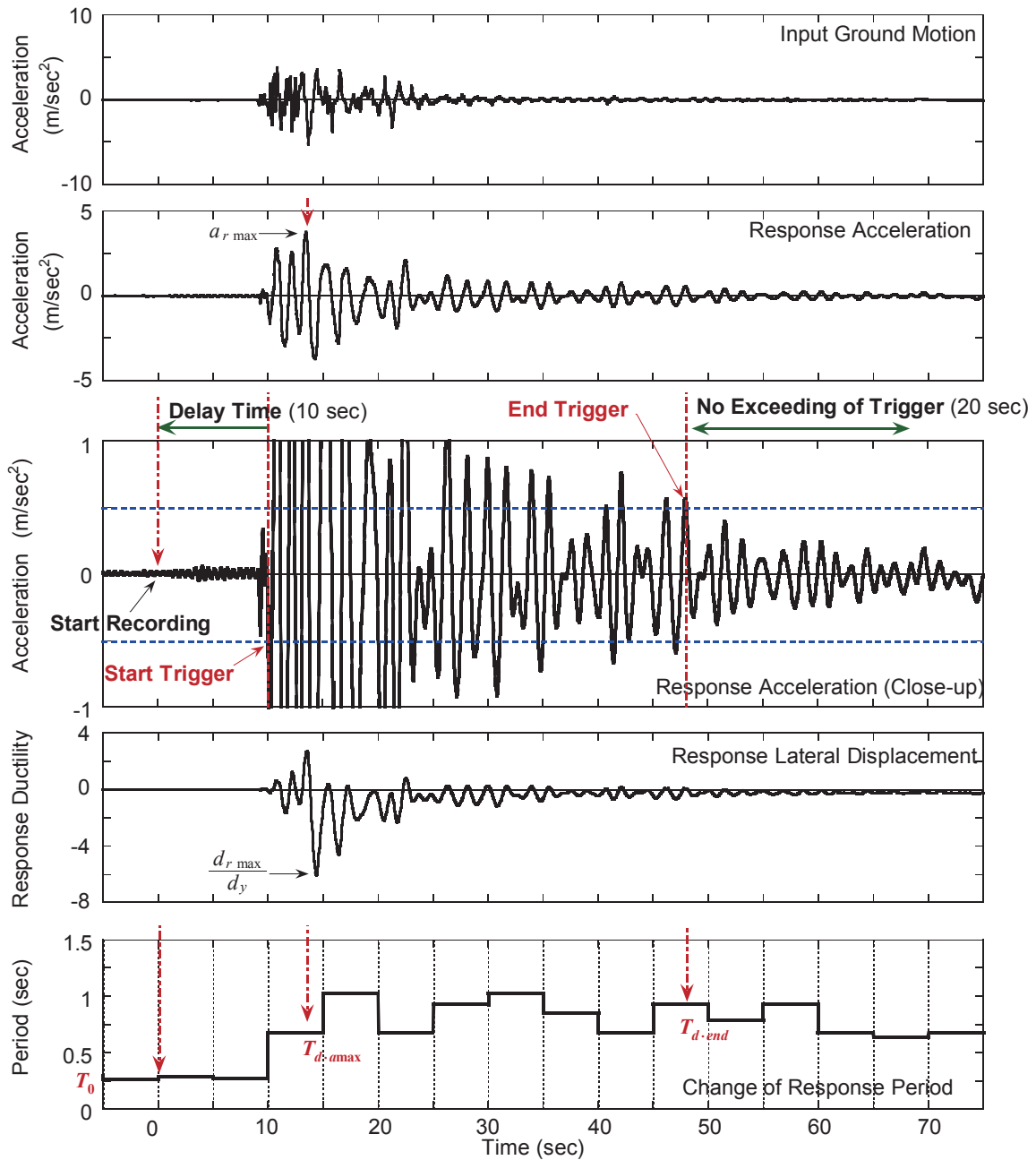


Figure 11 Definitions of Virgin Period and Damaged Period

measurements of vibrations that would be done when the sensor unit is installed at a site.

The start trigger should be set to a value that is larger than the acceleration induced by traffic vibrations because frequent start of the sensor unit will shorten the service life of the sensor. The value of the trigger may be dependent of the bridge structural type, bearing conditions, ground conditions, etc. From the seismic

response point view, it is unnecessary to record response acceleration smaller than  $0.5 \text{ m/sec}^2$  (50 gals) because such small acceleration would not affect the structural serviceability, much less structural safety. Therefore,  $0.5 \text{ m/sec}^2$  shall be used as the standard value for the start trigger. When the response acceleration induced by traffic is larger than  $0.5 \text{ m/sec}^2$ , special consideration should be made to determine the appropriate trigger.

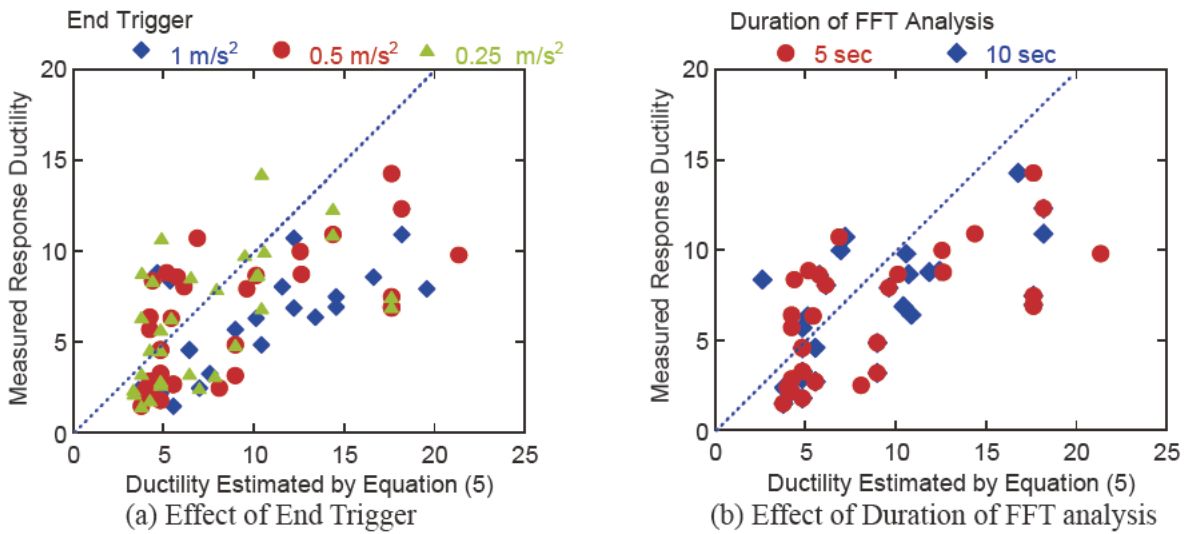


Figure 12 Effect of End Trigger and Duration of FFT analysis

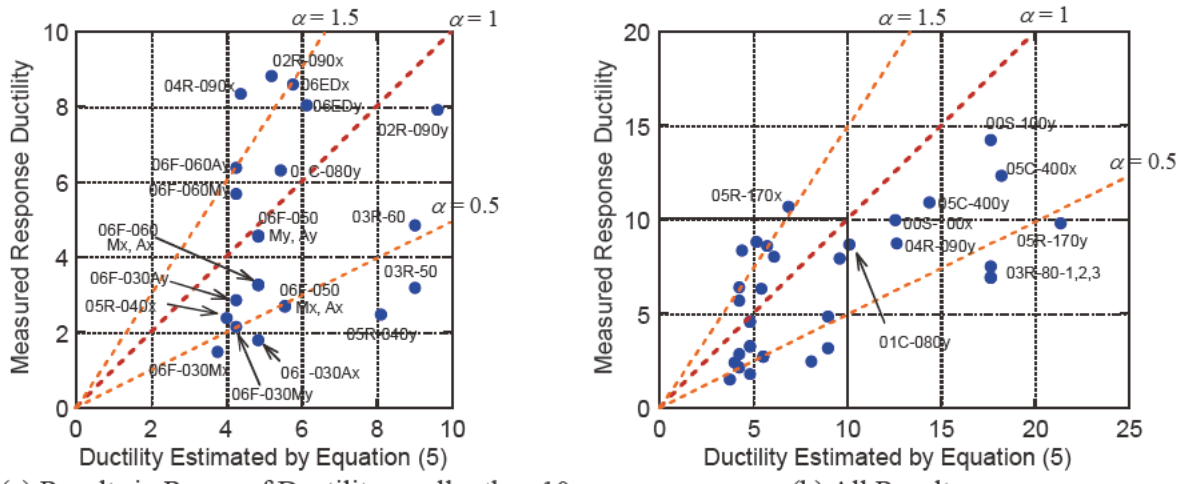


Figure 13 Accuracy of Proposed Method and Empirical Coefficient for Structural Properties  $\alpha$

The damaged response period is defined as the period at the end trigger, and the time at the end trigger is determined in the data processing by checking if the response acceleration does not exceed the trigger again for 20 seconds. The end trigger is determined based on the analysis of test results as described later.

### 3.5 Accuracy of Proposed Method

To evaluate the accuracy of the proposed method and to determine the empirical coefficient for structural properties  $\alpha$  for reinforced concrete bridge columns that fail in flexure at the bottom, the response ductility was calculated from Equation (5) and the accuracy of

the estimated response ductility was investigated. Figure 12 shows the correlation between the measured response ductility and the estimated response ductility from Equation (5).  $1 \text{ m/sec}^2$ ,  $0.5 \text{ m/sec}^2$ , and  $0.25 \text{ m/sec}^2$  were considered as the end trigger, and 5 seconds and 10 seconds were considered for the duration here to investigate the effects of the end trigger and the duration of the FFT analysis on the estimated values. The duration shown here are the converted values into real bridge size because the time of ground motions was scaled in the tests using a scale factor as described earlier.

Figure 12 shows that larger trigger is likely to result in larger estimated response ductility. This

is because the response includes the characteristics of the input ground motion. If 0.5 m/sec<sup>2</sup> and 0.25 m/sec<sup>2</sup> are used for the end trigger, Equation (5) provides almost similar accuracy for the estimated ductility, which indicates that input ground motion characteristics do not have significant effects when the trigger of smaller than 0.5 m/sec<sup>2</sup> is used. Consequently, the end trigger is set to the same value of the starting trigger, 0.5 m/sec<sup>2</sup> (50 gals). This can be used as the standard value for the start and end triggers unless the traffic vibration induces larger response acceleration.

The duration of the FFT analysis does not have significant effect on the accuracy. Because smaller duration captures changes of response periods better, the smaller duration, which is 5 seconds, is recommended.

Figure 13 shows the accuracy of the estimated ductility that is computed when 0.5 m/sec<sup>2</sup> and 5 seconds are used for the end trigger and the duration of the FFT analysis, respectively, and also shows the lines for the empirical coefficient for structural properties  $\alpha$  equal to 0.5, 1 and 1.5 for comparison. Values under these lines overestimate the response ductility by the proposed method while those over the lines underestimate. Figure 13 shows that the proposed method tends to estimate 2 times larger response ductility than the measured. Based on the regression analysis, 0.64 is obtained as the empirical coefficient for structural properties  $\alpha$ , and the coefficient of determination  $R^2$  is 0.22.

Figure 13 also shows that the method tends to underestimate the response ductility for the stronger axis of the columns of the rectangular section. This is because the effect of stiffness changes due to the seismic damage would be relatively small in stronger axis, which indicates the response of the column with the considerable earthquake damage tends to occur in the response in the weaker axis. Therefore, the regression analysis was conducted for the results excluding the response of the stronger axis of the rectangular columns. Consequently, the coefficient of determination  $R^2$  was improved

to 0.43, and 0.61 of the empirical coefficient for structural properties  $\alpha$  is obtained.

Based on this investigation, the empirical coefficient for structural properties  $\alpha$  equal to about 0.6 is recommended. When the empirical coefficient  $\alpha$  is preset for installation to a real column, the importance of the bridges in an emergency road network should also be considered. For example,  $\alpha = 1$  may be used if a target bridge has an important role in the emergency road network and underestimation of the degree of seismic damage can not be allowed.

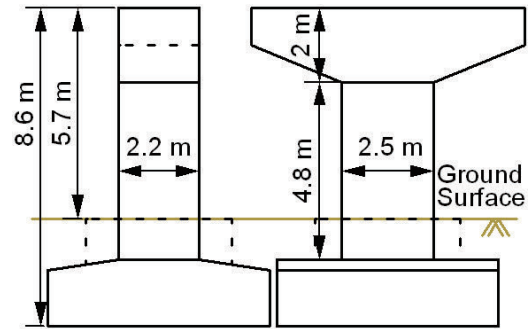
#### 4. FIELD MEASUREMENT OF TRAFFIC INDUCED VIBRATIONS BY MEANS OF INTELLIGENT SENSOR UNIT

##### 4.1 Bridges Measured

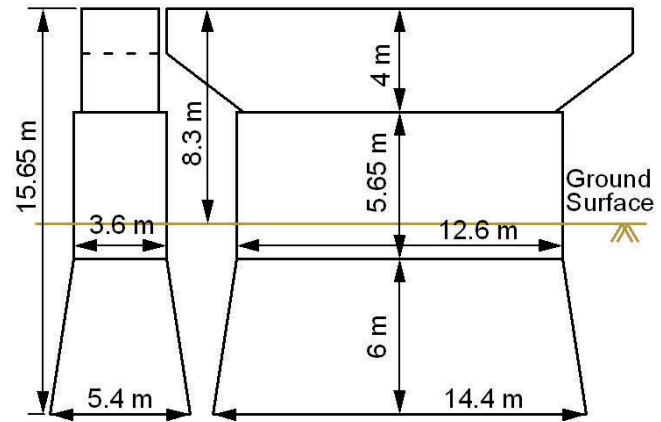
As described in 3.4, it is important to predetermine the start trigger to warrant the longer service life of an intelligent sensor unit. It is also important how the proposed method estimate the virgin period  $T_0$  under the effect of traffic induced vibrations. To investigate these matters, a series of field measurements were conducted using a prototype of the intelligent sensor unit on two reinforced concrete bridge columns supporting three-span continuous bridge that are in-service.

Figure 14 shows the target bridges and the dimensions of the bridge columns. Both bridges have one fixed/others free boundary condition. The fixed columns were selected for measurements. Column A has a rectangular cross section with a dimension of 2.5 m by 2.2 m. The bridge was constructed in 1988 and the column was retrofitted by steel jacketing. The bottom portion about 1.1 m from the bottom is embedded in the ground, and the column is supported by a pile foundation.

The cross section of Column B is a rectangular with a half-round at both ends. The dimensions in longitudinal and transverse directions are 14.4 m and 5.4 m at the bottom and the section size reduces to 12.6 m by 3.6 m at the height of 6 m from the bottom. The bridge was constructed in



(a) Column A



(b) Column B

Figure 13 Bridges Measured

1971, and the column was retrofitted by reinforced concrete jacketing. The bottom half portion is embedded in the ground, and the column is supported by a caisson foundation.

Two horizontal (longitudinal and transverse of bridge axis) accelerations were measured. The sensor was manually started for measurements. The duration of measurement and the sampling frequency were set to 120 seconds and 100 Hz, respectively, and 40 times of measurements were conducted for each column. The baseline shifting due to traffic vibrations included in the recorded data was eliminated in data processing.

#### 4.2 Double Amplitude of Response Acceleration

Figure 14 shows time histories of response acceleration. The results after baseline correction are shown here. Figure 14 also shows the change of natural period calculated from the FFT analysis with the duration of 5 seconds.

Figure 15 shows the maximum difference of the maximum and minimum response accelerations induced by the traffic vibrations. Here the maximum difference is defined as the double amplitude of response acceleration. The maximum double amplitude was  $0.18 \text{ m/sec}^2$  and  $0.06 \text{ m/sec}^2$  for Column A and B, respectively. These results also show the baseline drift due to traffic induced vibrations could be about  $0.2 \text{ m/sec}^2$  at most, and thus the possible maximum response acceleration may be about  $0.2$  to  $0.3 \text{ m/sec}^2$ . Based on these considerations, the start trigger of  $0.5 \text{ m/sec}^2$ , which is the standard value for the start and end triggers, can be used for these bridges.

#### 4.3 Virgin Period

As shown in Figure 14, the response period changes due to traffic conditions in 120 seconds. To determine the virgin period of the column for the proposed damage detection method, all the

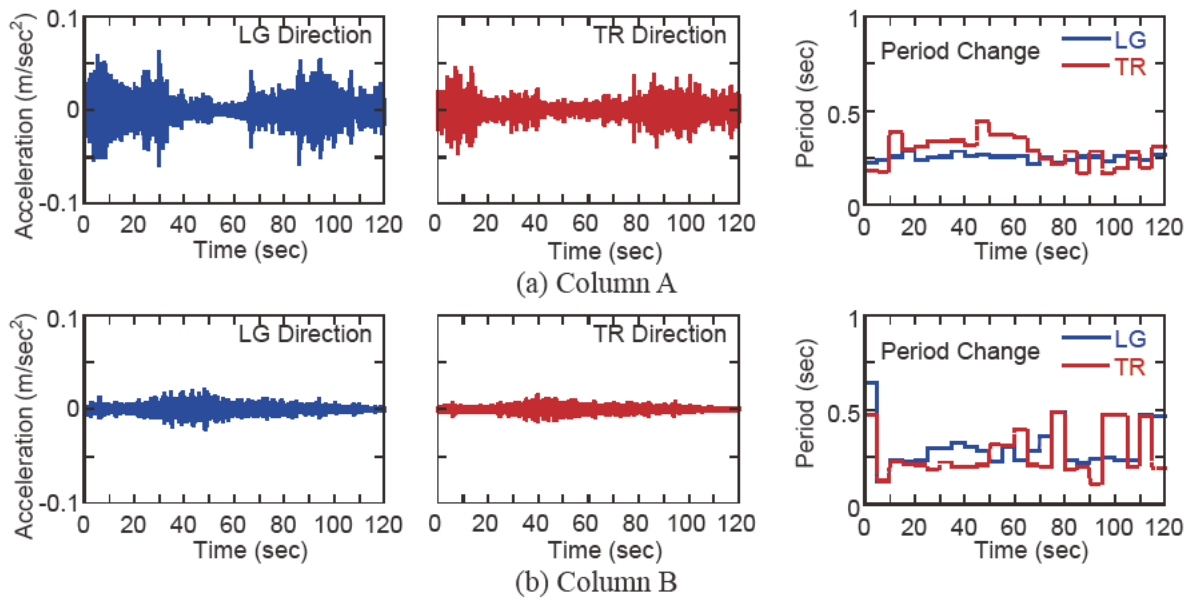


Figure 14 Response Accelerations Induced by Traffic and Changes of Response Period

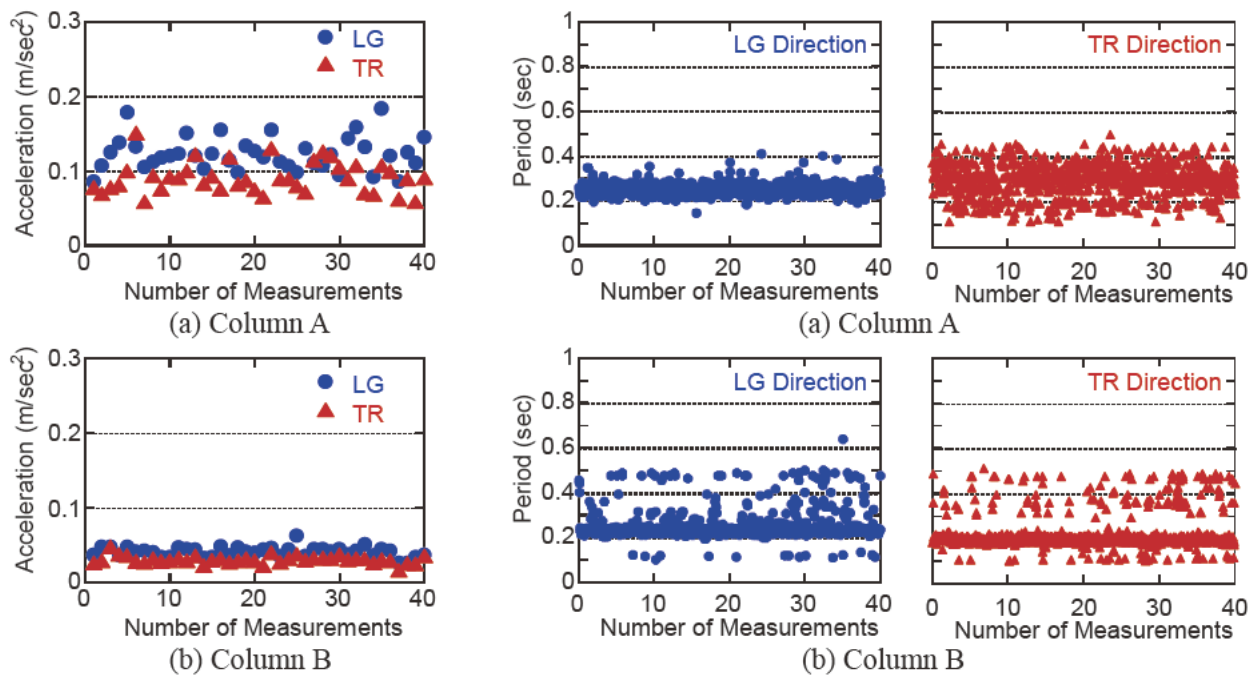


Figure 15 Double Amplitude Accelerations

Figure 16 Estimated Virgin Period

natural periods calculated for 5 second duration, which is 960 data from 40 measurements multiplied by 24 FFT analysis steps, are investigated.

Figure 16 shows all the period obtained for 960 cases. The periods of the longitudinal direction of Column A are mostly in the range of 0.23 to 0.27 seconds. The mean value is 0.25 seconds.

Those of the transverse direction scatters and the values take wider range, which is between 0.25 and 0.35 seconds. The mean value is 0.31 seconds. For Column B, the results take wider range than those of Column A. The mean values in the longitudinal and transverse directions are 0.23 and 0.2 seconds, respectively. The virgin period can be predetermined by such statistical analysis, but hundreds of datasets may be

needed because some scattering is included due to traffic conditions and this may depend on the bridge structural type, bearing conditions, ground conditions, etc. If the sensor unit is installed for an important bridge, and the scatter of the periods obtained from preliminary measurements is relatively large, special attention may be paid for predetermination of the virgin period. Smaller virgin period may be used in such a case to prevent underestimation of the damage because smaller virgin period results in larger estimated response ductility as shown in Equation (5).

## 5. CONCLUSIONS

To develop a quick detection system of earthquake damage for structures, an algorithm estimating changes of natural period has been proposed. The method estimating the earthquake damage was investigated through the analyses of shake table test data of reinforced concrete bridge column models. The field measurements were conducted to evaluate the efficacy and the applicability of the proposed method. Below are the conclusions determined from the study:

- 1) The response natural period increases after the flexural damage due to the large deformation of the columns. Seismic damage of reinforced concrete bridge columns can be evaluated using natural period change.
- 2) The method estimating the response ductility using response period before and after damage was proposed. The relation between the degree of damage and response ductility depending on the applied specifications, and the sequence of data processing were also proposed. This method can be used for any structural type by determining the empirical coefficient for structural properties.
- 3) Through the analyses of shake table test results, the empirical coefficient for structural properties for reinforced concrete bridge column that fails in flexure at the bottom was determined to be 0.6. The start and end triggers and the duration of FFT analyses were also determined to be  $0.5 \text{ m/sec}^2$  and 5 seconds.

- 4) Field measurements verified that the  $0.5 \text{ m/sec}^2$  for the start and end triggers are appropriate. It is also found that the virgin period can be predetermined by statistical analysis, but hundreds of datasets may be needed because some scattering is included due to traffic conditions.

## 6. REFERENCES

1. Sakai, J. and Unjoh, S.: Shake Table Tests for Development of Rapid Repair Method for Damaged Reinforced Concrete Bridge Columns, *Proc. 6th International Conference on Urban Earthquake Engineering*, pp. 601-606, Tokyo, Japan 2009.
2. Kiremidjian, A. S., Cheung, A., Sarabandi, P. and Nair, K.: Application of Damage Detection Algorithms to Bridge Filed Data, *Proc. 23rd US-Japan Bridge Engineering Workshop*, pp. 337-350, Tsukuba, Japan, 2007.
3. Seki, M., Nishimura, A., Sano, H. and Nakano, S.: Study on The Evaluation of Damage Levels of RC Rigid Frame Railway Bridges in The Case of Earthquake, *J. Structure Mechanics and. Earthquake Engineering., JSCE, 731/I-63, 51-64.*, 2003. (in Japanese)
4. Uehan, F. and Meguro, K.: Experimental Research on Inspection Method for Damaged Structure Using Microtremor Measurement, *Proc. of 11th Japan Earthquake Engineering Symposium*, pp.1975-1980, Tokyo, Japan, 2002. (in Japanese)
5. Uehan, F. and Meguro, K.: Development of Non-Contact Microtremor Measuring Method for Vibration Diagnoses of Railway Structure, *JSCE Journal of Earthquake Engineering*, Vol. 27, CD-ROM No. 272, 2003. (in Japanese)
6. Nihei, T., Sogabe, M., Tanimura, Y., Sasaya, T., Hirano, K., Miyamoto, N. and Hamada, H.: Development of Damage Level Sensor System for Railway RC Rigid-frame Viaduct, *J-RAIL 2007*, pp. 183-186, 2007. (in Japanese)
7. Wu, Z. S. and Takahashi, T.: Damage Detection with Hybrid Sensors of Fiber

- Optics and Composite Fibers, *Proc. of the Japan Concrete Institute*, Vol/24, No.1, pp.1647-1652, Vol.24, 2002. (in Japanese)
8. Chen, G., Mu, H., Pommerenke, D. and Drewniak, J. L.: Damage Detection of Reinforced Concrete Beams with Novel Distributed Crack/Strain Sensors, *Structural Health Monitoring*, Sage Publications, Vol.3 (3), pp. 225-243, 2004.
  9. Sonehara, K., Yokoyama, K., Harada, T. and Tanabe, K.: Laboratory Test on Seismic Damage Detection Using PVDF Film Sensor, *Proc. of 9th Motion and Vibration Control Symposium*, JSME, Vol. 2005, No.9, pp.444-448, 2005. (in Japanese)
  10. Kobayashi, H. and Unjoh, S.: Development of an earthquake damage detection system for bridge structures, *Proc. 20th US-Japan Bridge Engineering Workshop*, pp. 125-132, Washington D.C., USA, 2004.
  11. Sakai, J., Kobayashi H. and Unjoh, S.: Quick earthquake damage detection method for bridge structures, *Proc. of World Forum on Smart Materials and Smart Structures Technology*, Chongqing, China, 2007.
  12. Nishida, H. and Unjoh, S.: Dynamic response characteristic of reinforced concrete column subjected to bilateral earthquake ground motions, *Proc. of 13th World Conference on Earthquake Engineering*, CD-ROM No. 576, Vancouver, Canada, 2004.
  13. Nishida, H. and Unjoh, S.: Shake Table Test for Rectangular RC Column Subjected to Three Dimensional Excitation, *Proc. of 9th Symposium on Ductility Design Method for Bridges*, pp. 327-330, 2006. (in Japanese)
  14. Nishida, H. and Unjoh, S.: Applicability of fiber Model Analysis for Dynamic Response of Rectangular RC Column Subjected to Three Dimensional Excitation, *Proc. of 12th Japan Earthquake Engineering Symposium*, No. 0196, Tokyo, Japan, 2006. (in Japanese)
  15. Sakai, J. and Unjoh, S.: Earthquake Simulation Test of Circular Reinforced Concrete Bridge Column under Multi-directional Seismic Excitation, *Earthquake Engineering and Engineering Vibration*, Vol.5, No.1, pp. 103-110, 2006.
  16. Sakai, J. and Unjoh, S.: Shake Table Test for Development of Quick Repair Method for Seismic Damage of Reinforced Concrete Bridge Columns, *Civil Engineering Journal*, Public Works Research Center, Vol. 50, No. 9, pp. 30-35, 2008.
  17. Sakai, J. and Unjoh, S.: Earthquake Simulation Tests of Bridge Column Models Damaged during 1995 Kobe Earthquake, *Proc. of 14th World Conference on Earthquake Engineering*, CD-ROM No. S17-02-001, Beijing, China, 2008.

# Shake Table Testing of Bridge Reinforced Concrete Columns under Combined Actions

by

Juan G. Arias-Acosta<sup>1</sup> and David H. Sanders<sup>2</sup>

## ABSTRACT

Combined loadings (axial, shear, bending and torsion) can have significant effects on the force and deformation capacity of reinforced concrete bridge columns (RCC); these loads can result in unexpected large deformations and extensive damage. To study the impact of different loadings on both circular and non-circular sections (interlocking spirals), eight large-scale cantilever-type RCC specimens will be tested on the bidirectional shake table facility at University of Nevada, Reno (UNR). As part of the study, an inertial loading system was developed to test on shake table single RCC under biaxial ground motions. Two sets of circular and interlocking RCC will be subjected to different levels of biaxial, torsion and vertical loads through real time earthquake motions. The performance of the specimens will be assessed in terms of strength, deformation, and failure mode.

**KEYWORDS:** bridge engineering, reinforced concrete columns, combined loadings, shake table test

## 1.0 INTRODUCTION

During moderate to large earthquakes, reinforced concrete bridge columns are subjected to combinations of actions and deformations, caused by spatially-complex earthquake ground motions, structural configurations and the interaction between input and response characteristics. As a result, the seismic behavior of RCC will be seriously affected, and that in turn influences the performance of bridges as critical components of transportation systems. In addition, current analysis methods, behavior theories and design practices do not take into consideration the full range of interactions, due to the scarcity of

experimental data and a lack of behavioral understanding.

In order to address the complex behavior of bridge members under combined loadings and its impact on system response, a comprehensive project sponsored by the National Science Foundation was established in 2006. This project includes researchers from six institutions, and the objectives are to develop a fundamental knowledge of the impact of combined actions on column performance and their implications on system response through analytical and experimental research.

The work at UNR focuses on the development of refined analysis and shaking table tests of small-scale models of bridge columns subjected to different levels of biaxial, torsion and vertical loads through real time earthquake motions. The performance of the specimens will be assessed in terms of strength, deformation, energy dissipation and failure mode. These results will be used to validate analytical tools, developing new inelastic models for RCC under combined loadings and to propose new design methodologies. This paper highlights some of the preliminary work underway at UNR.

## 2.0 SPECIMEN DETAILS

Two sets of specimens of circular and interlocking columns were constructed using current bridge design details typical of bridges in California in accordance with the *Seismic Design Criteria* (CALTRANS, 2006). The structural configuration selected was similar to previous columns tested at UNR (Laplace *et al.*, 1999 and Correal *et al.*, 2004). For circular columns the scaling factor selected was 1/3. The diameter of the specimens was 406 mm (16 in) and the height 1830 mm (72

<sup>1</sup> Graduate Student, Dept. of Civil & Environmental Engineering, Univ. of Nevada, Reno, NV89557, USA

<sup>2</sup> Professor, Dept. of Civil & Environmental Engineering, Univ. of Nevada, Reno, NV89557, USA

in), thus the aspect ratio was 4.5, which allows for flexural dominated behavior. The columns were reinforced with 20 No.4 (D13) deformed longitudinal bars, distributed uniformly around the perimeter and fully developed with 90 degree hooks in the footing. This resulted in a longitudinal reinforcement ratio of 2%. The confinement consisted of a continuous spiral made from galvanized steel wire with a diameter of 6.25 mm (0.25 in) and a pitch of 38 mm (1.5 in). The clear cover was set to 19 mm and the resulting volumetric ratio of the spiral reinforcement was 0.92%. Details of circular specimens are shown in Fig. 1.

For interlocking columns a scale factor of 1/4 was used. Consequently, the height was 1800 mm (72 in) and the width in the short side was 305 mm (12 in), while that in the long dimension was 445 mm (17.5 in). The longitudinal reinforcement consisted of 32 No. 3 (D10) deformed bars, spaced evenly in two circular patterns and fully developed in the footing. The resulting reinforcement ratio was 2%, while the volumetric ratio of the spiral reinforcement was 1.0%. The confinement for each of the circular sections consisted of a continuous spiral made from galvanized steel wire with a diameter of 4.9 mm (0.192 in) and a pitch of 25 mm (1.0 in). The clear cover was set to 13 mm (0.5 in). Details of the interlocking specimens are shown in Fig. 2.

The design compressive strength of the concrete was set as 30 MPa (4.5 ksi), while the nominal yielding strength of the steel was 447 MPa (64 ksi) for deformed bars and 420 MPa (60 ksi) for steel wire. Table 1 shows the real properties of steel and concrete based on coupons and cylinders tests. The superstructure mass was defined as 356 kN (80 kips), which is equivalent to an axial load of 8% of  $A_g f_c'$ .

### 3.0 EXPERIMENTAL TEST SETUP

As part of the project a new inertial loading system was developed at UNR to test single cantilever-type columns on shake table under biaxial excitations. The aim of the test setup is to have a supporting structure that carries safely the vertical component of the inertial mass

(superstructure weight) but allows transfer the inertial forces from the structure to the specimen. A similar structure that allows dynamic excitation in one direction was developed at UNR ten years ago (Laplace, 1999). The new system is composed by a 3D four columns frame and a platform that sets on ball bearings located at the top of the columns. The platform is connected to the RCC specimen through links in two perpendicular directions, which transfer shear and torsion but not axial load (Fig. 3a). Additional mass is set on the platform to simulate the weight of a portion of the bridge superstructure and this can be distributed in an asymmetric configuration to induce torsion in the system. In addition, a safety system was designed to catch the platform in the event of large displacements or specimen collapse.

The axial load is applied directly to the specimen through a center-hole ram equipped with a servo-valve. The ram is connected to the specimen throughout an unbonded prestressed bar placed in an ungrouted conduit at the middle of the column and anchored at the footing. It is important to note that the main purpose of the prestressed bar is to induce the required level of axial load in the columns rather than increases its displacement capacity as has been found in other studies (Sakai *et al.*, 2006).

Since the designed system does not induce secondary moments (PD-effects) in the specimen and the unbonded prestressed bar inside the column would generate restoring lateral forces, additional dynamic actuators will be located at the top of the specimen to induce the equivalent force to have PD effects and to compensate the restoring force throughout hybrid simulation (Fig. 3b).

In view of the complexity of the system in terms of the active control of dynamic actuators, the test program was divided in two phases. At the beginning a set of two circular and two interlocking columns will be tested without any axial load or PD effects. A second phase will incorporate all the effects.

### 4.0 ANALYTICAL INVESTIGATION

Analytical models were developed to anticipate the seismic performance of the specimens and to

determine the appropriate input loadings to be used during the tests. Time history inelastic analysis have been performed using OpenSees (Mazzoni *et al.*, 2006). Analytical models of single cantilever-type columns with lumped mass as well models of the specimens including the inertial loading system were studied under different levels of earthquake excitations and mass distribution to determine limit states in the behavior of the columns during the tests. Fig.5. shows the analytical models used in this study.

The biaxial flexural behavior of the columns was simulated using a lumped plasticity model throughout uniaxial fiber elements (element beam-with-hinges in OpenSees). The stress-strain properties of the unconfined and confined concrete were simulated using the Mander's model (Mander *et al.*, 1988). For that, the actual strength of the concrete measured from cylinders at 28 days was used. Likewise, the longitudinal reinforcing steel was idealized using the uniaxial steel material model developed by Chang and Mander (1994). The actual stress-strain backbone curve measured from coupons was used as the input parameter for the steel material model. Also, the reinforcement slippage was included in the models in the form of additional rotation at the plastic hinge location.

Since inelastic fiber models for torsion are still under development (Mullapudi *et al.*, 2008), a reduction factor of 20% the elastic torsional stiffness (GJ) was used to take in account the torsional cracking of the concrete in agreement with the *Seismic Design Criteria* (CALTRANS, 2006).

To estimate the lateral load and displacement capacities of the specimens moment-curvature analysis were performed. Table 2 summarizes the capacities of the circular and interlocking columns. Once the capacity was estimated, a series of nonlinear time history analysis were conducted to select the input motion to be simulated in the shake table test.

As was mentioned before, five cases of mass distribution were studied to determine the largest torsional demand on the specimen. Fig. 4 shows

five cases of mass distribution at the top of the inertial frame.

#### 4.1 Ground Motions

The two horizontal components of the 1940 Imperial Valley earthquake (El Centro), the 1994 Northridge earthquake, the 1992 Cape Mendocino earthquake and the 1995 Hyogo-ken Nanbu earthquake (Kobe) were used as the input motions. The earthquake records for Northridge and Cape Mendocino were scaled to have a hazard level of 2% of exceedence in 50 years (Zhang and Xu, 2008).

The amplitude of the records was increased until the maximum capacity of the analytical model was achieved. Also, the time axis of the input motions was compressed to account for the specimen scale factor.

From the dynamic analysis, it was found that the record at Cape Mendocino amplified by a factor of 1.4 will induce the maximum displacement ductility demand on the specimens without exceeding the shake table capacity. The maximum accelerations imposed in both horizontal directions were 0.8g and 0.95g, respectively.

#### 5.0 ANALYTICAL RESULTS

Fig. 6 compares the displacement history and hysteresis (base shear-displacement) curves for the models of a single column and the specimen with the inertial load system, without taking in consideration the axial load. From the figure is clear that the inertial loading system does not change the behavior of the specimen.

In terms of the torsion, it was found that the load case 2 induces the largest demand on the circular specimen (64 kN-m), which is in between the values at cracking (26 kN-m) and ultimate (80 kN-m) calculated using the ACI code (ACI, 2008).

#### 6.0 CONCLUDING REMARKS

The new inertial mass system to be used on bidirectional shake table tests at UNR represent a significant advance in the simulation of single RCC

under simultaneous loads induced by real time earthquake motions. One of the most important characteristics of this system is that it allows the interaction between bending and torsion with or without axial load.

Preliminary analytical and experimental results found at UNR and by researchers from other institutions involved in the project have shown that the interaction between loads have a significant effect in the capacity of reinforced concrete bridge columns under seismic loads. These results are being used to develop analytical tools and new inelastic models for reinforced concrete columns that in turn will assist in the development of new design methodologies.

## 7.0 ACKNOWLEDGEMENTS

The research presented in this paper was founded by The National Science Foundation under Grant No.EMS – 0530737. The Assistance of Ian Buckle, Patrick Laplace and Chad Lyttle of the Large Scale Structural Laboratory at University of Nevada Reno is gratefully acknowledged.

## 8.0 REFERENCES

ACI Committee 318 (2008), "Building Code Requirements for Structural Concrete (ACI 318-08) and Commentary." American Concrete Institute, Farmington Hills, Michigan, USA, 465 pp.

California Department of Transportation. (2006) "Bridge Design Specifications." Engineering Service Center, Earthquake Engineering Branch, California, USA, 250 pp.

Chang, G. and Mander, J. (1994). "Seismic Energy Based Fatigue Damage Analysis of Bridge Columns: Part I – Evaluation of Seismic capacity." NCEER Technical Report 94-0006.

Correal, J.F., Saiidi, M.S., and Sanders, D.H. (2004). "Seismic Performance of RC Bridge Columns Reinforced with Interlocking Spirals." Report No. CCEER-04-6, Center for Civil Engineering Earthquake Research, Department of Civil Engineering, University of Nevada-Reno, USA, 438 pp.

Zhang, J. and Xu, S.Y. (2008). " Seismic Response Simulations of Bridges Considering Shear-Flexural Interaction of Columns. " Proceedings of the 6<sup>th</sup> National Seismic Conference on Bridges & Highways, Paper No. P29, Charleston, South Carolina, USA.

Mander J.B., Priestley, M.J.N. and Park, R. (1988). "Theoretical Stress-Strain Model for Confined Concrete." Journal of Structural Eng. 114 (8), pp 1804-1826.

Laplace, P., Sanders, D.H., and Saiidi, M.S. (1999). "Shake Table Testing of Flexure Dominated Reinforced Concrete Bridge Columns." Report No. CCEER-99-13, Center for Civil Engineering Earthquake Research, Department of Civil Engineering, University of Nevada-Reno, USA, 438 pp.

Mazzoni, S., McKenna, F., Scott, M., and Fenves, G.L. "Open System for Earthquake Engineering Simulation (OpenSees), 2006." User manual, version 1.7.3, Pacific Earthquake Engineering Research Center, University of California, Berkeley, California, USA, <http://opensees.berkeley.edu/OpenSees/manuals/usermanual/index.html>

Mullapudi, T.R., Ayoub, S. and Belarbi, A. (2008). "Effect of Coupled Shear-Bending Deformations on the Behavior of RC Highway Structures Subjected to Extreme Seismic Loading." Proceedings of the 6<sup>th</sup> National Seismic Conference on Bridges & Highways, Paper No. P19, Charleston, South Carolina, USA.

Sakai, J., Jeong H. and Mahin, S.A. (2006). "Reinforced Concrete Bridge Columns that Re-Center Following Earthquakes." Proceedings of the 8<sup>th</sup> U.S. National Conference on Earthquake Engineering, Paper No. 1421, San Francisco, California, USA.

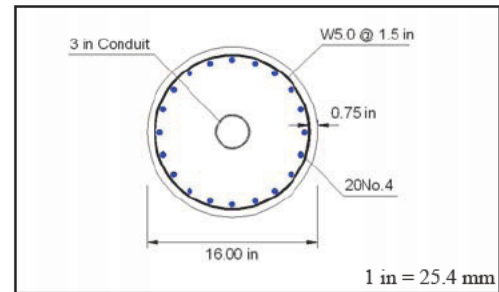
Table 1: Material properties

Days	Concrete Compressive Strength [MPa]			
	Circular		Interlocking	
	Footing	Column	Footing	Column
28	33	28	36	27

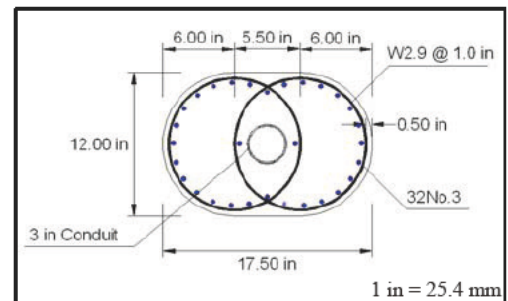
Steel Properties	No.3	No.4	W2.9	W5.0
Yield stress [MPa]	423	448	400	400
Yield strain	0.0022	0.0023	0.0024	0.0024
Strain at hardening	0.012	0.0075	N.A	N.A
Peak stress [MPa]	653	712	541	541
Strain at peak	0.124	0.115	0.115	0.126
Fracture stress [MPa]	561	687	537	484
Fracture strain	0.195	0.151	0.154	0.138

Table 2: Lateral load capacities of the specimens

Circular Columns P=0	
Properties	Radial
$\phi_y$	0.00034
$M_y$ (kN-m)	177
$\phi_u$	0.00584
$M_u$ (kN-m)	223
$\mu\Delta$	8.29
$V_u$ (kN)	122



Interlocking Columns P=0		
Properties	Short dimension	Long dimension
$\phi_y$	0.0004	0.0003
$M_y$ (kN-m)	158	229
$\phi_u$	0.00742	0.00431
$M_u$ (kN-m)	177	253
$\mu\Delta$	7.36	7.36
$V_u$ (kN)	98	138



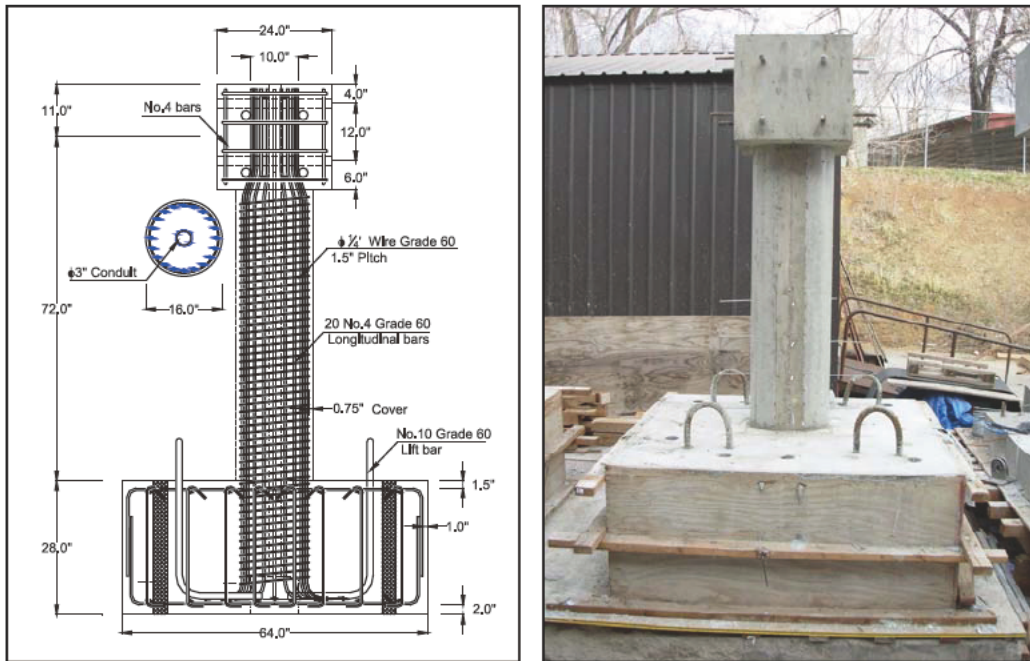


Figure 1: Geometric configuration and reinforcement for circular RCC\*.

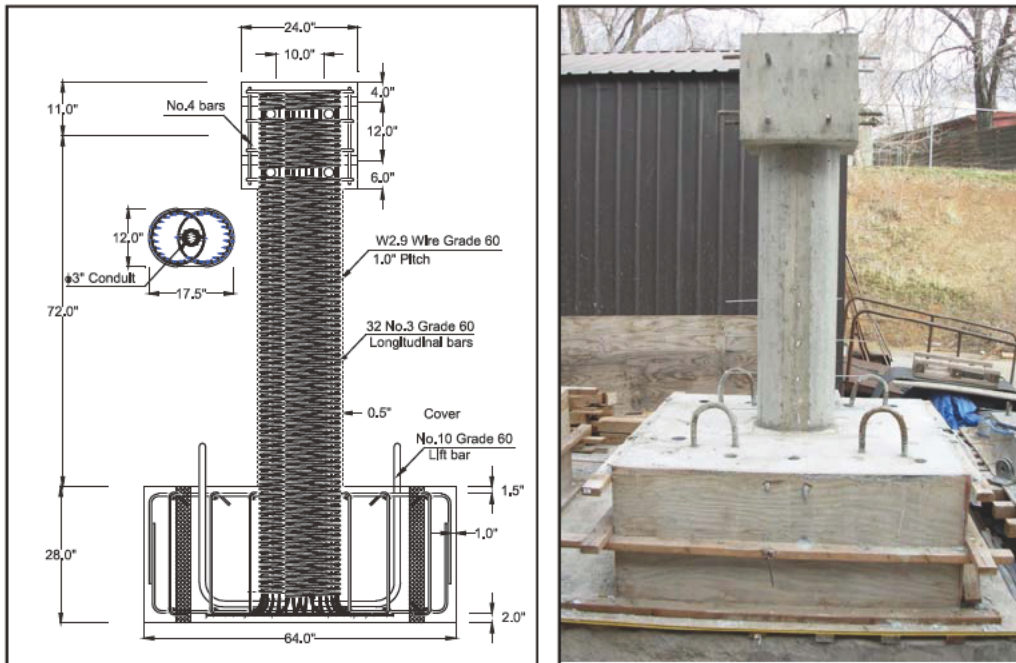
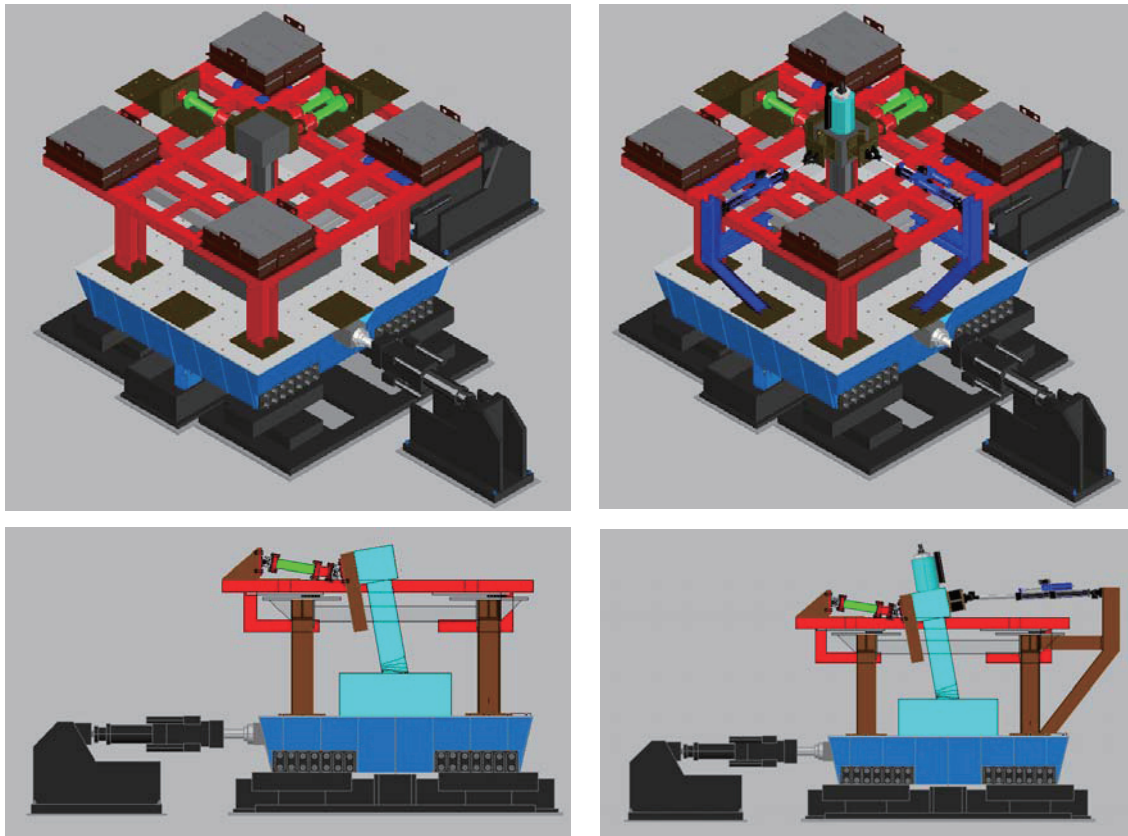


Figure 2: Geometric configuration and reinforcement for interlocking RCC\*.

\* Unit conversion 1 in = 25.4 mm.



a: Without axial load.

b: With axial load (prestressed bar + actuators)

Figure 3: Inertial loading system.

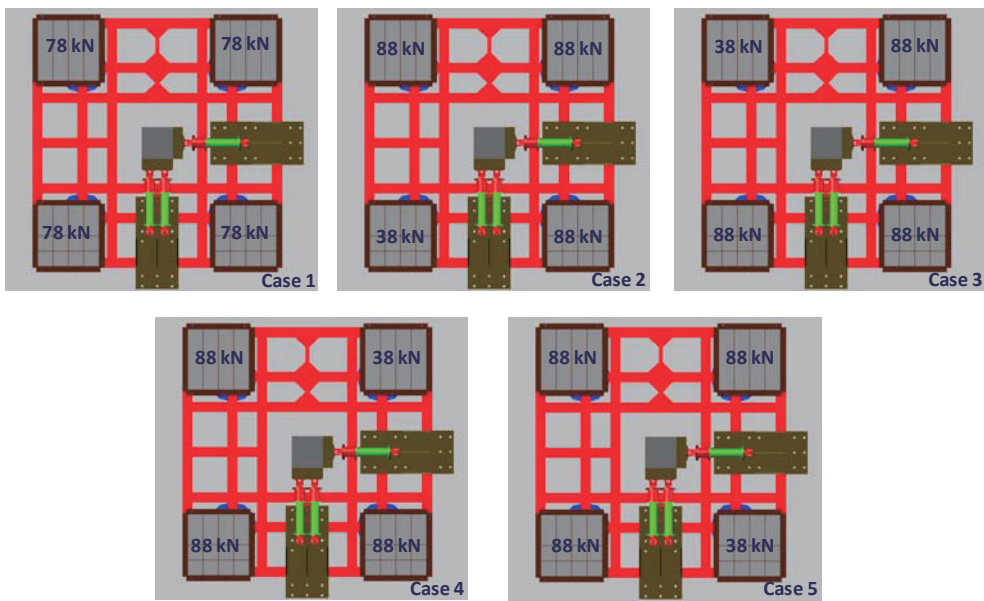


Figure 4: Mass distribution cases studied.

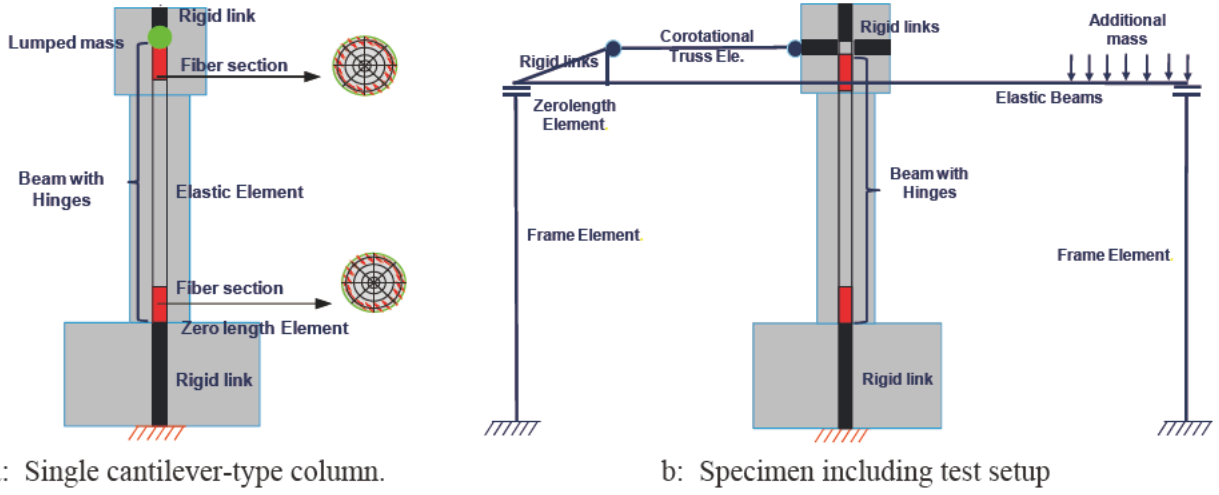


Figure 5: Analytical models.

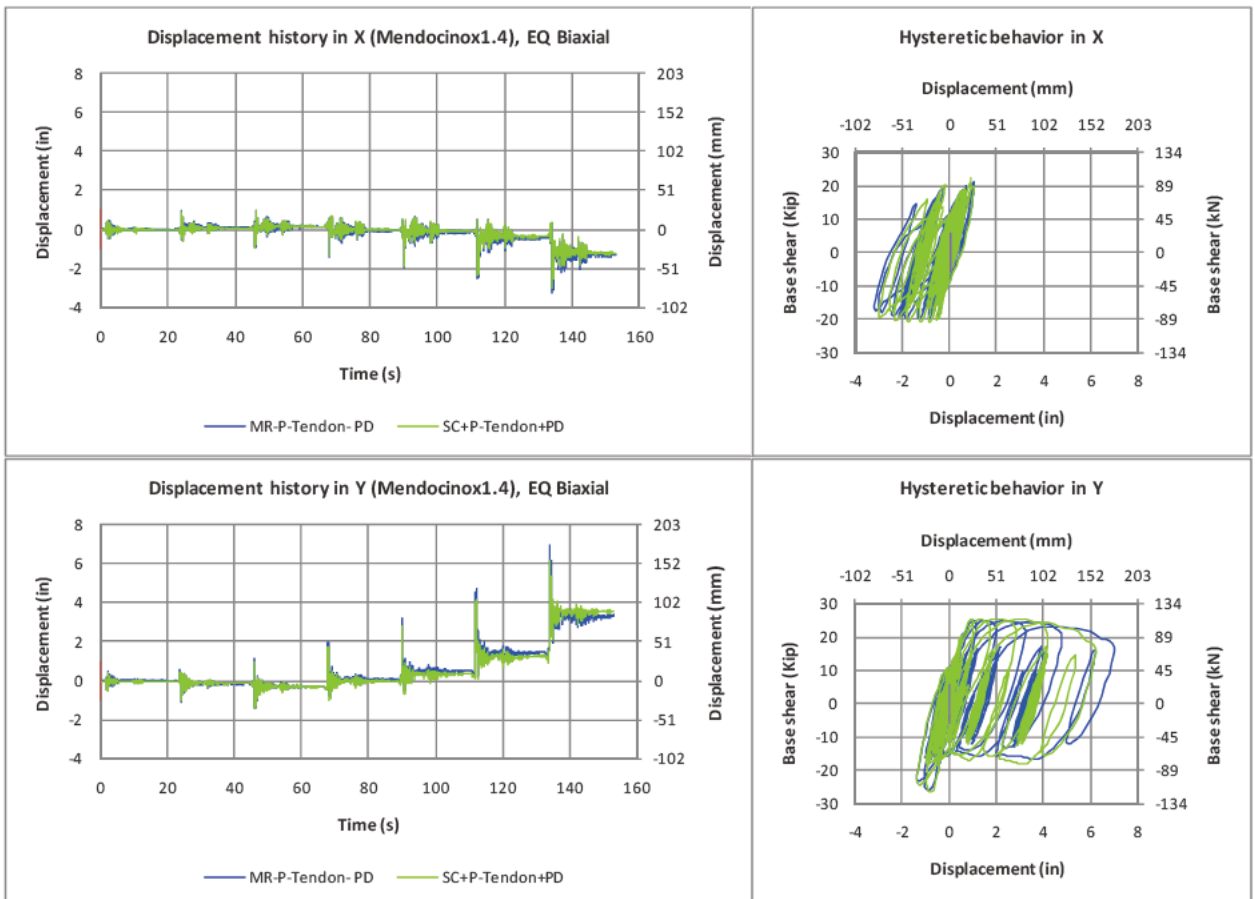


Figure 6: Analytical results, columns without axial load

# Shake table experiment on RC bridge columns using E-Defense

by

Kazuhiko Kawashima<sup>1</sup>, Tomohiro Sasaki<sup>2</sup>, Koichi Kajiwara<sup>3</sup>, Hiromichi Ukon<sup>4</sup>, Shigeki Unjoh<sup>5</sup>, Junichi Sakai<sup>6</sup>, Kenji Kosa<sup>7</sup>, Yoshikazu Takahashi<sup>8</sup>, Masaaki Yabe<sup>9</sup> and Hiroshi Matsuzaki<sup>10</sup>

## ABSTRACT

This paper presents preliminary results of a large scale shake table experiment conducted to study the failure mechanism of reinforced concrete bridge columns. E-Defense which was constructed by National Institute for Earth Science and Disaster Prevention was used to excite three columns; a typical flexural failure dominant column in the 1970s (C1-1 column), a typical shear failure dominant column in the 1970s (C1-2 column) and a typical column designed in accordance with the current design code (C1-5 column). They were 7.5 m tall 1.8-2.0 m diameter circular reinforced concrete columns. They were subjected to a near-field ground motion recorded during the 1995 Kobe, Japan earthquake. Preliminary results on the experiment and analytical correlation are presented.

## 1. INTRODUCTION

Bridges are a vital component of transportation facilities; however it is known that bridges are vulnerable to the seismic effect. Bridges suffered extensive damage in past earthquakes such as 1989 Loma Prieta earthquake, 1994 Northridge earthquake, 1995 Kobe earthquake, 1999 Chi Chi earthquake, 1999 Bolu earthquake and 2008 Wenchuan earthquake. A large scale bridge experimental program was initiated in 2005 in the National Research Institute for Earth Science and Disaster Prevention (NIED), Japan as one of the three US-Japan cooperative research programs based on NEES and E-Defense collaboration. In the bridge program, it was originally proposed to conduct experiments on two model types; 1) component models and 2) system models. They are called hereinafter as C1 experiment and C2 experiment, respectively [1].

The objective of the C1 experiment is to clarify the failure mechanism of reinforced concrete columns using models with as large section as possible. On the other hand, C2 experiment was proposed to clarify the system failure mechanism of a bridge consisting of decks, columns, abutments, bearings, expansion joints and unseating prevention devices.

C1 experiment was conducted for two typical reinforced concrete columns which failed during the 1995 Kobe earthquake (C1-1 and C1-2 experiments) and a typical reinforced concrete column designed in accordance with the current design requirements (C1-5 experiment). This paper shows preliminary results of the experiment and analysis on three C1 columns.

## 2. EXPERIMENTAL SETUP AND COLUMN MODELS

Photo 1 shows the experimental setup of three columns using E-Defense [2]. Two simply supported decks were set on the column and on the two steel end supports. A catch frame was set

---

<sup>1</sup> Professor, Department of Civil Engineering, Tokyo Institute of Technology, Meguro, Tokyo, Japan

<sup>2</sup> Graduate student, ditto

<sup>3</sup> Senior researcher, Hyogo Earthquake Engineering Research Center, National Research Institute for Earth Science and Disaster Prevention, Miki, Hyogo, Japan

<sup>4</sup> Research Fellow, ditto

<sup>5</sup> Chief Researcher, Center for Advanced Engineering Structural Assessment and Research, Public Works Research Institute, Tsukuba, Japan

<sup>6</sup> Senior Researcher, ditto

<sup>7</sup> Professor, Department of Civil Engineering, Kyushu Institute of Technology, Kita Kyushu, Japan

<sup>8</sup> Associate Professor, Disaster Prevention Research Institute, Kyoto University, Uji, Japan

<sup>9</sup> General Manager, Earthquake Engineering Division, Chodai, Tsukuba Science City, Japan

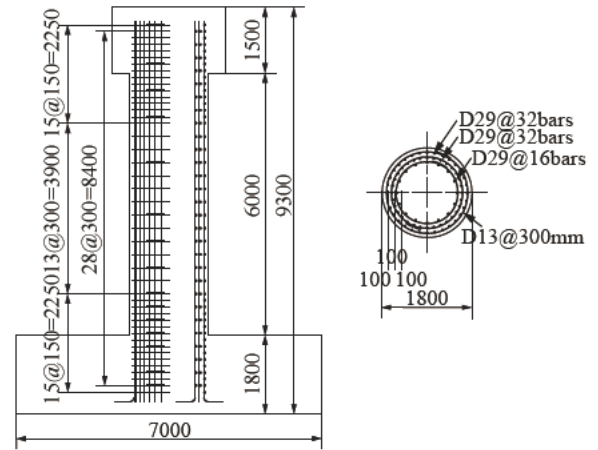
<sup>10</sup> Assistant Professor, Department of Civil Engineering, Tokyo Institute of Technology, ditto



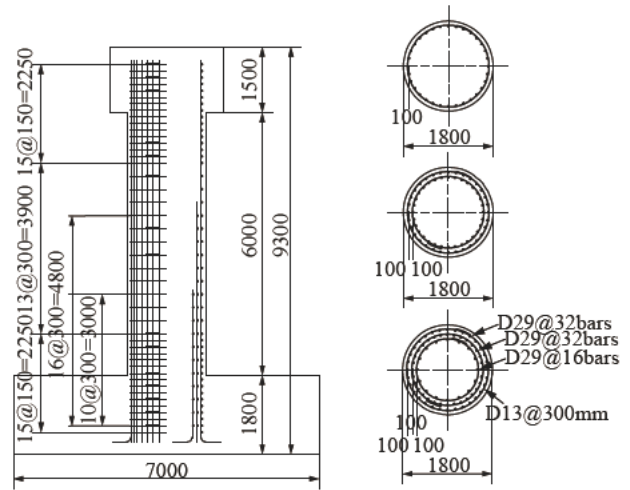
Photo 1 C1 on E-Defense

under the lateral beam of the column to prevent collapse of the column when it was excessively damaged. Tributary mass to the column by two decks including four weights was 307 t and 215 t in the longitudinal and transverse directions, respectively. The tributary mass was increased by 21 % from 307 t to 372 t in a part of C1-5 excitation.

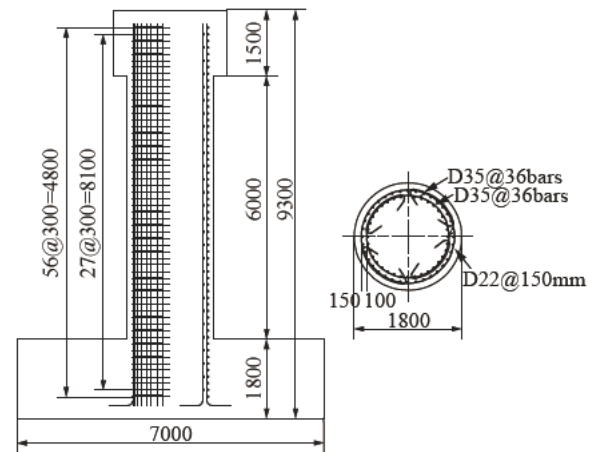
Three full-size reinforced concrete columns as shown in Fig. 1 were constructed for the experiment. Columns used for C1-1, C1-2 and C1-5 experiments, which are called hereinafter as C1-1, C1-2 and C1-5, respectively, are 7.5 m tall reinforced concrete columns with a diameter of 1.8 m in C1-1 and C1-2 and 2 m in C1-5. C1-1 and C1-2 are typical columns which were built in the 1970s based on a combination of the static lateral force method and the working stress design in accordance with the 1964 Design Specifications of Steel Road Bridges, Japan Road Association. Since it was a common practice prior to 1980 to terminate longitudinal bars at mid-heights, the inner and center longitudinal bars were cut off at 1.86 m and 3.86 m from the column base, respectively. The cut-off heights were determined by extending a length equivalent to a lap splicing length  $l_{ls}$  (about 30 times bar diameter) from the height where longitudinal bars became unnecessary based on the moment distribution. On the other hand, longitudinal bars were not cut-off in C1-1. C1-1 and C1-2 had the same shape, heights, bar arrangement and properties except the cut-off. As a consequence, C1-1 failed in flexure while C1-2 failed in shear, as will be described later. The shear failure due to cut-off was one of



(a) C1-1



(b) C1-2



(c) C1-5

Fig. 1 C1 column models

the major sources of the extensive damage of bridges in the 1995 Kobe earthquake [3].

Table 1 Seismic performance of C1-1 and C1-5 in longitudinal direction based on 2002 JRA code

Demand and Capacity	Model Columns	C1-1	C1-5(1)	C1-5(2) and C1-5(3)
Lateral Force	Design response acceleration $S_A$ (m/s <sup>2</sup> )	$1.75 \times 9.8 \text{ m/s}^2 = 17.16$		
	Force reduction factor $R = \sqrt{2\mu_d - 1}$	1.58	2.56	2.54
	Acceleration demand $S_A / R$ (m/s <sup>2</sup> )	10.83	6.70	6.77
Demand	Lateral force (kN)	3,271	2,023	2,824
	Lateral displacement $u$ (m) ( $\mu = u / u_y$ )	0.328	0.168	0.183
Capacity	Lateral force $P_u$ (kN)	1,614	2,341	2,371
	Yield displacement $u_y$ (m)	0.046	0.045	0.045
	Design displacement $u_d$ (m) ( $\mu_d = u_d / u_y$ )	0.081	0.169	0.166
	Ultimate displacement $u_u$ (m) ( $\mu_u = u_u / u_y$ )	0.099	0.231	0.227

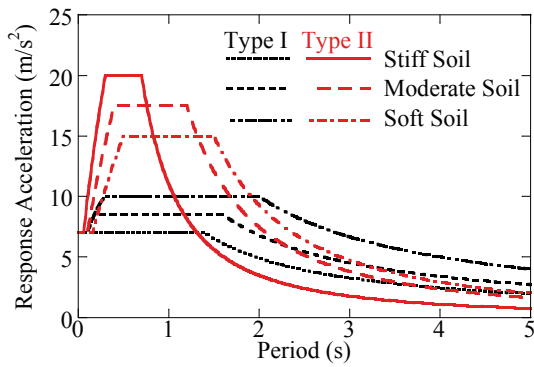


Fig. 2 Design response spectra (2002 JRA)

Combination of the lateral seismic coefficient of 0.23 and the vertical seismic coefficient of  $\pm 0.11$  (upward and downward seismic force) was assumed in the design of C1-1 and C1-2.

Deformed 13 mm diameter circular ties were provided at 300 mm interval, except the outer ties at the top 1.15m zone and the base 0.95 m zone where they were provided at 150mm interval in C1-1. Ties were only lap spliced with 30 times the bar diameter. Lap splice was a common practice by the mid 1980s. The longitudinal and tie bars had a nominal strength of 345 MPa (SD345), and the design concrete strength was 27 MPa. The longitudinal reinforcement ratio  $P_l$  was 2.02 % and the volumetric tie reinforcement ratio  $\rho_s$  was 0.32 % except the top 1.15 m and base 0.95m

zones where  $\rho_s$  was 0.42% in C1-1.  $P_l$  and  $\rho_s$  varied depending on the zones in C1-2; 2.02 % and 0.42 % at the base 0.95 m zone, 2.02 % and 0.32 % between 0.95 m and 1.86 m, 1.62 % and 0.21 % between 1.86 m and 3.86 m, 0.81 % and 0.11 % between 3.86 m and 4.85 m, and 0.81 % and 0.21 % at the top 1.15 m zone, respectively.

On the other hand C1-5 was designed in accordance with the 2002 JRA Design Specifications of Highway Bridges (JRA 2002) based on the design response spectrum as shown in Fig. 2. Sixty four deformed 35mm diameter longitudinal bars were provided in two layers. Deformed 22 mm diameter circular ties were set at 150 mm and 300 mm interval in the outer and inner longitudinal bars, respectively. The ties were developed in the core concrete using 135 degree bent hooks after lap spliced with 40 times the bar diameter. The nominal strength of longitudinal and tie bars and the design concrete strength were the same with those in C1-1 and C1-2 columns. The longitudinal reinforcement ratio  $P_l$  was 2.19 % and the volumetric tie reinforcement ratio  $\rho_s$  was 0.92 %

Table 1 shows the evaluation of the seismic performance of C1-1 and C1-5 in the longitudinal direction based on the 2002 JRA code. Because

the design response acceleration  $S_A$  is  $17.15 \text{ m/s}^2$  for both C1-1 and C1-5, the yield displacement  $u_y$  and ultimate displacement  $u_u$  are  $0.046 \text{ m}$  and  $0.099 \text{ m}$  in C1-1 and  $0.045 \text{ m}$  and  $0.231 \text{ m}$  in C1-5. The design displacement  $u_d$  is evaluated from  $u_y$  and  $u_u$  as

$$u_d = u_y + \frac{u_u - u_y}{\alpha} \quad (1)$$

in which  $\alpha$  depends on the type of ground motion (near-field or middle field ground motion) and the importance of the bridge. Assuming  $\alpha$  is  $1.5$  for a combination of the near-field ground motion category and the important bridges category, the design displacement  $u_d$  is  $0.081 \text{ m}$  in C1-1 and  $0.169 \text{ m}$  in C1-5.

On the other hand, the displacement demand  $u$  is  $0.328 \text{ m}$  in C1-1 and  $0.168 \text{ m}$  in C1-5 because the force reduction factor is  $1.58$  and  $2.56$  respectively. Consequently, C1-1 and C1-5 were evaluated to be unsafe and safe, respectively based on the current design code.

Three columns were excited using a near-field ground motion as shown in Fig. 3 which was recorded at the JR Takatori Station during the 1995 Kobe earthquake. It was one of the most influential ground motions to structures. However duration was short. Taking account of the soil structure interaction, a ground motion with 80% the original intensity of JR Takatori record was imposed as a command to the table in the experiment. This ground motion is called hereinafter as the 100 % E-Takatori ground motion. Excitation was repeated to clarify the seismic performance of the columns when they were subjected to near-field ground motions with longer duration and/or stronger intensity. Only C1-5 was excited using 125 % E-Takatori ground motion with 21 % increased deck mass to study the seismic performance under a stronger ground motion than the JR-Takatori Station ground motion.

### 3. SEISMIC PERFORMANCE OF C1-1 AND C1-5

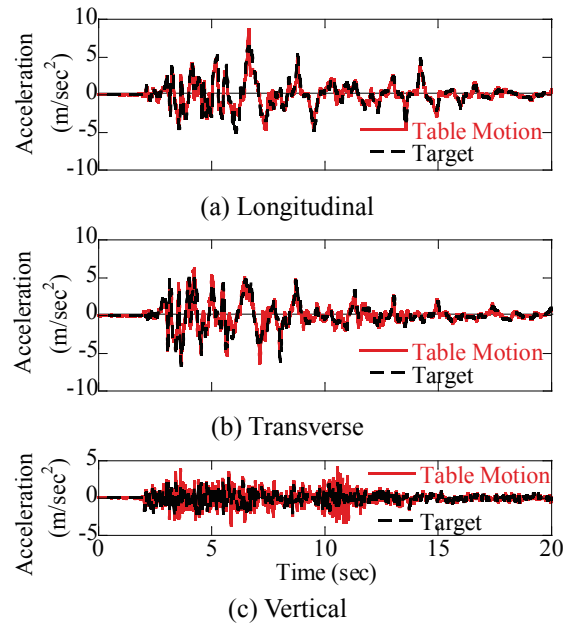


Fig. 3 100% E-Takatori ground motion (C1-5(1)-1 excitation)

#### 3.1 Progress of Failure

C1-1 was subjected to the 100 % E-Takatori ground motion twice. Photo 2 shows the progress of failure at the plastic hinge on the SW surface where damage was most extensive. NS and EW direction correspond to the transverse and longitudinal directions, respectively, of the model. During the first excitation (C1-1-1 excitation), at least two outer longitudinal bars from S to W locally buckled between the ties at  $200 \text{ mm}$  and  $500 \text{ mm}$  from the base. During the second excitation (C1-1-2 excitation), both the covering and core concrete suffered extensive damage between the base and  $0.7 \text{ m}$  from the base on the SW surface. Three ties from the base completely separated at the lap splices. Eleven outer and three center longitudinal bars locally buckled between ties at  $50 \text{ mm}$  and  $500 \text{ mm}$  from the base.

On the other hand, C1-5 was subjected to the 100% E-Takatori ground motion twice (C1-5(1)-1 and C1-5(1)-2 excitations). After the mass was increased by 21 % from  $307 \text{ t}$  to  $372 \text{ t}$ , C1-5 was subjected to the 100% E-Takatori ground motion once (C1-5(2) excitation). Then C1-5 was subjected to the 125% E-Takatori ground motion twice (C1-5(3)-1 and C1-5(3)-2 excitations).



(a) C1-1-1 excitation (8.35s)



(a) C1-5(2) excitation (8.80s)



(b) C1-1-2 excitation (7.71s)

Photo 2 Progress of damage of C1-1



(b) C1-5(3)-2 excitation (7.17s)

Photo 3 Progress of damage of C1-5

Photo 3 shows the progress of failure of C1-5 at the plastic hinge during C1-5(1)-1, C1-5(2) and C1-5(3)-2 excitations. During C1-5(1)-1 excitation, only a few flexural cracks with the maximum width of 1mm occurred around the column at the plastic hinge. Therefore it is noted that the seismic performance is enhanced in C1-5 than C1-1 under the first 100% E-Takatori excitation. The damage progressed during C1-5(2) excitation such that the covering concrete spalled off at the 500 mm base zone from WSW to SSW. During C1-5(3)-2 excitation, the failure extensively progressed. The core concrete crashed due to repeated compression, and blocks of crashed core concrete spilled out from the steel cages like explosion. Such a failure was never seen in the past quasi-static cyclic or hybrid loading experiments. Because the maximum aggregate size was 20 mm, the concrete blocks after crashed can be as small as 20-40 mm. Because the gaps of longitudinal bars and circular

ties were 132mm and 128mm, respectively, it was possible for the blocks of crashed core concrete to move out from the steel cages. Furthermore twelve outer longitudinal bars and nineteen inner longitudinal bars locally buckled on SW and NE-E surfaces. The 135 degree bent hooks developed in the core concrete still existed in the original position although the core concrete around the hooks suffered extensive damage.

### 3.2 Response Displacement and Moment Capacity

Figs. 4 and 5 show the response displacement at the top of C1-1 and C1-5, respectively, in the principal response direction (nearly SW-NE direction). The peak displacement of C1-1 was 0.179 m (2.4 % drift) during C1-1-1 excitation while the peak displacement of C1-5 was 0.084 m (1.1 % drift) during C1-5(1)-1 excitation. Because the ultimate displacement in accordance with JRA 2002 code was 0.100 m and 0.235 m in C1-1 and C1-5, respectively, the above peak response

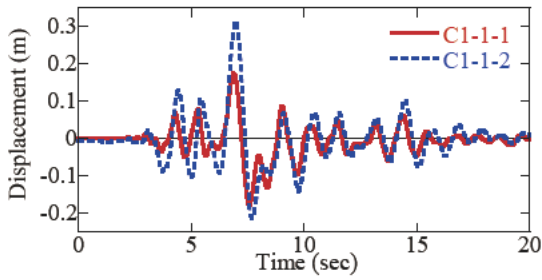


Fig. 4 Response displacement at the top of C1-1 in the principle response direction

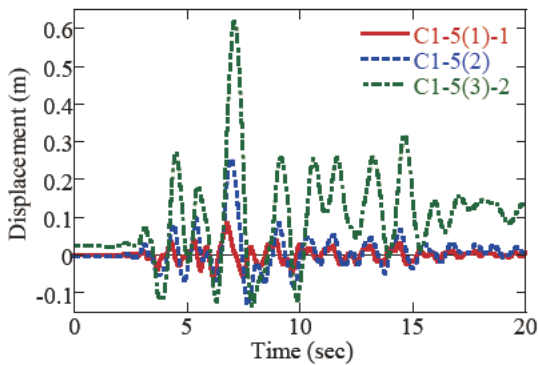


Fig. 5 Response displacement at the top of C1-5 in the principle response direction

displacements corresponded to 179 % and 36 % the ultimate displacement in C1-1 and C1-5, respectively.

Figs. 6 and 7 show the moment at the column base vs. lateral displacement at the column top hysteresses of C1-1 and C1-5, respectively, in the principal response direction. The computed moment vs. lateral displacement relations based on the 2002 JRA code are also shown here for comparison. The moment capacity of C1-1 during C1-1-2 excitation was 13.41 MNm which deteriorated by 19 % from the moment capacity during C1-1-1 excitation of 16.47 MNm. On the other hand, the moment capacity of C1-5 column progressed from 19.82 MNm during C1-5(1)-1 excitation to 20.14 MNm and 24.85 MNm during the C1-5(2) and C1-5(3)-2 excitations, respectively. However since the moment capacity of C1-5 during the C1-5(3)-1 excitation was 25.54 MNm, the moment capacity of C1-5 deteriorated by 3% during C1-5(3)-2 excitation. The computed moment capacities are close to the experimental values in both C1-1 and C1-5, however the

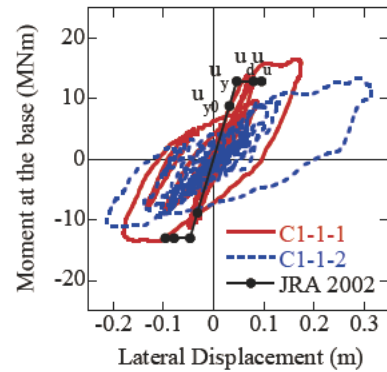


Fig. 6 Moment at the base vs. lateral displacement at the column top hysteresis of C1-1 in the principle response direction

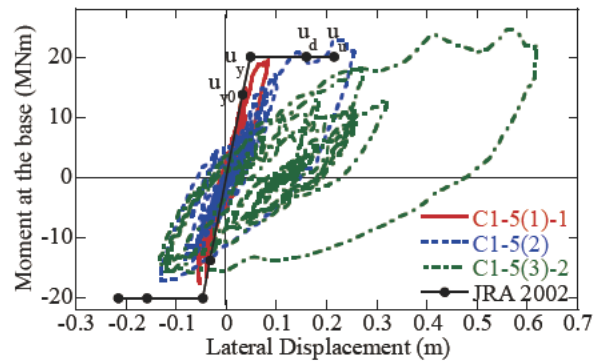


Fig. 7 Moment at the base vs. lateral displacement at the column top hysteresis of C1-5 in the principle response direction

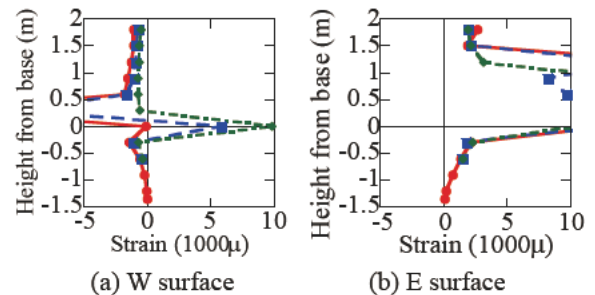


Fig. 8 Stains of longitudinal reinforcements at 6.9 s during C1-1-1 excitation

computed ultimate displacement are very conservative compared to the experiment.

### 3.3 Deformation of Longitudinal Bars

Fig. 8 shows the strain distribution of the longitudinal bars in the vertical direction in C1-1 during C1-1-1 excitation at 6.9s when the response displacement in the principal response

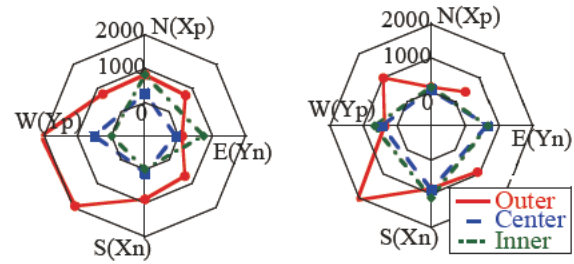
direction took a peak value. Strains in the longitudinal bars were over  $10,000 \mu$  in tension at the SE, E, NE, N and NW surfaces while they were over  $5,000 \mu$  in compression at the SW and W surfaces. The fact that large compression strains developed in the longitudinal bars implies that the core concrete had already been damaged allowing local buckling of longitudinal bars to occur. Strains in the longitudinal bars are extremely large between 0.25 m below and 1.5 m above the base of the column. Because the plastic hinge length is a half width of the column (0.9 m) based on the design code, it is important to note that longitudinal bars extensively yielded at the zone above the plastic hinge region.

### 3.4 Deformation of Circular Ties

Fig. 9 shows the strains of circular ties in C1-1 at 6.9 s during C1-1-1 excitation. In particular, strain distribution along ties at 350 mm and 650 mm from the base are shown. Strains of tie bars reached nearly  $2,000 \mu$ , slightly larger than the yield strain. Consequently the ties were still in the elastic or slightly inelastic range. It is important to note that strains in the outer ties are larger along the SW and W surfaces where the section is subjected to compression. As will be described later, this resulted from the local buckling of longitudinal bars at the SW surface.

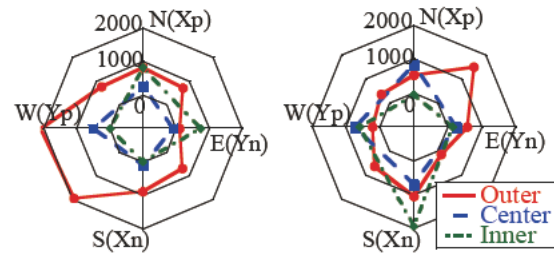
It should be noted in Fig. 9 that the lateral confinement by ties is very complex. The lateral confinement is not uniform around the ties as it is generally assumed when the lateral confinement is evaluated in design (JRA 2002). The tie strains are not the same among the three ties. For example, outer bars yielded at the SW and W surfaces while strains of center and inner ties are still less than  $1,000 \mu$  at 350 mm.

Fig. 10 shows strains of three ties at 350 mm from the base vary at 6.9 s and 7.6 s in C1-1. Strains are generally larger in the outer ties than the center and inner ties. It is noted that strain of a tie in a layer (outer, center or inner) becomes large independently with ties in other layers. For example, strain of an outer tie at 7.6 s is largest at NE ( $1,513 \mu$ ), but strains of center and inner ties are small. On the other hand, strain of an inner tie



(a) 350 mm from base (b) 650 mm from base

Fig. 9 Strains of ties at 6.9 s during C1-1-1 excitation



(a) 6.9 s (b) 7.6 s

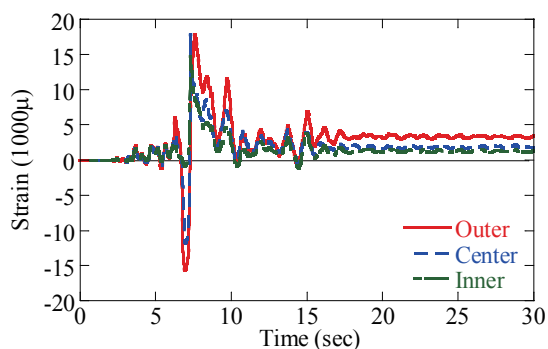
Fig. 10 Strains of Ties at 350 mm from base

at 7.6s is largest at S ( $1,925 \mu$ ) but strains of center and outer ties are small. Based on the current design code, the volumetric tie reinforcement ratio  $\rho_s$  is evaluated as

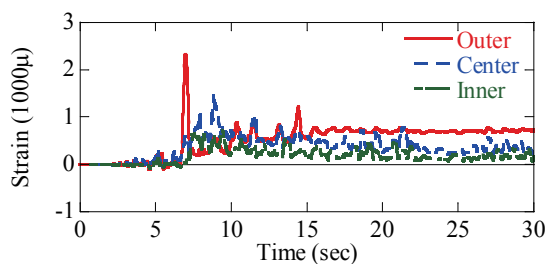
$$\rho_s = \rho_{sO} + \rho_{sC} + \rho_{sI} \quad (2)$$

where,  $\rho_{sO}$ ,  $\rho_{sC}$  and  $\rho_{sI}$  are volumetric tie reinforcement ratio of the outer, center and inner ties, respectively. However Fig. 10 shows that estimation of the volumetric tie reinforcement ratio by Eq. (2) can be overestimated. Mechanism of the lateral confinement by multi-layered ties should be critically clarified.

Fig. 11 shows the strains in the outer, center and inner layers of both longitudinal bars and tie bars. Because a compression strain over  $15,000 \mu$  developed in the outer longitudinal bar at 6.9 s, buckling of the outer longitudinal bar must have occurred at this time. It is important to note that strain of the outer tie reached  $2,300 \mu$  at the same time. This implies a mechanism that the outer tie restricted the local buckling of the outer longitudinal bar, and that this resulted in a sharp



(a) Longitudinal bars



(b) Tie bars

Fig. 11 Strains of longitudinal bars at 300 mm and tie bars at 350 mm from base at W surface

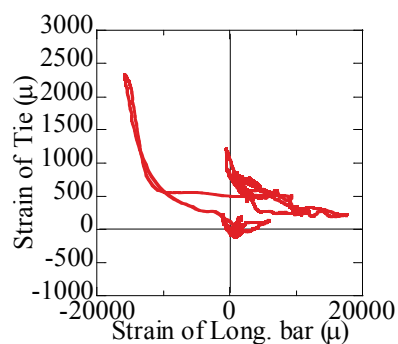
increase of strain in the outer tie.

Fig. 12 shows the interaction of a longitudinal bar 300 mm from the base and a tie bar 350 mm from the base at the W surface. Fig. 12 (a) shows the hysteresis of strains of the outer longitudinal bar and the outer tie. An increase of strain in the outer tie which resulted from restraining the local buckling of the outer longitudinal bar under high compression strain is clearly seen. On the other hand, such an increase of strain in the outer tie is not seen in the center and inner bars as shown in Fig. 12 (b) and (c) because longitudinal bars did not yet buckle.

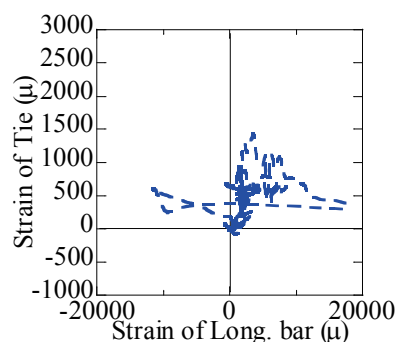
#### 4. SEISMIC PERFORMANCE OF C1-2

##### 4.1 Progress of Failure

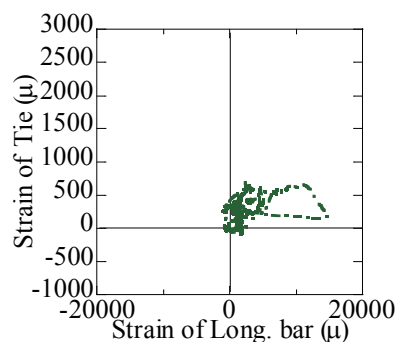
Photo 4 shows the progress of failure of C1-2 on NW and SE surfaces. A horizontal crack first developed at 4.10s along NW to E surface, and it progressed to a shear crack at 4.33 s. Another horizontal crack developed at 4.60s along W to SE surface, and it extended to at least two diagonal cracks at 4.87s. Among two diagonal cracks



(a) Outer layer



(b) Center layer



(c) Inner layer

Fig. 12 Longitudinal bar strain at 300 mm vs. tie bar strain at 350 mm from base at W surface

developed at 4.33 s, a crack on NW surface extended to W surface, and the other crack on SE surface extended to S at 5.37s. The core concrete started to crush due to shear, and the blocks of crashed core concrete started to move out from the inside of the column near the upper cut-off on N and NW surfaces at 6.04 s. The same but more extensive failure occurred on S and SW surfaces at 6.50 s. The blocks of crashed core concrete progressively moved out from steel cages associated with the column response in the SW



(a) NW



(b) SE

(1) 6.50s



(a) NW



(b) SE

(2) 6.87s

Photo 4 Progress of damage of C1-2

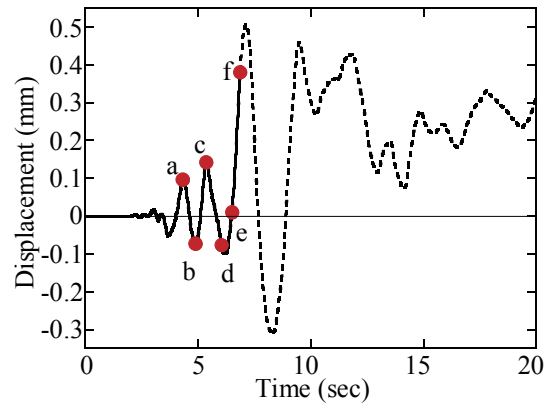


Fig. 13 Response displacement of C1-2 in the principal response direction

direction.

At 6.87 s, the bottom of lateral beam hit with the upper surface of catch frame due to excessive response displacement. Three circular tie bars completely separated at their lap splice and the longitudinal bars deformed in the outward direction. Extensive failure of core concrete and deformation of longitudinal bars progressed on W, NW, N, NE and E surfaces.

It should be noted in the above process that the failure of core concrete was extensive and a large numbers of blocks of crashed core concrete as well as deformed longitudinal bars moved out from inside of the column during very short time (less than 3 s). It was like an explosion.

#### 4.2 Response and Shear Capacity

Fig. 13 shows response displacement of C1-2 in the principal response direction. As described above, since bottom of the lateral beam hit with the upper surface of catch frame at 6.87 s, the column response after 6.87 s was affected by this contact. Without the catch frame, the column possibly overturned. Therefore the response displacement after this contact is plotted by dotted line in Fig. 13. At 7.125 s, right after the contact, the column response displacement reached its peak of 439.2 mm and 253.0 mm in the longitudinal and transverse directions, respectively. Residual drifts of 204.5 mm and 343.2 mm were developed after the excitation.

Fig. 14 shows the lateral force at the upper cut-off vs. lateral displacement at the column top hysteresis in the principal response direction. The hysteresis after the contact of the column with the catch frame is plotted by dotted line. The shear capacity of the column  $F_s$  was evaluated based on the truss theory as [4]

$$F_s = F_{sc} + F_{ss} \quad (3)$$

where

$$F_{sc} = c_c \tau_c b d \quad (4)$$

$$F_{ss} = \frac{A_h \sigma_{sy} d}{1.15s} \quad (5)$$

$$\tau_c = 0.72d^{-0.33} \left( \frac{24}{f_{c0}} \right)^{-1/3} \left( \frac{0.012}{pl} \right)^{-1/3} \quad (6)$$

in which  $F_{sc}$  and  $F_{ss}$ : shear capacity by concrete and ties (MN), respectively,  $\tau_c$ : averaged concrete shear strength (MPa),  $b$  and  $d$ : width and length of the concrete section (m),  $c_c$ : modification factor depending on loading condition,  $A_h$  and  $\sigma_{sy}$ : sectional area (m<sup>2</sup>) and the yield strength of a tie (MPa),  $f_{c0}$ : design strength of concrete (MPa),  $pl$ : longitudinal reinforcement ratio in tension, and  $s$ : interval of ties (m). The modification factor in accordance with loading condition  $c_c$  is a factor which takes account of the deterioration of concrete shear capacity under repeated cyclic loading;  $c_c$  is 1.0 under a static load, while it is 0.6 and 0.8 under Type I ground motion (long-duration middle-field ground motions generated by M8 subduction earthquakes) and Type II ground motion (short-duration near-field ground accelerations with long-period pulses), respectively.

Assuming Eq. (3), the shear stress at the upper cut-off vs. the lateral displacement at the column top relation was evaluated as shown in Fig. 15, in which  $\tau_c$  is normalized in terms of  $\alpha_c$  and  $\alpha_{pl}$  defined as

$$\alpha_c = \left( \frac{24}{f_c} \right)^{-1/3} ; \alpha_{pl} = \left( \frac{0.012}{pl} \right)^{-1/3} \quad (7)$$

In Fig. 15, shear stress evaluated for two 1.68m

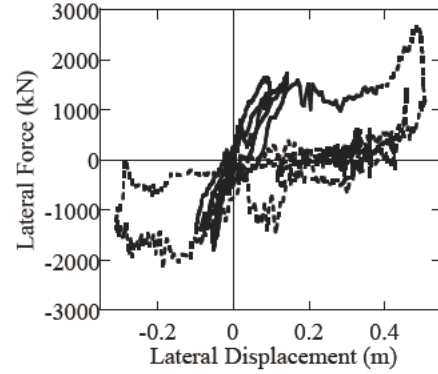


Fig. 14 Lateral force at upper cut-off vs. lateral displacement at the column top hysteresis in the principle response direction

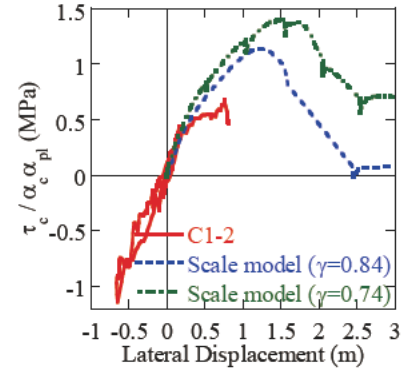


Fig. 15 Shear stress of concrete

tall 400mm diameter scaled model columns with different shear vs. flexure strength ratio is included for comparison [5]. It is seen in Fig. 15 that  $\tau_c / \alpha_c \alpha_{pl}$  of C1-2 is 0.68 MPa which is 15 % larger than the value (0.59 MPa) evaluated by Eq. (3).

## 5. ANALYTICAL CORRELATION FOR C1-5

### 5.1 Analytical Idealization

The column was idealized by a 3D discrete analytical model including  $P-\Delta$  effect as shown in Fig. 16. The column was idealized by fiber elements. A section was divided into 400 fibers.

The stress vs. strain constitutive model of confined concrete is assumed as [6]

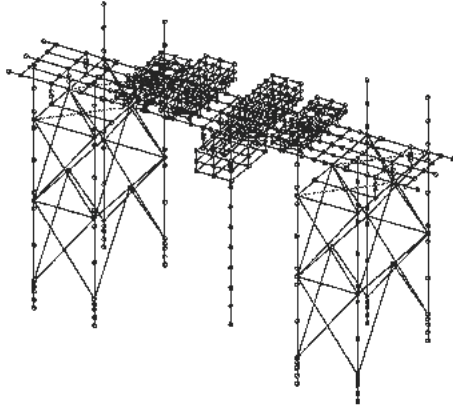


Fig. 16 Analytical model

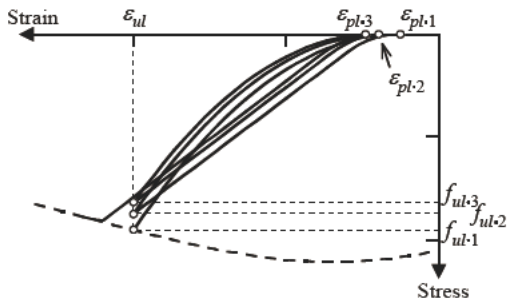


Fig. 17 Unloading and reloading paths of confined concrete

$$f_c = \begin{cases} E_c \varepsilon_c \left\{ 1 - \frac{1}{n} \left( \frac{\varepsilon_c}{\varepsilon_{cc}} \right)^{n-1} \right\} & (0 \leq \varepsilon_c \leq \varepsilon_{cc}) \\ f_{cc} - E_{des} (\varepsilon_c - \varepsilon_{cc}) & (\varepsilon_{cc} \leq \varepsilon_c \leq \varepsilon_{c0}) \\ a f_{cc} & (\varepsilon_{c0} \leq \varepsilon_c) \end{cases} \quad (8)$$

in which  $f_{cc}$  and  $\varepsilon_{cc}$  = strength and strain corresponding to  $f_{cc}$ ,  $E_c$  = elastic modulus of concrete,  $E_{des}$  = gradient at descending branch,  $a$  = residual strength factor depending on the confinement, and  $n = E_c \varepsilon_{cc} / (E_c \varepsilon_{cc} - f_{cc})$ . In Eq. (8),  $f_{cc}$ ,  $\varepsilon_{cc}$ ,  $E_{des}$ ,  $\varepsilon_{c0}$  and  $a$  are defined as

$$f_{cc} = f_{c0} + 3.8 \alpha \rho_s f_{sy} \quad (9)$$

$$\varepsilon_{cc} = 0.002 + 0.033 \beta \frac{\rho_s f_{sy}}{f_{c0}} \quad (10)$$

$$E_{des} = 11.2 \frac{f_{c0}^2}{\rho_s \cdot f_{sy}} \quad (11)$$

$$\varepsilon_{c0} = \varepsilon_{cc} + 0.8 f_{cc} / E_{des} \quad (12)$$

$$a = 0.2 \quad (13)$$

in which  $f_{c0}$  = design strength of concrete,  $f_{sy}$  = yield strength of tie bars,  $\alpha$  and  $\beta$  = shape factors ( $\alpha=1.0$  and  $\beta=1.0$  for circular piers), and  $\rho_s$  = volumetric ratio of tie bars. Stress vs. strain relation of covering concrete was evaluated by Eq. (3) assuming  $\rho_s = 0$  in Eqs. (9) and (10).  $E_{des}$ ,  $\varepsilon_{c0}$  and  $a$  are given as

$$E_{des} = \frac{f_{c0}}{\varepsilon_{c0} - \varepsilon_{cc}} \quad (14)$$

$$\varepsilon_{c0} = 0.005 \quad (15)$$

$$a = 0 \quad (16)$$

Unloading and reloading hystereses consist of combinations of full unloading, partial unloading, full reloading and partial reloading. For example, as shown in Fig. 17, unloading from an envelop curve and reloading from zero stress are idealized as [7]

$$f_c = f_{ul,1} \left( \frac{\varepsilon_c - \varepsilon_{pl,1}}{\varepsilon_{ul} - \varepsilon_{pl,1}} \right)^2 \quad (17)$$

$$f_c = \begin{cases} 2.5 f_{ul,n} \left( \frac{\varepsilon_c - \varepsilon_{pl,n}}{\varepsilon_{ul} - \varepsilon_{pl,n}} \right)^2 & 0 \leq \frac{\varepsilon_c - \varepsilon_{pl,n}}{\varepsilon_{ul} - \varepsilon_{pl,n}} < 0.2 \\ E_{c,rl} (\varepsilon_c - \varepsilon_{ul}) + f_{ul,n+1} & 0.2 \leq \frac{\varepsilon_c - \varepsilon_{pl,n}}{\varepsilon_{ul} - \varepsilon_{pl,n}} \leq \frac{\varepsilon_{re} - \varepsilon_{pl,n}}{\varepsilon_{ul} - \varepsilon_{pl,n}} \end{cases} \quad (18)$$

where

$$\varepsilon_{pl,1} = \begin{cases} 0 & 0 \leq \varepsilon_{ul} \leq 0.001 \\ 0.43 (\varepsilon_{ul} - 0.001) & 0.001 < \varepsilon_{ul} < 0.0035 \\ 0.94 (\varepsilon_{ul} - 0.00235) & \varepsilon_{ul} \geq 0.0035 \end{cases} \quad (19)$$

in which  $f_{ul,1}$  and  $\varepsilon_{ul}$  = unloading stress and strain on the envelope curve,  $f_{ul,n}$  = stress at the unloading point after  $n$  th unloading/reloading,  $\varepsilon_{pl,n}$  = plastic strain after  $n$  th unloading & reloading,  $\varepsilon_{re}$  = strain at the point where reloading path intersects the envelope curve, and  $E_{c,rl}$  = reloading modulus.

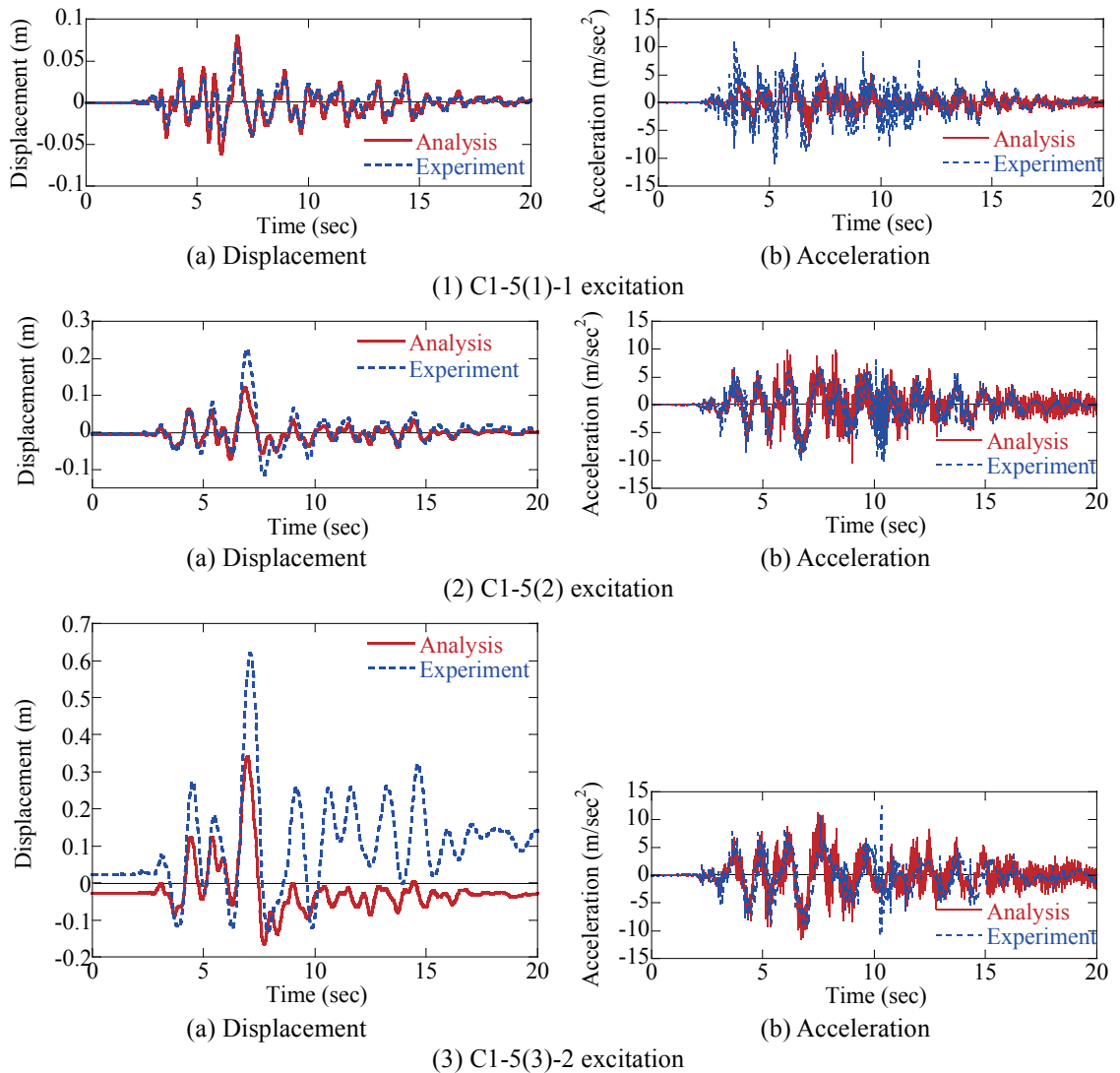


Fig. 18 Analytical correlation for the response displacements and accelerations at the column top in the principle response direction

Modified Menegotto-Pinto model was used to idealize the stress vs. strain relation of longitudinal bars [8, 9].

### 5.2 Analytical Correlation

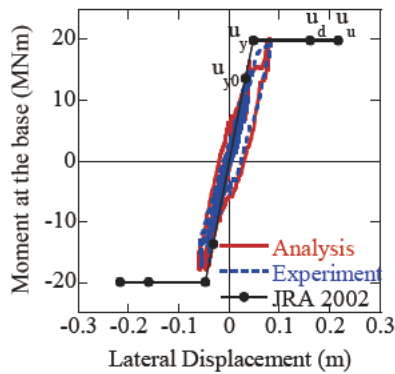
Fig. 18 shows the analytical correlation on the response displacements at the top of the column in the principal direction during C1-5(1)-1, C1-5(2) and C1-5(3)-2 excitations. Fig. 19 compares the measured and computed moment at the base vs. lateral displacement at the column top hysteresis during the three excitations. Because nonlinear hysteretic response was still limited during C1-5(1)-1 excitation, the computed response displacement and moment vs. lateral displacement

hysteresis are quite in good agreement with the experimental results, however as C1-5 suffered more damage, the accuracy of analytical prediction decreases.

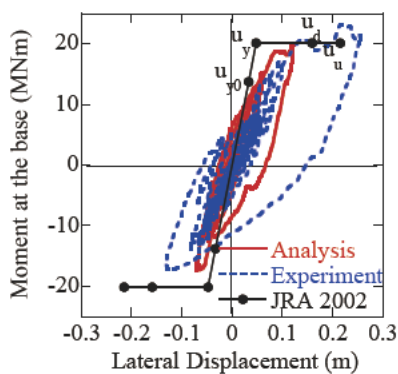
Consequently, it is required to develop an analytical model that can predict the response of the columns until collapse for realizing reliable performance based seismic design.

## 6. COCLUSIONS

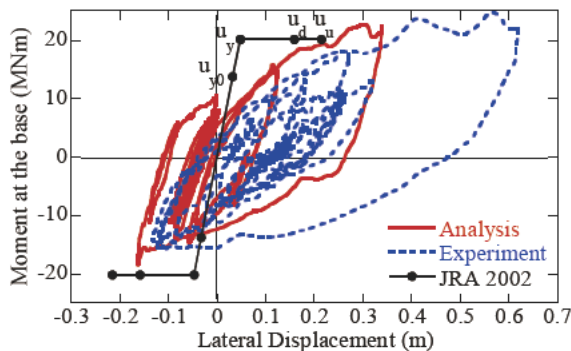
A preliminary result on a series of shake table experiment and analysis to three full-size reinforced concrete columns was presented. Based



(a) C1-5(1)-1 excitation



(b) C1-5(2) excitation



(c) C1-5(3)-2 excitation

Fig. 19 Moment at the base vs. lateral displacement at the column top hysteresis in principle response direction

on the results presented herein, the following tentative conclusions may be deduced;

1) C1-1 which is a typical column in the 1970s suffered extensive damage under C1-1-1 excitation. The progress of damage during C1-1-2

excitation was extensive even though it was anticipated before the experiment that damage would not progress unless the intensity of second excitation was much larger than that of the first excitation. This resulted from the extensive deterioration of the lateral confinement due to separation of ties at the lap splices. It is highly possible that columns without sufficient lateral confinement have a similar progress of damage during a long-duration near-field ground motion or strong aftershocks.

2) C1-5 which is a typical column in accordance with the current design criteria suffered only a few numbers of horizontal cracks with the maximum width of 1 mm under C1-5 (1)-1 excitation. The ultimate drift was 2.9 % which was 2.2 times larger than that of C1-1. Consequently, enhancement of the seismic performance of C1-5 compared to C1-1 is obvious. However the progress of failure of C1-5 was extensive when it was subjected to 25 % stronger excitation under 21% added mass (C1-5(3) excitations). Blocks of crashed core concrete spilled out like explosion from the steel cages. The seismic performance of C1-5 subjected to longer duration near-field ground motion has to be carefully evaluated.

3) C1-2 failed in shear at the upper cut-off. As soon as circular ties at the upper cut-off yielded, a small diagonal cracks developed. As they extended to several major diagonal cracks, C1-2 completely failed in shear within less than 2.5 s since the initiation of a couple of small diagonal cracks. Concrete blocks crashed by shear and deformed longitudinal bars extensively moved out from the inside of column.

4) The lateral confinement in the flexure dominant columns is not uniform around the ties as it is currently assumed in design. More importantly, the lateral confinement of multi layered ties is very complex. Strains of ties are not similar among the multi-layered ties, and they are related to the degree of constraint exerted for preventing local buckling of longitudinal bars. Strains are generally larger in the outer ties than the inner ties. This implies that the lateral confinement by Eq. (2) can be overestimated.

5) Computed response for the flexure dominant columns is satisfactory while response undergoes the moderate nonlinear range, however accuracy of the analytical prediction deteriorates once the columns undergo the strong nonlinear range. An analytical model which can predict response of the columns until failure should be developed for enhancing the reliability of the performance based seismic design.

#### ACKNOWLEDGEMENTS

The C1 experiment was conducted based on the extensive support of over 70 personnel in the Overview Committee (Chair, Professor Emeritus Hirokazu Iemura, Kyoto University), Executing Committee of Large-scale Bridge Experimental Program (Chair, Professor Kazuhiko Kawashima, Tokyo Institute of Technology), Analytical Correlation WG (Chair, Dr. Shigeki Unjoh, Public Works Research Institute), Measurements WG (Chair, Professor Yoshikazu Takahashi, Kyoto University), Dampers & Bearings WG (Chair, Dr. Masaaki Yabe, Chodai) and Blind Analysis WG (Chair, Professor Hiroshi Mutsuyoshi, Saitama University). Their strong support is greatly appreciated. Invaluable support and encouragement of Professor Stephen Mahin, University of California, Berkeley and Professor Ian Buckle, University of Nevada, Reno are greatly appreciated.

#### REFERENCES

1. Nakashima, M., Kawashima, K., Ukon, H. and Kajiwara, K.: Shake table experimental project on the seismic performance of bridges using E-Defense, S17-02-010 (CD-ROM), 14 WCEE, Beijing, China, 2008.
2. Kawashima, K. Sasaki, T., Kajiwara, K., Ukon, H., Unjoh, S., Sakai, J., Takahashi, Y., Kosa, K., and Yabe, M.: Seismic performance of a flexural failure type reinforced concrete bridge column based on E-Defense excitation, Proc. JSCE, A, Invited paper, 1-19, JSCE, 2009 (in print).
3. Kawashima, K. and Unjoh, S.: The damage of highway bridges in the 1995 Hyogo-ken nanbu earthquake and its impact on Japanese seismic design, Journal of Earthquake Engineering, 1(3), 505-542, 1997.
4. Kono, H., Watanabe, H. and Kikumori, Y.: Shear strength of large RC beams, Technical Note, 3426, Public Works Research Institute, Tsukuba, Japan, 1996.
5. Sasaki, T., Kurita, H. and Kawashima, K.: Seismic performance of RC bridge columns with termination of main reinforcement with inadequate development, S17-02-009 (CD-ROM), 14WCEE, Beijing, China, 2008.
6. Hoshikuma, J., Kawashima, K., Nagaya, K. and Taylor, A.W.: Stress-strain model for confined reinforced concrete in bridge piers, Journal of Structural Engineering, ASCE, 123(5), 624-633, 1997.
7. Sakai, J. and Kawashima, K.: Unloading and reloading stress-strain model for confined concrete, Journal of Structural Engineering, ASCE, 132 (1), 112-122, 2006.
8. Menegotto, M. and Pinto, P.E.: Method of analysis for cyclically loaded R.C. plane frames including changes in geometry and non-elastic behavior of elements under combined normalized force and bending, Proc. IABSE Symposium on Resistance and Ultimate Deformability of Structures Acted on by Well Defined Repeated Loadings, 15-22, 1973.
9. Sakai, J. and Kawashima, K.: Modification of the Giuffre, Menegotto and Pinto model for unloading and reloading paths with small strain variations, Journal of Structural Mechanics and Earthquake Engineering, JSCE, 738/I-64, 159-169. 2003.
10. Priestley, M.N.J., Seible, F. and Calvi, G.M.: Seismic design and retrofit of bridges, John Wiley & Sons, New York, USA, 1996.

Outline of the Damage of Transportation Facilities and Geotechnical Structures  
by the 2009 L'Aquila, Italy Earthquake

by

Kazuhiko Kawashima<sup>1</sup>, Omer Aydan<sup>2</sup>, Kazuo Konagai<sup>3</sup>, Atsushi Yamashita<sup>4</sup>, and Sven-Peter Teodori<sup>5</sup>

## ABSTRACT

This is a reconnaissance report on the damage to transportation facility and geotechnical structures caused by the 2009 L'Aquila, Italy earthquake. Site investigation was conducted by the authors during the period of April 18-21, 2009. Presented is a discussion on the damage of transportation facilities. Geotechnical damage and ground motions are also presented.

## 1. INTRODUCTION

A strong earthquake with  $M_L=5.8$  and  $M_W=6.2$  occurred near L'Aquila, Central Italy, at 03:32 local time on April 6, 2009 as a result of 15 km long NW-SE striking normal fault. The fault dips southwest and the city of L'Aquila is located on the hanging wall of the causative fault. Damage in L'Aquila and its vicinity was extensive with about 10,000-15,000 buildings heavily damaged. Approximately 294 people were killed, with over 1,000 injured.

The population of L'Aquila was about 70,000. The city center spreads over terrace of calcareous conglomerates while Aterno River cuts through the terrace down to lower elevations. The terrace is about 100 m higher than the elevations of lowland along Aterno River.

A joint reconnaissance damage investigation team consisting of ten members from Japan Society of Civil Engineers, Japanese Geotechnical Society, Architectural Institute of Japan and Japan Association for Earthquake Engineering was sent. The authors conducted a field investigation on the geotechnical and geological damage as well as investigation on the damage to transportation facilities and other structures in the regions of L'Aquila and its vicinity including Ocre, Onna,

Paganica and Coppito during April 18-21, 2009. Based on the field investigation, feature of the damage including their damage mechanisms are presented here.

It should be however noted that since the field investigation was conducted without prior information on design drawings and analysis, it is highly possible that the interpretation of the failure mechanism by the authors might not be accurate. Moreover, because access to the extensively damaged regions including the old city of L'Aquila, Onna and Paganica was restricted, there were a number of structures which could not be investigated thoroughly.

## 2. GEOLOGICAL AND SEISMOLOGICAL CONDITIONS

The stratigraphy of L'Aquila consists of schists, limestone, lacustrine deposits, conglomeratic deposits and Holocene deposits from bottom to top. Schists are best seen at the east portal of Gran-Sasso tunnel. Schists are overlain by limestone, which is the main rock unit constituting Gran-Sasso Mountain ridge. The basin of L'Aquila consists of lacustrine clayey deposits. Conglomeratic deposits cover these deposits. The inclusions of conglomeratic deposit originate from limestone and other rocks from nearby mountains. Matrix of conglomeratic deposits is clayey or calcareous, which can be easily dissolved by

---

1: Professor, Tokyo Institute of Technology, Tokyo, Japan

2: Professor, Tokai University, Shimizu, Japan

3: Professor, Institute of Industrial Science, University of Tokyo, Tokyo, Japan

4: Professor, Gifu University, Gifu, Japan

5: Researcher, Nippon Koei Consultants Company, Tsukuba, Japan

ground water flow. Fig. 1 shows the geological profile along the SW-NE cross section of L'Aquila. All these deposits are covered by Holocene deposits from Aterno River Valley. Holocene deposits are a mixture of clay, silt, sand and gravel, and they are widely distributed along Aterno River. Paganica, Onna and Fossa village where extensive damage was developed are on Holocene deposits.

Historically large earthquakes occurred in 1315, 1349, 1461, 1703, 1706 and 1915 in the vicinity of L'Aquila. The 1915 event named as Fucino earthquake ( $M_S=7$ ) resulted in victims of 33000. The most recent events were 1984 Greco earthquake ( $M_L=5.8$ ) and 1996 Umbria ( $M_S=6.1$ ). The nearest event occurred in 1461. Bagh et al. (2007) reported that earthquakes in the close vicinity of L'Aquila were either due to purely normal faulting or oblique faulting with a normal component. They pointed out that there was no large seismic event since the 1915 Fucino event, implying that the region might suffer a large event in near future.

Based on parameters by various seismological institutes worldwide, the L'Aquila earthquake was caused by a 15-20km long and 10-15km wide normal fault as shown in Fig. 2. The estimated rupture duration ranged between 6.8 and 14 s.

Surface ruptures were observed at Paganica, Lake Sinizzo, and two bridges at Onna and Fossa as shown in Fig. 3 and Photo 1. Surface ruptures were observed at three sites in Paganica. Most fractures at Paganica indicated the opening of surface cracks with a normal displacement. The authors also observed cracks on the road to Lake Sinizzo, which is thought to be the southeast end of the earthquake fault. There were also surface cracks in the vicinity of a bridge near Fossa (refer to Photo 11) as shown in Fig. 7. Some cracks were in compression while most of them were in tension.

### 3. STRONG MOTION RECORDS

Based on the Italian National Strong Motion Network (Accelerometric National Network (RAN)), 56 strong motion records triggered during the earthquake were so far released. In the

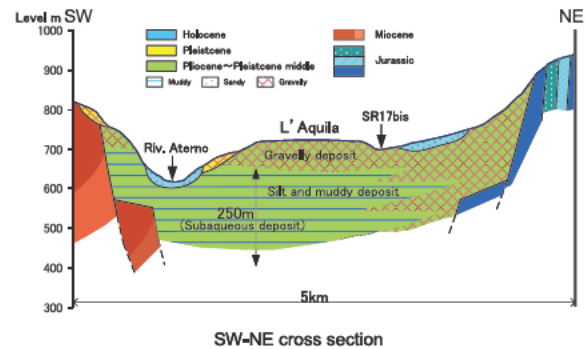


Fig. 1 Geological profile along the SW-NE cross section under L'Aquila

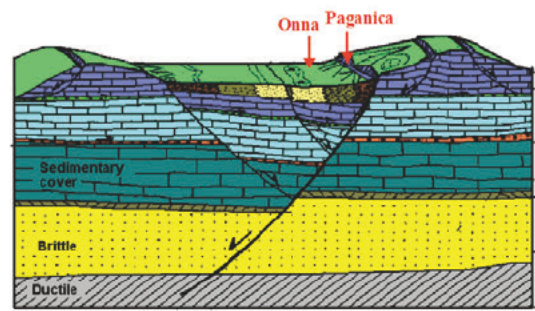


Fig. 2 Schematic illustration of size and surface effects of M6 class graben earthquakes (modified from Dramis and Blumetti, 2005)

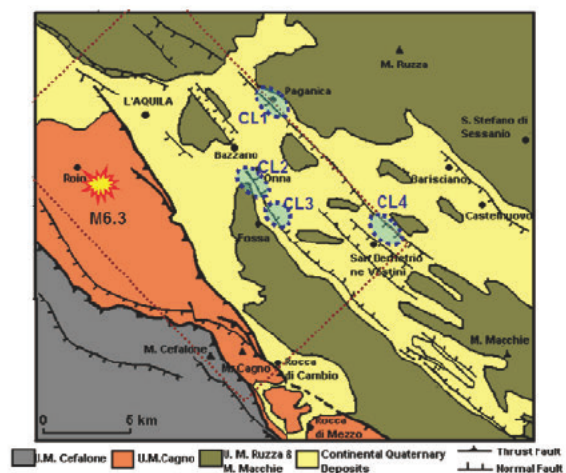


Fig. 3 Locations of surface ruptures



(a) CL1 (b) CL2 (c) CL3 (d) CL4  
 Photo 1 Surface ruptures in the area of Aterno River to the west of Onnna town  
 (refer to Fig. 3 for locations of CL1-CL4))

Table 1 Main strong motion records

Station name	Station code	Latitude	Longitude	Type of ground	$R_e$ (km)	$V_{s30}$ (m/s)	PGA ( $m/s^2$ )
Aquil Park	AQK	42.345	13.401	Conglomerate	5.6	455	3.66
V. F.Aterno	AQV	42.377	13.337	Fluvial	5.8	475	6.46
Colle Grilli	AQG	42.376	13.339	Limestone	4.3	1000	5.05
V.&F. Aterno	AQA	42.345	13.401	Fluvial	4.8	475	4.78

close vicinity of L'Aquila City, there are four strong motion stations as shown in Table 1; AQV (GX066-B), AQG (FA030-B), AQA (CU104-B) and AQK (AM043-C). They were all on the hanging wall side of the earthquake fault. The equivalent shear wave velocity between the ground surface and 30 m from the ground surface,  $V_{s30}$ , is in the range of 455-1000 m/s. The largest peak ground acceleration of  $6.46 m/s^2$  was recorded at AQV.

Fig. 4 shows the acceleration records at AQV and AQK stations. It is of great interest that the amplitude of ground accelerations are not symmetric and their forms are different each other although the epicentral distances and the equivalent shear wave velocity  $V_{s30}$  of ground are almost the same.

Fig. 5 shows the acceleration records at GSA and GSG stations, which are reportedly founded on Eocene limestone with a shear wave velocity of 1 km/s. The GSA station is at Assergi and the GSG station is located in an underground gallery. Although the epicentral distances and ground conditions are the same, the acceleration at ground surface is amplified almost 15 times that in the underground gallery.

Acceleration spectra at some selected strong motion stations (AQV, AQK, AQA, AQG, MTR, FMG, GSA and GSG) are shown in Fig. 6. The predominant periods of the recorded accelerations range between 0.05s and 0.4s in the lateral components. The predominant period of about 0.8 s at AQG station is noted as was pointed out by Luca et al. (2005). The spectral accelerations of vertical component are high at natural periods ranging between 0.05s and 0.1s.

#### 4. GEOTECHNICAL DAMAGE

##### 1) Horizontal movements and cracking in the area of Aterno River

Horizontal movements and cracking were observed in the area of Aterno River to the west of Onna town. The embankments on both sides of Aterno River moved towards the river creating separation cracks as well as some compression cracks in the vicinity of the damaged bridge on Aterno River as shown in Fig. 7 and Photo 2. The cracks and movements on the east side of the river were more intensive as the ground was inclined towards west. Nevertheless, any sand boiling was not observed in the area. It would be quite speculative on the cause of these movements.

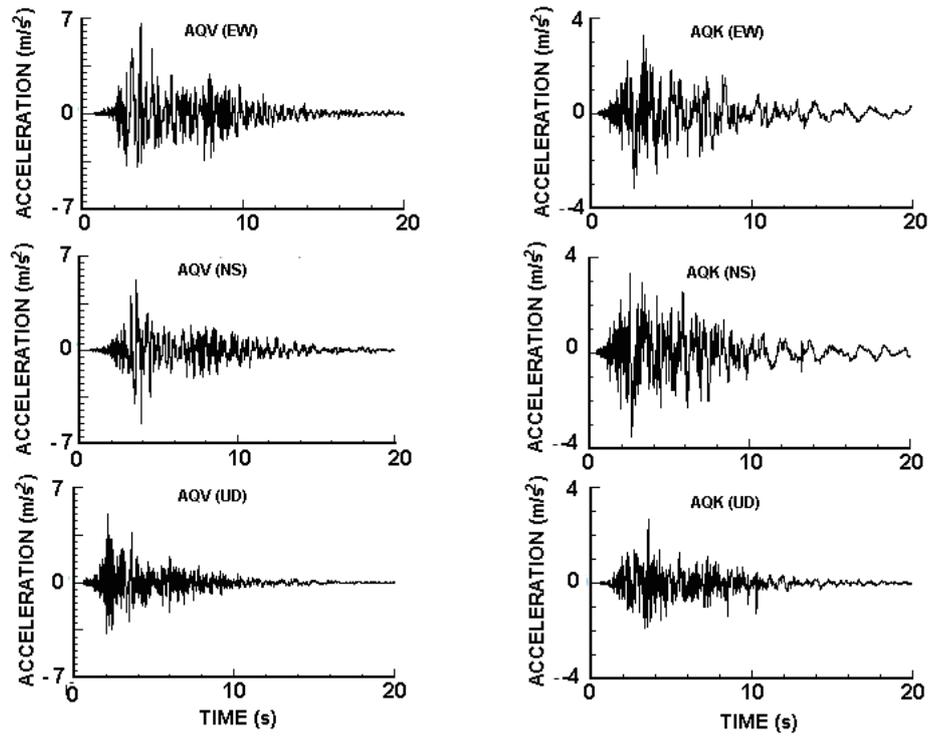


Fig. 4 Acceleration records at AOV and AQK stations

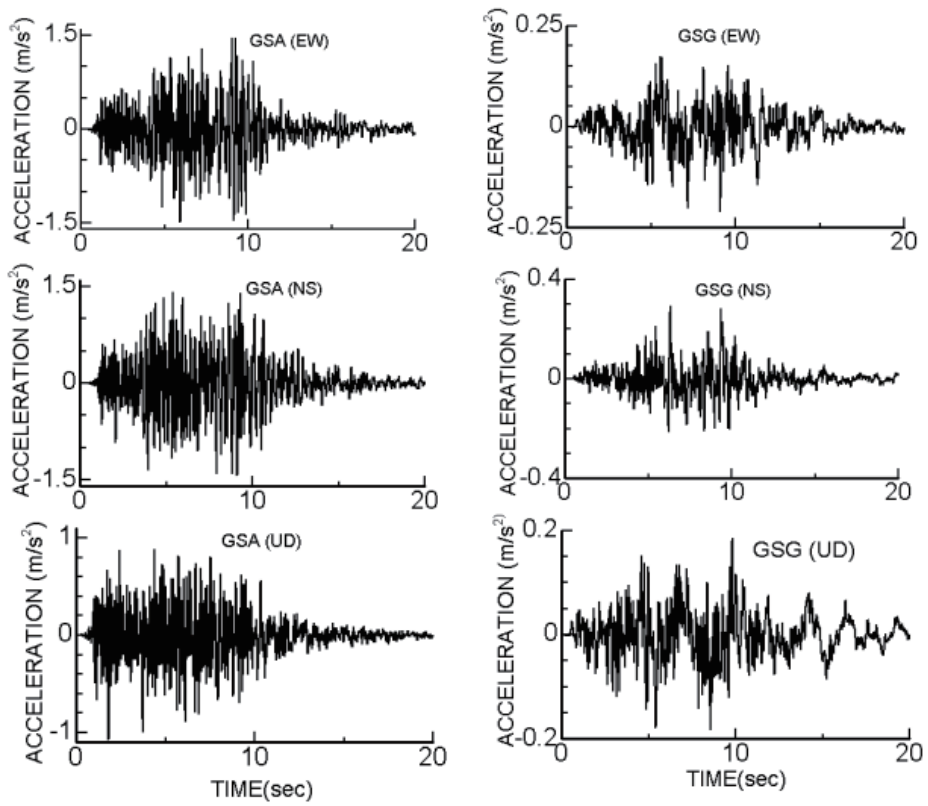


Fig. 5 Acceleration records at GSA and GSG strong motion stations

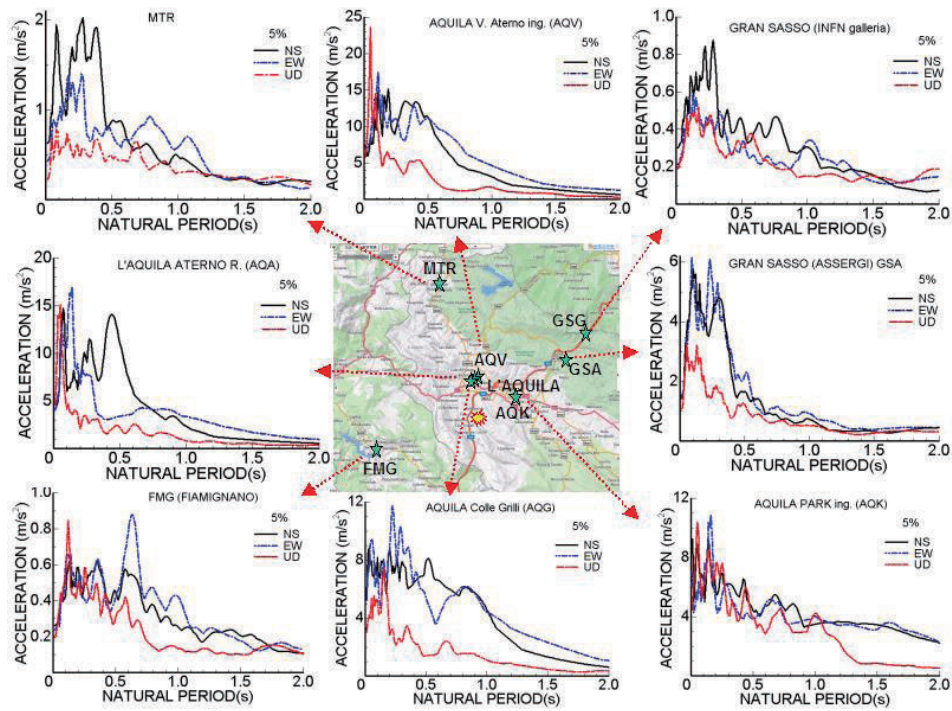


Fig. 6 Acceleration response spectra of selected strong motion stations

Based on InSAR evaluation, ground movements are large in the close vicinity of Aterno River near Onna town. Tectonic movements, ground liquefaction or both might cause the movement in this area. If ground liquefaction is involved, it is likely that there is a thick impermeable silty and clayey layer on top of the liquefiable ground below.

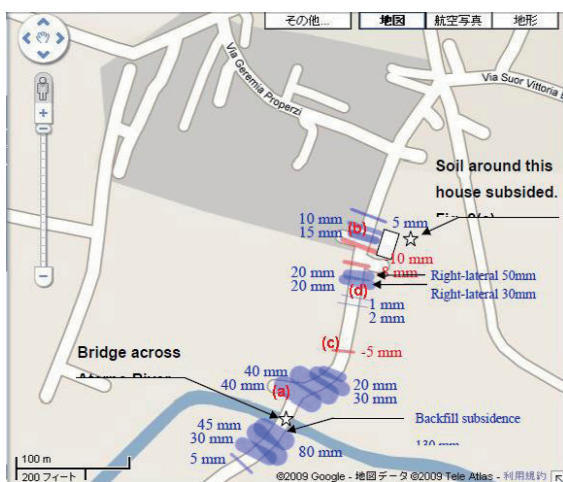


Fig. 7 Cracks in the vicinity of a damaged bridge on Aterno River (Refer to Photo 2)



Photo 2 Surface cracks on the east side of Aterno River (Refer to Fig. 7 for locations)

## 2) Lateral spreading and sliding along shoreline of Sinizzo Lake

There are a number of sinkholes in the vicinity of L'Aquila featuring the Karst topography of the area. Sinizzo Lake with about 120 m diameter is probably one of the sinkholes. Extensive lateral spreading occurred along the shoreline of Sinizzo Lake as shown in **Photo 3**. Around the north shore, several parallel blocks were bounded by continuous cracks due to large lateral spreading of the surface ground and they moved toward the lake as shown in **Photo 4**. The ground at the west shore moved 22 m towards the lake. Two famous beautiful springs at the north-eastern shore dried up after the earthquake, however a new spring was formed close to the original two springs. The fact that the original ground water flow paths were blocked and a new water flow path was formed due to ground deformation during the earthquake implies that the ground water table was high and close to the ground surface. Based on this evidence, it is considered that the lateral spreading was resulted from yielding of the ground due to intensive earthquake shaking as well as degradation of shear strength of the ground due to generation of the pore water pressure.

Extensive surface rock sliding on the mountain on east side of the lake was developed as shown in **Photo 5**.



Photo 3 Lateral spreading around Lake Sinizzo (added on Google map)



Photo 4 Separated blocks due to lateral spreading



Photo 5 Surface rock sliding on the mountain (east of the Sinizzo Lake)

## 3) Rock falls in Stiffe

Two large rock falls occurred in Stiffe. The estimated mass and size of one of the rock blocks was 12 t and 1.5m x 1.6m x 1.9m, respectively. This rock block hit and destroyed the wall of a small building in the park near Grotte di Stiffe as shown in **Photo 6**. **Photo 7** shows a broken tree, a shallow dent on the ground and the damaged wall, lined up along the path of the fallen rock block. The velocity and energy at the instance of collision is estimated in view of the jumping distance as 15 m/s and 2,700 kJ, respectively. The collision energy was large enough to destroy the wall of a building. The other fallen rock block reached the bottom of the park.

It is important to assess the sources of falling rocks so that stability of neighboring rock masses or isolated rocks remaining on a slope can be evaluated. By assessing the collision energy of possible unstable rock masses, the risk to human lives and properties can be evaluated. It may be effective to prepare a check sheet to record information on the height of rock fall sources, size, geological conditions, protection measures and possible fall path.



Photo 6 A 12 ton fallen rock with 1.9m long, 1.6m wide and 1.5m tall

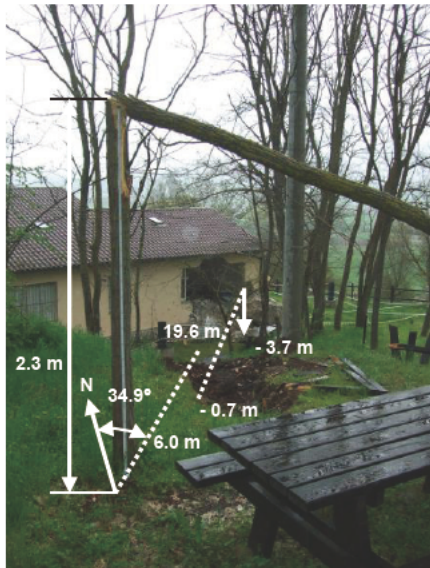


Photo 7 A broken tree, a shallow dent on the ground and a collapsed wall of the building along the path of a fallen rock.

It is noted that there are several large sinkholes and sparsely distributed gorges probably due to subterranean drainage in a mountainous terrain in the vicinity of the above rock fall. The good drainage indicates the presence of numerous cracks and caves in the soluble rock formation, and this may have contributing factor in rock falls. It is likely that there may be lots of unstable rocks in source areas. Detailed in-situ investigation to identify rock fall hazard locations will be necessary for a rational rehabilitation.

#### 4) Sinkholes on roads due to caving

In the old city of L'Aquila, two sinkholes appeared on roads due to the earthquake and a vehicle fell into a sinkhole as shown in Photo 8. One of the sinkholes was already back-filled with soils for stabilizing the surrounding ground. However the other sinkhole was only partially back-filled as shown in Photo 9 and the authors had the chance to investigate it. Fig. 8 shows the dimensions of the sinkhole. The deepest point from the road surface was measured as 13m near the east edge of the sinkhole. However the cave tended to become deeper towards west. The roof of the cave roughly consists of four horizontal layers. From the bottom to top, they are (1) well cemented calcareous conglomerate, (2) clayey conglomerate, (3) clay, and (4) backfill. It is noted that a sewage conduit was constructed after excavating a 3.7m deep vertical trench reaching to the level of the calcareous conglomerate. This trench excavation has eventually notched the upper surface of the conglomerate roof of the cave, which could further reduce its effective thickness. The scenario mentioned above may have been responsible for the formation of the sinkhole during the earthquake shaking.

After experiencing the intense shaking, there are probably a number of unstable thin roofed caves remaining underground in the old city of L'Aquila. Thorough sounding of the condition of foundation rock mass may be important for a safe and rational rehabilitation of the city. Among many techniques available, the surface wave tomography may be effective and it may yield shear wave velocities of ground, which are directly related to its mechanical properties.



Photo 8 Sinkhole immediately after the earthquake (from Web page)

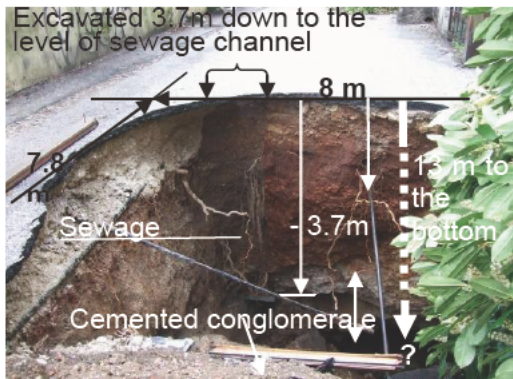
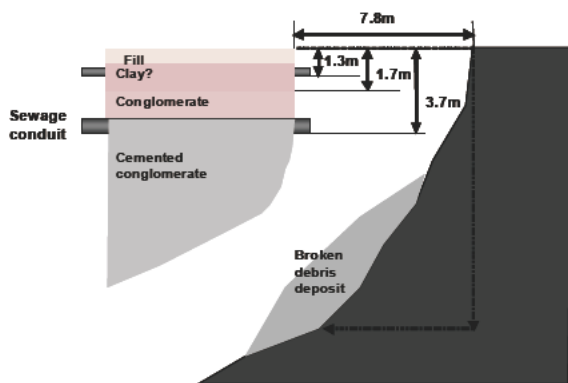


Photo 9 Sinkhole in a road, locality of A uila f r o Fi .



Section of a sinkhole (Refer to Photo 9)

### 5) Soil Liquefaction

Soil liquefaction is caused by the generation of the pore water pressure and it is often observed when r u c i s o u r s . Alluvium deposits are geologically formed along Aterno River in the epicentral area. During

investigations, the authors found sand boils along A e o c a i w just south of the hill on which the old downtown o ' i i s c a e . T i v e d s th r i e a v e u i n d deposits at those meanders. At Martini district liquefaction created many NE-SW trending f t a th i m a n m t a n they opened up as shown in Photo 10. Sand b i l i c k a s m v i o s l o e o e m f u d w a towards SE direction. Table 2 and Fig. 9 show s p y c r p t i e s a n d g r a i n s i z e d u s b i l s e c v , a s e d laboratory tests at Tokai University, Japan and Pam k a e U n e y k . B e a s e n u i t s r a n s i e i s i b t i o falls within the easily-liquefiable bounds a r r d r b u R e s r I s t e c l a s s i c a t i o n (1997).

T q e n i n a e l s p r a d i n g . Th s u m o f c r a c k o p e n i n g s f r o m t h e a d j a c e n t f i e l d t o d t h e r b k m e n t r a n g e d b e t w e e n 2 0 3 0 e r e r e p t - l i k structures and bridges for railways and roadways in the area where soil liquefaction was observed. H e r w a o v m e o e e structures probably because the foundations were r i n e e p s f o i l s .



to 1 L e a c i o t a t i n i d i s t r c t f L i l

Table 2 Properties of liquefied soil sample collected from sand volcanoes

Unit weight ( $\gamma$ ) (N/m <sup>3</sup> )	13.11-13.80
Moisture content (%)	-
Mean grain size $D_{50}$ (mm)	0.5-0.6
Friction angle (degree)	32-35

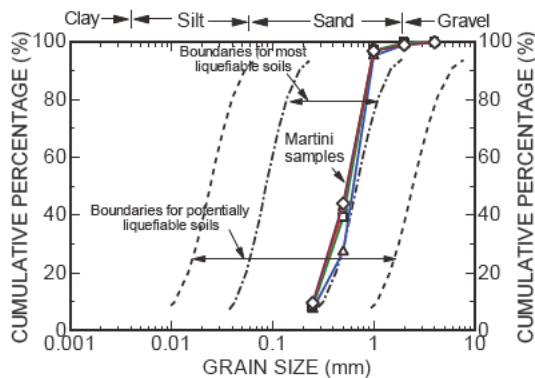


Fig. 9 Grain size distribution and comparison of liquefaction bounds

## 5. DAMAGE OF TRANSPORTATION FACILITIES

### 1) Damage of bridges

A 35 m long 5 m wide three-span continuous reinforced concrete bridge collapsed as shown in [Photos 11 and 12](#). It was located at the crossing of SR261 on Aterno River for approaching Fossa Town. Four reinforced concrete pile-bent columns with a hexagonal section failed at a height slightly above the river surface, and they shifted sideways and penetrated the deck slab as shown in [Photos 13 and 14](#). A column had six 17 mm diameter round main bars at each corner of the hexagonal section as shown in [Photo 15](#). Several 9 mm diameter round bars were also set to fix the top of columns to the reinforced concrete girders. 6 mm diameter round hoops were provided at about 300 mm interval. The strength of concrete in columns was most likely less than 20 MPa. [Photo 16](#) shows a broken pile-bent as well as a girder next to the bent at the right downstream column. Plastic hinge did not form in the column because of the low reinforcement. It seems that damage of the column which was induced prior to the earthquake progressed during the earthquake. Steel bars exposed due to very thin covering concrete were extensively corroded prior to the earthquake. Both left and right river dykes were protected by stone masonries at inside facing to river flow. The river dykes suffered almost no damage due to the earthquake. This feature of damage reminds us of a similar damage of the Struve Through Bridge in the 1989 Loma Prieta Earthquake, California, USA (Lew, 1990).



Photo 11 Collapse of a three span continuous bridge near Fossa Station



Photo 12 Section of the fallen deck



Photo 13 Damage of pile-bent pier



Photo 14 Pile-bent piers which punching sheared the deck slab



Photo 15 Top of a pile-bent pier



Photo 18 Damage of a frame reinforced concrete pier



Photo 16 Failure of a pile-bent pier

A 2 m long, 2.5 m tall stone masonry arch culvert collapsed and was temporarily repaired by filling crushed lime stone into the culvert as shown in [Photos 19 and 20](#). How the arch culvert suffered damage was not known because it was already repaired. However it is likely that a part of stone masonry arch members lost the equilibrium and collapsed during the earthquake. Because the embedment of the arch was shallow without covering masonries on the arch, the arch members had less stability.

A 20 m long 4 m wide three-span continuous bridge located in the suburbs of Onna Village suffered damage at the top of frame piers as shown in [Photos 17 and 18](#). Plastic hinge did not form at the beam-column connection. The damage which was developed prior to the earthquake progressed during the earthquake. Embankment right behind the abutment settled and a cast-iron water pipe attached on the bridge suffered damage at the connection between the bridge and the embankment. Several cracks occurred on the river dyke due to soil sliding.



Photo 19 Emergency repair of a stone masonry arc culvert (SR261)



Photo 17 A 20 m long bridge near Onna Village



Photo 20 Road temporarily repaired by filling crushed limestone

A part of the A24 viaduct in L'Aquila as shown in **Photo 21** also suffered damage. The viaduct is a 37 m long simply supported PC box-girder bridges supported by 11-20 m tall reinforced concrete columns. It is supported by steel fixed (sliding) and movable (roller) bearings or elastomeric bearings. The viaduct was separated in the upper and lower bound bridges. Vertical gaps as large as 200 mm were seen at numerous expansions as shown in **Photo 22**. A number of decks drifted by nearly 200 mm in the longitudinal and transverse directions as shown in **Photo 23**. The bearings where gaps occurred at expansion joints or decks drifted could hardly be investigated, but it is likely that the gaps at expansions were developed by failure of bearings. Drift of the decks is generally developed due to residual deformation of elastomeric bearings. A part of the covering concrete spalled as shown in **Photo 24** at the bottom of a pier. It is likely that the pier nearly yielded. **Photo 25** shows damage of a shear connector at the end of a deck.



Photo 23 Residual drift of two bridges in the longitudinal direction



Photo 24 Spalling of a part of covering concrete



Photo 21 A viaduct of A24 in L'Aquila



Photo 25 Damage of a shear connector



Photo 22 Gap at an expansion joint

## 2) Damage of retaining wall

Settlement of road surface occurred at a number of locations in the lowland along Aterno River. One of the two lanes of SS17 at the intersection with SR615 was partly restricted for traffic because the road embankment locally subsided by 350mm and the upper part of the stone masonry retaining wall leaned as shown in **Photos 26 and 27**. The retaining wall was propped by wood bars for resisting the earth pressure. The detour lane was being constructed adjacent to the affected lane.



Photo 26 Subsidence of a road embankment at the intersection of Route SS17 and Route SR615



Photo 27 Emergent repairing of damaged embankment

## 6. SUMMARY

The L'Aquila earthquake provided valuable lessons on how transportation facilities behaved under an  $M_w=6.2$  low probability and high consequence event. Historically L'Aquila and its vicinity were subjected to at least eight earthquakes since the 14th century. During this earthquake, extensive damage was developed in the old city of L'Aquila and the surrounding towns and villages including Onna, Paganica, Fossa and Ocre. The L'Aquila basin was covered by conglomeratic clayey or calcareous deposits underlay by lacustrine clayey deposits.

Inherent to the unique soil condition, settlements and sliding of ground and soil structures occurred at numerous locations in the lowland along Aterno River, and a number of sliding and rock fall occurred in the nearby mountainous regions. Two sinkholes were found in the old city of L'Aquila due to collapse of thin roofed caves in conglomeratic calcareous deposits.

As was apparent from the lessons in the past events, old unreinforced masonry buildings were extremely vulnerable to earthquake. In particular, unreinforced masonry buildings with soil joint suffered extensive damage.

Extensive corrosion of steel bars in reinforced concrete structural members was widely observed not only in bridges but also in buildings. Concrete cover was so thin for preventing corrosion. There were even cases when concrete cover was not virtually provided. Corrosion of bars resulted in direct loss of tension strength as well as loss of bond strength between concrete and bars.

A local and probably old three-span continuous short-span bridge collapsed, and several bridges suffered damage. At A24 viaduct in L'Aquila, residual drift of decks and vertical gaps of expansion joints occurred at number of spans possibly due to damage of bearings. Failure of shear connectors was also observed. However damage of bridges was generally less significant because most of bridges in the damaged area were small supported by short columns.

## ACKNOWLEDGEMENTS

The authors express their sincere appreciation to Professor Giovanni Barla, Torino Polytechnic University for hosting the JSCE/JGS/JAEE/AIJ joint Reconnaissance Team. Special appreciation is extended to Professor Mauro Dolce, Department of Civil Protection, Professor Michele Calvi, University of Pavia, and Professor Paolo Pinto, University of Rome, "La Sapienza". Without the kind support of a number of personnel, the reconnaissance damage survey could not be successfully conducted.

## REFERENCES

1. Bagh, S., L. Chiaraluce, P. De Gori, M. Moretti, A. Govoni, C. Chiarabba, P. Di Bartolomeo, M. Romanelli, (2007), "Background seismicity in the central Apennines of Italy: The Abruzzo region case study," *Tectonophysics*, 444, 80-92.
2. Bigi, G., Cosentino, D., Parotto, M., Sartori, M., and Scandone, P., (1990), "Structural model of Italy and gravity map, CNR – Progetto

- Finalizzato Geodinamica, Quaderni de “La Ricerca Scientifica” No. 114, 3.
3. Dramis, F. and Blumetti, A.M., (2005), “Some considerations concerning seismic geomorphology and paleoseismology,” *Tectonophysics*, 408, 177-191.
  4. Institute for Environmental Protection and Research, (2006), “Geologic Map of Italy, scale 1:50.000, Sheet No. 359-L'Aquila,” S.EL.CA. Firenze, Italy.
  5. Lew, H.S. (editor), (1990) “Performance of structures during the Loma Prieta earthquake of October 17, 1989,” NIST Special Publication 778, National Institute of Standards and Technology, Gaithersburg, MD, USA.
  6. Port and Harbor Research Institute, Japan, (1997), “Handbook on liquefaction remediation of reclaimed land,” Balkema, 312p.
  7. CEN, Eurocode 8, (1994), “Design provisions for earthquake resistance of structures, European ENV 1998,” Comité Européen de Normalisation, Brussels.
  8. Italian Strong Motion Network (RAN managed by the Italian Department of Civil Protection, DPC. (<http://www.protezionecivile.it/minisite/>).
  9. Luca, G. D., Marcucci, S., Milana, G., and Sano, T., (2005), “Evidence of low-frequency amplification in the city of L'Aquila, central Italy, through a multidisciplinary approach including strong- and weak-motion data, ambient noise, and numerical modeling,” *Bulletin of Seismological Society of America.*, 95, 1469 -1481.

## **THEME 5**

### **Storm Surge and Tsunami**

## Decision Making on Evacuation from the Tsunami Following the Earthquake off Kuril Islands in 2006

by

Yoshio Suwa<sup>1</sup> and Fuminori Kato<sup>2</sup>

### ABSTRACT

This paper builds and examines a model of decision making on evacuation from the tsunami in November 2006. A questionnaire survey on actions etc. after the evacuation order was conducted in Kushiro City, and the model was examined through a structural equation modeling. The results show that intention to evacuate was related to concern over inundation, resources on evacuation, and experiences of tsunami damage and evacuation, and that social capital had close relation to interest in disaster prevention.

**KEYWORDS:** Evacuation, Social Capital, Structural Equation Method, Tsunami

### 1. INTRODUCTION

Storm surge disaster has frequently occurred both in and out of Japan in the past several years, and large-scale tsunami disasters are expected to occur in the future. However, in reality, there are many residents who do not evacuate despite their recognition of the need to do so due to normalcy bias and other factors, even when a typhoon approaches or a tsunami warning is issued.

On the other hand, social capital is drawing attention in the context of disaster prevention, together with volunteers, community development activities, and international cooperation. Social capital is a characteristic of social organization, with others being "trust," "norms of reciprocity," and "network of civic engagement," and is known to enhance the efficiency of society by activating people's cooperative action.

In general the occurrence of tsunami is characterized by long intervals. Given this

characteristic, it is important to hand down the lessons learned from past disasters and communicate a picture of expected damage to residents in disaster prevention. It is necessary to have neighbors call out to each other to evacuate and to support mobility-impaired residents during evacuations, and to engage in local efforts toward restoration and rehabilitation after damage has been suffered. These actions cannot be easily realized without residents' having close ties with their neighbors and enthusiasm for participation in disaster drills. Accumulation of social capital is thus required.

For evacuation from a tsunami, it has been noted that people excessively depend on evacuation information or tsunami warnings when they make decisions about evacuation, that people tend to have too optimistic a view about danger, and that people's impressions of tsunami tend to be fixed based on their past experience [1]. A report from the Tokachi-oki Earthquake in 2003 indicates that those who, immediately after they felt a big tremor, clearly understood that they were in danger unless they evacuated were actually able to evacuate swiftly [2]. The Cabinet Office conducted a nation-wide survey on social capital [3] and reported some noteworthy findings about its relationship with disaster prevention. However, there are no reports where the action of evacuation from a tsunami was analyzed out of the need to consider social capital.

In this research, which views social capital as the basis for local people's historically formed disaster prevention capability, we surveyed evacuation decision-making factors for the purpose of reviewing measures to promote

---

<sup>1</sup> Head, Coast Division, National Institute for Land and Infrastructure Management, Asahi 1 Tsukuba-shi, Ibaraki-ken 305-0804 Japan

<sup>2</sup> Senior Researcher, Coast Division, ditto

evacuation.

## 2. SURVEY METHOD

### 2.1 Outline of Survey

On November 15, 2006, a tsunami warning was issued in the area of Hokkaido facing the Okhotsk Sea and the eastern coast facing the Pacific following an earthquake that occurred off the Kuril Islands. All local governments located in the concerned coastal areas issued an evacuation directive and order (to 130,804 residents). Kushiro City, where the seismic intensity was recorded to be only 1, issued an evacuation order, simultaneously with the tsunami warning (8:29 pm), to 2,561 households (4,675 residents) in the areas in which evacuation is necessary when a tsunami of 3 meters or less is expected based on the Tsunami Hazard Map of Kushiro City [4] and the Onbetsu area (i.e., the area seaward from the track of the Nemuro Main Line). The first tsunami waves hit the coast at a height of 0.2 meters at 9:43 pm; however, the waves never exceeded 0.3 meters in height, and no damage was done. At 11:30 pm. when the tsunami warning was switched to a tsunami advisory, the evacuation order was cancelled.

To clarify what factors differentiated those who evacuated from those who did not, a questionnaire survey was conducted that targeted residents in the area of Kushiro City, Hokkaido, that was subjected to the evacuation order.

### 2.2 Past Tsunamis in Kushiro and Present Measures

Kushiro City faces the Pacific Ocean. The Kushiro River, New Kushiro River and Akan River flow through the city area and drain into the sea. Learning from a flood of the Kushiro River that occurred in 1920 and inundated the city area, the government started excavation of a new water channel (to become the New Kushiro River in 1931). When the Tokachi-oki Earthquake occurred on March 4, 1952, Hamanaka Town, east of Kushiro City, were inflicted with serious damage by a resulting tsunami. While the height of this tsunami was

about 0.9 meters at Kushiro City, damage by the earthquake itself was greater. Tsunami damage was minor following the Chile Earthquake that occurred on May 24, 1960. The Kushiro-oki Earthquake on January 15, 1993, shook the city at a seismic intensity of about 6, and damage caused by the seismic motion was serious. When the Tokachi-oki Earthquake struck on September 26, 2003, the city was severely jolted, and 193 residents evacuated voluntarily.

As stated above, Kushiro's citizens have almost never experienced tsunami damage. Nonetheless, the Central Disaster Prevention Council predicts that major earthquakes with epicenters somewhere in the Kuril Trench occur at intervals of 500 years. In response, Kushiro City distributed a new hazard map based on tsunami-inundated areas predicted by Hokkaido Government in 2007. In addition, voluntary disaster prevention and mitigation activities are aggressively conducted, including surveys on citizens' awareness of tsunami evacuation and disaster "desk drills" by the Kushiro City Federation of Disaster Prevention Promotion Councils (a federation of voluntary disaster prevention organizations). However, these activities are experiencing some problems, including falling participation in disaster prevention efforts as well as fewer people taking the lead in disaster prevention due to hollowing out of the city center.

### 2.3 Survey Method

A questionnaire survey was conducted and recovered answers from respondents to questions on the following: the number of co-inhabitants; presence or absence of mobility-impaired people and car drivers; type of housing and number of stories; fear of seismic motion; anticipation of inundation and related danger; recognition of warnings and evacuation orders; intention to, preparation for, and action concerning evacuation; presence or absence of mutual alerting to evacuate; experience of disaster or evacuation; status of participation in disaster prevention drills; recognition of the circulated hazard map (Kushiro Anshin Map), shelters, and expected inundation areas; recognition of past disasters

and memories of past disasters; desire to live in the neighborhood permanently; and social capital (trust of others, neighborhood socialization, activities based on community bonds, individual activity, etc.). Questions about social capital included the same questions asked by the Cabinet Office survey [3] for comparison. The questionnaire also clearly stated that the subject earthquake, which occurred in November 2006, is different from another earthquake that occurred off the Kuril Islands on January 13, 2007, after which a tsunami warning and evacuation order were also issued, so that no confusion between them should occur.

In order to prevent biasing of samples by location or type of housing, the number of households to be candidate subjects of the questionnaire survey was allocated by a unit set by combining such attributes as the zone of elevation (below 2 meters and 2 meters or higher), expected inundation depth (below 1 meter and 1 meter or higher), and type of housing (detached or collective) for each block in the areas to which an evacuation order is to be issued, and the households to be surveyed were selected from those at random.

The questionnaire was handed in person to 557 households and delivered to 93 households from December 15 to 17, 2007. Questionnaire answers were returned by mail, postage collect. The recovery ratio was 46% (302 households); however, one questionnaire was left blank.

### 3. SURVEY RESULTS

#### 3.1 Attributes of Respondents

The sizes of the respondents' households were relatively small, as shown by the ratio of household size, or 31.2% for single-person households, 34.9% for two-person, and 18.6% for three-person. The survey revealed that 18.2% are households with residents who cannot easily evacuate on foot. As for types of housing, detached houses occupy 58.7%, while collective housing accounts for 42.2%. For the number of stories, flat houses occupy 5.0%, two-storied 65.4%, three-storied 4.3%, and four-storied or higher 24.9%. For the floor where respondents

stay the longest, the first floor accounts for 56.5%, 2nd floor 20.9%, 3rd floor 4.7%, 4th floor 5.3%, 5th floor 9.3%, and 6th floor or higher 2.3%.

#### 3.2 Information on Respondents' Locations

Information on the respondents' locations, loudspeaker car routes, and the locations of PA radio facilities were input into a geographical information system, and then the elevations of the residents' homes, expected inundation depth (in the case of a once-in-500-years earthquake), distance from the coastline, distance from the waterfront (i.e., the closest coastline or river), distance from the evacuation area, distance from loudspeaker car routes, and distance from disaster PA radio facilities (outdoor speakers) were measured. An outline of the results is provided below:

- For the elevation of the respondents' homes, homes below 1 meter in elevation account for 1.7%, 1 to 2 meters 60.5%, and 2 to 3 meters 29.2%.

- For the expected inundation depth, homes expected to be inundated to a depth of less than 0.5 meters account for 37.2%, 0.5 to 1.0 meters 42.9%, and 1.0 to 1.5 meters 11.0%. Of all respondents' houses, 5.6% have an expected inundation depth of zero meters.

- For distance from the coastline, 48.2% are over 1,000 meters away, meaning a relatively high number of homes are located away from the coastline. This is because it is expected to be flooded by tsunamis through the Kushiro River.

- For the distance from the waterfront, 19.9% are less than 100 meters away, 33.6% are 100 to 200 meters, and 28.2% are 200 to 300 meters. No households are beyond 1,000 meters.

- For the distance from the designated evacuation area, 88.0% are less than 400 meters away.

- For the distance from a loudspeaker car route, 91.0% are less than 100 meters away.

- For the distance from a disaster information PA radio facility, 27.6% are less than 100 meters away, 37.5% for 100 to 200 meters, and 17.3% for 200 to 300 meters.

#### 3.3 Simple Summation of the Responses

##### 3.3.1 Fear of Tremor

As shown in Figure 1, the tremor of the subject earthquake was no more fearful than that of an ordinary earthquake for over two-thirds of the respondents.

### 3.3.2 Expectation of Inundation and Danger to Life

As shown in Fig. 2, the respondents who thought their homes "would surely be inundated" or "would probably be inundated" in the subject earthquake together occupy only about 5%. Asked the depth to which they thought their homes would be inundated, 1.0% of the respondents answered "up to the 2nd floor," 2.3% "to the level of the floor," 5.3% "below the floor level," 24.9% "around the house," and 61.1% answered they "never thought the house could be inundated." For danger to life, as shown in Fig. 3, 5% of the respondents "thought I would not be safe unless I evacuate" or "thought I could die unless I evacuate." Thus, only a small number of respondents anticipated inundation or danger to life due to the earthquake.

### 3.3.3 Recognition of Warning and Evacuation Order

Of the respondents, 72.4% knew a tsunami warning was issued, and 23.9% did not. Those who knew were asked how they learned of the warning, with multiple answers allowed; of them, 85.3% said TV, 46.8% said loudspeaker car or fire engine, 14.2% said outdoor speaker, 14.2% said radio, and 4.6% said neighbors. The fact that many chose loudspeaker car, fire engine or outdoor speaker is probably due to the fact that many respondents lived near a loudspeaker car route or PA radio facility.

Of the respondents, 65.8% knew that an evacuation order was issued, while 26.6% did not. When those who knew were asked how they learned of the order, with multiple answers allowed, 82.8% indicated TV, followed by 56.1% for loudspeaker car or fire engine, 18.7% for outdoor speaker, 9.6% for radio, and 5.6% for neighbors. This trend is similar to that of warning, but compared with the case of warning, the ratio for TV is smaller, while those for outdoor speaker and neighbors were slightly

greater.

### 3.3.4 Intention and Preparation for Evacuation

The respondents were asked if they intended to evacuate following the subject earthquake regardless of whether or not they knew of the evacuation order. As shown in Fig. 4, those who "thought I must evacuate" and "thought I should evacuate" together accounted for about 30%.

Answering another question about whether they prepared for evacuation or not, 16.6% of respondents "checked the location of the evacuation area and prepared items to take," 26.9% "checked the location of the evacuation area but did not prepare items to take," and 50.8% "did not prepare for evacuation."

### 3.3.5 Evacuation, Starting Time, and Means of Transportation

Of all of the respondents, 28.6% evacuated and 67.8% did not; 3.7% gave no answer. The ratio of those who evacuated roughly agrees with the previously mentioned ratio of people who leaned toward evacuation.

Eighty-six respondents who evacuated were asked at what time they did so. As shown in Fig. 5, over three-fourths of the evacuees left their homes for an evacuation area by the time immediately after the issuance of the evacuation order.

For the means of transportation, 67.4% used cars, 24.4% walked, and 4.7% used bicycles. Thus, many respondents used cars for evacuation.

### 3.3.6 Motivating Factor for Evacuation and Reason not to Evacuate

The 86 evacuees were asked what motivated them to evacuate. As shown in Fig. 6, many of them gave the issuance of the tsunami warning or evacuation order. In addition to calls for evacuation from TV and radio stations, the city hall or fire department, a relatively large percentage of respondents said they decided to evacuate because neighbors called on them to evacuate together.

The 204 respondents who did not evacuate were

asked why they did not. As shown in Fig. 7, the most common answers were, in descending order, "did not think a big tsunami would occur," "monitored the situation on TV," and "no neighbors evacuated." Some answered "I have family members who are physically disabled" or "I could not evacuate by myself." This suggests the need to support residents who require care in evacuation.

### 3.3.7 Mutual Calls for Evacuation

Of the respondents, 9.6% were called on to evacuate by neighbors, while 62.8% were not. Conversely, 10.0% called on their neighbors to evacuate, while 79.1% did not.

### 3.3.8 Experience of Disaster and Experience of Evacuation

Respondents were asked about their experience with tsunami disasters, and 74.1% said they "had not experienced any tsunami damage," 5.3% "experienced tsunami damage caused by the Tokachi-oki Earthquake in 1952," and 5.0% "experienced tsunami damage caused by the Chile Earthquake in 1960." Asked about experience with damage other than tsunami, 40.9% "had not experienced any damage other than tsunami," and 27.6% "experienced damage caused by the shaking of an earthquake." Although few residents had suffered tsunami damage, a relatively large number of people had experienced earthquake damage other than tsunami.

To a question about their experience in evacuating from a tsunami, the majority of respondents, or 46.5%, answered they "had never evacuated from a tsunami." But 11.0 to 17.9% had evacuated following earthquakes, including the Hokkaido Toho-oki Earthquake in 1994, Tokachi-oki Earthquake in 2003, Kushiro-oki Earthquake in 1993, and Tokachi-oki Earthquake in 1952.

### 3.3.9 Interest in Disaster Prevention

Of the respondents, 70.8% had never participated in disaster drills, while 8.6% participate in them every year.

The percentage of respondents that had seen

Kushiro Anshin Map was 75.4%, which is far greater than the ratio of those who had not (20.6%).

Asked about the evacuation area, 76.7% answered it is "within walking distance," 5.3% said it is "beyond walking distance," and 12.6% "don't know where it is."

Asked if their home is in the expected inundation area or not, many respondents, or 77.1%, indicated that they know their home is in the expected inundation area, while those who did not know account for 13.6%.

When subject residents were asked about serious damage caused by a devastating flood in Kushiro in 1920, many of them, or 59.8%, had "never heard of it." Those who "know about it in detail" and "heard of it" only accounted for 3.3% and 34.6%, respectively.

### 3.3.10 Social Capital

When asked about their trust of others, 9.6% answered they "can trust most people," 40.9% think "there are more trustworthy people than not," 38.2% "cannot say either way," 6.3% said "there are more untrustworthy people than trustworthy people," and 1.7% "can't trust most people." Compared with the nation-wide survey done by the Cabinet Office, the sense of trust in others is higher in this survey.

When asked about degree of socialization with their neighbors, 13.6% said they "cooperate with neighbors in daily living; for example, in mutual consultation or lending/borrowing of daily commodities," 36.2% "socialize with neighbors on daily chatting terms," 42.2% "engage in a minimum level of socialization; e.g., are just on greeting terms," and 5.6% "do not socialize with neighbors." As for their desire to live in the neighborhood permanently, 33.6% "want to live permanently," 15.3% "would rather live permanently," 25.2% "can't say either way," 8.0% "would rather not live permanently," and 15.9% "don't want to live permanently." The results for degree of socialization with neighbors and desire to live in the neighborhood permanently are slightly lower than those of the

Cabinet Office's nation-wide survey.

Asked about participating in activities that are based on community bonds, many respondents, or 52.5%, "don't participate in such activities," 24.6% "participate a few times a year," and 7.0% "participate about once a month." The ratio of respondents who participate in volunteer activities, NPO, or civil activities is about 20%.

#### 4. ANALYSIS OF DETERMINING FACTORS IN EVACUATION DECISION-MAKING

##### 4.1 Analytical Method

The questionnaire survey asked questions about what made residents decide to evacuate or why they didn't evacuate. It is recognized that their answers may contain some bias that justifies their action. To clarify the relationship between various factors, including recognition of the evacuation order, and evacuation action, a covariance structure analysis was conducted using AMOS with such observed variables as the respondents' answers and locational information of the respondents compiled by the geographical information system.

As shown in Fig. 8, the hypothesis used in this verification was established based on the previous research results, with evacuation action separated from intention to evacuate, and the factors concerning intention to evacuate set as latent variables (surrounded by ovals). To increase the appropriateness of the model, the final path diagram of Fig. 9 was obtained by narrowing down the observed variables of the latent variables (surrounded by squares in Fig. 9) based on the results of factor analysis and eliminating the paths that lead to inappropriate solutions.

##### 4.2 Analysis Results

As indicated in Fig. 9, the path coefficients (arrow subscripts) indicate the correlation between factors. Since this figure is a standardized solution, the closer the absolute value of the path coefficient is to 1, the greater the correlation between factors. Since GFI and AGFI of the model are below 0.9, the model's appropriateness is not sufficiently high; however,

the model is still considered appropriate enough to estimate the relationship between factors.

Focusing on the path coefficients, we can clearly see a path leading from concern over inundation to intention to evacuate and from intention to evacuate to evacuation action; however, recognition of evacuation information has little to do with concern over inundation or intention to evacuate. While the part of the result where concern over inundation is connected to intention to evacuate agrees with the corresponding result of the survey made by Yoshii et al. [2], it is understood that concern was affected by previous experience and fear of tremors. Unlike the answers on motivating factor for evacuation, a certain tendency is suggested whereby recognition of a tsunami warning or evacuation order has little effect on evacuation action. Although recognition of the hazard map and evacuation areas and experience of participation in disaster drills are important, it is possible that interest in disaster prevention alone will not directly lead to evacuation.

Intention to evacuate has a relatively strongly relationship with previous experience and resources on evacuation as well as concern of inundation. This finding puts importance on sharing of disaster and evacuation experience, measures to support people who require assistance, and development of neighborhood evacuation areas when promoting evacuation.

Social capital is greatly related to interest in disaster prevention. Separately conducted factor analysis on all of the observed variables found that the observed variables related to social capital, excluding trust of others, (i.e., participation in activities based on community bonds, socialization with neighbors, and desire to live in the neighborhood permanently) are greatly affected by the same factors as the observed variables related to interest in disaster prevention, such as participation in disaster drills. This finding indicates that the part of social capital that is related to the local community may probably encourage recognition of evacuation information or evacuation action by enhancing residents' interest in disaster

prevention. Note that large path coefficients are also derived from calculation by reversing the arrows from social capital to interest in disaster prevention, suggesting close ties between them bilaterally.

## 5. CONCLUSIONS

As discussed above, our survey suggests the possibility that the evacuation information provided when the evacuation order was issued had little connection with concern over inundation or evacuation action. This indicates a disassociation between recognition of a tsunami warning or evacuation order and recognition of inundation risk. Elimination of such disassociation or reinforcement of factors related to intention to evacuate based on the assumption of such disassociation should work to encourage evacuation action. One step toward eliminating the disassociation would be thorough communication of the importance of tsunami warnings and evacuation orders. Promising actions to reinforce the factors related to intention to evacuate include simulated disaster experience through visualization of past or expected damage or participation in evacuation drills and improvement of the evacuation environment, including support for people who need assistance and reduction in evacuation distance. It is also important to accumulate social capital to enhance people's interest in disaster prevention.

**Acknowledgements:** This study was conducted under the guidance of Professor Haruo Hayashi of Disaster Prevention Research Institute, Kyoto University. We gratefully acknowledge the cooperation of the General Affairs Section, General Affairs Department, Kushiro City, and the Fire Headquarters of Kushiro City in our questionnaire survey. The Kushiro Municipal Federation of Disaster Prevention Promotion Councils provided us with questionnaire results as well as plenty of information on related local efforts. The Fire and Disaster Prevention

Division, Bureau of Crisis Management, Department of General Affairs, Hokkaido Government, provided us with the topographical data and expected tsunami data. Professor Hirotsugu Sato of Kushiro Junior College's Lifetime Education Center informed us of the history of Kushiro City. Assistant Professor Keiko Tamura of Niigata University's Research Center for Natural Hazards & Disaster Recovery provided us with advice on the design of the questionnaire. We received the cooperation of KCS Co., Ltd., in summation and analysis of the questionnaires. We would like to thank all of the above for their cooperation as well as the subject residents who answered the questionnaires during the busy year-end season.

## 6. REFERENCES

1. Katada, T., Kodama, M., Kuwasawa, T., and Koshimura, S.: Issues of Residents' Consciousness and Evacuation from the Tsunami - from Questionnaire Survey in Kesenuma City, Miyagi Pref. after the Earthquake of Miyagiken-oki, 2003, *Journal of Japan Society of Civil Engineers*, No. 789/II-71, 2005 (in Japanese).
2. Yoshii, H., Tanaka, A., Nakamura, I., Nakamori, H., and Mikami, T.: Questionnaire Survey to Citizens on Evacuation from Tsunami, 2003, *the Emergency Research Report on the Tokachi-oki Earthquake (edited by Tadashi Hirata)*, 2004 (in Japanese).
3. Quality-of-Life Policy Bureau, Cabinet Office: Survey entrusted by the Cabinet Office in 2002, "Social Capital: Toward Rich Human Relationship and Favorable Circulation of Citizen Activities," [http://www.npo-homepage.go.jp/data/report9\\_1.html](http://www.npo-homepage.go.jp/data/report9_1.html), 2003 (in Japanese).
- 4) General Affairs Section, Kushiro City: Once-in-500-Years Earthquake Tsunami Hazard Map, <http://www.city.kushiro.hokkaido.jp/www/contents/1141823239893/files/tsunami1.pdf>, etc. (in Japanese).

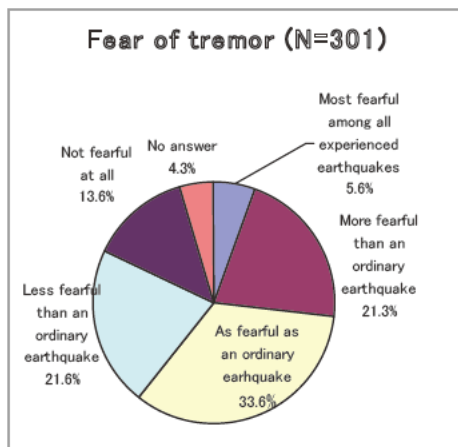


Fig.1 Fear of Tremor

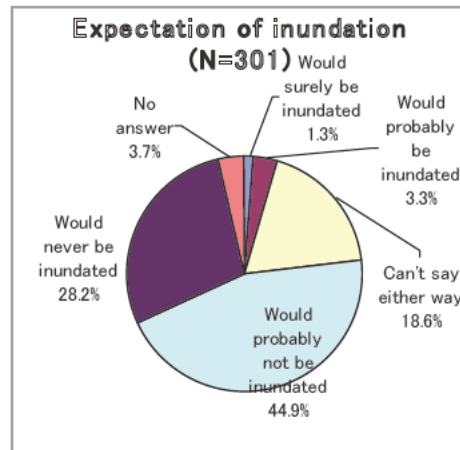


Fig.2 Expectation of Inundation

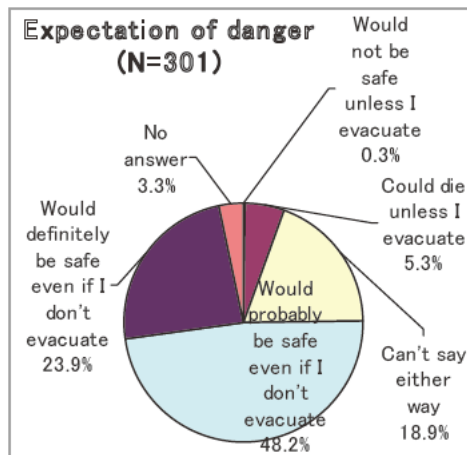


Fig.3 Expectation of Danger

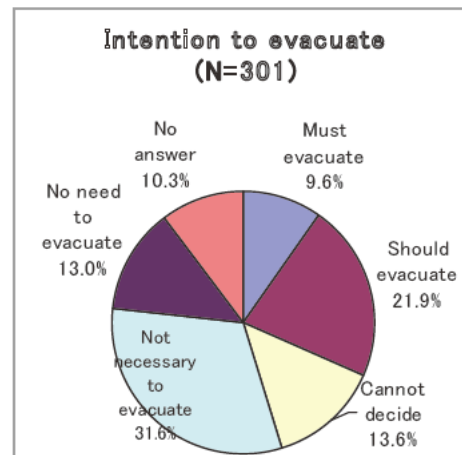


Fig.4 Intention of Evacuate

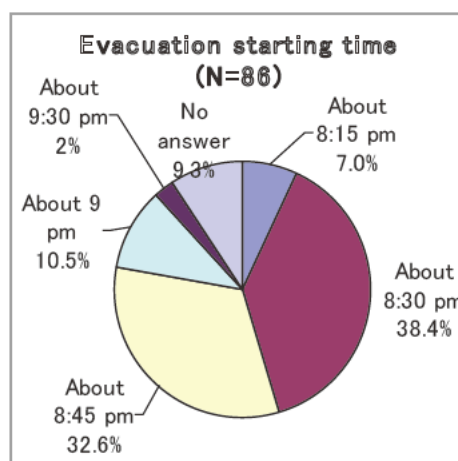


Fig.5 Evacuation Starting Time

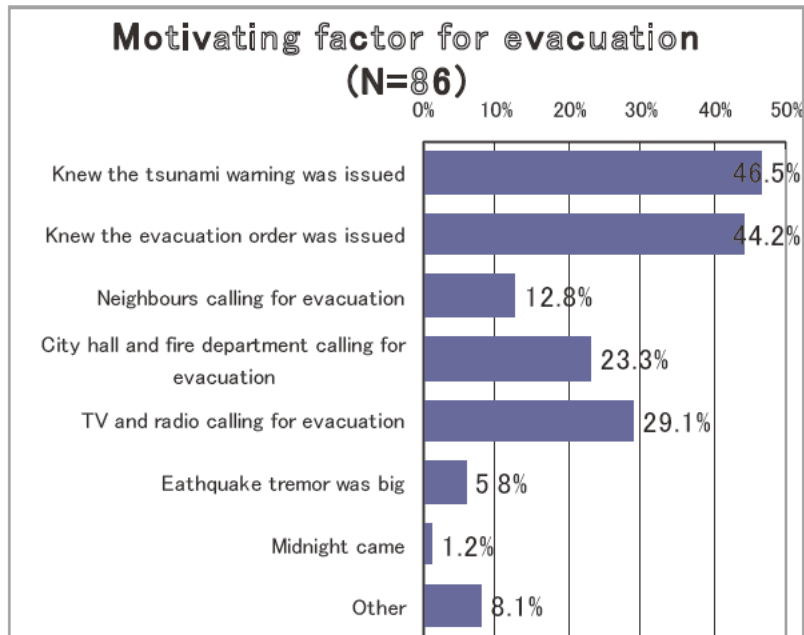


Fig.6 Motivating Factor for Evacuation (multiple answers allowed)

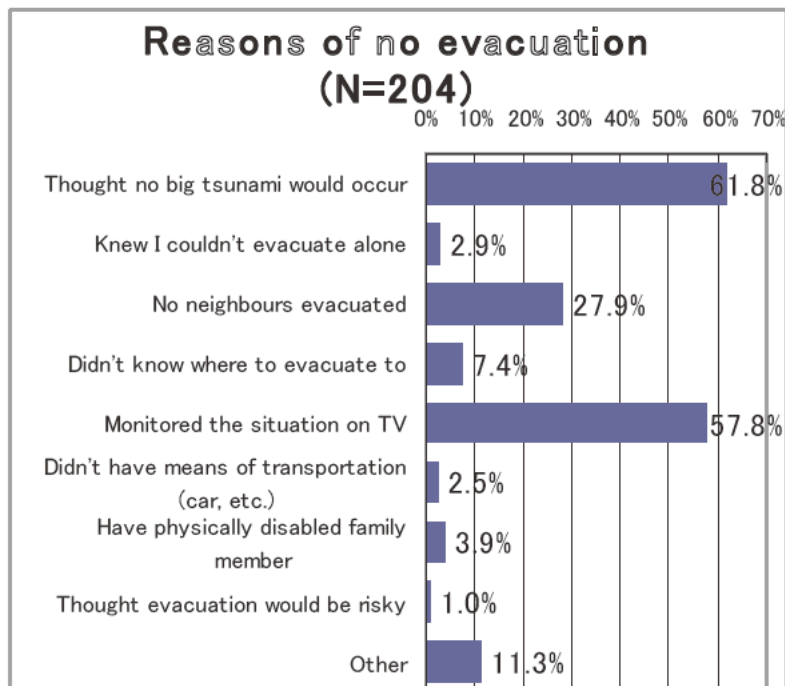


Fig.7 Reasons of No Evacuation (multiple answers allowed)

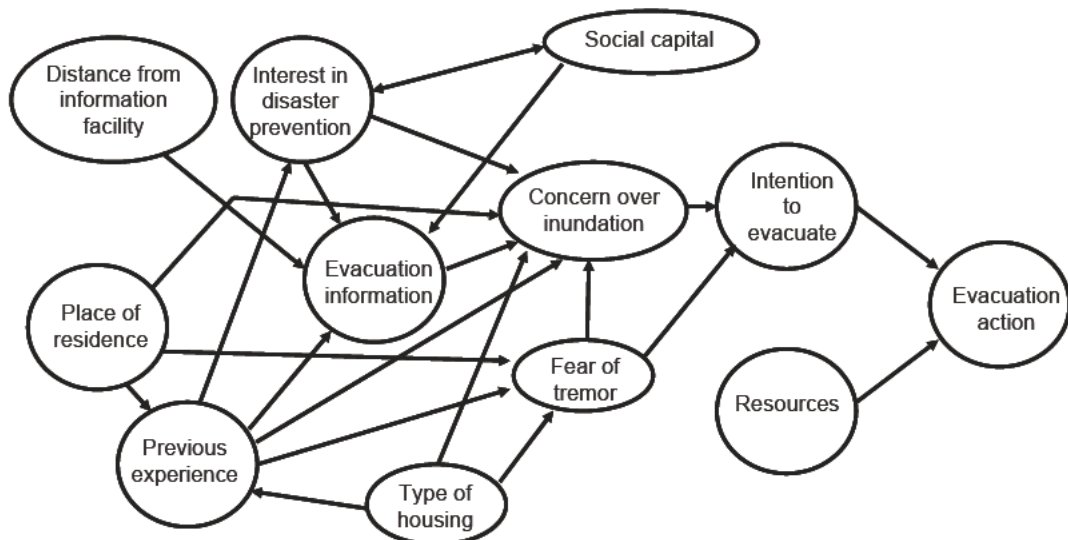


Fig.8 Hypothesis of Evacuation Action

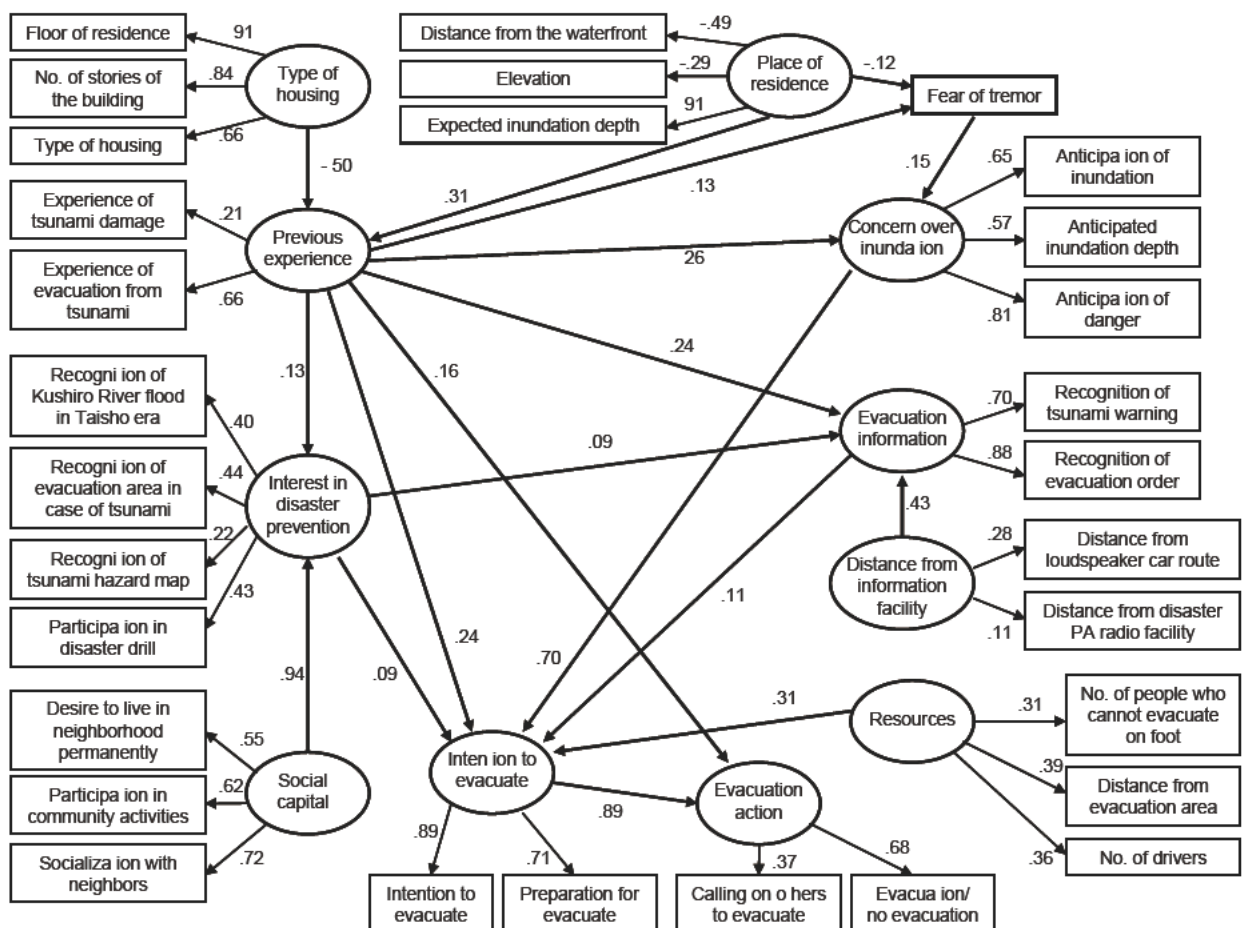


Fig.9 Final Model (Standard Solutions: GFI = 0.797; AGFI = 0.756; RMSEA = 0.059)

## Practical Model to Estimate Behavior of Tsunami-Drifted Bodies

by

Takashi Tomita<sup>1</sup> and Kazuhiko Honda<sup>2</sup>

### ABSTRACT

Historical records of tsunami damage have shown us that tsunamis cause various damages: inundation, destruction of houses, drift of vessels and others. If vessels are drifted by a tsunami, they have the potential to collide with houses and buildings and then to cause secondary damage to them in addition to the damage by tsunami fluid force. To control and mitigate the damages by the drifted-bodies, we should understand and predict the damages at first. We have, therefore, developed a numerical model to estimate behavior of multiple tsunami-drifted bodies practically. The present model calculates drift motion of each body in terms of drag and inertia forces acting on the body, and furthermore considers collision between drifted bodies and between the drifted body and any structure. After the present model is implemented into the STOC system which calculates tsunami damages in oceans and coastal areas, it is validated qualitatively in comparison with some simple test runs and applied to the calculation in a model area with actual bathymetry and topography.

**KEYWORDS:** Collision, Drifted Body, Numerical Modeling, Tsunami

### 1. INTRODUCTION

Japan has good system to issue tsunami warning. The Japan Meteorological Agency (JMA) is the organization in charge. Local governments also issue evacuation order and advisory if happen of tsunami damage is estimated in their regions. However, even if the tsunami warning and evacuation order are issued, many residents stay at their houses and offices to get further information of tsunami and do not evacuate actually. Is this good behavior? Each person decides finally whether he/she should evacuate

or not. Therefore, it is important that each person images tsunami disasters which he/she may suffer, before encounter of the tsunami.

To help the enhancement of people's imagination of tsunami disasters, we have developed numerical simulation and visualization system on tsunami damage, which is named the STOC system [1]. As introduced in the 40th panel meeting in the NIST, the STOC system consists of the numerical simulation model named STOC (Storm surge and Tsunami simulator in Oceans and Coastal areas) and a display tool which shows easily numerical results such as the variation of water surface elevation and water particle velocity as well as damage occurrence areas by using the moving images. Another feature of the display tool is that users of the tool can see the results from any viewpoint they want.

As shown in historical damage records, tsunamis cause inundation, destruction of houses as well as drift of many vessels and others. If vessels are drifted by a tsunami, they may collide with houses and buildings, and then cause secondary damage to them in addition to the damage by tsunami fluid force. To control and mitigate damages by the drifted bodies, we should understand and estimate their behavior. A new numerical model is, therefore, developed and implemented in the STOC system to estimate the behavior of tsunami-drifted bodies. The attractive features of the model are as follows: 1) it can deal with a large number of bodies, 2) calculate not only translational motion of each body but rotational motion in the horizontal plane, and 3) consider collision between the drifted bodies and between the body and any structure

---

<sup>1</sup> Research Director, Tsunami Research Center, Port and Airport Research Institute, 3-1-1 Nagase Yokosuka 239-0826, Japan

<sup>2</sup> Researcher, ditto.

## 2. NUMERICAL SIMULATOR OF STOC FOR ESTIMATION OF TSUNAMI DAMAGE

The STOC system is composed of two parts: numerical simulation model and display tool of its results. The simulation model also consists of 3 sub-models: STOC-ML, STOC-IC and STOC-DM. Figure 1 shows an example of arrangement of STOC-ML, STOC-IC and STOC-DM.

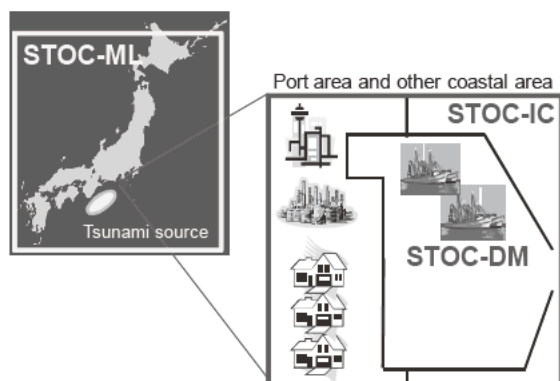


Fig. 1 Arrangement of STOC-ML, STOC-IC and STOC-DM in the numerical simulation model of the STOC system

STOC-ML [1] is a multi-level model which is developed with the use of hydrostatic pressure assumption, and therefore can be applied in wide area such as oceans. To consider vertical distribution of horizontal velocity, STOC-ML deals with a water basin vertically divided into some layer. STOC-IC [1] is the fully three-dimensional model, whose governing equations are the continuity equation to express the mass conservation and the Reynolds-Averaged Navier-Stokes (RANS) equations as the momentum equations in three dimensions. The porous body model by Sakakiyama and Kajima [2] is introduced in the discretized equations of the governing equations to consider the configuration of sea bottom and the shape of structures smoothly. The eddy viscosity is also considered in terms of implementation of the eddy viscosity coefficient which depends on velocity structure and a model coefficient in the same way as Fujima et al. [3]. Comparison with the hydraulic experiment, in

which tsunami reduction was investigated around a tsunami breakwater, showed that the tsunami was not sensitive to the model coefficient in the eddy viscosity coefficient [4]. Therefore, we may use the default value of the coefficient.

STOC-DM is the new model added into the STOC system to calculate the tsunami-drifted vessels, cars, containers and other. To calculate behavior of the tsunami-drift bodies, this model uses temporal and special variation data of water surface elevation and horizontal velocity calculated by STOC-ML and STOC-IC. The details of the model are in the next section.

Easy showing of numerical simulation results is important for residents who may not necessarily have enough knowledge to see the results. For

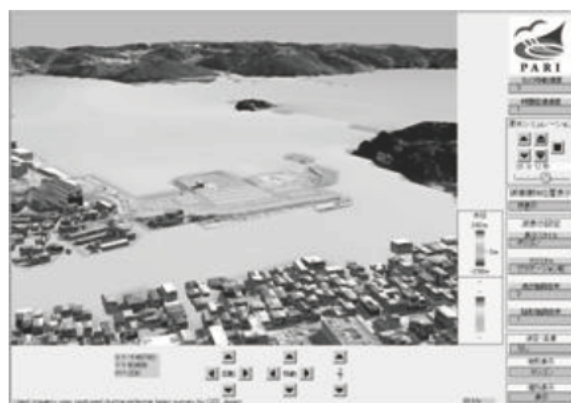


Fig. 2 Snapshot of display on water surface elevation using the STOC system

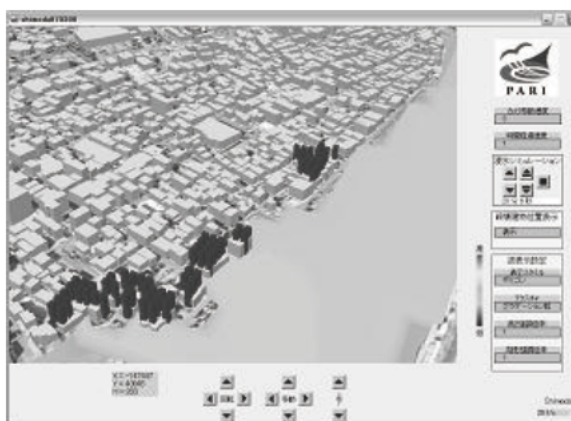


Fig. 3 Snapshot of display on damage occurrence areas using the STOC system (Black bars indicate damage occurrence areas)

example, a resident may want to see the result of tsunami damage estimation in the whole area of their city as well as in his/her residential area. To satisfy such a demand of each resident and disaster mitigation officer, the display tool of the STOC system has the function of showing the results from any viewpoints. Furthermore, the displayed results are not only inundation area and its depth but fluid velocity and wave pressure, which are calculated by the STOC system. Figures 2 and 3 show examples of tsunami inundation and tsunami-damaged areas indicated by the display tool. Actually the tool shows the results by the moving images, although the figures indicate snapshots.

### 3. NUMERICAL MODEL TO ESTIMATE DRIFT MOTION OF BODIES BY TSUNAMIS

#### 3.1 Drift Motion Model

To calculate drift motion of many bodies by a series of tsunami waves with less computational efforts, the numerical model to solve drift motion of bodies does not calculate water surface elevation and water particle velocity of tsunami directly, and utilizes the results on them which are calculated by the other numerical models of tsunami. Then, each body is horizontally moved by the tsunami-induced drag and inertia forces acting on each body.

For practical calculation, the shape of each drifted body is approximated by a rectangular solid. Three modes of motion are calculated in the model: surging, swaying and yawing, as shown in Fig. 4. It should be noted that the vertical motion of heaving is considered so as to keep draft of the body on the water surface. Therefore, the vertical motion is induced by the buoyancy force of the body.

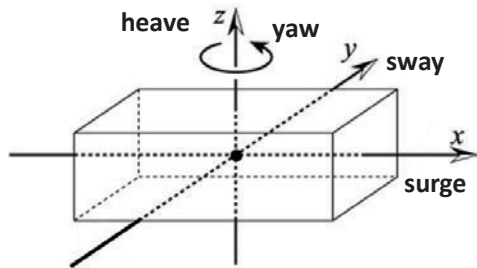


Fig. 4 Considered motion of drifted body

With reference to Ikeya et al. [5], horizontal forces in the surging and swaying directions,  $F_x$  and  $F_y$ , respectively, and momentum around the z-direction,  $M_z$ , are determined by the following equations:

$$\left. \begin{aligned} F_x &= (1-\omega)F_{DX1} + \omega F_{DX2} + F_{MX} \\ F_y &= (1-\omega)F_{DY1} + \omega F_{DY2} + F_{MY} \\ M_z &= (1-\omega)M_{DZ1} + \omega M_{DZ2} + M_{MZ} \end{aligned} \right\} \quad (1)$$

in which

$$\omega = \begin{cases} 1.0 - \frac{0.95}{0.2} \left( \frac{h}{D} - 1.0 \right) : & 1 < \frac{h}{D} \leq 1.2 \\ 0.05 : & 1.2 < \frac{h}{D} \end{cases} \quad (2)$$

$$\left. \begin{aligned} F_{DX1} &= + \frac{\rho}{2} \iint_{sm} C_{DX1,sm} U_{sm} |U_{sm}| dYdZ \\ &+ \frac{\rho}{2} \iint_{sn} C_{DX1,sn} U_{sn} |U_{sn}| dYdZ \\ F_{DY1} &= + \frac{\rho}{2} \iint_{ps} C_{DY1,ps} V_{ps} |V_{ps}| dXdZ \\ &+ \frac{\rho}{2} \iint_{sb} C_{DY1,sb} V_{sb} |V_{sb}| dXdZ \\ M_{DZ1} &= - \frac{\rho}{2} \iint_{sm} C_{DX1,sm} U_{sm} |U_{sm}| YdYdZ \\ &- \frac{\rho}{2} \iint_{sn} C_{DX1,sn} U_{sn} |U_{sn}| YdYdZ \\ &+ \frac{\rho}{2} \iint_{ps} C_{DY1,ps} V_{ps} |V_{ps}| XdXdZ \\ &+ \frac{\rho}{2} \iint_{sb} C_{DY1,sb} V_{sb} |V_{sb}| XdXdZ \end{aligned} \right\} \quad (3)$$

$$\left. \begin{aligned} F_{DX2} &= \frac{\rho}{2} C_{DX2} (U_G^2 + V_G^2) \frac{U_G}{|U_G|} BD \\ F_{DY2} &= \frac{\rho}{2} C_{DY2} (U_G^2 + V_G^2) \frac{V_G}{|V_G|} LD \\ M_{DZ2} &= l \sqrt{F_{DX2}^2 + F_{DY2}^2} \end{aligned} \right\} \quad (4)$$

$$\left. \begin{aligned} F_{MX} &= \frac{\rho}{2} C_M LD \left( \int_{sm} \frac{\partial U_{sm}}{\partial t} dY + \int_{sn} \frac{\partial U_{sn}}{\partial t} dY \right) \\ F_{MY} &= \frac{\rho}{2} C_M BD \left( \int_{ps} \frac{\partial V_{ps}}{\partial t} dX + \int_{sb} \frac{\partial V_{sb}}{\partial t} dX \right) \\ M_{MZ} &= - \frac{\rho}{2} C_M LD \left( \int_{sm} Y \frac{\partial U_{sm}}{\partial t} dY + \int_{sn} Y \frac{\partial U_{sn}}{\partial t} dY \right) \\ &+ \frac{\rho}{2} C_M BD \left( \int_{ps} X \frac{\partial V_{ps}}{\partial t} dX + \int_{sb} X \frac{\partial V_{sb}}{\partial t} dX \right) \end{aligned} \right\} \quad (5)$$

$L$ ,  $B$  and  $D$  are the length, width and draft depth of floating body, and  $h$  the water depth, as shown in Fig. 5. In Eq. 3,  $U_{sm}$ ,  $U_{sn}$ ,  $V_{ps}$  and  $V_{sb}$  are the distributed flow velocities on the side faces of body, as shown in Fig. 6. It is necessary that these velocities should be calculated in the situation of no drifted body. In Eq. 4,  $U_G$  and  $V_G$  are the flow velocities in the surging and swaying directions at the position of the center of gravity of the body as shown in Fig. 6. The first and second terms in the right-hand side of Eq. 1 mean drag forces induced by the flows going under the bottom of body and running through the sides, respectively. The third terms are for inertia force. In the calculation of  $F_{DXI}$ ,  $F_{DYI}$  and  $M_{DZI}$ , velocity distribution in the horizontal plane is considered, because eddies shedding from the bottom may not be uniform horizontally depending on the non-uniform velocity. It should be noted that  $M_{DZI}$  is modified because a drifted body with rotational motion and the same drift speed as the surrounding flow makes rotations indefinitely using the original  $M_{DZI}$  by Ikeya et al.

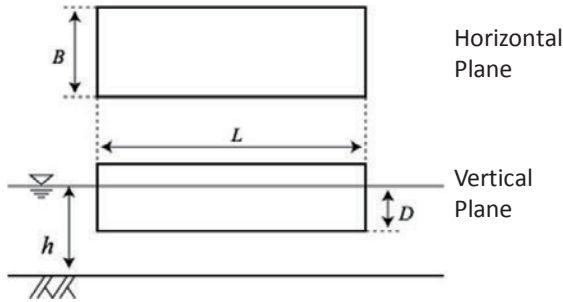


Fig. 5 Definition of size of body

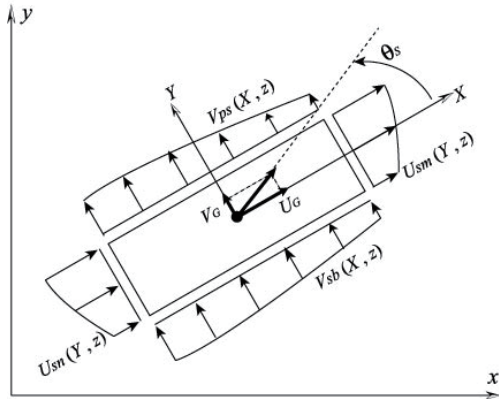


Fig. 6 Definition of flow velocities to calculate fluid forces

The coefficients such as  $C_{DXI,sm}$  and others are as follows:

$$\begin{aligned} C_{DXI,sm} &= \begin{cases} 0.4 & : U_{sm} \geq 0 \\ 0.8 & : U_{sm} < 0 \end{cases} \\ C_{DXI,sn} &= \begin{cases} 0.8 & : U_{sn} \geq 0 \\ 0.4 & : U_{sn} < 0 \end{cases} \\ C_{DYI,ps} &= \begin{cases} 0.4 & : V_{ps} \geq 0 \\ 0.8 & : V_{ps} < 0 \end{cases} \\ C_{DYI,sb} &= \begin{cases} 0.8 & : V_{sb} \geq 0 \\ 0.4 & : V_{sb} < 0 \end{cases} \end{aligned} \quad (6)$$

$$\begin{aligned} C_{CX2} &= 2.0(\cos^2 \theta_s + 1.2|\sin \theta_s \cos \theta_s|) \\ C_{CY2} &= 2.0(\sin^2 \theta_s + 2.2|\sin \theta_s \cos \theta_s|) \end{aligned} \quad (7)$$

$$C_M = 2.0 \quad (8)$$

$$l = \begin{cases} +0.09L|\sin(2\theta_s)|^{1/2} & : \sin(2\theta_s) \geq 0 \\ -0.09L|\sin(2\theta_s)|^{1/2} & : \sin(2\theta_s) < 0 \end{cases} \quad (9)$$

### 3.2 Collision Model

For easily searching a contact point of a drifted body to another body or a structure, it is assumed that a contact face is set so as to cover all main parts of the body, as shown in Fig. 7, which shows an example of a fishing boat. The horizontal shape of a ship which is inscribed in the rectangular indicated by the actual body length of  $L_C$  and actual body width of  $B_C$  is surrounded by a contact face line with circular curves with the radius of  $R_C$  (m) and parallel lines with the spacing of  $2R_C$  (m). The vertical section of contact face is the rectangular to covers main parts which may collide with anybody. It should be noted that the volume formed by the contact face is different from the volume for calculation of drift motion, which is indicated in terms of  $L$ ,  $B$  and  $H$  in Fig. 5. The values of  $L$  and  $B$  are determined by Eq. 10, considering Eq. 11. Eq. 10 expresses the balance of mass and buoyancy of the body, in which  $M$  is the mass of body,  $D$  the draft depth of body and  $\rho_w$  the density of water. In deed

$$M = \rho_w LBH \quad (10)$$

$$\left. \begin{aligned} L &\leq L_C \\ B &\leq B_C \\ H &\geq D \end{aligned} \right\} \quad (11)$$

At the moment that the drift body collides with anything, it is assumed that the moving speed of the drift body suddenly becomes zero in the normal direction of the contact face without deformation.

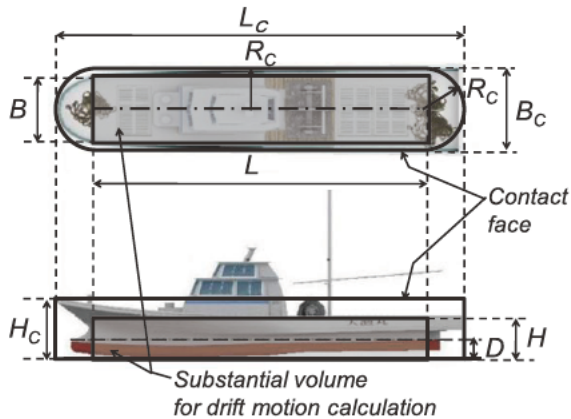


Fig. 7 Contact face and substantial volume of mass to calculate drift motion

#### 4. TEST CALCULATIONS IN SIMPLE CONDITIONS

Validation of the drift model is conducted under very simple calculation conditions. In the phase 1 of test runs, drift motion of a floating body in a uniform flow has been investigated, in which the initial body's angle in the flow, the partition number of the body to consider the velocity distribution in space, and ratio of water depth and draft depth have been changed. The number of test runs is eight. In the phase 2, a moving body contacting with a structure and two bodies colliding with each other have been checked. The number of test runs is seven. In total 15 runs, the developed drift model provided good results qualitatively.

Figure 8 show a result of the test calculation in the phase 2, in which a floating body is initially set in the flow of  $u = 0.5$  m/s in the x-direction and  $v = 0.5$  m/s in the y-direction. The body scales are 3 m in the x-direction, 15 m in the y-direction, and 1 m of draft depth, the mass of body is 45 t. In the figure, locations of the drifted body are indicated every 30 s. Before colliding with the structure, the angle of body

gradually turned to the flow direction as it is drifted by the uniform flow, and the moving speed of the body is also accelerated. After colliding with a corner of structure, the body rotates in anti-clockwise direction around the corner, and the body collides again with the side of structure. Figures 9 and 10 show the motion velocity of the drifted body and rotation angle, respectively. Until 350 s when the drifted body contacts the structure first, the direction of body changes toward  $45^\circ$  which is the flow direction, the motion speed is also accelerated toward the flow velocity. After colliding, the motion speed is suddenly down.

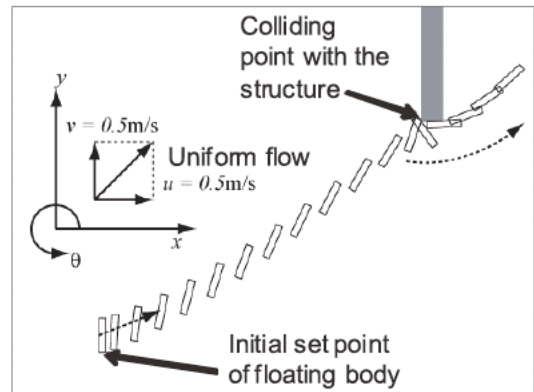


Fig. 8 Motion of the drifted body in a uniform flow (Case 1-1)

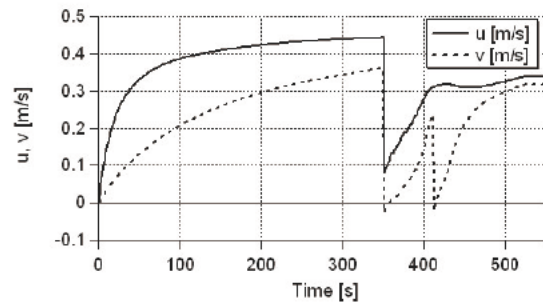


Fig. 9 Motion speed of the drifted body

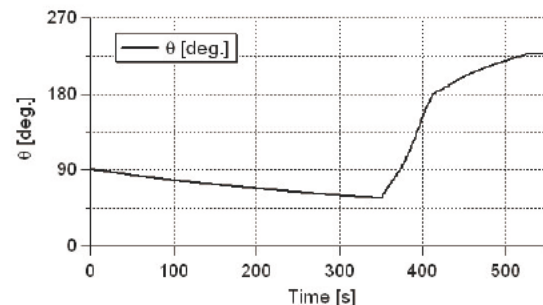


Fig. 10 Direction angle of the drifted body

## 5. APPLICATION OF STOC SYSTEM INCLUDING WITH DRIFT MODEL TO ACTUAL BATHYMETRY AND TOPOGRAPHY

The STOC system is applied to a model area with actual bathymetry and topography, as shown in Fig. 11. Many fishing boats are moored in the water area covered by the dashed thin line, as shown in Picture 1. Since air-born laser profiler data is available in the model area, we can use the calculation grid size of 2 m in the area surrounded by the dashed thick line in the figure where STOC-IC is applied to calculate the tsunami in detail. In the outer region, STOC-ML with a single layer is applied, and the grid size of 6 m is especially used in the area indicated in the figure. STOC-ML and STOC-IC is connected to conduct sequence of tsunami calculation.

The generated tsunami in the calculation has the tsunami height of 2 m approximately and wave period of 20 minutes at Point A in Fig. 11 in the situation of no breakwaters. If there are the breakwaters as shown in the figure, the tsunami does not overtop them, and they can reduce the tsunami intrusion into the harbor area. If a submerged breakwater is additionally installed in the opening section of the breakwaters, it is anticipated to reduce further the tsunami height in the harbor area. As a trial to check the performance of the STOC system, tsunami calculation by the STOC system is conducted in the situation of existence of the breakwaters with the submerged breakwater, because experimental validation of the STOC system has shown that it can solve the tsunami passing through breakwaters with the submerged breakwater [4, 5]. The calculation conditions are as follows: in Case 1 no breakwaters are installed, and in Case 2 there are breakwaters with the submerged breakwater which narrow their opening section area from 27,000 m<sup>2</sup> to 1,800 m<sup>2</sup>. The number of moored vessels is 158 in the harbor area. In this trial, only the first tsunami is picked up in a series of tsunami waves. The initial water surface level is 0.7 m above the mean water level.

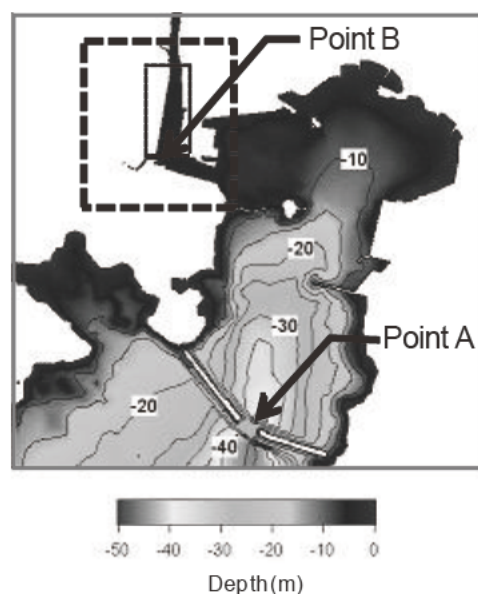


Fig. 11 Model area where the STOC system is applied



Picture 1 Moored vessels in the model area

Figure 12 shows variations of water surface elevation at Point A and Point B. The water surface elevation at Point B rises 3.2 m from the initial water surface level (3.9 m from the mean water level) in the case of no breakwaters. However, in the situation of existence of the breakwaters, it decreases to 2.2 m (2.9 m). Since the ground height is approximately 0.8 m above the initial water level (1.5 m above the mean water level) around Point B, the tsunami runs up on the land even if the breakwaters are installed. However, inundation depth is less than 2 m, and then may not cause severe destruction of houses by the tsunami. Indeed, Shuto [6] and damage reports on the 2004 Indian Ocean Tsunami have indicated that the tsunami of 2 m or more provides complete destruction of wooden houses.

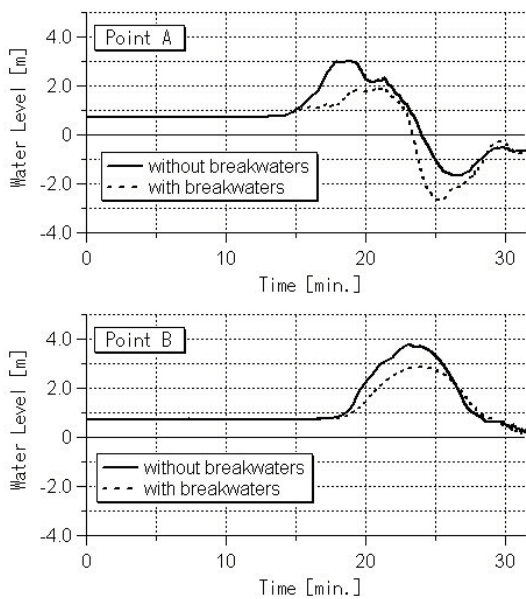


Fig. 12 Time variations of water surface elevation

The fluid velocity is also reduced from 3.5 m/s to 2.1 m/s, as shown in Fig. 13 by the installation of the breakwaters. However, it should be noted that at the opening section of breakwaters (at Point A) the fluid velocity is fastened depending on narrowing of the opening section. Therefore, we should consider such a fast fluid velocity for design of the breakwater.

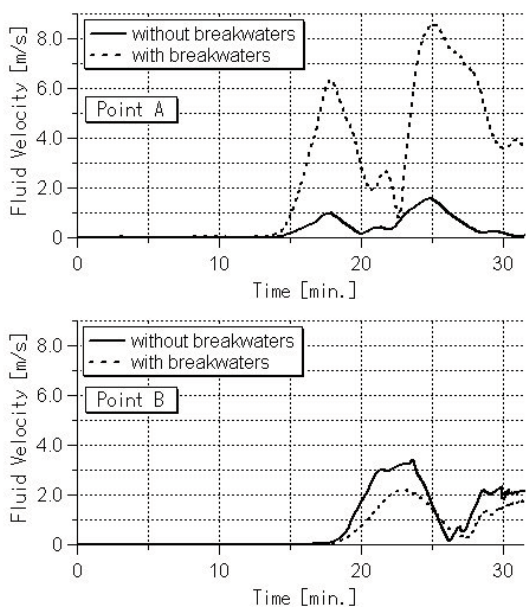
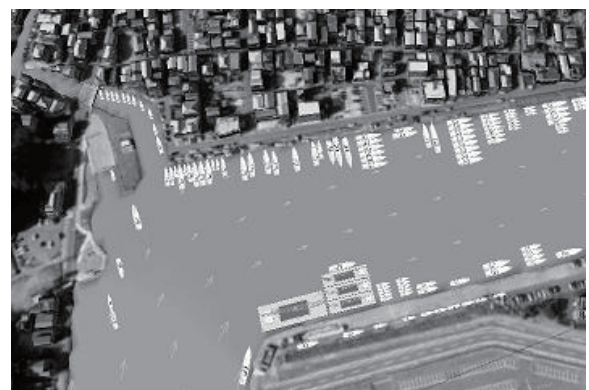


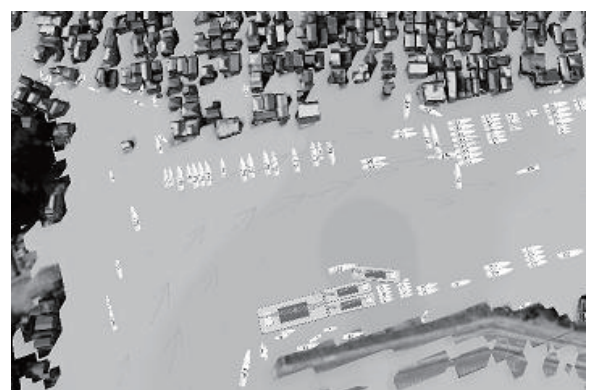
Fig. 13 Time variations of fluid velocity

The breakwaters have another function to control tsunami damage. In this trial, they delay the start of tsunami inundation 90 seconds in residential area near the coast line. This time duration provides evacuating people with advantages.

The reduction of water surface elevation and fluid velocity also provides reduction of the number of drifted vessels. Figure 14 shows the situations just before inundation starts and 3 minutes after the start of inundation. Both of them are of the case of no breakwaters. In the case of no breakwaters, the tsunami with high water surface elevation and fast fluid velocity drifts 56 vessels: 49 vessels broken the mooring system, and 7 vessels settled on the land. All boats are not necessarily swept by the tsunami in the case of no breakwaters. However, if the breakwater is installed, the first tsunami wave sweeps only 7 vessels on the land.



(1) Just before inundation starts



(2) 3.6 minutes after the start of inundation

Fig. 14 Snapshots of drifted vessels in the case of no breakwaters, using STOC's display tool

## 6. CONCLUDING REMARKS

The new numerical model is implemented in the STOC system to calculate the drift behavior of vessels and others by tsunamis. The model can deal with their collision with structures and another drifted body.

Validation of the model is conducted in the very simple test runs, and it is confirmed that the model gives us good results. Furthermore, we need to validate the model quantitatively.

As a trial to show how damage estimation we do by the STOC system including the drift model, the system is applied to a model area with actual bathymetry and topography. Existence of breakwaters, on which the STOC system is already validated in comparison with experimental results quantitatively, reduces inundation depth, fluid velocity in the harbor area and the number of drifted vessels, and delays the start of inundation.

## ACKNOWLEDGEMENT

We express sincere thanks to the Geographical Survey Institute Japan for supplying the airborne laser scanning survey data of the model area.

## REFERENCES

1. Tomita, T., K. Honda, and T. Kakinuma. 2007. Application of three-dimensional tsunami simulator to estimation of tsunami behavior around structures. *Proceedings of the 30<sup>th</sup> International Conference on Coastal Engineering*, ASCE, 1677-1688.
2. Sakakiyama, T., and R. Kajma. 1992. Numerical simulation of nonlinear wave interacting with permeable breakwater, *Proceedings of 23<sup>rd</sup> International Conference on coastal Engineering*, ASCE, 1517-1530.
3. Fujima, K., K. Masamura, and C. Goto. 2002. Development of the 2d/3d hybrid model for tsunami numerical simulation, *Coastal Engineering Journal*, JSCE, 44(4), 373-397.
4. Tomita, T. and K. Honda. 2009. Tsunami inundation simulation by three-dimensional model, *Proceedings of the 31<sup>st</sup> International Conference on Coastal Engineering*, ASCE (in press).
5. Ikeya, T., R. Asakura, N. Fujii, M. Ohmori, T. Takeda and K. Yanagisawa. 2005. Experiment on tsunami wave force acting on a floating body and development of an evaluation method, *Proceedings of Annual Journal of Coastal Engineering*, JSCE, 52, 761-765 (in Japanese).
6. Shuto N. 1993. Tsunami intensity and disasters. *In Tsunamis in the world*, edited by Tinti, S., Kluwer Academic Press, 197-216.

# Manual for Forecasting Earthquake and Tsunami Damage to Public Civil Engineering Facilities (proposal)

by

Osamu Okamoto<sup>1</sup>, Kentaro Kumagai<sup>2</sup>, Katsuya Oda<sup>3</sup>

## ABSTRACT

In order to reduce damage from earthquake and tsunami, while it is effective to forecast damage and to formulate and implement countermeasures based on such estimations, a method of forecasting earthquake and tsunami damage to public civil engineering facilities has not been established. This is a report on our proposal for a method of forecasting damage to port facilities and a policy manual for applying the damage forecast results.

**KEYWORDS:** Damage forecasting, Earthquake, Port facilities, Tsunami

## 1. INTRODUCTION

It is feared a large-scale earthquake accompanied by tsunami will occur within the next 30 years, such as a Tokai earthquake, a Tonankai earthquake, and Nankai earthquake. For this reason, the Central Disaster Prevention Council and local governments are forecasting damage from large-scale earthquakes which are presumed will occur in the future. While these damage forecasts estimate building damage and human damage caused by earthquakes and tsunami, a policy for the comprehensive planning of earthquake and tsunami countermeasures which assumes damage to public civil engineering facilities does not currently exist as a reference to prevent such damage and handle emergency goods transport. This manual presents methods for forecasting earthquake and tsunami damage and application guidelines as a reference. The details of these methods should conform with these guidelines, among other standards.

## 2. FORECASTING DAMAGE TO PORT FACILITIES

### 2.1 Forecasting damage

Forecasting damage by earthquake and tsunami requires data on the various external forces of phenomena (maximum acceleration, flood depth, etc.). In many cases, the earthquake motion and tsunami simulation results conducted by the Central Disaster Prevention Council and local governments are stored as numerical data, and it is possible to determine these external forces from this numerical data. In recent years, it is becoming relatively easier to conduct tsunami numerical simulations and detailed collection of elevation data for low-lying seaside areas is being conducted. Therefore, if the results of previously implemented simulations for use as reference cannot be obtained, implementing new tsunami simulations and determining external forces can be considered.

As well, other data required for damage forecasting will include strength of seismic movement, tsunami height, and facilities structure, among others. Provision of this data can be requested from the body implementing earthquake and tsunami damage forecasting, or a new estimation of strength of seismic movement and tsunami height can be performed.

### 2.2 Damage to facilities from earthquake motion

Damage to port facilities from earthquake motion will be forecasted based on the Technical standards and description of port facilities” revised in 2007[1]. Until now, earthquake-resistant design of port facilities has involved the application of a seismic coefficient method which replaces the dynamic action of earthquake motion with static inertia force. In dynamic analysis, earthquake response analysis employed seismic waveforms measured at points different from the points targeted for des-

---

<sup>1</sup> Senior Researcher, Coastal and Marine Department, National Institute of Land and Infrastructure Management, Yokosuka-city, Kanagawa-ken 239-0826 Japan

<sup>2</sup> Senior Researcher, Coastal and Marine Department, ditto

<sup>3</sup> Head, Coastal and Marine Department, ditto

ign such as by Hachinohe and Kobe. However, earthquake motion was dependent on the source properties, propagation path properties, and ground characteristics of target points, and earthquake response of facilities was dependent not only on the vibrational amplitude of input earthquake motion, but on the frequency characteristics of earthquake motion, ground, and structures. For this reason, when checking the aseismic capacity of port facilities, a method of calculating the action of earthquake motion is employed which considers the properties of subsurface ground and structures, based on the time history wave form of earthquake motion in the engineering bedrock derived by considering source properties, propagation path properties, and ground characteristics (site characteristics).

The following points are described for port standards.

1. With respect to level 1 earthquake motion (earthquake motions with the probability of occurring once or twice during the operation of facilities), the stochastic time history wave form should be appropriately determined based on measured values of earthquake motion, and considering source properties, propagation path properties, and site properties.

2. With respect to level 2 earthquake motion (earthquake motions possessing the maximum intensity imaginable at the targeted points from the present to the future), the time history wave form should be appropriately determined based on measured values of earthquake motion and assumed earthquake source parameters etc., and considering source properties, propagation path properties, and site properties.

Figure 1 shows methods of forecasting damage to port facilities from earthquake motion.

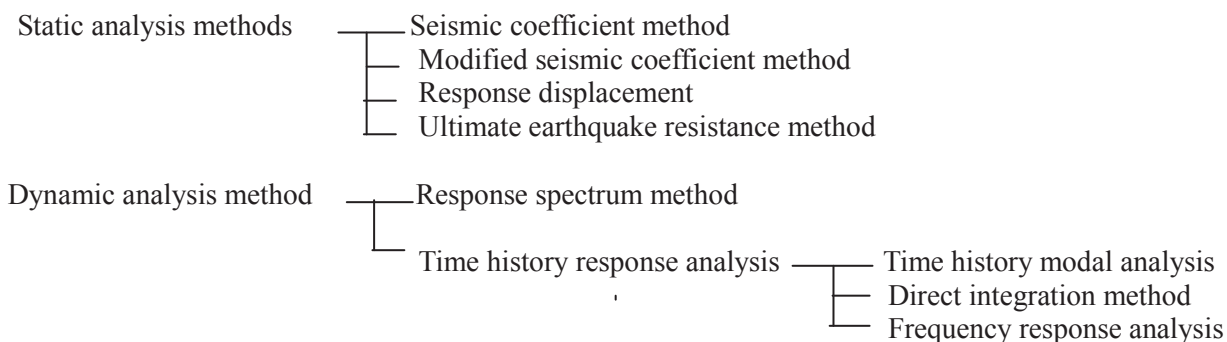


Fig.1 Methods of forecasting damage to port facilities from earthquake motion

As well, Table 1 shows the results of considering the adaptive flexible of methods of forecasting earthquake damage to various port facilities.

### 2.3 Damage to breakwaters by earthquake motion and tsunami

The cross-section of breakwaters is generally determined according to the external force of ocean waves, a consideration of level 1 earthquake motion is often omitted. However, in cases where the installation water depth is deep and design wave height is small, consideration of external force due to level 1 earthquake motion becomes predominant. For this reason

the necessity of checking aseismicity is judged from the relationship between cross-sectional data determined by the external force of ocean waves and level 1 earthquake motion. The checking of aseismicity is conducted if it is judged necessary according to port standards shown in the “necessity judgment diagram of aseismicity checking.” When checking sliding and toppling capacity is deemed necessary, such methods will be conducted in accordance with port standards.

Damage to breakwaters from tsunami consists of deformation due to tsunami wave force,

Table 1 Adaptive flexibility port facility earthquake damage forecasting methods

Damage forecasting methods	Target facilities	Structural format
Simple forecasting method	Pier, embankment	Gravity structure earth fill
Seismic coefficient method	Pier, embankment, flood gate, land lock, drainage pump station, shed, warehouse	Gravity structure, sheet-pile type structure, earth fill
Ultimate earthquake resistance method	Pier, road bridge	Vertical pile pier
Response displacement method	Tunnel lifeline	Shield tunnel Water supply, sewage line, common ducts, etc.
Response spectrum method	Railroad facility	
Dynamic response analysis (total stress)	Tunnels All structures	Submerged tube Almost all structural formats
Dynamic response analysis (effective stress)	All structures	Almost all structural formats (when liquefaction is considered)

deformation due to ocean flow, and deformation due to a combination of wave force and ocean flow, and is similar to deformation chain architecture by ocean waves. In particular, problematic damage from tsunami can be evaluated according to items 1)–3) below.

1) Stability of breakwaters in the event of tsunami

Tsunami wave force and uplift pressure are considered the external forces when investigating breakwater dislocation due to sliding, breakwater dislocation due to toppling, and breakwater dislocation due to lack of mound bearing capacity. The tsunami wave pressure formula proposed by Tanimoto et al. is used for this investigation.[2]

2) Scattering of the breakwater covering rock

To investigate the scattering of breakwater covering rock on the port side (leeward side) and on the ocean-facing side, the relationship between current drift in the mound vicinity and the weight stability limit of the covering rock etc. is considered utilizing the Isbash formula[1] to derive the stable mass of covering materials in relation to current velocity. Scattering is judged will occur in the event that the weight of the covering rock used is less than stable mass.

3) Movement and scattering of breakwater wave breaking works

An evaluation formula regarding the scattering of wave breaking works due to tsunami does not exist. Thus, scattering experiment results relating to deformed block levees due to tsunami soliton fission[3] will be useful as reference. The results of these experiments show that the destructive force of tsunami is dramatically greater than normal ocean waves.

2.4 Embankment deformation due to earthquake motion and tsunami

To quantitatively check the volume of structural deformation such as slanting of the embankment, it is necessary to employ Time History Response Analysis methods as indicated in Figure 1. Time History Response Analysis methods can be divided into the total stress analysis method and the effective stress analysis method. Typical analysis programs for the total stress analysis method include “SHAKE” and “FLUSH,” and typical analysis programs for the effective stress analysis method include “FLIP” and “LIQCA.” It is necessary that they be chosen according to the amount of excess hydrostatic pressure which occurs.

As shown in Figure 2, tsunami damage to embankments can be categorized into 3 types: damage due to wave force; damage from scouring of the frontal side; and damage from scouring of the leeward side. In estimating

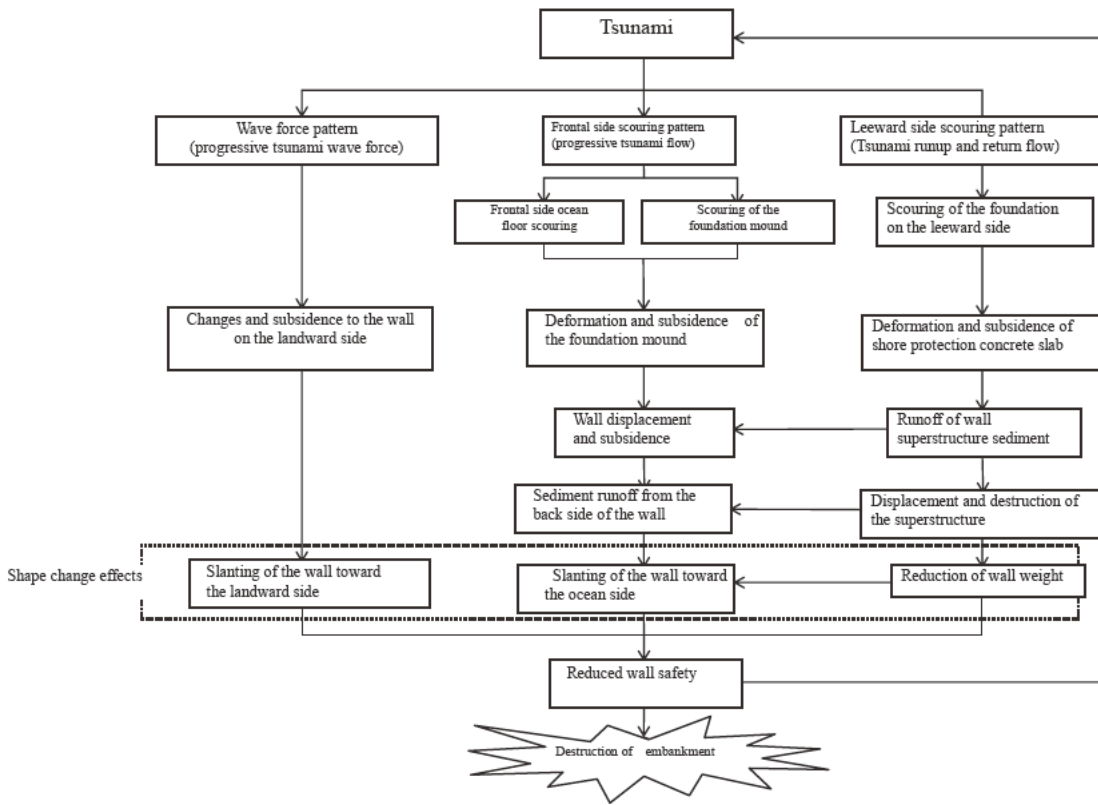


Fig.2 Major chain of damages to gravity revetment due to tsunami

damage, it is necessary to accurately forecast embankment displacement and subsidence until sloping occurs, and shape changes from the scouring of the ground foundation etc. through appropriate methods. Specifically, regarding damage from scouring to the leeward side (due to return flow of tsunami run-up), the results of considering ground scouring of the leeward side of the embankment, and caisson wall and superstructure stability despite the load of return flow drag applied, will serve as reference. [4]

### 2.5 Assessment of driftage

Main driftage which is observed when a tsunami hits a port region includes maritime containers, wood materials, and boats etc. The driftage area is forecast using driftage simulation methods which can accurately replicate driftage behavior. The behavior of driftage can be calculated by solving the motion equation of driftage. This is accomplished by applying the results of flat surface two-dimensional tsunami analysis as the external force of driftage such as maritime containers, wooden materials, and boats etc.

In addition, by judging the contact between driftage and structures as well as considering colliding force, the drift and collision behavior of driftage can be more accurately considered, including the collision phenomenon. Figure 3 is a flowchart of driftage behavior forecasting due to tsunami.

By calculating the drift and collision behavior of driftage, this data can be applied to check the safety of structures such as berth facilities and shore protection structures from driftage collision, understand how risk of spillage can be reduced by adequately developing and consolidating storage locations for maritime containers etc., and understand the effect of developing facilities to prevent spillage etc. Regarding methods of calculating collision force by driftage, various previous research can be referenced such as the study by Matsutomi et al. targeting driftwood, and the study by Mizutani et al. on maritime containers. As for methods of calculating drift and collision behavior of driftage due to tsunami, there are also studies which combine the flat surface two-dimensional

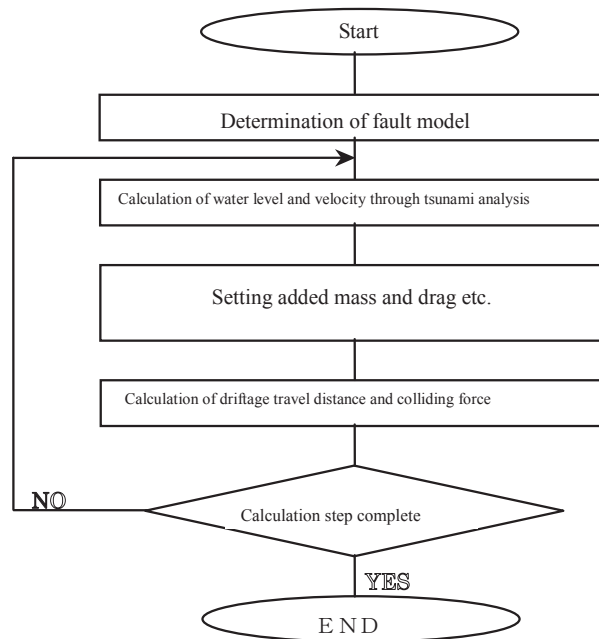


Fig.3 Flowchart of driftage behavior forecasting due to tsunami

tsunami numerical simulation with a shape representation and collision analysis of driftage employing a distinct element method. When checking the safety etc. of structures, it is desirable that an appropriate calculation method be adopted based on the results of conducting trial calculations using these various calculation methods. [5][6][7][8]

### 3. Policy course for applying damage forecast results

#### 3.1 Creation of a damage forecast map

By creating a damage forecast map showing the results of forecasting damage to public civil engineering facilities and flooded areas due to earthquake and tsunami, and upon considering geographical conditions etc. according to area, it will be possible to consider specific earthquake and tsunami countermeasures in collaboration with related agencies. As well, by indicating the locations of important bases in the event of disasters and public agencies on the map, it will be possible not only to consider hard infrastructural countermeasures (development and reinforcement of public civil engineering

facilities), but to consider measures for mitigating damage by applying soft infrastructural measures (information provision and improvement of initial response system).

As an example, Figure 4 shows a damage forecast map focused around Susaki Port in Kochi prefecture. In addition to the results of assessing damage to various facilities and flooded areas etc., the map indicates tsunami arrival time, flooded regions, the position of government facilities and hospitals, damage to humans and buildings evaluated based on bridge reinforcement methods etc., which will be useful as reference in formulating earthquake and tsunami countermeasures. As for tsunami protection facilities such as tidal barrier, creating maps of damage to flooded areas and hinterland areas before and after implementing reinforcement and new facilities construction countermeasures will serve as reference for judging the necessity of implementing such countermeasures.

By creating such maps, it will be possible to consider specific measures relating to the implementation of emergency drills, the provisioning of information, evacuation routes, evacuation space, preliminary plans to carry out

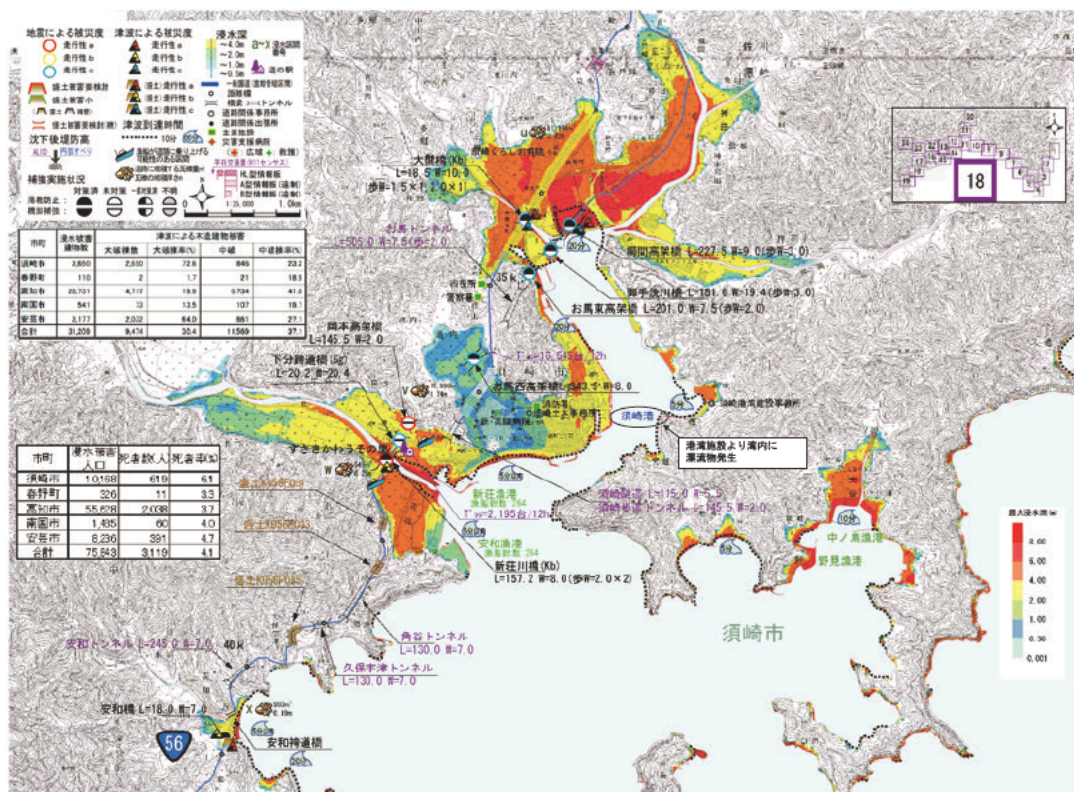


Fig.4 Damage forecast map (Susaki Port)

efficient emergency and recovery activities, tsunami protection facilities which are particularly effective to mitigate damage, and facilities which should be prioritized for reinforcement.

However, damage forecasting is at most a starting point for considering specific measures, and there will also be situations where actual damage will not occur according to forecasts. Therefore, in formulating countermeasures, it is necessary that planning be conducted flexibly considering that unforeseen events may also occur.

### 3.2 Sharing and application of damage forecast results

In planning earthquake and tsunami countermeasures, it is also important that the results of damage forecasts to public civil engineering facilities etc. be shared with related agencies. As forecasted damage to coastal and riverside facilities and countermeasures by public civil engineering facilities will influence forecasts on flooded areas, this will lead to functional impairment of port facilities. As well,

it will also be necessary to consider the effect of driftage from port facilities when planning countermeasures. Therefore, by having related agencies exchange information relating to damage forecasts and earthquake and tsunami countermeasures etc., it will be possible to formulate a highly effective and comprehensive plan for countermeasures. Specifically, it is desirable that related agencies discuss countermeasures including their respective apportionment of responsibilities at disaster prevention conventions etc.

As well, consensus-building with citizen involvement is now underway from the planning stages of disaster prevention activities. By appropriately conducting damage forecasts utilizing this manual, as well as for the sake of confirming the effectiveness and thinking behind the planning of countermeasures, not only can the smooth implementation of activities be anticipated, but it is surmised this will contribute to raising the government's responsibility to explain its policy measures to the public etc.

While there may be cases where port plans etc.

may be changed depending on the disaster activities included within countermeasure plans, it is surmised that damage forecast results will also be effective as basic materials for explaining the necessity of the positioning of such activities within the plan. As the level of damage as a result of developing facilities or not developing facilities can be estimated by applying the damage forecasting method indicated in this manual, it can also be applied when evaluating public works.

#### 4. CONCLUSIONS

This manual has organized and systematized various research results relating to earthquakes and tsunamis. While research relating to earthquakes has made great headway, much progress in research relating to tsunamis can be anticipated from future research by relevant parties.

#### 5. ACKNOWLEDGEMENTS

In compiling this paper, we received a great deal of cooperation from the people at the Coastal Development Institute of Technology, as well as from related consultants in this field. As well, we received valuable opinions from Professor Shuto of Nihon University regarding tsunami damage forecasts on concrete armor units. We would like to extend our warmest regards and appreciation to all involved.

#### 6. REFERENCES

1. Japan Port and Harbor Association. *Technical standards of port facilities and explanations*. 2007.
- 2) Tanimoto, K., Matsutomi, H., Tsuruya, H., Takahashi, S., Goto, C., Nagai, T., Hashimoto,

N., Nagao, T., Hosoyamada, T., Shimosako, K., Goto, M., and Asai, T.

Characteristics and Damage of the 1993 Hokkaido Southwest Offshore Earthquake and Tsunami. *Port and Harbour Research Institute materials*, No.775, pp.225, 1994.

3. Tomikashi, H., Hirayama, K., and Sugiyama, M. Destructive mechanism of soliton fission tsunami run-up on concrete armor unit levee. *Coastal Engineering collected papers*, volume 34, pp517–521, 1987.

4. Okamoto, O., Oda, K., and Kumagai, K. Study on scour by tsunamis—example of port and harbor structures. *ICSE-4*, 2008.

- 5) Matsutomi, H. and Ikeda, H. Evaluation method of driftwood collision force based on large-scale experiments. *Coastal Engineering collected papers*, volume 43, pp.781–785, 1996.

- 6) Mizutani, N., Takagi, Y., Shiraishi, K., Miyajima, S., and Tomita, T. Study relating to tsunami power and driftage colliding force on berth containers. *Coastal Engineering collected papers*, volume 52, pp.741–745, 2005.

- 7) Kumagai, K., Oda, K., Fujii, N. Applicability of container drift behavior simulation model due to tsunami. *Coastal Engineering collected papers*, volume 53, pp.241–245, 2006.

- 8) Kumagai, K., Oda, K., Fujii, N. Evaluation of container drift and collision simulation and colliding force due to tsunami. *Coastal Engineering collected papers*, volume 54, pp.236–240, 2007.

## **THEME 6**

# **Sustainable Design for Buildings and Infrastructure - Focus on Natural Disaster Prevention**

# Earthquake Disaster Management in Japan

by

Koji Ikeuchi<sup>1</sup> and Masamitsu Waga<sup>2</sup>

## ABSTRACT

This paper presents the earthquake disaster management in Japan. General disaster management has been promoted in an integrated and well-planned manner by the central, prefectural and municipal governments, and public utilities in their capacity according to Disaster Countermeasures Basic Act. In addition, building and improvement of facilities of high priority which help reduce damage by earthquakes have been promoted according to 5 year plans based on Act on Special Measures for Earthquake Disaster Countermeasures to prepare for earthquakes that occur anywhere at anytime. On the other hand, countermeasures have been formulated individually against devastating large-scale earthquakes. One of the examples is Tokyo Inland Earthquakes, which is outlined in detail. There have been some developments in earthquake disaster management policy for Tokyo Inland Earthquakes. Following, “Policy Framework”, “Earthquake Disaster Reduction Strategy” and “Guidelines for Emergency Response Activities”, “Specific Plan for Emergency Response Activities” was formulated by “Central Disaster Management Council (CDMC)” chaired by the prime minister. Specific measures for massive evacuees and the stranded generated by Tokyo Inland Earthquakes were also formulated and proposed measures have been further considered and pursued.

Current situation of several other initiatives are also outlined in this paper such as building quake-proofing, Early Earthquake Warning (EEW) and Disaster Management Information Systems.

**KEYWORDS:** Building quake-proofing, Early Earthquake Warning (EEW), Large-scale earthquakes, Measures for evacuees and the stranded, Tokyo Inland Earthquakes

## 1. INTRODUCTION

Japan has suffered from frequent natural disasters of almost all kinds due to its geographical, topological and meteorological conditions and has undergone losses of human lives and properties in years. Protecting lives and properties from natural disasters is a high priority and one of the most important responsibilities of the central government.

This paper presents the earthquake disaster management in Japan. Section 2 summarizes the earthquake proneness of Japan. Section 3 outlines policy frameworks for earthquake disaster countermeasures, Disaster Countermeasures Basic Act, Act on Special Measures for Earthquake Disaster Countermeasures and framework for countermeasures against devastating large-scale earthquakes. The Disaster Countermeasures Basic Act sets a general framework for disaster management to be organized and implemented in an integrated and well-planned manner, and the Act on Special Measures for Earthquake Disaster Countermeasures is to encourage local governments to build and/or improve facilities of high priority while countermeasures against devastating large-scale earthquakes have been considered and formulated individually. Section 4 and Section 5 detail countermeasures against Tokyo Inland Earthquakes and measures for evacuees and the stranded as a result of Tokyo Inland Earthquakes respectively. Section 6 details current situation of building quake-proofing. Section 7 outlines the Early Earthquake Warning and lessons learnt from recent earthquakes. Section 8 presents Disaster Management Information Systems, IT systems developed to estimate damage using only data

---

<sup>1</sup> Director for Earthquake, Volcanic and Large-scale Disaster Management, Disaster Management Bureau, Cabinet Office, 1-2-2 Kasumigaseki, Chiyoda-ku, Tokyo 100-8969 Japan

<sup>2</sup> Deputy director, ditto

which are available beforehand or readily available when earthquakes occur and, streamline information flow and strengthen information sharing.

## 2. EARTHQUAKES IN JAPAN

Japan is located on and near plate boundaries of the North American plate, Eurasian plate, Philippine Sea plate and Pacific plate as illustrated in Fig.1 [1]. This explains why Japan is one of the most earthquake-prone countries in the world. Fig. 2 [2] shows the distribution of focuses of earthquakes measuring 5.0 or greater from 1996 to 2005, which illustrates that a large number of earthquakes have occurred around Japan. In addition, Japan accounts for 20% of earthquakes with magnitude of 6.0 or greater from 1996 to

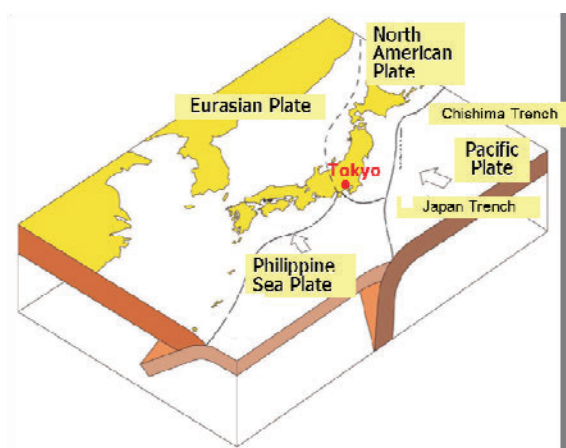


Fig.1 Plates around Japan

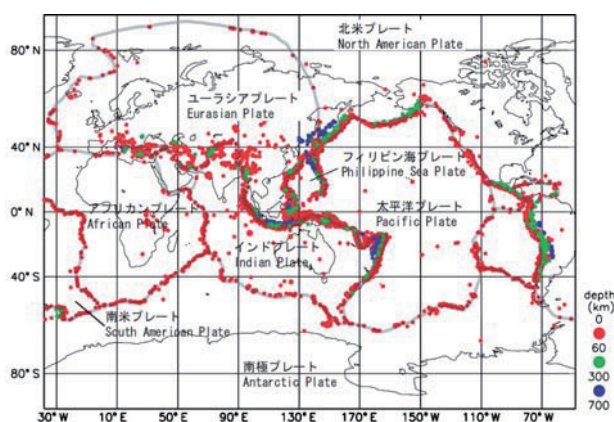


Fig.2 Earthquake Focus Distribution  
Magnitude 6.0 or Greater

2005.

There are mainly two different mechanisms that cause earthquakes in Japan;

1) Earthquakes generated near convergent boundaries

Earthquakes occur when the continental plates, i.e.) Eurasian Plate or North American Plate bounce back from the tension by the subduction of oceanic plates, i.e.) Philippine Sea Plate or Pacific Plate.

2) Earthquakes generated by active faults

Should these earthquakes occur right under cities, they cause enormous damage even if their magnitudes are insignificant.

## 3. FRAMEWORKS OF EARTHQUAKE DISASTER COUNTERMEASURES

### 3.1 Disaster Countermeasures Basic Act

The act was enacted in 1961 and has reflected lessons learnt in earthquakes since then. It states obligations, authorities and/or responsibilities of the central government, local governments, public utilities and citizens. It mandates that central government should establish CDMC comprising the prime minister as chairperson, other ministers and several other members, and that local governments should establish similar councils so that disaster management is organized in an integrated manner. Furthermore, it requires CDMC to formulate Basic Disaster Management Plan and disaster management entities such as central government ministries and agencies, local governments and public utilities to formulate Disaster Management Operation Plan or Local Disaster Management Plan to promote disaster management in a well-planned manner.

### 3.2 Act on Special Measures for Earthquake Disaster Countermeasures

In 1995, the Great Hanshin-Awaji Earthquake occurred and caused devastating damage. As a result, the Act on Special Measures for Earthquake Disaster Countermeasures was enacted to promote preparation for earthquakes that occur anywhere in Japan. The act encourages governors of local prefectural

governments, in consultation with mayors of municipal governments to formulate a 5 year plan of building and/or improving facilities of urgent priority in view of earthquake disaster management. All prefectural governments have been pursuing further improvements since 2006, the beginning of 3rd 5 year plan. Financial assistance from the central government is available to certain types of facilities scheduled in the 5 year plans.

### 3.3 Countermeasures against Large-scale Earthquakes

Measures against devastating large-scale earthquakes are considered individually by the CDMC according to the flowchart depicted in Fig.3 [3]. Measures against the following earthquakes, illustrated in Fig.4 [3] were or have been considered;

- Tokai Earthquake
- Tonankai and Nankai Earthquakes
- Trench type Earthquakes in the Vicinity of the Japan and Chishima Trenches
- Tokyo Inland Earthquakes
- Chubu and Kinki Inland Earthquakes

Firstly, things that determine characteristics of earthquakes are determined, such as earthquake focuses and earthquake models. Then, seismic

intensity distribution is estimated. With the seismic intensity distribution as an input, the number of collapsed buildings, death toll and economic loss are estimated. Based on the damage estimates, Policy Framework which serves as a master-plan covering disaster preparedness, emergency response and recovery is formulated. Following the Policy Framework, Earthquake Disaster Reduction Strategy and Guidelines for Emergency Response Activities are formulated. The former stipulates quantitative disaster reduction objectives and specific measures to achieve them. The latter is a set of guidelines for emergency response activities by organizations concerned. Specific Plan for Emergency Response Activities specifies emergency response activities such as dispatch of search and rescue units, and shipment of emergency goods of predetermined quantity region by region based on the damage estimates. This enables emergency response activities to be implemented as soon as devastating earthquakes occur even when no detailed information on the damage is available. The emergency response activities will be adjusted as more information becomes available.

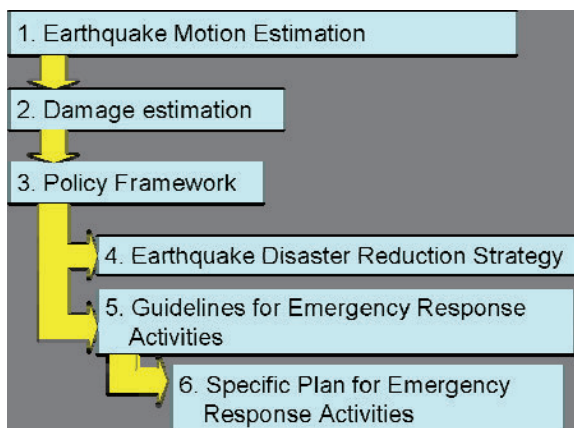


Fig.3 Flowchart of Formulation of Countermeasures against Large-scale Earthquakes

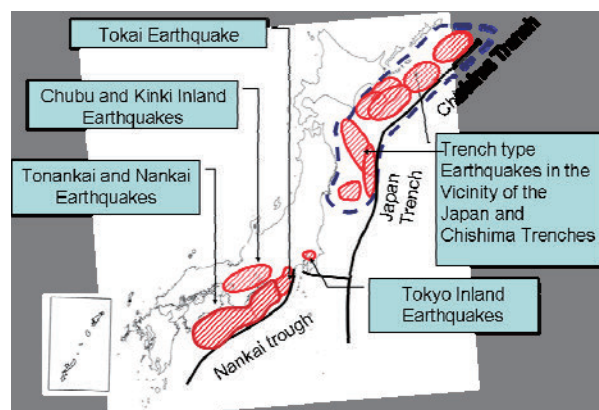


Fig.4 Large-scale Earthquakes

#### 4. COUNTERMEASURES AGAINST TOKYO INLAND EARTHQUAKES

The largest earthquake which struck Tokyo metropolitan area within a century is the Great Kanto Earthquake in 1923 measuring 7.9 magnitude. This caused tremendous damage, totaling more than 100,000 deaths and missing persons combined. Earthquakes with magnitude of around 8 occur periodically at intervals of 200 to 300 years in the area. It is unlikely that an earthquake of this magnitude will occur in 100 years however inland earthquakes of magnitude 7 class occur several times between two magnitude 8 class earthquakes. Therefore, countermeasures against Tokyo Inland Earthquakes of magnitude 7 class have been considered according to the flowchart outlined in 3.2.

An earthquake was selected, out of 18 simulated earthquakes as a target to consider countermeasures against because it is relatively imminent, it strikes central Tokyo heavily and the impacts widespread as illustrated in Fig. 5 [4]. As a result of the earthquake, it is estimated that 850,000 buildings could collapse or burn down, and that 11,000 people could die in the disaster. Economic loss is estimated to reach 112 trillion yen (approximately 1.12 trillion US dollars).

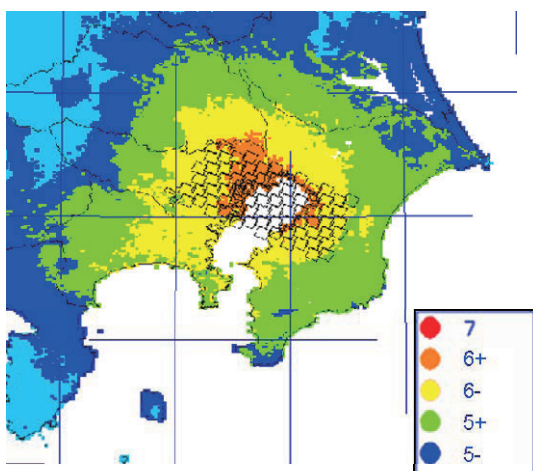


Fig.5 Seismic Intensity Distribution Tokyo Inland Earthquake

Policy Framework which serves as a master-plan covering disaster preparedness, emergency response and recovery was formulated in 2005 and sets policy direction to reduce the influence of the disruption of functions as the political, administrative and economic center, and the influence of enormous damage. Earthquake Disaster Reduction Strategy was formulated in 2006 and stipulates quantitative disaster reduction objectives, which are to reduce the estimated death toll by 50% and economic loss by 40% in 10 years. It also stipulates specific measures to achieve the disaster reduction objectives.

Specific Plan for Emergency Response Activities was recently formulated in 2008 following Guidelines for Emergency Response Activities formulated in 2006 which is a set of guidelines for emergency response activities by organizations concerned.

Specific Plan for Emergency Response Activities specifies emergency response activities such as the dispatch of search and rescue units, and the shipment of emergency goods of predetermined quantity, region by region based on the damage estimates. This enables emergency response activities to be implemented as soon as devastating earthquakes occur even when no detailed information on the damage is available. The emergency response activities will be adjusted as more information becomes available. Fig. 6 and 7 [5] show the Specific Plan for Emergency Response Activities.

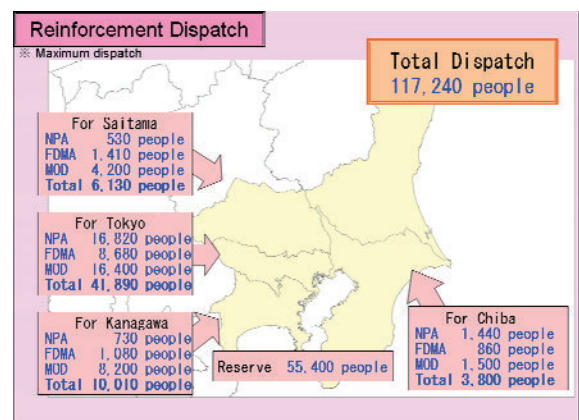


Fig.6 Reinforcement Dispatch Plan, Specific Plan for Emergency Response Activities

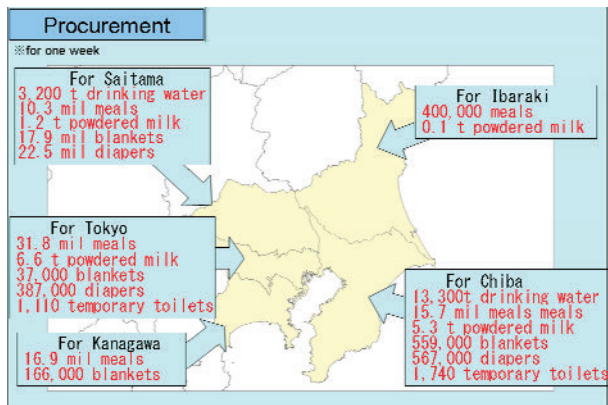


Fig.7 Procurement Plan, Specific Plan for Emergency Response Activities

### 5. MEASURES FOR EVACUEES AND THE STRANDED

The Tokyo Inland Earthquake is estimated to devastate the area forcing up to 7 million people to evacuate home, 4.6 million of them need shelters, and affecting 14 million people certain distance away from home, 6.5 million of them would find it difficult to walk such a long distance home. The Policy Framework for Tokyo Inland Earthquakes refers to this problem leaving specific measures for evacuees and the stranded to be considered. A committee to work on problems as a result of the massive evacuees and the stranded was established and produced a report which analyzes problems quantitatively and proposes measures.

#### 5.1 Measures for Evacuees

There will be shortage of shelters for 600,000 evacuees in total provided that each Ward of Tokyo needs to accommodate evacuees from its residents. A first thing to be considered to cope with the shelter shortage is to reduce the number of evacuees needing shelters. One of the proposed measures is to examine promptly if the buildings are safe from collapse by aftershocks and to encourage evacuees to return home whose housing is proved to be safe. It is also proposed that evacuees be encouraged to find shelters at parents', relatives' or places offered outside of the area if possible. For the supply side, it is proposed that each Ward make use of public and private facilities to ensure capacity in its district and to coordinate evacuation with other Wards. Furthermore, measures related to the supply of essentials, operation of shelters and provision of useful information for evacuees are referred to in the Policy Framework.

#### 5.2 Measures Concerning Temporary Emergency Dwellings

If the Tokyo Inland Earthquake occurs, it is estimated that up to 1.62 million temporary emergency dwellings is demanded in the region. It is estimated that housing for about 1.35 million households can be arranged 6 months after the earthquake, 120,000 of them by temporary housing, 310,000 by repairing damaged dwellings, 2,000 by public housing, and 920,000 by undamaged private houses and apartments for let in the region, which falls short

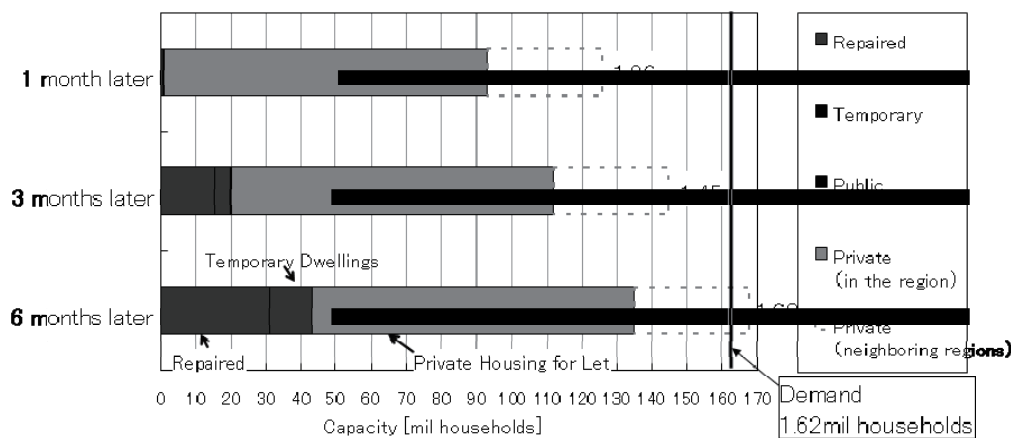


Fig.8 Supply of Temporary Emergency Dwellings

of the demand by 270,000 households. Thus, it seems difficult to meet the demand in the region alone. Capacity for 330,000 households found in the neighboring regions could fill the gap as illustrated in Fig. 8 [6]. Thus, it is important to make arrangements such that damaged dwellings will be repaired promptly, provisionally or permanently so that evacuees could return home, vacant capacity, public or private will be made available, and emergency temporary housing will be provided.

### 5.3 Measures for the Stranded

As for the stranded, simulations were implemented to understand their behaviors, degree of road congestion caused by the stranded, time it takes for the stranded to return home on foot, and the like. The simulation model was developed using a random utility model and road network model. The random utility function assumes that people choose the option which gives the highest expected utility, i.e.) either to stay where they are, to go home on foot, to take a rest at a shelter, or to keep walking. The model also incorporates factors such as the availability of information about the family and their safety, distance to home, and degree of congestion. The utility function was derived from answers to 24,500 questions from 200 examinees.

The simulation was implemented to see the effects of the following factors;

- types of available roads, trunk roads with/without semi-trunk roads
- weather
- bottlenecks of roads
- building collapse
- fire
- availability of information on road congestion
- time taken to obtain information on family
- time to commence returning home

The simulation suggests that without any measures to alleviate, roads will be terribly crowded (more than 6 people / m<sup>2</sup> which is almost as crowded as trains during rush hours in Japan) as illustrated in Fig. 9, 10 [6] and as many as 2 million people will have to undergo

this terrible congestion for more than 3 hours. This naturally leads to concerns that not a few people may need medical attention and that there will be huge demand for rest rooms and places for rest on their way home. Some policy implications are also derived from the simulations. The number of people stranded in a heavy congestion for more than 3 hours is reduced to;

- 50% or 25% respectively if 1/3 or half of the stranded commence returning home next day,
- 80% or 2/3 respectively if staggered return is arranged within 3 hours or 6 hours,
- 90% if the information on the family is available in 6 hours instead of 24 hours,
- 40% if the information on the road congestion is available,
- 30% if there is no fire or building collapse.

Based on the findings, measures for the stranded are proposed. It is extremely dangerous for the stranded to head home at once as this overcrowds roads and places near railway stations, and increases chances of being involved in mass falling and of dying from fire and falling objects. Also, this clogs roads and impedes emergency response such as search and rescue, fire fighting, emergency shipment and medical transfer. It should become widely known that it is important that people refrain from heading home immediately and things be arranged so that family safety could be confirmed promptly when disasters occur. It is also proposed that companies and schools be prepared for and arrange things for their employees and students to stay there for a while to allow for their return on the following day and staggered return. It should be arranged such that information on roads is readily available for the stranded.

In addition, assistance for the stranded returning home on foot is proposed including traffic restricting and directing at dangerous and/or congested areas, provision of information on roads, medical assistance, and places for rest on their way home. Local authorities are encouraged to coordinate the assistance.

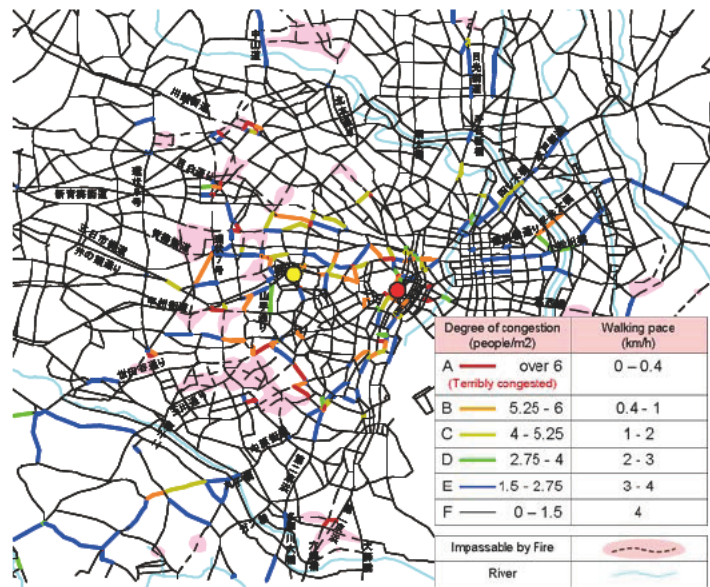


Fig.9 Road Network and its Congestion (3 hours after the earthquake)

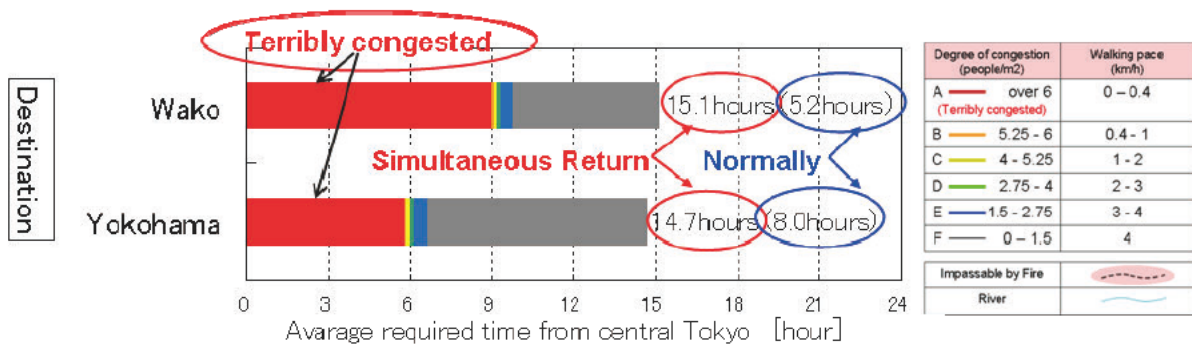


Fig.10 Degree of Congestion and its Duration to Destinations

#### 5.4 Measures for Shortage of Rest Rooms

Demand for rest rooms and places for rest will be enormous as both evacuees and the stranded need them.

Supply of and demand for rest rooms were estimated based on the results from the simulation to understand the behaviors of the stranded.

Demand was estimated based on the frequency per hour of passersby and evacuees, which are assumed to be 0.5 times /hour/person and 5 times/24 hours/person respectively from literature review.

Supply was estimated based on the number of rest rooms for emergency use and fixed rest

rooms at places such as convenience stores, gas stations, restaurants, shelters and public space in 23 Wards of Tokyo under certain assumptions allowing for their capacity and availability/hour, and disruption of water supply.

Fig. 11 illustrates the demand-supply gap of rest rooms along route 246 in Setagaya Ward. Shortage of rest rooms could continue for 17 hours [7].

It is proposed that local authorities stockpile portable rest rooms and make necessary arrangements such that the stranded could use rest rooms of public and private facilities.

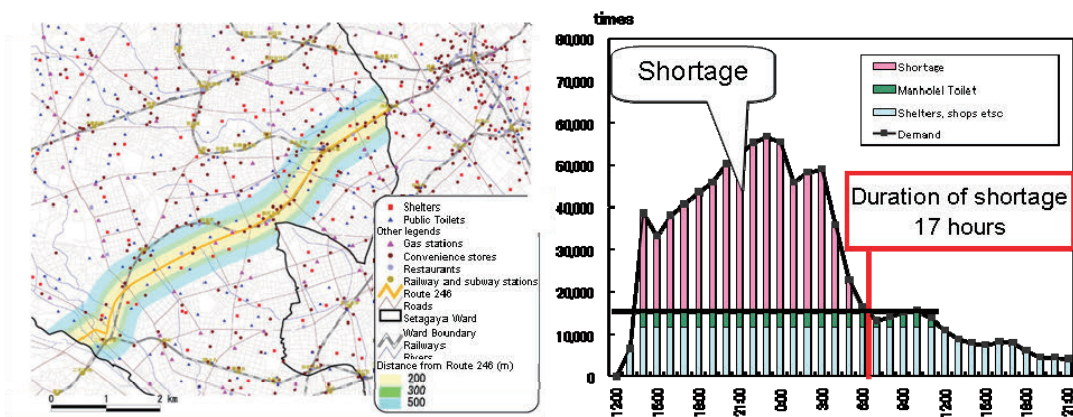


Fig.11 Shortage of Rest Rooms

## 6. BUILDING QUAKE-PROOFING

In Great Hanshin-Awaji Earthquake, it was reported that 83.3% of 5,500 [8] deaths immediately after the earthquake were caused by building collapse and/or furniture falling. It is estimated that 4,200 people die due to building collapse in a Tokyo Inland Earthquake provided that the earthquake occurs at 5 o'clock in the morning according to damage estimation undertaken by CDMC. It became clear from series of damage estimations that building collapse not only causes deaths but also facilitates outbreak and spread of fire, generates evacuees, impedes search and rescue, and generates debris. Thus, building quake-proofing has been considered and promoted as a high priority in earthquake disaster management.

Objectives of building quake-proofing are summarized in table1 [9], [10].

### 6.1 Acts Related to Earthquake Resistance of Buildings

In addition to the Act on Special Measures for Earthquake Disaster Countermeasures outlined in 3.2, following acts are also related to earthquake resistance of buildings;

#### a) Building Standard Law

The law stipulates minimum standards on building sites, structures, facilities and use to protect lives, health and properties of the citizens. The law was enacted in 1950 and has been amended. The Earthquake Resistance Standards based on the law have been amended

in response to major earthquakes. The epoch-making amendments to the Standards which have served as a basis of the current Standards were introduced in 1981 and have been called "New Earthquake Resistance Standards". Standard was introduced that buildings must be designed so as not to collapse completely after being struck by an earthquake of seismic intensity 6+ to 7, to the then-existing standard that buildings must be designed to maintain sound structure after being struck by an earthquake of seismic intensity 5+.

Table1 Objectives of Quake-proofing

Use	Proportion of buildings with earthquake resistance	Objective
Buildings	75% (2003)	Raising the proportion to 90% by 2015
Public elementary and junior high schools	58.6% (2007)	Quake-proofing 10,000 schools with high possibility of collapse by FY2011
Hospitals	43% (2005)	Quake-proofing 50% of hospitals with insufficient earthquake resistance by FY2010

The law also stipulates that buildings must be examined before the commencement of, during the construction of and after the completion of the buildings to ensure that the buildings are built in conformity with related acts.

b) Housing Quality Assurance Act

This act was enacted in 2000 to assure the quality of housing, to protect the interests of housing purchasers and to settle disputes related to housing swiftly and properly by introducing the following schemes;

-Warranty against defects

Contractors and vendors of new housing are held liable for warranty against defects affecting the structural performance for at least 10 years.

-Housing Performance Indication System

Housing Performance Indication Standards have been introduced to enable would-be purchasers to compare housing performance before contract and third party institutions have been established to evaluate the performance indicators.

-Dispute settlement scheme

c) Act for Execution of Defect Warranty Liability under Housing Quality Assurance Act

This act was enacted to mandate that contractors and vendors of new housing should either deposit the sum according to the number of housing supply or contract insurance to ensure funding necessary to redeem warranty against defects for 10 years stipulated in the Housing Quality Assurance Act.

d) Act on Promotion of the Earthquake-proof Retrofit of Buildings

This act is to enhance building safety by promoting earthquake-proof retrofit of building to protect lives, safety and properties of the citizens from building collapse.

The act was amended in 2006 to promote quake-proofing buildings further. One of the major amendments was the introduction of a scheme that the central government formulates basic guidelines and each local government formulates a plan based on the guidelines to promote the building earthquake resistance

evaluation and building quake-proofing. It was also stipulated that local governments may announce that owners of designated buildings instructed to have them examined and/or quake-proofed fail to do so.

6.2 Assistance

Financial assistance available to earthquake resistance evaluation and building quake-proofing has been expanded as in table 2 [11].

Table2 Assistance Scheme for Building Quake Proofing

Measures	Subsidy rates and conditions
Evaluation	<ul style="list-style-type: none"> <li>-Undertaken by private sector 2/3</li> <li>-Undertaken by public sector Residence 1/2, Others 1/3 (Buildings on emergency transportation roads 1/2)</li> </ul>
Quake-proofing	<ul style="list-style-type: none"> <li>• Entitled buildings               <ul style="list-style-type: none"> <li>-Single family homes in built up areas whose collapse may cause road blocks</li> <li>-Collective housing and non-residential buildings in densely inhabited areas</li> <li>-Single family homes with income less than 40 percentile</li> </ul> </li> <li>• Subsidy rate               <ul style="list-style-type: none"> <li>15.2% (undertaken by private sector)</li> </ul> </li> </ul> <p>The rate is increased to</p> <ul style="list-style-type: none"> <li>-2/3 for buildings on emergency transportation roads</li> <li>-2/3 for buildings used as shelters</li> <li>-1/3 for Collective housing on evacuation routes</li> <li>- 23% for single family homes with income less than 40 percentile</li> </ul>

Quake-proofing promotion tax incentives are also in effect [11].

#### Residential buildings

-10% of expense up to 200,000 yen (approx. 2,000 USD) is deductible from income tax subject to certain conditions

-Real estate tax (up to 120m<sup>2</sup> equivalence) is reduced to 50% for the duration of;

3 years if the building is quake-proofed between 2006 and 2009

2 years if the building is quake-proofed between 2010 and 2012

1 year if the building is quake-proofed between 2013 and 2015

#### Commercial buildings

10% of expense for quake-proofing may be added to tax depreciation for the initial year for income and corporate taxes.

#### 6.3 Earthquake Insurance System

Fire insurance does not cover losses by fire caused by earthquakes and losses expanded by earthquakes. Earthquake insurance optional rider to fire insurance is necessary for these losses to be covered. The central government reinsures part of the risk borne by insurers of earthquake insurance and manages funds in a special account to pay insurance in case devastating earthquakes occur which private insurers alone are unable to insure.

Earthquake insurance only covers residential buildings and household goods. Insurance premium is calculated according to the structures and locations of insured buildings and buildings accommodating insured household goods. Insurance premium per insurance payment of 10 million yen is from 5,000 yen (approx. 50 USD) to 31,300 yen (approx. 313 USD) per annum. Discount is available as follows:

-10% for buildings built after June 1st 1981,

-10%, 20%, 30% for buildings of earthquake resistance grade 1, 2 and 3 respectively according to the Housing Performance Indication Standards stipulated in Housing Quality Assurance Act or guidelines for earthquake resistance evaluation formulated by MLITT,

-30% for seismic isolated buildings defined in Housing Quality Assurance Act,

-10% for buildings proved to meet Earthquake Resistance Standards stipulated in Building Standard Law.

Furthermore, insurance premium is deductible from income tax (up to 50,000 yen) and residential tax (up to 25,000 yen) [12].

#### 6.4 Public School Quake-proofing

Act on Special Measures for Earthquake Disaster Countermeasures presented in 3.2 was amended in 2008 and subsidy rates have been raised from 1/2 to 2/3 for reinforcing public schools and from 1/3 to 1/2 for rebuilding public schools if inevitable. It has been mandated that municipalities evaluate the earthquake resistance of schools and announce the results.

In addition, 280 billion yen (approx. 2.8 billion USD) in total was appropriated in the first and second supplementary budgets for FY2008 and initial budget for FY2009. Quake-proofing 10,000 building with high possibility of collapse have been rescheduled to be completed by FY2011, one year earlier than previous schedule [10].

#### 6.5 Hospital Quake-proofing

Financial assistance for hospital quake-proofing has been increased as follows;

- Private hospitals designated as a disaster base hospital: from 1/3 to 1/2
- Other private hospitals scheduled in 5 year plans based on the Act on Special Measures for Earthquake Disaster Countermeasures: from 1/3 to 1/2
- Public hospitals designated as a disaster base hospital: from 60% to 65%
- Other public hospitals scheduled in 5 year plans based on the Act on Special Measures for Earthquake Disaster Countermeasures for earthquake disaster countermeasures: from 30% to 65%

### 7. EARTHQUAKE EARLY WARNING

#### 7.1 Purpose and Mechanism of EEW

Earthquake Early Warning (EEW) is to provide the public with the warning of earthquakes so that the public could take precautions before the

secondary wave arrives. First, a seismograph near the earthquake focus, out of 1,000 seismographs all over Japan detects quakes by the primary wave. The wave is then analyzed to estimate the location of the earthquake focus and its magnitude. Then, the distribution of seismic intensity is predicted. EEW is issued for the general public if the maximum predicted seismic intensity reaches 5- and more than one seismograph detect the earthquake. EEW is also issued for Specific Users who wish to receive the warning as soon as possible and understand its limitation if the predicted magnitude is greater than or equal to 3.5 or the maximum predicted seismic intensity is greater than or equal to 3.

Fig. 12 illustrates how EEW works [13].

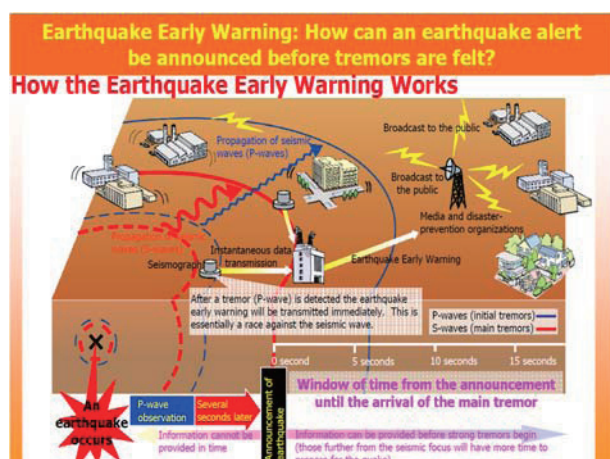


Fig.12 Outline of Earthquake Early Warning

## 7.2 User Response to EEW in Actual Earthquakes

EEW has been in operation for Specific Users since August 2006 and for the general public since October 2007 respectively. EEW has been issued for the general public against 9 earthquakes and for Specific Users against more than 1,600 earthquakes respectively.

A survey was conducted against offices located in Tohoku area where two large earthquakes struck in 2008, Iwate-Miyagi inland earthquake with magnitude 7.2 and maximum seismic intensity 6+ and Iwate northern coast earthquake with magnitude 6.8 and maximum seismic intensity 6-. This is undertaken to understand

the perception of and actual response to EEW.

In the case of Iwate-Miyagi inland earthquake, EEW was issued for the Specific Users and for the general public 3.5 seconds and 4.5 seconds after the earthquake was first detected respectively. Fig. 13 illustrates the time between the issue of EEW and the arrival of the secondary wave. The EEW did not arrive before the secondary wave in regions near the earthquake focus however it was in time in other regions. Precautions were taken in response to EEW such as halting machines or elevators in factories, alerting employees, and having children under desks at a kindergarten.

In the case of Iwate northern coast earthquake,

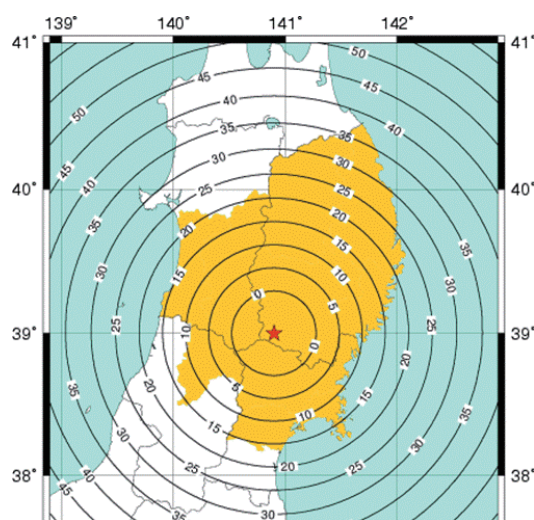


Fig.13 Time between the issue of EEW and the arrival of the secondary wave in Iwate-Miyagi Inland Earthquake

the percentage of people who took precautions was slightly less than Iwate-Miyagi inland earthquake as Iwate northern coast earthquake occurred at midnight. EEW was issued for the Specific Users after 4.1 seconds however EEW was not issued for the general public until 20.8 seconds after the earthquake. This was because maximum predicted seismic intensity did not reach the criterion, seismic intensity of 5- until then.

JMA has established a working group to improve EEW so that EEW would be more accurate and issued sooner.

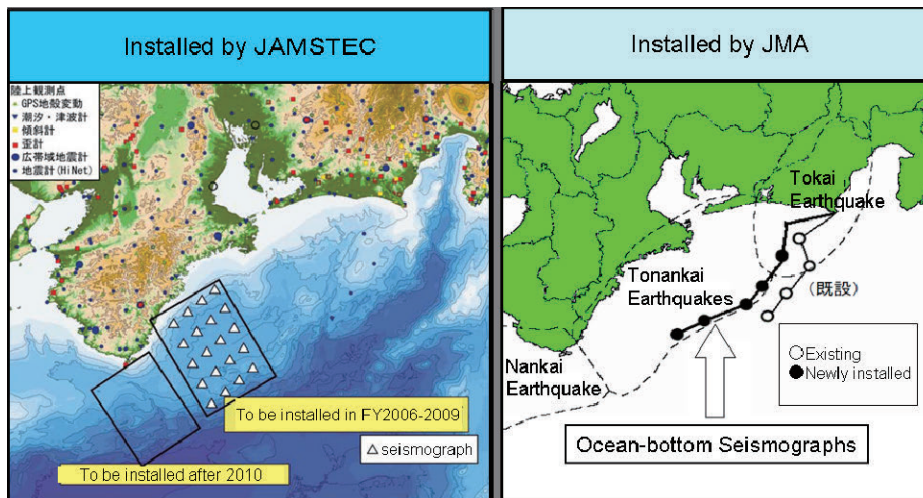


Fig.14 Ocean-bottom Seismographs and Tsunami Gauges

### 7.3 Ocean-bottom Seismographs and Tsunami Gauges

Ocean-bottom seismographs and tsunami gauges have been installed in assumed focal areas of Tokai Earthquake, and Tokai and Tonankai Earthquakes as in Fig.14. The ocean-bottom seismographs are to detect earthquakes which occur under the ocean at the depth of 1-2 km and the tsunami gauges are to detect tsunamis generated by earthquakes measuring the difference in the water pressure coming from the fluctuation of the ocean surface at the bottom. This is expected to detect earthquakes immediately and facilitate more accurate and prompt EEW against earthquakes under the ocean and tsunami warnings/advisories respectively. Also, this is expected to help understand details of earthquakes under the ocean, enhance the capacity to watch the signs of Tokai Earthquake, and contribute to the understanding of the mechanism of Tokai and Tonankai Earthquakes.

## 8. DISASTER MANAGEMENT INFORMATION SYSTEMS

### 8.1 Disaster Information System

The development of Disaster Information System (DIS) dates back to 1995 when the Great Hanshin-Awaji Earthquake struck Japan. In addition to the extensive damage and disrupted means of communication and transportation, the

lack of framework to report and share information made it difficult and time-consuming to collect and share information necessary for effective emergency response activities. Various initiatives have been undertaken to improve disaster management since then. One of such initiatives is the development of an IT system to estimate damage with only the data available beforehand and observed seismic intensities transmitted soon after earthquakes occur to help organize and initiate emergency response activities.

When an earthquake occurs, seismic intensities observed by seismographs of about 4,300 all over Japan are transmitted to DIS. If the maximum seismic intensity reaches 4, DIS is initiated automatically. Firstly, observed seismic intensities are transformed into velocities of the secondary waves on the surface, which are in turn transformed into velocities at the seismic bedrock with site amplification calculated beforehand from geological data. Then, distribution of velocities at the seismic bedrock are estimated for areas of 1 square kilometers based on the transformed velocities. The distribution of seismic intensities are estimated from the distribution of velocities at the seismic bedrock backwards. Then, the number of collapsed buildings is estimated from the distribution of seismic intensities and the relation between rate of collapsed buildings and

seismic intensity derived from past earthquakes. Lastly, death toll is estimated from the estimated number of collapsed buildings and the relation between the number of collapsed buildings and the death tolls derived from past earthquakes. Although it depends on the scales of earthquakes, the estimation is completed about 10 minutes after the earthquakes occur. The results are then transmitted to central government ministries and agencies.

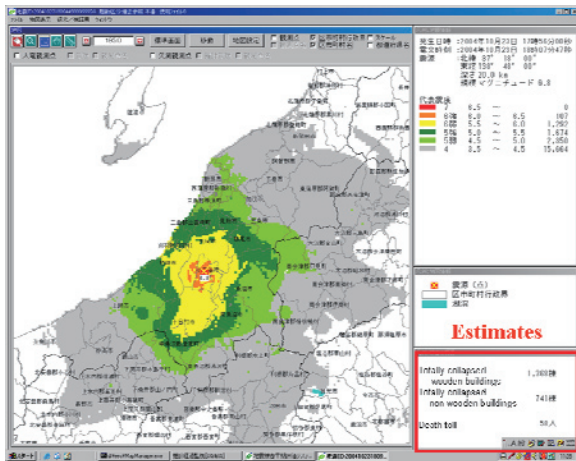


Fig.15 Distribution of seismic intensities estimated by DIS

consolidate disaster information gathered by organizations responsible for disaster management on a base map using Geographical Information System and share the information among central government ministries and agencies. It has been developed since 2005.

Different pieces of information from different organizations are stored on different layers. This enables users to choose layers of their interests and have them overlaid and displayed. In this way, information is used and shared easily and graphically.

The information is transmitted to the Platform automatically without data entry by integrating systems wherever possible. Keeping the workload of information transmission such as data entry minimum releases valuable resources for other activities in time of emergency, which is one of the main objectives of the Platform.

Information on the following items is currently available on the Platform.

- Weather
- Estimated distribution of seismic intensities and damage
- Satellite images
- Disruption of electricity and gas supply in certain regions
- Rivers

## 8.2 Disaster Information Sharing Platform

Disaster Information Sharing Platform is to

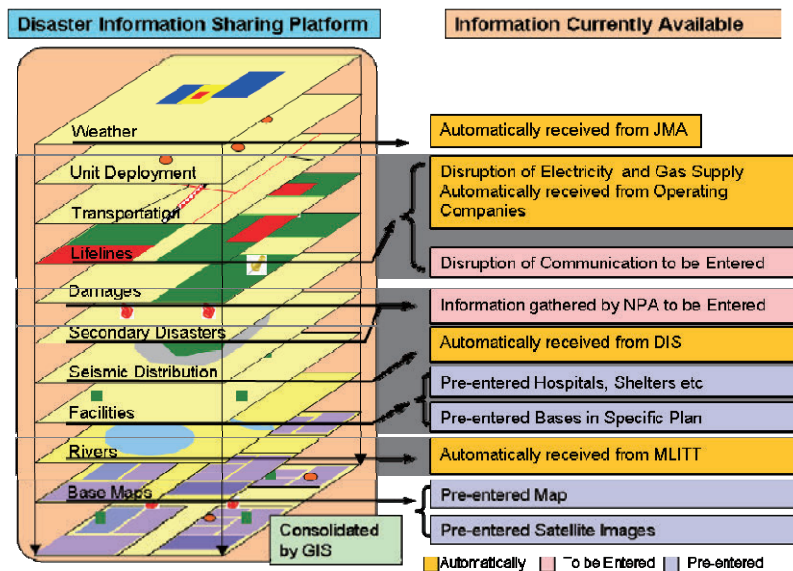


Fig.16 Information currently available on Disaster Information Sharing Platform

In addition, the number of casualties and damaged buildings, and disruption of communication facilities can be entered in the Platform.

Other information will be further consolidated on the Platform automatically by integrating IT systems managed by other organizations as far as possible.

## 9. CONCLUSION

This paper presented earthquake disaster management in Japan. Japan has suffered from earthquakes as large earthquakes occur anywhere at anytime in Japan. Disaster management has been promoted in an integrated and well-planned manner according to the Disaster Countermeasures Basic Act and facility improvement in preparation for earthquakes has been furthered according to 5 year plans based on the Act on Special Measures for Earthquake Disaster Countermeasures. On the other hand, comprehensive measures have been considered and undertaken against imminent devastating large-scale earthquakes individually. Tokyo Inland Earthquakes above all, striking Tokyo, is estimated to cause tremendous damage. Reducing the damage and maintaining political, administrative and economic functions as the Capital are two pillars of disaster management stated in the Policy Framework. Measures against Tokyo Inland Earthquakes have been promoted according to Earthquake Disaster Reduction Strategy. In addition, continuity of operation plans and business continuity plans, Specific Plan for Emergency Response Activities have been formulated to ensure administrative and business operation, and prompt and efficient emergency response to earthquakes.

The central government has institutionalized building earthquake resistance by legislation, increased subsidy rates appropriating supplementary budget for FY 2008 in addition to initial budget, and has arranged tax incentives to strongly promote building quake-proofing.

In addition to the measures proposed for massive evacuees and the stranded generated by Tokyo Inland Earthquakes, there are still some

issues to be worked on. For example, measures should be coordinated by the central government, local governments and media to gather, share and provide information for those who need it such as the evacuees and the stranded. Also, schemes should be arranged for organizations concerned to coordinate wide-area evacuation.

While all levels of governments play important roles in disaster management, the disaster management also requires for every single member of the society to be involved, play its part and help each other for better respond to disasters.

Specifically, each person should prepare for and take actions against disasters by doing things such as quake-proofing the home, fixing furniture to prevent it from falling to avoid being hurt, stockpiling emergency goods, food and water enough for the first few days, and examining ways to shelters.

Actions should be taken to encourage local communities to restore and strengthen the solidarity, to facilitate involvement of volunteers in disaster management, to expand and strengthen voluntary disaster prevention units of local communities, to encourage private companies to provide assistance for local communities and to encourage those individuals and groups to coordinate their initiatives to maximize disaster management capacity.

In addition to its disaster management, the central government has arranged measures to support these activities by arranging things such as various assistance scheme for building quake-proofing and EEW. It is extremely important that these activities should be furthered to strengthen disaster resistance of the country.

## 10. REFERENCES

1. Cabinet Office: Earthquake in Japan, [http://www.bousai.go.jp/jishin/chubou/taisaku\\_gaiyou/pdf/hassei-jishin.pdf](http://www.bousai.go.jp/jishin/chubou/taisaku_gaiyou/pdf/hassei-jishin.pdf)
2. Cabinet Office: Disaster Management in Japan, 2007
3. Ikeuchi, K. and Isago, N.: Natural Disaster Mitigation Policy in Japan, *Proc. 40th Joint Meeting of U.S. – Japan Panel on Wind and Seismic Effects UJNR*, 2008.
4. Cabinet Office: Results of damage estimation concerning Tokyo Inland Earthquakes, 2005, [http://www.bousai.go.jp/jishin/chubou/taisaku\\_syuto/pdf/higaisoutei/gaiyou.pdf](http://www.bousai.go.jp/jishin/chubou/taisaku_syuto/pdf/higaisoutei/gaiyou.pdf)
5. Cabinet Office: Summary of Specific Plan for Emergency Response Activities concerning Tokyo Inland Earthquakes, 2008, [http://www.bousai.go.jp/jishin/chubou/taisaku\\_syuto/pdf/081212/081212\\_01.pdf](http://www.bousai.go.jp/jishin/chubou/taisaku_syuto/pdf/081212/081212_01.pdf)
6. A Technical Committee on Measures for Evacuees and the Stranded concerning Tokyo Inland Earthquakes, Central Disaster Management Council: Report, 2008, <http://www.bousai.go.jp/jishin/chubou/shutohinan/081027/siry03.pdf>
7. Cabinet Office: Summary of Estimates of Supply and Demand Gap of Toilets Based on the Simulation for Behaviors of the Stranded, 2008, <http://www.bousai.go.jp/jishin/chubou/shutohinan/081027/siry06.pdf>
8. National Institute for Land and Infrastructure Management: Guidelines for Special Permissions in the Zoning Code under the Building Standard Law, *Technical Note of National Institute for Land and Infrastructure Management*, No.368, 2007, <http://www.nilim.go.jp/lab/bcg/siryoutnn/tnn0368pdf/ks0368.pdf>
9. Cabinet Office: Comprehensive Plan to Achieve Zero Victims in Natural Disasters, 2008, <http://www.bousai.go.jp/chubou/22/shiryo4-2.pdf>
10. Ministry of Education, culture, Sports, Science and Technology: Acceleration of School Facility Quake-proofing according to Comprehensive Emergency Measures, [http://www.mext.go.jp/b\\_menu/soshiki/daijin/shionoya/08101606.htm](http://www.mext.go.jp/b_menu/soshiki/daijin/shionoya/08101606.htm)
11. Ministry of Land, Infrastructure, Transport and Tourism: Assistance Scheme for Building Quake-proofing, <http://www.mlit.go.jp/jutakukentiku/build/taisinsen1.pdf>
12. Ministry of Finance: Summary of Earthquake Insurance, <http://www.mof.go.jp/jouhou/seisaku/jisin.htm>
13. Japan Meteorological Agency: Earthquake Early Warning, <http://www.jma.go.jp/jma/en/Activities/how.pdf>,

# Study on Landslide Orientation Bias Triggered by 1994 Northridge Earthquake

by

Hiroshi P. Sato<sup>1</sup>

## ABSTRACT

Previous studies reported that the 1994 Northridge earthquake triggered 11,000 landslides in 10,000 km<sup>2</sup>; however, no study has investigated the landslide orientation bias in the wider area than the Santa Susana quadrangle map, i.e., 124 km<sup>2</sup>. I selected 3,200 km<sup>2</sup> on the mountain slope and found that the bias shows the direction from south to west. I also investigated the relation between the landslide slope orientation and ground acceleration direction of initial and peak sliding acceleration (ISA and PSA), using simulated horizontal and vertical ground acceleration data. As a result, it was found that PSA gives better explanation than ISA for the landslide orientation bias of southwest; however, since north-facing slopes also showed the highest accumulated PSA, I could not state the reason why many landslides did not occur on the north-facing slopes.

**KEYWORDS:** Aspect, California, Ground Acceleration, Landslide, Northridge Earthquake, Slope

## 1. INTRODUCTION

On 17 January 1994, Northridge earthquake (Mw 6.7) occurred 18 km beneath the Northridge, Southern California [1], neighborhood in the city of Los Angeles. The earthquake resulted from more than 3 m of reverse slip on a 15-km-long south-dipping thrust fault that raised the Santa Susana Mountains by as much as 70 cm [2].

Northridge earthquake triggered 11,000 landslides over 10,000 km<sup>2</sup> [3][4]. They described that deep landslide was rare and almost all of the landslides were shallow disrupted rock slide, and tell that the landslides were concentrated primarily in the Santa Susana Mountains and the mountains north of the Santa

Clara River Valley. Since no rain had fallen for several month before the earthquake; hence, pore-pressure effect were not a factor in triggering landslides [3][4].

Harp and Jibson [3][4] also reported that the earthquake induced-landslide were concentrated more on south (S)- than north (N)- slope aspect (the direction which the slope faces) in Santa Susana Mountains. Parise and Jibson [5] also said that the landslides have Southeast (SE)~Southwest (SW) orientation bias in the 124 km<sup>2</sup> area using 10-m-resolution digital elevation model (DEM) prepared by U.S. Geological Survey (USGS).

Such the bias was also shown in the other cases of earthquakes; e.g., the bias of SW [6] in the 2005 Northern Pakistan earthquake (M7.6), the bias of S [7] in the 1999 Chi-Chi earthquake (Mw 7.6) in Taiwan, and the bias of SE [7] in the 1993 earthquake (Mw 6.9) in Finisterre Mountain, Papua New Guinea. It is thought that the relation between slope aspect and ground acceleration direction has close relation to trigger landslides. However, previous studies have not investigated the relation between them enough.

Time-series ground acceleration shows different directions in each measurement time, and slope aspect is variable among the different sites. Furthermore, steep slope angle is an important factor to induce landslides. Since time-series sliding acceleration [8] in each site is also calculated from the ground acceleration, I investigated the relation between slope aspect and the time-series sliding acceleration, inducing landslides.

## 2. STUDY AREA

---

<sup>1</sup> Senior Researcher, Geography and Crustal Dynamics Research Center, Geographical Survey Institute, Tsukuba-shi, Ibaraki-ken 305-0811 Japan

## 2.1 Topography

Study area is shown in Fig.1a, where elevation ranges from 0 m, at the coast facing Pacific Ocean, to the summit 2,248 m at the site A. Figure 1a also depicts the model fault plane [9] whose upper edge is shown as D. The position B-B' in Fig. 1a shows the Susana Mountains.

Figure 1b shows the mapped landslides [3][4] as red dots. The site C in Fig.1a shows Simi Hills where Cretaceous hard sandstone lies, and the landslide density in the Simi Hills was smaller than in Santa Susana Mountains [3][4][5]. Figures 1c and 1d depict slope angle and aspect calculated from 40-m-resolution DEM. In this study I deal landslides occurred on mountain slope, therefore, I limited the study area where slope angle is 5° and more; Figures 1c and 1d shows just the area, 3,200 km<sup>2</sup>. Furthermore, I selected the landslide whose area is more than 40 m by 40 m, this is because I thought that large landslides clearly shows their orientation (the directions that the landslides face on the slopes).

## 2.2 Landslide Orientation Bias

I overlaid the slope aspect in Fig.1d on the mapped landslides in Fig.1b; I calculated the landslide area ratio among eight orientations. As a result, the radar chart in Fig.2a showed the SW orientation bias.

To confirm slope steepness effect on the bias, I overlaid the slope angle in Fig.1c on the mapped landslides; I calculated the average slope angle among eight orientations. As a result, Fig.2b does not show remarkable slope angle changes among them and it means that slope steepness does not control the landslide orientation bias in the whole study area.

Next, to confirm geologic unit effect on the bias, I overlaid the geologic map [10] on the mapped landslides; I calculated the landslide area ratio among both eight orientations and the 18 kinds of geologic unit, from Pre-Cambrian granite to Holocene sediments. All units except Miocene continental sedimentary rocks showed S, SW, and west (W) orientation bias and it means that

geologic unit does not control the landslide orientation bias in the whole study area.

## 3. METHOD

### 3.1 Simulated Ground Acceleration Data

Jibson and Jibson [11] showed the 84 seismometer instruments in and around the study area. I drew the instrument-centered 2-km-radius sampling circles on the landslide polygons; however, almost all of the sampling circles did not have the enough numbers of landslide polygon because the instruments are not always installed in the mountains. Only the four instruments of FSD, WPI, PDD, and PDA in Fig.1c (PDA is in the same place as PDD) showed over 1% landslide area ratio in each sampling circle.

However, the number of the sampling circles is not enough to consider landslide orientation bias in the whole study area. Therefore, in this study I did not use the real ground acceleration data [11] but I used the simulated ground acceleration data at the 4-km-spacing 144 sites, from the site #1 to #144. The data have northing, easting, and up components and whose sampling time and period is 0.04 second and 50 seconds, respectively. Since the simulated data [12] originally provides ground velocity, I calculated the acceleration from the velocity data. In calculating the velocity Wald et al. [12] considered substrate stiffness differences between hard and soft rock; however, they did not consider topographic seismic-wave amplification effect; hence, calculated acceleration does not contain this effect.

On the mapped landslides I overlaid 2-km-radius sampling circles whose centers are the 144 sites, and I investigated landslide area ratio within the sampling circles. As a result, I selected 12 sampling circles where the landslide area ratio is over 1%. Figure 1d shows these 12 sampling circles of #64, #65, #76~#78, #81, #89, #98~#101, and #112. Within the 12 sampling circles I overlaid the slope aspect on the mapped landslides, calculated 2,072 landslide DEM cells number ratio among eight orientations (Fig.3a). Again, I could find the S~SW orientation bias.

Figure 3b shows the whole DEM cells distribution ratio in the 12 sampling circles; however, no orientation bias was found in the radar chart.

### 3.2 Sliding acceleration calculation

In this study we assumed that any DEM cells in each sampling circle have the same ground acceleration. In each sampling circle I calculated sliding acceleration [8] using the simulated ground acceleration data. As an example, at the DEM cell (SW slope aspect in a landslide polygon, within the sampling circle #77), I show the easting  $a_E$ , northing  $a_N$ , and up  $a_V$  components of the ground acceleration in Figs.4a, 4b, and 4c, respectively.

For calculating sliding acceleration, in Fig.5 Huang et al. [8] assumed free landslide body whose mass is  $m$  on the basement. Relative to the inertial frame of reference, the basement moves with acceleration  $a_n$  in the direction of normal to the slide surface (positive away from the slope),  $a_d$  tangential to the slide surface along the dip (positive down dip), and  $a_s$  tangential to the slide surface along the strike. In Fig.5,  $a_s$  is not written because it is vertical to the page (positive up-away from the page). Eqs.(1) and (2) shows how to calculate  $a_n$  and  $a_d$  [8].

$$a_n = a_E \sin \delta \cos \varphi_s - a_N \sin \delta \sin \varphi_s + a_V \cos \delta \quad (1)$$

$$a_d = a_E \cos \delta \cos \varphi_s - a_N \cos \delta \sin \varphi_s - a_V \sin \delta \quad (2)$$

Where,  $\delta$  and  $\varphi_s$  is slope angle and slope strike direction from north measured clockwise, which is equal to slope aspect minus  $90^\circ$ , respectively. The  $a_n$  and  $a_d$  calculated from  $a_E$ ,  $a_N$ , and  $a_V$  is shown in Figs.4d and 4e.

Finally, sliding acceleration  $S_a$  was calculated by Eq.(3). The  $S_a$  calculated from  $a_n$  and  $a_d$  is shown in Fig.4f. If  $S_a$  is positive, it will move the slope surface; if not, the surface will stay.

$$S_a = (g \sin \delta - a_d) - \mu_s (g \cos \delta + a_n) - c' / mA \quad (3)$$

Where,  $g$ ,  $\delta$ ,  $\mu_s$ ,  $c'$ ,  $A$  is gravity, slope angle, the

coefficient of static friction, effective cohesive strength across the sliding surface, and area of the sliding surface, respectively. The coefficient of static friction  $\mu_s$  was calculated from  $\mu_s = \tan(\varphi')$ , where  $\varphi'$  is effective friction angle. The values of  $\varphi'$  and  $c'$  in each geologic unit [10] were determined by Jibson et al. [13] referring to the lithologic facies of the geologic units.

### 3.3 Initial and Peak Sliding Acceleration (ISA and PSA) Selection

Time-series sliding acceleration was calculated at each DEM cells, whose number is 2,072 landslide cells and 54,289 no-landslide cells. In each DEM cell slope aspect was calculated. If original  $a_E$  and  $a_N$  in Figs.4b and 4c are referred to, I can calculate the ground acceleration direction from  $a_E$  and  $a_N$  in any time in Fig.4f. Therefore, in each cell I selected the two kinds of positive sliding acceleration and compared slope aspects with ground acceleration direction in each case.

First, I selected the ISA that moves slope surface for the first time; e.g., in Fig.4f, initial positive  $S_a$  is 0.03 m/s/s and the recorded time is 4.84 second. This is because I expected that ground acceleration direction of ISA would determine the landslide orientation. Next, I extracted PSA; e.g., in Fig.4f, PSA is 0.99 m/s/s and the recorded time is 8.72 second. This is because I thought that ISA may be small to move slope surface in practice and PSA is effectively working to move it. In the both cases, I recorded not only the ISA and PSA but also whose original ground acceleration direction at the time and slope aspect at the cell.

However, in the two cases, it is not efficient to consider the relation between the slope aspect and ground acceleration direction at each DEM cell, because the number of DEM cells is totally 56,361; therefore, I accumulated the ISA and PSA among the slope aspect and ground acceleration directions in the whole sampling circle.

## 4. RESULTS

### 4.1 Initial Sliding Acceleration (ISA)

Figure 6a shows the accumulated ISAs at 2,072 landslide DEM cells among slope aspects and ground acceleration directions. Generally speaking, high accumulated ISAs are concentrated on and around the diagonal line between slope aspect N, ground acceleration direction S and slope aspect NW, ground acceleration direction SE. The highest accumulated ISA recorded 19.3 m/s/s in the slope aspect SW, ground acceleration direction NE. The fourth highest accumulated ISA recorded 10.0 m/s/s in the slope aspect N, ground acceleration direction S. Since the landslide DEM cells face more SW than N (Fig.2a), I thought that more ISAs were accumulated on the SW-facing DEM than on the N-facing DEM.

Figure 6b shows the accumulated ISAs at both 2,072 landslide DEM cells and 54,289 no-landslide DEM cells, i.e., at the all 56,361 DEM cells within the whole sampling area. The highest accumulated ISA recorded 138.6 m/s/s in the slope aspect N, ground acceleration direction S. The second highest accumulated ISA recorded 84.3 m/s/s in the slope aspect SW, ground acceleration direction NE. And it looks like two peaks of accumulated ISA around the slope aspect N, ground acceleration S, and slope aspect SW, ground acceleration NE.

To normalize Fig.6a, I divided Fig.6a by Fig.6b. The result is shown in Fig.6c; it shows 100% in the slope aspect SW, ground acceleration direction SW, and in the slope aspect W, ground acceleration direction S. Furthermore, 99.4% recorded in the slope aspect N, ground acceleration direction NW; however, Fig.6c does not show that higher accumulated ISAs were added on the landslide SW-facing slope, regardless of ground acceleration direction.

#### 4.2 Peak Sliding Acceleration (PSA)

Figure 6d shows the accumulated PSA at 2,072 landslide DEM cells among slope aspects and ground acceleration directions. The highest accumulated PSA recorded 83.3 m/s/s in the slope aspect SW, ground acceleration direction NE. The seventh highest accumulated PSA recorded 40.0 m/s/s in the slope aspect N,

ground acceleration direction S.

Figure 6e shows the accumulated PSAs at the all 56,361 DEM cells. The highest accumulated PSA recorded 341.4 m/s/s in the slope aspect N, ground acceleration direction S. The second highest accumulated PSA recorded 289.2 m/s/s in the slope aspect SW, ground acceleration direction NE. And it also shows two peaks of accumulated PSA around the first and second highest accumulated PSA.

Figure 6f shows the normalized accumulated PSA by dividing Fig.6d by Fig.6e; it was found that the slope aspect SW tended to experience relatively higher ratio than the other slope aspects, regardless of ground acceleration direction. Comparing Fig.6f with Fig.3a, I found that landslide orientation bias is closely related with the normalized accumulated PSA among the slope aspects. However, if we focus on the slope aspect N and SW in Fig.6e, we cannot state the reason why landslides did not occur at the slope aspect of N.

## 5. CONCLUSIONS

In this study I revealed that the 1994 Northridge earthquake-induced landslides have the orientation bias of SW over the whole mountain area, 3,200 km<sup>2</sup>. Next, I stated that the bias is not controlled by the slope steepness and geologic units. I also stated that PSA (peak sliding acceleration) gives better explanation than ISA (initial sliding acceleration) for the SW landslide orientation bias. However, we could not state the reason why landslides did not occur at the N-facing slope where the highest accumulated PSA recorded in Fig.6e.

## 6. ACKNOWLEDGEMENT

Support for my research at the U.S. Geological Survey facilities in Golden, CO was provided by a grant from the Ministry of Education, Culture, Sports, Science and Technology of Japan.

## 7. REFERENCES

1. Wald, D.J., Heaton, T.H.: A Dislocation of the 1994 Northridge, California Earthquake

- Determined from Strong Ground Motions, *U.S. Geological Survey Open-File Report*, No. 94-278, 1996.
2. U.S. Geological Survey and the Southern California Earthquake Center: The Magnitude 6.7 Northridge, California, earthquake of January 17, 1994, *Science*, Vol.266, 389-397, 1994.
  3. Harp, E.L., Jibson, R.W.: Inventory of landslides triggered by the 1994 Northridge, California earthquake, *U.S. Geological Survey Open-File Report*, No. 95-213, 1995.
  4. Harp, E.L., Jibson, R.W.: Landslides triggered by the 1994 Northridge, California earthquake, *Bulletin of the Seismological Society of America*, Vol.86(1B), S319-S332, 1996.
  5. Parise, M., Jibson, R.W.: A Seismic Landslide Susceptibility Rating of Geologic Units based on Analysis of Characteristics of Landslides Triggered by the 17 January, 1994 Northridge, California Earthquake, *Engineering Geology*, Vol.58, 251-270, 2000.
  6. Sato, H.P., Hasegawa, H., Fujiwara, S., Tobita, M., Koarai, M., Une, H., Iwahashi, J.: Interpretation of Landslide Distribution Triggered by the 2005 Northern Pakistan Earthquake using SPOT5 Imagery, *Landslides*, Vol.4, 113-122, 2007.
  7. Meunier, P., Houvius, N., Haines, J.A.: Topographic Site Effects and the Location of Earthquake Induced Landslides, *Earth Planetary Science Letters*, Vol.275, 221-232, 2007.
  8. Huang, C.C., Lee, Y.H., Liu, H.P., Keefer, D.K., Jibson, R.W.: Influence of Surface-Normal Ground Acceleration on the Initiation of Jih-Feng-Erh-Shan Landslide During the 1999 Chi-Chi, Taiwan, Earthquake, *Bulletin of the Seismological Society of America*, Vol.91, 953-958, 2001.
  9. Wald, D.J., Heaton, T.H., Hudnut, K.W.: The Slip History of the 1994 Northridge, California, Earthquake Determined from Strong-motion, Teleseismic, GPS, and Leveling Data, *Bulletin of the Seismological Society of America*, Vol.86(1B), S49-S70, 1996.
  10. Jennings, C.W.: Geologic Map of California (Scale 1:750,000), State of California, 1977.
  11. Jibson, R.W., Jibson, M.W.: Java Programs for Using Newmark's Method and Simplified Decoupled Analysis to Model Slope Performance During Earthquakes, *U.S. Geological Survey Open-File Report*, No.03-005, 2003.
  12. Wald, D.J., Hudnut, K.W., Heaton, T.H.: Estimation of Uniformly Spaced, Near-source, Broadband Ground Motions for the 1994 Northridge Earthquake from Forward and Inverse Modeling, *Proceedings of the CUREe Northridge Earthquake Research Conference, Los Angeles, 1997.* (<http://pasadena.wr.usgs.gov/office/wald/CUREe.html>)
  13. Jibson, R.W., Harp, E.L., Michael, J.A.: A Method for Producing Digital Probabilistic Seismic Landslide Hazard Maps: an Example from the Los Angeles, California, Area, *U.S. Geological Survey Open-File Report*, No.98-113, 1998.

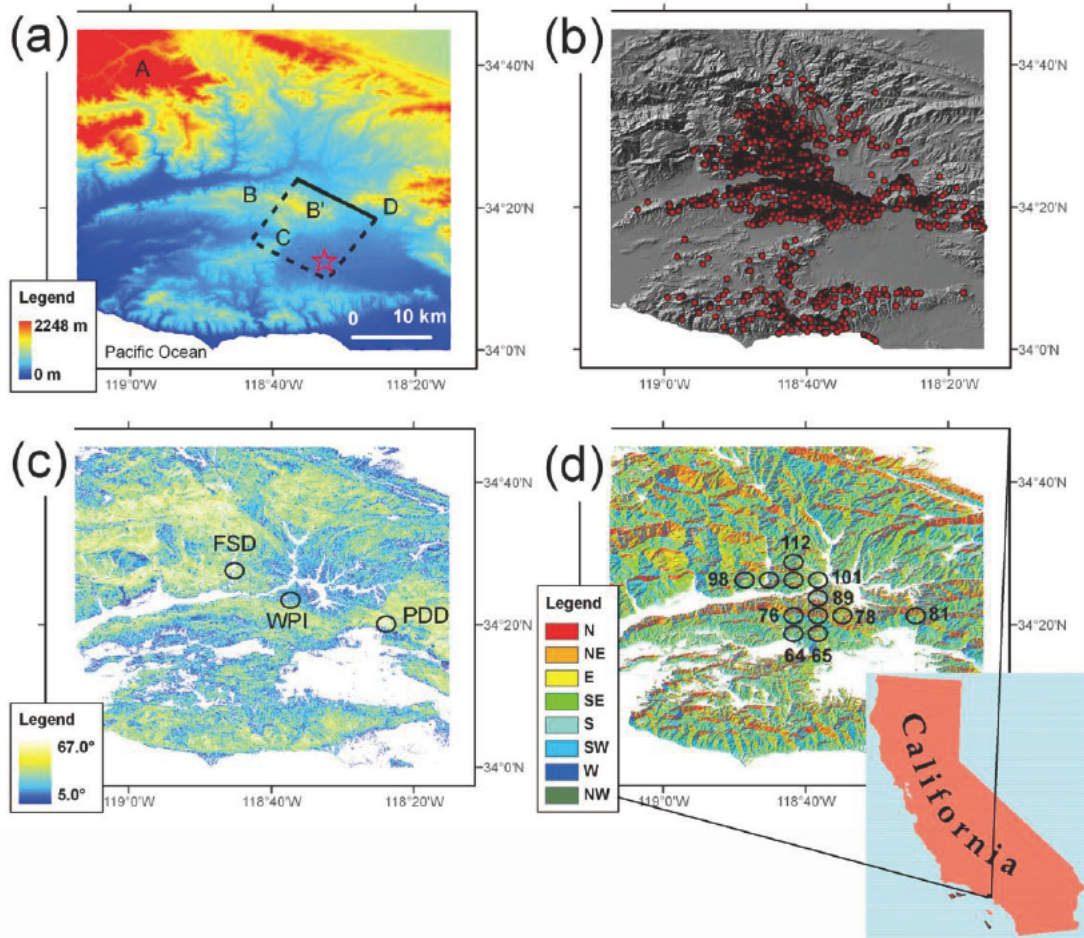


Fig.1 Study Area

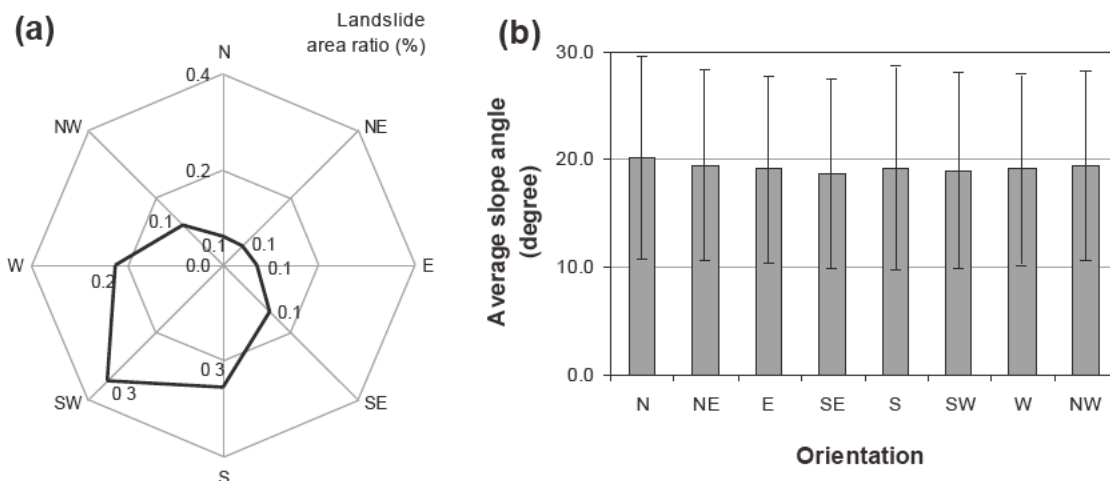


Fig.2 (a) Landslide Area Ratio among Eight Orientations and (b) Average Slope Angle (Error Bar Means Standard Deviation) among Eight Orientations in the Whole Study Area

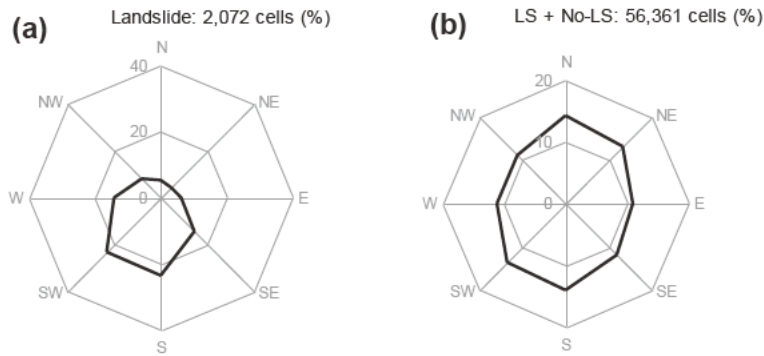


Fig.3 Orientation Ratio in (a) 2,072 Landslide Cells, (b) Whole Cells (2,072 Landslide Cells + 54,289 No-landslide Cells)

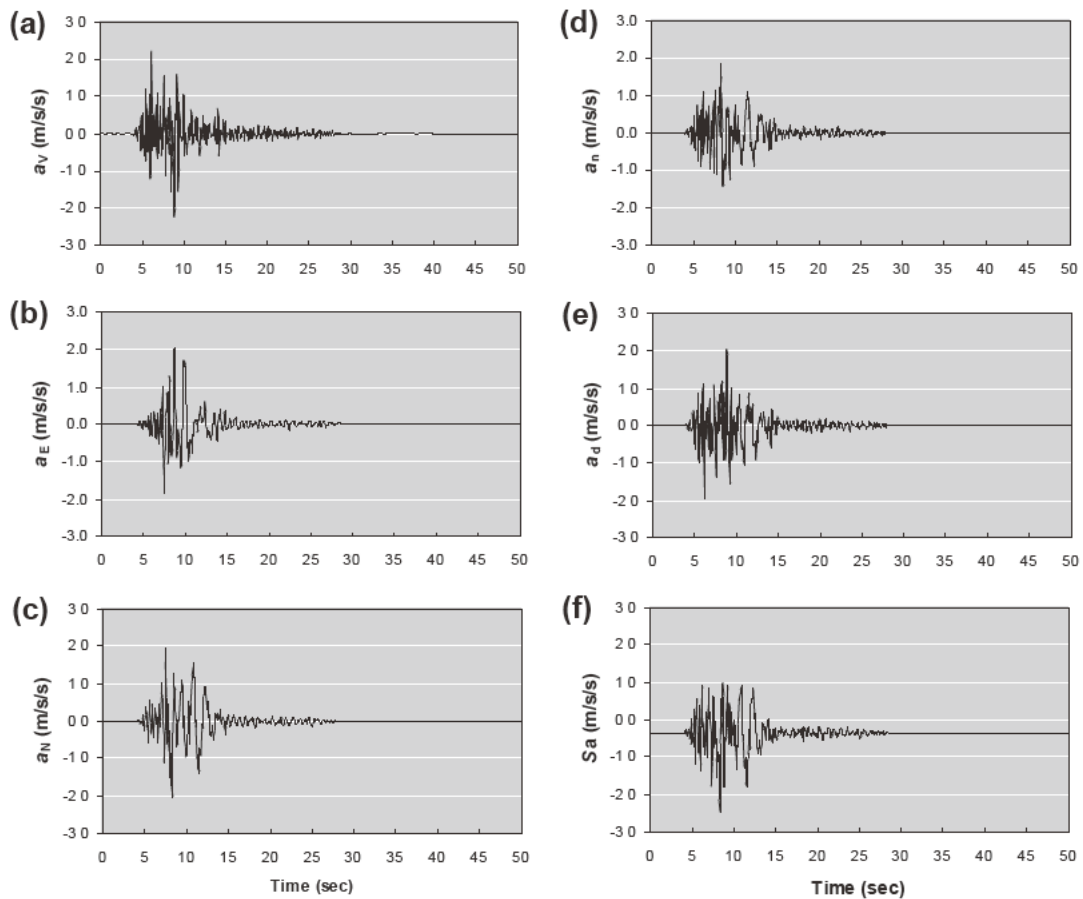


Fig.4 (a), (b), and (c) are the Examples of Ground Acceleration, Up ( $a_v$ ), Easting ( $a_E$ ), and Northing ( $a_N$ ) Component, Respectively at the Cell (Slope Angle and Slope Aspect is  $53.8^\circ$  and  $206.6^\circ$ , Respectively) in the Sampling Circle #77 (in Fig.1d). Ground Acceleration  $a_d$  in Tangential to the Slide Surface along the Dip (Positive Down Dip) shows (d), and (e) is  $a_n$  in the Direction of Normal to the Slide Surface (Positive Away from the Slope) in Landslide Area. The (f) is Sliding Acceleration Calculated from  $a_n$  and  $a_d$ .

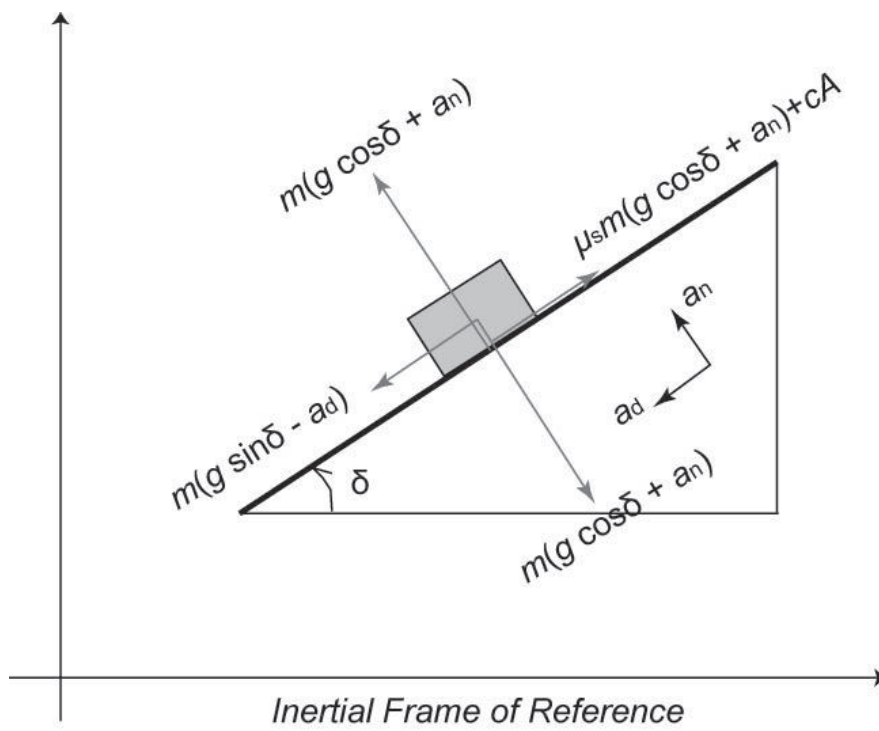


Fig.5 Free Landslide Body Diagram about Mountain Body under Earthquake Ground Motion and Critically Balanced Conditions ([8] was simplified)

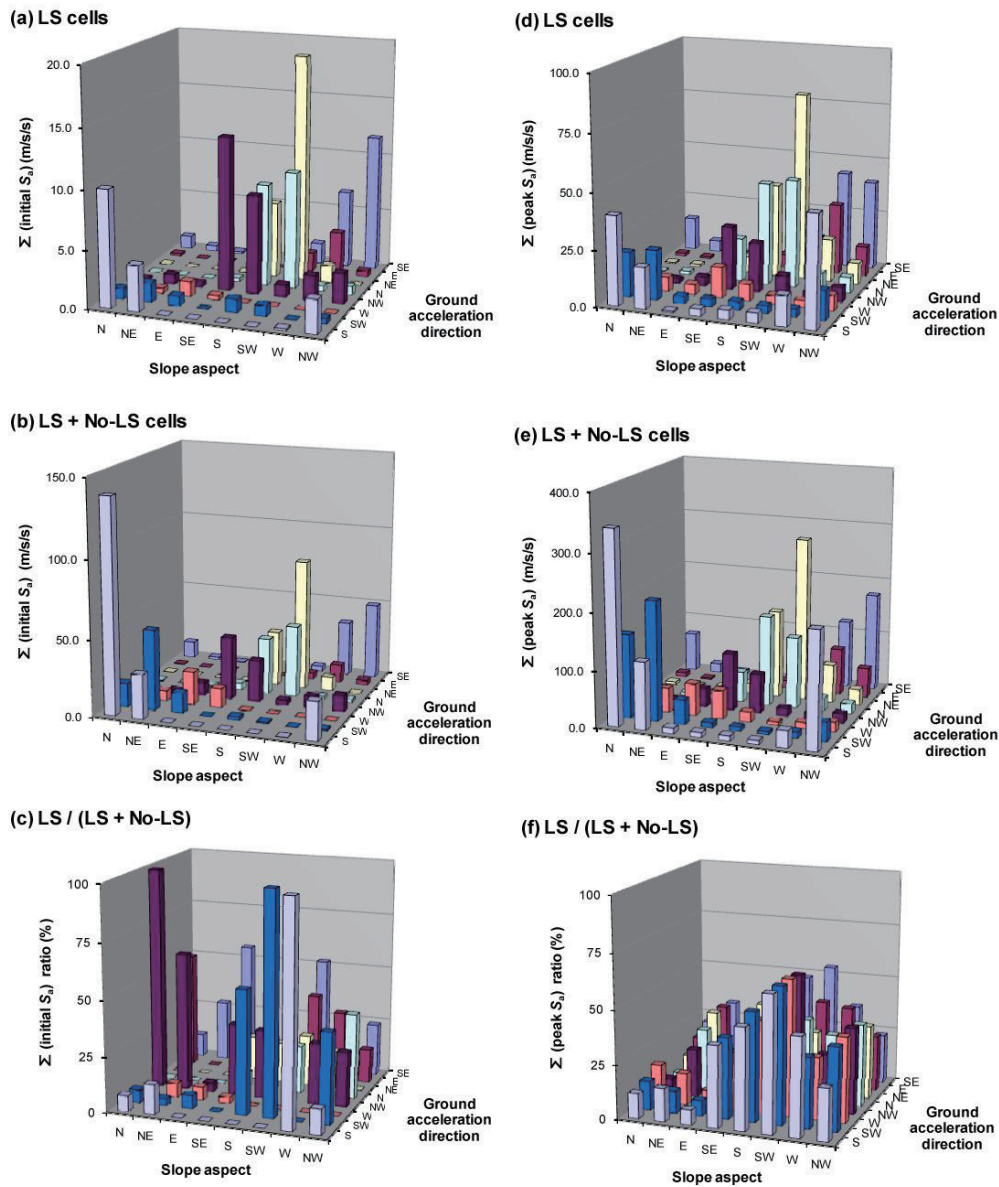


Fig.6 Accumulated Initial Sliding Acceleration (ISA) between Slope Aspects and Ground Acceleration Direction in (a) 2,072 Landslide Cells, (b) Whole Cells (2,072 Landslide Cells + 54,289 No-landslide Cells), (c) Normalized Accumulated ISA. Accumulated Peak Sliding Acceleration in (d) 2,072 Landslide Cells, (e) Whole Cells, (f) Normalized Accumulated PSA.

## **THEME 7**

# **Disaster Resilient Buildings and Infrastructure**

# On the Variation of Fundamental Frequency (Period) of an Undamaged Building – A Continuing Discussion

by

M. Çelebi<sup>1</sup>

## ABSTRACT

Variation of fundamental period (frequency) of undamaged structures has been the subject matter of numerous studies. Recently, this topic is rekindled with the premise but repeat of the well known conclusion that fundamental period (frequency) varies with amplitude of shaking. Some researchers appropriately called this “wandering” of the natural frequencies of a structure. Although due to various sources of excitation and time-varying environmental conditions, variation of the fundamental period (frequency) of even an undamaged structure should not be a surprise to many, it is important to understand why such variation is important for practical purposes. In this paper, we investigate the fundamental frequencies of an undamaged building for which there are numerous studies of several sets of vibration data, including forced vibration testing, strong shaking due to a distant large earthquake, and low-amplitude shaking due to ambient excitations as well as several small nearby earthquakes. It is shown that the fundamental frequency “wanders” in a consistent way with the level of shaking, and that the significant difference between low-amplitude and strong shaking is attributed to soil-structure interaction during stronger shaking

**KEYWORDS:** fundamental frequency (period), accelerations, earthquake response, spectra, building,

## 1.0 INTRODUCTION

### 1.1 General

Reasonably accurate assessment of fundamental period (frequency) of a structure is an essential part of design and analysis processes. It is also known that variation of fundamental period (frequency) of undamaged structures has been subject matter of numerous studies – too long to cite herein. Recently, with advanced technologies and methods to acquire and analyze vibration data from structures excited by natural and man-made sources, study of the subject matter is rekindled with the premise that fundamental period (frequency) varies with the amplitude of shaking (e.g. Calvi et al, 2006, Dunand et al, 2006, Todorovska et al, 2006). Clinton and others (2006) appropriately called this “wandering” of the natural frequencies of a structure. While due to various sources of excitation and time-varying environmental conditions, variation of the fundamental period (frequency) of even an undamaged structure should not be a surprise to many, but nonetheless it is important to understand and dwell upon as to whether such variation is important for practical purposes. It is also important to mention that accurate assessment of fundamental frequency is important to establish a baseline linear elastic behavior of a structure in order to interpret its nonlinear elastic or nonlinear inelastic behavior that may be observed in future events. The objective of this paper is to investigate the fundamental frequencies of the undamaged Pacific Park Plaza Building in Emeryville, CA, for which there are numerous studies of numerous sets of vibration data, including forced

<sup>1</sup> Earthquake Hazards Team, USGS (MS977),  
345 Middlefield Rd., Menlo Park, Ca, 94025

vibration testing, strong shaking due to a far distance large earthquake, and low-amplitude shaking due to ambient excitations as well as several small nearby earthquakes. It is repeated herein that the particular building being studied has not been damaged but, as shown in this study that its fundamental period (frequency) is observed to “wander” in a consistent way with the level of shaking. The scope of the paper is based on findings using actual data and does not include mathematical modeling of the building (except in reference to existing analyses by others). In the case of this building, the significant change in the value of fundamental period (frequency) between low-amplitude and strong shaking is attributed to soil-structure interaction (SSI) during stronger shaking. However, detailed SSI investigation of the building is beyond the scope of this paper but has been reported elsewhere (Kagawa et al, 1993a, b, Aktan et al, 1992, Kambhatla et al, 1992, Çelebi, 1992, 1998). This paper introduces additional results from new data that reinforces this argument.

## 1.2 The Building, Design Spectra and Instrumentation

The Pacific Park Plaza (PPP) Building is an equally-spaced three-winged, cast in place, thirty-story, 312 ft. (95.1 m) tall, ductile reinforced concrete moment-resisting frame building. The three wings of the building are constructed monolithically and are equally spaced at angles of 120 degrees around a central core. Shear walls in the center core and wings extend to the second floor level only, but column lines are continuous from the foundation to the roof. The foundation is a 5-foot-thick concrete mat supported by 828 (14-inch-square) pre-stressed concrete friction piles, each 20-25 m in length, in a primarily soft-soil environment that has an average shear-wave velocity between 250 and 300 m/s and a depth of approximately 150 ft (~50 m) to harder soil. A three-dimensional schematic of the building and its seismic instrumentation is shown in Figure 1. The instrumentation integrates arrays for the structure, surface, and downhole, and comprises a 30-channel accelerometer deployment uniquely

designed to capture (a) the translational motions of the wings of the building relative to its core, (b) the vertical motions of the mat foundation slab at the ground floor level, and (c) free-field motions at the surface and at a downhole depth of 200 ft (61 m). The South Free-field (SFF) station is often referred to as the Emeryville (EMV) ground site. This building is selected for this study because there is a variety of old and new data and because there is no evidence that it experienced any damage during the various levels of shaking described in this paper.

## 1.3 Site Conditions

Based on a relatively recent geologic log and shear-wave velocity profile (Gibbs et al, 1994), the soils at the site consist of artificial fill, soft silty clay (Holocene Bay Mud), and stiff to very stiff, undifferentiated deposits composed of numerous layers of clay, loam, sand, and gravel. The layer of Holocene Bay Mud, clearly evident on the shear-wave velocity profile shown in Figure 2, begins at about 16 ft. (5 m) depth and is approximately 10 ft. (3 m) thick. Stiff deposits with shear-wave velocity ( $V_s$ ) of approximately 820 ft/s (0.25 km/s) extend from below the Holocene Bay Mud to a depth of approximately 80 ft. (24 m). Very stiff Pleistocene deposits with  $V_s$  approximately equal to 1300 ft/s (0.4 km/s) extend to a depth of about 155 ft (48 m). The computed site transfer function, corresponding to the shear-wave velocity profile in Figure 2, using Haskell’s shear-wave propagation method (Haskell, 1953, 1960) and coded by Mueller (*pers. comm.* 2002) is also provided in Figure 2, and indicates a site frequency at approximately 0.7 Hz.

## 1.4 Design Spectra and Significant Shaking Experienced

To date, the most significant shaking recorded by the building arrays was during the 1989 Loma Prieta (LPE), CA earthquake ( $M_s=7.1$ ). The data set from LPE is extensively used in several studies as well as in this investigation that specifically dwells upon the variation of fundamental period with level of shaking. As previously mentioned, the building was not damaged.

Responses of the building and the surface free-field recorded during the strong shaking caused by

the LPE earthquake exhibit distinct amplification of motions (Figures 3a) at the site of the building as compared to the motions at Yerba Buena Island, both approximately 100 km (and at similar azimuths) from the epicenter of the LPE. The east-west components of acceleration recorded at the roof and the ground floor of the structure and at the associated free-field station (SFF in Figure 1) are shown in Figure 3a. The motion at Yerba Buena Island (YBI), the closest rock site, had a peak acceleration of 0.06 g, and is also shown for comparison. The response spectra (Figure 3b) clearly demonstrate that the motions at Emeryville (SFF) were amplified by as much as five times when compared with YBI. This is also inferred by the amplitude of the peak accelerations (0.26 g for SFF and 0.06 g for YBI). Furthermore, the differences in peak acceleration at SFF (0.26 g) and at the ground floor of the building (0.21 g) (Fig. 3a) suggest the possibility of significant soil-structure interaction. Figure 3c shows a comparison of actual response spectra with site-specific design response spectra (based on the probabilistic earthquakes related to levels of performance) used in the design of the building: (a) the maximum probable earthquake (50 % probability of being exceeded in 50 years with 5 % damping) anchored at zero period acceleration (ZPA) of 0.32g. [curve A in Figure 3c], and two maximum credible earthquakes both with 10 % damping but 10 % probability of being exceeded in (b) 100 years (ZPA of 0.63 g) [Curve B in Fig. 3c] and (c) 50 years [ZPA of 0.53 g]<sup>2</sup>. The spectra of the EW components of recorded motions at the ground floor and SFF are also shown in Figure 3c. At 100 km from the epicenter, even though the recorded EW peak acceleration at SFF (0.26 g) is smaller than the ZPA of the postulated maximum probable earthquake (0.32 g), the spectral accelerations of the EW component of SFF is considerably higher than the maximum probable earthquake for periods >0.6 seconds – that is, practically the first three modes of the building. This implies that, when large earthquakes occur closer to the structure, the level of shaking and the response spectra of motions are likely to be higher (for some period bands) than the design response spectra, and, in many cases, the code design

response spectrum (e.g. the 1979 Uniform Building Code).

## 2.0 SUMMARY OF STUDIES RELATED TO THE BUILDING

### 2.1 Data Sets

Extensive data sets from this building include not only the Loma Prieta earthquake response data but also those from smaller earthquakes and from forced and ambient vibration tests (Stephen et al, 1985, Çelebi et al, 1993). Table 1 summarizes the events (including LPE) that have been recorded by the building array and are used in this study. Those related to LPE and test data are summarized in Table 2.

### 2.2 Pre-1991 Data sets including LPE and Studies

The building has been studied in detail or as part of a larger investigation by several researchers (Çelebi and Safak, 1992, Safak and Çelebi, 1992, Anderson et al, 1991, Bertero et al, 1992, Kagawa et al, 1993a, b, Aktan et al, 1992, Kambhatla et al, 1992, Çelebi, 1992, 1998). Using different methods, including spectral analyses, system identification techniques (Çelebi, 1998), and mathematical models, the majority of the investigators are in agreement that, for the 1989 Loma Prieta earthquake data, the predominant three response modes of the building and the associated frequencies (periods) are 0.38 Hz (2.63 s), 0.95 Hz (1.05 s), and 1.95 Hz (0.51 s). These three modes of the building are torsionally-translationally coupled (Çelebi, 1998) and are depicted in the cross-spectra ( $S_{xy}$ ) of the orthogonal records obtained from the roof, ground floor and SFF (the south free-field site) and the normalized cross-spectra of the orthogonal records (Figure 4). The site frequency at 0.7 Hz (1.43 s) observed in the cross-spectrum of the roof (Figure 4a) appears as the dominant peak in the cross-spectra of the ground floor and the south free-field (SFF) (Figure 4b and 4c). This site frequency has been also confirmed by the wave propagation method using site borehole data by Gibbs and others (1994) as shown in Figure 2. Justification of the site frequency as determined from this set of records are reported in Çelebi (2003).

<sup>2</sup> Not shown in the figure

Dynamic characteristics of the building extracted from the data sets are summarized in Table 2 and show considerable differences in the fundamental frequency determined from strong shaking versus low-amplitude shaking and analyses. The differences are attributed to SSI effects during strong shaking (Çelebi, 1998, Kagawa et al, 1993a, b, Aktan et al, 1992, Kambhatla et al, 1992), and frequencies from recorded motions can be matched when SSI is incorporated into the mathematical models (Kagawa et al, 1993a, b). Furthermore, a study of the building for dynamic-pile-group interaction (Aktan et al, 1992, Kambhatla et al, 1992) indicates that there is significant interaction. The study shows that computed responses of the building using state-of-the-art techniques for dynamic-pile-group interaction compares well with the recorded responses. Clearly, the mathematical models developed at that time needed improvements (Stephen et al, 1985). This conclusion could only be reached because we have recorded on-scale motions.

In addition, system identification techniques, when applied to the records of this building, yielded very large damping ratios corresponding to the 0.38-Hz first-mode frequency. These are 11.6 percent (north-south) and 15.5 percent (east-west) [Table 2] (Çelebi, 1996, 1998). Such unusually high damping ratios have been attributed to radiation damping that commonly occurs for buildings with large mat foundations in relatively soft geotechnical environment (Çelebi, 1996).

Anderson and others (1991) compared the design criteria, code requirements, and the elastic and nonlinear dynamic response of this building due to the earthquake. They also found the fundamental frequency of the building to be  $\sim 0.37$ - $0.39$  Hz. However, contrary to others, but based only on comparison of ground level motions with those at the free-field, they concluded that soil-structure interaction was insignificant for this building during this earthquake.

### 2.3 Recent Data, Analyses and Discussion

Analyses of subsequent data sets listed in Table 1 show that for shaking much lower than caused by

LPE, the fundamental frequency (period) is significantly lower (longer) than that determined using the LPE record. In Figure 5, for each of the 1998, 2000, 2003 and 2006 earthquakes (Table 1), plots of acceleration time history and corresponding amplitude spectra are shown for the 30<sup>th</sup> floor and ground floor of the building. Consistently, a structural fundamental frequency (period) of  $\sim 0.48$  Hz ( $\sim 2.08$  s) is identified. This identified frequency is also confirmed by system identification method. For the sake of brevity, only a sample system identification plot is presented for the 2006 event (Figure 6) which clearly shows the fundamental frequency at 0.48 Hz. For all events and tests to date, Table 3 summarizes the level of shaking (acceleration in g's) and identified dynamic characteristics (frequencies and damping ratios). These results are also graphically depicted in Figure 7. Both Table 3 and Figure 7 complements and reinforces the argument that the fundamental frequency varies significantly with the level of shaking even if the building may not be damaged. In the case of Pacific Park Plaza Building, the variation is attributable to SSI.

As noted in this paper, there is significant difference between the 0.38 Hz and 0.48 Hz frequencies (approximately 20% less for LPE if 0.48Hz is considered as the baseline and even more if 0.59 Hz is considered). In many studies, establishment of baseline frequency can be an issue and therefore ought to be carefully assessed to prevent erroneous interpretation. Another point to be made is that, in reaching the conclusions in this paper, most of the data analyses were made with data with time increments of 0.005 seconds. It was observed during the data analyses that overdecimating and oversmoothing the data can lead to significant differences in the assignments of values to the fundamental frequencies.

## 4.0 CONCLUSIONS

Recorded responses of structures serve to expose unusual and unexpected response characteristics that require detailed analyses in order to improve or validate analytical models and design processes and to identify possible methods for retrofit of the structure if necessary. Significant

findings, although not limited by the list below, are summarized as:

1. It is shown that there are significant differences in the fundamental frequencies of Pacific Park Plaza Building determined from strong shaking as compared to low-amplitude shaking. Thus, the variation of fundamental frequency (period) is dependent on the amplitude of shaking.
2. System identification procedures are very useful in extracting the dynamic characteristics; in particular, the modal damping ratios (for the defined level of shaking) which otherwise are difficult to determine as they are not constant and increase with the level of shaking.
3. Soil-structure interaction, although neglected in the design-analysis process of this building and as is also neglected for most non-critical buildings, plays a significant role in altering dynamic characteristics and therefore the response of buildings. For this building, the variation of the fundamental period (frequency) is quite substantial.

Additional conclusions may also be stated as:

4. As expected, higher modes are excited for this building during the earthquake events.
5. It is shown in this paper (as also in previous papers) for this building that the translational and torsional responses are coupled. This conclusion may be generalized for buildings with irregularities.
6. In certain cases, as for this building, response spectra of recorded motions exceed design response spectra within some (lower) frequency bands that include structural frequencies. In determination of design response spectra, effect of lower frequency ground motions must be taken into account.
7. Finally, particularly in areas of high seismicity, deployment of seismic monitoring systems particularly for complex and irregular buildings and other types of structures are strongly

encouraged since records obtained during future events reveal response characteristics that are not always envisioned or taken into account during design and analysis processes.

## 5.0 REFERENCES

- Aktan, H., Kagawa, T., Kambhatla, A., and Çelebi, M.(1992). "Measured and analytical response of a pile supported building," in Proceedings, Tenth World Conference on Earthquake Engineering: A.A.Balkema, Rotterdam, v. 3, p. 1791-1796.
- Anderson, J.C., Miranda, E., and Bertero, V.V., and Kajima Project Research Team. 1991, "Evaluation of the seismic performance of a thirty-story RC building", Earthquake Engineering Research Center, University of California, Berkeley, Report: UCB/EERC-91/16, 254 p.
- Bertero, V.V., Miranda, E., and Anderson, J.C.(1992)."Evaluation of seismic response of two RC buildings," in Structures Congress '92 compact papers: American Society of Civil Engineers, New York, p. 408- 411.
- Calvi, G. M., Pinho, R., and Crowley, H., 2006, "State-of-the-knowledge on the period elongation of RC buildings during strong ground shaking", PROC (CD) First European Conference on Earthquake Engineering and seismology, Geneva, Switzerland, 3-8 Sept. 2006.
- Çelebi, M.(1992). "Highlights of Loma Prieta responses for four tall buildings", in Proceedings, of the Tenth World Conf. on Earthquake Engineering, A.A. Balkema, Rotterdam, v. 7, p. 4039-4044.
- Çelebi, M., and Şafak, E.(1992)."Recorded Seismic Response of Pacific Park Plaza: Part I--Data and Preliminary Analysis." ASCE Journal of Structural Engineering, June 1992.
- Çelebi, M., Phan, L. T., and Marshall, R. D.(1993). "Dynamic characteristics of five tall buildings during strong and low-amplitude motions," Journal of the Structural Design of Tall Buildings (John Wiley & Sons), v. 2, 1-15, 1993.
- Çelebi, M.(1996). "Comparison of damping in buildings under low-amplitude and strong motions", Journal of Wind Engineering and Industrial Aerodynamics, 59, pp. 309-323.
- Çelebi, M., 1998, "Performance of Building structures - A Summary", in The Loma Prieta, California, Earthquake of October 17, 1989 -

- Building Structures (M. Çelebi, editor), USGS Prof. Paper 1552-C, p. c5-c76.
- Çelebi, M., 2003, "Identification of Site Frequencies from Building Records", Journal of EERI, *Earthquake Spectra*, v.19, Issue 1, pp.1-23.
- Clinton, J. F., Bradford, S. C., Heaton, T. H., and Favela, J., 2006, "The Observed Wander of the Natural Frequencies in a Structure", Bull. Seism. Soc. of Am. , v.96, no.1, pp 237-257, Feb. 2006.
- Dunand, F., Guegen, P., Bard, P-Y, Rodgers, J., and Celebi, M., 2006, "Comparison of the dynamic parameters extracted from weak, moderate and strong motion recorded in buildings", PROC (CD) First European Conference on Earthquake Engineering and seismology, Geneva, Switzerland, 3-8 Sept. 2006.
- Gibbs, J. F., Fumal, T. E., and Powers, T. J.(1994). Seismic velocities and geologic logs from borehole measurements at seven strong motion stations that recorded the 1989 Loma Prieta, California, earthquake: U.S. Geological Survey Open-File Report 94-222, 104 p.
- Haskell, N. A.(1953). "The dispersion of surface waves on multilayered media", Bulletin of the Seismological Society of America, v. 43, no. 1, p. 17-34.
- Haskell, N. A.(1960). "Crustal reflection of plane SH waves", Journal of Geophysical Research, v. 65, no. 12, p. 4147-4150.
- International Conference of building Officials (1979), Uniform Building Code [1979 Edition]: Whittier, California.
- Kagawa, T., Aktan, H., Çelebi, M.(1993). "Evaluation of soil and structure model using measured building response during the Loma Prieta earthquake": Report of the Dept. of Civil Engineering, Wayne State University, Detroit, Michigan, 169 p.
- Kagawa, T., and Al-Khatib, M. A.(1993). "Earthquake response of a 30-story building during the Loma Prieta earthquake", in Third Int'l Conf. On Case Histories of Geotechnical Engineering, Univ. of Missouri-Rolla, p. 547-553.
- Kambhatla, A., Aktan, H. M., Kagawa, T. and Çelebi, M.(1992)."Verification of simple soil-pile foundation-structure models," in Structures Congress '92, ASCE, NY, p.721-724.
- Şafak, E., and Çelebi, M. (1992). "Recorded Seismic Response of Pacific Park Plaza: Part II--System Identification." ASCE Journal of Structural Engineering, June 1992.
- Stephen, R., M., Wilson, E.L., and Stander, N., 1985, Dynamic properties of a thirty-story condominium tower building: Univ. of California, Berkeley, EERC Report 85-03, 100p.
- Todorovska, M., Trifunac, M., and Hao, T-Y, 2006, "Variation of apparent Building Frequencies - Lessons from Full-Scale Earthquake Observation," PROC (CD) First European Conference on Earthquake Engineering and seismology, Geneva, Switzerland, 3-8 Sept. 2006.

Table 1. Events that have been recorded by the PPP arrays

Event/ Date	UTC	Lat. (N)/ Long. (E)	Dist. (km)	Azim. (deg)	Depth (km)	Mag.
Loma Prieta 10/18/1989	04:15	37.036 -121.883	96	157	18.0	M <sub>s</sub> 6.9
El Cerrito 12/04/1998	12:16	37.920 -122.290	9	4	6.8	M <sub>w</sub> 4.0
Yountville 09/03/2000	08:36	38.379 -122.413	61	350	10.1	M <sub>w</sub> 5.0
Piedmont 09/05/2003	01:39	37.845 -122.222	7	85	12.4	M <sub>w</sub> 3.9
Berkeley 03/02/2006	06:08	37.863 -122.245	5	96	11.4	M <sub>d</sub> 2.8

Table 2. Peak Accelerations and System Identification Results for (Pre-1991) PPP Data

Peak Accelerations (A[g])				
	Loma Prieta Eq. (1989) [See Refs]		Low-Amp. Tests & Analyses [See Refs]	
	NS	EW	NS	EW
Roof	0.24	0.38	<0.01	<0.01
Gr. Fl.	0.17	0.21	<0.01	<0.01
FF	0.21	0.26	-	-
Dynamic Characteristics (System Identification)				
f <sub>0</sub> (Hz)	0.38	0.38	0.48-0.59	
T <sub>0</sub> (s)	2.63	2.63	1.69-2.08	
ξ(%)	11.6	15.5	0.6-3.4	

Table 3. Summary - Events, Levels of Shaking (in g's) and Identified Dynamic Characteristics

Tests, Analyses or Events												
	1985 Tests/ analyses	1989 LPE		1990 Tests	1998 EQ. (1204_ 1216)		2000 EQ. (0903- 0836)		2003 EQ (0905_ 0139)		2006 EQ (0302_ 0608)	
Peak Accelerations (A[g]) [NS & EW represents 350° and 260° respectively]												
	NS/EW	NS	EW	NS/EW	NS	EW	NS	EW	NS	EW	NS	EW
Roof	<0.01	0.24	0.38	<0.01	.025	.016	.01	.007	.056	.067	.004	.003
Gr.Fl.	<0.01	0.17	0.21	<0.01	.016	.037	.005	.004	.037	.041	.003	.003
SFF	-	0.21	0.26	-	.022	.028	-	-	.039	.031	.003	.006
Dynamic Characteristics (System Identification & Spectral Analyses)												
f <sub>0</sub> (Hz)	0.59	0.38	0.38	0.48	.48	.48	.48	0.48	0.48	0.48	0.48	0.48
T <sub>0</sub> (s)	1.69	2.63	2.63	2.08	2.08	2.08	2.08	2.08	2.08	2.08	2.08	2.08
ξ(%)	.6-3.4	11.6	15.5	.6-3.4	-	-	-	-	.5-2.	.5-2.	.5-2.	.5-2.



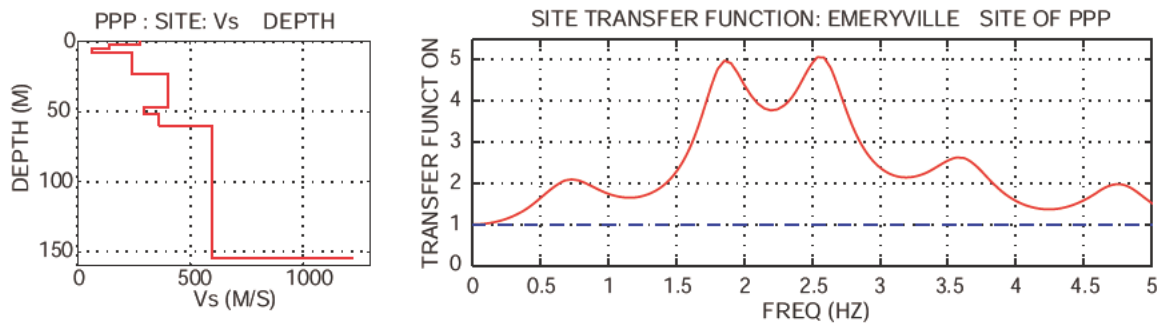


Figure 2. Shear-wave velocity profile and the computed site transfer function. 0.7 Hz is the fundamental frequency and other peaks belong to higher modes.

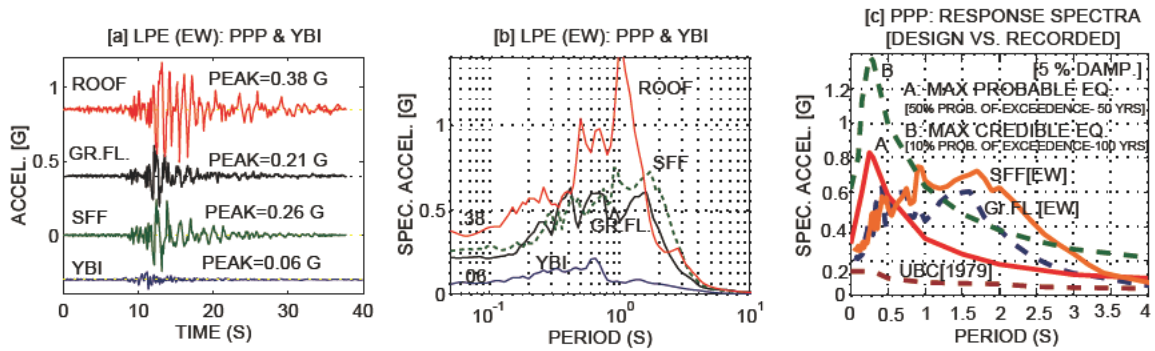


Figure 3. (a,b) Amplified (EW) motions and their corresponding response spectra (5% damped) at the South Free-Field (SFF), ground floor and roof of the Pacific Park Plaza array as compared to the motions at Yerba Buena Island (YBI) at approximately the same epicentral distance as PPP. (c) Design response spectra and response spectra of recorded motions at the ground floor and SFF of Pacific Park Plaza. Also shown is the 1979 UBC response spectrum for comparison. [Note: Curve B is for 10% damping].

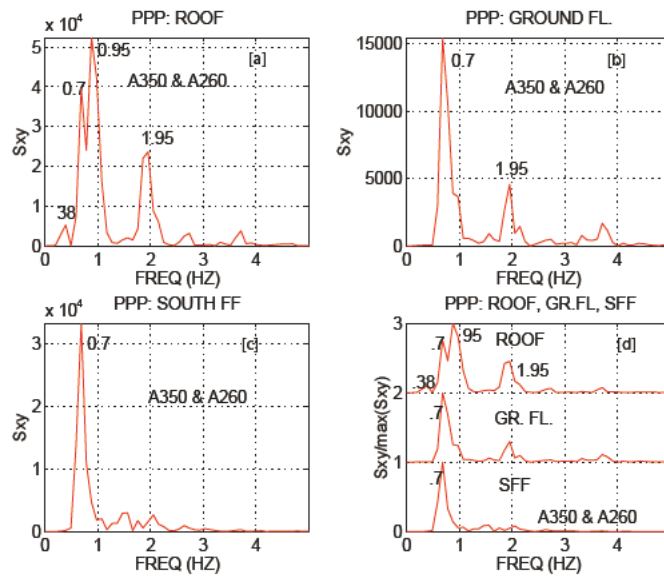


Figure 4. Cross-spectra of orthogonal motions at the [a] roof, [b] ground floor, [c] free-field of PPP, and [d] the normalized cross-spectra depicting structural and site frequency peaks.

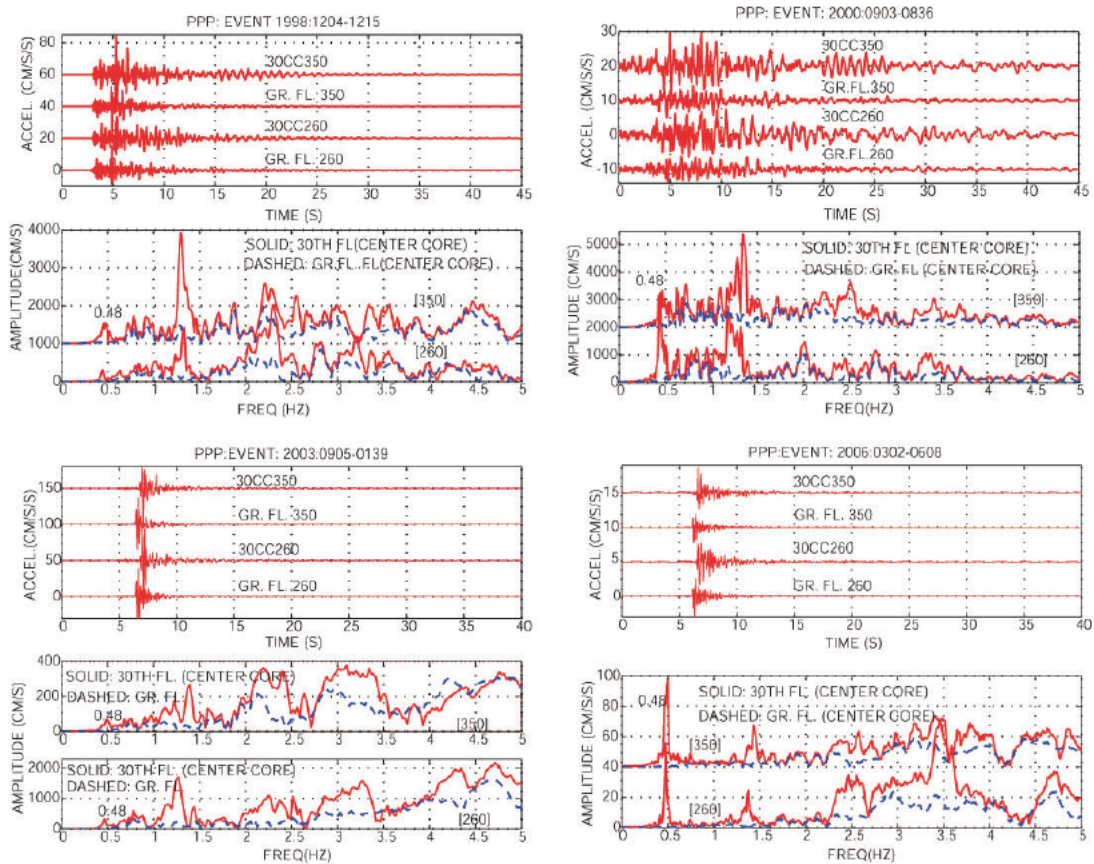


Figure 5. Recorded accelerations at 30<sup>th</sup> and ground floors and corresponding amplitude spectra.

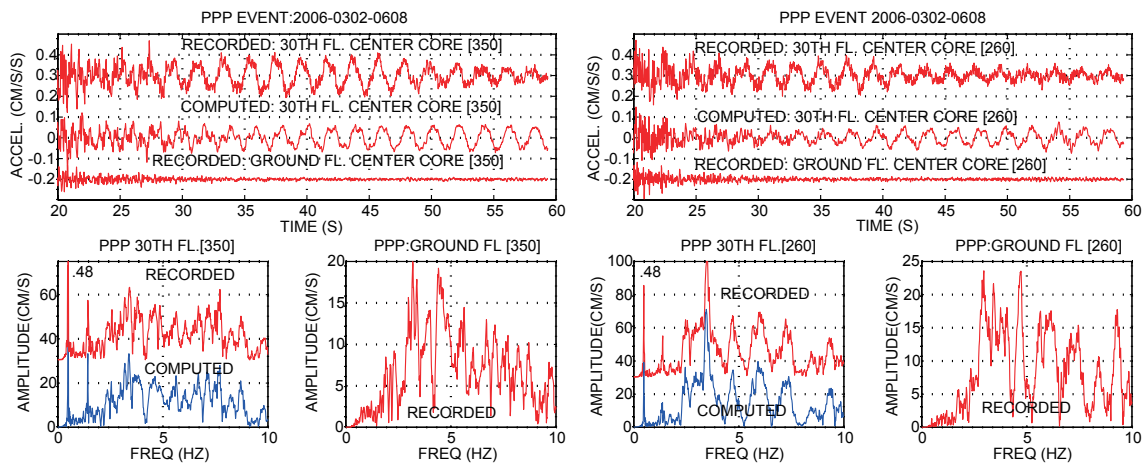


Figure 6. System identification for 2006 event using 40-second window of acceleration data. Ground level motions are used as input and 30<sup>th</sup> floor motions are used as output.

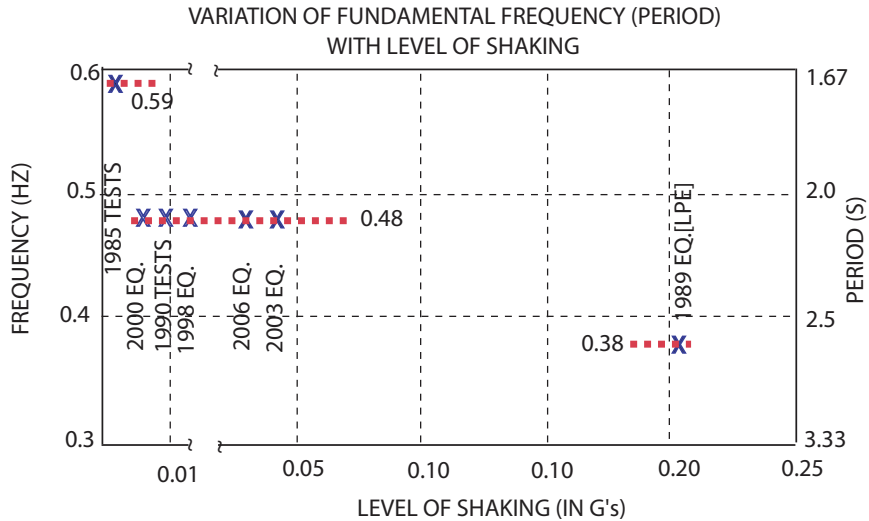


Figure 7. Plot showing variation of fundamental frequency with level of shaking (in g's).

# System Dynamics Modeling and Simulation of Disaster Recovery Process of Interdependent Infrastructure Systems

by

Shojiro Kataoka<sup>1</sup>

## ABSTRACT

A simulation model is developed for disaster recovery process of infrastructure systems. The model is based on the system dynamics and the interdependency among infrastructures is taken into account. Disaster recovery process of the infrastructure system in the Tokyo metropolitan area, where the infrastructures are highly interdependent, is simulated using the model and the effects of the interdependency are investigated.

**KEYWORDS:** Infrastructure System, Influence Diagram, System Dynamics, Interdependency

## 1. INTRODUCTION

Infrastructures such as roads, railroads, electric power, gas, and water supplies, sewerage, and telecommunications are vital for our daily lives and industrial activities. Natural and human disasters, however, have damaged the infrastructures and the damage has caused social and economic losses from time to time. The longer the disaster recovery takes, the larger the losses become; thus, prompt recovery is important to mitigate the losses.

Since the infrastructures are interdependent and compose a highly complex system, especially in urban areas, damage to one of the infrastructures may affect the others (damage spreading). For example, if the electric power supply is damaged, the road traffic capability is deteriorated until the electric power recovers traffic lights. If the gas supply and the road network are damaged, the recovery of the gas supply is delayed because road traffic is necessary for the recovery works.

Tsuruta *et al.* (2008) surveyed interdependency of the infrastructure system during past disasters

and developed a damage propagation model based on matrix equation [1]. Though the case study simulation using the model successfully demonstrated the earthquake damage spreading among infrastructures, dynamic behavior such as recovery process of the infrastructure system was not investigated.

In this study, the disaster recovery process of the infrastructure systems is modeled based on the system dynamics and the time history of the recovery process from a hypothetical earthquake (M7.3) in the Tokyo metropolitan area is simulated taking account of the interdependency.

## 2. SYSTEM DYNAMICS MODELING

First, the functions and components of infrastructures and their relationships are organized as influence diagrams. A base model that shows relationships among facilities, resources, and infrastructures necessary for disaster recovery is developed for each of infrastructures. Then the base models are assembled into a system dynamics model of disaster recovery process of the infrastructure system. The details of the modeling are described in Kataoka *et al.* (2009).

The influence diagrams illustrate the functions and components of infrastructures and their relationships; the diagram of the gas supply system is shown in Fig. 1 as an example. The gas supply system consists of many facilities but only the low pressure pipes are assumed to be damaged during earthquakes. Not only the facilities managed by gas suppliers but also the electric power are necessary to maintain the gas supply function.

---

<sup>1</sup> Senior Researcher, Earthquake Disaster Prevention Division, National Institute for Land and Infrastructure Management, Tsukuba 305-0804, Japan

Then, based on the influence diagrams, the base models are developed taking account of facilities, resources, and infrastructures that are necessary for disaster recovery. For example, the base model of the gas supply system is developed as shown in Fig. 2. The road traffic and telecommunication functions are considered necessary for the disaster recovery of the gas supply function. Since the electric power is required to maintain the gas supply function, either backup electric power or physical recovery of substations is necessary for the recovery of the system.

The system dynamics model is constructed by assembling the base models of all infrastructures. Given the initial damage to the infrastructures, the disaster recovery process of the whole infrastructure system can be simulated using the model.

### 3. SIMULATION CASE STUDY

Disaster recovery process of the infrastructure system in the Tokyo metropolitan area, where the infrastructures are highly interdependent, is simulated using the system dynamics model.

#### 3.1 Initial Damage and Interruption

Central Disaster Management Council (CDMC) announced the estimated damage due to Tokyo metropolitan earthquakes in 2005 [3]. The most disastrous one is the hypothetical northern Tokyo Bay earthquake (M7.3), which causes strong ground motion with JMA seismic intensity of 6 upper in the eastern half area of the 23 special wards of Tokyo as shown in Fig. 3. Following CDMC, Tokyo Metropolitan Government (TMG) also conducted estimation of damage caused by the earthquake [4]. In this study, the damage to the infrastructures estimated by TMG is used as the initial damage in the simulation. Table 1 shows the damage in Chiyoda and Sumida wards and the 23 wards in total.

Railroads are ordered a halt for inspection just after earthquakes even though no damage is reported. Road traffic is also controlled and only emergency vehicles can be admitted to path

through disaster areas. Thus, the initial interrupted ratios are assumed as follows:

- 100% for the railroad network (all lines are once halted for inspection of the damage),
- 0% everywhere for emergency vehicles,
- 100% in “the road traffic prohibited area” and 50 % in the other area with seismic intensity of 6 upper for non-emergency vehicles.

Once a Tokyo metropolitan earthquake occurs, Metropolitan Police Department regulates the traffic so that non-emergency vehicles are prohibited to pass through “the road traffic prohibited area”, which covers 75% of the area of the 23 special wards. In this study, the traffic regulation is assumed to last for 10 days.

#### 3.2 Recovery Rate without Interdependency

CDMC surveyed the recovery rates of the infrastructures based on interviews and obtained the following results [3]:

- 95% of electric power recovers in 6 days,
- 95% of telecommunications recovers in 14 days,
- 80% of gas supply recovers in 55 days,
- 95% of water supply recovers in 30 days,
- 95% of sewerage pipes recover in 30 days.

The recovery rates for railroads and roads are assumed as follows:

- 100% of railroads are available in 1 day in the area with seismic intensity of 5 upper (no damage and only inspection),
- 90% of railroads are available in 1 day, then 95% recover in 5 days in the area with seismic intensity of 6 lower,
- 80% of railroads are available in 1 day, then 95 % recover in 15 days in the area with seismic intensity of 6 upper,
- 95% of roads recover in 18 days in the area with seismic intensity of 6 upper.

These rates are assumed to be those when the recovery process is not influenced by the interdependency among infrastructures and used as initial recovery rates. For example, the “recovery rate of low pressure pipe” in Fig. 2 is set to be the recovery rate of the gas supply mentioned above.

### 3.3 Simulation Results

Fig. 4 shows the time histories of recovered ratios of the infrastructures in Chiyoda and Sumida wards. In this simulation, 10% of the vehicles used for the disaster recovery work are assumed to be the emergency vehicles. Thus, 90% of them are affected by the traffic regulation or interruption. The recovery of the infrastructures is delayed significantly compared with the recovery rates mentioned in 3.2. The delays are longer in Sumida wards because it suffers greater damage than Chiyoda wards (Table 1).

Fig. 5 is the same as Fig. 4 but 90 % of the vehicles used for the disaster recovery work are assumed to be the emergency vehicles. In Fig. 5, the delays still exist but much shorter than those in Fig. 4. To achieve this improvement, road facilities must not collapse during earthquakes so that the road networks maintain the traffic at least for emergency vehicles.

### 4. CONCLUSIONS

A simulation model is developed to investigate the effects of the interdependency among infrastructures on the recovery process of the infrastructure system. The simulation case

study shows the importance of smooth traffic of emergency vehicles for prompt disaster recovery of the highly interdependent infrastructure systems.

Further research and investigation are needed to improve accuracy and actuality of the simulation model and data in order to discuss the simulation results quantitatively.

### 5. REFERENCES

1. Tsuruta, M., Goto, Y., Shoji, Y. and Kataoka, S.: Damage propagation caused by interdependency among critical infrastructures, *14th World Conference on Earthquake Engineering*, 2008.
2. Kataoka, S., Tsuruta, M. and Shoji, Y.: Model development of interdependency among critical infrastructures and simulation of earthquake damage spreading, *Technical Note of National Institute for Land and Infrastructure Management*, No. 510, 2009.
3. Central Disaster Management Council: Documents of the 15th Tokyo metropolitan earthquake disaster management council, 2005.
4. Tokyo Metropolitan Government: Estimated damage in Tokyo due to the Tokyo metropolitan earthquakes, 2006.



Fig. 1 Influence diagram of the gas supply system.

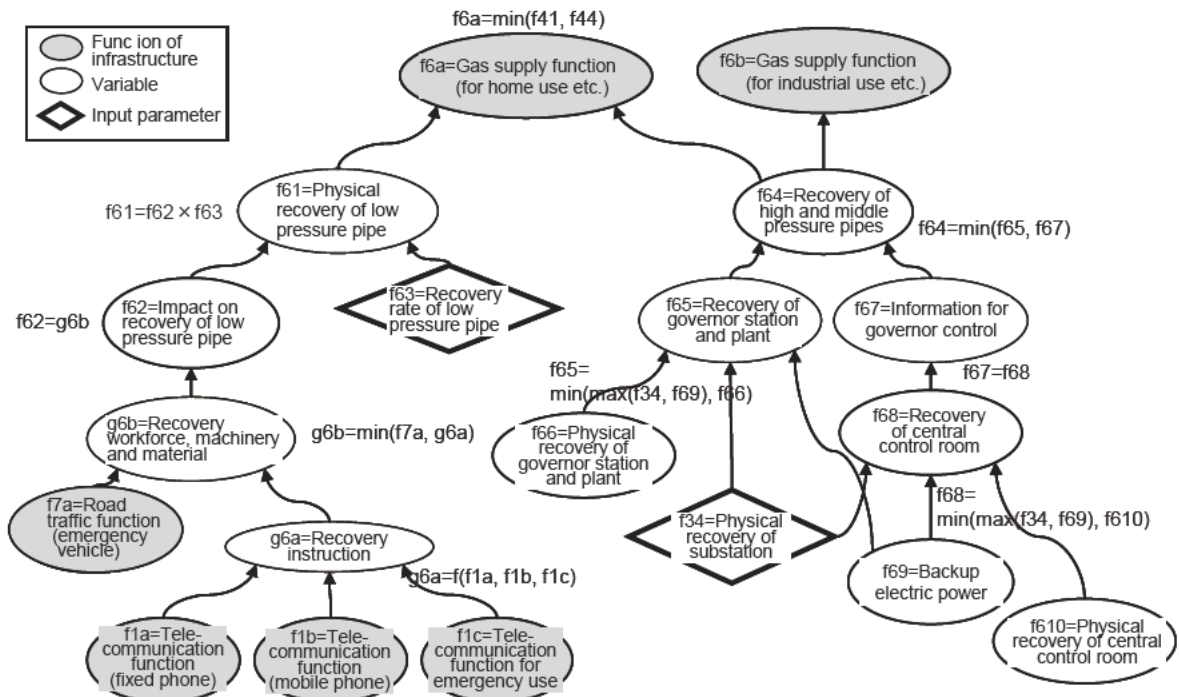


Fig. 2 Base model showing relationships among facilities, resources, and infrastructures necessary for disaster recovery of the gas supply system.

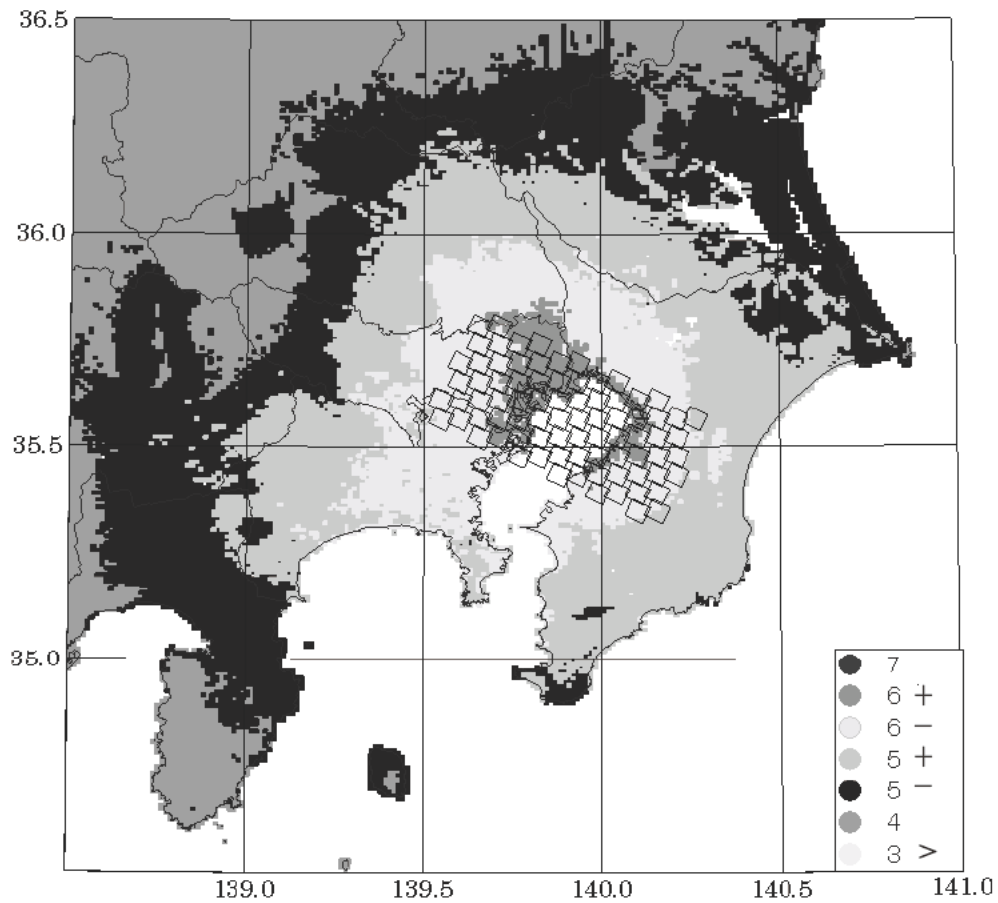


Fig. 3 Map of Kanto region showing JMA seismic intensity due to the northern Tokyo Bay earthquake (M7.3) and its source fault (Central Disaster Management Council, 2005)[3].

Table 1 Estimated damage to infrastructures caused by the northern Tokyo Bay earthquake (M7.3) in Chiyoda and Sumida wards and the 23 wards in total (Tokyo Metropolitan Government, 2006)[4].

Wards	Electric power supply (power failure ratio)	Telecommunications (interrupted ratio)	Gas supply (cut off ratio)	Water supply (cut off ratio)	Sewerage (ratio of damaged pipe)
Chiyoda	6.1%	0.9%	59.4%	37.4%	23.3%
Sumida	48.6%	17.6%	100.0%	79.5%	31.8%
23 wards total	22.9%	13.2%	22.9%	46.3%	25.4%

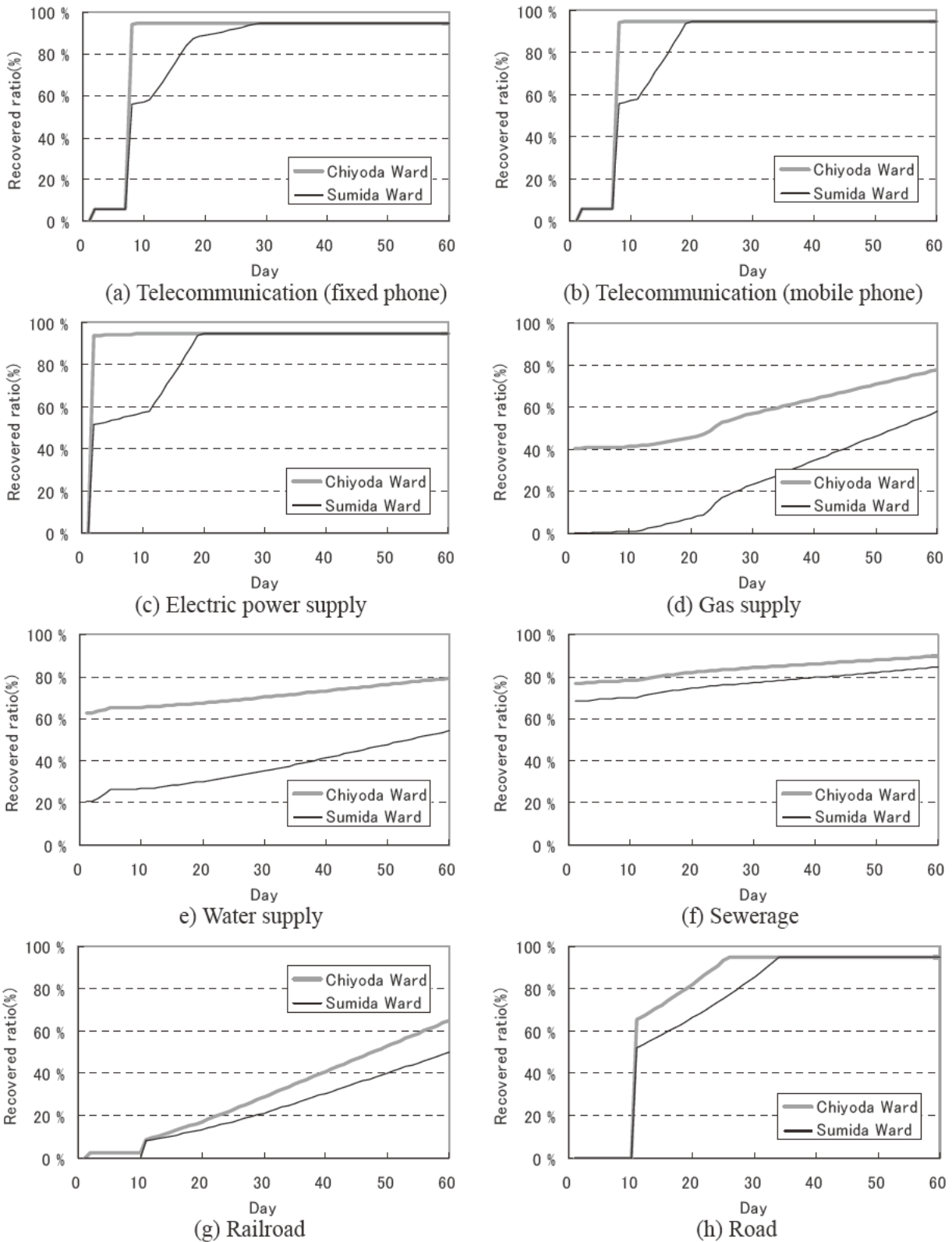


Fig. 4 Time histories of recovered ratios of the infrastructures in Chiyoda and Sumida Wards. 10% of the vehicles used for disaster recovery work are assumed to be the emergency vehicles.

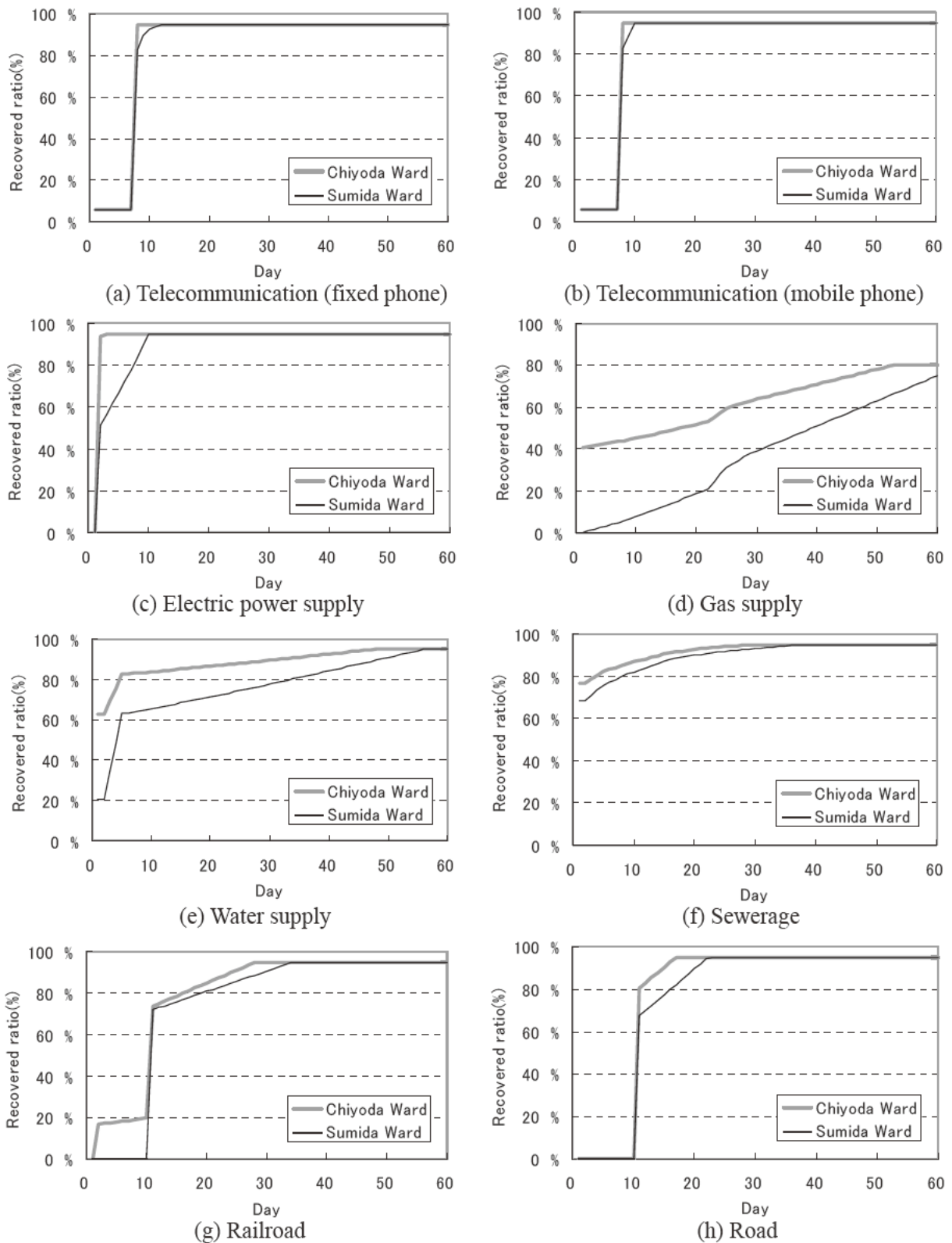


Fig. 5 Time histories of the recovered ratios of the infrastructures in Chiyoda and Sumida Wards. 90% of the vehicles used for disaster recovery work are assumed to be the emergency vehicles.

# Modal-Pushover-based Ground Motion Scaling Procedure for Nonlinear Analysis of Structures

by

Erol Kalkan<sup>1</sup> and Anil K. Chopra<sup>2</sup>

## ABSTRACT

Earthquake engineering practice is increasingly using nonlinear response history analysis (RHA) to demonstrate performance of structures. This rigorous method of analysis requires selection and scaling of ground motions appropriate to design hazard levels. Presented herein is a modal-pushover-based scaling (MPS) method to scale ground motions for use in nonlinear RHA of buildings. In the MPS method, the ground motions are scaled to match (to a specified tolerance) a target value of the inelastic deformation of the first-mode inelastic SDF system whose properties are determined by first-mode pushover analysis. Appropriate for first-mode dominated structures, this approach is extended for structures with significant contributions of higher modes by considering elastic deformation of higher-mode SDF systems in selecting a subset of the scaled ground motions. Based on results presented for three actual buildings—4-story, 6-story, and 13-story—the accuracy and efficiency of the MPS procedure are established and its superiority over the ASCE-7 scaling procedure is demonstrated.

**KEYWORDS:** nonlinear analysis; seismic effects; drift; performance-based earthquake engineering.

## 1.0 INTRODUCTION

The maximum span of long-span bridges has been Seismic evaluation of existing structures and of proposed design of new structures is usually based

on nonlinear static (or pushover) analysis procedures, but nonlinear response history analysis (RHA) is now being increasingly used. In the latter approach, the seismic demands are determined by nonlinear RHA of the structure for several ground motions. Procedures for selecting and scaling ground motion records for a site-specific hazard are described in building codes and have been the subject of much research in recent years.

Current performance-based design and evaluation methodologies prefer intensity-based methods to scale ground motions over spectral matching techniques that modify the frequency content and/or phasing of the record to match its response spectrum to the target spectrum. In contrast, intensity-based scaling methods preserve the original non-stationary content and only modify its amplitude. The primary objective of intensity-based scaling methods is to provide scale factors for a small number of ground motion records so that nonlinear RHA of the structure for these scaled records is accurate, i.e., it provides an accurate estimate in the median value of the engineering demand parameters (EDPs), and is efficient, i.e., it minimizes the record-to-record variations in the EDP. Scaling ground motions to match a target value of peak ground acceleration (PGA) is the earliest approach to the problem, which produces inaccurate estimates with large dispersion in EDP values for structures responding in nonlinear range [Nau and Hall 1984; Miranda 1993; Vidic et al. 1994; Shome and Cornell 1998]. Other scalar intensity measures (IMs) such as: effective peak acceleration, Arias intensity and effective peak velocity have also been found to be inaccurate and

---

<sup>1</sup> Senior Research Engineer, United States Geological Survey, Menlo Park, CA 94025, USA

<sup>2</sup> Professor, Dept. of Civil and Env. Engineering, University of California, Berkeley, CA 94720, USA

inefficient [Kurama and Farrow 2003]. None of the preceding IMs consider any property of the structure to be analyzed.

Including a vibration property of the structure led to improved methods to scale ground motions, e.g., scaling records to a target value of the elastic spectral acceleration,  $A(T_1)$  from the code-based design spectrum or PSHA-based uniform hazard spectrum at the fundamental vibration period of the structure,  $T_1$ , provides improved results for structures whose response is dominated by their first-mode [Shome et al. 1998]. However, this scaling method becomes less accurate and less efficient for structures responding significantly in their higher vibration modes or far into the inelastic range [Mehanny 1999; Alavi and Krawinkler 2000; Kurama and Farrow 2003]. To consider higher mode response, a scalar IM that combines the spectral accelerations  $A(T_1)$  and  $A(T_2)$  at the first two periods and vector IM comprised of  $A(T_1)$  and the ratio of  $A(T_1)/A(T_2)$  have been developed [Bazzurro 1998; Shome and Cornell 1999]. Although this vector IM improves accuracy, it remains inefficient for near-fault records with a dominant velocity pulse [Baker and Cornell 2006].

To recognize the lengthening of the apparent period of vibration due to yielding of the structure, a scalar IM defined as a combination of  $A(T_1)$  and  $A(cT_1)$  where  $c > 1$ , has been considered [Mehanny 1999; Cordova et al. 2000]; alternatively, scaling earthquake records to minimize the difference between its elastic response spectrum and the target spectrum has been proposed [Kennedy et al. 1984; Malhotra 2003; Alavi and Krawinkler 2004; Naeim et al. 2004; Youngs et al. 2007].

International Building Code (IBC) [ICBO 2006] and California Building Code (CBC) [ICBO 2007] require that earthquake records be scaled according to the ASCE-7 provisions [ASCE 2005]. For two dimensional analyses of regular structures, ground motions are scaled such that the average value of the 5%-damped elastic response

spectra for a set of scaled motions is not less than the design response spectrum over the period range from  $0.2T_1$  to  $1.5T_1$ . For structures having plan irregularities or structures without independent orthogonal lateral load resisting systems, where three-dimensional analyses need to be performed, ground motions should consist of appropriate horizontal components.

All the preceding scaling methods utilize IMs based on elastic response of the structure, but do not explicitly consider its inelastic response. They lead to scale factors that depend only on the structural period(s), independent of the structural strength. The elastic-response-based IMs may not be appropriate for near-fault sites where the inelastic spectral deformation can be significantly larger than corresponding elastic spectral deformation [Bozorgnia and Mahin 1998; Alavi and Krawinkler 2000; Baez and Miranda 2000; Chopra and Chintanapakdee 2004]. This limitation has been overcome in recently proposed IMs based on the inelastic deformation spectrum, leading to improved estimate of the median EDPs, and reduced dispersion of EDPs [Bazzurro and Luco 2004; Luco and Cornell 2007]. Based on incremental dynamic analyses response of generic frames to different intensity levels of near-fault ground motions demonstrated that scaling records with the IM defined as the inelastic deformation of the first-mode inelastic SDF system is accurate, efficient and sufficient compared to elastic-response-based IMs [Tothong and Luco 2007; Tothong and Cornell 2008]. Required in this approach are attenuation relationships for the inelastic deformation with given ground motion properties (magnitude, closest fault distance, site condition, etc.) and mean rate of occurrence of that hazard level [Tothong and Cornell 2008].

The objective of this paper is to develop a new method for selecting and scaling earthquake ground motion records in a form convenient for evaluating existing structures or proposed designs for new structures. The procedure presented explicitly considers structural strength and is based on the standard IM of spectral acceleration that is available from the USGS seismic hazard maps, where it is mapped for periods of 0.2 s and 1.0 s for the entire U.S. to facilitate construction of site-

specific design spectrum [Petersen et al. 2008], or it can be computed from the uniform hazard spectrum obtained by probabilistic seismic hazard analysis (PSHA) for the site.

Based on modal pushover analysis, the procedure presented herein explicitly considers the strength of the structure, obtained from the first-mode pushover curve and determines scaling factors for each record to match a target value of the deformation of the first-mode inelastic SDF system estimated by established procedures. Appropriate for first-mode dominated structures, this approach is extended for structures with significant contributions of higher modes. Based on results presented for three actual buildings—4-, 6-, and 13-story—the effectiveness of this scaling procedure is established and its superiority in terms of accuracy and efficiency over the ASCE-7 procedure is demonstrated.

## 2.0 MODAL-PUSHOVER-BASED SCALING

In the modal pushover-based scaling (MPS) procedure, each ground motion record is scaled by a scale factor selected to ensure that the peak deformation of the first-mode inelastic SDF system due to the scaled record is close enough to a target value of the inelastic deformation. The force-deformation relation for the first-mode inelastic SDF system is determined from the first-mode pushover curve. The target value of the inelastic deformation is the median deformation of the inelastic SDF system for a large ensemble of (unscaled) earthquake records compatible with the site-specific seismic hazard conditions. Nonlinear RHA of the inelastic SDF system provides the peak deformation of the system to each record in the ensemble, and the median of the data set provides the target value. Alternatively, the median deformation of the inelastic SDF system can be estimated as the deformation of the corresponding linearly elastic system, known directly from the target spectrum, multiplied by the inelastic deformation ratio; empirical equations for this ratio are available for systems with known yield-strength reduction factor [e.g., Ruiz-Garcia and Miranda 2002; Chopra and Chintanapakdee 2004].

For first-mode dominated structures, scaling earthquake records to the same target value of the inelastic deformation is expected to be sufficient. Because higher vibration modes are known to contribute significantly to the seismic response of mid-rise and high-rise buildings, the MPS procedure checks for higher-mode compatibility of each record by comparing its scaled elastic spectral displacement response values at higher-mode vibration periods of the structure against the target spectrum. This approach ensures that each scaled earthquake record satisfies two requirements: (1) the peak deformation of the first-mode inelastic SDF system is close enough to the target value of the inelastic deformation; and (2) the peak deformation of the higher-mode (i.e., second-mode) elastic SDF system is not far from the target spectrum.

### 2.1 MPS Procedure: Summary

The MPS procedure is summarized below in a step-by-step form:

1. For the given site, define the target pseudo-acceleration response spectrum either as the PSHA-based uniform hazard spectrum, or code-based design spectrum, or the median pseudo-acceleration spectrum for a large ensemble of (unscaled) earthquake records compatible with the site-specific seismic hazard conditions.
2. Compute the frequencies  $\omega_n$  (periods  $T_n$ ) and  $\phi_n$  of the first few modes of elastic vibration of the structure.

#### First-mode Dominated Structures

3. Develop the base shear-roof displacement  $V_{b1}-u_{r1}$  relation or pushover curve by nonlinear static analysis of the structure subjected to gradually increasing lateral forces with an invariant force distribution  $s_1^* = \mathbf{m}\phi_1$ , associated with the first-mode, where  $\mathbf{m}$  is the structural mass matrix. Gravity loads, including those present on the interior (gravity) frames, are applied before starting the pushover analysis.

4. Idealize the pushover curve and select a hysteretic model for cyclic deformations, both appropriate for the structural system and materials [Han and Chopra 2005; Bobadilla and Chopra 2007]. Determine the yield-strength reduction factor  $R_y$  (equals strength required for the structure to remain elastic divided by the yield strength of the structure) from:  $R_y = M_1^* \bar{A}_1 / V_{b1y}$ , where  $M_1^*$  is the effective modal mass and  $V_{b1y}$  is the yield point value of base shear determined from the idealized pushover curve.
5. Convert the idealized pushover curve to the force-deformation  $F_{s1}/L_1 - D_1$  relation of the first-mode inelastic SDF system by utilizing  $F_{s1}/L_1 = V_{b1} / M_1^*$  and  $D_1 = u_{r1} / \Gamma_1 \phi_{r1}$  in which  $L_1 = \phi_1^T \mathbf{m} \mathbf{1}$ ,  $\phi_{r1}$  is the value of  $\phi_1$  at the roof,  $\Gamma_1 = (\phi_1^T \mathbf{m} \mathbf{1}) / (\phi_1^T \mathbf{m} \phi_1)$  and each element of the influence vector  $\mathbf{1}$  is equal to unity.
6. For the first-mode inelastic SDF system, establish the target value of deformation  $\bar{D}_1'$  from  $\bar{D}_1' = C_R \bar{D}_1$ , where  $\bar{D}_1 = (T_1/2\pi)^2 \bar{A}_1$  and  $\bar{A}_1$  is the target pseudo-spectral acceleration at period  $T_1$ , and  $C_R$  is determined from an empirical equation (shown in the next section) for the inelastic deformation ratio corresponding to the yield-strength reduction factor  $R_y$ , determined in Step 4.
7. Compute the peak deformation  $D_1' = \max |D_1(t)|$  of the first-mode inelastic SDF system defined by the force deformation relation developed in Steps 4 and 5, and damping ratio  $\zeta_1$ . The initial elastic vibration period of the system is  $T_1 = 2\pi (L_1 D_{1y} / F_{s1y})^{1/2}$ . For a SDF system with known  $T_1$  and  $\zeta_1$ ,  $D_1'$  can be computed by nonlinear RHA due to one of the selected ground motions  $\ddot{u}_g(t)$

multiplied by a scale factor  $SF$ , to be determined to satisfy Step 8, by solving

$$\ddot{D}_1 + 2\zeta_1 \omega_1 \dot{D}_1 + F_{s1} [D_1, \dot{D}_1] / L_1 = -(SF) \ddot{u}_g(t) \quad (1)$$

8. Compare the normalized difference between the target value of the deformation  $\bar{D}_1'$  of the first-mode inelastic SDF system (Step 6) and the peak deformation  $D_1'$ , determined in Step 7 against a specified tolerance,  $\varepsilon$

$$\Delta_1 = |\bar{D}_1' - D_1'| / \bar{D}_1' < \varepsilon \quad (2)$$

9. Determine the scale factor  $SF$  such that the scaled record  $(SF) \ddot{u}_g(t)$  satisfies the criterion of Eq. (2). Because Eq. (1) is nonlinear,  $SF$  cannot be determined *a priori*, but requires an iterative procedure starting with an initial guess. Starting with  $SF = 1$ , Steps 7 and 8 are implemented and repeated with modified values of  $SF$  until Eq. (2) is satisfied. Successive values of  $SF$  are chosen by trial and error or by a convergence algorithm, e.g., Newton-Raphson iteration procedure. For a given ground motion, if the Eq. 2 is satisfied by more than one  $SF$ , the  $SF$  closest to one should be preferred.

Repeat Steps 7 and 8 for as many records as deemed necessary; obviously the scaling factor  $SF$  will be different for each record. These scaling factors will be shown to be appropriate for structures that respond dominantly in the first-mode.

#### Higher-mode Considerations

10. Establish target values of deformation of higher-mode SDF systems, treated as elastic systems, from the target spectrum  $\bar{D}_n = (T_n/2\pi)^2 \bar{A}_n$ , where the mode number  $n = 2$ . We have found that the second-mode is mostly adequate for buildings susceptible to higher-mode effects.

11. By linear RHA, calculate the peak deformation  $D_2 \equiv \max_t |D_2(t)|$  of the  $n$ th-mode elastic SDF system with known  $T_2$  and  $\zeta_2$  due to a selected ground motion  $\ddot{u}_g(t)$  multiplied by its scale factor  $SF$  determined in Step 9.
12. Compute the normalized difference between the target value of deformation  $\bar{D}_2$  (Step 10) and the peak deformation determined in Step 11.

$$\Delta_2 = |\bar{D}_2 - D_2| / \bar{D}_2 \quad (3)$$

and rank the scaled records based on their  $\Delta_2$  value; the record with the lowest average  $\Delta_2$  is ranked the highest.

13. From the ranked list, select the final set of records with their scale factors determined in Step 9 to be used in nonlinear RHA of the structure.

### 3.0 ESTIMATING SDF-SYSTEM INELASTIC DEFORMATION

The inelastic deformation ratio  $C_R$  is required in Step 6 to estimate the deformation of the inelastic SDF system. Such equations were first developed by Veletsos and Newmark [1960] as a function of elastic vibration  $T_n$  and ductility factor  $\mu$ . However, in selecting and scaling ground motion records for nonlinear RHA of an existing building or of a proposed design of a new building, the inelastic deformation ratio should be expressed as a function of  $T_n$  and the yield-strength reduction factor  $R_y$ ; these quantities are determined in Steps 7 and 4, respectively. The inelastic deformation ratio can be expressed as a function of elastic vibration period and yield-strength reduction factor  $R_y$ . Response data for 216 ground motions recorded on NEHRP site classes B, C, and D demonstrated that the mean inelastic deformation ratio is influenced little by soil condition, by magnitude if  $R_y < 4$  (but significantly for larger  $R_y$ ), or by site-to-fault

distance so long as it exceeds 10 km [Ruiz-Garcia and Miranda 2002]. Regression analysis of these data led to an equation for the inelastic deformation ratio as a function of  $T_n$  and  $R_y$ ; this equation is restricted to elastoplastic systems.

Median values of  $C_R$  have been presented for non-degrading bilinear hysteretic systems subjected to seven ensembles of far-fault ground motions (each with 20 records), representing large or small earthquake magnitude and distance, and NEHRP site classes, B, C, or D; and for two ensembles of near-fault ground motions. Regression analysis of these data led to the empirical  $C_R$  equation [Chopra and Chintanapakdee 2004]:

$$C_R = 1 + \left[ (L_R - 1)^{-1} + \left( \frac{a}{R_y^b} + c \right) \left( \frac{T_1}{T_c} \right)^d \right]^{-1} \quad (4)$$

in which, the limiting value of  $C_R$  at  $T_n = 0$  is:

$$L_R = \frac{1}{R_y} \left( 1 + \frac{R_y - 1}{\alpha} \right) \quad (5)$$

where  $\alpha$  is the post-yield stiffness ratio and  $T_c$  is the period separating the acceleration and velocity-sensitive regions of the target spectrum; the parameters in Eq. (4) are:  $a=61$ ,  $b=2.4$ ,  $c=1.5$ , and  $d=2.4$ .

Equations (4) and (5) and values of their parameters are valid for far-fault ground motions, independent of (1) earthquake magnitude and distance; and (2) NEHRP site class B, C, and D; and also for near-fault ground motions.

### 4.0 CODE-BASED SCALING PROCEDURE

The procedures and criteria in the 2006 IBC and 2007 CBC for the selection and scaling of ground motions for use in nonlinear RHA of structures are based on the ASCE-7 provisions [ASCE 2005]. According to ASCE-7, earthquake records should be selected from events of magnitudes, fault distance and source mechanisms that comply with the maximum considered earthquake. If the required number of appropriate records is not

available, appropriate simulated ground motions may be included to make up the total number required.

For two-dimensional analysis of symmetric-plan buildings, ASCE-7 requires intensity-based scaling of ground motion records using appropriate scale factors so that the average value of the 5%-damped response spectra for the set of scaled records is not less than the design response spectrum over the period range from  $0.2T_1$  to  $1.5T_1$ . The design value of an EDP—member forces, member deformations or story drifts—is taken as the average value of the EDP over seven (or more) ground motions, or its maximum value over all ground motions, if the system is analyzed for fewer than seven ground motions.

The ASCE-7 scaling procedure does not insure a unique scaling factor for each record; obviously, various combinations of scaling factors can be defined to insure that the average spectrum of scaled records remains above the design spectrum (or amplified spectrum in case of 3-D analyses) over the specified period range. Because it is desirable to scale each record by the smallest possible factor, an algorithm is developed and used in applying the code-scaling procedure in the evaluation section. This algorithm is provided at Kalkan and Chopra (2008).

## 5.0 GROUND MOTIONS & SYSTEMS ANALYZED

A total of twenty one near-fault strong earthquake ground motions were compiled from the Next Generation of Attenuation project earthquake ground motion database [Power et al. 2006]. These motions were recorded during seismic events with moment magnitude,  $M \geq 6.5$  at closest fault distances,  $R_{cl} \leq 12$  km and belonging to NEHRP site classification C and D. The selected ground motion records and their characteristic parameters are listed in Table 1. Shown in Fig. 1a are the pseudo-acceleration response spectrum for each ground motion and the median of the 21 response spectra. The median spectrum is taken to be the design spectrum for purposes of evaluating the MPS and ASCE-7 scaling procedures. The median spectrum of the ground motion ensemble is

presented next in Fig. 1b as a four-way logarithmic plot, together with its idealized version (dashed-line). The idealized spectrum is divided logically into three period ranges: the long-period region to the right of point  $d$ ,  $T_n > T_d$ , is called the displacement-sensitive region; the short-period region to the left of point  $c$ ,  $T_n < T_c$ , is called the acceleration-sensitive region; and the intermediate-period region between points  $c$  and  $d$ ,  $T_c < T_n < T_d$ , is called the velocity-sensitive region [Chopra 2007; Section 6.8]. Note that the velocity-sensitive region is unusually narrow, which is typical of near-fault ground motions.

The buildings selected to evaluate the efficiency and accuracy of the MPS method are existing four-, six-, and thirteen-story steel special moment resisting frame (SMRF) buildings representative of low-rise and mid-rise building-types in California. The six and thirteen-story buildings are instrumented, and their motions have been recorded during past earthquakes. The first three natural vibration periods and modes of each building are shown in Fig. 2 and the first-mode pushover curves in Fig. 3, where P- $\Delta$  effects are included. A description of these buildings and complete details of their analytical models are reported at Kalkan and Chopra (2008).

## 6.0 EVALUATION OF MPS PROCEDURE

The efficiency and accuracy of the MPS and ASCE-7 scaling procedures will be evaluated. A scaling procedure is considered efficient if the dispersion of EDPs due to the scaled records are small; it is accurate if the median value of the EDPs due to scaled ground motions is close to the benchmark results, defined as the median values of EDPs, determined by nonlinear RHA of the building to each of the 21 unscaled ground motions. In this section, the median values of EDPs determined from a set of 7 ground motions, scaled according to MPS and ASCE-7 scaling procedures, will be compared. The median value  $\hat{x}$ , defined as the geometric mean, and the dispersion measure,  $\delta$  of  $n$  observed values of  $x_i$  are calculated from

$$\hat{x} = \exp \left[ \frac{\sum_{i=1}^n \ln x_i}{n} \right] \quad \delta = \left[ \frac{\sum_{i=1}^n (\ln x_i - \ln \hat{x})^2}{n-1} \right]^{1/2} \quad (4)$$

The EDPs selected are peak values of story drift ratio, i.e., peak relative displacement between two consecutive floors normalized by story height; floor displacements normalized by building height; column and beam plastic rotations. Fig. 4 shows the benchmark EDPs for all three buildings; results from individual records are also included to demonstrate the large dispersion. Almost all of the excitations drive all three buildings well into the inelastic range as shown in Fig. 3 where the roof displacement values due to 21 ground motions are identified on the first-mode pushover curve. Also shown is the median value.

### 6.1 Evaluation of MPS Concept

As a first step in evaluating the concept underlying the MPS procedure, the target value of deformation  $\bar{D}_1^I$  is computed not as described in Step 6 of the procedure, but as the median value of peak deformation of the first-mode inelastic SDF system due to 21 ground motions determined by nonlinear RHA. The MPS method utilizing this  $\bar{D}_1^I$  value is denoted henceforth as MPS\*. The 21 ground motions are divided into 3 sets each containing 7 records (Table 1). The records in each set are selected randomly from at least 3 different earthquakes to avoid any dominant influence of a single event on the ground motion set. An appropriate scale factor for each record is determined by implementing Steps 1-8 of the MPS procedure.

Efficiency and accuracy of the MPS\* procedure are evaluated for each ground motion set, separately by comparing the median values of EDPs determined by nonlinear RHA of the building due to the 7 scaled records against the benchmark EDPs. Representative comparisons are depicted in Fig. 5 for the three buildings considering Ground Motion Set 1. Included are the EDPs due to each of the 7 scaled ground motions to show the dispersion of the data. Ground Motion Set 2 and 3 yield identical results [Kalkan and

Chopra 2008].

These results identifies that the median values of EDPs due to every small (7) subset of scaled ground motion closely match the benchmark results, which were determined from a large (21) set of ground motions. The dispersion of the EDP values due to the 7 scaled records about their median value is much smaller compared to the data for the 21 unscaled records in Fig. 4. These results collectively demonstrate that the concept underlying the MPS procedure is accurate and efficient in scaling records for nonlinear RHA of buildings.

### 6.2 Evaluation of MPS and Code-Based Scaling Procedures

The preceding implementation of the MPS concept is the same as the MPS procedure described earlier, except for how  $\bar{D}_1^I$  was computed. Previously, the exact value of  $\bar{D}_1^I$  was determined by nonlinear RHA of the first-mode inelastic SDF system, but it will now be estimated according to Step 6, using an empirical equation for  $C_R$ , in accordance with the MPS procedure. In utilizing  $C_R$  equation, zero post-yield stiffness is assumed, although the idealized first-“mode” SDF systems have negative post-yield stiffness. This choice is dictated by the fact that the original  $C_R$  equation was determined for stable systems with non-negative post-yield stiffness ratio [Chopra and Chintanapakdee 2004]. In  $C_R$  equation, using zero post-yield stiffness seems to be plausible, because the variability in the peak displacement demand is not affected significantly by the hysteretic behavior (Kurama and Farrow, 2003; Gupta and Kunnath, 1998). Fig. 6 compares the “exact” target value of deformation  $\bar{D}_1^I$  (continuous horizontal line) with estimated target value of deformation  $\bar{D}_1^I$  (dashed horizontal line) using the  $C_R$  equation with zero post-yield stiffness;  $D_1^I$  values from individual records for each of the three buildings are also included. The difference between the “exact” and estimated values of  $\bar{D}_1^I$  is 4, 9, and 12% of “exact”  $\bar{D}_1^I$  values for the 4-, 6-, and 13-story buildings, respectively.

An appropriate scale factor for each record is then determined in accordance with two procedures: Steps 1-8 of the MPS procedure and the ASCE-7 procedure. The EDPs determined by nonlinear RHA of the structure due to a set of 7 ground motions scaled according to MPS and ASCE-7 procedures are compared against the benchmark EDPs. Figs. 6-8 present such comparisons for the three buildings considering Set 1 ground motions. The other two sets provide visually identical results [Kalkan and Chopra 2008].

These results demonstrate that the MPS procedure is much superior compared to the ASCE-7 procedure for scaling ground motion records. This superiority is apparent in two respects: First, for each building and each ground motion set, the ground motions scaled according to the MPS procedure lead to median values of EDPs that are much closer to the benchmark values than the corresponding results based on the ASCE-7 procedure. Second, the dispersion in the EDP values due to the 7 scaled records around the median value is much smaller when the records are scaled according to the MPS procedure compared to the ASCE-7 scaling procedure. However, even with MPS scaling, the dispersion of EDPs for the upper stories of 6- and 13-story buildings is noticeable (particularly for Ground Motion Set 2 as shown later), indicating that the higher-mode contributions to the seismic demands are significant. These factors will be considered later in Steps 10-13 of the MPS procedure.

An alternative way of comparing MPS and ASCE-7 scaling methods is based on the ratio of the EDP value due to a scaled record and the benchmark value. The deviation of the median  $\Delta$  of this ratio from unity is an indication of the error or bias in estimating the median EDP value, and the dispersion  $\sigma$  of this ratio is an indication of the scatter in the individual EDPs, determined from the scaled ground motions. Included also in the comparison is the MPS\* procedure based on “exact” values of  $\bar{D}_1^f$  instead of Step 6.

Fig. 9 presents the median  $\Delta$  of the EDP ratio for story drifts determined from records scaled according to the MPS\*, MPS, and ASCE-7 scaling

methods. Comparing these  $\Delta$  values against 1.0, it is apparent that the MPS\* method is most accurate (least biased), the MPS method is only slightly less accurate. The bias in the MPS methods is generally less than 20%. The ASCE-7 method is least accurate generally overestimates the EDPs, with the overestimation exceeding 50% in some cases.

Fig. 10 presents the dispersion of the EDP ratio for story drifts determined from records scaled according to the MPS\*, MPS, and ASCE-7 scaling methods. It is apparent that the MPS\* scaling method leads to the smallest dispersion, and it becomes only slightly larger in the MPS method. Dispersion is largest in the ASCE-7 scaling method, becoming unacceptably large for some combinations of buildings and ground motion sets.

## 7.0 MULTI-MODE CONSIDERATIONS

As demonstrated in preceding section, the MPS method based solely on the first-mode inelastic SDF system (steps 1-9 of the method) is superior over the ASCE-7 scaling method. Considering the higher modes of vibration is expected to improve the method further for mid-rise and high-rise buildings [Tothong and Cornell, 2008; Tothong and Luco, 2007; Luco and Cornell 2007].

The 21 records scaled based on the first-mode response only (steps 1-9 of the method) are ranked by accounting for higher mode response according to steps 10-13 of the method. Only one higher mode, the second mode, was considered for the 6 and 13-story buildings. The seven records with the highest ranks (see step-12) were defined as Ground Motion Set 4. Note that this set is different for each building.

Considering higher modes in selecting ground motions in the MPS method provides accurate estimates of the median EDPs and reduces the record-to-record variability (compared to the results achieved by Ground Motion Sets 1-3). This improved accuracy and efficiency is demonstrated in Figure 11, where the  $\Delta$  and  $\sigma$ —the median value of the ratio of the estimated story drift to its benchmark value, and dispersion of this ratio—are

plotted for the four set of ground motions. It is apparent that Ground Motion Set 4 is more accurate and efficient than Ground Motion Sets 1 through 3.

The improvement achieved for these buildings is modest because the higher-mode computations are not especially significant in the response of selected buildings. Such improvement is expected to be more pronounced in the case of taller buildings responding significantly in their higher modes.

## 8.0 CONCLUSIONS

A modal-pushover-based scaling (MPS) method has been developed to scale ground motions for use in nonlinear response history analysis (RHA) of buildings. In the MPS method, the ground motions are scaled to match (to a specified tolerance) a target value of the inelastic deformation of the first-mode inelastic SDF system—its properties determined by first-mode pushover analysis—and the elastic deformation of higher-mode SDF systems are considered in selecting a subset of the scaled ground motions.

The median values of engineering demand parameters (EDPs)—floor displacement, story drifts, and plastic rotations—due to three sets of 7 ground motions scaled by two methods—MPS and ASCE-7—were computed by nonlinear RHA of the building and compared against the benchmark values of EDPs, determined by nonlinear RHA of the building for 21 unscaled records. Presented for 4-, 6-, and 13-story existing steel-SMRF buildings, such comparison led to the following conclusions:

1. Even for the most intense near-fault ground motions, which represent a severe test, the MPS method estimates the median value of seismic demands to a good degree of accuracy (within 20% of the benchmark value). In contrast, the ASCE-7 scaling method overestimates the demand by 20 to 50% for 4-, 6-, and 13-story building, and its overestimation exceeds 50% for 13-story building. The dispersion of responses due to ground motion

scaled by the MPS method is much smaller compared to the ASCE-7 scaling method; in the latter method, dispersion is unacceptably large for some combinations of buildings and ground motions sets. Thus, the MPS method is much more accurate, as well as efficient (as defined earlier) compared to the ASCE-7 scaling method.

2. Using the exact value of target deformation (as in MPS\*), defined as the median deformation of the first-mode inelastic SDF system for a large ensemble of unscaled records determined by nonlinear RHA, leads to the most accurate and efficient version of the MPS method. Because this rigorous approach is not suitable for practical application, the target deformation may be estimated from the deformation of the corresponding linear system, available from the design spectrum, and empirical equations for the inelastic deformation ratio. The increase in bias and dispersion resulting from this approximation is small. The resulting practical version of the MPS method uses attenuation relations for elastic spectral ordinates that are currently available; new attenuation relations for inelastic spectral deformation are not required.
3. For first-mode dominated structures, scaling earthquake records to the target value of the inelastic deformation is sufficient in producing accurate estimates of median EDPs and in reducing the dispersion of EDPs due to individual ground motions. For mid-rise and high-rise buildings where higher vibration modes are known to contribute significantly to the seismic response, the MPS method requires an additional step to rank the scaled ground motions based on the closeness of the elastic deformation of higher-mode elastic SDF systems to their target values. Selecting a subset of highest-ranked ground motions leads to a method that is more accurate and efficient for estimating seismic demands for taller buildings.

This study has focused on developing the MPS method for scaling ground motions and its initial evaluation, which has been limited to low- and mid-rise steel SMRFs; stable force deformation

relations were considered and P- $\Delta$  effects were excluded.

## 9.0 ACKNOWLEDGMENT

Dr. Kalkan wishes to acknowledge the generous support of the Earthquake Engineering Research Institute for providing him the 2008 EERI/FEMA NEHRP Professional Fellowship in Earthquake Hazard Reduction for the research study "Preparation of practical guidelines to select and scale earthquake records for nonlinear response history analysis of structures".

## 10.0 REFERENCES

Alavi, B., and Krawinkler, H. (2000). "Consideration of near-fault ground motion effects in seismic design," Proc. of the 12th World Conference on Earthquake Engineering, Paper No. 2665, Auckland, New Zealand.

Alavi, B., and Krawinkler, H. (2004). "Behavior of moment-resisting frame structures subjected to near-fault ground motions," Eq. Eng. and Str. Dyn., Vol. 33, No. 6, pp. 687-706.

American Society of Civil Engineers (2005), ASCE-7 Minimum Design Loads for Buildings, Reston, VA.

Anderson, J., and Bertero, V. V. (1991). "Seismic performance of an instrumented six-story steel building," Earthquake Engineering Research Center, University of California, Berkeley, Report No. 1991-11, 134 p.

Báez, J. I., and Miranda, E. (2000). "Amplification factors to estimate inelastic displacement demands for the design of structures in the near field," Proc. of the Twelfth World Conf. on Eq. Eng., Paper No. 1561, Auckland, New Zealand.

Baker, J. W., and Cornell, A. C. (2006). "Spectral shape, epsilon and record selection," Earthquake Engineering & Structural Dynamics, Vol. 35, No. 9, pp. 1077-1095.

Bazzurro, P., 1998. Probabilistic Seismic Demand Analysis, Ph.D. thesis, Dept. of Civil and Env.

Eng., Stanford University, CA. (Available online at <http://www.stanford.edu/group/rms/Thesis/index.html>; last accessed on 06/2008).

Bazzurro, P., and Luco, N. (2004). "Parameterization of Non-Stationary Acceleration Time Histories. Lifelines Program Project 1G00 Addenda. Pacific Earthquake Engineering Research (PEER) Center, University of California: Berkeley, CA, 83 p.

Bazzurro, P., and Luco, N. (2006). "Do scaled and spectrum-matched near-source records produce biased nonlinear structural responses," Proc. of the 8th National Conf. on Eq. Eng., Paper No. 1029, San Francisco, CA.

Bozorgnia, Y., and Mahin, S. A. (1998). "Ductility and strength demands of near-fault ground structure-specific scalar intensity measures 389 motions of the Northridge earthquake," Proceedings of the 6th U.S. National Conf. on Eq. Eng., Seattle, WA.

Chopra, A.K. (2001). Dynamics of Structures: Theory and Applications to Eq. Eng., 2nd Ed., Prentice Hall, Englewood Cliffs, N.J.

Chopra, A. K., and Chinatanapakdee, C. (2004). "Inelastic Deformation Ratios for Design and Evaluation of Structures: Single-Degree-of-Freedom Bilinear Systems," J. of Str. Eng. (ASCE), Vol. 130, No. 9, pp. 1304-1319.

Cordova, P. P., Deierlein, G. G., Mehanny, S. S. F., and Cornell, C. A., 2000. Development of a two-parameter seismic intensity measure and probabilistic assessment procedure, Proceedings of the 2nd U.S.-Japan Workshop on Performance-Based Seismic Design Methodology for Reinforced Concrete Building Structures, PEER Report 2000/10, Pacific Earthquake Engineering Research Center, University of California, Berkeley, CA.

International Conference of Building Officials (2006). International Building Code, Whittier, CA.

International Conference of Building Officials (2007). California Building Code, Whittier, CA.

Kalkan, E., and Chopra, A. K. (2008). "Modal-Pushover-based Ground Motion Scaling Procedure," Eq. Eng. Res. Center. Report, University of California Berkeley, CA, p. 49.

- Krawinkler, H., and Al-Ali, A. (1996). "Seismic demand evaluation for a 4-story steel frame structure damaged in the Northridge earthquake," *The Structural Design of Tall Buildings*, Vol. 5, No. 1, pp. 1-27.
- Kennedy, R. P., Short, S. A., Merz, K. L., Tokarz, F. J., Idriss, I. M., Power, M. S., and Sadigh, K. (1984). "Engineering characterization of ground motion-task 1: Effects of characteristics of free-field motion on structural response," NUREG/CR-3805, U.S. Regulatory Commission, Washington, D.C.
- Kurama, Y., and Farrow, K. (2003). "Ground motion scaling methods for different site conditions and structure characteristics," *Eq. Eng. and Str. Dyn.*, Vol. 32, No. 15, pp. 2425-2450.
- Lilhand, K., and Tseng, W. S. (1989). "Development and application of realistic earthquake time histories compatible with multiple damping design spectra," *Proc. of the 9th World Conf. on Eq. Eng. Tokyo-Kyoto, Japan*, Vol. 2, pp. 819-830.
- Luco, N., and Cornell, A. C. (2007). "Structure-Specific Scalar Intensity Measures for Near-Source and Ordinary Earthquake Ground Motions," *Earthquake Spectra*, Vol. 23, No. 2, pp. 357-392.
- Malhotra, P. K. (2003). "Strong-Motion Records for Site-Specific Analysis," *Earthquake Spectra*, Vol. 19, No. 3, pp. 557-578.
- Mehanny, S. S. F. (1999). "Modeling and Assessment of Seismic Performance of Composite Frames with Reinforced Concrete Columns and Steel Beams," Ph.D. thesis, Dept. of Civil and Env. Eng., Stanford University, California.
- Miranda, E. (1993). "Evaluation of site-dependent inelastic seismic design spectra," *J. of Str. Eng. (ASCE)*, Vol. 119, No. 5, pp. 1319-1338.
- Naeim, F., Alimoradi, A., and Pezeshk, S. (2004). "Selection and scaling of ground motion time histories for structural design using genetic algorithms," *Earthquake Spectra*, Vol. 20, No. 2, pp. 413-426.
- Nau, J., and Hall, W. (1984). "Scaling methods for earthquake response spectra," *J. of Str. Eng. (ASCE)*, Vol. 110, No. 91-109.
- OpenSEES. Open Source finite element platform for earthquake engineering simulations 2006. University of California Berkeley, Pacific Earthquake Engineering Center. (Available online at <http://opensees.berkeley.edu/>; last accessed on 06/2008).
- Petersen, M. D., Frankel, A. D., Harmsen, S. C., Mueller, C. S., Haller, K. M., Wheeler, R. L., Wesson, R. L., Zeng, Y., Boyd, O. S., Perkins, D. M., Luco, N., Field, E. H., Wills, C. J., and Rukstales, K. S., (2008). "Documentation for the 2008 Update of the United States National Seismic Hazard Maps," U.S. Geological Survey Open-File Report 2008-1128, 61 p. (Available online at: <http://pubs.usgs.gov/of/2008/1128/>; last accessed on 06/2008).
- Power, M., Chiou, B., Abrahamson, N., and Roblee, C. 2006. "The Next Generation of Ground Motion Attenuation Models" (NGA) project: An overview," In *Proc. of the Eighth National Conf. on Eq. Eng.*, Paper No. 2022, San Francisco, CA.
- Ruiz-Garcia, J., and Miranda, E. (2002). "Inelastic displacement ratios for evaluation of existing structures," *Eq. Eng. and Str. Dyn.*, Vol. 31, No. 3, pp. 539-560.
- Shome, N., and Cornell, A. C. (1998). "Normalization and scaling accelerograms for nonlinear structural analysis," *Prof. of the 6th U.S. National Conf. on Earthquake Engineering*, Seattle, WA.
- Shome, N., Cornell, C. A., Bazzurro, P., and Carballo, J. E., 1998. Earthquakes, records, and nonlinear responses, *Earthquake Spectra*, Vol. 14, No.3, pp. 469-500.
- Shome, N., and Cornell, C. A., 1999. Probabilistic Seismic Demand Analysis of Nonlinear Structures, Reliability of Marine Structures Program Report No. RMS-35, Dept. of Civil and Env. Eng., Stanford University, CA. (Available online at <http://www.stanford.edu/group/rms/Thesis/index.html>; last accessed on 06/2008).
- Tothong, P., and Cornell, A. C. (2008). "Structural performance assessment under near-source pulse-

like ground motions using advanced ground motion intensity measures,” *Eq. Eng. and Str. Dyn.* Vol. 37, No. 7, pp. 1013-1037.

Veletsos, A. S., and Newmark, N. M. (1960). “Effect of inelastic behavior on the response of simple systems to earthquake motions,” *Proc. of the Second World Conf. on Eq. Eng.*, Tokyo, Japan, Vol. II, pp. 895–912.

Vidic, T. Fajfar, P., and Fischinger, M. (1994). “Consistent inelastic design spectra: Strength and displacement,” *Eq. Eng. and Str. Dyn.*, Vol. 23, No. 5, pp. 507-521.

Youngs, R. Power, M., Wang, G., Makdisi, F., and Chin, C. C. (2007). “Design Ground Motion Library (DGML) – Tool for Selecting Time History Records for Specific Engineering Applications (Abstract),” *SMIP07 Seminar on Utilization of Strong-Motion Data*, pp. 109 – 110. (Available online at [http://www.conservation.ca.gov/cgs/smip/docs/seminar/SMIP07/Pages/Paper8\\_Youngs.aspx](http://www.conservation.ca.gov/cgs/smip/docs/seminar/SMIP07/Pages/Paper8_Youngs.aspx); last accessed on 06/2008).

Table 1: Selected Earthquake Ground Motions

No.	Earthquake	Year	Station	M	$R_{cl}$ (km)	$V_{S30}$ (m/s)	PGA (g)	PGV (cm/s)	PGD (cm)	Ground Motion Set No.
1	Tabas, Iran	1978	Tabas	7.4	2.1	767	0.85	110.3	61.1	2
2	Imperial Valley	1979	EC Meloland Overpass FF	6.5	0.1	186	0.31	79.3	28.1	2
3	Imperial Valley	1979	El Centro Array #7	6.5	0.6	211	0.42	80.2	41.0	3
4	Superstition Hills	1987	Parachute Test Site	6.5	1.0	349	0.46	74.8	36.3	1
5	Loma Prieta	1989	LGPC	6.9	3.9	478	0.78	77.2	42.7	3
6	Erzincan, Turkey	1992	Erzincan	6.7	4.4	275	0.49	72.9	24.8	2
7	Northridge	1994	Jensen Filter Plant	6.7	5.4	373	0.75	77.8	31.9	1
8	Northridge	1994	Newhall - W Pico Canyon Rd	6.7	5.5	286	0.39	76.6	43.1	3
9	Northridge	1994	Rinaldi Receiving Sta	6.7	6.5	282	0.63	109.2	28.3	3
10	Northridge	1994	Sylmar - Converter Sta	6.7	5.4	251	0.75	109.4	45.8	2
11	Northridge	1994	Sylmar - Converter Sta East	6.7	5.2	371	0.68	87.3	31.7	1
12	Northridge	1994	Sylmar - Olive View Med FF	6.7	5.3	441	0.71	97.4	22.4	3
13	Kobe, Japan	1995	Port Island	6.9	3.3	198	0.26	62.3	29.6	2
14	Kobe, Japan	1995	Takatori	6.9	1.5	256	0.65	118.8	33.4	1
15	Kocaeli, Turkey	1999	Yarimca	7.4	4.8	297	0.31	60.5	54.7	1
16	Chi-Chi, Taiwan	1999	TCU052	7.6	0.7	579	0.35	131.9	183.2	2
17	Chi-Chi, Taiwan	1999	TCU065	7.6	0.6	306	0.68	99.5	81.8	1
18	Chi-Chi, Taiwan	1999	TCU068	7.6	0.3	487	0.54	206.1	336.3	3
19	Chi-Chi, Taiwan	1999	TCU084	7.6	11.2	553	0.79	92.7	28.8	2
20	Chi-Chi, Taiwan	1999	TCU102	7.6	1.5	714	0.24	93.9	65.7	1
21	Duzce, Turkey	1999	Duzce	7.2	6.6	276	0.42	71.0	46.3	3

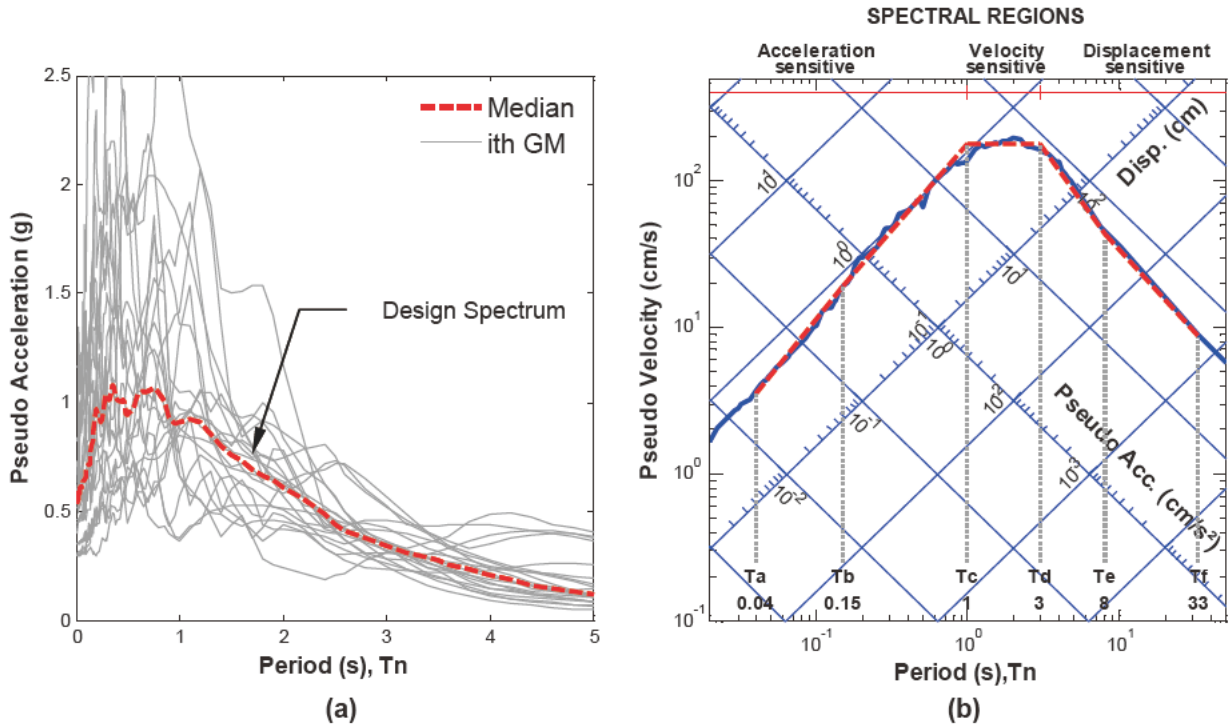


Figure 1: (a) Median elastic response spectrum for the selected ensemble of ground motions shown by a solid line, together with its idealized version in dashed line; spectral regions are

identified; (b) Individual response spectra for 21 ground motions and their median response spectrum;  $\zeta = 5\%$ .

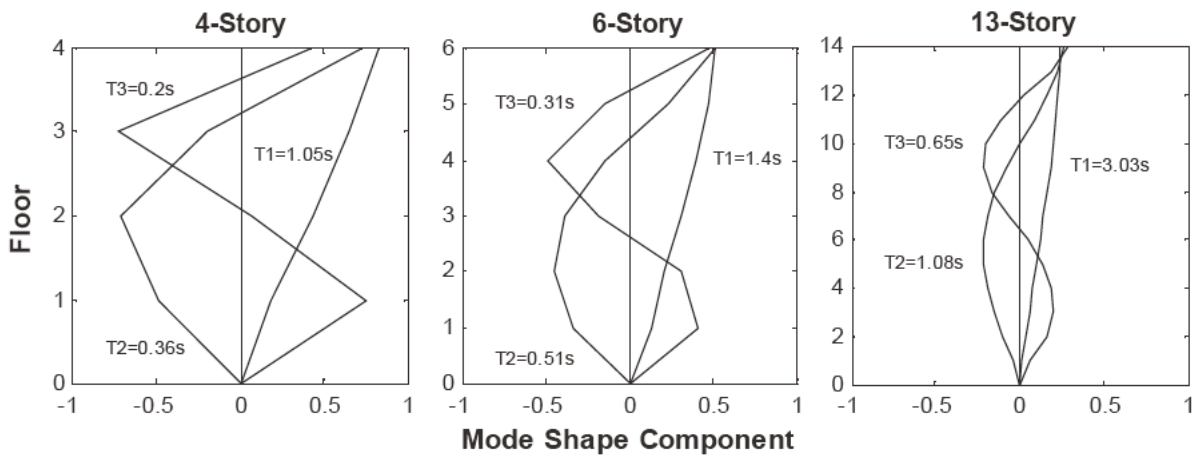


Figure 2: Natural vibration periods and modes of four-, six-, and thirteen-story buildings.

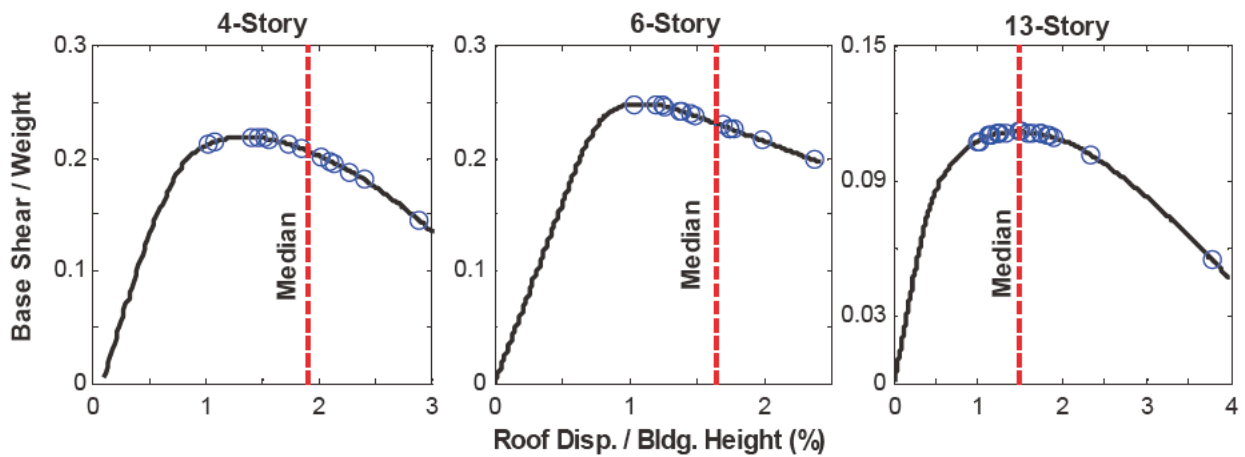


Figure 3: Roof displacements determined by nonlinear RHA of three buildings for 21 ground motions identified on first-mode pushover curves.

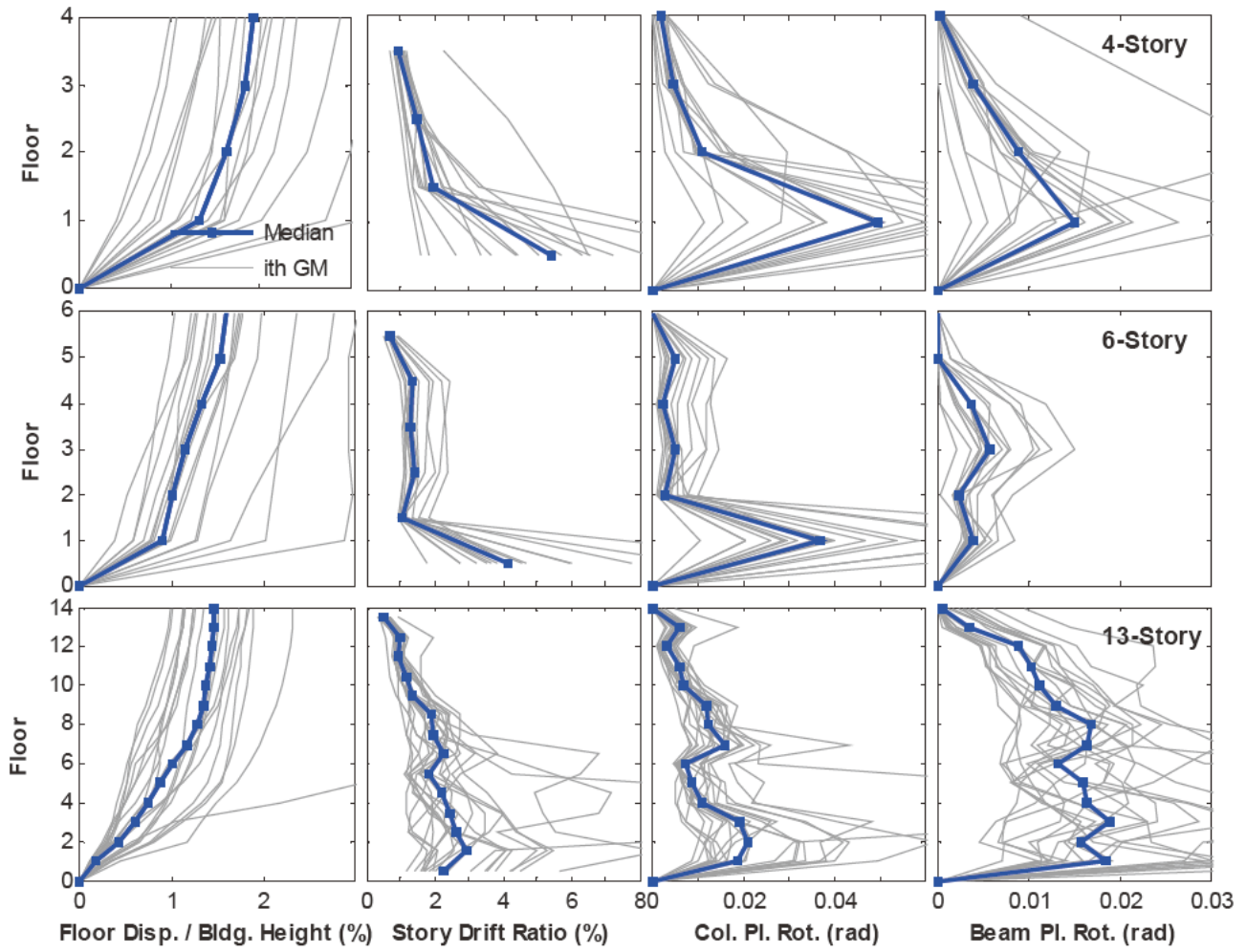


Figure 4: Median values of EDPs determined by nonlinear RHA of three buildings for 21 ground motions; results for individual ground motions are also included.

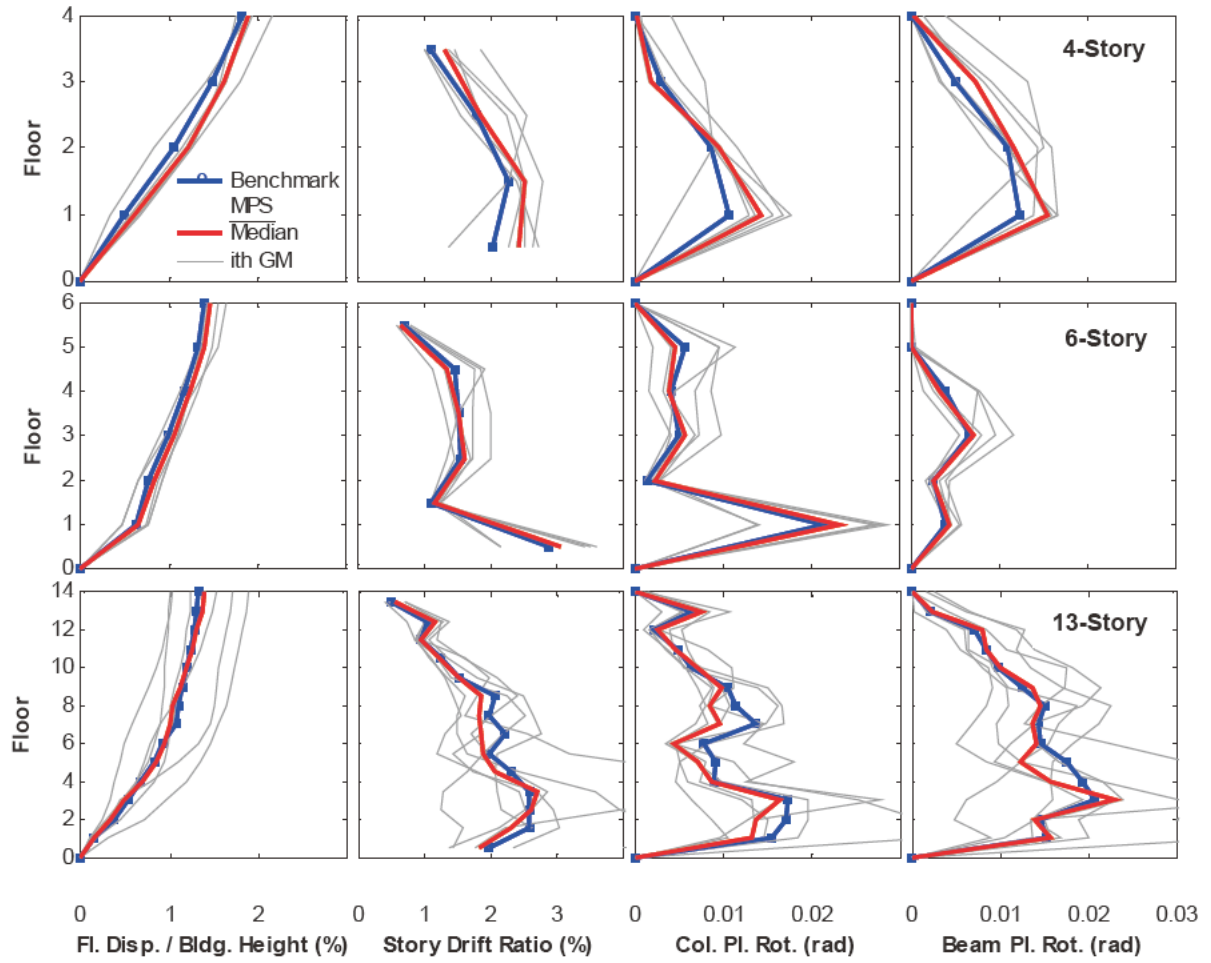


Figure 5: Comparison of median EDPs based on the MPS concept with benchmark EDPs for the 4-, 6-, and 13-story buildings for Ground Motion Set 1; individual results for each of the seven scaled ground motions are also presented.

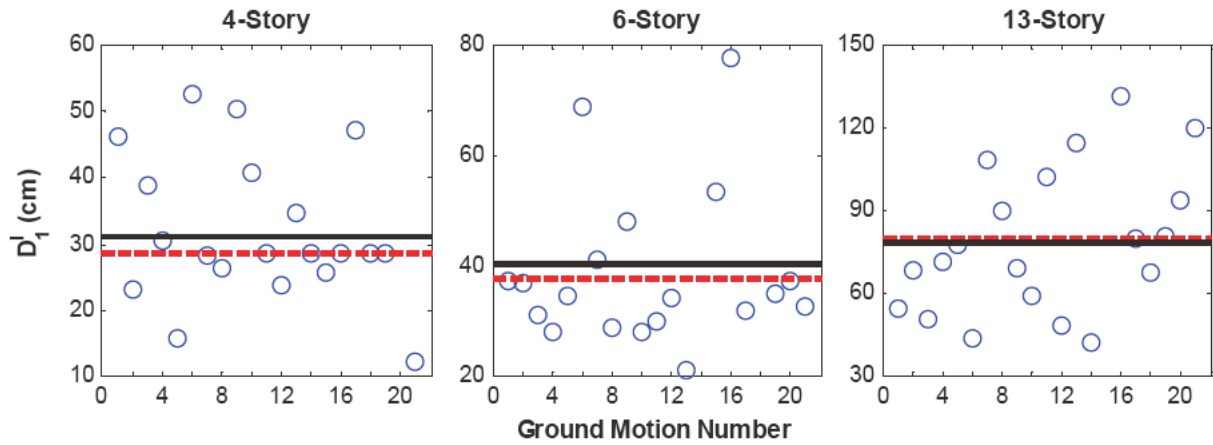


Figure 6: Peak deformation  $\bar{D}_1^I$  values of the first-“mode” inelastic SDF system for 21 ground motions for 4-, 6-, and 13-story buildings; “exact” target value of deformation  $\bar{D}_1^I$  is identified by horizontal continuous line; horizontal dashed line indicates target value of deformation  $\bar{D}_1^I$  established by  $C_R$  equation.

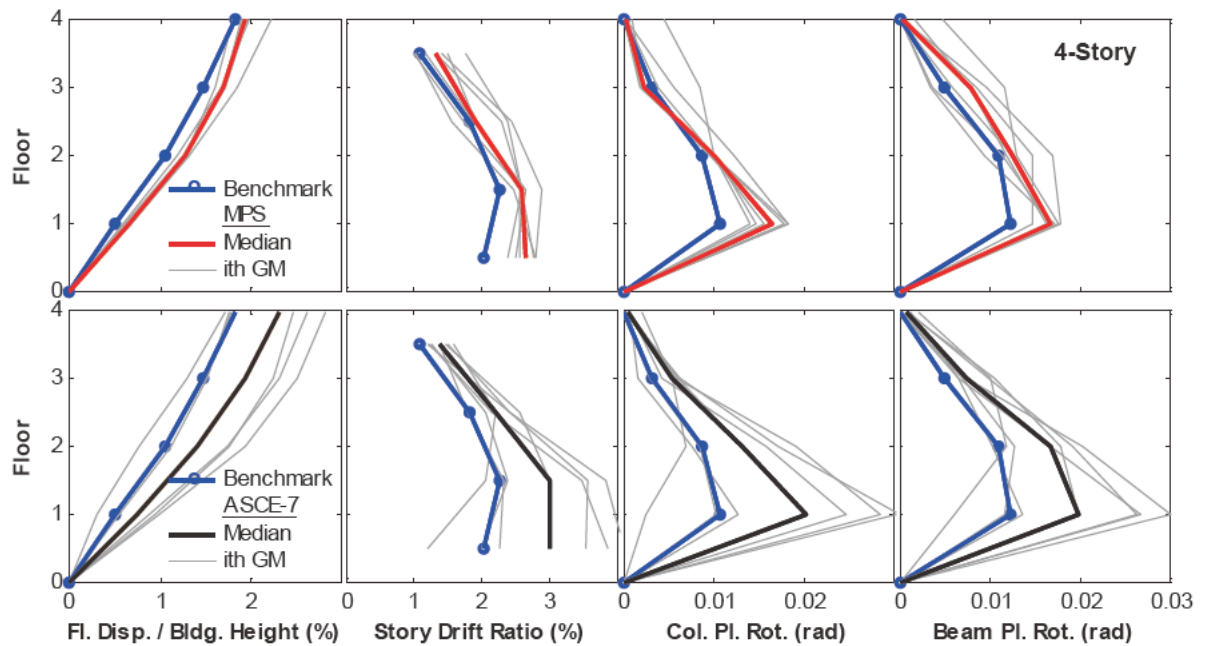


Figure 6: Comparison of median EDPs for Ground Motion Set 1 scaled according to MPS (top row) and ASCE-7 (bottom row) scaling procedures with benchmark EDPs; individual results for each of seven scaled ground motions are also presented. Results are for the 4-story building.

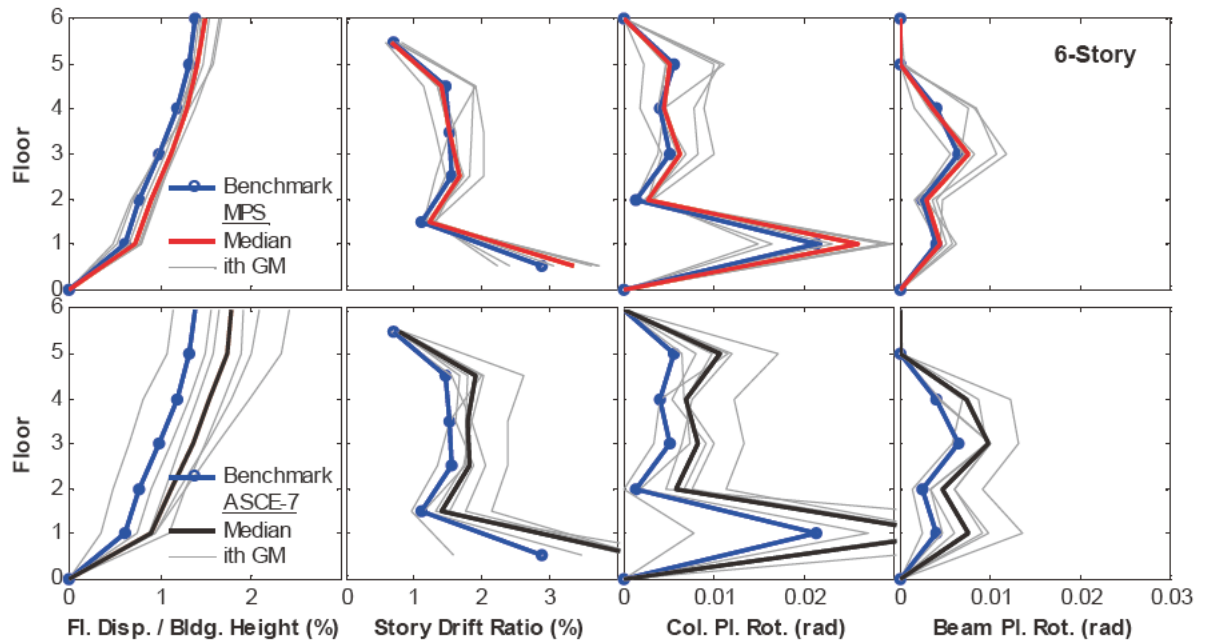


Figure 7: Comparison of median EDPs for Ground Motion Set 1 scaled according to MPS (top row) and ASCE-7 (bottom row) scaling procedures with benchmark EDPs; individual results for each of seven scaled ground motions are also presented. Results are for the 6-story building.

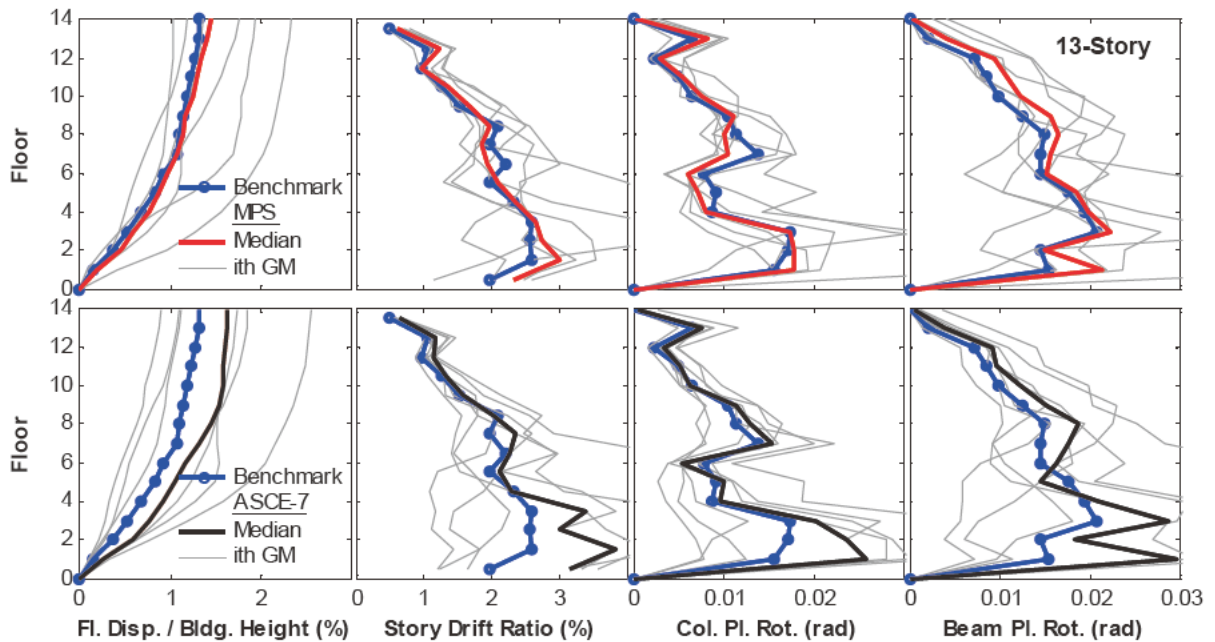


Figure 8: Comparison of median EDPs for Ground Motion Set 1 scaled according to MPS (top row) and ASCE-7 (bottom row) scaling procedures with benchmark EDPs; individual results for each of seven scaled ground motions are also presented. Results are for the 13-story building.

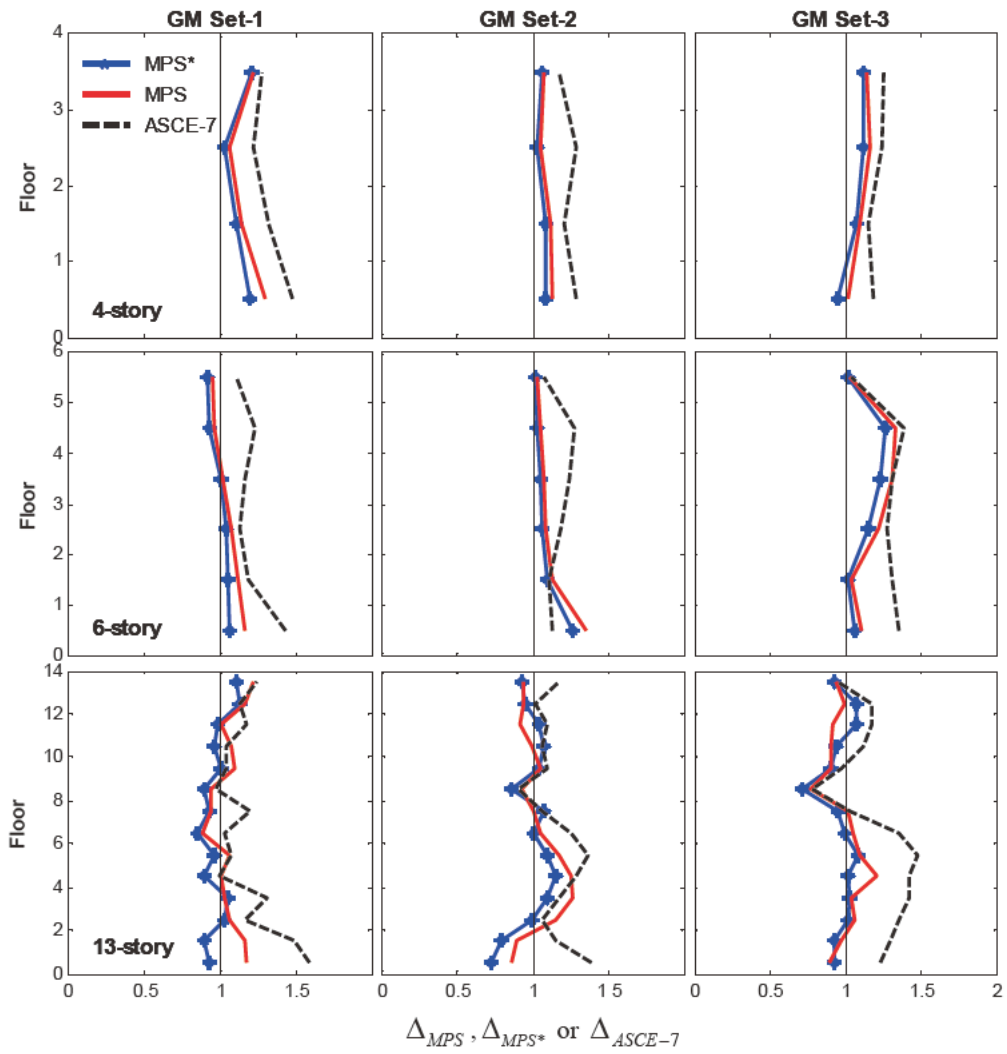


Figure 9: Median story drift ratios  $\Delta_{MPS}$ ,  $\Delta_{MPS^*}$  and  $\Delta_{ASCE-7}$  for three ground motions sets and for three buildings.

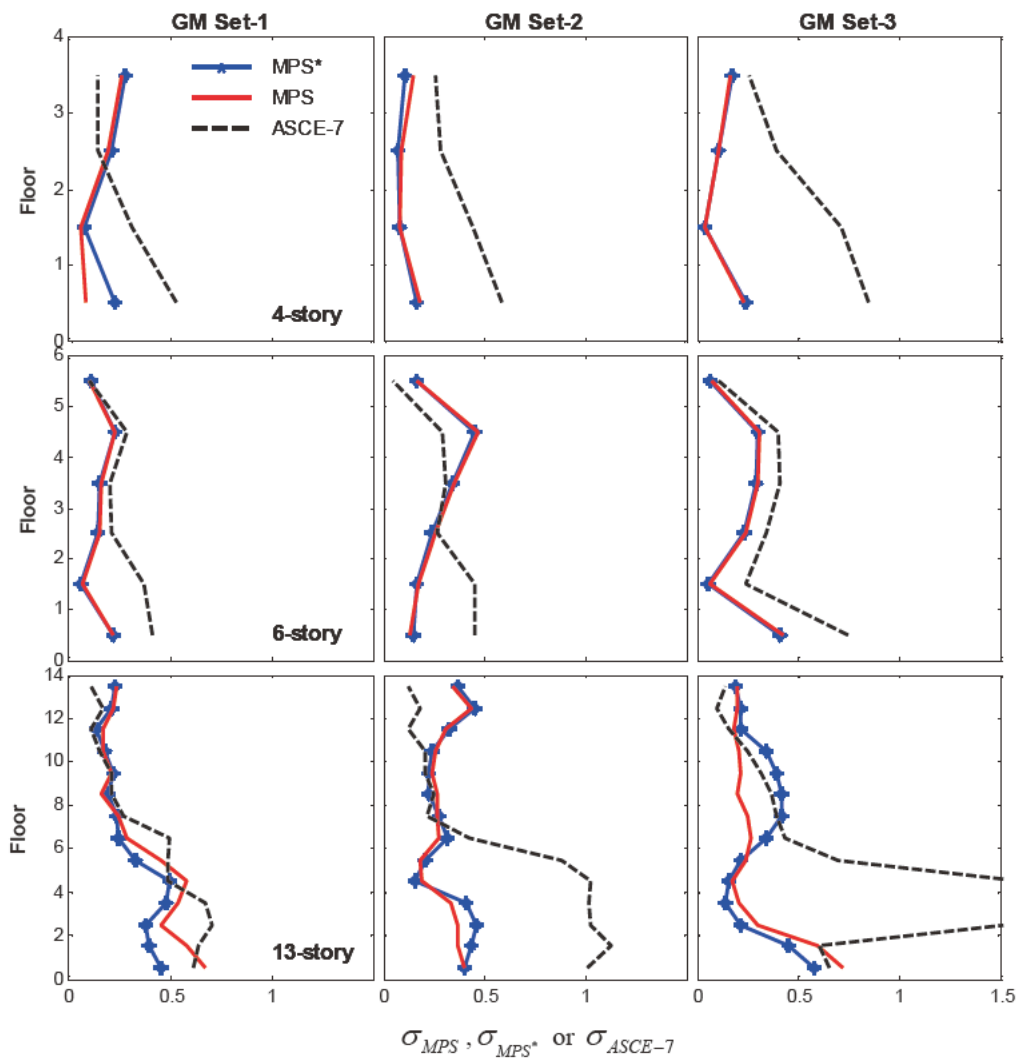


Figure 10: Dispersion of story drift ratios  $\sigma_{MPS}$ ,  $\sigma_{MPS^*}$  and  $\sigma_{ASCE-7}$  for three ground motions sets and for three buildings.

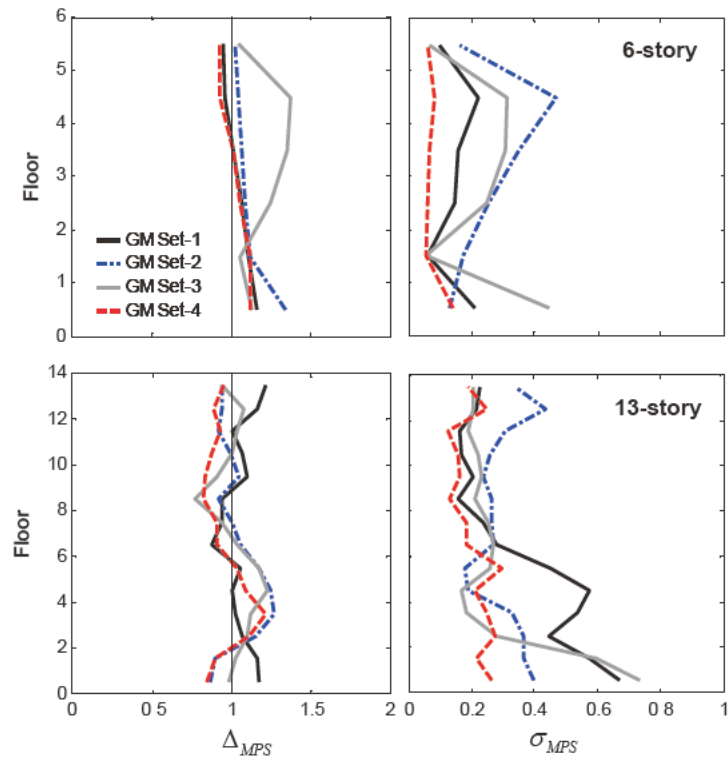


Figure 11: Median  $\Delta_{MPS}$  and dispersion  $\sigma_{MPS}$  of story drift ratios for four ground motions sets and for two buildings.

# Climate Change Adaptive Strategies for Buildings and Public Health

by

Fuyuen Yip, Josephine Malilay, George Luber, and Paul Garbe<sup>1</sup>

## ABSTRACT

Reducing the impact of climate change on buildings and public health will require ongoing preparation and action. Much effort thus far has emphasized mitigation activities to decrease a building's greenhouse gas emissions into the environment. However, buildings need to also adapt to accommodate the growing effects of heat waves and urban heat islands, and subsequent energy demands, especially cooling. While the public health effort to adapt to climate change will be critical, the building sector will also be instrumental in helping to reduce the impact of climate change on buildings and the built environment, and to ensure that the needs of occupants are met.

## KEYWORDS

Built environment, buildings, climate change, public health, adaptation

## 1.0 INTRODUCTION

The accumulation of greenhouse gases (GHGs) has been a dominant cause of climate change. The Intergovernmental Panel on Climate Change's recent Fourth Assessment Report<sup>1</sup> shows that there is growing evidence that global warming is associated with changes in the climate. These changes include increased frequencies of natural disasters, more extreme weather events, and rising sea levels from the widespread melting of snow and ice.<sup>1</sup> These climactic changes can affect public health in many ways.<sup>2,3,4</sup> Accordingly, societies need to prepare for, and effectively respond to, the changing climate. Two strategies are commonly identified to manage the effects of climate change: mitigation, which is

associated with reducing climate change, especially GHG emissions, and adaptation, which includes designing, implementing, monitoring, and evaluating strategies to reduce the effects of climate change. Both strategies address technological, institutional, and behavioral options.<sup>1</sup> While mitigation approaches to reduce GHG are often emphasized, a concomitant effort to work on public health adaptation to climate change will also be important to help prepare the public for ongoing changes.<sup>5</sup> Thus, it is critical to consider both mitigation and adaptation activities for reducing long-term, potentially hazardous effects on human health. We attempt to describe the important role that buildings and the built environment, collectively, should also be considered within this public health and climate change framework.

Mitigation strategies are continually being developed to reduce GHG from the built environment, yet there are opportunities to simultaneously integrate adaptation strategies (e.g., material selection, energy use, building design, etc.). These efforts can assure the resilience of the building sector to more effectively respond to increasing climate variability. Furthermore, as the building sector and overall built environment influence human health and welfare both in the indoor and outdoor environment, they are an integral part of the process.<sup>6</sup>

The anticipated health effects to climactic changes can include morbidity and mortality associated with temperature extremes and air pollution-related exposures. Effects of vector-borne and zoonotic diseases, especially on those organisms that are sensitive to and disrupted by climactic factors, may also emerge in areas where they had been limited.<sup>2</sup> The implications and threats of climate change to the overall

<sup>1</sup>National Center for Environmental Health, Centers for Disease Control and Prevention, Atlanta, GA, USA

infrastructure, including the building sector, are also becoming better understood. The estimated global anthropogenic GHG emissions (in carbon dioxide [CO<sub>2</sub>] equivalents) contributed by residential and commercial buildings was 7.9% in 2004<sup>1</sup> and efforts have primarily focused on reducing GHG from buildings. However, the impact of global warming over time on physical structures and their ability to adapt to changing climactic conditions should also be considered. With the increasing number of heat waves and the effect of the urban heat island, for example, the building sector will need to adapt to rising energy demands for cooling while maintaining indoor comfort and a healthy environment.

## 2.0 EFFECTS OF CLIMATE CHANGE ON HUMAN HEALTH: HEAT WAVES

There has been considerable research on the health effects associated with extreme heat. These health effects, along with periods of elevated temperatures outside the normal range of climate variability are projected to increase in frequency throughout the world and become more intense in the future.<sup>7</sup> Therefore, heat-related health effects are increasing in public health significance. In fact, many cities have reported excess mortality that has been attributed to extreme heat. Heat wave events are typically marked with sustained high temperatures that are often hotter than those to which the population is accustomed. These exposures can cause mild symptoms, such as heat stress or exhaustion, or exacerbate existing respiratory and cardiovascular conditions, which can lead to more severe health effects or be fatal. In the United States, heat waves kill more people than other natural disasters including hurricanes, tornadoes, floods, and earthquakes combined.

In 2003, Europe reported experiencing abnormally high temperatures in the summer and observed an unprecedented number of deaths—35,000 in the region.<sup>8</sup> In France alone, 14,800 deaths were reported between

two weeks in August, and many were among persons >75 years of age.<sup>9</sup> During this time in France, peak temperatures of 104°F (40°C) were recorded and remained elevated for two weeks.<sup>10</sup>

Vulnerable populations, which often include the elderly, young children, those with underlying medical conditions, and those without air conditioning, are disproportionately affected during heat waves as they may be more sensitive to temperature extremes.<sup>11,12, 13</sup> With a growing elderly U.S. population, these trends suggest that temperature-related morbidity and mortality are likely to increase in the future.

Vulnerability can also vary by geographic area, especially among those expected to experience the greatest changes in average temperatures.<sup>13</sup> As in Europe, these changes may be the most significant among residents in more temperate zones who may not be as acclimated to high temperatures and may be at greater risk.<sup>14</sup> In addition, these regions may also have increased concentrations of ozone and other air pollutants that are influenced by rising temperatures.<sup>15</sup> High levels of ozone can exacerbate existing respiratory and cardiovascular diseases.

## 3.0 EFFECTS OF CLIMATE CHANGE ON URBAN ENVIRONMENTS: URBAN HEAT ISLAND EFFECT

The urban “built” environment adds to the climate change-driven increases in temperature. Cities and climate are evolving together in a manner that will intensify both the effect of heat and the vulnerability of urban populations to heat-related death.

More than 50% of the world now lives in cities, and urban areas are gaining an estimated 67 million people per year. Further estimates suggest that approximately 5 billion people, or 60% of the projected global population, will be living in urban areas by 2030.<sup>16</sup> This rapid urbanization transitions communities to engineered

infrastructures that increase thermal-storage capacity, resulting in significant changes in the urban climate compared to neighboring rural regions. This is known as the urban heat island (UHI) effect. There is growing concern that the UHI effect can intensify and prolong the duration of extreme heat events.<sup>16</sup>

UHI has increased air temperatures in cities 2°F–8°F compared to surrounding suburban and rural areas, often due to solar energy absorbed by dark paved surfaces and buildings, fewer vegetation and trees, heat emitted from buildings and vehicles, and reduced air flow around buildings. UHI absorbs heat during the daytime, causing the surface temperatures of urban structures to become 50°F–70°F (10°C–21°C) warmer than ambient air temperatures.<sup>16</sup> In the evening, the energy is radiated out, raising nighttime minimum temperatures in the urban environment and keeping them relatively high.<sup>17</sup> This phenomenon makes it more difficult for the population to recover, which contributes to general discomfort, respiratory difficulties, heat cramps and exhaustion, nonfatal heat stroke, and heat-related mortality. Harlan et al. (2006),<sup>14</sup> found that Phoenix, Arizona residents living in warmer neighborhoods experienced increased health risks from heat stress.

Rising temperatures are likely to increase the demand for air conditioning and other sources of cooling. Research has shown that for every 1°F (0.6°C) increase in air temperatures (starting from 68°F–77°F [20°C–25°C]), cooling increases the demand for electricity by 1.5%–2.0%. This suggests that 5%–10% of community-wide demand for electricity is used to compensate for the UHI effect.<sup>18</sup> Demand may also increase pollutant emissions from regional power plants and other power sources that can contribute to the formation of ozone and other air pollutants,<sup>20</sup> thereby affecting public health.

#### 4.0 ADAPTATION AND MITIGATION: BUILDINGS SECTOR

The Fourth Assessment Report<sup>1</sup> detailed mitigation-related activities to reduce GHG emissions from the building sector. Energy use in buildings is typically high and inefficient, so efforts to reduce carbon emissions have often targeted buildings. Various design strategies have been developed to reduce carbon emissions, such as changing the building stock, using natural ventilation<sup>20</sup>, and better insulation and windows to improve thermal performance. Integrating approaches to increase energy efficiency and renewable energy, such as adopting the Leadership in Energy and Environmental Design (LEED) standards into building design, can reduce annual average carbon dioxide emissions by 350 metric tons (385 tons) in the United States.<sup>21</sup>

However, there has been less discussion in the Fourth Assessment Report about adapting residential and commercial buildings to climate change. Future approaches should therefore consider the ability of the building sector to adapt to climate variability and also to protect the health of the occupants and the public. After the heat wave in 2003, French researchers indicated that the quality of the built environment was an important factor in understanding the causes of excess mortality.<sup>10</sup> These adaptations can include modifying the building's energy use, peak demand, equipment life, and building stock.<sup>22</sup>

Thus, when selecting technologies to mitigate the effects of GHG, it is important to consider adapting building regulations, materials, and construction techniques to ongoing events associated with climate change. Smith and Levermore (2008)<sup>23</sup> suggested that approaches such as altering a building's façade (e.g., use of high-reflectivity materials), green roofs, urban greening, and design to allow cooling winds, can help lower the temperature in the urban micro-environment by reducing its heat absorption and emission. Adapting building codes, for example, to address these changes

can help to guide better building practices and can also lead to public health benefits. Further, the changing pattern of energy use and rising energy demand will likely continue to influence the design and efficiency of building services, especially those supporting the increasing need for cooling and heating.<sup>23,24</sup>

A growing body of technology helps maintain the thermal comfort of people in urban environments. Other existing technology, such as sensor arrays have often been used to monitor the health of buildings, and may also serve as a useful tool to help assess the ability of the building sector to withstand climate variability over time and the resiliency of the building materials.

## 5.0 BUILDING SECTOR INFRASTRUCTURE AND PUBLIC HEALTH

Several heat-related events, such as the 1995 heat wave in Chicago<sup>25</sup> and 2003 heat wave in Europe revealed that the existing infrastructure lacked the capacity to deal with the impact of these disasters. The failure to adapt, such as reducing UHIs, meeting electricity and cooling demands, and reducing population vulnerability to heat stress, may leave a community poorly prepared to cope with adverse changes, which can lead to severe consequences.<sup>2,5</sup>

Building design, its impact on local climate, and its ability to maintain human comfort—both short- and long-term changes, and on a micro- and macro-scale—will therefore be significant.

A driving force for adapting to climate change is to ensure basic public health protection. Adaptation is a process, so it is important to understand local and regional vulnerability, the adaptive capacity of the population, and future potential climate risks.<sup>5</sup>

## 6.0 COLLABORATIVE EFFORTS AND NEXT STEPS

Great complexity surrounds climate change. In order to effectively plan for these events, increased efforts to develop, mitigate and adapt strategies at the urban level requires a multi-disciplinary approach through collaborating with engineering, architecture, construction, community/urban planning, and public health professionals.

The health effect of extreme weather events is influenced by the vulnerability of the environment, the population, and its ability to recover from them. These factors rely on the resiliency of the building sector and its ability to protect the health of the population. Therefore, the challenge is to support the design, development and growth of new and existing urban environments in a sustainable manner that promotes public health. Further, policy and planning should be implemented and maintained to reduce the future vulnerability of urban populations to events such as extreme heat.<sup>23</sup>

The building community has an important role in adapting to climate change for there are co-benefits of better designed buildings for sustainability and health. Advancing efforts for adaptation will be challenging, but essential and require ongoing assessment and action. Thus, the building community will need to be engaged in and aware of the design, implementation, and monitoring of building resiliency and indoor comfort. This will be important in not only assuring the sustainability of the buildings and the community over time, but this will also protect public health and overall population vulnerability from events such as extreme heat.

## 7.0 REFERENCES

1. IPCC, Climate Change 2007: Synthesis Report. Contribution of Working Groups I, II and III to the Fourth Assessment Report of the Intergovernmental Panel on Climate Change (IPCC; Core Writing Team, Pachauri, RK and Reisinger A.

- [editors]). IPCC, Geneva, Switzerland, 104 pp.
2. Haines A, Kovats R, Campbell-Lenrum D, Corvalan C. Climate change and human health: impacts, vulnerability, and mitigation. *Lancet* 2006 367:2101–09.
  3. Patz J, Campbell-Lendrum D, Holloway T, and Foley J. Impact of regional climate change on human health. *Nature* 2005 438:310–317.
  4. Greenough G, McGeehin M, Bernard S, Trtanj J, Riad J, Engelberg D. The potential impacts of climate variability and change on health impacts of extreme weather events in the United States. *Environ. Health. Perspect.* 2001 109:191–8.
  5. Ebi K, Semenza J. (2008) Community-based adaptation to the health impacts of climate change. *Am. J. Prev. Med.* 35(5):501–7.
  6. Younger M, Morrow-Almeida H, Vigdigni S, and Dannenberg A. The Built Environment, Climate Change, and Health Opportunities for Co-Benefits. *Am. J. Prev. Med.* 2008;35(5):517–526).
  7. Meehl G, Tebaldi C. More intense, more frequent, and longer lasting heat waves in the 21<sup>st</sup> century. *Science*. 2004 305:994–7.
  8. Confalonieri U, Menne B, Akhtar R, et al. Human Health. Climate Change 2007: Impacts, Adaptation and Vulnerability. Contribution of Working Group II to the Fourth Assessment Report of the Intergovernmental Panel on Climate Change. Parry ML, Canziani OF, Palutikof JP, van der Linden PJ, Hanson CE, eds. Cambridge University Press, Cambridge UK, 391–431.
  9. Pirard P, Vandentorren S, Pascal M, et al. Summary of the mortality impact assessment of the 2003 heat wave in France. *Euro. Surveill.* 2005 10(7):153–6.
  10. Salagnac J-L. Lessons from the 2003 heat wave: a French perspective. *Building Research and Information.* 2007 35(4):450–7.
  11. CDC. Heat-related deaths—United States, 1999—2003. *MMWR* 2006 55(29):796–8.
  12. Patz J, McGeehin M, Bernard S, et al. The potential health impacts of climate variability and change for the United States: executive summary of the report of the health sector of the U.S. national assessment. *Environ. Health. Perspect.* 2000 108(4):367–76.
  13. McGeehin M, Mirabelli M. The potential impacts of climate variability and change on temperature-related morbidity and mortality in the United States. *Environ. Health. Perspect.* 2001 109(Suppl2):185–9.
  14. Harlan S, Brazel A, Prashad L, Stefanov W, Larsen L. Neighborhood microclimates and vulnerability to heat stress. *Soc. Sci. Med.* 2006 63(11):2847–63.
  15. Bernard S, Samet J, Grambsch A, Ebi K, Romieu I. The potential impacts of climate variability and change on air pollution-related health effects in the United States. *Environ. Health. Perspect.* 2001 109(suppl 2):199–209.
  16. Golden J. The built environment induced urban health island effect in rapidly urbanizing arid regions—a sustainable urban engineering complexity. *Environ. Sci.* 2004 1(4):321–49.
  17. Sailor D, Pavlova A. Air conditioning market saturation and long term response of residential cooling energy demand to climate change. *Energy. Int. J.* 2003 28:941–51.
  18. Akbari H. Energy saving potentials and air quality benefits of urban heat island mitigation (PDF). 2005.

- Lawrence Berkeley National Laboratory.
19. U.S. EPA. Assessment of the Impacts of Global Change on Regional U.S. Air Quality: A Synthesis of Climate Change Impacts on Ground-Level Ozone (An Interim Report of the U.S. EPA Global Change Research Program). 2008. U.S. Environmental Protection Agency, Washington, DC, EPA/600/R-07/094F.
  20. Short C, Lomas K, Woods A. Design strategy for low-energy ventilation and cooling within an urban heat island. *Build. Res. Inf.* 2004 32(3):187–206.
  21. U.S. Green Building Council. Building design leaders collaborating on carbon-neutral buildings by 2030. 2007. [www.usgbc.org/News/PressReleaseDetails.aspx?ID=3124](http://www.usgbc.org/News/PressReleaseDetails.aspx?ID=3124).
  22. Crawley D. Impact of Climate Change on Buildings. Proceedings of the 2003 CIBSE/ASHRAE Conference. [www.cibse.org](http://www.cibse.org).
  23. Smith C, Levermore G. Designing urban spaces and buildings to improve sustainability and quality of life in a warmer world. *Energy Policy.* 2008 36(12):4558–62.
  24. Vidrih B, Medved S. The effects of changes in the climate on the energy demands of buildings. *Int. J. Energy. Res.* 2008 32(11):1016–29.
  25. Semenza J, Rubin C, Falter K, et al. Heat-related deaths during the July 1995 heat wave in Chicago. *N. Engl. J. Med.* 1996 335:84–90.

# **APPENDIX**

# **TASK COMMITTEE REPORTS**

**Report of Task Committee B**  
**NEXT-GENERATION BUILDING AND INFRASTRUCTURE SYSTEMS**

**Date:** 18 May 2009

**Place:** National Institute for Land and Infrastructure Management, Tsukuba, Japan

<b>Attendees:</b>	U.S. Side --	H. S. Lew	NIST
		Mehmet Celebi	USGS
		Erol Kalkan	USGS
		M. P. Singh (Co-Chair) (by e-mail)	NSF
	Japan Side --	Hiroshi Fukuyama (Co-Chair)	BRI
		Takashi Kaminosono	CBL
		Koichi Morita	BRI
		Yoshihiro Iwata	BRI

### 1. Objective and Scope of Work

#### (1) Objective

The objectives of the Task Committee are to enhance the development and implementation of innovative and new 1) structural and non-structural materials; 2) enabling technologies such as structural health monitoring and multi-hazard performance based engineering; 3) evaluation, analysis, design, construction, and maintenance methods through cooperative analytical and experimental approaches for the next-generation building and infrastructure systems. Opportunities during the next five years include topics on multi-hazard resilient buildings, embedded systems for the health and productivity of occupants, sustainability, and collaborations with other researchers and practitioners.

#### (2) Scope of Work

- a) Conduct joint workshops and meetings to identify research opportunities and new projects including multi-hazard risk reduction strategies and measures.
- b) Encourage the development and application of new technologies, smart sensors, intelligent materials, and sustainability to improve the health, safety, and productivity of construction workers and building occupants.
- c) Develop new materials and technologies for condition assessment, retrofit of existing buildings, and design of new buildings.
- d) Coordinate development of databases, test procedures, and guidelines for interpretation of test results and their applications.
- e) Coordinate joint research including the utilization of experimental facilities.
- f) Enhance the exchange of information and personnel.

### 2. Accomplishments

Task Committee B developed a five-year strategic research plan in February 2007 that addresses high-performance buildings' abilities to better resist the effects from extreme wind, earthquakes, and fire loads and to effect informed decisions about design procedures that incorporate environmental quality and sustainability of occupant health and life cycle systems. However, final achievements through joint research are not clearly defined since this plan covered very wide area.

### 3. Future Plans

Current research interests and activities in both sides will be compiled and presented for exchange information to find particular topics appropriate for collaborative research. Possible topics for collaboration will be disaster

resilient building, seismic retrofit, and structural renewal and/or remodeling of existing buildings. A suitable opportunity for exchange of information focusing on specific topics will be coordinated jointly.

**Appendix:** Future plans in the 2008 Task Committee report

Formulate an action plan for joint research on disaster resilient building systems/functions (reference Figure 1) with targeted research activities, together with estimated schedule, milestones, and needed resources by October of 2008. The possibility of partnering with TC D, Wind Engineering and other Task Committees will be explored in the formulation of the plan. The basic elements of this plan are as follows:

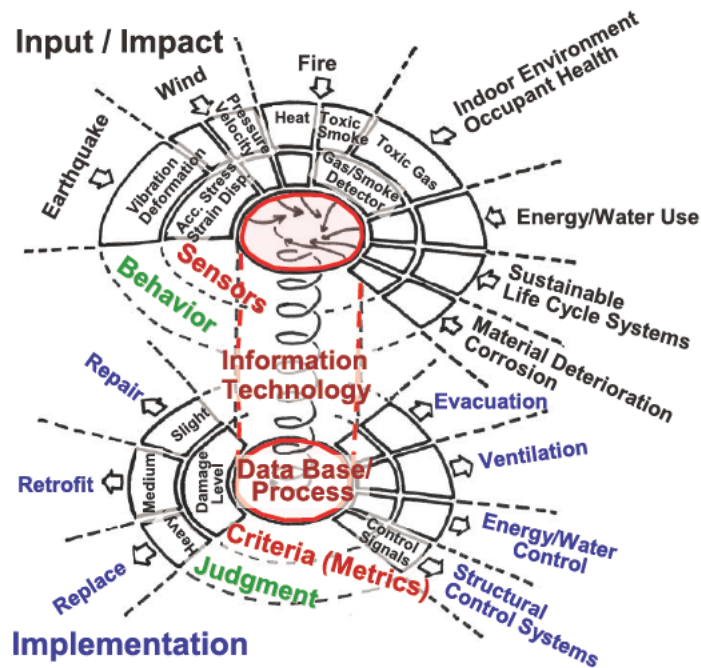


Figure 1

Figure 1. Diagram for creating high-performance buildings that better resist extreme winds, earthquakes, and fire loads resulting in informed decisions about design procedure incorporate environmental quality and sustainability of occupant health and life cycle systems. The initial TC focus is on sensors followed by subsequent actions to be determined during the next six months.

- (1) Develop and evaluate a framework to quantify the resilience of buildings. Seek expanded membership from both sides with expertise in sensors, information technology, and sustainability issues to collectively address the research involved in disaster resiliency for buildings and building systems (next generation buildings).
- (2) Identify the common elements in the work being performed by BRI's research on *Development of Performance Evaluation Systems for Structural Resilience and Functional Continuity of Buildings After Disasters*, and the MCEER/University at Buffalo's research on disaster resilient buildings and functional systems and other related on-going US-Japan research on this topic.
- (3) Identify the information needed for resilience evaluation. Create a database on building's performance and functionality considering physical attributes, public health issues following disasters, and environmental issues for use in the Quantification Framework. Refine metrics as required. The research is expected to identify and classify functionality of buildings considering the performance of the structural and nonstructural components and equipment and their impacts on the health of

- occupants and environmental consequences and impact. Check performance sensitivity based on costs, recovery time, and resources needed
- (4) Explore with TC D, Wind Engineering and other TCs the feasibility of their participation in this proposed joint research in disaster resilient buildings.
  - (5) Identify institutional and financial resources from organizations that can be used to jointly address this research problem such as:
    - a) United States - MCEER/University at Buffalo, National Science Foundation, Centers for Disease Control and Prevention, Arlington County's Department of Environmental Services and Facilities, Green Buildings Council, Virginia Polytechnic Institute and State University, Corps of Engineers - Military Construction Directorate.
    - b) Japan - Building Research Institute, National Institute for Land and Infrastructure Management, University of Tokyo, Nagoya University
  - (6) Finalize the US-Japan TC B research plan by October 2009 working through teleconference and email.

## Report of Task Committee C DAMS

**Date:** 18 May 2009

**Place:** National Institute for Land and Infrastructure Management, Tsukuba, Japan

**Attendees:**

U.S. Side --	Michael Sharp (Acting Chair)	USACE
	Robert Cris Hughes	USDHS
Japan Side --	Yoshikazu Yamaguchi (Chair)	PWRI
	Tomoya Iwashita	PWRI
	Hiroyuki Satoh	PWRI

### 1. Objective and Scope of Work

To develop technical insights into better understanding of the response of dams to seismic effects, the T/C will plan, promote, and develop research initiatives to assist in assuring seismic safety and economical protective countermeasures against earthquake loading for these critical structures.

The scope of work includes:

- (1) Develop methods of analysis for seismic design of dams including outlet works.
  - a) Comparative analysis of design methods and evaluation criteria used by U.S. and Japan.
  - b) Development of "Design Earthquake Ground Motions" for analysis and evaluation of dams.
  - c) Assessment of models and numerical procedures used for seismic dynamic analysis.
- (2) Perform research to better understand the dynamic characteristics of dam construction materials and site conditions.
  - a) Strength and deformation characteristics of concrete, soil and rock materials during earthquakes.
- (3) Evaluate observed performance of dams and outlet works during earthquakes.
  - a) Develop a database that contains measured ground accelerations and dynamic response of dams and outlet works during earthquakes, and other related information necessary to evaluate their seismic behavior, such as experimental and/or analytical data with description of test and analysis procedures used.
  - b) Investigation of damage mechanisms due to earthquake loading.
  - c) Application of the analysis of the observed dynamic behavior to the improvement of design criteria.

### 2. Accomplishments

- (1) Technical exchange and collaborative research on "*Non-linear response analysis of concrete dams*" has been conducted between the U.S. (U.S. Army Engineer Research and Development Center) and Japan (Public Works Research Institute). The shaking table experiments for crack-segmented concrete specimens considering the uplift pressure in a crack were made at PWRI in 2008. The U.S. Bureau of Reclamation is continuing to conduct shaking table tests at different scales and non-linear response analyses, and the joint comparison and evaluation of test and analysis results will be extremely beneficial to advance the state of the art in constitutive modeling of mass concrete structures.
- (2) Technical exchange and collaborative research on "*Experimental characterization of non-linear tensile behavior of mass concrete*" has been conducted between U.S. (U.S. Army Engineer Research and Development Center & U.S. Bureau of Reclamation) and Japan (Public Works Research Institute).

### 3. Future Plans

- (1) The Proceedings of the "**4th U.S.-Japan Workshop on Advanced Research on Dams**" will be published in 2009. In view of the importance of cooperative research programs on earthquake engineering for dams, the Task Committee will hold the "**5th U.S.-Japan Workshop on Advanced Research on Dams**" in USA in autumn of 2010. Specific location and time of the Workshop will finally be determined through correspondence between the Chairs of the Task Committee on Dams.
- (2) The Task Committee will continue the current efforts focused on the development of improved mechanisms to facilitate the continuous exchange of results of research activities and general technical information related to dam earthquake engineering.
- (3) The Task Committee will coordinate exchange visits of scientists and engineers from the U.S. and Japan. A series of case histories of mutual interest will be identified and prioritized and they will serve as the focus for this exchange program.
- (4) The Task Committee will promote the development of joint research programs. The following topics have been identified as areas for future collaborative research:
  - a) **Non-linear response analysis of concrete dams:**  
The Task Committee will continue their collaboration in this research to include both analytical and experimental data.
  - b) **Global stability analysis of concrete dams:**  
The Task Committee will conduct a review of the minimum requirements for sliding and overturning stability currently in use in the U.S. and Japan. The Task Committee recognizes the importance of this collaborative effort, as the corresponding guidelines are currently subject to revision and update both in the U.S. and Japan. The results of this effort will be summarized and published. "**Engineer Manual No. 1110-2-2100: Stability Analysis of Concrete Structures**" published by The U.S. Army Corps of Engineers in December 2005 (4. (2)) contains this problem.
  - c) **Criteria for seismic analysis progression:**  
The Task Committee will review and compare the state of practice in the U.S. and Japan regarding current recommendations for progression of seismic analysis based on stages of increasing complexity. The results of this effort will be summarized and published.
  - d) **Seismic evaluation of embankment dams:**  
The Task Committee will review criteria and guidelines for post-earthquake stability and deformation analysis of embankment dams. The results of this effort will be summarized and published.
  - e) **Dam-foundation interaction:**  
The Task Committee will develop collaborating research efforts to review and develop improved numerical models for dam-foundation interaction.

The activities corresponding to the four areas indicated above will be addressed sequentially and the corresponding schedule will depend on the progress of the corresponding guidance documents, some of which are currently under discussion, development and/or review in the U.S. and Japan.
- (5) Following large earthquakes in the U.S. or Japan, the Task Committee will assemble a joint reconnaissance team to investigate the performance of concrete dams, earth and rockfill dams, and outlet works.

#### 4. Related Activities

- (1) The Ministry of Land, Infrastructure and Transport (MLIT), Japanese Government completed the "**Guidelines for Seismic Safety Evaluation of Dams (Draft)**" in March 2005. This document was applied to four existing dams during the fiscal year of 2005 and three other existing dams during the fiscal year of 2006 to 2008 in order to verify and revise it. The final draft of the revised version of the guidelines is now being reviewed by the headquarters of the MLIT for the final approval.
- (2) Japanese dam engineers travelled to China in order to investigate the damage to dams and repair works of the damaged dams due to Wenchuan Earthquake, which occurred on 12 May 2008.

## **Report of Task Committee D WIND ENGINEERING**

**Date:** 18 May 2009

**Place:** National Institute for Land and Infrastructure Management, Tsukuba, Japan

<b>Attendees:</b>	U.S. Side --	John Gaynor (Co-Chair)	NOAA
		Partha Sarkar	ISU
	Japan Side --	Yasuo Okuda (Co-Chair)	BRI
		Jun Murakoshi (Co-Chair)	PWRI
		Hitomitsu Kikitsu	NILIM
		Hiroshi Katsuchi	YNU
		Mitsuru Ueno	MRI

### **1. Objective and Scope of Work**

To exchange technical information and to jointly plan, promote, and foster research and dissemination, in order to improve understanding of wind and its effects on structures, to establish more rational wind-resistant design procedures for structures, and to contribute collaboratively and synergistically to wind hazard mitigation. Specific objectives for the Task Committee include:

- (1) Strategically and collaboratively, identify research needs in wind hazard mitigation in the areas of new technology, basic and applied research in wind and structural engineering, and in social and economic impacts of wind events.
- (2) Facilitate cooperation and collaborative research between U.S. and Japanese researchers in wind engineering.
- (3) Identify and exchange successes in wind engineering and wind hazard mitigation.

The scope of the US-Japan collaboration includes:

- (1) Characterization of strong wind, especially boundary layer extreme winds.
- (2) The study of wind effects including wind loading on and wind-induced response of structures.
- (3) Performance of experimental and analytical research to predict wind effects.
- (4) Sharing damage surveys, and wind hazard and risk assessments.
- (5) Development of new technologies for wind hazard mitigation.

### **2. Accomplishments**

- (1) The results of an international comparison of wind-tunnel based wind effects on a typical low-rise industrial building were published ("International Comparison of Wind Tunnel Estimates of Wind Effects on Low-Rise Buildings: Test-related Uncertainties", W. P. Fritz, B. Bienkiewicz, B. Cui, O. Flamand, T. C. E. Ho, H. Kikitsu, C. W. Letchford, and E. Simiu, *J. Struct. Engrg.* 134, 1887 (2008)). In addition to NIST and BRI, other participants included the Univ. of Western Ontario, Colorado State Univ., Clemson Univ., TTU, and the Centre Scientifique et Technique du Batiment, Nantes, France. The ratios between maximum and minimum wind-induced internal forces in building frames were as high as three.
- (2) In March 2008 conducted joint experiments on the simulation of transient loads on buildings using Miyazaki multi-fan wind tunnel are underway under the collaboration between the University of Notre Dame, COE, Tokyo Polytechnic University, and Miyazaki University. A paper was recently presented at an international Fluid Mechanics Conference and Sixth International Colloquium on Bluff Body Aerodynamics and Applications in Milan, July 2008. A benchtop multi-fan wind tunnel and a wind tunnel with a flat plate to simulate transient events are being used at the University of Notre Dame to better capture the aerodynamics in transient conditions to assess their impact in downbursts.

- (3) Professor Tetsuro Tamura, Tokyo Institute of Technology and Dr. Y. Okuda, BRI are preparing numerical simulation of the LES model to evaluate wind environment of the urban area, Tokyo and Chicago, as a joint research with Professor A. Kareem, University of Notre Dame. Trial calculations using hybrid method of LES model and meso-meteorological model (MM-5) for several examples in Tokyo were carried out. The difference of urban shape based on buildings and streets between Tokyo and Chicago were clarified.
- (4) Several papers and reports have resulted from the US-Japan collaboration between Professors P. Sarkar, F. L. Haan Jr. et al. in Iowa State University (ISU) in the US and Drs. H. Kikitsu, H. Sato, J. Murakoshi in BRI/PWRI/NILIM in Japan within the last year, April 2008 to May 2009. They are included in Appendix A.
- (5) Professor Jones, Dr. DeLong, and Professor Shirato exchange data on stay cable vibrations.

### 3. Future Plans

- (1) A wind engineering symposium for meteorologists and wind engineers led by Iowa State University and NOAA that was originally scheduled for 2009 will be held in conjunction with the Fifth International Symposium on Computational Wind Engineering (CWE2010) to be held from May 24 - 29, 2010 at Chapel Hill, North Carolina, USA. More details will be posted soon on the CWE2010 website. It is suggested that the symposium will include storm surge in collaboration with TC-H.
- (2) The Fifth US-Japan Workshop on Wind Engineering will be held in second half of 2010 subject to availability of support from the US NSF.
- (3) As opportunities arise, seek additional opportunities to pursue collaborative research on the following topics:
  - a) Wind effects on buildings and wind energy systems
  - b) Wind effects on bridges
  - c) Evolving Technologies
- (4) Exchange technical information on the following topics.
  - a) Wind characteristics and wind hazards
  - b) Wind pressures, loadings and performance of buildings
  - c) Wind-induced response of flexible, cable-suspended bridges and their components
  - d) New prediction and mitigation techniques for wind effects
  - e) Share data base of storm damage assessments.
- (5) Engage in more regular interaction and communication among Task Committee members. Use email and exchange visits between full Panel meetings were suggested as a means of facilitating and coordinating collaborative activities.
- (6) Strategically and collaboratively construct a vision and plan for wind engineering research needs for the next decade, and formulate collaborative activities around those plans.

## Appendix A:

Papers and reports from the US-Japan collaboration between Iowa State University (ISU) in the US and BRI/PWRI/NILIM in Japan within the last year, April 2008 to May 2009

- A damage survey of the Parkersburg EF-5 Tornado of May 25, 2008 was conducted by Dr. Hitomitsu Kikitsu, BRI, Japan and Dr. Partha Sarkar, ISU, USA along with personnel from the Office of National Weather Service, NOAA, Des Moines, IA on May 26-27, 2008. Both English and Japanese versions of the damage survey report are available on request from its co-authors. The Japanese version of the report "Damage to Buildings by EF5 Tornado in Iowa, U.S., on May 25, 2008" by H. Kikitsu and P. P. Sarkar is published in the Journal of Wind Engineering, JAWE, Vo. 33 (4), October 2008.
- A paper "Comparative and sensitivity study of flutter derivatives of selected bridge deck sections, Part 1: Analysis of inter-laboratory experimental data" by P. P. Sarkar, L. Caracoglia, F. L. Haan, Jr., H. Sato and J. Murakoshi, was published in Engineering Structures (Elsevier) 31 (2009), pp 158-169.
- Another paper "Comparative and sensitivity study of flutter derivatives of selected bridge deck sections, Part 2: its Implications on the aeroelasticity of slender- bridges aeroelasticity", by L. Caracoglia, P. P. Sarkar, F. L. Haan, Jr., H. Sato and J. Murakoshi is accepted for publication in Engineering Structures (Elsevier) and soon be available online (in press).
- A paper "United States-Japan Benchmark Study of Flutter Derivatives of Selected Bridge Decks" by P. P. Sarkar, L. Caracoglia, F. L. Haan, Jr., H. Sato and J. Murakoshi, was presented by Prof. Caracoglia at the 40th Joint Panel Meeting held at NIST, May 19-21, 2008.
- A paper titled, "Experimental study of internal pressure and debris strike for improved tornado-induced loads of low-rise buildings" by Partha Sarkar, ISU and Hitomitsu Kikitsu, BRI will be presented by Partha Sarkar at the 41st Joint Panel Meeting of the UJNR Wind and Seismic Effects at Tsukuba, Japan from May 18-20, 2009.
- A paper titled (tentative), "Damage to Buildings by EF5 Tornado in Iowa, U.S. in May, 2008" by H. Kikitsu and P. P. Sarkar will be presented by Hitomitsu Kikitsu at the 41st Joint Panel Meeting of the UJNR Wind and Seismic Effect at Tsukuba, Japan from May 18-20, 2009.
- A paper, "Characteristics of Tornado-induced wind load on low-rise building using tornado simulator" by Hitomitsu Kikitsu, Partha Sarkar, and Fred Haan will be presented by Dr. Kikitsu at the Annual Meeting of the Japanese Association for Wind Engineering (JAWE) in May 2009.
- A paper, "Evaluation on Structural Risk by Wind-Borne Debris Using Tornado Simulator" by Hitomitsu Kikitsu and Partha Sarkar will be presented by Dr. Kikitsu at the 58th National Congress of Theoretical and Applied Mechanics in Japan, June 2009.

## **Report of Task Committee G TRANSPORTATION SYSTEMS**

**Date:** 18 May 2009

**Place:** National Institute for Land and Infrastructure Management, Tsukuba, Japan

**Attendees:**

U.S. Side --	W. Phillip Yen (Chair)	FHWA
	David Sanders	UNR
Japan Side --	Atsushi Yoshioka (Chair)	PWRI
	Shoichi Nakatani	PWRI
	Jun-ichi Hoshikuma	PWRI
	Junichi Sakai	PWRI
	Masahiro Shirato	PWRI

### **1. Objective and Scope of Work**

The objectives of work include:

- (1) To plan, promote and foster research on the behavior of transportation facilities when subjected to wind and seismic forces, and
- (2) To disseminate research results and provide specifications and guidelines based on the Task Committee's findings.

The scope of work includes:

- (1) To investigate existing and new bridges design, the behavior of whole bridge systems and/or single component of a bridge without limitation on their size and function.

### **2. Accomplishments**

- (1) The 24th US-Japan Bridge Engineering Workshop was held during 22 - 24 September 2008, in Minneapolis, MN, US. 19 U.S. and 25 Japanese participants attended the workshop. 42 technical papers were presented and discussed on the following main topics: a) Seismic design/retrofit and b) Maintenance.
- (2) The proceedings of the 24th US-Japan Bridge Engineering Workshop will be printed and will be distributed soon. The program and papers of the workshop will be posted on the web-site of the UJNR at the PWRI ([http://www.pwri.go.jp/eng/ujnr/tc/g/tc\\_g.htm](http://www.pwri.go.jp/eng/ujnr/tc/g/tc_g.htm)) and FHWA.
- (3) Both side conducted post earthquake damage evaluation studies, and the information has been exchanged.

### **3. Future Plans**

- (1) The 25th US-Japan Bridge Engineering Workshop will be held in October 19-21, 2009, in Tsukuba, Japan. Specific program and itinerary will be proposed by the Japan-side Task Committee G with the concurrence of the US-side Task Committee.
- (2) Following a devastating earthquake or hurricane (typhoon) in the US or Japan, the committee will form a joint reconnaissance team to investigate the performance of transportation systems.
- (3) With increasing concerns over structural member fractures of older bridges in the US and Japan, the committee will conduct joint efforts to investigate detection methods, causes and repairs. The joint efforts should be initiated by the hosting side.
- (4) Both sides agreed to conduct joint researches on the following topics.
  - a) Strategy to determine design criteria, design loads, and load factors that consider ductility and redundancy for multiple hazards

- b) Collaboration to develop feasible and practical non-destructive test techniques for bridge inspection
- (5) Both sides agreed to conduct information sharing on the following topics.
  - a) Best and poor practices in bridge design and maintenance
  - b) Post earthquake response and repair
  - c) Study on policy making to set different performance levels of routes and allocate resources for seismic upgrading/retrofit, bridge inspection, and rehabilitation based on the assigned characteristics

#### **4. Related Activities**

- (1) Both side's committee members participate a NIED/NEES cooperative experimental research in full scale Bridge Column shaking table tests.

**Report of Task Committee H  
STORM SURGE AND TSUNAMI**

**Date:** 18 May 2009

**Place:** National Institute for Land and Infrastructure Management, Tsukuba, Japan

**Attendees:** U.S. Side -- Solomon Yim (Co-Chair) OSU  
(via e-mail correspondence)

Japan Side -- Takashi Tomita (Chair) PARI

**1. Objective and Scope of Work**

The objectives of work include:

- (1) To exchange scientific and technical information
- (2) To jointly plan, promote and foster research and dissemination of knowledge
- (3) To develop measures to prevent and mitigate damages from storm surges and tsunamis

The scope of work includes:

- (1) Perform joint research on storm surge and tsunami occurrences, generation, propagation, and coastal effects. Develop database on storm surge, tsunami and wave measurements.
- (2) Improve coordination of strategies and systems for observations of storm surges and tsunamis by field surveys, satellites, and in-situ measurements.
- (3) Exchange results and status of storm surge and tsunami mitigation activities including analysis of the problem, planning, warning, and engineering approaches.
- (4) Exchange information on development of technologies including numerical models to predict propagation processes, land-fall locations, inundation and run-up heights, and wave characteristics, improved instrumentation, and use of satellite communication for detection and warning.
- (5) Facilitate research result and technology development disseminations through exchange of literature, technical reports at joint meetings, special workshops, joint projects, and direct interaction among participants.
- (6) Develop planning, design and construction guidelines in storm surge and tsunami flooding zones to serve as a model for international standards.
- (7) Provide technical support to develop storm surge and tsunami mitigation programs worldwide.
- (8) Encourage conduct of joint investigation following storm surge and tsunami events.

**2. Accomplishments**

- (1) The 5th International Workshop on Coastal Disaster Prevention was held on July 22, 2008 in Jogjakarta, Indonesia in cooperation with Port and Airport Research Institute (PARI), Coastal Development Institute of Technology, Ministry of Land, Infrastructure, Transport and Tourism, Japan, Ministry of Marine Affairs and Fisheries, Indonesia, and University of Gadjah Mada. Participants include not only T/C H members of this panel but engineers, natural and social scientists and NGO members. The number of participants was 220. Both Japan and US side chairs, Drs. Tomita and Yim, gave invited presentations on recent research activities on tsunami and storm surge effects on coastal structures.
- (2) Professor Daniel Cox of Oregon State University (OSU) and Japan side chair, Dr. Tomita, are collaborating on an experimental project on tsunami inundation of an Oregon coastal city. OSU will conduct the physical experiment at the Hinsdale Wave Research Laboratory (HWRL) and Dr. Tomita will use numerical models at PARI to simulate the results. Other numerical researchers in the US and Europe including Professors Solomon Yim of OSU and Patrick Lynett of Texas A & M University also are conducting numerical simulations for comparison and evaluation of their models.

### 3. Future Plans

- (1) Create joint research between the US and Japan to develop and improve numerical models of storm surge and tsunami dynamics and to exchange experimental and field data. The following topics have been identified as areas of future research collaboration on storm surges and tsunamis:
  - a) field observation
  - b) characterization
  - c) physical experiment models
  - d) numerical simulation models
  - e) effects on coastal structures and damage estimations
  - f) design of protective structures for different levels
  - g) hazard maps development and warning system design
  - h) storm surge and tsunami information communication and warning systems development
  - i) risk assessment including hazard beyond designed levels
- (2) Develop database for existing and planned experiments including description and parameters of experiments to maximize overall available experimental data for understanding of physical behavior, numerical model validation and structural design.
- (3) Include the effects of global warming on atmospheric and oceanographic environmental conditions leading to changes in the probability of occurrence and intensity of typhoons, cyclones and hurricanes, and sea level rise. These changes in typhoon and sea level characteristics will directly influence the characteristics and induced damages of future storm surges and tsunamis.
- (4) Plan to hold the 6th International Workshop on Coastal Disaster Prevention in Japan, in late 2009.
- (5) The US side co-chair, Professor Solomon Yim, will contact the co-chair, Dr. Eddie Bernard and the US side co-chair of T/C D, Mr. John Gaynor, regarding the study of storm surge, and the US side chair of T/C G, Dr. Phillip Yen, regarding storm surge and tsunami effects on bridges.

### 4. Related Activities

- (1) Both Japan and US side chairs, Drs. Tomita and Yim, partially wrote "Recommendations with regard to the design and construction of maritime structures in tsunami prone areas," which was the report of Working Group 53 of Maritime Navigation Commission of the International Navigation Association (PIANC).
- (2) US side researchers at OSU are conducting numerical and experimental modeling of storm wave effects on coastal bridges. A series of experiments of a 1/5-scale highway bridge section subjected to storm waves have been conducted at the Large Wave Flume at the HWRL. Final tests were completed in July 2008. The experimental results are being used to help develop design guidelines and calibrate numerical models developed in house.
- (3) The third and fourth Japan-U.S. seminars on Tsunami Disasters were held at PARI on October 28, 2008 and March 4, 2009, respectively, welcoming Professors Harry Yeh and Daniel Cox of OSU. Many engineers and researchers participated in the both seminars.
- (4) Japan side T/C members have cooperative research activities in Technical Committee on Technologies to Estimate and Reduce Tsunami Damages, Japan Society of Civil Engineers.
- (5) US side T/C members have several on-going research projects on tsunami and storm surge numerical modeling and experiments at the HWRL of OSU. OSU will hold a training workshop on 8-10 July 2009.

# **TECHNICAL SITE VISITS**

## HIGHLIGHTS OF THE TECHNICAL SITE VISITS

During the 41st Joint Panel Meeting the delegation visited seven sites. Highlights follow:

### 1. Tokyo Rinkai Oh-hashhi Bridge

The Tokyo Rinkai Oh-hashhi Bridge also tentatively named the Tokyo Port Seaside Bridge is 1,618 m long over the water and 2,933 m long in its entirety. It connects reclaimed land outside the central breakwater and the Wakasu area of Tokyo. When it is opened in 2011, the Tokyo Port Seaside Road will facilitate commercial highway transportation in and around the Tokyo Port easing traffic congestion in roads serving the Tokyo Bay area.

The uniqueness of this bridge design is its requirements not to interfere with the flight patterns of Haneda Airport and yet be high enough over the shipping channel to accommodate cargo ships. If this bridge's height was not controlled by the flight limits, a suspension-type design would have been the most economic choice. The selected design was a high strength steel (70 ksi) truss bridge with structural height of 87.8 m and headroom (distance below substructure) of 54.6 m. The bridge's lower foundation is the main pier that supports the bridge's 760 m composite box truss (160 m end spans and 440 m center span). Soft clay covers the bottom of the Tokyo Bay where the pier is located. This continuous and composite bridge poses a huge challenge of its substantial self weight and high corrosion resistance requirement area. Steel coating and welding standards are much higher than required. The clay layer is about 30 m thick. A "steel pipe sheet pile well foundation," was used in which temporary steel pipe sheet pile cofferdams serve as the foundation. Truss members are installed by various cranes (land and floating). The truss will be transported by barge using one of Japan's three largest floating cranes. When in place the upper deck truss will be installed using a 450 ton crane to lift members to the deck. Sliding bearings are installed for seismic isolation and the piers. The bridge is orthotropic steel to limit the fatigue with 0.5 m steel expansion finger joints. The bridge is designed for a 100 year life. The bridge cost is estimated to be 98 B yen (\$1 B).



Group Photograph of the Delegation at Tokyo Rinkai Oh-hashhi Bridge

## **2. Tokyo International Airport (Haneda) New Runway Design and Construction**

Haneda Airport is constructing a fourth runway (off shore) to accommodate the spiraling increase in demand for air mass transportation. A new Passenger Terminal 2 was conducted in February 2007. This fourth runway (Runway D) will serve domestic and international flights easing congestion at Narita International Airport about 60 km northeast of Tokyo. The new 2,500 m runway is a combination of land fill reclamation and a bridge. The landfill is located in Tokyo Bay and its adjoining bridge is in the Tama River estuary at Tokyo Bay. The runway elevation ranges from 14 m to 17 m above sea level. This runway is connected to Haneda Airport by a 260 m bridge section.

The bridge pier jackets are 1.6 m diameter by 80 m long. Bridge deck sections are prefabricated in sets of six piers each with its superstructure measures 63 m by 45 m with cross bracing to resist the flow of the Tama River. These sections are floated to site. When placed, the weight of the sections sinks about 20 m into the sea bed. They are then vibrated to a depth of 70 m. The piers are aluminum with stainless steel jackets starting 1.5 m below the splash zone and to the deck steel substructure that is covered with titanium plates. The superstructure runway is super high strength precast fiber concrete. One hundred eighty nine jackets make up the bridge. The expected life of the bridge is 100 years.

The landfill consists of sand compaction piles in alluvium clay layer, riprap perimeter serves as wave dissipaters, and 12 m to 20 m deep dredged earth mixed with cement is placed over a sand mat with compacted sand around the perimeter. The landfill is expected to sink about one meter over its life time. The runway connection to the bridge is by a roller leaf connection. The cost of the runway is about 600 trillion yen (about \$6 trillion at May 2009 conversion).

## **3. Disaster Management Center (DMC)**

The new national disaster management center at Ariake, Tokyo, is a regionally based, state-of-the-art, multi-function emergency management facility. When a disaster strikes, such as a major earthquake, the DMC functions as a disaster management center and a medical treatment-shelter facility. The facility includes an evacuation zone, evacuation center, stockpiling base, relief goods collection location, debris yard, emergency/restoration operation center, emergency headquarters facility, and a “spare” facility. Here, administrative agencies gather information and direct regional operations. The operation room is equipped with large-screen monitors, terminal devices, and communication equipment. The facilities include a meeting room, a napping room, and rooms for staff on standby. The design of the DMC site includes a number of features such as a water collection and reuse system that uses permeable pavement (green technology), plantings of large trees strategically positioned in the overflow area of the grounds that will serve as a field hospital in temporary tents, and decorative fountain that recedes into the ground to provide a level pathway for access to and from the field tent hospital and to the new Cancer Hospital located adjacent to the DMC.

The DMC coordinates disaster relief efforts with the Tokyo Metropolitan Area and with the Tokyo Metropolitan Disaster Relief Center in Shinjuku, Tokyo. The Center uses dedicated communication systems

to communicate with its officials and staff during emergencies. Pagers worn by staff are triggered with seismic intensity of 5 or greater on the Japan Meteorological Agency intensity scale. The Center operates with three contingency plans to assist the disaster relief staff get to their offices - 1) through designated roads, 2) designated metro trains, and 3) helicopters from its rooftop heliport respectively. The DMC serves a dual function during the non disaster periods as a learning center for general public disaster awareness about earthquake disaster education and demonstrations on a day-to-day basis that help prepare local residents for disaster response. The DMC provides outdoor recreation space in the surrounding park (evacuation zone).

#### **4. Takenaka Corporation Tokyo Main Office, Tokyo**

Takenaka Corporation's Tokyo seven story main office building opened in 2004 as a sustainable office building. Wall mounted monitors display the building's energy consumption and CO<sub>2</sub> emissions. This building uses natural light and wind for ventilation. Its HVAC ducts are made of used and recycled cardboard materials with an added aluminum coating. Its rooftop is designed with greenery, a large rain tank is located in the basement as a water source for toilet flushing and as emergency water supply, and an IT-based energy use management system records CO<sub>2</sub> emissions that are 25 percent lower than an average office building today. The building is designed to allow north-south winds to bring air into the building with greenery around the base of the building. Their "Comprehensive Assessment System for Building Environmental Efficiency (CASBEE)", akin to the US LEED (Leadership in Energy and Environmental Design) environmental efficiency rating scheme, awarded this building an environmental efficiency rating of 4.9 (5.0 is the highest rating). The office spaces on the 2nd story and above have open layout and its three center cores allows sunlight into the building's interior through its cathedral glass ceiling. The building incorporates solar collectors on the building exterior for heating and ventilation and features a hybrid air conditioner using conditioned air with natural ventilation that flows through louvers in the outer walls and through a porous floor. The conditioned air is cooled during the day using ice produced during evenings in its roof top thermal storage units. The cafeteria accommodates 350 persons and can be used as a general purpose room for large meetings and conferences. Building temperatures are maintained near 24 degrees Celsius. The building is designed to be operational for a one week period following a major disaster and serves as a disaster relief center for its staff.

The structural framing system consists of an outer braced structure and a universal floor beam with buckling resistant braces. The steel beams are coated with fire resistant calcium silicate sheets. Building equipment is tightly fixed to the building's structural system permitting the building to be operational after an earthquake. The structure uses a uniform span measuring 10.8 m by 10.8 m made up of CFT columns with a diameter of 500 mm, an "external bracing structure" with buckling-restrained braces laid out, and "universal floor beams" made up girders and beams of a uniform beam depth of 450 mm. With a disperse layout of air conditioners in the exterior brace sections, outside air is directly drawn in from the exterior wall louvers, exhausting through the light wells, the building uses a four-mode hybrid air-conditioning system using natural ventilation. With the universal floor beams, the air-conditioning ducts do not penetrate the beams, but are hung under the beams, so with a standard office building floor height of 4.1 m, a

minimum 3 m ceiling height has been maintained. The direct ceiling “new ceiling system” consists of punching metal underneath covers and lighting fixtures.

### **5. Shimizu Institute, Shimizu Corporation**

The Shimizu Corporation’s Research Institute Headquarters was built in 2003 using Green Building Concepts that demonstrated a 43% savings in energy costs and a 35% reduction in CO<sub>2</sub> emission during the building’s first 5 years of operation. The research institute is designed in a campus like setting with various testing facilities. For example, its structural testing laboratory is equipped with a 6 MN testing machine, a reaction floor, and vibration testing systems. The wind tunnel testing laboratory is a return boundary-layer wind tunnel 3.5 m wide, 2.5 m high, and 20.3 m long that generate wind up to 35 m/s. Included are a multi-point wind velocity and direction measuring system, a 512-point simultaneous pressure measuring system, and various simulation systems. Also the tunnel is equipped to simulate snow drift on the roofs and around buildings. A 1,940 m biotope (pond with fish and birds) is located in the foundation space of the original building that was demolished for construction of the campus of individual research laboratories.

The main office building adjacent to its labs was designed for energy savings technologies. Air is supplied through the floor carpets reducing the need for ducts. The office work space incorporates “personal air diffusers” under desks to help cool the workers legs. Room air temperatures average 24 degree celsius. Task and ambient lighting and information systems optimizes energy use and electricity. The ice storage system cools water in the evening for use during warm summer days for cooling. Gradation blinds help reflect the sunlight away from the building. The building’s CASBEE rating is 3.2. Paper waste and biomass are used to generate electricity through an energy conversion system. The building is installed on seismic isolators installed in an underground reservoir that isolates the building through buoyancy. The six main columns are installed with rubber bearing base isolators. The core suspended system on one of its buildings employs isolators on the roof with the building suspended around a central core. This technique is similar to those used for pagodas.

Of particular interest is Shimizu’s research into a Green Float Botanical Future City. This concept involves erecting a series of 1000 m towers (inverted cones) where residents live in about 150 m<sup>2</sup> - 200 m<sup>2</sup> units starting at the 700 m level and research and plant factories are located below the residential level. The towers are constructed on 3 km diameter floating artificial islands located in the equatorial Pacific Ocean. A waterside resort is at the oceanfront. A cluster of islands could accommodate 1 million persons. This botanical city design concept is aimed at the 2025 time frame having the intent to: provide living spaces for the increasing population; reduce CO<sub>2</sub>; conserve energy; reduce waste products; and preserve the environment. Ocean thermals and solar energy is expected to be the primary energy source. Cooling will be from several thousand meter high pipes in the atmosphere and also in deep ocean water. CO<sub>2</sub> will be dumped into the ocean using a 1 km to 1.5 km deep pipe. The inverted cone tower is proposed to be constructed of honeycomb materials using magnesium from the sea. Shimizu philosophy in developing their proposed living base addresses Albert Einstein’s quote, “We can not solve problems using the same kind of thinking we used when we created them”.

## **6. Japan Meteorological Agency**

The visit was divided into three topics: seismic, tsunami, and volcano warnings.

**Seismic Warnings.** Japan experiences about 100,000 earthquakes per year - most of them small. Earthquakes which can be felt by the population average about 2,000 per year. There are in excess of 4,248 seismic intensity observing stations in Japan operated by JMA, local governments (the majority of stations), and NIED. Seismic warnings are sent out through multiple communication channels within 2 minutes after the event for earthquakes estimated to be equal to or greater than 3 on the Japanese intensity scale. The levels of response are scaled with the intensity of the earthquakes. A simple shake map of the predicted timing and intensity of the earthquake is used for the forecasts and seismic stations are used for verification. Currently, there is a project called the Tokai Earthquake Prediction Project designed to provide early prediction of a possible 8 or greater magnitude earthquake in a region west of Tokai that would severely impact the Tokyo region. The project is attempting to simulate pre-seismic strain rates 1 or 2 days prior to a major event using a large array of strain gages in the region. If the strain indicates that an earthquake is imminent, this information is given to high level government authorities.

**Tsunami Warnings.** If the estimated height of the tsunami exceeds 3 m, a warning is given within 2 or 3 minutes of the seismic event. For estimated heights below 3 m, a tsunami advisory is given. JMA also provides tsunami information for the Northwest Pacific region and to most Asian countries.

**Volcano Information Service.** There are currently 108 active volcanoes in Japan. They are monitored by combinations of seismic sensors, TV cameras, and GPS monitoring (for large ground motion). Warnings are provided if necessary. There are 5 levels of warning, with level 5 being the highest, meaning a large eruption is imminent or underway and evacuation is necessary. JMA also provides volcanic ash advisories to civil aviation for aircraft safety. JMA is one of only nine stations in the world offering such advisories.

## **7. Nippon Life Insurance Company, Marunouchi Building**

This headquarters building of Nippon Life Insurance recently received an award for its energy and environmental savings. Its façade (the base of the building's front) corresponds to Tokyo's historic 31 m height line with the main building office tower body set back. Seismic vibration control is by "w-pair Mullions" installed in the exterior walls. These paired precast columns (w-paired mullions) are hinged at their connections to the top and bottom structural beams with vibration control panels installed between the granite precast columns. The building's seismic damping system is located in the top floor. The building is not designed against terrorist attacks or for fire loads. During disasters occupants either descend to street or ascent to the roof for evacuation by helicopters. Sunshine heat gain is reduced by auto blinds and mullions and eaves in the façade. Energy savings are through greater use of natural lighting and light control sensors. The building achieved a 34 percent energy savings during 2006-2007 over the standard value calculated for a typical office building. The building's CASBEE rating is 3.2. The building was designed for a 100 year life.